

A LITHOGEOCHEMICAL STUDY OF HYDROTHERMAL ALTERATION  
ASSOCIATED WITH MAFIC HOSTED AND BESSHI-TYPE  
MASSIVE SULPHIDE DEPOSITS

by

HRISTO SIMEONOV STOYNOV

B.Sc., Institute of Mining and Geology, Sofia, Bulgaria, 1986  
M.Sc., University of Minnesota, Minneapolis, USA, 1995

A THESIS SUBMITTED IN PARTIAL FULFILLMENT  
OF THE REQUIREMENTS FOR THE DEGREE OF  
DOCTOR OF PHILOSOPHY

in

THE FACULTY OF GRADUATE STUDIES  
(Department of Earth and Ocean Sciences)

We accept this thesis as conforming  
to the required standard

THE UNIVERSITY OF BRITISH COLUMBIA

April 2003

© Hristo Simeonov Stoyanov, 2003

In presenting this thesis in partial fulfilment of the requirements for an advanced degree at the University of British Columbia, I agree that the Library shall make it freely available for reference and study. I further agree that permission for extensive copying of this thesis for scholarly purposes may be granted by the head of my department or by his or her representatives. It is understood that copying or publication of this thesis for financial gain shall not be allowed without my written permission.

Department of Earth and Ocean Sciences

The University of British Columbia  
Vancouver, Canada

Date April 25, 03



## **Abstract**

Pearce element ratio (PER) analysis was proposed in 1968 as a graphical method to be applied in petrology. Using major element chemical compositions of rocks, it allows for the determination of primary mineral parageneses. The application of the technique was later expanded to include studies of hydrothermal alteration associated with mineral deposits. This study tests the applicability of PER analysis and the related generalized element ratio (GER) analysis methods to the study of alteration associated with two classes of Volcanic-Hosted Massive Sulphide deposits. Presented are case studies of the Chu Chua and the Konuto Lake Mafic-Hosted Massive Sulphide deposits and the Goldstream Besshi-type deposit.

Molar element ratio techniques (PER and GER) are used to identify altered samples and to differentiate between individual chemical alteration types. It is demonstrated that the technique is capable of identifying the exact alteration reaction for an individual sample or for a coherently altered group of samples. The format in which the chemical analytical data are presented allows for a convenient interpretation of the mineralogical effects of alteration. Thus, the validity of the conclusions based on major element lithogeochemistry can be independently verified by petrographic methods.

The most typical chemical alteration types found in the three studied deposits are silica mobility (loss and addition), loss of Ca and Na and addition of Fe and Mg. Mineralogically, the alteration process involves the destruction of plagioclase and pyroxene, local deposition of quartz and deposition of iron sulphides. At Chu Chua, extreme Fe-Mg addition caused the characteristic talc-magnetite assemblage whereas at Goldstream Fe and Mg-rich clays were deposited in a seafloor hydrothermal vent setting. Mobilized Ca, Na and excess  $\text{SiO}_2$  were exhaled on the seafloor, giving rise to exhalative chert deposits, carbonate and clay minerals.

The tested technique allows the degree of alteration to be quantified in each individual sample. The geographic coordinates of altered samples are then plotted to reveal the spatial patterns of alteration. The outlined alteration anomalies coincide spatially with the known ore bodies and are significantly larger in overall dimensions. Thus, in an exploration context, they would represent intermediate targets. The study proposes exploration parameters, which can be used in similar geologic settings.

## **Table of Contents**

Abstract.....	ii
Table of contents.....	iii
List of figures.....	vii
List of plates.....	xiii
List of tables.....	xiv
Acknowledgements.....	xv
<b>Chapter 1. Introduction .....</b>	<b>1</b>
Alteration zones associated with VHMS deposits.....	1
Lithogeochemical approaches to studying alteration zones.....	9
<i>Empirical alteration indices</i> .....	10
<i>Material transfer-based techniques</i> .....	12
<i>Residual-based techniques</i> .....	13
<i>Pearce element ratio analysis</i> .....	14
<i>Generalized element ratio analysis</i> .....	15
Problem statement.....	16
Research objectives.....	18
References.....	20
<b>Chapter 2. Major element lithogeochemistry of alteration associated with the Goldstream Besshi type Volcanogenic Massive Sulphide deposit, British Columbia.....</b>	<b>31</b>
Abstract.....	32
Introduction.....	33
Geologic Setting.....	34
<i>Regional geology</i> .....	34
<i>Stratigraphy, lithologies and metamorphism</i> .....	36
<i>Structure</i> .....	40
<i>Metallogeny</i> .....	42
<i>Mineralization</i> .....	43
Lithogeochemistry.....	44

<i>Sampling and analytical quality control</i> .....	44
<i>Background compositional variability and controlling factors</i> .....	45
<i>Conserved elements</i> .....	51
Conserved element test results.....	51
Interpretations and conclusions following from the conserved element test	58
<i>Molar element ratio analysis</i> .....	60
Characteristics and spatial distribution of alteration.....	73
Conclusions.....	78
References.....	81
<b>Chapter 3. Lithogeochemical data from the Chu Chua copper massive sulphide deposit and the adjacent Chinook Mountain property near Barriere, British Columbia</b> .....	87
Abstract.....	88
Introduction.....	88
Geologic setting.....	89
<i>Regional geology</i> .....	89
<i>Local geology</i> ,.....	91
<i>Structure</i> .....	95
<i>Metallogeny</i> .....	96
<i>Mineralization</i> .....	96
Lithogeochemistry.....	97
<i>Sampling and analytical quality control</i> .....	97
<i>Conserved elements and REE</i> .....	99
Interpretation of the property scale geology based on geochemistry....,,...	105
REE abundances.....	107
<i>PER analysis</i> .....	109
Composition of fractionating phases.....	109
PER analysis applied to Chu Chua basalts.....	111
<i>Effect of Mg and Fe addition</i> .....	114
<i>Effect of Na and Ca loss</i> .....	116
<i>Dual nature and effect of silica</i> .....	116

Spatial patterns of alteration of basalts.....	120
PER analysis applied to Chu Chua siliceous rocks.....	124
Discussion.....	127
Conclusions.....	130
References.....	133
<b>Chapter 4. Major element lithogeochemistry of alteration at the</b>	
<b>Konuto Lake group copper-zinc Volcanic Hosted Massive Sulphide</b>	
<b>deposits, Flin Flon mining camp, Manitoba and Saskatchewan.....</b>	<b>136</b>
Abstract.....	137
Introduction.....	137
Geologic setting.....	139
<i>Regional geology</i> .....	139
<i>Local Geology</i> .....	143
Birch Lake assemblage basalt flows.....	143
Clinopyroxene-phyric gabbro.....	149
Ruth Lake ultramafic sill.....	150
Granodiorite and quartz-plagioclase porphyritic dacite.....	151
Mosher Lake basalt flows and Cable Lake gabbro sill.....	152
<i>Structure</i> .....	152
<i>Metamorphism</i> .....	154
<i>Metallogeny</i> .....	155
Zn-Cu, basalt and rhyolite-hosted deposits.....	155
Cu-rich, predominantly basalt-hosted deposits.....	155
Gold deposits.....	156
Porphyry mineralization.....	156
<i>Konuto Lake deposit</i> .....	156
Lithogeochemistry.....	157
<i>Sampling and analytical quality control</i> .....	157
<i>Conserved elements</i> .....	159
Conserved Element Test Results.....	159
<i>Molar element ratio analysis</i> .....	164

Birch Lake assemblage basalt and gabbros.....	165
<i>Spatial patterns of alteration</i> .....	173
Ruth Lake ultramafic sill.....	176
Mosher Lake basalt and Cable Lake sill gabbro.....	180
Conclusions.....	183
References.....	187
<b>Chapter 5. Conclusions</b> .....	192
MER analysis: Modus operandi.....	192
<i>Conditions</i> .....	192
<i>Formation of molar ratios (MER)</i> .....	193
<i>Construction of MER diagrams</i> .....	194
<i>Interpretation of MER diagrams</i> .....	196
Applicability of MER analysis to mineral exploration problems.....	198
<i>Chemostratigraphy</i> .....	198
<i>Characterization of hydrothermal metasomatism</i> .....	199
<i>Contribution to the genetic/deposit model</i> .....	200
References.....	202
Appendix 1. Samples and analytical data used in the study of the Goldstream deposit.	203
Appendix 2. Estimates of analytical precision of the geochemical analyses performed by Chemex Laboratories Ltd. on samples from the Goldstream deposit.....	229
Appendix 3. Samples and analytical data used in the study of the Chu Chua deposit.	252
Appendix 4. Estimates of analytical precision of the geochemical analyses of samples from the Chu Chua deposit.....	293
Appendix 5. Samples and analytical data from the area of the Konuto Lake deposit...	301
Appendix 6. Estimates of analytical precision of the geochemical analyses of samples from the Konuto Lake and adjacent deposits.....	317
Appendix 7. Petrographic database.....	324
Appendix 8. Spatial distribution of alteration associated with the Konuto group deposits according to various lithogeochemical parameters.....	342
Appendix 9. Location of selected mapping samples and drillholes.....	353
Appendix 10. Microprobe data for minerals from the Konuto Lake and Chu Chua VHMS deposits .....	354

## List of Figures

Figure 2.1. Location of the Goldstream deposit.....	33
Figure 2.2 General geologic setting and principal mineral deposits of the Goldstream area.....	35
Figure 2.3. Regional and local stratigraphy of the Goldstream area.....	36
Figure 2.4. Local geology of the Goldstream mine area.....	38
Figure 2.5. Phases of deformation of the Goldstream stratigraphy and ore body.....	41
Figure 2.6. Ternary diagram showing the major chemical components in all 303 samples from the area of the Goldstream massive sulphide deposit in reference to selected mineral compositions.....	48
Figure 2.7. Ternary diagram showing the major chemical components in all 303 samples from the area of the Goldstream massive sulphide deposit in reference to selected mineral compositions.....	50
Figure 2.8. $\text{TiO}_2$ vs. Zr (potentially conserved element) plot, utilizing data for all 303 lithogeochemical samples from the Goldstream massive sulphide deposit area .....	52
Figure 2.9. Nb vs.Zr (potentially conserved element) plot, utilizing data for all 303 lithogeochemical samples from the Goldstream massive sulphide deposit area .....	53
Figure 2.10.a. $\text{SiO}_2$ vs. Zr plot, utilizing data for all 303 lithogeochemical samples from the Goldstream massive sulphide deposit area.....	54
Figure 2.10.b. $\text{SiO}_2$ vs. $\text{TiO}_2$ plot, utilizing data for all 303 lithogeochemical samples from the Goldstream massive sulphide deposit area.....	55
Figure 2.10.c. $\text{SiO}_2$ vs. Nb plot, utilizing data for all 303 lithogeochemical samples from the Goldstream massive sulphide deposit area.....	56
Figure 2.11. $\text{TiO}_2$ vs. Nb (potentially conserved element) plot, utilizing data for all 303 lithogeochemical samples from the Goldstream massive sulphide deposit area...	57
Figure 2.12. A generalized element ratio plot of 253 pelitic and calcareous samples from the Goldstream massive sulphide deposit area shown in reference to selected mineral compositions.....	62

Figure 2.13. Pearce element ratio plot of $\text{Al}_2\text{O}_3$ vs. $\text{SiO}_2$ with $\text{TiO}_2$ as the conserved denominator component for 152 pelegic samples of Goldstream area rocks.....	63
Figure 2.14. Pearce element ratio plot of $\text{Al}_2\text{O}_3$ vs. $\text{K}_2\text{O}$ with $\text{TiO}_2$ as the conserved denominator component for 243 metapelitic samples of Goldstream area rocks. ....	65
Figure 2.15.a. Pearce element ratio plot of $\text{Al}_2\text{O}_3$ vs. $\text{Na}_2\text{O}$ with $\text{TiO}_2$ as the conserved denominator component for 243 metapelitic samples of Goldstream area rocks.....	66
Figure 2.15.b. Pearce element ratio plot of $\text{Al}_2\text{O}_3$ vs. $\text{Na}_2\text{O}$ with $\text{TiO}_2$ as the conserved denominator component for 243 metapelitic samples of Goldstream area rocks showing also relative $\text{MgO}$ , $\text{Fe}_2\text{O}_3$ , S, $\text{SiO}_2$ and Ca concentrations.....	67
Figure 2.16. Pearce element ratio plot of $\text{Al}_2\text{O}_3$ vs. $\text{Fe}_2\text{O}_3$ with $\text{TiO}_2$ as the conserved denominator component for 243 metapelitic samples of Goldstream area rocks.....	69
Figure 2.17. Pearce element ratio plot of $\text{Al}_2\text{O}_3$ vs. $\text{MgO}$ with $\text{TiO}_2$ as the conserved denominator component for 243 metapelitic samples of Goldstream area rocks... ..	70
Figure 2.18. Pearce element ratio plot of $\text{MgO}$ vs. $\text{Fe}_2\text{O}_3$ with $\text{TiO}_2$ as the conserved denominator component for 243 metapelitic samples of Goldstream area rocks.....	71
Figure 2.19. Generalized element ratio plot of ferromagnesian component vs. $\text{Na}_2\text{O}$ for 243 metapelitic samples of Goldstream area rocks.....	72
Figure 2.20. Figure 2.25. Major element alteration model of the Goldstream deposit with a proposed position of the “C” zone.....	75
Figure 2.21. Spatial distribution of Si addition based on $\text{SiO}_2$ vs. $\text{Al}_2\text{O}_3$ Pearce element ratio .....	76
Figure 2.22. Spatial distribution of Mg addition based on $\text{MgO}$ vs. $\text{Al}_2\text{O}_3$ Pearce element ratio .....	76
Figure 2.23. analysis Spatial distribution of Fe addition based on $\text{FeO}(\text{total})$ vs. $\text{Al}_2\text{O}_3$ Pearce element ratio analysis .....	77
Figure 2.24. Spatial distribution of K mobility based on $\text{K}_2\text{O}$ vs. $\text{Al}_2\text{O}_3$ Pearce element ratio .....	77
Figure 2.25. Spatial distribution of Na addition based on Na vs. Al Pearce element ratio analysis.....	78
Figure 3.1. Location of the Chu Chua deposit.....	89

Figure 3.2. Conserved element plot of $\text{TiO}_2$ vs. $\text{Al}_2\text{O}_3$ .....	100
Figure 3.3. Conserved element plots of Zr vs. $\text{TiO}_2$ and Zr vs. Y.....	101
Figure 3.4. Spatial position of the various sampled rock types and a geological interpretation.....	103
Figure 3.5. Total alkalis vs. $\text{SiO}_2$ diagram for samples from the Chu Chua deposit area.....	104
Figure 3.6. Interpretation of the deposit scale geology based on spatial distribution of rock types as defined by chemical composition.....	106
Figure 3.7. Chondrite-normalized plot of REE abundances.....	108
Figure 3.8. Composition of pyroxenes from Chu Chua basalts.....	110
Figure 3.9. PER plot of $\text{SiO}_2$ vs. cations for basalt samples from the Chu Chua deposit area.....	112
Figure 3.10. PER plot of $\text{SiO}_2$ vs. cations for Low-Ti basalts from the Chu Chua deposit area.....	113
Figure 3.11. Vectors of individual effects and total vector of reaction in the composition-space defined by figure 3.9.....	118
Figure 3.12. A PER diagram quantifying the mobility of silica in each sample as the abscissa of the data point.....	119
Figure 3.13. A PER diagram quantifying the loss of Ca and Na in Chu Chua rocks....	119
Figure 3.14. A PER diagram quantifying the addition of Fe and Mg in Chu Chua rocks.....	120
Figure 3.15. $\text{SiO}_2$ mobility in Chu Chua basalts.....	121
Figure 3.16. Fe, Mg addition in Chu Chua basalts.....	122
Figure 3.17. Ca, Na loss in Chu Chua basalts.....	123
Figure 3.18. Aluminum balance diagram using data for Chu Chua banded cherts....	125
Figure 3.19. Phyllosilicate mineralogy of impurities in banded cherts from the Chu Chua deposit area.....	127
Figure 3.20.a. PER discrimination diagram showing proportions of main phyllosilicate minerals in cherts.....	128
Figure 3.20.b. Spatial distribution of secondary phyllosilicate minerals with respect to structural features.....	128



Figure 4.1. Location of the Konuto Lake deposit.....	138
Figure 4.2. Regional geologic setting of the Konuto Lake deposit.....	140
Figure 4.3. Konuto Lake and Birch Lake area geology.....	142
Figure 4.4. Total alkalis vs. SiO <sub>2</sub> diagram for the mafic and ultramafic rocks of the Konuto Lake and Birch Lake areas.....	144
Figure 4.5. TiO <sub>2</sub> vs. Zr scatterplot.....	160
Figure 4.6. Y vs. Zr scatterplot .....	161
Figure 4.7. Y vs. TiO <sub>2</sub> scatterplot .....	161
Figure 4.8. Location of samples taken from mafic and ultramafic rocks, Konuto and Birch Lake areas.....	162
Figure 4.9. Classification based on cation percentages of Al, (Fe <sub>total</sub> +Ti) and Mg for the basaltic rocks occurring in the area of the Konuto and Birch lakes.....	163
Figure 4.10. Plagioclase, clinopyroxene and orthopyroxene fractionation model plot of Birch Lake basalt and gabbro.....	166
Figure 4.11. Plagioclase, clinopyroxene and olivine fractionation model plot of Birch Lake basalt and gabbro.....	167
Figure 4.12. Plagioclase and clinopyroxene fractionation model plot of Birch Lake basalt and gabbro.....	169
Figure 4.13. Plagioclase-clinopyroxene phase discrimination plot. Birch Lake basalt.	170
Figure 4.14. GER plot of Birch Lake basaltic andesite and gabbro.....	171
Figure 4.15. GER plot of Birch Lake basaltic andesite and gabbro projecting from silica.....	172
Figure 4.16. Spatial distribution of hydrothermal alteration in the vicinity of the Konuto Lake deposit, based on the GER plot (Fig. 4.15.).....	174
Figure 4.17. Spatial distribution of hydrothermal alteration in the vicinity of the Birch Lake and Flexar deposit, based on the GER plot (Fig. 4.15.).....	175
Figure 4.18. Plagioclase, clinopyroxene and olivine fractionation model plot of Ruth Lake ultramafic rocks.....	177
Figure 4.19. Plagioclase, clinopyroxene and orthopyroxene fractionation model plot of Ruth Lake ultramafic rocks.....	178

178	Figure 4.20. Plagioclase - clinopyroxene phase discrimination plot for the Ruth Lake ultramafic rocks.....	179
	Figure 4.21. Plagioclase - olivine phase discrimination plot for the Ruth Lake ultramafic rocks.....	179
	Figure 4.22. Plagioclase, clinopyroxene and orthopyroxene fractionation model plot for the Sandy Bay assemblage rocks.....	180
	Figure 4.23. Plagioclase and clinopyroxene fractionation model plot for the Sandy Bay assemblage rocks .....	181
	Figure 4.24. Plagioclase - clinopyroxene phase discrimination plot for the Sandy Bay assemblage rocks .....	182
	Figure 4.25. GER plot for the Sandy Bay assemblage rocks.....	182
	Figure A8.1. Spatial distribution of hydrothermal alteration in the vicinity of the Konuto Lake deposit, based on the plagioclase-clinopyroxene phase discrimination plot (Fig. 4.13).....	343
	Figure A8.2. Spatial distribution of hydrothermal alteration in the vicinity of the Birch Lake and Flexar deposits, based on the plagioclase-clinopyroxene phase discrimination plot (Fig. 4.13).....	344
	Figure A8.3. Spatial distribution of hydrothermal alteration in the vicinity of the Konuto Lake deposit, based on a plot projecting from plagioclase.....	345
	Figure A8.4. Spatial distribution of hydrothermal alteration in the vicinity of the Birch Lake and Flexar deposits, based a plot projecting from plagioclase.....	346
	Figure A8.5. Spatial distribution of hydrothermal alteration in the vicinity of the Konuto Lake deposit, based on a plot modeling plagioclase and clinopyroxene fractionation (Fig. 4.11).....	347
	Figure A8.6. Spatial distribution of hydrothermal alteration in the vicinity of the Birch Lake and Flexar deposits, based a plot modeling plagioclase and clinopyroxene fractionation (Fig. 4.11).....	348
	Figure A8.7. Spatial distribution of hydrothermal alteration in the vicinity of the Konuto Lake deposit, based on a plot modeling plagioclase, clinopyroxene and olivine fractionation (Fig. 4.11).....	349

Figure A8.8. Spatial distribution of hydrothermal alteration in the vicinity of the Birch Lake and Flexar deposits, based a plot modeling plagioclase, clinopyroxene and olivine fractionation (Fig. 4.11).....	350
Figure A8.9. Spatial distribution of hydrothermal alteration in the vicinity of the Konuto Lake deposit, based the GER plot (Fig. 4.14).....	351
Figure A8.10. Spatial distribution of hydrothermal alteration in the vicinity of the Birch Lake and Flexar deposits, based the GER plot (Fig. 4.14).....	352
Figure A9.1. Locations of selected mapping samples and drillholes.....	353
Figure A10.1. Composition of pyroxenes from the host rocks to the Chu Chua VHMS deposit.....	354
Figure A10.2. Composition of feldspars from the host rocks to the Chu Chua VHMS deposit.....	355
Figure A10.3. Composition of amphiboles from the host rocks to the Konuto Lake VHMS deposit.....	356
Figure A10.4. Composition of feldspars from the host rocks to the Konuto Lake VHMS deposit.....	357

## **List of Plates**

Plate 2.1. View of the Goldstream area looking south.....	31
Plate 3.1. View north from the Rea gold deposit towards the Chu Chua Mountain.....	87
Plate 3.2. Chloritized basalt.....	91
Plate 3.3. Chert.....	93
Plate 3.4. Bedded chert.....	93
Plate 3.5. Authigenic carbonate in chert.....	94
Plate 3.6. Basalt intruded into soft siliceous sediment, peperitic texture.....	94
Plate 4.1. The rocky banks of Konuto Lake.....	136
Plate 4.2. Felsic lapilli in a basaltic lava flow.....	143
Plate 4.3. Interface between tops and bottoms of basalt flows.....	146
Plate 4.4. Basaltic flow bottoms.....	146
Plate 4.5. Pipe vesicles in basaltic flow bottoms.....	147
Plate 4.6. Basaltic flow tops.....	148
Plate 4.7. Pillow basalt.....	149
Plate 4.8. Gabbro, Konuto Lake sill.....	150
Plate 4.9. Felsic rocks occurring in the Konuto Lake area.....	151
Plate 4.10. Amygdaloidal basalt.....	154

## **List of Tables**

Table 1.1. Alteration indices in common use in lithogeochemical exploration	11
Table 3.1. Matrix equation for calculating axes coefficients for a PER diagram.....	111
Table A1.1. Sample location and field identification.....	205
Table A1.2. Major element concentrations.....	211
Table A1.3. Concentrations of various additional components.....	217
Table A1.4. Trace element concentrations.....	223
Table A2.1. Analyses of internal (MDRU) standards.....	231
Table A2.2. Precision (relative error) of determination of “accepted values” for MDRU standards analyzed by Chemex Laboratories Ltd. ....	235
Table A2.3. Analytical precision based on duplicate pulps of Goldstream deposit samples analyzed by Chemex laboratories.....	248
Table A3.1. Sample location and identification.....	254
Table A3.2. Major element concentrations.....	267
Table A3.3. Trace element and additional components concentrations.....	280
Table A4.1. Internal (MDRU) and laboratory standards and laboratory duplicates...	295
Table A4.2. Precision (relative error) of “accepted values” for MDRU standards analyzed by XRAL.....	297
Table A4.3. Analytical precision based on duplicate pulps of Chu Chua deposit samples analyzed by Chemex laboratories.....	299
Table A5.1. Sample location and identification.....	302
Table A5.2. Major element concentrations.....	307
Table A5.3. Trace elements and additional components concentrations.....	312
Table A6.1. Internal (MDRU) and laboratory standards and laboratory duplicates...	319
Table A6.2. Analytical precision based on duplicate pulps of Konuto Lake deposit samples analyzed by Chemex laboratories.....	321
Table A10.1. Major element concentrations in pyroxenes from the wall rocks to the Chu Chua deposit.....	355
Table A10.2. Major element concentrations in plagioclase from the wall rocks to the Chu Chua VHMS deposit.....	358

Table A10.3 Major element concentrations in amphiboles from the wall rocks to the Chu Chua VHMS deposit.....	360
Table A10.4 Major element concentrations in plagioclase from the wall rocks to the Konuto Lake VHMS deposit.....	365

## Acknowledgements

This thesis has benefited from the assistance and expertise of many people and the involvement of a number of organizations. It was made possible by the support of the Mineral Deposit Research Unit (MDRU) of the Department of Earth and Ocean Sciences and was jointly sponsored by the mining industry, the Science Council of British Columbia and the National Science and Engineering Research Council of Canada.

First and foremost I wish to thank my academic advisor, Alastair Sinclair, who directed and oversaw the research and was always available to assist with ideas, advice and critical review at all stages of the research. His care about academic, administrative and even personal issues relating to the thesis work is greatly appreciated.

Many thanks go out to Cliff Stanley for his valuable help in the processing and interpretation of the lithogeochemical data and use of PER methodology as well as for directing and assisting my fieldwork in the summer of 1996. Thanks are also extended to the graduate research committee members K Fletcher, Kelly Russell and Mati Raudsepp, and to the external reviewer David Lentz for critically reviewing the manuscript and suggesting valuable additions and edits to the text.

Trygve Hoy and Jim Logan from the Ministry of Energy and Mines of British Columbia are thanked for sharing analytical data and for offering valuable comments on the thesis text. Thanks are extended to Kurt Grimm for reviewing the sections of this thesis pertaining to sedimentology.

I wish to acknowledge the assistance of Arne Toma for the dependable logistical assistance he offered as MDRU resource centre coordinator as well as the assistance of Mark Coolbaugh in collecting samples from the Goldstream deposit. It is impossible to name all the colleagues at MDRU and the Department of Earth and Ocean Sciences alongside whom I had the pleasure of working, but the valuable stimulus of interacting with them is very much appreciated.

The kind support of Inmet Mining Co., Bethlehem Resources, Ltd. and Hudson Bay Exploration and Development Co. who allowed access to core and offered logistic support during work on their properties is greatly appreciated. Personal thanks are extended to Gary Wells, Kelly Gilmore, Jim Pickell and David Price of the above named companies for the field assistance, stimulating discussions and review of the manuscript.

# **A Lithogeochemical Study of Hydrothermal Alteration Associated with Mafic-Hosted and Besshi Type Massive Sulphide Deposits**

## **Chapter 1**

### **Introduction**

#### **Alteration zones associated with Volcanic-hosted Massive Sulphide (VHMS) deposits**

In many VHMS deposits complex alteration zones, identified in the footwall of the stratiform ore body, were documented as early as 1930 in the Noranda area of Canada (Walker, 1930) and 1954 in the Kuroko area of Japan (Iwao and Kishimoto, 1954). These metasomatic zones are, in many cases, larger than the deposits themselves and, thus, constitute intermediate-sized exploration targets for mineral deposits. For this reason, much attention has been paid to the alteration zones (*e.g.*, Riddell, 1953; Lickus, 1965; Sakrison, 1967; Sangster, 1972; MacGeehan, 1978; MacGeehan and MacLean, 1980; Riverin and Hodgson, 1980; Finlow-Bates and Stumpfl, 1981; Franklin *et al.* 1981; Knuckey *et al.* 1982; Gibson *et al.* 1983; Urabe *et al.* 1983; Franklin, 1984; Groves, 1984; Morton and Nebel 1984; Morton *et al.* 1985; Franklin, 1986; Morton and Franklin, 1987; Osterberg *et al.* 1987) and their most general characteristics are well studied and reasonably well understood. Some of the most detailed descriptions of metasomatic effects are those concerning deposits in the Abitibi Belt in Canada (*e.g.*, Franklin *et al.* 1975; Urabe *et al.* 1983; Morton *et al.* 1985; Morton *et al.* 1991; Larocque and Hodgson, 1993; Doucet *et al.* 1998; Barrie *et al.* 1999) and the Kuroko deposits in Japan (*e.g.*, Iijima, 1974; Shirozu, 1974; Hashiguchi and Usui, 1975; Ishikawa *et*



*al.* 1976; Saeki and Date, 1980; Date *et al.* 1983; Urabe *et al.* 1983). Two major types of alteration were recognized with respect to mineralogy, mineral distribution, morphology and structure (Morton and Franklin, 1987):

1. Discordant alteration zones (pipes) that immediately underlie the stratiform massive sulphide body and can host significant amounts of stringer mineralization (*e.g.*, Riddell, 1953; Gilmour, 1965; Lickus, 1965; Sakrison, 1967; Sangster, 1972; Richards *et al.* 1989; Gemmell and Fulton, 2001). At most deposits the alteration pipe consists of an inner chloritized core, commonly surrounded by a sericitized periphery (*e.g.*, Franklin, 1995). The mineralogy of the core reflects major addition of ferromagnesian elements and depletion of Ca, Na and Si, due to the destruction of feldspars present in the original rock (mafic or felsic). Strong silicification is characteristic of the uppermost parts of many deposits, particularly the Kuroko deposits in Japan (*e.g.*, Urabe *et al.* 1983) and the VHMS deposits of Cyprus (Lydon, 1984a,b). Potassium is also depleted from the central chloritic zone, but is enriched in the surrounding sericitic zone. However, cases have been described (*e.g.*, Walford and Franklin, 1982; Lydon, 1984a; Franklin, 1995) where potassium is contained in minerals other than sericite. Generally, the gradational change from the core of the alteration pipe outwards to the "fresh" footwall rocks suggests that the zonation pattern is due to a single metasomatic gradient imposed by the ore-forming solution. It has also been noted that individual veins and their selvages display the same metasomatic zonation (Riverin and Hodgson, 1980). Extreme cases of metasomatic progression are represented by talc-actinolite (Roberts and Reardon, 1978), talc-magnetite (Aggarwal and Nesbitt, 1984) or talc-magnetite $\pm$ biotite $\pm$ phlogopite (Costa *et al.* 1983) assemblages developed in the immediate footwall of the mineralization through intense removal of Al<sub>2</sub>O<sub>3</sub>. Quartz, chlorite, sericite, talc and magnetite, where present, are clearly shown to be metasomatic minerals. The components for their formation were supplied, at least in part, by the hydrothermal solutions; another source being *in situ* redistribution. Atypical, but not uncommon, is the occurrence in the alteration halos of low-temperature phases such as clay minerals (or metamorphic aluminosilicates: kyanite and andalusite) and zeolite. Alunite, and more generally acid alteration, is present in the wall rocks of gold-rich massive sulphide deposits (Poulsen and Hannington, 1995).

2. Stratigraphically, semiconformable alteration zones are developed more deeply (down to several hundred metres) into the footwall of the deposit, typically of lower contrast and larger lateral extent (up to several kilometres) than both the discordant alteration zone and the ore body (*e.g.*, Descarreaux, 1973; MacGeehan, 1978; MacGeehan and MacLean, 1980; Gibson *et al.* 1983; Groves, 1984; Morton and Franklin, 1987; Galley and Jonasson, 1992; Galley, 1993; Gibson and Watkinson, 1999; Gemmell and Fulton, 2001). These zones are described as patchy in character, being restricted to the more permeable rock types. Mineralogically the semiconformable alteration is represented by albite, chlorite (either Mg- or Fe-rich), epidote, quartz, calcite and ankerite. Actinolite-tremolite or kyanite occur in metamorphosed rocks (Morton and Franklin, 1987). Gibson and Watkinson (1999) in their description of the semiconformable alteration beneath the VHMS deposits of the Noranda area, Quebec delineate several petrographic subtypes of semiconformable alteration, differing in mineralogy, texture and spatial distribution:

(1) Spilitic alteration is widespread and pervasive. It is characterized by the assemblages chlorite-albite-epidote-quartz in andesite, or sericite-albite-epidote-quartz in rhyolite. These minerals replace the groundmass of the flows, while original textures are preserved. Altered rocks are enriched in Na<sub>2</sub>O and depleted in CaO.

(2) Epidote-quartz alteration occurs exclusively in intermediate and mafic volcanic rocks. It occurs as grey to grey-green, distinct, resistant-to-weathering, irregular amoeboid spots or patches up to several metres in diameter. In addition to epidote and quartz, calcite, chlorite and opaque minerals may also be present. The texture of the alteration is granular (original textures are obliterated). Altered rocks are enriched in CaO and depleted in MgO, Na<sub>2</sub>O and K<sub>2</sub>O, whereas SiO<sub>2</sub>, Al<sub>2</sub>O<sub>3</sub> and Fe<sub>2</sub>O<sub>3(total)</sub> remain relatively constant.

(3) Silicification is typically restricted to certain flows or stratigraphic horizons within the volcanic sequences. Petrographically, the effect of alteration ranges from the occurrence of scattered blebs of granular quartz to pervasive silicification, which, however, preserves albite phenocrysts and microlites.

Gemmell and Fulton (2001), in their study of the Hellyer VHMS deposit in Tasmania, recognize that the mineral assemblage of the conformable alteration zone depends on the temperature of the hydrothermal fluids and on the water/rock ratios:

(1) Close to the seafloor the water/rock ratios are high and alteration assemblages, including adularia, Mg-smectite and zeolite, attest to relatively low temperatures (50-140°).

(2) Deeper into the volcanic pile, where water/rock ratios drop to less than 5 and temperatures are in the 150-300 °C range, the characteristic alteration minerals are Mg-smectite, chlorite, quartz and albite.

(3) At temperatures exceeding 300° the alteration minerals are chlorite, actinolite, epidote and albite.

The semiconformable zones of alteration are commonly depleted in base metals (MacGeehan, 1978; Franklin, 1995). Because of its distal position with respect to ore, low contrast and similarity to regional metamorphism of lower grades, this type of alteration has received less attention than has the discordant variety. From a practical perspective, areas of spilitized, epidote-quartz-altered and silicified rocks are indicative of a high temperature hydrothermal system. They represent a larger exploration target than proximal chlorite and sericite alteration. Variability in the distribution and intensity of epidote-quartz alteration and silicification can point to synvolcanic faults and intrusions that might have controlled the location of VHMS deposits.

In cases where the semiconformable-type alteration is recognized, the discordant-type alteration is contained within it. The described patterns of spatial occurrence and the depletion/enrichment in base metals imply a genetic and functional relationship between the two types of alteration. The rocks of the semiconformable zone are interpreted to represent a hydrothermal reservoir, capped by impermeable silicified rocks (*e.g.*, Hodgson and Lydon, 1977; Gibson *et al.* 1983; Morton and Franklin, 1987; Gibson and Watkinson, 1999). The circulating hydrothermal fluids become enriched in (among other components) base and precious metals (Spooner and Fyfe, 1973; Spooner, 1977; Richards *et al.* 1989). The fluids are then tapped and transported to the site of ore deposition at the seafloor or immediately

below via conduits comprising the discordant alteration pipe, while altering the wall rocks in the process.

The morphology, dimensions, structure, geochemistry and mineralogy of both types of alteration vary widely, depending on a number of factors, the most important being: (1) water depth, (2) wall-rock permeability and (3) wall-rock composition (controlling the chemistry of the hydrothermal reactions). Based on these variables, a two-fold classification has been suggested for Archean Cu-Zn VHMS deposits (Morton and Franklin, 1987). The two types of deposits are named after the Noranda mining area in Quebec and the Mattabi deposit at Sturgeon Lake, Ontario. The Noranda-type deposits are formed at water depths of more than 500 m (Gibson *et al.* 1986). They are characterized by: (1) a well-defined discordant alteration zone, (2) a semiconformable alteration zone of actinolite-epidote-quartz-rich rocks, (3) dominantly mafic and felsic flows and hyaloclastites and (4) high Fe/Mg ratios in chlorites and presence of Fe-carbonates. The Mattabi-deposits are thought to have formed at depths less than 500 m (Groves *et al.* 1984; Morton, 1984). They are characterized by: (1) broader, but less sharply delineated alteration pipes, (2) large, mineralogically well-defined semiconformable alteration zone, (3) association with predominantly fragmental rocks and (4) low Fe/Mg ratios in chlorites and the presence of other Mg-bearing minerals. Felsic rocks are more abundant in the footwall of the Mattabi-type deposits.

Alteration of the hanging wall has been described in association with Phanerozoic deposits such as the Kuroko deposit (Shirozu, 1974), the Madenkoy deposit in Turkey (Franklin *et al.* 1975) and the Hellyer deposit in Tasmania (Gemmell and Fulton, 2001). Hanging wall alteration is of low intensity and is characterized by (in order of increasing distance above the ore body): Mg-chlorite, sericite, clay minerals (montmorillonite, kaolinite and mixed-layer clays), carbonates (dolomite and calcite), feldspars (K and Na), zeolites and cristobalite. Gemmell and Fulton (2001) describe a different concentric lateral zonation for the hanging wall of the Hellyer deposit in Tasmania, Australia. From the highest-temperature central zone outward the alteration assemblages include: chromian muscovite, carbonate-chlorite,

quartz-albite and sericite. Hanging wall alteration is interpreted as the result of a continuing, albeit waning, hydrothermal activity after the formation of the massive sulphide ore body.

A large number of VHMS deposits occur in metamorphic terranes. Some of the most productive mining areas in Canada such as the Flin Flon camp in Manitoba and Noranda in Quebec contain deposits hosted by rocks of relatively high metamorphic grade. The effects of metamorphism superimposed on the alteration zones include deformation and changes in their mineralogy and texture. Deformation may complicate and sometimes completely detach the alteration zones from the massive sulphide deposits and can also cause significant solution transfer and, hence, mass transfer (Lentz, 1999). The mineralogy of the alteration zones depends on the original mineralogy (primary and alteration), the metamorphic conditions and on the amount of tectonic deformation of the rocks (Koo and Mossman, 1975).

The alteration types and zones described above retain their pre-metamorphic chemical signatures (Walford and Franklin, 1982). Thus, the chloritic cores of the discordant alteration zones are rich in Fe and Mg silicates, aluminosilicates and phyllosilicates and are devoid of alkali-bearing minerals (with the possible exception of albite) (Walford and Franklin, 1982). Typical minerals include cordierite, anthophyllite (or gedrite), gahnite, biotite, chlorite, kyanite, actinolite and tourmaline (Franklin *et al.* 1981; Walford and Franklin, 1982; Bernier and MacLean, 1993). The occurrence of the paragenesis cordierite - anthophyllite +/- talc is consistent with the finding that these minerals are formed from the breakdown of Mg-chlorite and quartz at temperature of 580° and pressure of 2 kb (Akella and Winkler, 1966). Recognition of the cordierite-antophyllite zones as potential ore horizons in highly metamorphosed terranes may thus be a useful exploration tool (Franklin *et al.* 1981).

The sericitic halo of the discordant alteration zone is typically metamorphosed to a muscovite schist, commonly containing biotite, quartz and andalusite. At high metamorphic grades (*e.g.*, in the Anderson Lake and Snow Lake area of the Flin Flon belt, Manitoba), zincian staurolite and garnet occur in the outer shell of the discordant alteration zone (Walford and

Franklin, 1982; Zaleski and Halden, 1988; Galley *et al.* 1993). Sericite and chlorite are superimposed on all of the above parageneses during retrograde metamorphism.

Metamorphism of the various alteration zones causes the development of coarse textures as well as garbenschiefer and "dalmatianite" (spotty) textures (Walker, 1930; Elliott-Meadows and Appleyard, 1991).

A number of contributions have been made to the problem of rare earth element (REE) participation in water-rock interaction in zones associated with VHMS deposits. Many of these studies present evidence that REE and particularly the light REE (LREE) have been mobile in the alteration zones associated with massive sulphide deposits (Baker and de Groot, 1983; Campbell *et al.* 1984; Bence and Taylor, 1985; MacLean, 1988; Schneider *et al.* 1988; Dergachev *et al.* 1989; Schade *et al.* 1989; Barrett *et al.* 1990; MacLean and Hoy, 1991; Barrett, 1992). The most notable example is that of Winston Lake, Ontario, where, across a lithologic contact, the rhyolite is depleted by 90% and the basalt is enriched up to 150 times in REE (Schandl and Gorton, 1991; Gorton and Schandl, 1995). Apart from this extreme example, the reported additions were typically tens to hundreds of ppm (*e.g.*, at the Phelps Dodge ore body in Quebec; MacLean, 1988). Coupled depletion and enrichment in LREE are reported for the Kidd Creek deposit, Ontario (Campbell *et al.* 1984) and the Horne mine, Quebec (MacLean and Hoy, 1991). In both cases, the LREE were interpreted to have been leached from distal parts of the alteration zone and deposited immediately beneath the ore body. After a critical mass of publications reported REE mobility in alteration zones of VHMS deposits, Schandl *et al.* (1995) suggested that REE geochemistry could be used as an exploration tool.

There has been serious controversy, however, regarding important issues, such as the timing of the transfer, the geochemical mechanism of mobilization and precipitation of REE, the REE mineralogy of the source rocks and the type of hydrothermal fluid involved. Geochronological evidence (U-Pb dating of monazite by Schandl and Gorton, 1991) indicates that at Winston Lake, Kidd Creek and Geko deposits, Ontario, monazite and xenotime

precipitation occurred 50-70 Ma after the ore deposition. Thus, according to this study, REE mobility was unrelated to the process of ore deposition.

Based on theoretical calculations, Wood and Williams-Jones (1994) concluded that if hydrothermal vent fluids were chemically analogous to modern ones, they could not have transported enough REE to account for the observed enrichments and depletions. Their studies, however, assumed monazite as the source mineral, whereas other phases (volcanic glass, feldspar) could also have served as the source for the REE. Other authors have suggested that orthomagmatic fluids (Schade *et al.* 1989, on the example of the Prieska massive sulphide deposit, South Africa), or metamorphic fluids (Gorton and Schandl, 1995; Schandl *et al.* 1996) were responsible for the observed REE mobility.

Most VHMS deposits are hosted by predominantly mafic to intermediate volcanic sequences, but in the best-studied and most productive areas (*e.g.*, Noranda, Kuroko), the deposits occur in close spatial association with felsic rocks. There exists, however, a subtype of VHMS deposits hosted by essentially mafic volcanic sequences without felsic rocks. These are typically Cu-Zn deposits and occur in various tectonic settings and stratigraphic levels and in different parts of the world. These differences justify assigning them to a separate subclass within the broader class of VHMS deposits. Individual deposits of this subclass such as Hellyer in Australia (Gemmell *et al.* 1990; Gemmell and Fulton, 2001), Chu Chua in British Columbia (Vollo, 1974; McMillan, 1979; Aggarwal, 1982; Aggarwal and Nesbitt, 1984), the deposits hosted by the Birch Lake assemblage in the Flin Flon camp, Saskatchewan (Morgan, 1995; Reilly, 1995; Robinson, 1996; Gilmore and Pickell, 2000), *etc.*, have been studied in significant detail. Generalizations about this subclass of deposits are not available with the exception of the understanding about the specificity of the association of metallic elements occurring in the ores.

## **Lithogeochemical approaches to studying alteration zones**

Various approaches have been used in studying lithogeochemical variability in rocks caused by metasomatism, among other processes. These approaches were based on a variety of compositional data: major element concentrations (including water, carbon dioxide and sulphur), minor and trace element concentrations, REE concentrations and isotopic ratios (oxygen, sulphur, lead and other isotopic systems). Many of the proposed methods have proven their value in specific contexts but some of these methods have a larger potential for broad use than do others.

Lithogeochemical exploration techniques utilizing isotopic and REE data are generally expensive, time consuming and unproven. Their widespread use is hindered by the high analytical costs. Although indispensable in some petrochemical research applications, they have not been proven suitable for routine lithogeochemical exploration tasks.

Utilization of minor or trace element data has its legitimate place in some contexts of exploration for ore deposits. They are widely and successfully used in studying secondary anomalies in soils, water, bioaccumulations, *etc.* The large geochemical contrast these elements exhibit and the ease of direct interpretation of anomalies makes them indispensable in certain scales and contexts of exploration. Lithogeochemical anomalies are formed either through: (1) deposition of disseminated mineralization (*e.g.*, in porphyry deposits and some magmatic deposits), or (2) secondary dispersion (*e.g.*, diffusion) of ore components away from the ore body. The first process is not typical for the VHMS class of deposits, with the exception of stringer mineralization (mainly Fe and Cu), which is generally laterally restricted compared to the associated exhalative massive sulphide deposit. The effects of the second process have been shown to attenuate exponentially away from the ore body (*e.g.*, Silverman *et al.* 1962; Turek *et al.* 1976; Prins and Venter, 1978) and is, thus, incapable of producing significant anomalies.



Major elements are generally considered to be the most useful discriminators in studying the complete alteration system that is broadly developed, including low intensity wall rock alteration. Despite their relatively low contrast and their sensitivity to obscuring closure effects (a mathematical artifact due to the use of percent concentration data, see Chayes, 1971), major element data provide the most useful information for characterizing and quantifying metasomatic products and processes. Losses and additions of major elements during metasomatism are directly related to the alteration mineral assemblage, which, in turn, can be easily observed and interpreted. Furthermore, modern techniques for major element or whole-rock analysis (X-Ray Fluorescence and Inductively Coupled Plasma) are accurate, precise, inexpensive and rapid.

The general discriminatory statistical approach to lithogeochemical data analysis (Govett, 1983) will not be considered here. It assumes little or no previous knowledge about the nature of geochemical variations in the rocks and thus is of highest value when such knowledge is not available. This is not the case in the studies reported here, which are concerned with deposits for which geological contexts and genetic models are well constrained.

Deterministic approaches fall in one of the following categories:

- (1) elemental and molecular ratios formulated using empirical alteration indices based on general geological knowledge;
- (2) material transfer techniques based on mathematical models for net mass and volume change;
- (3) numerical procedures helping to visualize and explain observed lithogeochemical variations (residual based techniques, *e.g.*, Stanley and Madeisky, 1996).

### ***Empirical alteration indices***

Empirical alteration indices developed from detailed case studies (*e.g.*, Hashiguchi and Usui, 1975; Ishikawa *et al.* 1976; Spitz and Darling, 1978; Sacki and Date, 1980; Date *et al.* 1983; Hashiguchi *et al.* 1983) have been used widely in the exploration for VHMS deposits. They

are formulated as ratios of major oxide concentrations (or their sums), supposed to be added (numerator) and removed (denominator) during hydrothermal alteration. The indices are examined spatially to define anomalies and, thus, identify exploration targets. The formulation of ratios offers an advantage by eliminating the effect of closure (Nicholls, 1988). This also limits the set of elements deemed responsible for the observed anomaly and thus allows petrogenetically coupled processes more specifically associated with the mineralization event to be targeted. However, this approach suffers from a number of weaknesses. Being empirical and formulated on case histories from specific mining camps, they have uncertain and limited application in other VHMS systems. The indices proposed for use in the exploration for VHMS deposits contain up to four elements (*e.g.*, the chlorite index –  $[\text{Fe}_2\text{O}_3^{\text{T}} + \text{MgO}] / [\text{Fe}_2\text{O}_3^{\text{T}} + \text{MgO} + \text{CaO} + \text{Na}_2\text{O}]$ ). The multielement nature of these types of indices makes anomalous responses difficult to interpret in terms of alteration assemblages and processes. It also allows anomalies to be erroneously defined based on processes not associated with mineral deposit formation. Material transfers of small magnitude are obscured by wider variations and are not recognized although they may be important. As the formulated ratios commonly include suites of elements that are involved in coupled (addition and removal) metasomatic processes, the natural variation of any index is artificially and dramatically magnified, as are background variability and measurement error.

Table 1.1 Alteration Indices in Common Use in Lithogeochemical Exploration

Alteration Index Name	Alteration Index formula	Reference
Ishikawa/Date	$(\text{MgO} + \text{K}_2\text{O}) / (\text{MgO} + \text{K}_2\text{O} + \text{CaO} + \text{Na}_2\text{O})$	Ishikawa <i>et al.</i> (1976), Date <i>et al.</i> (1983)
Chlorite	$(\text{Fe}_2\text{O}_3^{\text{T}} + \text{MgO}) / (\text{Fe}_2\text{O}_3^{\text{T}} + \text{MgO} + \text{CaO} + \text{Na}_2\text{O})$	Saeki and Date, (1980)
Alkali	$(\text{CaO} + \text{Na}_2\text{O}) / (\text{CaO} + \text{Na}_2\text{O} + \text{K}_2\text{O})$	Saeki and Date, (1980)
Hashiguchi	$\text{Fe}_2\text{O}_3^{\text{T}} / (\text{Fe}_2\text{O}_3 + \text{MgO})$	Hashiguchi and Usui, (1975), Hashiguchi <i>et al.</i> (1983)
Sericite	$\text{K}_2\text{O} / (\text{Na}_2\text{O} + \text{K}_2\text{O})$	Saeki and Date, (1980)
Spitz/Darling	$\text{Al}_2\text{O}_3 / \text{Na}_2\text{O}$	Spitz and Darling, (1978)

### ***Material transfer-based techniques***

Material transfer-based techniques of lithogeochemical exploration involve a model explaining the concentration differences observed in a suite of rocks. They all are based on the fundamental material transfer equation:

$$S_p x_{ip} + dX_i = S_d x_{id} \quad (1)$$

where  $S_p$  and  $S_d$  denote, correspondingly, the sizes of the parent rock and the daughter rock,  $x_{ip}$  and  $x_{id}$  are the concentrations of element  $X$  in the two rocks ( $i=1$  to  $n$  where  $n$  is the number of elements in the rocks) and  $dX_i$  is the amount of element  $i$  added or removed from the parent rock by the material transfer process. For all the elements in the rock,  $n$  equations can be written, containing  $n+1$  unknowns (as  $x_{ip}$  and  $x_{id}$  are measurable and either  $S_p$  or  $S_d$  can be arbitrarily set at any value). For the equations to be solved simultaneously a value must be assigned to one more unknown. This is justified by knowing or assuming a value for one of the following: (1) system size change ( $S_p = mS_d$ ); (2) the amount of one element added or removed in the course of the process ( $dX_i = p$ ; or that one element did not participate in material transfer -  $dX_i = 0$ ); (3) a functional relation between the additions or removals of two elements ( $dX_i = r dX_j$ ). With one such critical assumption the material transfers can be determined from the compositional data. Studies that contributed to the various aspects of the theory are, for example: Akella (1966), making use of the conserved constituent assumption; Gresens (1967) - using the volume factor; Pearce (1968) - developing a molar ratio diagram procedure and applying it to modeling fractionation in igneous rocks; Grant (1986) - adding a graphical approach to mass change factor calculations; Brimhall and Dietrich (1987) - strain accommodating material transfer; Brimhall *et al.* (1988) - porosity accommodating material transfer; De Pangher (1988) - conserved constituent identification; Stanley (1994) - element ratio analysis without conserved element denominator. The number of authors and studies developing and applying the practical procedures involving the material transfer approach is much greater.

Most of the approaches accounting for material transfer balance rely heavily on the use of an assumed "parent rock" composition as a constraint for the solution of the material transfer equation (1). This is based on a variety of criteria: petrologic and geochemical evidence for lack of alteration (MacLean and Barrett, 1993), adherence to theoretical models for the genesis of the fresh host rocks - differentiation lines (MacLean, 1990) and thermodynamically constrained stable assemblages (Brown and Skinner, 1974; Capitani and Brown, 1987). Despite the positive results that have been achieved by this approach, none of the above criteria used in the crucial step of identifying the "parent rock" composition can be shown to be universally valid. An additional limitation of the approach is due to the common variability introduced by primary processes, which make the identification of a single "parent rock" impossible. Unfortunately, all but one (Pearce, 1968) technique employ calculations in terms of mass (density, volume) and, thus, have an inherent impediment in accounting for the mineralogical aspects of alteration as mineral formulae are normally expressed in terms of moles rather than mass. Without the possibility of accounting for the mineralogical effects, primary and secondary variability are difficult to distinguish from one another. A combination of the mass balance and the mineral norm calculation approaches was recently proposed (Cheng and Sinclair, 1994; Cheng and Sinclair, 1995), which optimizes the approaches for use with metasomatically altered rocks. This methodology also requires the conversion of the typically used weight units into molar amounts, providing convenience in integrating mineralogical and geochemical information.

### ***Residual-based techniques***

The residual based techniques represent another group of empirical graphical approaches that recognize and try to accommodate different sources of geochemical variability. They all model primary variations in rock composition by developing fractionation models expressed as curved lines. The residuals (deviations of composition from the model line) are ascribed to the effects of metasomatism. Whereas Nichol *et al.* (1977) make no attempt to accommodate the effects of closure, the logarithms of ratios used by Beswick and Soucie (1978) avoid them. In this way, the logarithm ratio diagrams are influenced by only three rather than by all elements. However, both approaches use nonlinear models, making

quantification of metasomatism difficult. In the case of the Beswick and Sousie (1978) approach, the logarithmic scale used, which further impedes quantification of the processes as the magnitude of the residual corresponds to varying amounts of material transfer.

### ***Pearce-element-ratio analysis***

The Pearce-Element-Ratio Analysis (PER) combines the advantages of many of the approaches mentioned so far. Originally presented by Pearce (1968) as a procedure of investigating material transfer produced by igneous processes, the method has been expanded (*e.g.*, Stanley and Russell, 1989; Fowler, 1990; Russell and Nicholls, 1988, Russell and Stanley, 1990; Stanley and Madeisky, 1993; Stanley, 1994; Nicholls and Gordon, 1994; Stanley and Madeisky 1996) into a methodology that is soundly based on material transfer theory and uses residual variations to distinguish between primary and metasomatic processes. The denominator of the ratios is chosen to be a conserved element, which serves as the necessary additional constraint ( $dX_i = 0$ ) for the solution of the set of material transfer equations (1). It is evident that the choice of the denominator element is a crucial step in the procedure. The existence of at least one conserved element in the set of analyzed elements is one of the two fundamental assumptions that have to be justified before PER analysis can be undertaken. The second assumption is that all the rocks in the data set are cogenetic. The two assumptions are tested using bivariate scatterplots of potentially conserved elements (see Stanley and Russell, 1989).

PER analysis involves the use of ratios, which eliminates the effect of closure and, as an additional advantage, allows for the use of partial rather than full lithogeochemical analyses. In terms of graphical representation, the advantage of using ratios is that trends describing material transfer are a function only of the transfer process stoichiometry ( $dX_i / dX_j$ ) and are thus linear with a constant slope for a given process. The mass concentrations typically reported by labs are converted to the more convenient element or oxide mole concentrations. In this way material transfers are directly related to mineral and exchange component formulae and chemical reactions. Solid solutions can be easily accommodated by simple linear combinations of PERs. Fractionation effects of several minerals can be forced to vary

in a colinear fashion on a diagram, which ensures that the developed fractionation models are linear, as opposed to curvilinear in other approaches. Thus, it is possible to decouple the process of metasomatism from primary processes, which constitute background “noise”, from an explorationists’ point of view. Consequently, the PER method is particularly well suited to detecting low-contrast geochemical variations and thus applicable to the study of alteration aureoles of mineral deposits.

### ***Generalized element ratio analysis***

It is clear that the requirement for the existence of a conserved element is an unwanted limitation and the absence of conserved elements may render the PER analysis method inappropriate. Some examples of geological processes leading to this situation are magmatic assimilation, large degrees of partial melting, intense hydrothermal alteration and sedimentation of coarse material. Where this is the case, the generalized element ratio analysis (GER), an approach related to PER analysis, is applicable (Stanley, 1995). It requires no assumptions about element conservation or the size of the system. To solve the set of material transfer equations (1), it uses petrologic constraints in the form of a linear relationship between the amounts of material transfer of two elements:

$$dX_i = r dX_j, \text{ or: } r = dX_i/dX_j, \quad (2)$$

where  $dX_i$  and  $dX_j$  are the amounts of elements  $i$  and  $j$  added or removed from the parent rock by the material transfer process and  $r$  is the relationship constant. This results in a more complicated behavior of graphical expression of material transfer trends, depending on both the rock composition and the material transfer process stoichiometry.

### **Problem statement**

Several subtypes of VHMS deposits, excluding the most typical ones, have not been studied in considerable detail. Study of their metasomatic aureoles with respect to geochemical characteristics and spatial distribution is warranted from both a theoretical and practical

perspective. The deposits chosen for this study and exemplifying the subtypes in question are The Chu Chua and Goldstream deposits in British Columbia and the Konuto Lake deposit near the Manitoba-Saskatchewan border. They also offer an excellent opportunity to test the recently expanded and enriched methodology of Molar Element Ratio (MER) analysis.

With the realization of the significance of VHMS deposits as a source of various base and precious metals during the last decades, a multitude of articles have been published on their characteristics, genesis, exploration parameters and other features. Scientific interest and development of genetic concepts were stimulated also by the relatively recent discoveries of what are believed to be contemporary analogues of the environments of formation of VHMS deposits. Appreciating the importance of alteration patterns surrounding the sulphide mineralization, both for the development of the models and for exploration practice, extensive research was devoted to their characterization. However, the wealth of ensuing publications, while revealing many important attributes of VHMS deposits, also posed new questions.

Two of the preeminent mining camps in the world are situated in the Abitibi belt in Canada and in the Green Tuff belt in Japan. It is logical that the deposits of these two areas have received the most attention in the geological literature. Although deposits in these and other comparable mining areas are hosted largely by mafic volcanic sequences, they are more directly associated with felsic differentiates such as dacites or rhyolites. VHMS deposits associated with felsic rocks are shown to have different characteristics (Lydon, 1984a,b) than deposits contained exclusively in mafic volcanic rocks. Deposits contained exclusively in mafic volcanic rocks account for a smaller part of the discovered VHMS deposits. They are characterized by higher Cu / (Cu+Zn) ratios of the ores and very low (uneconomic) Pb contents. At the same time, in this subtype of VHMS deposits Au and Ag typically exhibit elevated concentrations. Due to their (at least apparent) relative rarity and less spectacular size, they have not been studied as exhaustively as have the felsic volcanic-associated VHMS deposits. Two the proposed study areas - the Chu Chua and Konuto Lake deposits where

several small but high grade Cu-Zn VHMS deposits have been found with little or no relation to felsic magmatism, provides insight into alteration associated with this deposit subclass.

Judging by the marked difference in the association of ore metals in the two types of VHMS deposits, as well as in the host rocks, it is reasonable to expect that differences exist also with respect to the associated alteration halos. Their mineralogies, the patterns of redistribution of major and trace elements and volume parameters (length, width, vertical extent, shape) are worth comparing and contrasting. Knowledge about the specific characteristics of the alteration zones surrounding mafic-hosted VHMS deposits is important both from theoretical (refining and enriching descriptive and genetic models) and practical (aiding exploration in exclusively mafic volcanic terraines) points of view.

The PER methodology is a relatively new tool capable of solving the complicated problem of distinguishing between the effects of superimposed geochemical processes, especially after its more recent developments. It was tested on a limited number of rock types of relatively simple mineralogy: mafic volcanic rocks (*e.g.*, Russell and Stanley, 1990; Pearce and Stanley, 1991) and felsic volcanic rocks (Madeisky and Stanley, 1993; Stanley and Madeisky, 1994). Applying the PER analysis in mineralogically and geochemically more complicated environments will be an important test of its potential.

The Besshi type deposits (*e.g.*, Fox, 1984; Slack, 1993), hosted by mixed assemblages consisting of pelitic sedimentary and mafic volcanic rocks, represent another subtype of the larger and diverse category of VHMS deposits and a link to the sediment-hosted massive sulphide deposits (SHMS). Although formed in a distinctly different environment, they exhibit marked similarities to the "VHMS-proper" deposits in terms of morphology and mineral composition. Although these deposits have been mined for decades, little is known about the characteristics of their associated alteration aureoles. Comparing and contrasting them to alteration associated with other subtypes of VHMS deposits will contribute to the understanding of their genesis. In addition, the pelitic sedimentary environment is another area in which the PER analysis is still to be tested.



## **Research objectives**

Two major objectives were set for the proposed research:

- (1) To characterize, quantify and compare geochemical variations in major element concentrations in various host rocks for VHMS mineralization. These host rocks include mafic volcanic and pelitic-dominated sequences that were subjected to low to medium grade metamorphism.
- (2) To test MER analysis techniques as a tool for the characterization of subtle and multi-source geochemical variations in the environments mentioned above. Both Pearce Element Ratio (PER) and general element ratio (GER) approaches will be used where appropriate.

The objective of characterization and quantification of chemical variations in host rocks to VHMS deposits includes partitioning the variations in their major components - primary (fractionation), secondary (metasomatic) and tertiary (metamorphic) in the case of metamorphosed host rocks. Emphasis is placed on the comprehensive characterization of the hydrothermal component of the geochemical variations as they are directly related to the genesis of the associated mineralizations. It is recognized that metasomatism may, and most probably is, manifested in more than one way in different locations of the same aureole and several stages of the processes may have been superimposed on the same rocks. Separation and identification of the individual processes will be sought, as well as their characterization with respect to the following:

- (1) Chemistry of the process - identification of the main chemical reactions and their mineralogical manifestation.
- (2) Intensity - what proportion of the rock has been influenced by the process?
- (3) Morphology - whether alteration was pervasive or discrete?
- (4) Spatial parameters - what is the physical extent of the alteration halo?
- (5) Contrast - how significant is the induced variation compared to variations due to other sources, including errors?

The objective of testing the PER and GER methodologies involves the evaluation of the following qualities:

- (1) The ability to solve the problem of extracting the metasomatic component from the total geochemical variability.
- (2) The ability to provide insight into complicated mineralogies of the alteration zones involving solid solution minerals with broadly varying mineral chemistries such as amphiboles, chlorites, garnets, clay minerals, *etc.*
- (3) The ability to quantify intensity of alteration through residuals from fractionation lines.

The research presented here is part of a project titled: "Lithogeochemical Exploration for Metasomatic Alteration Zones Associated with Hydrothermal Mineral Deposits" (Sinclair and Stanley, 1995), completed in 1999. It was undertaken with support from the Mineral Deposit Research Unit (MDRU) of the Department of Earth and Ocean Sciences, the University of British Columbia. The work was jointly sponsored by the mining industry, the Science Council of British Columbia (SCBC) and the Natural Sciences and Engineering Research Council of Canada (NSERC). Dr. Alastair J. Sinclair directed the project and Dr. Clifford R. Stanley was the project coordinator.

The research objective was to investigate alteration zones of several subtypes of mafic volcanic-hosted massive sulphide deposits (VHMS) in order to: (1) help develop enhanced strategies and tools for the exploration of VHMS deposits and (2) improve descriptive and genetic models for these alteration zones. This study is based on two well studied mineral deposits hosted in mafic volcanic rocks of varying metamorphic grade (Chu Chua in the the Canadian Cordillera and Konuto Lake in the Flin Flon mining camp, Manitoba and Saskatchewan) and one Besshi type deposit (Goldstream, in the Canadian Cordillera). The deposits were chosen in part because general genetic models for them were already established. This offered the opportunity of concentrating on a detailed lithogeochemical study of their associated alteration zones.

## References

- Aggarwal, P.K., (1982) Geochemistry of the Chu Chua massive sulphide deposit, British Columbia: M.Sc. thesis, University of Alberta, Edmonton, AB, 81 p.
- Aggarwal, P.K. and Nesbitt, B.E., (1984) Geology and geochemistry of the Chu Chua massive sulphide deposit, British Columbia: *Economic Geology*, 79, p. 815-825.
- Akella, J., (1966) Calculation of material transport in some metasomatic processes: *Neues Jahrbuch fur Mineralogie, Abhandlungen*. 104, p. 316-329.
- Akella, J. and Winkler, H.G.F., (1966) Orthorhombic amphibole in some metamorphic reactions: *Contributions to Mineralogy and Petrology*, 12, p. 1-12.
- Baker, J.H. and de Groot, P.A., (1983) Proterozoic seawater - felsic volcanics interaction, W. Bergslagen, Sweden – Evidence for high REE mobility and implications for 1.8 Ga seawater compositions: *Contributions to Mineralogy and Petrology*, 82, p. 119-130.
- Barrie, C.T., Hannington, M.D. and Bleeker, W., (1999) The giant Kidd Creek volcanic-associated massive sulphide deposit, Abitibi Subprovince, Canada: *Reviews in Economic Geology*, 8, p. 247-269.
- Barrett, T.J., (1992) Mass changes in the Galapagos geothermal mounds: Near axis sediment transformation and mineralization: *Geology*, 20, p. 1075-1078.
- Barrett, T.J., Jarvis, I. and Jarvis, K.E., (1990) Rare earth element geochemistry of massive sulfides-sulfates and gossans from the Southern Explorer Ridge: *Geology*, 18, p. 583-586.
- Bence, A.E. and Taylor, B.E., (1985) Rare earth systematics of West Shasta metavolcanic rocks: petrogenesis and hydrothermal alteration: *Economic Geology*, 80, p. 2164-2176.
- Bernier, L.R. and MacLean, W.H., (1993) Lithogeochemistry of a Metamorphosed VMS Alteration Zone at Montauban, Grenville Province, Quebec: *Exploration and Mining Geology*, 2, p. 367-386.
- Beswick, A.E. and Soucie, G., (1978) A correction procedure for metasomatism in an Archean greenstone belt. *In*: Trendall, A.F., (editor) *Precambrian Research*, 6, p. 235-248.
- Brimhall, G.H. and Dietrich W.H., (1987) Constitutive mass balance relations between chemical composition, volume, density, porosity and strain in metasomatic hydrochemical systems: results on weathering and pedogenesis: *Geochimica et Cosmochimica Acta*, 51, p. 567-587.

- Brimhall, G.H., Lewis, C.J., Ague, J.J., Dietrich, W.E., Hampel, J., Teague, T. and Rix, P., (1988) Rare-Earth Element Mobility in Alteration Pipes Below Massive Cu-Zn Sulphide Deposits: *Chemical Geology* 65, No. 12, p. 181-202.
- Brown, T.H. and Skinner, B.J., (1974) Theoretical prediction of equilibrium phase assemblage in multicomponent systems: *American Journal of Science*, 274, p. 961-986.
- Campbell, I.H., Leshner, C.M., Coad, P., Franklin, J.M., Gorton, M.P. and Thurston, P.C., (1984) Rare earth element mobility in alteration pipes below massive Cu-Zn-sulphide deposits: *Chemical Geology*, 45, p. 181-202.
- Capitani, C. and Brown, T.H., (1987) The computation of chemical equilibrium in complex systems containing non-ideal solutions: *Geochimica et Cosmochimica Acta*, 51, p. 2639-2652.
- Chayes, F., (1971) *Ratio Correlation*. University of Chicago Press, Chicago, 99 p.
- Cheng, X. and Sinclair, A.J., (1994) Optimizing norm calculations for metasomatic rocks. *In*: Chung, C.F., (editor) *International Association for Mathematical Geology Proceedings, 1994 Annual Meeting, Mt. Tremblant, Quebec*, p. 81-86.
- Cheng, X. and Sinclair, A.J., (1995) Metasomatic Norms and Mass Balance Chemico-mineralogic Models of Hydrothermal Alteration Systems: *Exploration and Mining Geology*, 4, p. 365-379.
- Costa, U.R., Barnett, R.L. and Kerrich, R., (1983) The Mattagami Lake mine Archean Zn-Cu sulphide deposit, Quebec: hydrothermal coprecipitation of talc and sulphides in a seafloor brine pool – evidence from geochemistry,  $^{18}\text{O}/^{16}\text{O}$  and mineral chemistry: *Economic Geology*, 78, p. 1144-1203.
- Date, J., Watanabe, Y. and Saeki, Y., (1983) Zonal alteration around the Fukazawa Kuroko deposits, Akita Prefecture, Northern Japan. *In*: Ohmoto, H and Skinner, B.J., (editors) *Economic Geology Monograph* 5, p. 313-334.
- Dergachev, A.L., Sergeyeva, N.Y. and Dergacheva, A.A., (1989) Possibility of rare earth mineral formation during hydrothermal sedimentary massive sulphide deposition: *Doklady Akademii Nauk SSSR*, 304, p. 1213-1217.
- Descarreaux, J., (1973) A petrochemical study of the Abitibi volcanic belt and its bearing on the occurrences of massive sulphide ores: *Canadian Institute of Mining and Metallurgy Bulletin*, 66; 730, p. 61-69.

De Pangher, M. (1988) Quantitative Assessment of Composition - Volume Changes During Metasomatism: New Techniques for Identifying Protoliths and Conserved Elements: Ph.D. thesis, University of Utah, Salt Lake City, UT, 50 p.

Doucet, P., Mueller, W and Chartrand, F., (1998) Alteration and ore mineral characteristics of the Archean Coniagas massive sulphide deposit, Abitibi Belt, Quebec: Canadian Journal of Earth Sciences, 35, p. 620-636.

Elliott-Meadows, S.R. and Appleyard, E.C., (1991) The Alteration Geochemistry and Petrology of the Lar Cu-Zn Deposit, Lynn Lake Area, Manitoba Canada: Economic Geology, 86, p. 486-505.

Finlow-Bates, T. and Stumpfl, E.E., (1981) The behaviour of so-called immobile elements in hydrothermally altered rocks associated with volcanogenic submarine-exhalative ore deposits: Mineralium Deposita, 16, p. 319-328.

Fowler, A.D., (1990) Rock alteration; a further application of Pearce diagrams and related techniques. *In*: Russell, J.K. and Stanley, C.R., (editors) Theory and application of Pearce element ratios to geochemical data analysis: Geological Association of Canada Short Course Notes, 8, p. 235-241.

Franklin, J.M., (1984) Characteristics of alteration associated with Precambrian massive sulphide deposits. *In*: Morton, R.L. and Groves, D.A., (editors) Volcanic rocks, hydrothermal alteration and associated massive sulphide and gold deposits: University of Minnesota – Duluth, Short Course notes, p. 92-105.

Franklin, J.M., (1986) Volcanic associated massive sulphide deposits – an update: Irish Association of Economic Geology Special Publication, 4, p. 49-69.

Franklin, J.M., (1995) Volcanic associated massive sulphide base metals: *In*: Eckstrand, O.R., Sinclair, W.D. and Thorpe, R.I., (editors) Geology of Canadian mineral deposit types: Geological Survey of Canada, Geology of Canada, 8, p. 158-183.

Franklin, J.M., Kasarda, J. and Poulsen, K.H., (1975) Petrology and chemistry of the alteration zone of the Mattabi massive sulphide deposit: Economic Geology, 70, p. 63-79.

Franklin, J.M., Lydon, J.W. and Sangster, D.M., (1981) Volcanic associated massive sulphide deposits: Economic Geology 75 Anniversary Volume, p. 485-627.

Fox, J.S., (1984) Besshi-type volcanogenic deposits; a review: Canadian Institute of Mining and Metallurgy Bulletin, 77; 864, p. 57-68.

Galley, A.G., (1993) Characteristics of semi-conformable alteration zones associated with volcanic massive sulphide districts: Journal of Geochemical Exploration, 48, p. 175-200.

Galley, A.G. and Jonasson, I.R., (1992) Semi-conformable alteration and volcanogenic massive sulphide deposits. *In*: Simmons, S.F., Newson, J. and Lee, K.C., (editors) Proceedings 14-th New Zealand Geothermal Workshop, p. 279-284.

Galley, A.G., Bailes, A. H. and Kitzler, G., (1993) Geological Setting and Hydrothermal Evolution of the Chisel Lake and North Chisel Zn-Pb-Cu-Ag-Au Massive Sulphide Deposits, Snow Lake, Manitoba: Exploration and Mining Geology, 2, p. 271-295.

Gemmell, J.B., Large, R.R., McArthur, G.J., Drown, C.G. and Downs, R.C., (1990) Formation of the alteration pipe and stringer zone beneath the Hellyer volcanogenic massive sulphide deposit, Tasmania: Geological Association of Australia Special Publication, 25, p. 8-9.

Gemmell, J.B. and Fulton, R., (2001) Geology, Genesis and Exploration Implications of the Footwall and Hanging-Wall Alteration Associated with the Hellyer Volcanic-Hosted Massive Sulphide Deposit, Tasmania, Australia: Economic Geology, 96, p. 1003-1035.

Gibson, H.L., Watkinson, D.H. and Comba, C.D.A., (1983) Silicification: Hydrothermal alteration in an Archean geothermal system within the Amulet Rhyolite Formation, Noranda, Quebec: Economic Geology, 78, p. 954-971.

Gibson, H.L., Lichtblau, A.P., Comba, C.D.A. and Watkinson, D.H., (1986) Subaqueous rhyolite flows of the central mine sequence, Noranda, Quebec: Geological Association of Canada Programs with Abstracts, 11, p. 72.

Gibson, H.L. and Watkinson, D.H., (1999) An Archean subseafloor hydrothermal system, regional semiconformable alteration and massive sulphide deposits, Noranda, Quebec, Canada: *In*: Franklin, J.M. and Gibson, H.L., (editors) Exploration tools for volcanogenic massive sulphide deposits: Mineral Deposits Division, Geological Association of Canada and MDRU, University of British Columbia - Short Course notes.

Gilmore, K.V. and Pickell, J.R., (2000) The Konuto Lake VMS Deposit: Hudson Bay Exploration and Development Co. Ltd. Report, 44 p.

Gilmour, P.C., (1965) The origin of massive sulphide mineralization in the Noranda district, northwestern Quebec: Geological Association of Canada Proceedings, 16, p. 63-81.

Gorton, M.P. and Schandl, E.S., (1995) An unusual sink for rare earth elements: The rhyolite-basalt contact of the Archean Winston Lake volcanogenic massive sulphide deposit, Superior province, Canada: Economic Geology, 90, p. 2065-2072.

Govett, G.J.S., (1983) Handbook of Exploration Geochemistry, Volume 3: Rock Geochemistry in Mineral Exploration: Elsevier, New York, 461 p.

Grant, J.A., (1986) The isocon diagram: a simple solution to the Gresens equation for metasomatic alteration: *Economic Geology*, 81, p. 1976-1982.

Gresens, R.L., (1967) Composition – volume Relationships of Metasomatism: *Chemical Geology*, 2, p. 47-65.

Groves, D.A., (1984) Stratigraphy, lithology and hydrothermal alteration of volcanic rocks beneath the Mattabi massive sulphide deposit, Sturgeon Lake Ontario: M.Sc. thesis, University of Minnesota, Duluth, MN, 141 p.

Groves, D.A., Morton, R.L. and Franklin, J.M., (1984) Stratigraphy of the footwall volcanic rocks beneath the Mattabi massive sulphide deposit, Sturgeon Lake, Ontario: *Geological Association of Canada, Programs with Abstracts*, 9, p. 69.

Hashiguchi, H. and Usui, H., (1975) An Approach to Delimiting Targets for Prospecting of the Kuroko Ore Deposits: On the Sulphur and Magnetic Susceptibility Haloes: *Mining Geology*, 25, p. 293-301.

Hashiguchi, H., Yamada, R. and Inoue, T., (1983) Practical Application of Low  $\text{Na}_2\text{O}$  Anomalies in the Footwall Acid Lava for Delimiting Promising Areas Around the Kosaka and Fukazawa Kuroko Deposits, Akita Prefecture, Japan: *Economic Geology Monograph* 5, p. 387-394.

Hodgson, C.J. and Lydon, J.V., (1977) The geological setting of volcanogenic massive sulphide deposits and active hydrothermal systems: some implications for exploration: *Canadian Institute of Mining and Metallurgy Bulletin*, 70; 786, p. 95-106.

Iijima, A., (1974) Clay and zeolitic alteration zones surrounding Kuroko deposits in the Hokuroko district, Northern Akita, as submarine hydrothermal-diagenetic alteration products: *Society of the Mining Geologists of Japan, Special Issue* 6, p. 267-290.

Ishikawa, Y., Sawaguchi, T., Iwaya, S. and Horiuchi, M., (1976) Delineation of Prospecting Targets for Kuroko Deposits Based on Models of Volcanism of Underlying Dacite and Alteration Haloes: *Mining Geology*, 26, p. 105-117.

Iwao, S. and Kishimoto, F., (1954) Wall rock alteration of the Kosaka mine, Akita Prefecture, Japan: *Japan Geological Survey, Report* 162, p. 1-31.

Knuckey, M.J., Comba, C.D.A. and Riverin, G., (1982) Structure, metal zoning and alteration at the Millenbach deposit, Noranda, Quebec. *In*: Hutchinson, R.W., Spence, C.D. and Franklin, J.M., (editors) *Precambrian sulphide deposits: Geological Association of Canada Special Paper* 25, p. 255-297.

- Koo, J. and Mossman, D.J., (1975) Origin and metamorphism of the Flin Flon stratabound Cu-Zn sulphide deposit, Saskatchewan and Manitoba: *Economic Geology*, 70, p. 48-62.
- Larocque, A.C.L. and Hodgson, C.J., (1993) Carbonate-rich footwall alteration at the Moburn Mine, a possible Mattabi-type VMS deposit in the Noranda Camp: *Exploration and Mining Geology*, 2, p. 165-169.
- Lentz, D.R., (1999) Deformation-induced mass-transfer in felsic volcanic rocks hosting the Burnswick No. 6 Massive sulphide deposit, New Brunswick: Geochemical effects and petrogenetic implications: *The Canadian Mineralogist*, 37, p. 489-512.
- Lickus, R.J., (1965) Geology and geochemistry of the ore deposits at the Vauze mine, Noranda district, Quebec: Ph.D. thesis, McGill University, Montreal, PQ, 48 p.
- Lydon, J. W., (1984a) Some observations on the mineralogical and chemical zonation patterns of volcanogenic massive sulfide deposits of Cyprus. *In: Current Research, Part A: Geol. Survey Canada, Paper 84-1A*, p. 611-616.
- Lydon, J. W., (1984b) Ore Deposit Models -8. Volcanogenic Massive Sulfide Deposits, Part1: A Descriptive Model: *Geoscience Canada*, 11, p. 195-202.
- MacGeehan, P.J., (1978) The geochemistry of altered rocks at Matagami, Quebec: a geothermal model for massive sulfide genesis: *Canadian Journal of Earth Sciences*, 15, p. 551-570.
- MacGeehan, P.J and MacLean, W.H., (1980) Tholeiitic Basalt-rhyolite magmatism and massive sulfides at Matagami, Quebec: *Nature*, 283, p. 153-157.
- MacLean, W.H., (1988) Rare earth element mobility at constant inter-REE ratios in the alteration zone at the Phelps Dodge massive sulphide deposit, Matagami, Quebec: *Mineralium Deposita*, 23, p. 231-238.
- MacLean, W.H., (1990) Mass change calculations in altered rock series: *Mineralium Deposita*, 25, p. 44-49.
- MacLean, W.H. and Hoy, L.D., (1991) Geochemistry of hydrothermally altered rocks at the Horne mine, Noranda, Quebec: *Economic Geology*, 86, p. 506-528.
- MacLean, W.H. and Barrett, T.J., (1993) Lithogeochemical techniques using immobile elements: *Journal of Geochemical Exploration*, 48, p. 109-133.
- Madeisky, H.E. and Stanley, C.R., (1993) A study of the footwall metasomatic zones associated with the Rio Tinto massive sulphide and stockwork deposits using Pearce element



ratio analysis: Geological Association of Canada Programs with Abstracts, Mineralogical Association of Canada; Canadian Geophysical Union, Joint Annual Meeting 1993, p. 65.

McMillan, W.J., (1980) CC Prospect, Chu Chua Mountain: Geological Fieldwork, 1980-1, p. 37-48.

Morgan, J., (1995) Geological Mapping of the Area of Denare Beach – Konuto Lake – Birch Lake: Hudson Bay Exploration and Development Co. Ltd. Report, 42 p.

Morton, R.L., (1984) Subaqueous volcanism. *In*: Morton, R.L. and Groves, D.A., (editors) Volcanic rocks, hydrothermal alteration and associated massive sulphide and gold deposits: University of Minnesota – Duluth, Short Course Notes, p. 15-45.

Morton, R.L. and Nebel, M.L., (1984) Hydrothermal alteration of felsic volcanic rocks at the Helen siderite deposit, Wawa, Ontario: *Economic Geology*, 79, p.1319-1333.

Morton, R.L., Groves, D.A. and Franklin, J.M., (1985) Volcanic stratigraphy and nature of the conformable alteration zone beneath the Mattabi massive sulphide deposit, Sturgeon Lake, Ontario: Lake Superior geology, Institute on Lake Superior Geology Proceedings and Abstracts, Annual Meeting. 31, p. 62-63.

Morton, R.L. and Franklin, J.M., (1987) Two-fold classification of Archean volcanic-associated massive sulphide deposits: *Economic Geology*, 82, p.1057-1063.

Morton, R.L., Hudak, G.J., Walker, J.S. and Franklin, J.M., (1991) Open-File Report – Geological Survey of Canada, p.74-94.

Nichol, I., Bogle, E.W., Lavin, O.P., McConnell, J.W. and Sopuck, V.J., (1977) Lithogeochemistry as an aid in massive sulphide exploration. *In*: Davis, G.R. (editor) Prospecting in areas of glaciated terrain, p. 63-71.

Nicholls, J., (1988) The Statistics of Pearce Element Diagrams and the Chayes Closure Problem: *Contributions to Mineralogy and Petrology*, 108, p. 212-218.

Nicholls, J. and Gordon, T., (1994) Procedures for the calculation of axial ratios on Pearce element-ratio diagrams: *Canadian Mineralogist*, 32, p. 969-977.

Osterberg, S.A., Morton, R.L. and Franklin, J.M., (1987) Hydrothermal alteration and physical volcanology of Archean rocks in the vicinity of the Headway-Coulee massive sulphide occurrence, Onaman area, northwestern Ontario: *Economic Geology*, 82, p. 1505-1520.

Pearce, T.H., (1968) A contribution to the theory of variation diagrams: *Contributions to Mineralogy and Petrology*, 19, p. 142-157.

- Pearce, T.H. and Stanley, C.R., (1991) The validity of Pearce element ratio analysis in petrology; an example from the Uwekahuna laccolith, Hawaii: *Contributions to Mineralogy and Petrology*, 108, p. 212-218.
- Poulsen, K.H. and Hannington, M.D., (1995) Volcanic associated massive sulphide gold. *In*: Eckstrand, O.R., Sinclair, W.D. and Thorpe, R.I., (editors) *Geology of Canadian mineral deposit types: Geological Survey of Canada, Geology of Canada*, 8, p. 183-196.
- Prins, P. and Venter, J.P., (1978) Primary Dispersion Aureoles Associated with Copper-bearing Mafic bodies, Namaqualand. *In*: Verwoerd, W.S., (editor) *Mineralization in metamorphic terranes: Geological Society of South Africa Special Publication 4*, p. 331-344.
- Reilly, B.A., (1995) The Geological setting of mineral deposits of the Flin Flon – Amisk Lake area: Summary of Investigations 1995, Saskatchewan Geological Survey, Saskatchewan Ministry of Energy, Mines Miscellaneous Report, 95-4, p. 3-12.
- Richards, H.G., Cann, J.R. and Jensenius, J., (1989) Mineralogical zonation and metasomatism of the alteration pipes of Cyprus sulphide deposits: *Economic Geology*, 84, p. 91-115.
- Riddell, J.E., (1953) Wall-rock alteration around base-metal sulphide deposits of northwestern Quebec: Ph.D. thesis, McGill University, Montreal, PQ, 122 p.
- Riverin, G. and Hodgson, C.J., (1980) Wall-rock alteration at the Millenbach Cu-Zn mine, Noranda Quebec: *Economic Geology*, 75, p. 424-444.
- Roberts, R.G. and Reardon, E.G., (1978) Alteration and ore forming processes at Mattagami Lake mine, Quebec: *Canadian Journal of Earth Sciences*, 15, p. 1-21.
- Robinson, M., (1996) Birch Lake Assemblage, Spring and Fall, 1995: Hudson Bay Exploration and Development Co. Ltd. Report, 57 p.
- Russell, J.K. and Nicholls, J., (1988) Analysis of Petrologic Hypotheses with Pearce Element Ratios. *Contributions to Mineralogy and Petrology*, 99, p. 25-35.
- Russell, J.K. and Stanley, C.R., (1990) Origins of the 1954-1960 lavas of Kilauea Volcano; constraints on shallow reservoir magmatic processes: *In*: *Continental Magmatism Abstracts*. New Mexico Bureau of Mines and Mineral Resources Bulletin, 131, p. 320.
- Saeki, Y. and Date, J., (1980) Computer Application of the Alteration Data for the Footwall Dacite Lava at the Ezuri Kuroko Deposits, Akita Prefecture: *Mining Geology*, 30, p. 241-250.

Sangster, D.F., (1972) Precambrian volcanogenic massive sulphide deposits in Canada: A review: Geological Survey of Canada Paper, 72-22, 44p.

Sakrison, H.C., (1967) Chemical studies of the host rocks of the Lake Dufault mine, Quebec: Ph.D. thesis, McGill University, Montreal, PQ, 138 p.

Schade, J., Cornell, D.H. and Theart, H.F.J., (1989) Rare earth element and isotopic evidence for the genesis of the Prieska massive sulphide deposit, South Africa: *Economic Geology*, 84, p. 49-63.

Schandl, E.S. and Gorton, M.P., (1991) Postore mobilization of rare earth elements at Kidd Creek and other Archean massive sulphide deposits: *Economic Geology*, 86, p. 1546-4553.

Schandl, E.S., Gorton, M.P. and Wasteneys, H.A., (1995) Rare earth element geochemistry of the metamorphosed volcanogenic massive sulphide deposits of the Manitouwadge mining camp, Superior Province, Canada; a potential exploration tool?: *Economic Geology*, 90, p. 1217-1236.

Schandl, E.S., Gorton, M.P. and Wasteneys, H.A., (1996) Rare earth element geochemistry of the metamorphosed volcanogenic massive sulphide deposits of the Manitouwadge mining camp, Superior Province, Canada; a potential exploration tool? A reply: *Economic Geology*, 91, p. 473-476.

Schneider, N., Ozcur, N., Palacios, C.M., (1988) Relationship between alteration, rare earth element distribution and mineralization of the Murgul copper deposit, Northeastern Turkey: *Economic Geology*, 83, 1238-1246.

Shirozu, H., (1974) Clay Minerals in Altered Wall Rocks of the Kuroko-type Deposits: *Mining Geology Special Issue*, 6, p. 303-310.

Silverman, A., Wehrenberg, J.P. and Behre Jr., C.H., (1962) Selected studies of base metal dispersion and implication in ore-deposit theory: *Economic Geology*, 57, p. 1013.

Sinclair, A.J. and Stanley, C.R., (1995) Lithogeochemical Exploration for Metasomatic Alteration Zones Associated with Hydrothermal Mineral Deposits: University of British Columbia, MDRU Research Proposal, 7 p.

Slack, J.F., (1993) Descriptive and Grade-tonnage models for besshi-type polymetallic massive sulphide deposits. *In*: Kirkham, R.V., Sinclair, W.D., Thorpe, R.I. and Duke J.M., (editors) *Mineral deposit modeling: Geological Association of Canada Special Paper*, 40, 343-371.

Spitz, G. and Darling, R., (1978) Major and Minor Element Lithogeochemical Anomalies Surrounding the Louvem Copper Deposit, Val d'Or, Quebec: Canadian Journal of Earth Sciences, 15, p. 1161-1169.

Spooner, E.T.C., (1977) Hydrodynamic model for the origin of the ophiolitic cupriferous pyrite ore deposits of Cyprus. *In: Volcanic Processes in Ore Genesis: Institute of Mining and Metallurgy, London, Special Publication, 7, p. 58-71.*

Spooner, E.T.C. and Fyfe, W.S., (1973) Sub-sea floor metamorphism, heat and mass transfer: Contributions to Mineralogy and Petrology, 42, p. 287-304.

Stanley, C.R., (1994) Graphical investigation of lithogeochemical variations using ratio diagrams: Geological Society of America Abstracts with Programs, 26; 7, p. 355.

Stanley, C.R., (1995) Graphical Investigations of Lithogeochemical Variations Using Molar Element Ratio Diagrams: Theoretical Foundation: University of British Columbia, MDRU Lithogeochemistry Technical Document 3, 40 p.

Stanley, C.R. and Russell, J.K., (1989) Petrologic hypothesis testing with Pearce element ratio diagrams; derivation of diagram axes: Contributions to Mineralogy and Petrology, 103, p. 78-89.

Stanley, C.R. and Madeisky, H.E., (1993) Lithogeochemical exploration for metasomatic halos around mineral deposits using Pearce element ratio analysis: Geological Association of Canada Programs with Abstracts, p. 99.

Stanley, C.R. and Madeisky, H.E., (1996) Lithogeochemical Exploration for Metasomatic Zones Associated with Hydrothermal Mineral Deposits Using Pearce Element Ratio Analysis: University of British Columbia, MDRU Short Course notes, 98 p.

Turek, A., Tetley, N.W. and Jackson, T., (1976) A study of metal dispersion around the Fox orebody in Manitoba: Canadian Institute of Mining and Metallurgy Bulletin, 69; 770, p. 104-110.

Urabe T., Scott, S.D. and Hattori, K., (1983) A comparison of footwall alteration and geothermal systems beneath some Japanese and Canadian volcanogenic massive sulphide deposits. *In: Ohmoto, H. and Skinner, B.J., (editors) The Kuroko and related volcanogenic Massive Sulphide Deposits: Economic Geology Monograph 5, p. 345-364.*

Vollo, N., (1974) Geology and regional setting of the Chu Chua copper deposit, South-central British Columbia: Canadian Institute of Mining and Metallurgy Bulletin, 74; 833, 60 p.

Walford, D.C. and Franklin, J.M., (1982) The Anderson Lake mine, Snow Lake, Manitoba: *In*: Hutchinson, R.W., Spence, C.D. and Franklin, J.M., (editors) Precambrian Sulfide Deposits: Geological Association of Canada, 25, p. 481-523.

Walker, T.L., (1930) Dalmatianite, the spotted greenstone from the Amulet mine, Noranda, Quebec: University of Toronto Studies, Geology Series, 29, p. 9-12.

Wood, S.A. and Williams-Jones, A.E., (1994) The aqueous geochemistry of the rare earth elements and yttrium: 4. Monazite solubility and REE mobility in exhalative massive sulphide depositing environments: *Chemical Geology*, 115, p. 47-60.

Zaleski, E.S. and Halden, N.M., (1988) Reconstruction of synvolcanic alteration associated with the Linda massive sulphide deposit, Snow Lake, Manitoba: Geological Survey of Canada, Paper 88-1C, p. 73-81.

Zaleski, E.S. and Peterson, V.L., (1996) Rare earth element geochemistry of the metamorphosed volcanogenic massive sulphide deposits of the Manitouwadge mining camp, Superior Province, Canada; a potential exploration tool? *A discussion: Economic Geology*, 91, p. 469-473.

## Chapter 2

### Major-element lithogeochemistry of alteration associated with the Goldstream Besshi-type Volcanogenic Massive Sulphide deposit, British Columbia



Plate 2.1. View of the Goldstream Mine area looking south.

## **Abstract**

The Goldstream Cu-Zn deposit in British Columbia is hosted by predominantly metapelitic rocks. Primary and secondary geochemical variability in the host rocks was studied using 180 samples analyzed by X-Ray Fluorescence analysis (XRF) and an additional suite of 123 donated samples analyzed by a variety of methods. Molar Element Ratio analysis techniques were used to quantify the alteration and to characterize it chemically, mineralogically and spatially.

The chemical compositions of the rocks bear the signatures of pelagic and turbiditic sedimentation along with that of a paleo-seafloor hydrothermal system. These geochemical signatures are distinguishable using binary plots of conserved elements, Zr, Ti and Nd versus  $\text{SiO}_2$ . Pearce Element Ratio (PER) Analysis and Generalized Element Ratio (GER) analysis were used to identify the most likely initial mineral paragenesis in the metapelitic rocks: quartz, montmorillonite (diagenetically altered to illite) and chlorite. The presence of the latter in the unaltered sediment is weak, but pervasive.

Samples influenced by the hydrothermal system, either through metasomatism, or through chemical sedimentation of exhalites, are identified by anomalously high Fe, Mg and silica addition and by the two-way mobility of the alkali metals. Mineralogically, the alteration is manifested by the formation of quartz, iron sulphides, chlorite, saponite, nontronite, sericite and albite, superseding the primary pelitic assemblage (probably montmorillonite and/or illite).

The hydrothermal signature is restricted to the stratigraphic footwall of the deposit. Spatial patterns at the western "C" zone are less clear and correlation with the main ore zone is speculative.

## Introduction

The Goldstream Cu-Zn deposit in the northern Selkirk Mountains in southeastern British Columbia (Fig. 2.1) is a concordant massive sulphide layer within a predominantly metapelitic and calcareous rock succession of probable early Paleozoic age (Hoy, 1979). Mineralization was discovered in 1972, during the construction of a logging road. Diamond drilling by Noranda Mines Ltd. outlined reserves of 3.175 million tonnes of ore grading 4.49 % Cu and 3.12 % Zn with significant silver grades. The ore body was mined in the 1980s of the last century by Noranda Inc. After an interruption due to depressed metal prices, Bethlehem Resources Corporation and Goldneve Resources Inc. resumed the operation until the mine was closed in 1996.

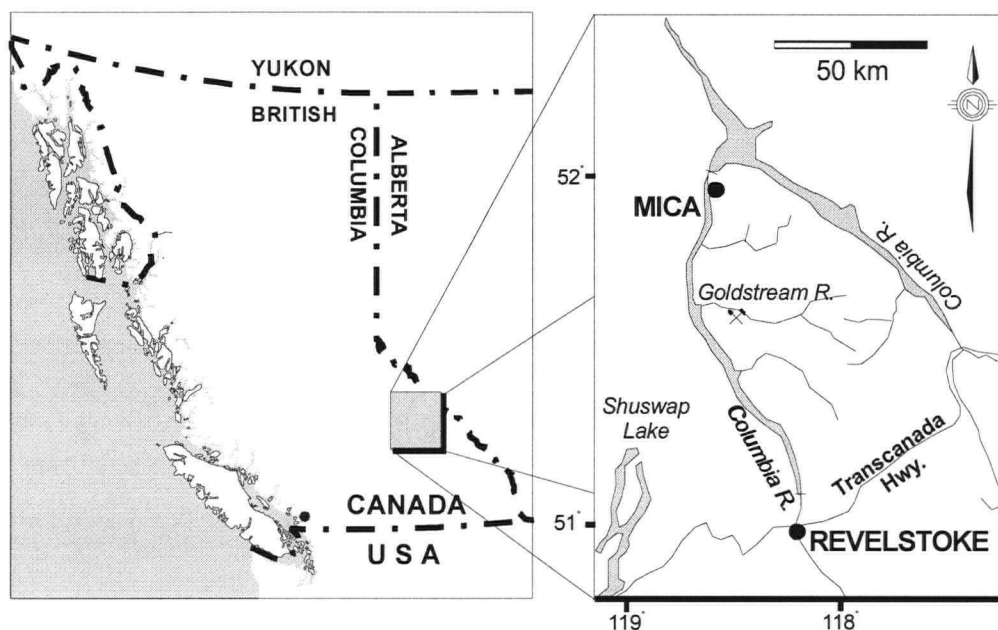


Fig. 2.1. Location of the Goldstream deposit, British Columbia

The work done on the Goldstream massive sulphide deposit is a part of a broader study of the lithogeochemistry of alteration zones associated with volcanic-hosted and volcanic-related massive sulphide deposits. Their lithogeochemical characteristics were studied using various techniques, but primarily using Pearce element ratio (PER, Pearce, 1968; Russell and Stanley, 1990; Stanley and Madeisky, 1993; Stanley, 1996) analysis. In the case of the Goldstream deposit variability in major-element concentrations was caused by numerous



geochemical processes, both preceding and following the deposit formation, thus masking the effects of ore-related hydrothermal alteration. The goal of this study is to quantitatively characterize the effects of metasomatism related to sulphide deposit formation. To achieve this goal, it was necessary to separate hydrothermal metasomatism effects on rock chemistry from the effects of other rock-forming processes, such as sorting of the pelitic clastic material and its dilution by carbonate chemical precipitates during sedimentation, diagenetic redistribution of elements and metamorphic recrystallization.

## **Geologic Setting**

### ***Regional geology***

The Goldstream deposit (Fig. 2.1) lies in the northern Kootenay arc, within the Omineca physiographic belt, west of the folded miogeoclinal rocks of the ancestral North American continent. The mineralized units are part of the pericratonic Kootenay terrane (Wheeler and McFeely, 1991; Wheeler *et al.* 1991), which consists of miogeoclinal Paleozoic rocks and younger (up to Mesozoic) sedimentary and volcanic rocks. The terrane was deformed in the Middle Jurassic and intruded by four granitic suites, varying in age from Mississippian to post-Late Cretaceous (Logan and Friedman, 1997). To the west the area borders the Monashee Complex, the older, metamorphosed Precambrian to Paleozoic section of the Omineca belt. The east-dipping Columbia River fault zone, within the deep North-South-trending Columbia River valley, is a major extensional structure of Eocene age that separates the Kootenay terrane from the Monashee Complex (Read and Brown, 1979).

The strata hosting the Goldstream deposit (Fig. 2.3) comprise Paleozoic metasedimentary and metavolcanic rocks, ranging in age from Upper Cambrian to Lower Mississippian (Logan and Drobe, 1994). They were deformed, metamorphosed, then intruded by the complex monzonitic Goldstream pluton of probable Middle Cretaceous age (Logan and Colpron, 1995; Logan and Friedman, 1997).

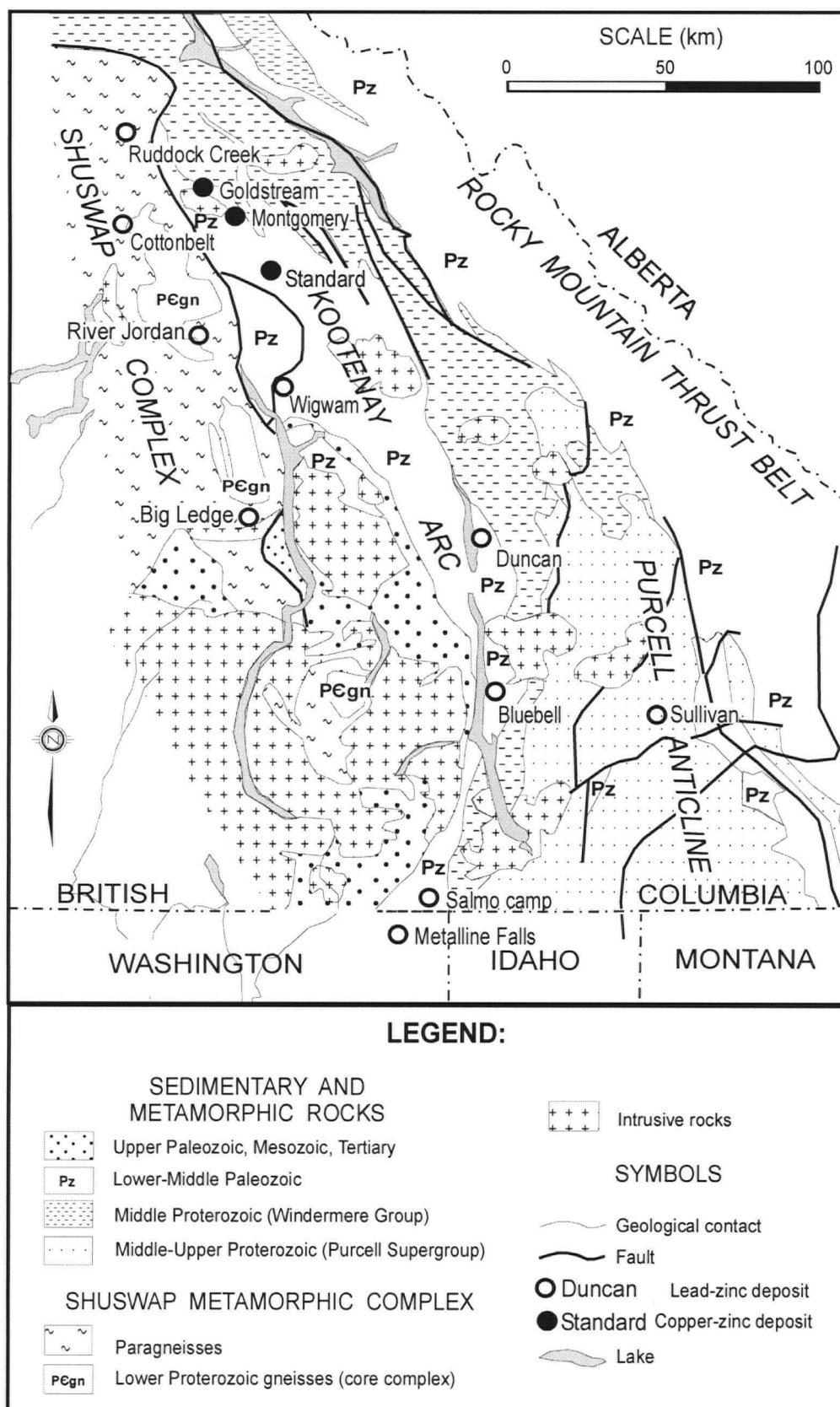


Fig. 2.2. General geologic setting and principal mineral deposits of the Goldstream area (modified from Hoy *et al.*, 1985)

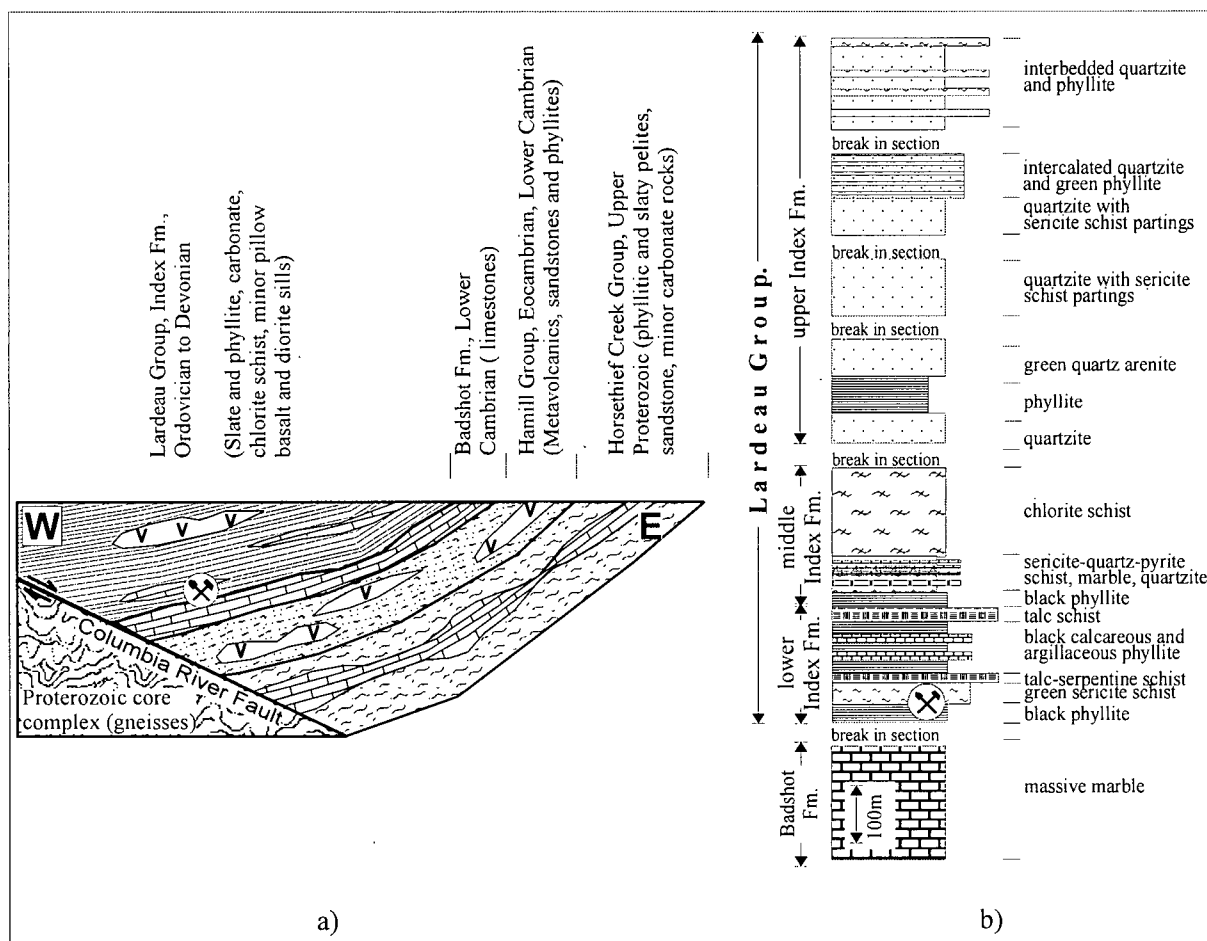


Fig. 2.3. Regional and local stratigraphy of the Goldstream area.

a). Regional stratigraphy (modified from Fyles, 1970)

b). Goldstream area stratigraphy, shown upright (Logan and Colpron, 1995)

### ***Stratigraphy, lithologies and metamorphism***

The stratigraphy of the Goldstream area (Fig. 2.3) is dominated by metapelitic rocks, which are commonly carbonate-rich. Quartzite, marbles, greywacke, and mafic metavolcanic rocks are also present. Stratigraphic and structural interpretations in the vicinity of the mine are difficult because: (1) the Goldstream structural slice is entirely fault bounded; (2) fossil-bearing strata are absent; (3) many of the stratigraphic units in the Kootenay arc are lithologically similar; and (4) repeated deformation of the rocks caused structural complexities. Thus, correlations with stratigraphic units defined in the southern part of the Kootenay arc are uncertain (Logan and Drobe, 1994).

Rocks north of the Goldstream River are assigned to the Late Proterozoic Horsethief Group by some authors (Franzen, 1974; Brown *et al.*, 1977; Wheeler *et al.*, 1991) and to the Paleozoic Hamill Group, Badshot Formation and Lardeau Group by others (Gibson and Hoy, 1985). Galena-lead model ages acquired from the Rift stratiform lead-zinc showing, occurring in possibly equivalent stratigraphy north of the Goldstream area, support the younger age for the strata (*ca.* 0.52Ga; Hicks, 1982).

The stratigraphy south of the Goldstream River is assigned to the Horsethief Creek Group (Upper Proterozoic), the Hamill Group and the Badshot Formation (Lower Cambrian), and the Index and Broadview formations of the Lardeau Group (Ordovician to Devonian) by various authors (Campbell, 1972; Brown *et al.*, 1976; Lane, 1977; Hoy, 1979). Hoy (1979) also recognized the Mohican Formation, which forms the upper part of the Hamill Group in the Kootenay arc in the Goldstream area. This stratigraphy was shown to be largely traceable in the area between Carnes Creek and Goldstream River (Brown *et al.*, 1983; Hoy *et al.*, 1984; Brown and Lane, 1988; Gibson, 1989; Brown 1991)

Recent and detailed work in the area (Logan and Colpron, 1995) recognizes three lithologically distinct units in the vicinity of the Goldstream deposit. This and other work (*e.g.*, Lane, 1977; Brown *et al.*, 1977; Hoy, 1979; Hoy *et al.*, 1984; Logan and Drobe, 1994) describe the stratigraphic section as inverted and correlate it with parts of the Lower to Middle Paleozoic stratigraphy (the Badshot Formation and the Index and Broadview Formations of the Lardeau Group) based on lithologic similarities. The inverted-section concept was also supported by lead isotope data from Goldstream galena and similarities with other lead-zinc deposits in the area (Hoy *et al.*, 1984).

The lithologies hosting the massive sulphide mineralization at Goldstream (Fig. 2.4) are best exposed in the east wall of the open pit, where they dip moderately to steeply north. Starting from the structural hanging wall, they include (names of the lithologic units and their abbreviations used by the mine geologists are adopted for the purposes of this study for their accuracy and simplicity):

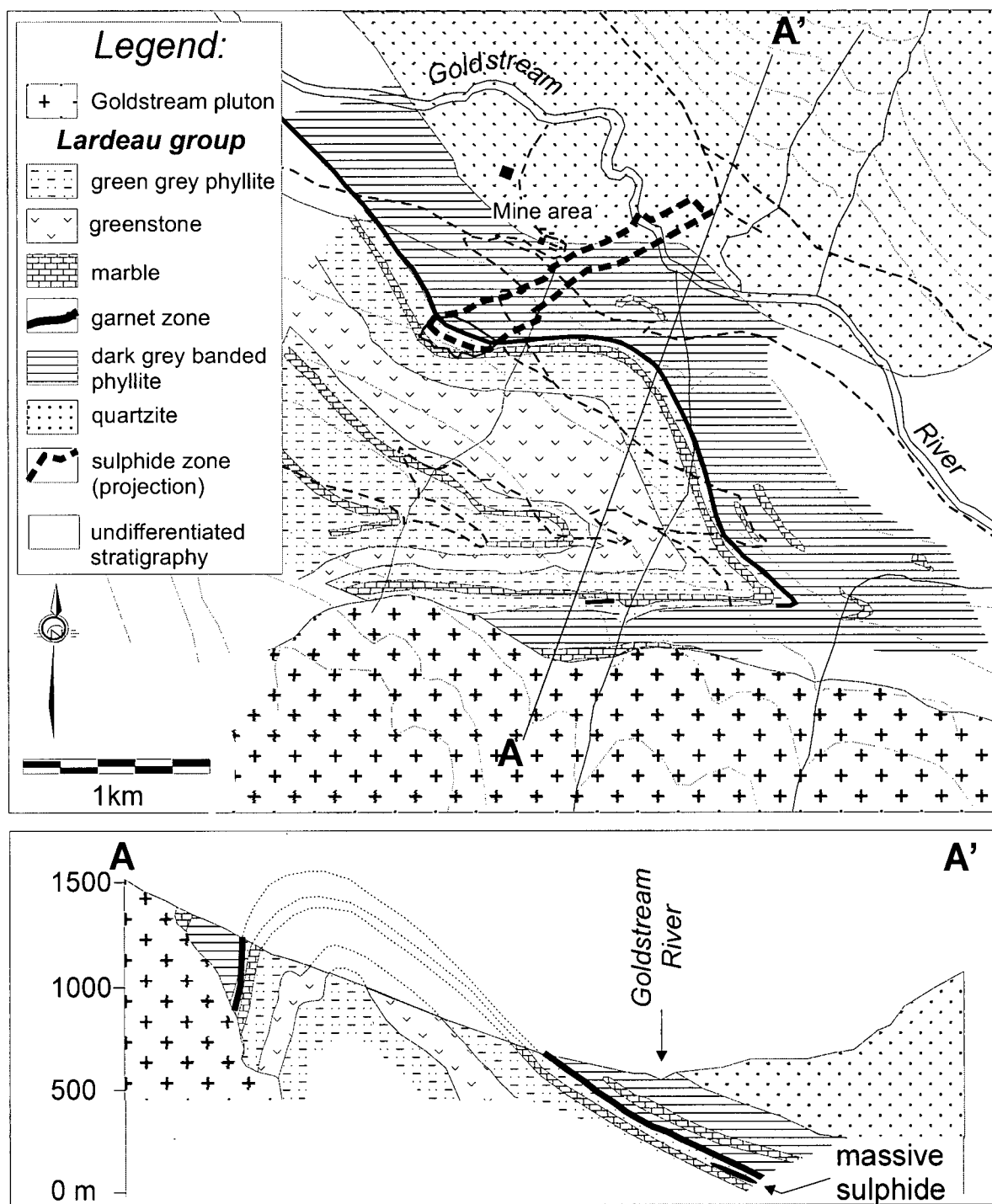


Fig. 2.4. Local geology of the Goldstream mine area adopted, with minor changes, from Logan and Colpron (1995)

1. The Dark Grey Banded Phyllite (DGBP) is a unit that comprises thinly bedded, graphitic and calcareous rocks (Hoy *et al.* 1984) spanning the range between calcareous phyllite and phyllitic marble. This rock type makes up most of the structural hanging wall from a few tens of metres above the ore horizon to the surface and commonly contains quartz veins and augen and local sulphide lenses.
2. The Garnet zone (GZ) is made up of garnetiferous, graphitic pelites containing an appreciable amount of wispy pyrrhotite and thin cherty layers. It forms a blanket of up to a few tens of metres in the hanging wall of the deposit and occurs in close proximity to the ore body. The manganese content of the garnets (Hoy *et al.* 1984; Bradshaw, 1996), the relatively higher silica concentrations and the spatial association of these rocks with the ore body are consistent with their interpretation as a manganiferous and cherty exhalite layer (Hoy *et al.* 1984).
3. The immediate hanging and footwall of the deposit is made up of grey-green, thinly bedded phyllite (Green Grey Phyllite, GGP). Muscovite (sericite) is as abundant in these rocks as in the DGBP and the paler colour of the rock is due to its low graphite concentrations. The contacts of this lithologic unit are gradational both with the overlying and underlying lithologies.
4. The deeper footwall of the ore body, beyond the few metres of GGP consists of impure limestone heavily interbedded with phyllite (Footwall Marble, FM). The phyllite component of this rock is so significant that in appearance (texture and colour) the rock is almost identical to the DGBP and GGP units.
5. Massive and schistose, fine-grained greenstone is exposed at the west end of the open pit. It is composed of large porphyroblasts of actinolite, chlorite, epidote, sericite and albite (Hoy *et al.* 1984). A rock of a similar composition was sampled in a drill hole northwest of the deposit.

Mineralogically, the lithologic units described above are fairly simple and similar, with few exceptions. Both the DGBP and GGP and the abundant phyllitic component in the GZ and FM contain quartz as the main constituent, phyllosilicate minerals (biotite, muscovite and chlorite) and calcite. Epidote and amphibole (grunerite) are rare. Amphibole, which

indicates metamorphic temperatures in excess of 600°C (Bucher and Frey, 1994), is identified in two samples, in close proximity to the Goldstream pluton. Pyrrhotite occurs in varying abundance as lenses stretched into foliation planes in all lithologic units. In the GZ unit and in the margins of the ore body, the concentration of pyrrhotite reaches several percent. Mn-bearing garnet (Hoy *et al.* 1984; Bradshaw, 1996) distinguishes the garnet zone from the otherwise identical DGBP. Graphite occurs in partings and less commonly as irregular masses in the GGBP, the GZ and the FM. Given the similar mineral composition and texture of the phyllitic component in the rocks, graphite provides a means for distinction between DGBP and GGP.

The Goldstream pluton is an elliptical, east-trending intrusive complex. It consists of monzodiorite, quartz monzonite and granite phases and pendants of layered and foliated country rock. The abundance and structural continuity of pendants, as well as the metamorphic mineral assemblages in the contact aureole of the pluton, suggest high-level emplacement. The age of the pluton is estimated as Cretaceous by  $^{40}\text{Ar}/^{39}\text{Ar}$  (hornblende: 114 +/- 4.5 Ma, biotite: 100 +/- 1 Ma; Logan and Colpron, 1995) and U-Pb (zircon: 104.3 +/- 1.4/- 1.8 Ma; Logan and Friedman, 1997) methods.

The rocks in the vicinity of the Goldstream deposit have undergone greenschist facies (chlorite zone) regional metamorphism and contact metamorphism. The typical mineral assemblage in the phyllites (quartz + chlorite + muscovite +/- biotite) as well as the presence of spessartine (Hoy, 1979; Bradshaw, 1996) in the GZ is a result of the mild thermal effect of the Goldstream pluton at relatively low pressures (Bucher and Frey, 1994).

### ***Structure***

Accretion of allochthonous terranes at the western edge of the North American plate during the Mesozoic (Monger *et al.* 1994) was associated with polyphase folding and faulting, now recognizable in the Northern Selkirk Mountains.

The most recent work on the Goldstream area (Logan and Colpron, 1995) recognizes two generations of structures. The earlier generation (phase 1, Fig. 2.5) is represented by northwest-trending, southwest-verging tight isoclinal folds and thrust faults. These are common in the west flank of the Selkirk fan structure and are assigned to a syn-metamorphic Middle Jurassic (*e.g.*, Parrish and Wheeler, 1983; Brown *et al.* 1992) tectonic event. The pronounced foliation and the elongation of the ribbon-shaped Goldstream ore body are attributable to this tectono-metamorphic event (Hoy *et al.* 1984). Outside of the study area, these folds are reported to deform earlier nappe structures (Hoy, 1979; Brown *et al.* 1983; Hoy *et al.* 1984; Brown and Lane, 1988) and contraction faults (Logan and Colpron, 1995).

A later generation of structures, recognized in the vicinity of the Goldstream mine, consists of easterly trending open folds that plunge gently eastwards (phase 2, Fig. 2.5). An antiform fold, belonging to this phase of deformation and developed in the overturned section of an earlier tight isoclinal fold, hosts the Goldstream sulphide ore body in its less-steep, north limb (Fig. 2.4). Thus, the mine strata are overturned (Hoy, 1979; Hoy *et al.* 1984).

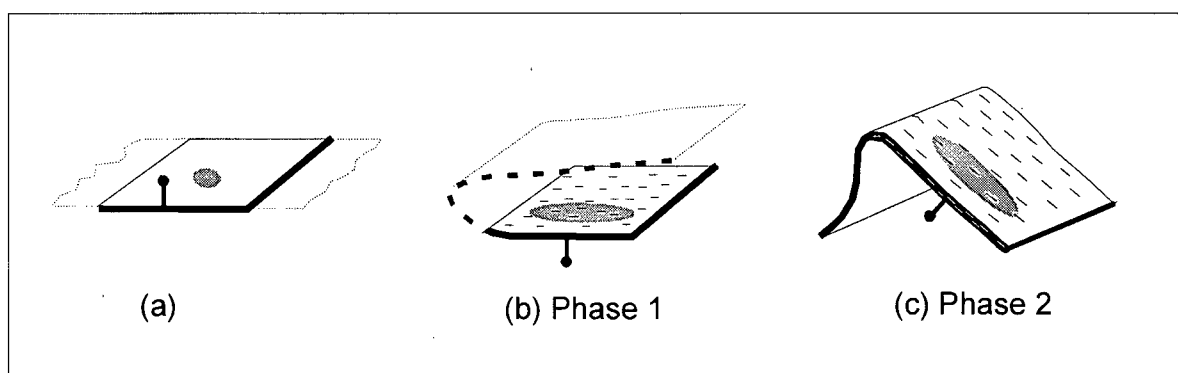


Fig. 2.5. Phases of deformation of the Goldstream stratigraphy and ore body according to Logan and Colpron (1995): The sedimentary strata, including a tabular body of massive sulphide (a) are stretched, foliated and overturned by isoclinal folding (b). They are in turn deformed by a more open, eastward-plunging antiform fold (c)



## ***Metallogeny***

The Kootenay arc and the adjacent Shuswap Complex and Purcell Anticlinorium are known to host a number of diverse lead-zinc and copper-zinc deposits, including the unique Sullivan ore body (Hoy, 1989; Lydon *et al.*, 2000). This massive sulphide-rich terrane of southeast British Columbia is part of a larger metallogenic province extending into Idaho and Montana (Fig. 2.2). It is recognized as one of the great base-metal metallogenic provinces of the world (Weissenborn *et al.*, 1970).

The Badshot Formation in the Kootenay arc is an extensive Lower Cambrian shallow water carbonate sequence, which hosts a number of deformed stratabound lead-zinc deposits. Among them are the Reeves MacDonald, H.B., Jersey, and Jackpot in the Salmo area, located north of the United States border. The ores have impregnated the host limestones after the latter were dolomitized, silicified, and deformed (Fyles, 1970). The Bluebell, in which the ore is fracture-controlled (Hoy, 1980), Duncan (Fyles, 1964), and Wigwam (Thompson, 1978) lead-zinc deposits are located in the same host rocks farther north in the Kootenay arc (Fig. 2.2). Similar, although undeformed, stratigraphy in Washington State hosts the Metaline Falls stratabound replacement Pb-Zn deposits (Fyles, 1970).

A number of large stratabound lead-zinc deposits, including Ruddock Creek, Cottonbelt, Jordan River, CK, and Big Ledge (Hoy, 1982) are located in the Shuswap Complex, to the west of the Goldstream area. They are hosted by platformal quartzite, marble, and paragneiss succession, which unconformably overlies a series of early Proterozoic metamorphic core complexes.

The Goldstream, Standard, and Montgomery copper-zinc deposits occur in basic metavolcanic rocks and dark calcareous phyllite. They are unique to an area that typically hosts lead-zinc deposits. This atypical metallogenic character of the Goldstream area can be attributed to the mafic volcanic rocks occurring, although not dominantly, in the host succession. The Keystone deposit (Hoy *et al.*, 1985), a lead-zinc-copper showing in the Goldstream area, has mid-Cretaceous lead isotopes (J. Logan, pers. comm.). Thus, it cannot

be directly compared with the Paleozoic deposits in the area. However, the atypical metal assemblage may be linked to the host-rock lithology, which is quartzitic rather than containing greenstone and metapelites (Franklin *et al.* 1981; Sverjensky, 1989). The stratabound Rift zinc-lead showing (Gibson and Hoy, 1985), located 30 km north of Goldstream is hosted by pelitic schists and is at least spatially associated with bimodal volcanic rocks. Economically important silver grades are typical for the deposits in the area regardless of the main ore components.

### ***Mineralization***

The Goldstream ore body and its mineralogy, structure, zonation, *etc.* are not specifically the object of this study. A relatively detailed description is available in Hoy *et al.* (1984). Only a few background facts and highlights that are related to the discussion of the associated alteration are presented below.

1. The ore body is over 1200 m long, 400 m wide and up to 3 m thick in its central part. It has been drilled to a depth of about 500 m under the Goldstream river valley and may continue further down dip to the northeast (Logan and Colpron, 1995). Its western limit is well defined, but it thins gradually and metal grades drop off to the east. The upper and lower contacts are sharp-to-gradational, smooth-to-highly-contorted and locally brecciated (Hoy *et al.* 1984).
2. Sulphide mineralization in the wall rocks is more abundant and extensive in the structural hanging wall. Sulphides occur in the form of disseminations and small lenses either stretched into foliation or occurring in fractures cross-cutting the schistosity.
3. The ore mineral assemblage consists of pyrrhotite, chalcopyrite, sphalerite, less commonly pyrite and locally galena. Subrounded inclusions of vein quartz and wall rock are abundant and commonly have a fine-grained, recrystallized sulphide matrix swirled around them. This feature, together with crude banding and gneissic and mylonitic textures attest to the extent of tectonic reworking and regional metamorphism of the ore body. Coarse-grained equigranular textures are preserved in the central parts of the deposit.
4. Metal concentrations are higher in the central, thicker part of the ore lens. The relative concentration of Pb and Zn (relative to Cu) increases to the east. Vertical zonation is not

apparent, but the horizontal zonation pattern may be due to shearing of an initially vertically zoned ore body (Hoy *et al.* 1984). The structural footwall contains more mineralization than the hanging wall, both in terms of thickness and grade. The hanging wall and footwall have a higher Zn/(Zn+Cu) ratio than the ore body. However, metal zoning is not sufficiently diagnostic by itself to support any interpretation of the direction of stratigraphic tops.

## **Lithogeochemistry**

### ***Sampling and analytical quality control***

This study utilized lithogeochemical data from 180 samples (Appendix 1), collected from outcrops and drillholes in the immediate and more distal vicinity of the ore body, as well as regional samples from lithologies correlated with the mine sequence (J. Logan, pers. comm.). The sampling was designed to characterize both background variability through distal and regional samples and the alteration halo of the ore body utilizing samples from within several tens of metres into the footwall and hanging wall of the deposit. Data from an additional 123 samples, provided by Jim Logan and Trygve Hoy, augment the data set. Use of this additional data was limited due to incomplete analytical compatibility with the main data set in terms of analytical errors, quality control and the suite of elements analyzed.

The samples from the main data set were analyzed for the major oxides (SiO<sub>2</sub>, TiO<sub>2</sub>, Al<sub>2</sub>O<sub>3</sub>, total iron as Fe<sub>2</sub>O<sub>3</sub><sup>T</sup>, MgO, MnO, CaO, Na<sub>2</sub>O, K<sub>2</sub>O and P<sub>2</sub>O<sub>5</sub>), a set of 6 trace elements (Ba, Rb, Sr, Y, Zr and Nb), H<sub>2</sub>O<sup>+</sup>, CO<sub>2</sub>, total S, FeO and T.O.C (total organic carbon). The analytical work was completed by Chemex Labs Ltd. in Vancouver. Major oxides and trace elements were determined by X-ray fluorescence. Fused Li-tetraborate discs were used for the major oxides and pressed pellets for the trace elements. More information about the sampling and analytical procedures employed is available in Appendix 1.

Analytical quality control was exercised according to the procedure developed for the Lithogeochemical Exploration Research Project of MDRU (Sinclair and Stanley, 1995; Stanley, 1997a). The relative errors of the analyses are estimated based on data from seven

quadruplicate analysis of reference materials (internal MDRU standards) submitted together with the lithogeochemical samples. The analytical errors were calculated and graphed using the THPLOT Matlab program (Stanley, 1997b) to obtain relative and absolute error terms and effective detection limits for each element analyzed (Appendix 2, Table A2.1, Figs. A2.1 through A2.11). Precision of the analyses is quoted as the departure (one standard deviation) from the accepted values of the internal MDRU standards (Stanley, 1997a; Appendix 2, Table A2.2). Recognizing that MDRU reference materials were prepared for analysis (crushed, pulverized and homogenized) separately from the samples, an additional study of 20 pulp duplicates from the Goldstream samples was used to characterize possible errors introduced at this stage of the analytical procedure. The analytical errors calculated for the pulp duplicates (Appendix 2, Table A2.3) are similar to that of the MDRU reference materials.

Analytical data acquired from T. Hoy and J. Logan was obtained either by X-ray fluorescence analysis, or by other analytical methods (wet chemistry with atomic absorption finish or ICP with atomic emission spectrometry). Most of these samples were not analyzed for  $\text{H}_2\text{O}^+$ ,  $\text{CO}_2$ , total S, FeO and T.O.C., which limited their usefulness in the lithogeochemical investigation. No information is available on the analytical quality of these donated data.

### ***Background compositional variability and controlling factors***

In order to understand and characterize the signature of metasomatic processes superimposed on the rocks, it is essential first to consider primary variability governed by sedimentary and diagenetic processes. The contribution of regional metamorphism to local geochemical variability is ignored because (1) it is considered to be largely an isochemical process and (2) it is a large scale process, unlikely to produce variations on a small scale comparable to that of ore-related hydrothermal alteration. The Goldstream ore body is hosted by metapelitic and calcareous rocks, originally deposited in a pericratonic basin along with minor mafic volcanic rocks and local exhalative sediments related to hydrothermal activity (Hoy, 1979). The original sediment, by analogy with turbidites elsewhere, most

likely contained quartz and feldspar as coarser clastic grains and various clay minerals, such as illite, montmorillonite, chlorite, kaolinite and mixed-layer clays, depending on climatic and physiographic conditions of source areas (Chamley, 1989; Greensmith, 1989; Stanley, 1997b). Hydraulic sorting processes during sediment transport and deposition cause variations in the proportions of clastic grains and clay minerals that are related to the position of the sample within the turbidite bed (Walker, 1992). The turbidite bed bottoms are, thus, coarse-grained and quartz-rich, whereas the turbidite bed tops are fine-grained and clay-rich. The argillaceous protolith of the phyllites hosting the massive sulphide mineralization at Goldstream was also enriched in calcite and other carbonate minerals by sedimentary and diagenetic processes (Hesse, 1986). Formation of pyrite and preservation of organic matter were favoured by anoxic conditions on, or just below, the seafloor. Seafloor alteration of the basaltic rocks produces clay minerals, calcite and zeolites and Fe hydroxides (Valsami *et al.* 1994; Staudigel *et al.* 1996). The latter coprecipitate with silica, barite, anhydrite, carbonate and sulphide minerals as a result of high temperature seafloor hydrothermal exhalation (Bonatti, 1981; Thompson, 1983). The occurrence and varying proportions of the above minerals likely produced the premetasomatic chemical variability in the sampled rocks. Hydrothermal alteration, diagenetic transformation and metamorphism further modified the rocks to produce the presently observed chemical compositions and variations.

Samples from the vicinity of the Goldstream deposit are classified in five main groups, based on visual distinctions and the HCl test for calcite: (1) Dark Grey Banded Phyllite, (2) Grey Green Phyllite, (3) Marble, (4) Garnet zone and (5) Volcanic rocks. Although the rocks can be subdivided into distinct visual classes, chemical classification is less clear. Chemically, the samples, with the exception of those representing volcanic rocks, can be viewed as a continuum involving several end-member components (Fig. 2.6). In terms of chemistry it is practical to restrict the components to four major-element oxides or combinations of these. Clay minerals, making up a significant proportion of the primary sedimentary assemblage and thus strongly influencing the geochemical variability, can be represented by means of the components  $\text{SiO}_2$ ,  $\text{Al}_2\text{O}_3$  and  $\text{Fe}_{(\text{total})} + \text{MgO} + \text{MnO} + \text{Na}_2\text{O} + \text{K}_2\text{O}$  (Fig. 2.6). Phyllosilicates

prevailing in sediments, such as montmorillonite, illite, kaolinite (Chamley, 1989), contain little calcium. Other important minerals such as quartz and iron sulphides (mainly pyrrhotite) and oxides (hematite, goethite) are also represented in this system. The metapelites (DGBP and GGP) and marbles cannot be distinguished chemically in this system. Differences between them, leading to their classification as separate groups are due to calcite and carbonaceous matter contents. Neither of these is reflected on Fig. 2.6. Similarities, however, are much more pronounced. Most of the pelitic and calcareous rocks, classified as DGBP, GGP and marbles have chemical compositions interpretable as a mixture of quartz and one or more clay minerals. The pelitic component is prevalent in the majority of the samples. Relatively few samples can be classified as wackes and only 6 – as arenites (Fig. 2.6).

The approximate molar ratio of components making up the clay mineral (or minerals) is:



This bulk composition is closest to montmorillonite with a formula

$(\text{Na},\text{Ca})_{2/3}(\text{Mg},\text{Fe})_{2/3}\text{Al}_3\text{Si}_8\text{O}_{20}(\text{OH})_4$ . Other minerals that likely comprise the actual assemblage are chlorite and illite.

Five samples of volcanic rocks have similar compositions with approximately 45-50%  $\text{SiO}_2$  and 14%  $\text{Al}_2\text{O}_3$  (black triangles on Fig. 2.6). A group of pelitic and intensely calcareous samples (dashed triangle on Fig. 2.6) have major-element compositions intermediate between the volcanic rocks and the main group of pelitic and calcareous rocks. These rocks occur in two distinct localities in the east and the west portions of the study area and in both places are spatially associated with sulphide mineralization. They are interpreted to be metasomatized host rocks, based on evidence presented and discussed in the next two sections.

A large number (55) of GZ samples were collected to characterize this distinctive unit of the local stratigraphy. On Fig. 2.6, they are represented as a linear trend (open squares) between two end-member compositions:

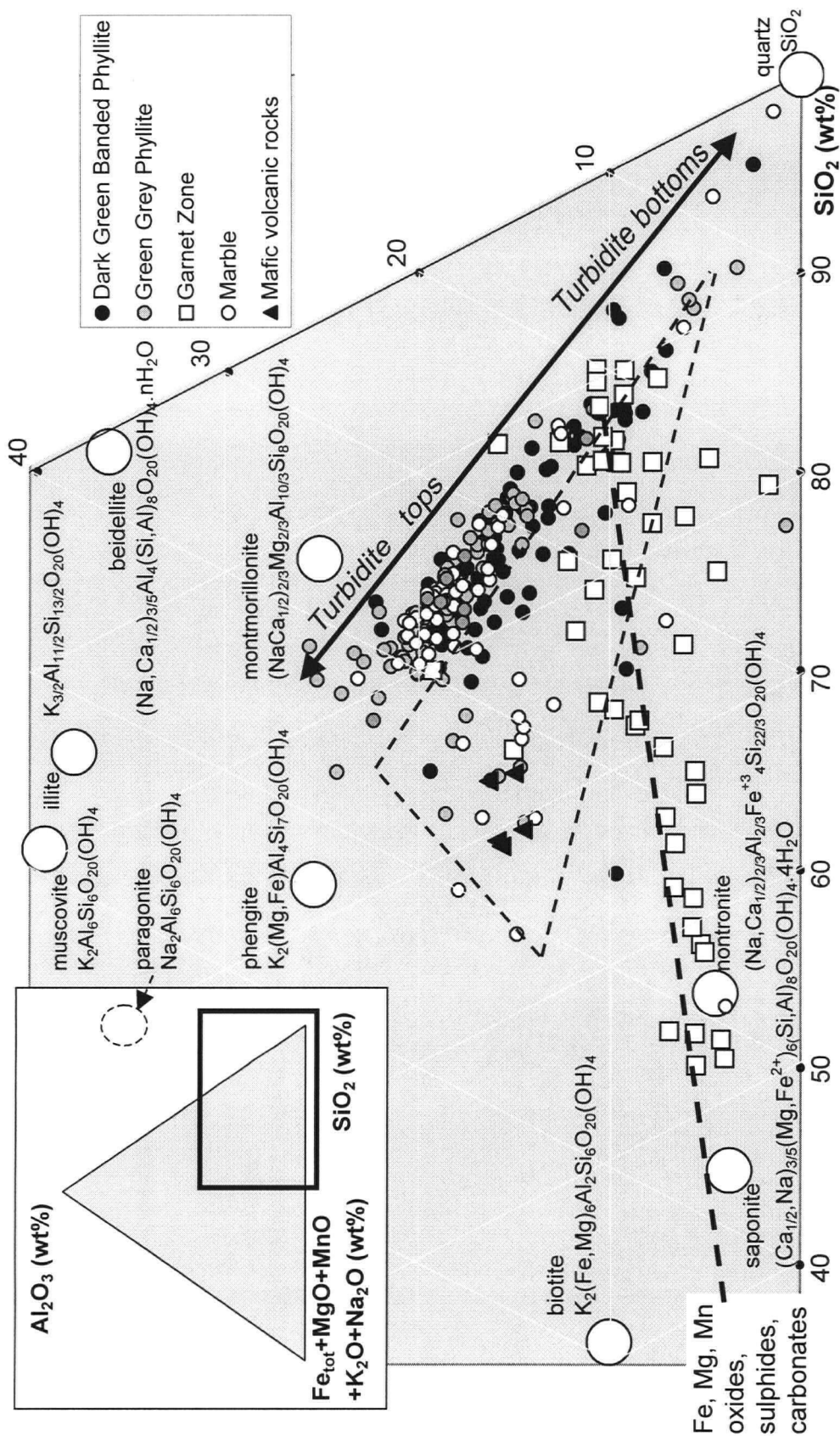


Fig. 2.6. Ternary diagram showing the major chemical components in all 303 samples from the area of the Goldstream massive-sulphide deposit in reference to selected mineral compositions (large circles).

1. Pelitic rocks from the silica-rich part of the spectrum. The garnet zone is considered a ferruginous exhalite horizon (Hoy *et al.* 1984; Logan and Colpron, 1995). Amorphous silica, precipitated biogenically or chemically is an essential component in exhalites (*e.g.*, Haymon and Kastner, 1981; Kuroda, 1983). Thus, it is argued that the prevalence of silica in the garnet zone is not explained by fractionation of coarser clastic quartz from turbidite flows, but rather by precipitation from silica-bearing seafloor hydrothermal exhalites.
2. Iron and manganese oxides, carbonates and/or iron sulphides of hydrothermal origin. Thus, the garnet zone is interpreted as a typical siliceous and ferruginous precipitate of hydrothermal origin ("coticule" horizon, Kramm, 1976), variously diluted with turbidite sediment.

A fourth major component, CaO, represents the mineral calcite, which is common in virtually all rock types near the deposit. According to Fig. 2.7, most of the samples classified as marbles are actually calcareous pelites. Most of the samples represent pelites with less than 15% CaO. The DGBP are more calcareous than the GGP. On this plot, montmorillonite stands out as the most likely clay mineral comprising the rock, possibly along with illite and phengite. Calcium carbonate is ubiquitous in the GZ and even more so in the intensively metasomatized rocks. Alternative explanations could be (1) contamination by mafic or intermediate volcanic material (*i.e.*, incorporation of pyroxene-containing debris in the sediment) and (2) ferromagnesian metasomatism. Both of these explanations are consistent with the overall chemical similarity and spatial association of these samples with metavolcanic rocks.

Based on the conclusion that background geochemical variability in DGBP, GGP and marbles (M) represents a continuum and that the pelitic component is prevalent, the lithologies are further studied as a single group of rocks, best described by the term "calcareous metapelites" or more generally "metapelites". Visual distinctions within this group, and hence field classifications, are not chemically significant. Reclassification of the samples taking into account chemical criteria is necessary for the further study of compositional variability within the metapelites.



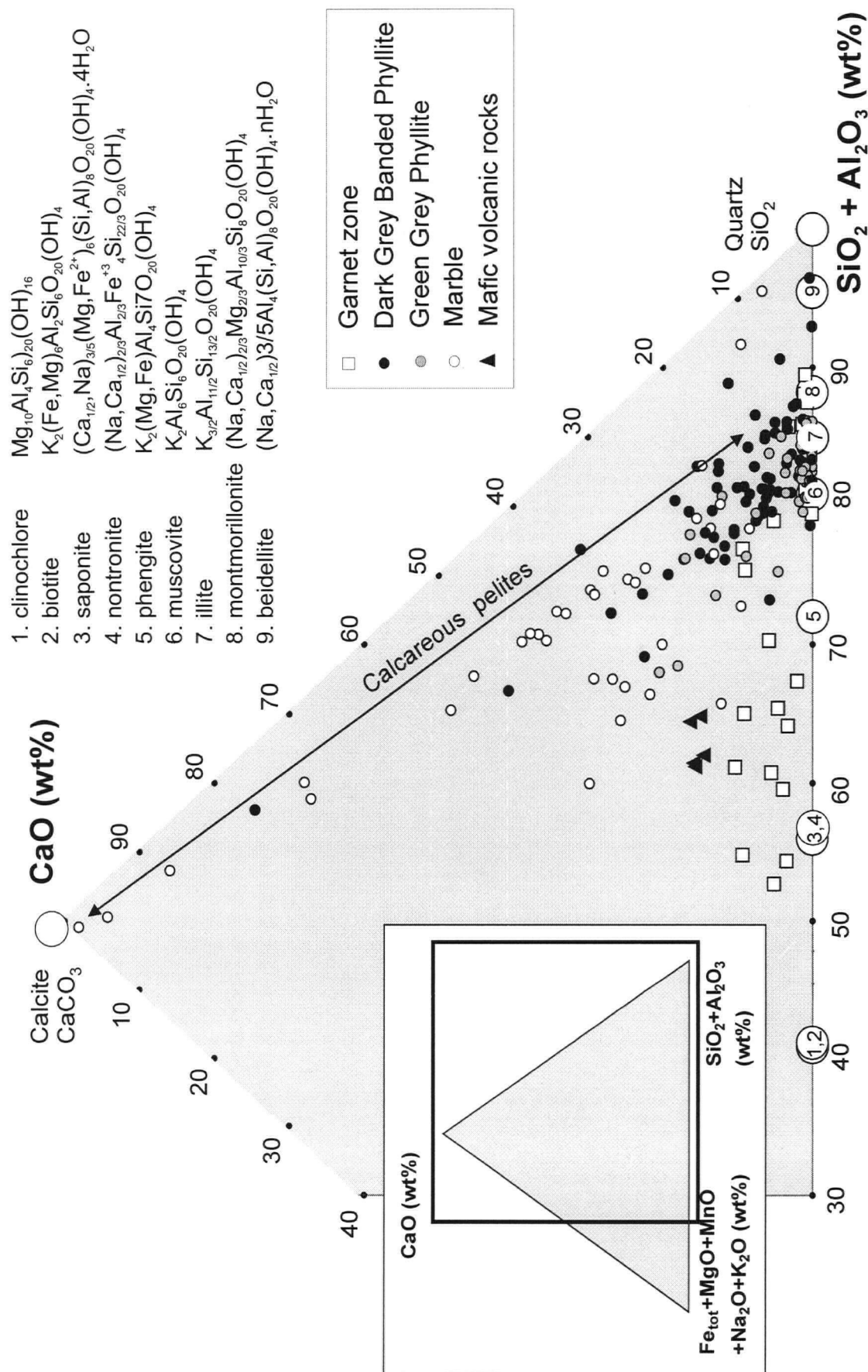


Fig. 2.7. Ternary diagram showing the major chemical components in all 303 samples from the area of the Goldstream massive sulphide deposit in reference to selected

mineral compositions (large circles). Carbonate as calcite is ubiquitous in the Goldstream pelitic rocks, adding another dimension to the background variability (Fig. 2.6).

### ***Conserved elements***

Elements or oxide components that do not participate in material transfer processes (magmatic or sedimentary fractionation, metasomatism *etc.*) affecting the system are defined as ***conserved*** (Stanley and Russell, 1989). Their concentrations are used as denominators in Pearce Element Ratios (Pearce, 1968). Thus, conserved element identification is a step toward justifying the application of PER analysis of the lithogeochemical data. Strictly speaking, the conserved character of components cannot be proven. A procedure is available, however, that can rigorously prove that the components involved are ***not conserved***. In this study an element or oxide component is considered conserved if the test (discussed below) fails to prove the contrary (Stanley and Russell, 1989).

A set of potentially conserved elements or oxide components, involving  $\text{TiO}_2$ , Zr, Nb and Y, are tested using binary scatterplots (Figs. 2.8 through 2.11). If both elements involved in the test are conserved, the data should plot on a single line that passes through the origin (Russell and Stanley, 1990). If a linear trend exists, but has a non-zero intercept, the element on the axis not intercepted is likely to be more conserved (Stanley and Madeisky, 1993). Here data points are considered following a linear trend if they are within two standard deviations of analytical errors (Appendix 2) from the trend line. Binary plots of some of the same elements against silica (Fig. 2.10a, b, c) were found to be useful in the process of reclassification of the metapelitic samples into groups with distinct chemistry, reflecting their origin.

### **Conserved element test results**

In the few available samples of mafic metavolcanic rocks (Figs. 2.8 and 2.11) all the tested incompatible (in igneous fractionation) elements, Zr, Ti, Nb and Y behave as conserved. This suggests that the volcanic rocks belong to one homogenous suite and that their chemistries have not undergone any extreme post-magmatic changes. Their silica concentrations (Fig. 2.10a, b) vary between 45 and 50%, which is compatible with a basaltic precursor.

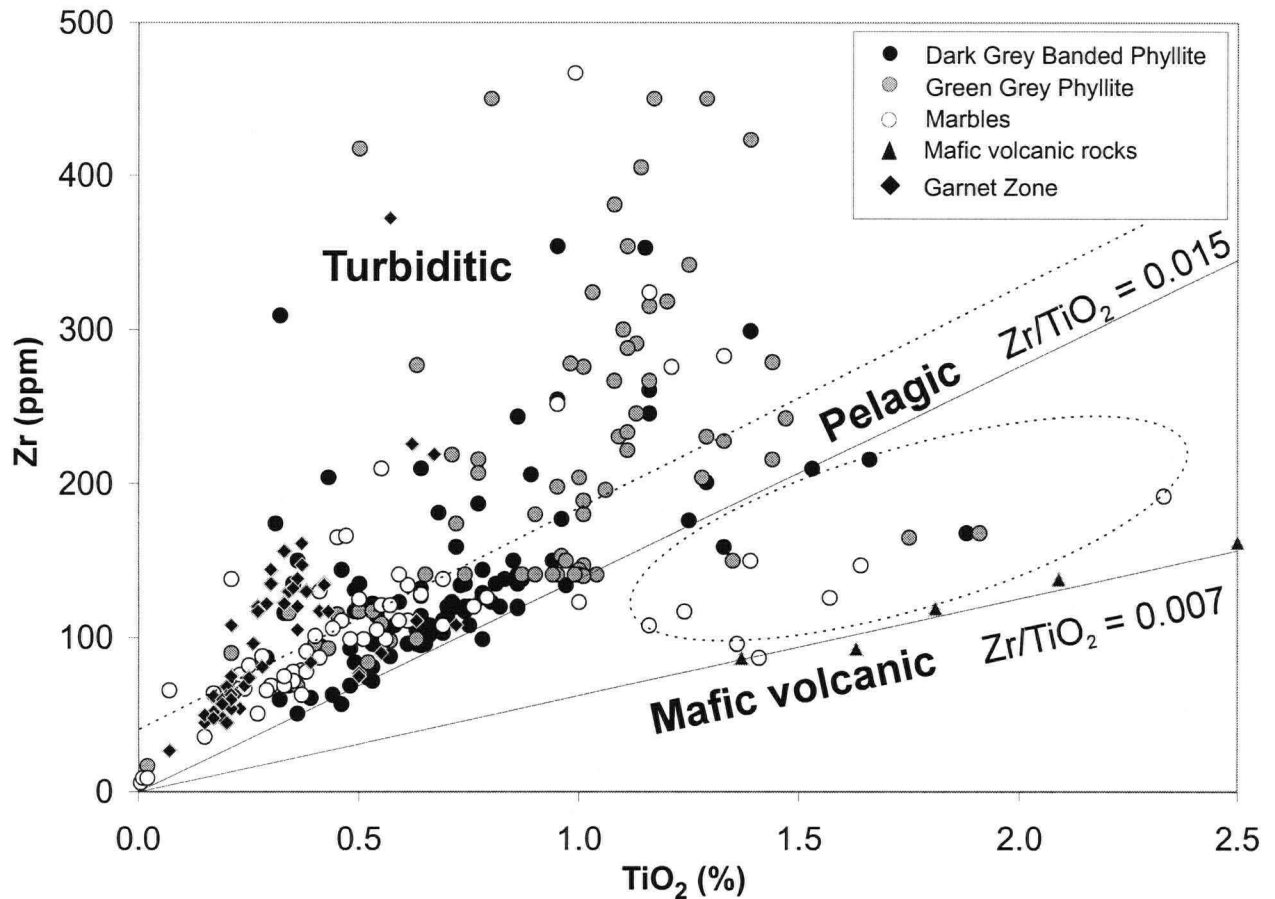


Fig. 2.8.  $\text{TiO}_2$  vs. Zr (potentially conserved elements) plot utilizing data for all 303 lithogeochemical samples from the Goldstream massive sulphide deposit area. Two standard deviations of measurement error is smaller than, or equal to symbol size. Zr and  $\text{TiO}_2$  are conserved in the volcanic rocks and in some metapelite rocks, yielding linear trends (solid lines), passing through the origin. A group of metapelite rocks deviate from the linear trend significantly and are separated from the first group by a dashed line.

The behavior of Zr,  $\text{TiO}_2$ , Nb and Y in the metapelite samples, however, is more complicated. This is due to the superimposition of several sedimentary and locally, post-depositional processes in which the tested elements participated in different ways. A large group of metapelites, mostly DGBP and Marbles, display relatively constant  $\text{TiO}_2/\text{Zr}$  and Nb/Zr ratios (Figs. 2.8 and 2.9), suggesting a common process of sedimentary fractionation. A significant number of samples, however, most of them GGP, have distinctly higher concentrations of Zr, while another group of samples show elevated  $\text{TiO}_2$  and Nb concentrations.

The binary diagrams of potentially conserved elements (Zr, TiO<sub>2</sub>, Nb) vs. SiO<sub>2</sub> (Fig. 2.10a, b, c) reveal two crude linear trends. The first trend is characterized by low ratios (shallow slopes on Fig. 2.10a, b, c) of Zr, TiO<sub>2</sub> and Nb to SiO<sub>2</sub>. The samples defining the trend are the same ones that display relatively constant Ti/Zr and Nb/Zr ratios (Figs. 2.8 and 2.9). The trend passes through the origin, justifying the conclusion that SiO<sub>2</sub> and Zr are conserved in this group of samples.

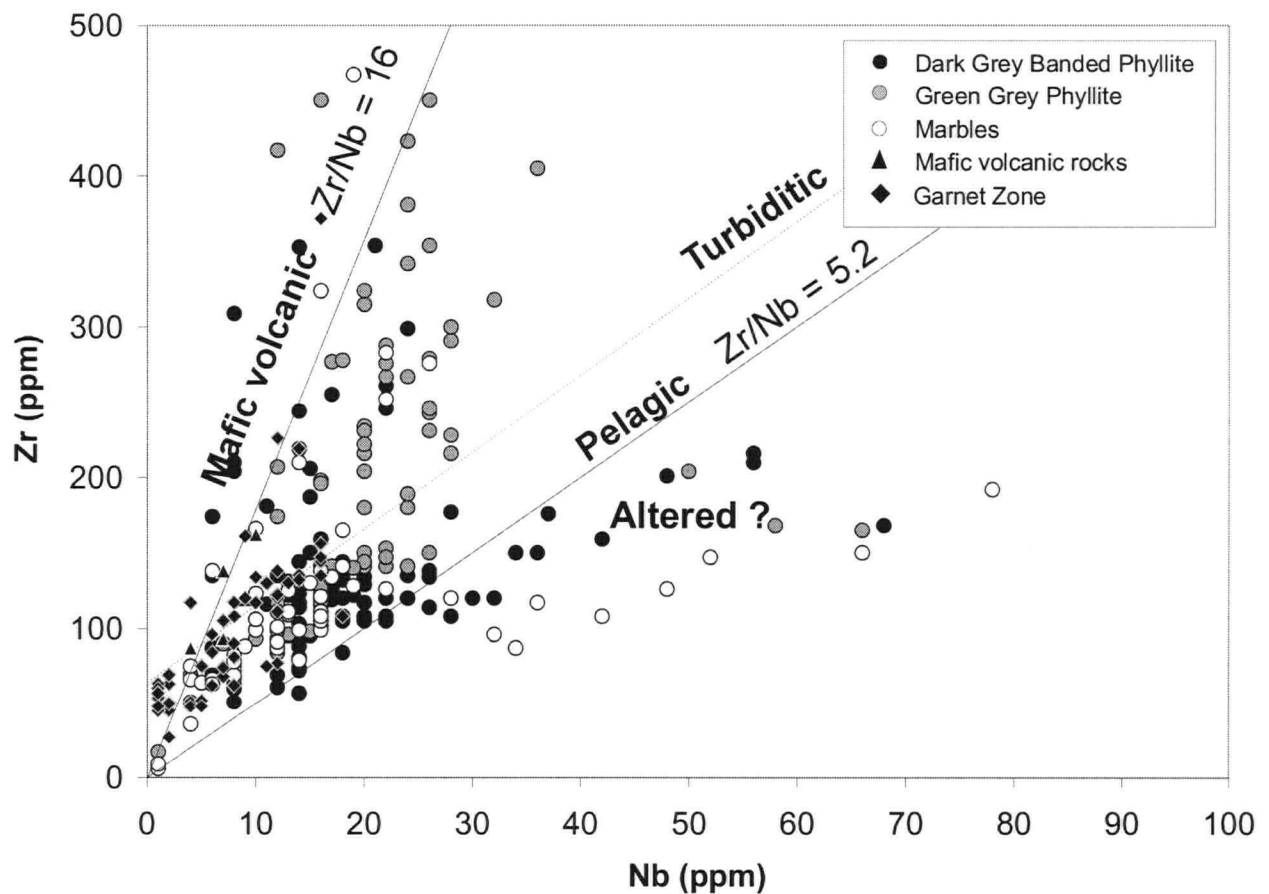


Fig. 2.9. Nb vs. Zr (potentially conserved elements) plot, utilizing data for all 303 lithogeochemical samples from the Goldstream massive sulphide deposit area. Two standard deviations of measurement error is smaller than, or equal to symbol size. Nb and Zr are conserved in the volcanic rocks and in the pelagic metapelites (solid lines). Turbiditic rocks deviate from the trend significantly and are separated on this plot from the pelagic metapelites by a dashed line.

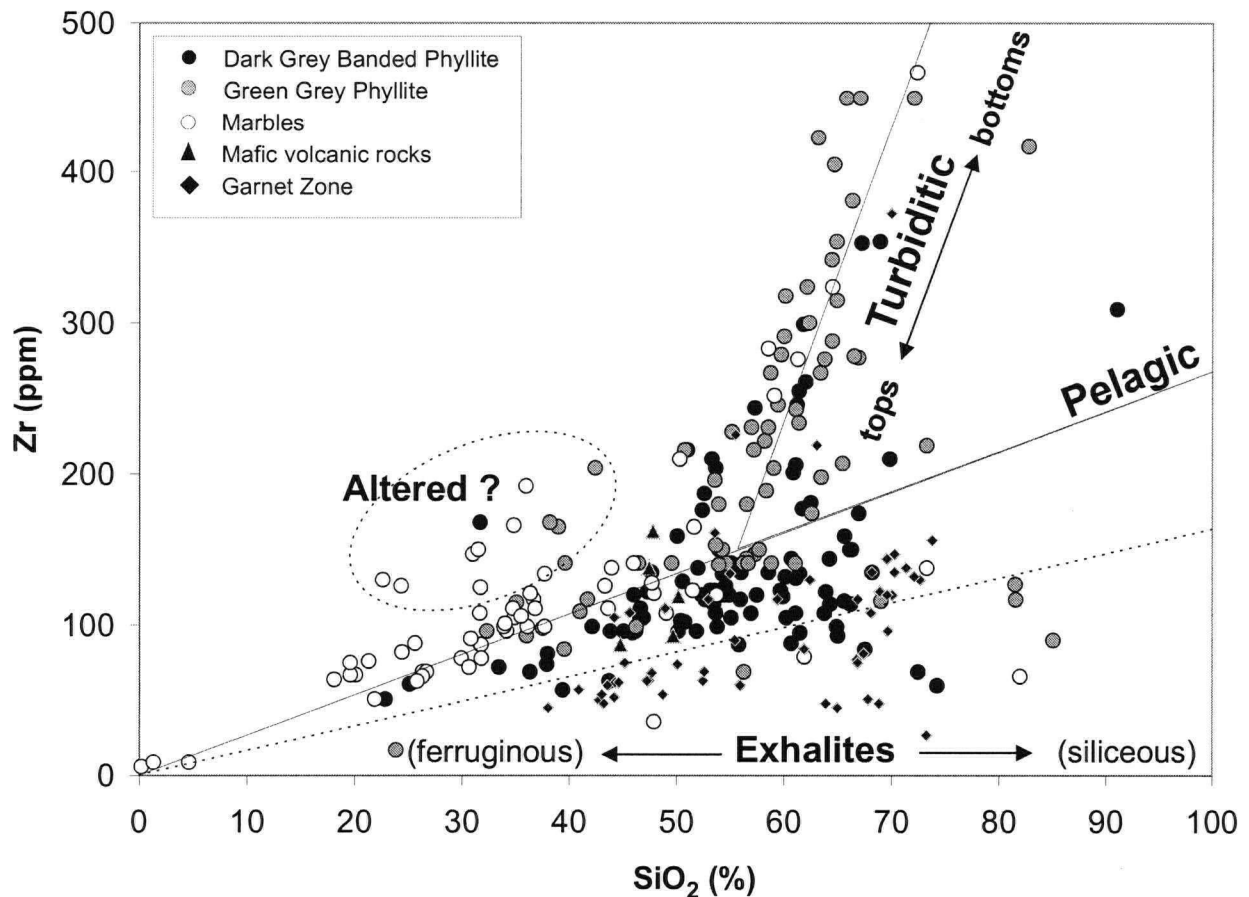


Fig. 2.10a.  $\text{SiO}_2$  vs. Zr plot utilizing data for all 303 lithogeochemical samples from the Goldstream massive sulphide deposit area. Two standard deviations of measurement error is smaller than, or equal to symbol size. Silica and zirconium are conserved in some metapelitic rocks, defining a trend passing through the origin of the plot. Three groups of samples deviate from this main trend (shallow-slope solid line).

1. A group of metapelitic rocks define a separate, steeper trend;
2. Some data (separated by a dashed line) plot below the main trend;
3. A few samples display high Ti concentrations.

The second trend is characterized by a steeper slope. It is best developed in the Zr vs.  $\text{SiO}_2$  plot (Fig. 2.10a), less so in the  $\text{TiO}_2$  vs.  $\text{SiO}_2$  plot (Fig. 2.10b) and almost non-existent in the Nb vs.  $\text{SiO}_2$  plot (Fig. 2.10c). The samples defining the trend are those previously identified to have excess Zr (Fig. 2.8, 2.9). In both trends silica is positively correlated with Zr, Ti and Nb (Fig. 2.10a, b, c). The two groups of samples constituting the trends also define distinct slopes on the Ti vs. Nb binary diagram (Fig. 2.11).

A group of samples, including the GZ samples, plot below the first trend (Fig. 2.10 a,b,c). Their silica concentrations vary but, in some samples, are as high as 90%. On the binary plots not involving silica (Figs. 2.8, 2.9 and 2.11) this group of samples behaves similarly to the pelites. Another, smaller group of samples (Figs. 2.8, 2.9), display elevated concentrations of  $\text{TiO}_2$  and Nb and low to moderate Zr concentrations. On the plots involving silica (Fig. 2.10a, b, c) these samples plot distinctly from the previously described trends.

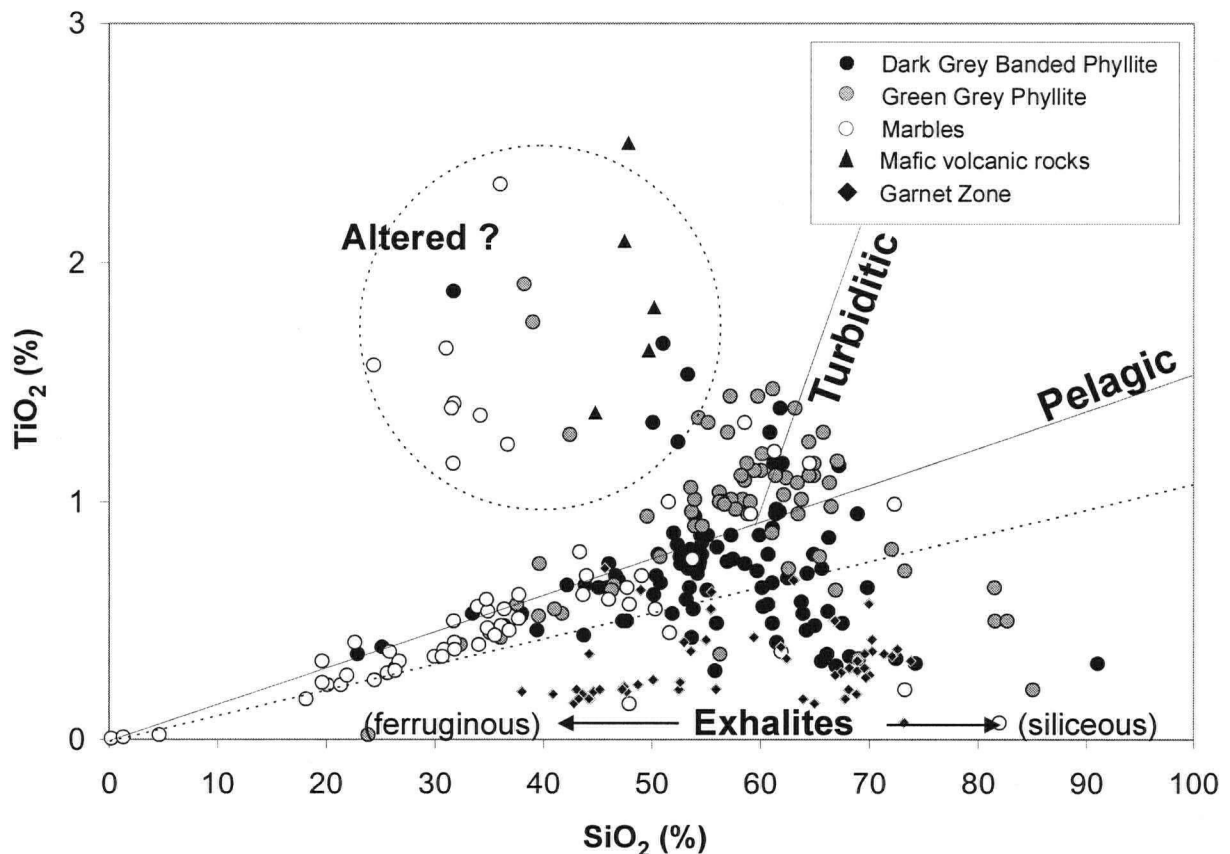


Fig. 2.10b.  $\text{SiO}_2$  vs.  $\text{TiO}_2$  plot utilizing data for all 303 lithogeochemical samples from the Goldstream massive sulphide deposit area. Two standard deviations of measurement error is smaller than, or equal to symbol size. Silica and titanium are conserved in most of the metapelites, defining a linear trend. Three groups of samples deviate from this main trend (shallow-slope solid line).

1. A group of metapelitic rocks define a separate, steeper trend, similar, but less pronounced than the one in the silica vs. Zr plot (Fig. 2.10a);
2. Some data (separated by a dashed line) plot below the main trend;
3. A few samples display high Ti concentrations.

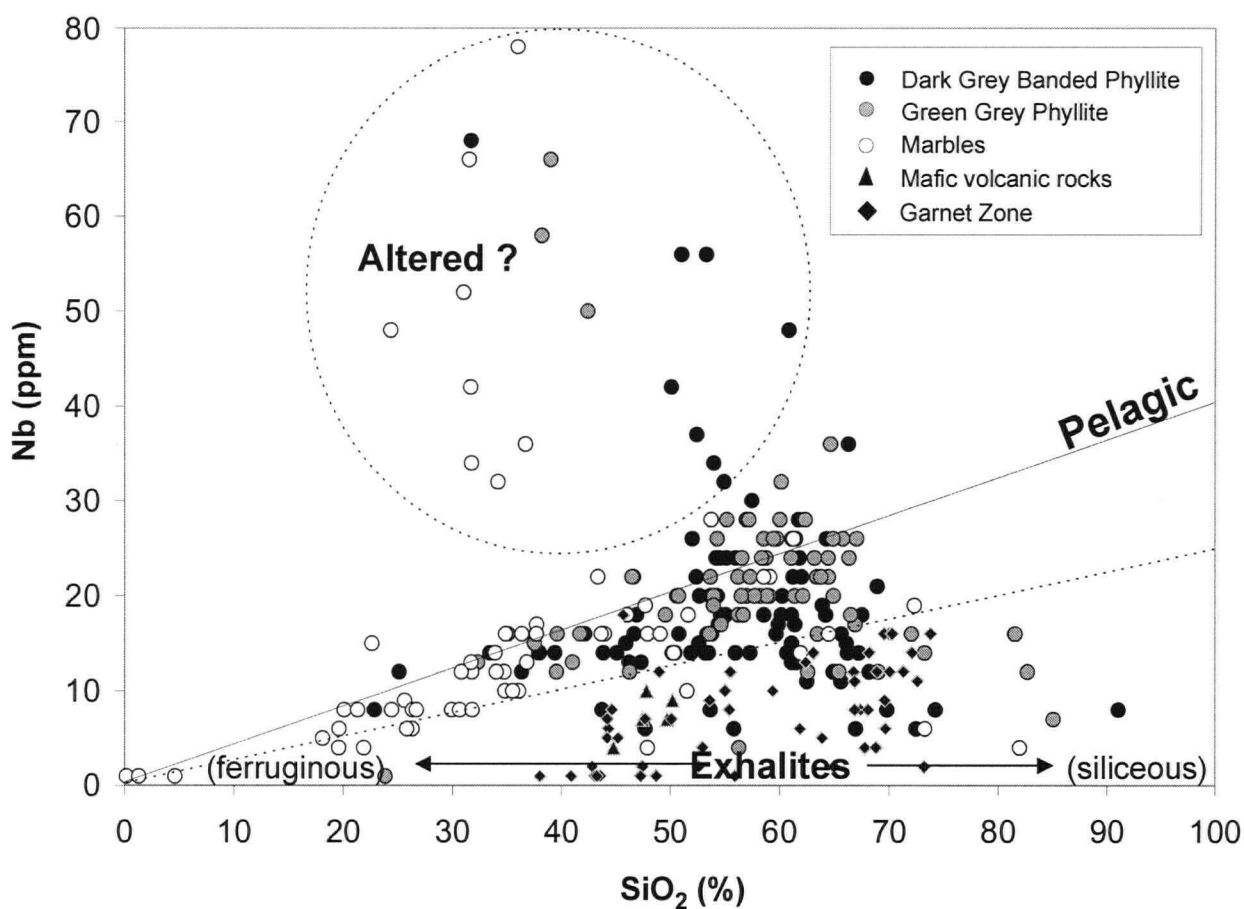


Fig. 2.10c. SiO<sub>2</sub> vs. Nb plot, utilizing data for all 303 lithogeochemical samples from the Goldstream massive sulphide deposit area. Silica and niobium are conserved in the in most metapelites, defining a linear trend. Two groups of samples deviate from this main trend (solid line).

1. Some data (separated by a dashed line) plot below the main trend;
2. A few samples display high Ti concentrations.

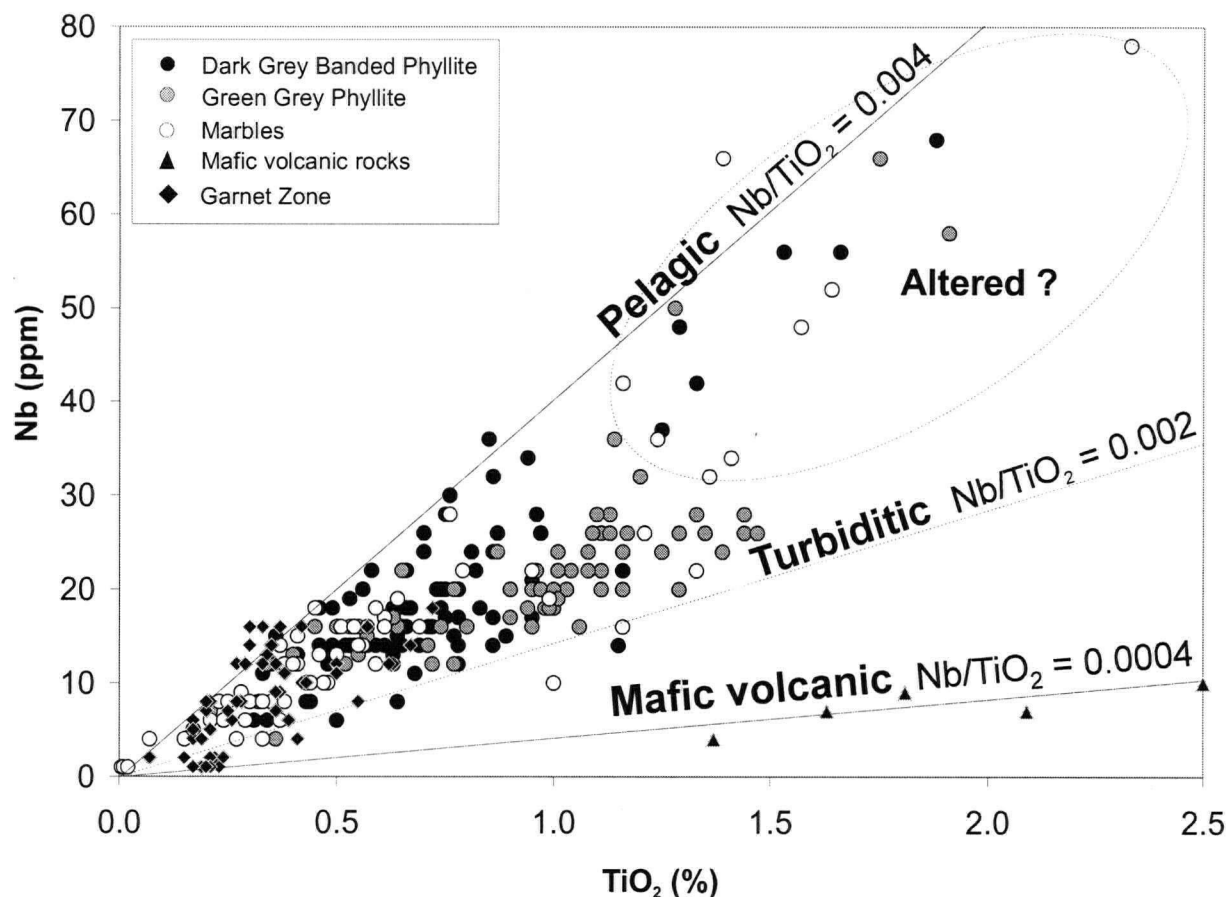


Fig. 2.11. TiO<sub>2</sub> vs. Nb (potentially conserved elements) plot utilizing data for all 303 lithogeochemical samples from the Goldstream massive sulphide deposit area. Two standard deviations of measurement error is smaller than, or equal to symbol size. TiO<sub>2</sub> and Nb are conserved in the volcanic rocks and in both the pelagic and turbiditic metapelites, defining linear trends (solid lines). However, the populations belonging to the two groups of pelitic rocks overlap on this plot and are hard to separate (dashed line). Rocks having unusually high Ti and Nb concentrations occur in two spatially restricted locations and are tentatively interpreted as altered.



### **Interpretations and conclusions following from the conserved element test**

The conserved element test helps identify four groups of samples in the data set having distinct chemical signatures. The distinctions are the result of the following mass transfer processes responsible for the observed rock chemistries:

1. ***Pelagic sedimentation*** in the pericratonic basin operated during times of a low energy hydrodynamic environment. The sediments represent a mixture of two end-member compositions: carbonate, which plots at the origin (Figs. 2.8 through 2.11) and clay minerals. Zr, TiO<sub>2</sub> and Nb are contained exclusively in the clay fraction and thus are positively correlated with it. Silica also is positively correlated with the clay fraction, reaching maximum concentrations of 55 to 60 wt.%, consistent with the composition of the montmorillonite-like clay mineral, empirically defined in the previous section. Linear trends passing through the origin of the plots (Figs. 2.8 through 2.11) suggest a conserved character for Zr, Ti, Nb and Si in this group, as well as their immobility in subsequent processes. Prevalence of dark coloured rocks (DGBP) in this group of samples is explained by the common enrichment of pelagic sediments in organic matter and CaO (Greensmith, 1989). Metapelites bearing the premetamorphic geochemical signature of pelagic sedimentation are further referred to as "pelagic metapelites".

2. ***Turbiditic deposition*** periodically interrupted pelagic sedimentation. Clastic material enriched in quartz, feldspar and heavy minerals was incorporated in the turbiditic flow bottoms. The enrichment in zirconium (Fig. 2.10a) was much more pronounced than that of titanium, niobium (Fig. 2.10b, c) and yttrium (not shown). This fact is attributable to the relative resistance of the corresponding heavy minerals (*e.g.*, titanite, rutile, ilmenite, monazite, columbite, tantalite) to weathering and abrasion during transport. Turbidite tops, containing exclusively clay minerals, are chemically indistinguishable from the clay-rich pelagic metasediments. GGP rocks prevail in this group, which reflects the initial enrichment in coarser quartz-feldspar component and relatively low concentration of carbonaceous matter ultimately resulting in paler colour. Metapelites exhibiting

premetamorphic geochemical features attributable to turbiditic sedimentation are further referred to as “turbiditic metapelites”.

3. *Seafloor hydrothermal activity* is reflected by those samples plotting below the pelagic trend (Fig. 2.10a,b,c) and having  $\text{SiO}_2/\text{Zr}$  ratios higher than approximately  $0.5 \times 10^4$  (or higher than 1/2, if  $\text{SiO}_2$  is measured in % and Zr is measured in ppm). Silica enrichment of these rocks is interpreted to have resulted from silica-rich exhalations (e.g., Tivey and Singh, 1997) in modern active seafloor hydrothermal-vent areas. Siliceous exhalites are least diluted in time intervals of reduced clastic sedimentation and thus have low Zr concentrations. The rocks belonging to this category were formed by a combination of pelagic and hydrothermal sources. Consequently, they plot along a series of mixing lines extending from the pelagic trend to the high end of the abscissa, where pure silica plots (Fig. 2.10a,b,c). The ferruginous hydrothermal component present in the typical GZ samples complicates the pattern by displacing data points toward the origin. Based on this discussion, the ratio of Si/Zr can be used as a simple geochemical parameter reflecting hydrothermal silica addition in pelagic sedimentary rocks.

4. A sub-group of samples is distinguished by higher  $\text{TiO}_2$ , Nb, (Figs. 2.8, 2.9, 2.10b, 2.10c and 2.11) and P (not shown) concentrations than both groups of metapelites. Ti/Nb ratios and Zr and silica concentrations are not significantly different than those of the pelagic metapelites (Figs. 2.8 through 2.11). Carbonate concentration in these rocks is up to twice that of typical Goldstream metapelites. The rocks occur in two distinct areas, both in proximity to sulphide mineralization. As described, the Zr and Nb concentrations of the rocks are not consistent with their interpretation as volcanoclastic material, due to higher Nb and Zr concentrations than occur in the local volcanic rocks. A possible explanation for the unusual concentrations of these elements could be alteration of extreme intensity, which involved, among other elements, the usually immobile Ti and Nb.

Pelagic and turbiditic metapelites are recognized in the data set as the most abundant rock type. Because neither of the two processes of deposition operated completely in isolation

from the other, there is a significant overlap between the two groups on all plots (Figs. 2.8 through 2.11) resulting in poorly defined trend lines. For the purposes of the PER analysis the two groups are distinguished using the  $\text{TiO}_2$  vs. Zr plot (Fig. 2.8). Because the samples described as siliceous exhalites are not distinguished on this plot and because of their small number and similarity with the pelagic metapelites with respect to Zr,  $\text{TiO}_2$  and Nb concentrations they will be further considered together with this group. To avoid complications due to mixing between multiple end member compositions, the GZ rocks are excluded from the molar ratio analysis. The samples tentatively interpreted as metasomatically altered are studied further as a separate group. Thus, the samples are reclassified in three cogenetic groups for the needs of the molar ratio analysis: (1) pelagic metapelites, (2) turbiditic metapelites and (3) altered metapelites.

Zr and  $\text{SiO}_2$  are conserved in the pelagic metapelites, whereas this is not true for the group of turbiditic metapelites (Fig. 2.10a). Thus Zr and  $\text{SiO}_2$  are inappropriate for use as denominators in the PER analysis.  $\text{TiO}_2$  is marginally enriched in the turbiditic metapelites and Nb is not enriched. These behave as conserved within each of the groups of samples, as illustrated by the linear trends on the  $\text{TiO}_2$  vs. Nb plot (Fig. 2.11). Ultimately,  $\text{TiO}_2$  was chosen, in preference to niobium, for a PER denominator because of its smaller analytical error (Appendix 2).

### ***Molar Element Ratio analysis***

PER analysis and GER (Generalized Element Ratio, Stanley, 1996) analysis confirm and supplement the conclusions about main mineralogical controls, done using simple binary and ternary plotting of the sample compositions. The analyses are further used to characterize and eventually quantify alteration, visualized as departures from background trends. For PER analysis of the metapelitic rocks,  $\text{TiO}_2$  is used as the axes denominator for the following reasons:

1. Although  $\text{TiO}_2$  is not conserved in the metapelites as a whole, it is shown, together with Zr and Nb, to be sufficiently conserved within both the pelagic and turbiditic varieties of these rocks (Figs. 2.10b, 2.11) taken separately.

2.  $\text{TiO}_2$  analytical errors are smaller than those for Zr and Nb (Appendix 2).

No element was shown to be conserved for the altered metapelites. Thus, strictly speaking, they should not be subjected to PER analysis. However, they will appear on the PER plots together with the rest of the samples to aid qualitative conclusions. Calcite, which significantly influences sample compositions (Fig. 2.7), is not a subject of the molar ratio analysis and all plots discussed in this section implicitly (by its not being included in the axis coefficients) project from this mineral. Thus, any influence of carbonate mineralogy, direct or through the effect of closure, is avoided.

Silica control is evident on various molar element ratio plots (Figs. 2.12 and 2.13). GER and PER plots alone, although helpful in determining the original mineralogy of the rocks provide no clear evidence about the origin of the minerals. Part of the silica may be related to a hydrothermal system, either as stringer mineralization or as a paleo-seafloor exhalite. Another part originates through clastic deposition in the bottoms of turbidite beds. To avoid interference of clastic silica deposition, a group of essentially pelitic samples is considered in the evaluation of hydrothermal silica addition (Fig. 2.13). The group includes pelagic metapelites and tops of turbidite beds. The latter are distinguished by their lower Zr concentrations ( $\text{Zr} < 150$  ppm, Fig. 2.10a). The style of the addition (crosscutting stringer type or seafloor exhalation) is impossible to decipher from the chemical data for the samples. Notwithstanding, being hydrothermal in origin, silica addition can be used as an exploration vector. It is quantified by the parameter  $(\text{SiO}_2 - 12/5 * \text{Al}_2\text{O}_3) / \text{TiO}_2$ , corresponding to the residuals from the montmorillonite line (Fig. 2.13).

Clay minerals are another important control on the rock compositions. Conclusions about the clay mineralogy made in previous sections are confirmed by PER and GER analysis. Currently, the bulk of the silicate mineralogy is a mixture of quartz, muscovite and chlorite and, correspondingly, data points plot in the triangular area defined by the three phases (Fig. 2.12). According to the interpretation of the rocks as metapelites and turbidites the precursor mineralogy consisted mostly of quartz and one or more phyllosilicate phases.

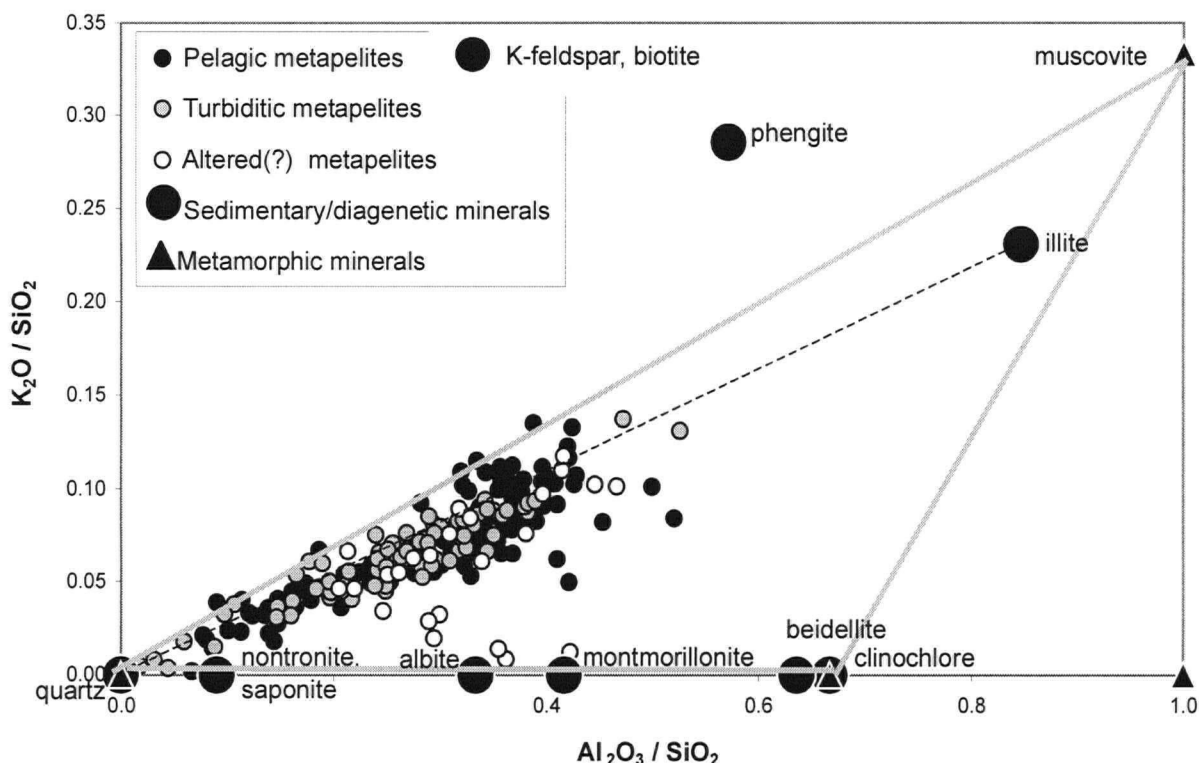


Fig. 2.12. A Generalized Element Ratio plot of 253 metapelitic and calcareous samples from the Goldstream massive sulphide deposit area (Garnet zone and volcanic samples are excluded from consideration), shown in reference to selected mineral compositions. Metapelites define a mixing line between quartz and a pelitic phase (dashed line). The line has a  $K_2O / Al_2O_3$  ratio of approximately 3/11, corresponding to illite and an  $Al_2O_3 / SiO_2$  ratio of approximately 5/12, corresponding to montmorillonite. A group of samples, mostly altered(?) metapelites, are strongly controlled by chlorite, gravitating to the mixing line between quartz and chlorite. All samples lie within a triangle defined by the minerals quartz, muscovite, and chlorite, which closely reflects the current mineralogy.

Unimodal patterns of data point clusters on molar element ratio graphs (Figs. 2.12 through 2.19) indicate that either the phyllosilicate phase was single or that multiple phyllosilicate phases were deposited in consistent ratios throughout the basin.

Conclusions about the characteristics of the phyllosilicate phase(s) drawn earlier in this text are confirmed and enhanced using molar element ratio diagrams. The plots show an  $Al_2O_3 / SiO_2$  ratio approximately equal to 14/32 (Figs. 2.12 and 2.13), which is consistent with montmorillonite, a clay mineral that is a common component of pelitic sediments. The

$K_2O/Al_2O_3$  ratio of 3/11 (Figs. 2.12, 2.14), however, suggests the clay mineralogy is dominated by illite. This apparent contradiction is explained by the diagenetic smectite-illite transition described by a number of authors (*e.g.*, Hower *et al.* 1976; Pearson and Small, 1988; Greensmith, 1989). In accordance with this concept, montmorillonite was the dominant mineral at the time of deposition. With burial it was diagenetically transformed into illite by incorporation of potassium from K-feldspar present mostly in bottoms of turbidite beds. During the process the system was closed with respect to alumina and silica (Hower *et al.* 1976) and thus an Al/Si ratio corresponding to montmorillonite was preserved.

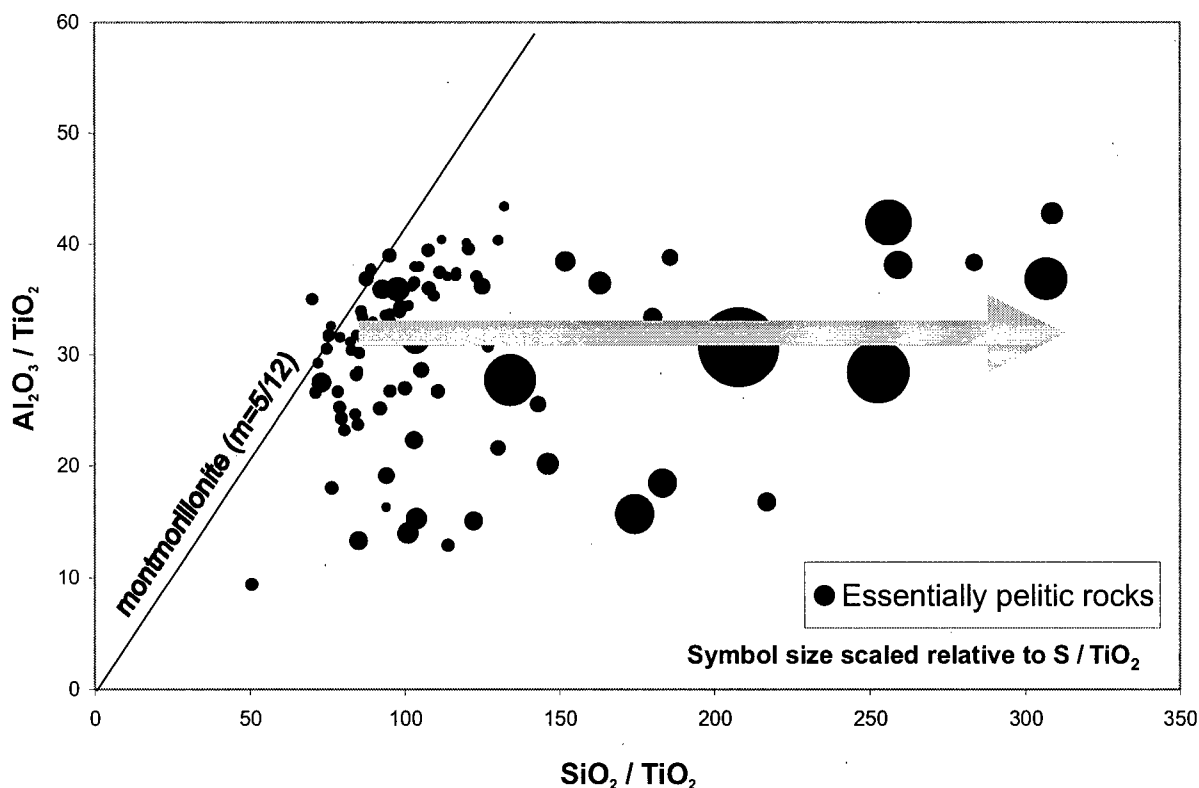


Fig. 2.13. Pearce Element Ratio plot of  $Al_2O_3$  vs.  $Na_2O$  with  $TiO_2$  as the conserved denominator component for 152 pelagic (turbidite tops, no elastic silica input) samples of Goldstream area rocks. Symbol size increases with increasing sulphur concentration. Arrow represents a data point-displacement vector corresponding to the effect of silica addition. The observed background ratio of  $Al_2O_3 / SiO_2$  is 5/12. The plot shows association between silica addition and elevated S concentrations. Silica addition is quantified by the parameter  $(SiO_2 - 12/5 * Al_2O_3) / TiO_2$ .

Alkali metals in the metapelites hosting the Goldstream deposit were concentrated originally in the clay fraction and in clastic feldspar grains, the latter being preferentially deposited in turbidite bottoms. After diagenesis, K was contained exclusively in illite. During regional metamorphism, illite was in turn transformed to muscovite, which is observed in the current mineralogy as the only K-bearing mineral. However, during this transformation the illite signature is preserved in the metapelites (Fig. 2.14) indicating that the system was closed to  $K_2O$  and  $Al_2O_3$ . The same controlling composition applies to the samples tentatively reclassified as altered, supporting their interpretation as initially cogenetic with the rest of the metapelites.

The decrease in K is evident as residuals from the illite line (Fig. 2.14) or from the ideal illite-quartz mixing line (Fig. 2.12), which is interpreted as a result of leaching. Because this metasomatic effect is not pervasive and because spatial association with the Goldstream pluton is not evident, K-loss is not considered a manifestation of regional or contact metamorphism. It influences many metapelite samples, but is best represented in the samples classified as both altered and spatially associated with sulphide mineralization. For this reason, loss of K is interpreted as a consequence of hydrothermal alteration related to ore formation. Alumina and silica, released during the destruction of illite, are reconstituted into new minerals forming *in situ*, such as quartz and chlorite (Figs. 2.12 and 2.19). Thus, the loss of potassium is expressed mineralogically in the rocks as chloritization and silicification. Slight loss of aluminum accompanying K loss is evident only in the group of altered samples (Fig. 2.14). Some scatter of data arises because of variations of the actual illite composition with respect to the ideal mineral stoichiometry.

A few samples have  $K_2O/Al_2O_3$  ratios higher than that of illite (3/11) and corresponding to muscovite (1/3). This can be explained by: (1) incomplete destruction of K-feldspar during diagenesis; and/or (2) addition of K during metamorphism or by hydrothermal fluids (sericitization). Lithogeochemistry alone cannot help discriminate between these hypotheses. The possibility that excess K is a result of hydrothermal sericitization will be

explored further in the next section by studying the spatial distribution of the affected samples.

The effect of K mobility can be quantified by the parameter  $(K_2O - 3/11 * Al_2O_3) / TiO_2$ , corresponding to the residuals from the illite line (Fig. 2.14). This parameter has a negative sign for K-loss (chloritization) and positive sign for K-addition (sericitization).

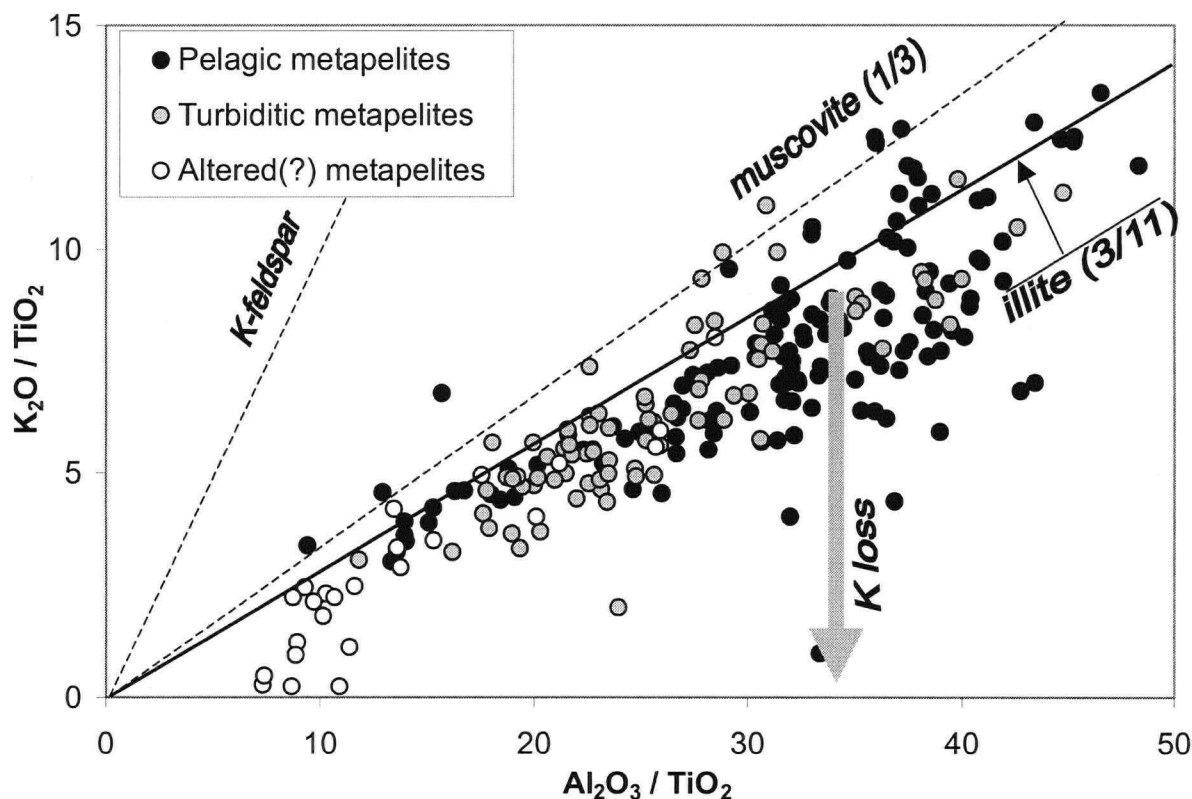


Fig. 2.14. Pearce Element Ratio plot of  $Al_2O_3$  vs.  $K_2O$  with  $TiO_2$  as the conserved denominator component for 243 metapelitic samples of Goldstream area rocks. Arrow represents a data point-displacement vector corresponding to the effect of K-loss. Current  $K_2O / Al_2O_3$  ratios of approximately 3/11 (solid line) are indicative of illite. Some samples display considerable loss of K. The samples most affected by this process are the ones classified as "altered(?) metapelites". Another group of samples display elevated K concentrations consistent with the mineral muscovite. K mobility is quantified by the parameter  $(K_2O - 3/11 * Al_2O_3) / TiO_2$ .



Mineralogical controls on Na (Fig. 2.15) are multiple, mutually interfering and difficult to distinguish. It is likely that albite, paragonite and montmorillonite were the minerals carrying this element into the original sediments, thus defining its background variability. Montmorillonite control is represented (Fig. 2.15a) as a crude linear trend with a slope of 1/11. Unlike K-feldspar, albite survives the diagenetic transformations (Hower *et al.* 1976) and its signature is superimposed on that of montmorillonite. Data points are displaced along a series of lines with a slope of unity, emanating from the montmorillonite trend. Because feldspar was deposited in the pelitic Goldstream sediment in limited amounts compared to clays, the signature of albite is subordinate to that of montmorillonite (Fig. 2.15a).

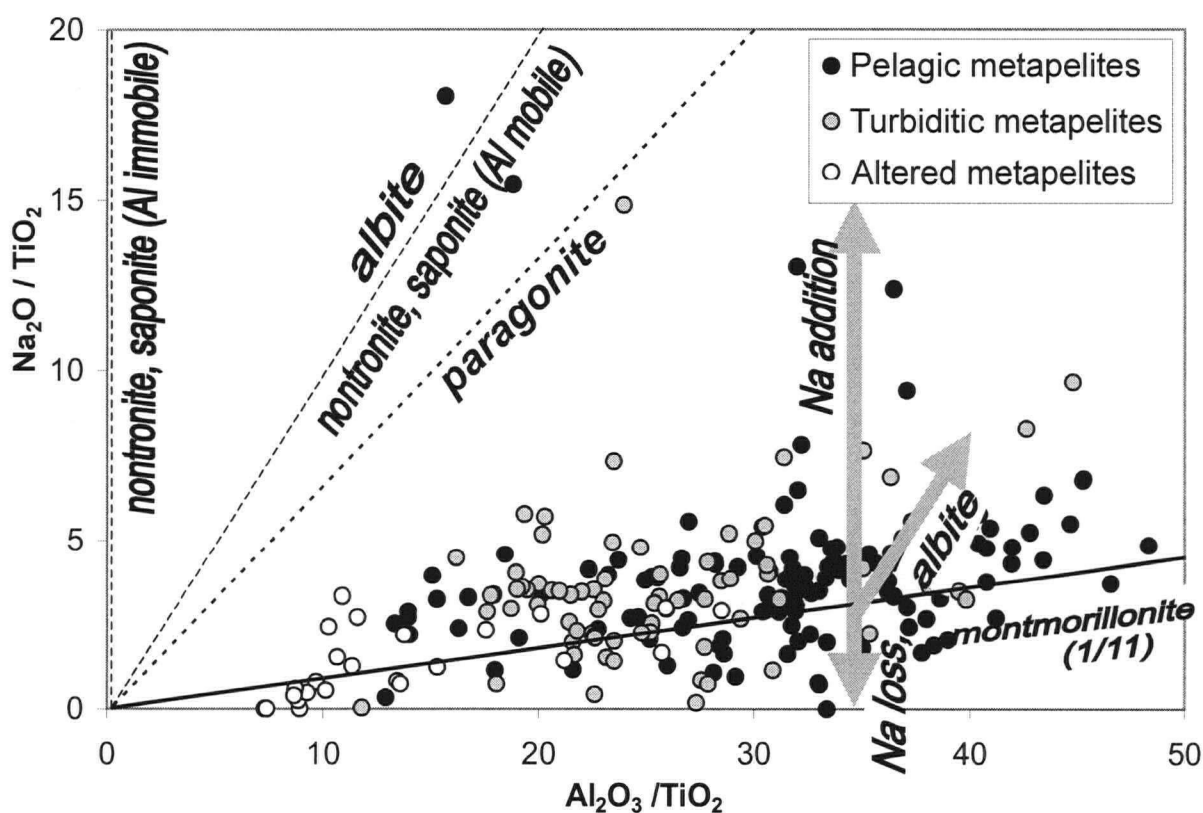


Fig. 2.15a. Pearce Element Ratio plot of  $\text{Al}_2\text{O}_3$  vs.  $\text{Na}_2\text{O}$  with  $\text{TiO}_2$  as the conserved denominator component for 243 metapelite samples of Goldstream area rocks. Arrows represent data point-displacement vectors corresponding to various processes/mineral effects. The samples define a background trend with a slope of approximately 1/11, which is close to the  $\text{Na}_2\text{O}/\text{Al}_2\text{O}_3$  ratio of montmorillonite.

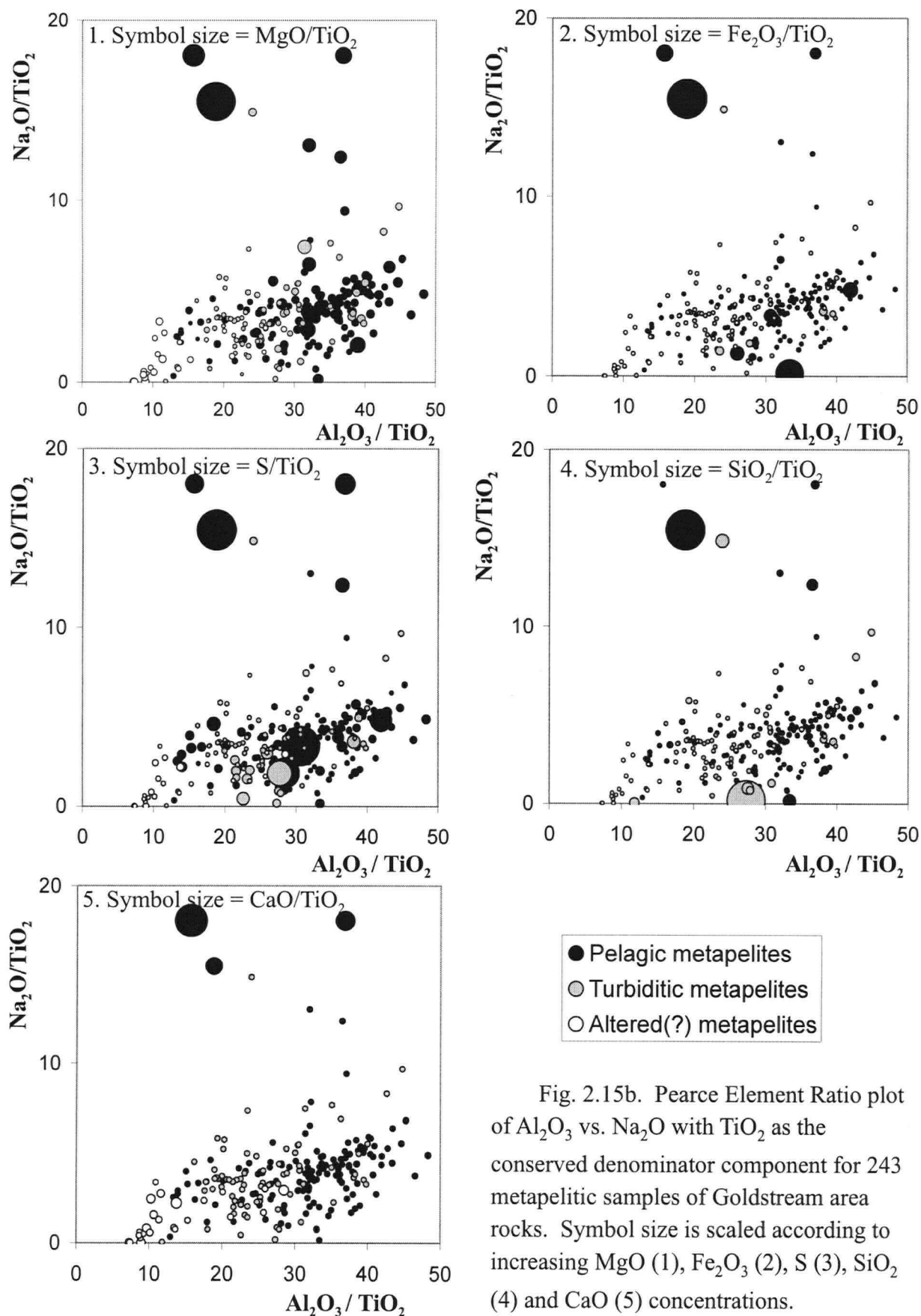


Fig. 2.15b. Pearce Element Ratio plot of  $\text{Al}_2\text{O}_3$  vs.  $\text{Na}_2\text{O}$  with  $\text{TiO}_2$  as the conserved denominator component for 243 metapelite samples of Goldstream area rocks. Symbol size is scaled according to increasing  $\text{MgO}$  (1),  $\text{Fe}_2\text{O}_3$  (2),  $\text{S}$  (3),  $\text{SiO}_2$  (4) and  $\text{CaO}$  (5) concentrations.

Superimposed on this background and largely masked by it, are the effects of Na mobility. By analogy with K it can be argued that Na-loss occurred as a result of hydrothermal alteration. However, the effect of other processes, such as diagenesis and regional metamorphism, cannot be ruled out. In fact, Na-mobility is reported to occur during seafloor alteration in association with volcanism (*e.g.*, Morton and Franklin, 1987; Franklin, 1995; Franklin *et al.* 1999) and diagenesis (*e.g.*, Hower *et al.* 1976). The magnitude and direction of Na mobility depends on many parameters, the most important being water/rock ratio, temperature and salinity. In the rocks hosting the Goldstream ore body, Na-loss, coupled with Fe and Mg addition (discussion below), is expressed mineralogically as chloritization of plagioclase.

Several samples display elevated Na concentrations accompanied by addition of Fe, Mg, Si and S. Their positions on molar ratio plots (Fig. 2.19) suggest that nontronite and/or saponite existed in the original sediment. These minerals are typical of seafloor exhalation environments where they commonly associate with calcareous ooze (Barrett, 1992). Association of high Na concentrations with calcite is observed in the Goldstream rocks as well (Fig. 2.15b No.5). Anomalously high concentrations of albite in the original sediment interfere with the hydrothermal signature of Na, thus preventing quantification of Na mobility. The effect of Na addition is microscopically undetectable in the present mineralogy of the rocks, likely because the added Na is in the form of a paragonite component in the ubiquitous white mica.

Hydrothermal addition of ferromagnesian component in the host rocks commonly accompanies VHMS deposits. It is identified in the Goldstream rocks, superimposed on the background of the low primary concentrations of Fe and Mg, attributable to montmorillonite, the primary clay mineral in the original sediment (Figs. 2.16, 2.17). As suggested by molar ratio analysis, anomalous concentrations are consistent with the presence of chlorite (Figs. 2.16, 2.17, 2.19). Influences of other minerals, such as Fe-sulphides, nontronite and/or saponite are also inferred from the lithogeochemical data. The latter two minerals are characterized by  $\text{Na}_2\text{O}/\text{Al}_2\text{O}_3$  molar ratios which are much higher than those of

typical sedimentary clay minerals. Thus, nontronite-controlled samples are also Na-enriched (Fig. 2.13).

Fe-Mg addition in the wall rocks of the Goldstream deposit is a sum of two spatially and chemically distinct processes:

1. Mainly Fe-addition: This process influences equally all types of metapelites (Fig. 2.16, 2.17). Most of the affected samples display high concentrations of S (Figs. 2.16, 2.18.a), which indicates pyrite and/or pyrrhotite formation either beneath or at the sea floor. A few samples display high concentrations of Na (Figs. 2.17, 2.18b), which may be attributed to the formation of nontronite. The possibility that nontronite (or its Mg variety saponite) controls, in part, the observed Fe (Mg) and Na addition is suggested also by GER analysis (Fig. 2.19).

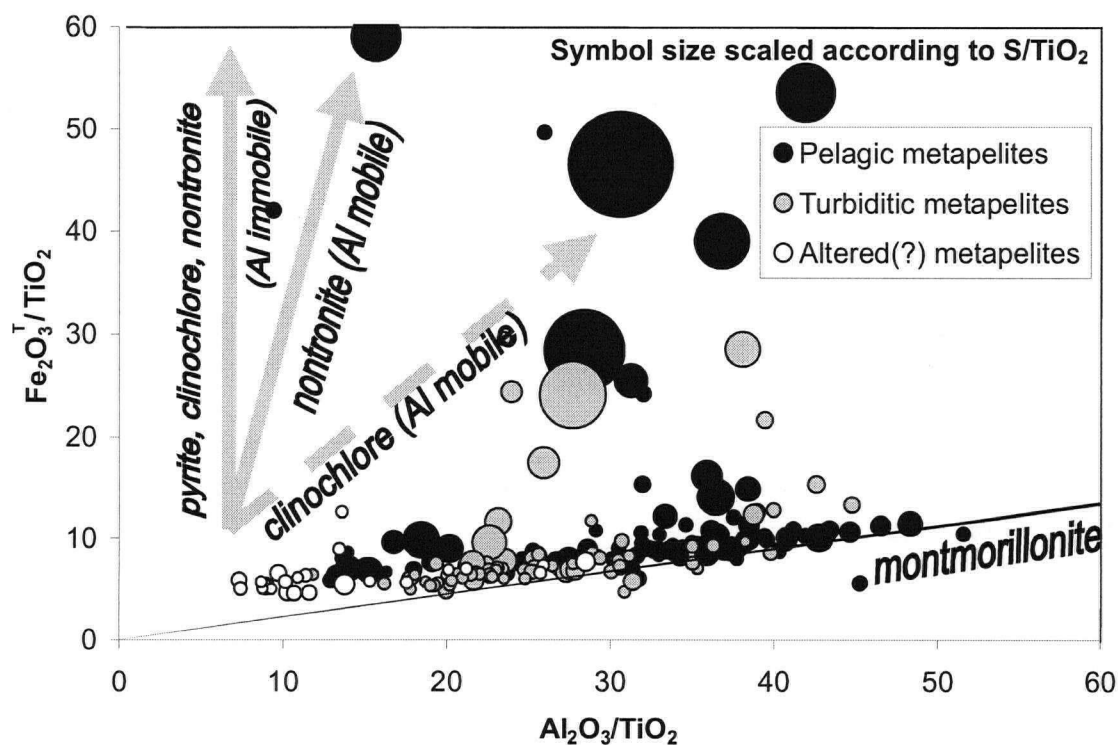


Fig. 2.16. Pearce Element Ratio plot of  $\text{Al}_2\text{O}_3$  vs.  $\text{Fe}_2\text{O}_3^T$  with  $\text{TiO}_2$  as the conserved denominator component for 243 metapelitic samples of Goldstream area rocks. Symbol size is proportional to sulphur concentration. Arrows represent data point-displacement vectors corresponding to various mineral effects. Background samples display a  $\text{Fe}_2\text{O}_3^T / \text{Al}_2\text{O}_3$  ratio of 12/50 (solid line). Combined with a  $\text{MgO}/\text{Al}_2\text{O}_3$  ratio of 8/50 (see Fig. 2.17) the ratio of the ferro-magnesian component to alumina is 2/5, which corresponds to the mineral montmorillonite.

2. Mainly Mg-addition ( $\text{Fe}/\text{Mg}$  approximately equal to  $\frac{1}{2}$ , Fig. 2.18a, b): This process influences predominantly pelagic metapelites and altered (?) metapelites. It is developed in a significantly larger proportion of the rocks than are affected by Fe-addition, but in most cases Mg-addition is weakly expressed. Thus, it can be suggested that Mg addition is a process of pervasive alteration transforming montmorillonite into chlorite through addition of Fe and Mg, whereas the essentially Fe addition is a discrete process, depositing sulphide in a more limited volume, possibly in stringer zones.

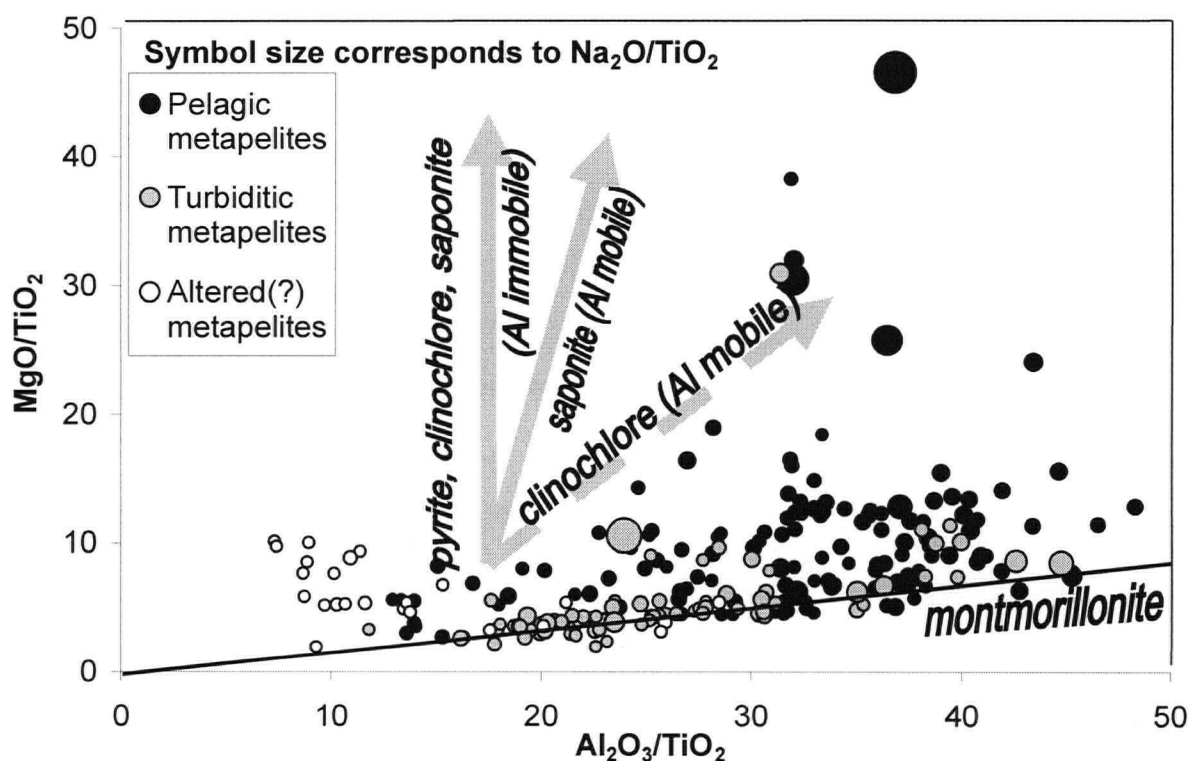


Fig. 2.17. Pearce Element Ratio plot of  $\text{Al}_2\text{O}_3$  vs.  $\text{MgO}$  with  $\text{TiO}_2$  as the conserved denominator component for 243 metapelitic samples of Goldstream area rocks. Symbol size is scaled according to  $\text{Na}_2\text{O}$  concentration. Arrows represent data point-displacement vectors corresponding to various mineral effects. Background samples display a  $\text{MgO}/\text{Al}_2\text{O}_3$  ratio of  $8/50$  (solid line). Combined with a  $\text{Fe}_2\text{O}_3/\text{Al}_2\text{O}_3$  ratio of  $12/50$  (Fig. 2.16), the ratio of the ferromagnesian component to alumina adds up to  $2/5$ , which corresponds to the mineral montmorillonite.

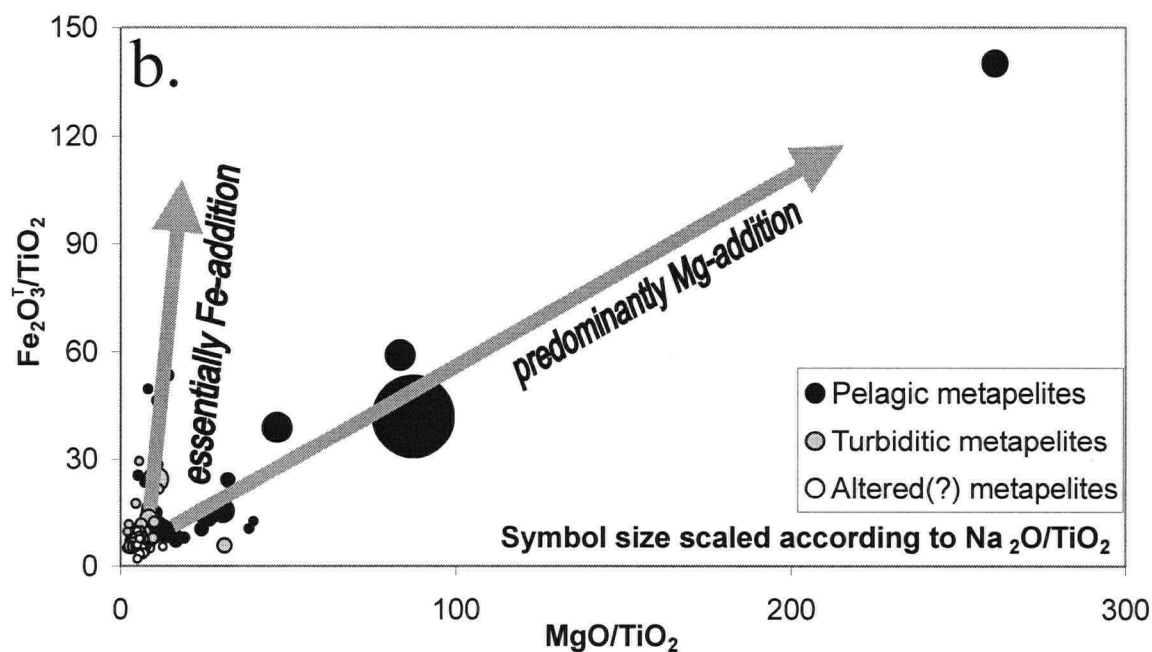
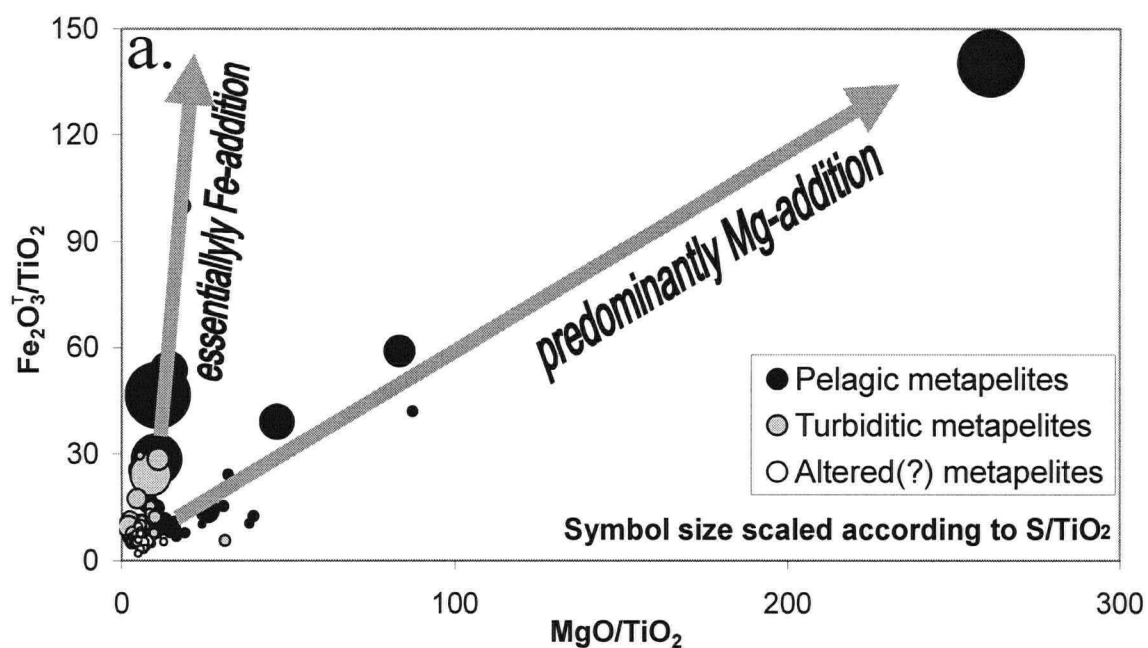


Fig. 2.18. PER plot of  $\text{MgO}$  vs.  $\text{Fe}_2\text{O}_3^{\text{T}}$  with  $\text{TiO}_2$  as the conserved denominator component for 243 metapelitic samples of Goldstream area rocks with symbol size scaled according to S (a) and  $\text{Na}_2\text{O}$  (b) concentrations. Arrows represent data point-displacement vectors corresponding to Fe-, and Mg additions.

Fe-Mg addition can take place as one of two end-member reactions or a combination of them: (1) with addition of both Fe and Mg and Al (if aluminium is mobile) and (2) with addition of Fe and Mg only, whereas aluminium is redistributed in situ between primary montmorillonite and the secondary mineral: chlorite or nontronite (*i.e.*,  $\text{Al}_2\text{O}_3$  is immobile). Positions of anomalous data points support the interpretation that Fe enrichment occurred either through the second end-member process alone, or through a combination of the two processes.

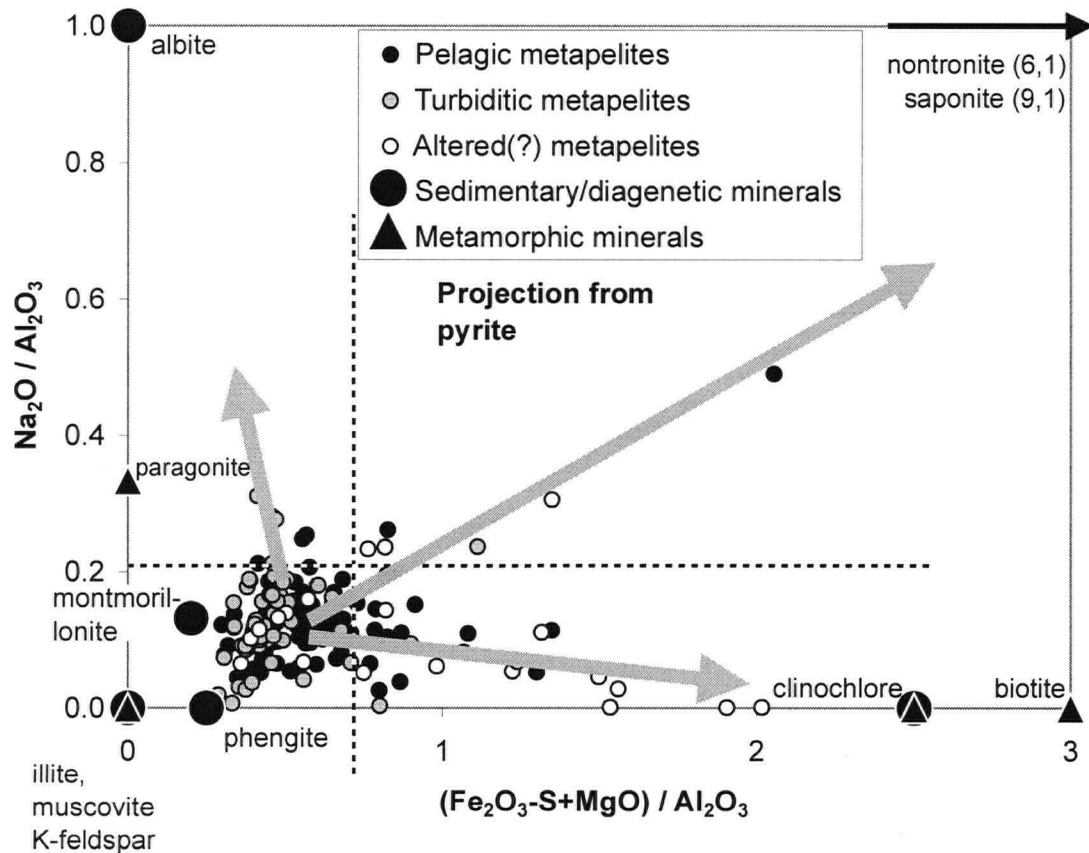


Fig. 2.19. Generalized Element Ratio plot of ferromagnesian component vs.  $\text{Na}_2\text{O}$  with  $\text{Al}_2\text{O}_3$  denominator for 243 metapelitic samples of Goldstream area rocks. Arrows represent data point-displacement vectors. The plot is an implicit projection from quartz and calcite and an explicit projection from sulphide (pyrite), allowing the illustration of compositional variability in clay fraction alone. Two distinct groups of samples display enrichment in Fe and Mg, controlled by (1) clinocllore, and (2) nontronite and/or saponite. Both processes influence strongly the altered(?) metapelites, less so the pelagic metapelites and only weakly the rocks of turbiditic origin. A small group of samples are enriched in Na. Dashed lines separate the fields, corresponding to background variability and the three mineralogical styles of alteration.

Results of PER analysis indicate that Fe- and Mg-addition can be described by the respective parameters  $(\text{Fe}_2\text{O}_3 - 12/50 * \text{Al}_2\text{O}_3) / \text{TiO}_2$  and  $(\text{MgO} - 8/50 * \text{Al}_2\text{O}_3) / \text{TiO}_2$ , which are numerically equivalent to the residuals from the background (montmorillonite) line (Figs. 2.16, 2.17). Because Fe-sulphide can also precipitate by sedimentary and diagenetic processes, its validity as an indicator of a hydrothermal alteration process is arguable.

### **Characteristics and spatial distribution of alteration**

The hydrothermal activity responsible for the formation of the Goldstream ore body transformed the country rocks by mobilizing a number of major elements, such as Mg, Fe, Si, Na and K. Indications exist (Figs. 2.8, 2.9) that relatively inert elements such as Ti and Nb also were involved locally in the process. The mobility of the major elements, as revealed by means of molar ratio analysis, is used to characterize the various alteration styles, their interrelations and spatial distribution. The term alteration is applied here in a broad sense to indicate rock compositions influenced by hydrothermal activity, not restricted to a cross-cutting, metasomatic mineralization. This allows for the inclusion in the discussion of lithogeochemical anomalies of syngenetic exhalative origin, present in the Goldstream rocks.

When spatial aspects of alteration at Goldstream are considered, a note of caution about the representativity of the available samples is necessary. Exploration drilling in most cases did not proceed much beyond the massive sulphide layer and, thus, the structural footwall of the Goldstream ore body was undersampled. Stratigraphic correlation between the mine area and the western section of the study area, where the massive sulphide and the garnetiferous layers were not intersected by drilling, is unclear.

The structural styles of alteration in the mine area and in the western "C" zone are significantly different. In the eastern section the alteration is diffuse and restricted exclusively to the stratigraphic footwall. It is not clear whether the pervasive character of alteration in the mine area is a primary feature of the hydrothermal system or is due to



intensive shearing, which obliterated the cross cutting alteration features in the stratigraphic footwall of the Goldstream ore body. Lack of alteration in the stratigraphic hanging wall can be due to waning of the hydrothermal activity after deposition of the sulphide mineralization. The following model (Fig. 2.20) is proposed, based on the spatial distribution of alteration and mineralization in the mine area:

1. Footwall alteration consists of ferro-magnesian addition, K loss and weak to spotty silica addition, identifiable at distances of at least 50 m (stratigraphically) below the sulphide ore body. The intensity of Si (Fig. 2.21), Mg (Fig. 2.22) and Fe (Fig. 2.23) addition peaks in the mineralized horizon, whereas K loss (Fig. 2.24) is characteristic for the stratigraphically deeper parts of the section.
2. Alkali (K and Na) addition (Figs. 2.24 and 2.25) is restricted to within 10-15 m from the mineralized layer.
3. A manganiferous, cherty layer, metamorphosed to a garnetiferous rock, occurs up to 20 m (stratigraphically) below the massive sulphide layer. Although the cherty layer is spatially associated with the sulphide ore body, the genetic relations are controversial. Due to its unusual occurrence stratigraphically below the massive sulphide body, some workers (T. Hoy, pers. comm.) consider it a result of a separate pulse of hydrothermal activity. Stratigraphic, hanging-wall samples, though limited in number, show no signs of major element mobility.

In contrast to the mine area, the "C" zone is characterized by discrete chloritic stringer zones, intersecting the stratigraphic sequence at high angles. Stratiform mineralization and/or the garnetiferous layer do not occur in this part of the study area. Alteration in the form of Fe, Mg, Si and K addition and alkali loss (Figs. 2.21 through 2.23) is identified to a depth of more than 100 m, which is as deep as the rocks were sampled by drilling. Potassium was leached from the deeper portions of the stratigraphy and deposited up-section, a feature observed also in the footwall of the Goldstream ore body. Widespread Na loss deviates from the model developed for the eastern section, but conforms to observations of other authors describing this process as commonly occurring in the footwall of VHMS deposits (*e.g.*, Morton and Franklin, 1987; Franklin, 1995; Franklin, 1999). Lack of



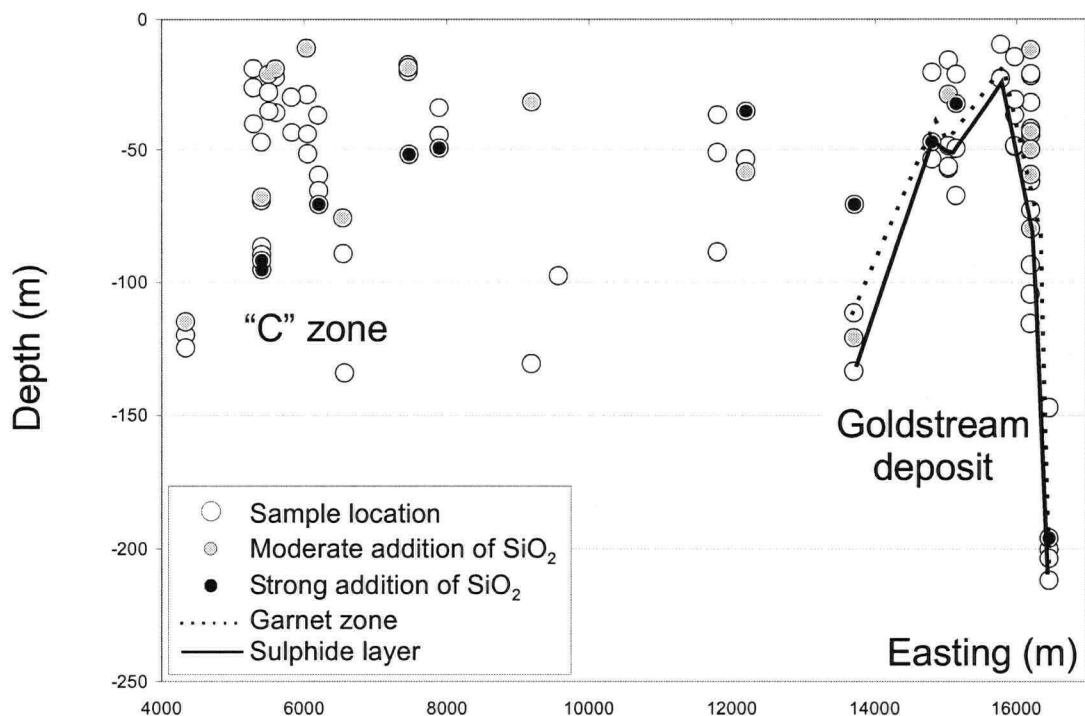


Fig. 2.21. Spatial distribution of  $\text{SiO}_2$  addition based on Pearce Element Ratio plot of  $\text{Al}_2\text{O}_3$  vs.  $\text{SiO}_2$  with  $\text{TiO}_2$  as the conserved denominator (Fig. 2.13). Moderate addition:  $[(\text{SiO}_2/\text{TiO}_2)/(\text{Al}_2\text{O}_3/\text{TiO}_2)] > 4$ , Strong addition:  $[(\text{SiO}_2/\text{TiO}_2)/(\text{Al}_2\text{O}_3/\text{TiO}_2)] > 7$ .

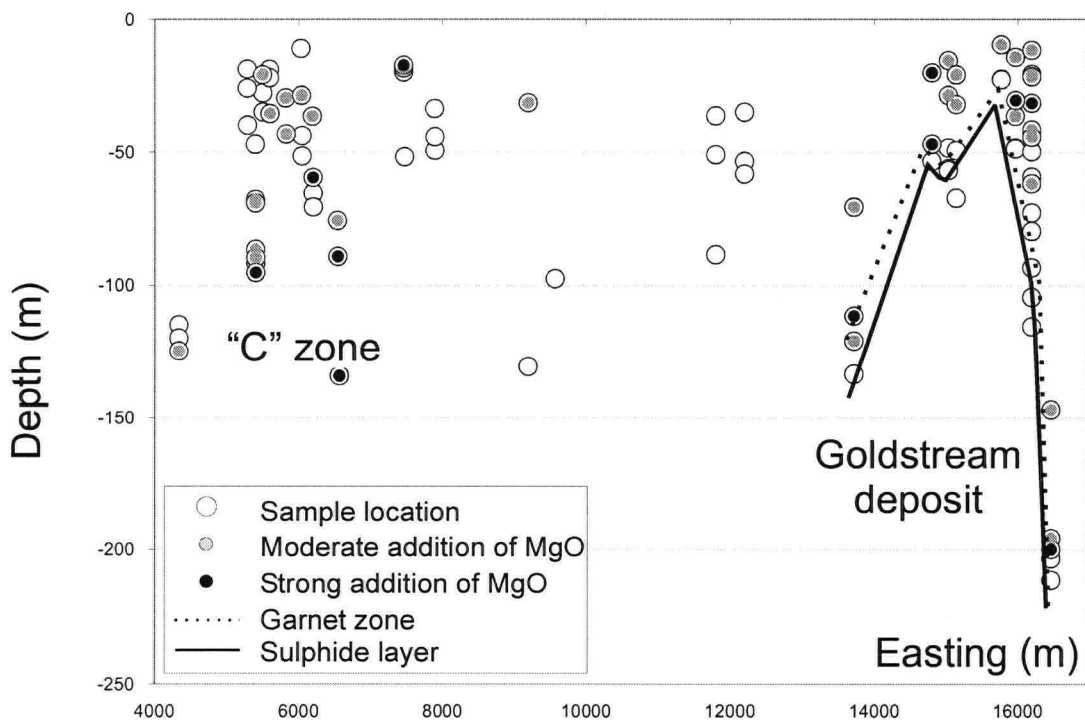


Fig. 2.22. Spatial distribution of  $\text{MgO}$  addition based on  $\text{MgO}$  vs.  $\text{Al}_2\text{O}_3$  with  $\text{TiO}_2$  as the conserved element denominator (Fig. 2.17). Moderate addition:  $[(\text{MgO}/\text{TiO}_2) / (\text{Al}_2\text{O}_3/\text{TiO}_2)] > 3$ , Strong addition:  $[(\text{MgO}/\text{TiO}_2) / (\text{Al}_2\text{O}_3/\text{TiO}_2)] > 2$ .

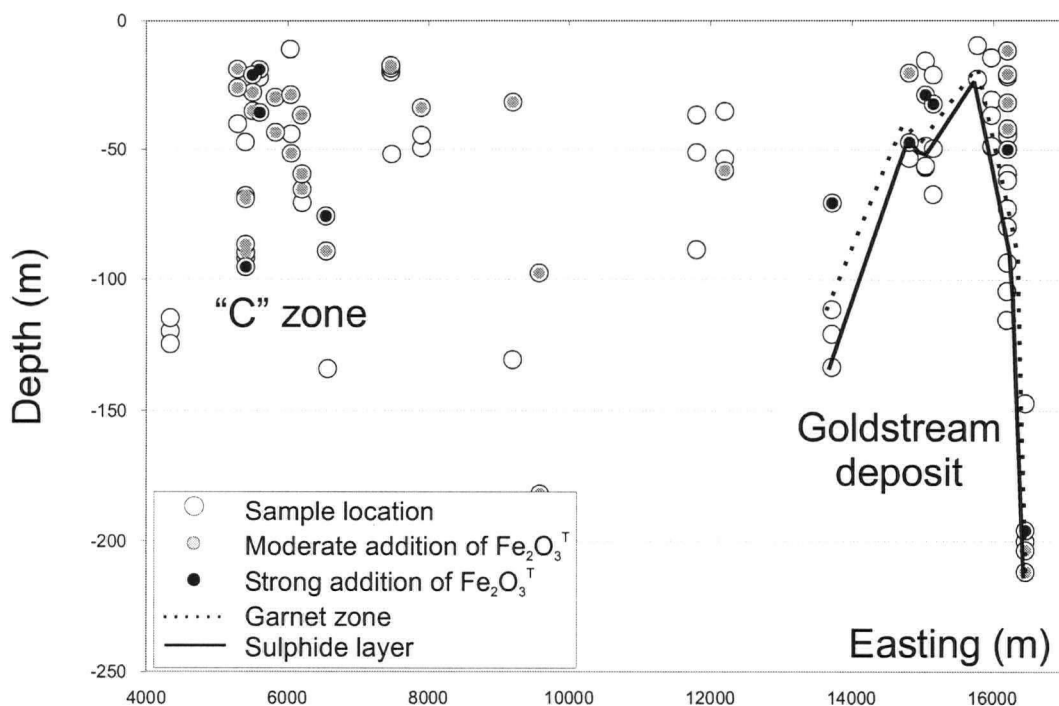


Fig. 2.23. Spatial distribution of  $\text{Fe}_2\text{O}_3^{\text{T}}$  addition based on Pearce Element Ratio analysis of  $\text{Fe}_2\text{O}_3^{\text{T}}$  vs.  $\text{Al}_2\text{O}_3$  with  $\text{TiO}_2$  as the conserved element denominator (Fig. 2.16).

Moderate addition:  $[(\text{Fe}_2\text{O}_3^{\text{T}}/\text{TiO}_2) / (\text{Al}_2\text{O}_3/\text{TiO}_2)] > 1/3$

Strong addition:  $[(\text{Fe}_2\text{O}_3^{\text{T}}/\text{TiO}_2) / (\text{Al}_2\text{O}_3/\text{TiO}_2)] > 3/4$

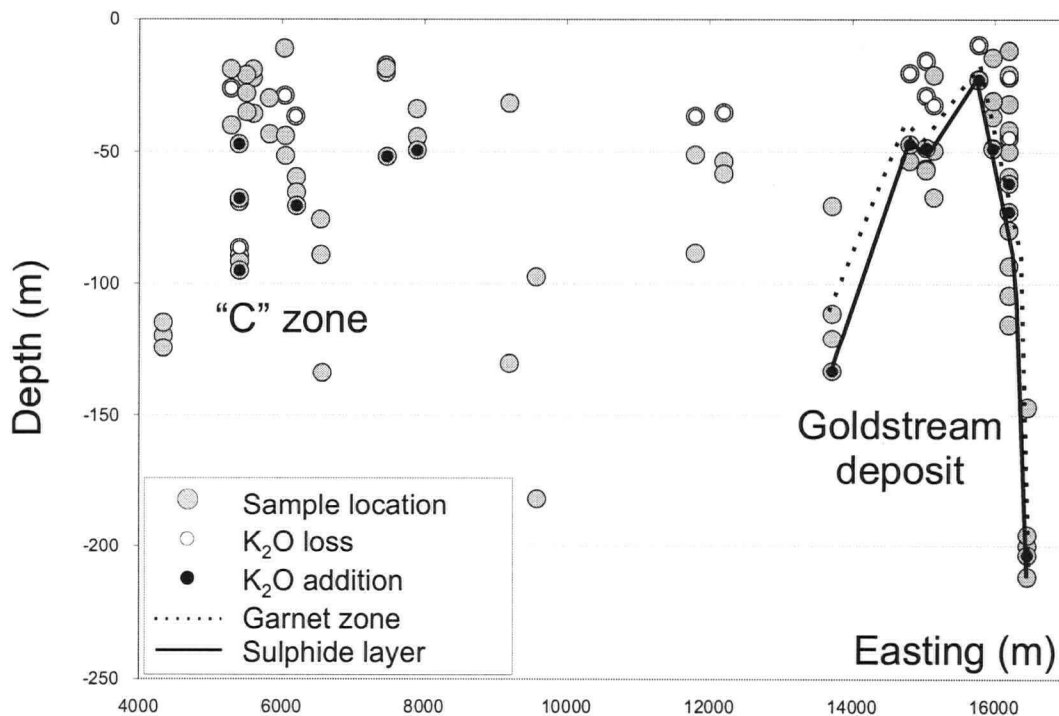


Fig. 2.24. Spatial distribution of  $\text{K}_2\text{O}$  mobility, based on Pearce Element Ratio analysis of  $\text{K}_2\text{O}$  vs.  $\text{Al}_2\text{O}_3$  with  $\text{TiO}_2$  as the conserved element denominator (Fig. 2.14).

Loss:  $[(\text{Al}_2\text{O}_3/\text{TiO}_2) / (\text{K}_2\text{O}/\text{TiO}_2)] > 5$

Addition:  $[(\text{Al}_2\text{O}_3/\text{TiO}_2) / (\text{K}_2\text{O}/\text{TiO}_2)] < 3$

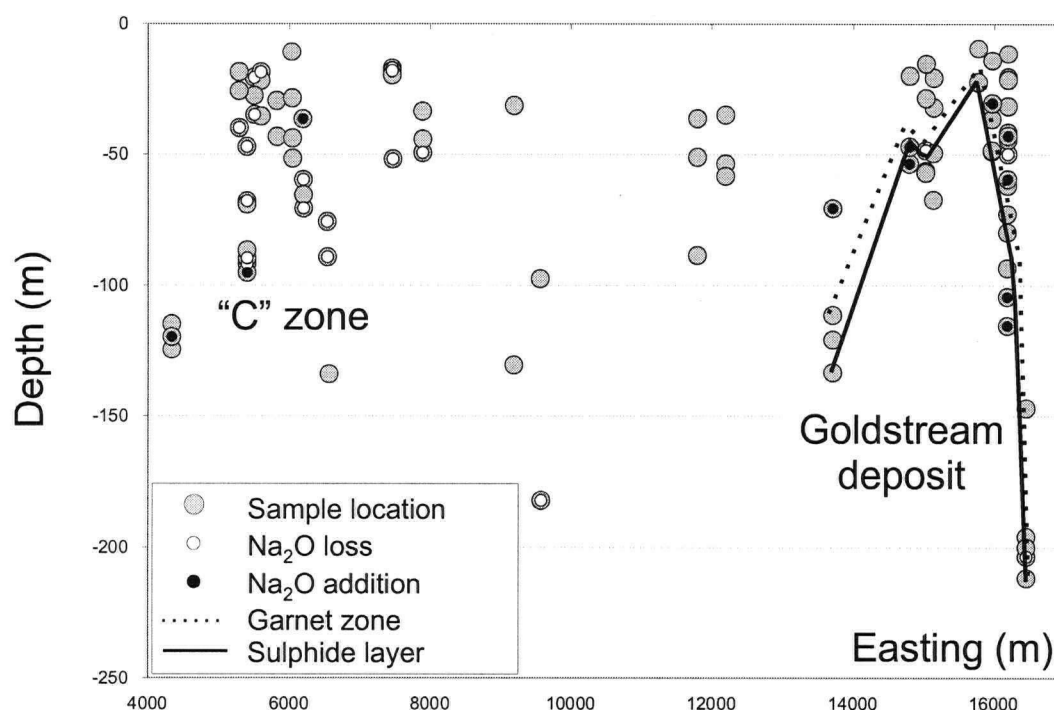


Fig. 2.25. Spatial distribution of Na<sub>2</sub>O mobility, based on Pearce Element Ratio analysis of Na<sub>2</sub>O vs. Al<sub>2</sub>O<sub>3</sub> with TiO<sub>2</sub> as the conserved element denominator (Fig. 2.15a).  
 Loss:  $[(Al_2O_3/TiO_2) / (Na_2O/TiO_2)] > 20$   
 Addition:  $[(Al_2O_3/TiO_2) / (Na_2O/TiO_2)] < 4$

## Conclusions

1. Despite their widely varying compositions and physical distinctions, the metamorphic rocks at Goldstream, with the exception of the metavolcanic rocks, can be viewed as a continuum of seafloor deposits dominated by a pelitic component. The following processes and their interaction are responsible for the observed chemical variability:
  - a) Pelagic sedimentation was active during quiescent periods and deposited clay and calcareous sediments in varying proportions.
  - b) Turbiditic sedimentation dominated the depositional process intermittently, at times of enhanced influx of terrigenous material into the basin. It resulted in two end member types of sediments: psammites and pelites. The latter are common members of both pelagic and turbiditic deposits.

c) Seafloor hydrothermal exhalations deposited siliceous and ferruginous material.

Similarly to pelagic deposits, exhalites constitute a significant proportion of the sediment only in quiescent periods when turbidite sedimentation is negligible.

Siliceous exhalites may occur separately, whereas ferruginous exhalites are accompanied by a significant silica component and display elevated Mn concentrations.

Thus, the Goldstream metapelites originated as a combination of various proportions of pelitic, psamitic, calcareous, ferruginous and siliceous components of pelagic, turbiditic and exhalative origin.

2. Background compositional variability in metapelitic rocks hosting the Goldstream deposit indicates that a mineral similar to montmorillonite dominated the clay mineral assemblage at the time of sedimentation. During diagenesis the clay mineral was transformed to illite by incorporation of potassium from hydrolyzed K-feldspar. The latter is originally present in turbiditic flow bottoms and as it is destroyed, K is redistributed locally causing convergence in compositions (with respect to K and Al) of turbidite bottoms and tops. Subordinate amounts of chlorite, possibly related to volcanoclastic material of mafic to intermediate composition, were also present in the sediment either as a separate phase or as interlayers in the structure of the clay mineral. Locally, clay minerals of exhalative origin, such as nontronite and saponite, were deposited. They indicate time intervals of relatively slow clastic sedimentation and intensive hydrothermal activity. Those periods were favourable also for the accumulation of ore, hence, the spatial correlation of Na-, Fe- and Mg-rich clay minerals and massive sulphides.
3. The molar ratio methodology used in the processing of the lithogeochemical data allows elucidation of both the primary and alteration mineralogy and detecting and quantifying alteration effects. MER analysis is not always capable of deciphering the original mineralogical composition of rocks that have gone through a series of diagenetic and

metamorphic transformations. It can, however, help to identify viable hypotheses, which can be further evaluated using other constraints.

Using MER methodology, major element anomalies were identified up to 100 m into the stratigraphic footwall. In the case of the Goldstream deposit, the limited availability of drill core did not allow a full testing of the sensitivity limitations of the MER. The method is insensitive to the superimposed effect of regional metamorphism, assuming the latter involves mostly isochemical phase transformations.

4. The following Pearce Element ratios are judged to be the most useful parameters in the study of the alteration associated with the Goldstream deposit:
  - a)  $(\text{Fe}_2\text{O}_3 - 12/50 * \text{Al}_2\text{O}_3) / \text{TiO}_2$  and  $(\text{MgO} - 8/50 * \text{Al}_2\text{O}_3) / \text{TiO}_2$  are used in the quantification of chloritization;
  - b)  $(\text{K}_2\text{O} - 3/11 * \text{Al}_2\text{O}_3) / \text{TiO}_2$  and  $(\text{Na}_2\text{O} - 1/11 * \text{Al}_2\text{O}_3) / \text{TiO}_2$  quantify alkali mobility.
  - c)  $(\text{Si} - 12/5 * \text{Al}) / \text{Ti}$  is used to characterize silica addition.
  - d)  $\text{Si/Zr}$  is used to distinguish between turbiditic and pelagic metapelites.
5. Several types of alteration are identified in the vicinity of the Goldstream deposit (Fig. 2.20) and interpreted as being genetically associated with mineralization. Large volumes of metapelitic rocks in the deeper stratigraphic footwall of the mineralized horizon lost their alkalis due to recrystallization of the clay mineral. Magnesian chlorite ( $\text{Mg/Fe} = 10/6$ ) and quartz formed *in situ*, utilizing the aluminum and silica from the destruction of clay minerals. Magnesium (originating from seawater) and iron and silica (leached from the country rocks) were added by the hydrothermal solutions, resulting in broad and locally intensive silicification and chloritization.

In the immediate footwall of the massive sulphide body, as well as in stringer zones, K-addition is well defined. Its initial mineralogical expression was most likely sericitization, however its petrographic signature is masked by the metamorphic

transformation of the pelitic rocks yielding abundant muscovite. The immediate footwall of the ore body is enriched also in Na, possibly deposited in the form of nontronite and/or saponite. After the regional metamorphic event, Na was incorporated in other rock-forming minerals, mostly as paragonite component in white micas, therefore the alteration is impossible to detect petrographically. Magnesium and iron addition, manifested mineralogically as chloritization, are detectable much deeper into the deposit's stratigraphic footwall but peak at the base of the massive sulphide layer. Where the thermal effect of the Goldstream pluton caused metamorphic grades to be higher, chlorite is superseded by biotite.

6. Alteration at the "C" zone bears similarities (ferro-magnesian and silica addition and K loss) with that identified in the footwall of the Goldstream ore body approximately 10 km to the East. Deviation from the model devised for the deposit, namely extensive Na loss present at the "C" zone, can be explained in one of two ways:

- a) The erosion is more advanced at the mine area, leaving only up to 100 m of the footwall (in the plane of the cross section, Figs. 21 through 25); and/or
- b) the mineralogical composition of the original pelitic rocks may have been different, including plagioclase, which is subject to hydrolysis and, thus is more reactive than clay minerals. The current mineral composition of the metapelitic rocks, however, does not bear any evidence to that effect.

If the model is applied to the "C" zone, possible massive sulphide mineralization should occur at deeper (stratigraphically shallower) levels. Judging by the intensity of Mg and Si addition and the indications of K and Na addition towards the bottoms of the drill holes, a sulphide-mineralized horizon may be present within another 50 to 100 m depth.

## References

Barrett, T. J., (1992) Mass Changes in the Galapagos Hydrothermal Mounds: Near-axis Sediment Transformation and Mineralization: *Geology*, 20, p. 1075-1078.



Bonatti, E., (1981) Metal Deposits in the Oceanic Lithosphere. *In*: Emiliani, C. (editor) *The Sea*: John Wiley and Sons, New York, p. 639-686.

Bradshaw, G.D., (1996) Compositional Variability in Mn-rich Garnets Hosted by a Ferruginous Chert Horizon, Goldstream Cu-Zn Mine, British Columbia: B.S. thesis, University of British Columbia, Vancouver, BC, 83 p.

Brown, R.L., (1991) Geological Map and Cross Section, Downie Creek Map Area (82 M/8) British Columbia: Geological Survey of Canada, Open File 2414.

Brown, R.L., Hoy, T. and Lane L.S., (1976) Stratigraphy and Structure South of Goldstream River, Selkirk Mountains: Geological Fieldwork, 1976, B.C. Ministry of Energy, Mines and Petroleum Resources, p. 17-22.

Brown, R.L., Perkins, M.J. and Tippet, C.R., (1977) Structure and Stratigraphy of the Big Bend Area, British Columbia: Current Research, Part A, Geological Survey of Canada, Paper 77-1A, p. 273-275.

Brown, R.L., Lane, L.S., Psutka, J.F. and Read, P.B., (1983) Stratigraphy and Structure of the Western Margin of the Northern Selkirk Mountains: Downie Creek Map Area: Current Research, Part A, Geological Survey of Canada, Paper 83-1A, p. 203-206.

Brown, R.L. and Lane, L.S., (1988) Tectonic Interpretation of West-verging Folds in the Selkirk Allochthon of the Southern Canadian Cordillera: Canadian Journal of Earth Sciences, 25, p. 292-300.

Brown R.L., McNicoll, V.J., Parrish, R.R. and Scammell R.J., (1992) Middle Jurassic Plutonism in the Kootenay Terrane, Northern Selkirk Mountains, British Columbia. Radiogenic Age and Isotopic Studies: Report 5, Geological Survey of Canada, Paper 91-2, p. 135-141.

Bucher, K. and Frey, M., (1994) Petrogenesis of Metamorphic Rocks: Springer-Verlag, Berlin, Heidelberg, 318 p.

Campbell, R.B., (1972) Geological Map of part of the Southeastern Canadian Cordillera. Structural Styles of the Southern Canadian Cordillera: XXIV International Geological Congress, Field Excursion X01-A01.

Chamley, H., (1989) Clay Sedimentology: Springer-Verlag Berlin Heidelberg, 623 p.

Franklin, J.M., (1995) Volcanic Associated Massive Sulphide Base Metals. *In*: Eckstrand, O.R., Sinclair, W.D. and Thorpe, R.I., (editors) *Geology of Canadian Mineral Deposit Types*: Geological Survey of Canada, Geology of Canada, 8, p. 158-183.

Franklin, J.M., (1999) Systematic Analysis of Lithogeochemical Data. *In*: Franklin, J.M., Gibson, H, (editors): Exploration Tools for Volcanogenic Massive Sulphide Deposits, Short Course notes: University of British Columbia, MDRU Short Course, Vancouver, Jan 24 & 25, 1999, 34 p.

Franklin, J.M., Lydon, J.W and Sangster, D.F., (1981) Volcanic-Associated Massive Sulphide Deposits. *In*: Skinner, B.J., (editor) Economic Geology: Seventy-Fifth Anniversary Volume, p. 485-627.

Franzen, J.P., (1974) Structural Analysis in the Selkirk Fan Axis near Argonaut Mountain, Southeastern British Columbia: M.Sc. thesis, Carleton University, Ottawa, ON 55 p.

Fyles, J.T., (1964) Geology of the Duncan Lake Area, Lardeau District, British Columbia. B.C. Ministry of Energy, Mines and Petroleum Resources Bulletin, 49, 87 p.

Fyles, J.T., (1970) Geological Setting of the Lead-zinc Deposits in the Kootenay Lake and Salmo Areas of British Columbia. Lead-zinc Deposits in the Kootenay arc, Northeastern Washington and Adjacent British Columbia: State of Washington Division of Mines and Geology Bulletin, 61, p. 41-53.

Gibson, G., (1989) Geological and Geochemical Report on the Brew Property: B.C. Ministry of Energy, Mines and Petroleum Resources, Assessment Report 19, 580 p.

Gibson, G. and Hoy, T., (1985) Rift, a Zinc-Lead Massive Sulphide Deposit in Southeastern British Columbia, (82M/15): Geological Fieldwork 1984, B.C. Ministry of Energy, Mines and Petroleum Resources, Paper 1985-1, p. 105-119.

Greensmith, J.T., (1989) Petrology of the Sedimentary Rocks: Unwin Hyman, London, 241 p.

Haymon, R.M. and Kastner, M., (1981) Hot Spring Deposits on the East Pacific Rise at 21°N: Preliminary Description of Mineralogy and Genesis: Earth and Planetary Science Letters, 53, p. 363-381.

Hesse, R., (1986) Diagenesis. Early Diagenetic Pore Water/Sediment Interaction. Modern Offshore Basins: Geoscience Canada, 13; 3, p. 165-197.

Hicks, K.E., (1982) Geology and Mineralogy of the "Rift" Zinc-Lead Massive Sulphide Deposit, Southeastern British Columbia: B.Sc. thesis, University of British Columbia, Vancouver, BC, 84 p.

Hower, J., Eslinger, E.V., Hower, M.E. and Perry, E.A., (1976) Mechanism of Burial Metamorphism of Argillaceous Sediment. 1. Mineralogical and Chemical Evidence: Geological Society of America Bulletin, 87, p. 725-737.

Höy, T., (1979) Geology of the Goldstream area: B.C. Ministry of Energy, Mines and Petroleum Resources Bulletin, 71, 49 p.

Höy, T., (1980) Geology of the Riondel area, Central Kootenay Arc, Southeastern British Columbia: B.C. Ministry of Energy, Mines and Petroleum Resources, 89 p.

Höy, T., (1982) Stratigraphic and Structural Setting of Stratabound Lead-Zinc Deposits in Southeastern B.C.: Canadian Institute of Mining and Metallurgy Bulletin, 75; 840, p. 114-134.

Höy, T., (1989) The Purcell Supergroup and the Sullivan Massive Sulfide Deposit. Geologic Guidebook for Washington and Adjacent Areas: State of Washington, Department of Natural Resources Information Circular, Division of Geology and Earth Resources, p. 55-62.

Höy, T., Gibson, G. and Berg, N.W., (1984) Copper-zinc Deposits Associated with Basic Volcanism, Goldstream Area, Southeastern British Columbia: Economic Geology, 79, p. 789-814.

Höy, T., Berg, N. Fyles, J.T., Delaney, G.D., McMurdo, D. and Ransom, P.W., (1985) Stratabound Base Metal Deposits in Southeastern British Columbia. Trip 11. *In*: Tempelman-Kluit, D.J., (editor) Field Guides to Geology and Mineral Deposits in the Southern Canadian Cordillera, p. 11.1-11.32.

Kramm, U., (1976) The Coticule Rocks (Spessartine Quartzites) of the Venn-Stavelot Massif, Ardennes, a Volcaniclastic Metasediment?: Contributions to Mineralogy and Petrology, 56, p. 135-155.

Kuroda, H., (1983) Geologic Characteristics and Formation Environments of the Furutobe and Matsuki Kuroko Deposits, Akita Prefecture, Northeastern Japan. *In*: Ohmoto, H. and Skinner, B.J. (editors) The Kuroko and Related Volcanogenic Massive Sulfide Deposits: Economic Geology Monograph 5, p. 149-146.

Lane, L.S., (1977) Structure and Stratigraphy, Goldstream River – Downie Creek Area, Selkirk Mountains, British Columbia: M.Sc. thesis, Carleton University, Ottawa, ON, 140 p.

Logan, J.M. and Drobe, J.R., (1994) Summary of Activities, North Selkirk Project Goldstream River and Downie Creek Map Areas (82M/8,9 parts of 10): Geological Fieldwork, 1993; A Summary of Field Activities and Current Research, Paper 1994-1, p. 153-169.

Logan, J.M. and Colpron, M., (1995) Northern Selkirk Project – Geology of the Goldstream River Map Area (82M/9 and Parts of 82M/10): Geological Fieldwork, 1994; A Summary of Field Activities and Current Research, Paper 1995-1, p. 215-241.

Logan, J.M. and Friedman, R.M., (1997) U-Pb Ages From the Selkirk Allochthon, Seymour Arm Map area, Southeast British Columbia (82M 8 and 9): Geological Fieldwork, 1996; a Summary of Field Activities and Current Research, Paper 1997-1, p. 17-23.

Lydon, J.W., Höy, T., Slack, J. and Knapp, M., (editors) (2000) The Geological Environment of the Sullivan Deposit, British Columbia: Geological Association of Canada, Mineral Deposits Division, Special Publication, 1, 834 p.

Monger, J.W.H., Clowes, R.M., Cowan, D.S., Potter, C.J., Price R.A. and Yorath, C.J., (1994) Continent-Ocean Transitions in Western North America Between Latitudes 46 and 56 Degrees: Transects B1, B2, B3. *In*: Speed, R.C. (editor), Evolution of North American Continent – Ocean Transitions: Geological Society of America, DNAG Continent – Ocean Transect Volume, p. 357-397.

Morton, R.L. and Franklin, J.M., (1987) Two-fold Classification of Archean Volcanic-Associated Massive Sulphide Deposits: Economic Geology, 82, p.1057-1063.

Parrish, R.R. and Wheeler, J.O., (1983) A U-Pb Zircon Age from the Kuskanax Batholith, Southeastern British Columbia: Canadian Journal of Earth Sciences, 20, p. 1751-1756.

Pearce, T.H., (1968) A Contribution to the Theory of Variation Diagrams: Contributions to Mineralogy and Petrology, 19, p. 142-157.

Pearson, M.J. and Small, J.S., (1988) Illite-smectite Diagenesis and Paleotemperatures in Northern North Sea Quaternary to Mesozoic Shale Sequences: Clay Minerals, 23; 2, p. 109-132.

Read, P.B. and Brown, R.L., (1979) Inverted Stratigraphy and Structures, Downie Creek, Southern British Columbia: Geological Survey of Canada Current Research, Part A, p. 33-34.

Russell, J.K. and Stanley, C.R., (1990) Material Transfer Equations and Chemical Variation Diagrams. *In*: Russell, J.K., Stanley, C.R., (editors), Theory and Application of Pearce Element Ratios to Geochemical Data Analysis: Geological Association of Canada Short Course Notes, 8, p. 23-54.

Sinclair, A.J. and Stanley, C.R., (1995) Lithogeochemical Exploration for Metasomatic Alteration Zones Associated with Hydrothermal Mineral Deposits: University of British Columbia, MDRU Research Proposal, 7 p.

Stanley, C.R., (1996) Graphical Investigation of Lithogeochemical Variations Using Molar Element Ratio Diagrams: Theoretical Foundation. *In*: Lithogeochemical Exploration for

Metasomatic Zones Associated with Hydrothermal Mineral Deposits: Mineral Deposits Research Unit, Lithogeochemical Research Project, Annual Technical Report Year 1, 40 p.

Stanley, C. R., (1997a) Analytical Quality Control and Assessment for the MDRU Lithogeochemical Exploration Research Project. *In: Lithogeochemical Exploration for Metasomatic Zones Associated with Hydrothermal Mineral Deposits: Mineral Deposits Research Unit, Lithogeochemical Research Project. Annual Technical Report, Years 1 and 2*, 32 p.

Stanley, C. R., (1997b) THPLOT.M, A Matlab Function to Implement Generalized Thompson-Howarth Error Analysis Using Replicate Data. *In: Lithogeochemical Exploration for Metasomatic Zones Associated with Hydrothermal Mineral Deposits: Mineral Deposits Research Unit, Lithogeochemical Research Project. Annual Technical Report, Years 1 and 2*, 51 p.

Stanley, C.R., (1997b) Sedimentologic, Diagenetic, Metamorphic and Metasomatic Controls on the Lithogeochemical Composition of Pelitic Sediments that Contain Sediment Hosted Massive Sulphide Deposits. *In: Lithogeochemical Exploration for Metasomatic Zones Associated with Hydrothermal Mineral Deposits: Mineral Deposits Research Unit, Lithogeochemical Research Project. Annual Technical Report, Year 3*, 27 p.

Stanley, C.R. and Russell, J.K., (1989) Petrologic Hypothesis Testing with Pearce Element Ratio Diagrams: Derivation of Diagram Axes: Contributions to Mineralogy and Petrology, 103, p. 78-89.

Stanley, C.R. and Madeisky H.E., (1993) Pearce Element Ratio Analysis: Applications in Lithogeochemical Exploration: Mineral Deposit Research Unit, Short Course No.13 Notes, Vancouver, British Columbia, Canada, 540 p.

Staudigel, H, Plank, T., White, B. and Schmincke, H.U., (1996) Geochemical Fluxes During Seafloor Alteration of the Basaltic Upper Oceanic Crust; DSDP Sites 417 and 418. *In: Bebout G.E., Scholl D.W., Kirby S.H. and Platt J.P., (editors): Geophysical Monograph 96*, p. 19-38.

Sverjensky, D.A., (1989) Chemical Evolution of Basinal Brines that Form Sediment-hosted Cu-Pb-Zn deposits. *In: Boyle, R.W, Brown, A.C., Jefferson, C.W., Jowett, E.C. and Kirkham, R.V., (editors) Sediment-hosted Stratiform Copper Deposits: Geological Association of Canada Special Paper, 36*, p. 127-134.

Tivey, M.K. and Singh, S., (1997) Nondestructive Imaging of Fragile Sea-floor Vent Deposit Samples: *Geology*, 25, p. 931-934.

Thompson, R.I., (1978) Geology of the Alkolkolex River area: British Columbia Ministry of Energy, Mines and Petroleum Resources Bulletin, 60, 77 p.

Thompson, G., (1983) Hydrothermal Fluxes in the Ocean. *In*: Riley, J.P. and Chester, R., (editors) Chemical Oceanography: Academic Press, New York, 8, p. 271-337.

Valsami, E., Cann, J.R. and Rassios, A., (1994) The Mineralogy and Geochemistry of a Hydrothermal Alteration Pipe in the Othris Ophiolite, Greece: Chemical Geology, 114, p. 235-266.

Walker, R.G., (1992) Turbidites and Submarine Fans. *In*: Walker, R. G. and James, N. P., (editors) Facies Models. Response to Sea Level Change: p. 239-263.

Weissenborn, A.E., Armstrong, F.C. and Fyles, J.T., (1970) Lead-zinc Deposits in the Kootenay Arc, Northeastern Washington and Adjacent British Columbia: Introduction: State of Washington Division of Mines and Geology Bulletin, 61, p. 3-4.

Wheeler, J.O. and McFeely, P., (1991) Tectonic Assemblage Map of the Canadian Cordillera and adjacent parts of the United States of America: Geological Survey of Canada, Map 1712A, 1:2 000 000.

Wheeler, J.O., Brookfield, A.J., Gabrielse, H., Monger, J.W.H., Tipper, H.W. and Woodsworth, G.J., (1991) Terrane Map of the Canadian Cordillera: Geological Survey of Canada, Map 1713A, 1:2 000 000.

## Chapter 3

### Applicability of Molar Ratio Analysis for Quantitative Characterization of Alteration Related to Volcanogenic Massive Sulphide Mineralization

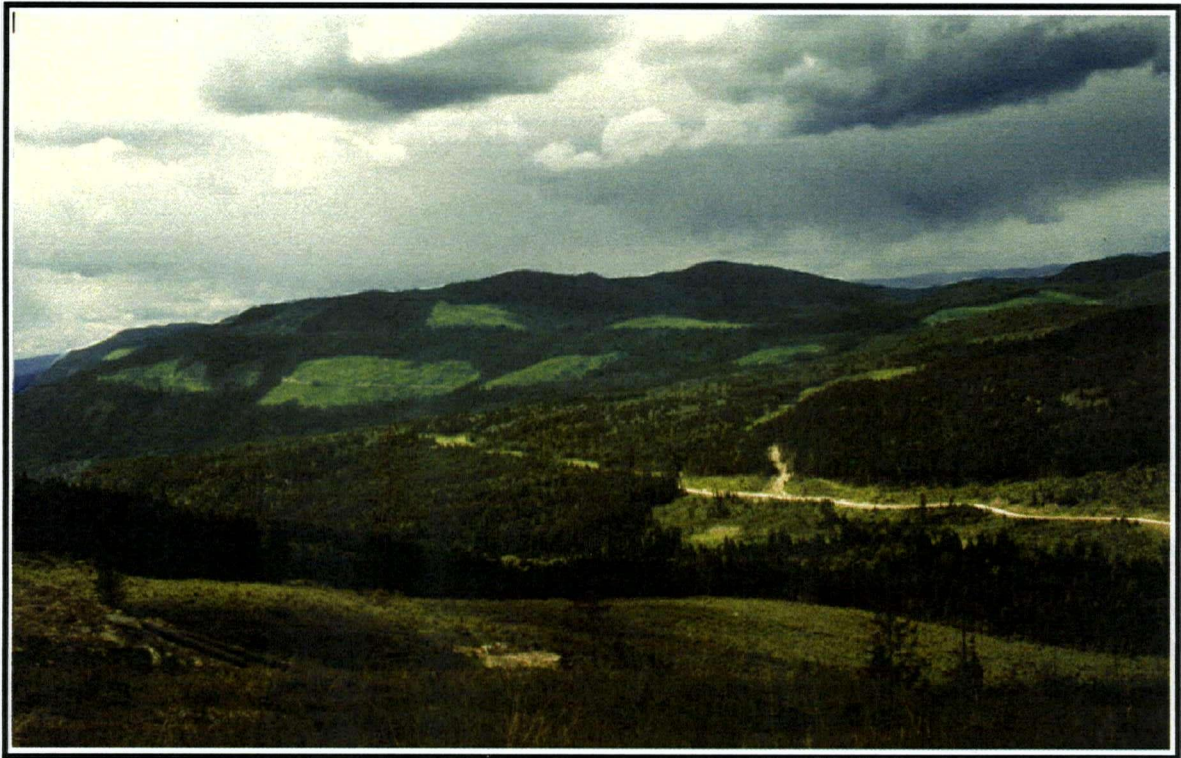


Plate 3.1. View North from the Rea gold deposit towards the Chu Chua Mountain.

## **Abstract**

The Chu Chua volcanogenic-hosted massive sulphide (VHMS) showing in British Columbia is hosted by mafic volcanic rocks and volcanic-related sedimentary rocks of Paleozoic age. Primary and secondary compositional variability in the host rocks was studied using 115 samples from all occurring rock types analysed by X-Ray Fluorescence analysis (XRF), and a supplementary data set of 533 donated samples analysed by various techniques. The compositional data were used to quantify the alteration of the host rocks and to characterize it chemically, mineralogically and spatially using Pearce Element Ratio (PER) Analysis.

Chemical compositions of the rocks are used to subdivide them into several types: basalt of two distinct compositions, silicic rocks interpreted as chert of exhalative origin, felsic dikes, and extreme ferromagnesian (magnetite-talc) metasomatites. Some samples represent physical mixtures of basalt and chert with peperitic textures. Spatial relations between the rock types indicate the existence of a synvolcanic normal fault focusing the paleo-hydrothermal system responsible for the exhalative sulphide mineralization.

Several chemical types of alteration were recognized: Ca and Na loss, Fe-Mg addition and SiO<sub>2</sub> mobility. Mineralogically, the alteration is expressed as destruction of plagioclase and pyroxene in the mafic volcanic rocks, pervasive chloritization, local magnetite-talc alteration and sericitization. Large amounts of SiO<sub>2</sub>, released in the process of alteration of the primary mineral assemblage, were exhaled on the seafloor and deposited as chert in a half-graben depression. The quantitative PER methodology used in this study allows the alteration reactions to be constrained. The hydrothermal process produced relatively small (a few tens of meters) alteration halos to the massive sulphide deposit.

## **Introduction**

The Chu Chua deposit is located about 20 km north-northeast of Barriere in south-central British Columbia. It was discovered in 1987 by prospecting up the slope from a large, copper-rich, transported gossan, located on the south slope of Chu Chua Mountain. Subsequently, various mining companies have owned the property, carrying out several



drilling programs between the late 1980s and early 1990s of the last century, the most recent being Inmet Mining Corporation. Resources of approximately 5 million tons of sulphide grading 1.5% copper with some zinc, gold, and silver eventually were outlined, but the deposit has never been put into production.

The research done on the Chu Chua deposit is a part of a lithogeochemical study of a group of mafic-hosted volcanogenic massive sulfide deposits. Their lithogeochemical characteristics were studied using various techniques, but with an emphasis on Pearce Element Ratio (PER) analysis (Pearce, 1968). The goal was to test the applicability of molar ratio analysis for quantitative characterization of alteration related to volcanogenic massive-sulphide mineralization in predominantly mafic rocks.

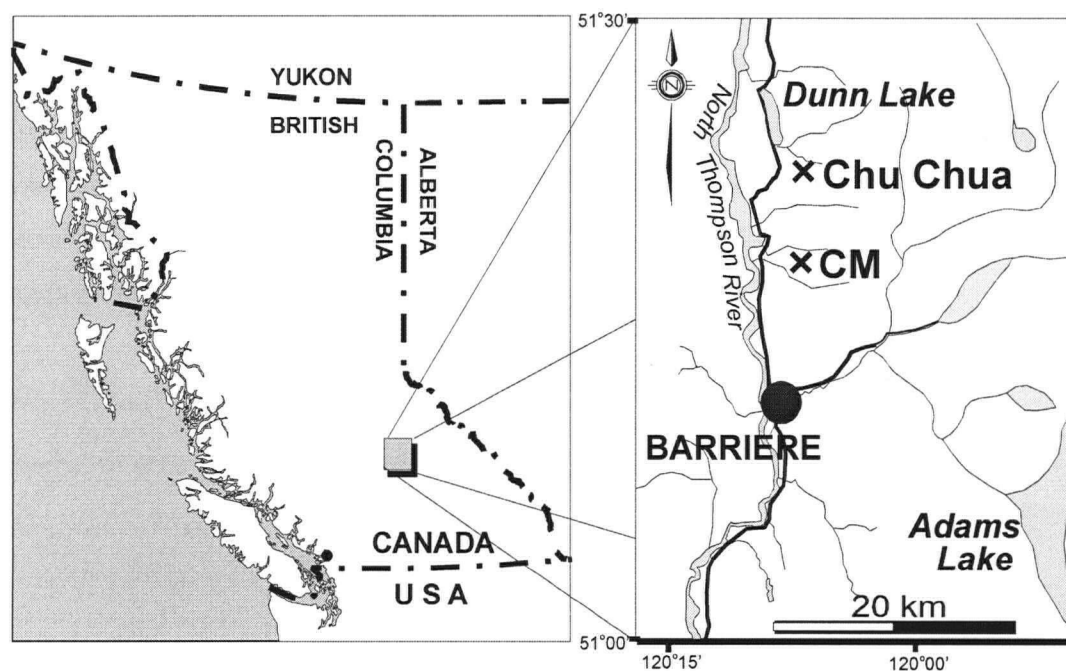


Fig. 3.1. Location of the Chu Chua deposit, British Columbia

## Geologic setting

### *Regional geology*

The area of study is on the western edge of the Omineca Belt, eastern British Columbia, and is underlain by the Upper Paleozoic Fennel Formation of the Slide Mountain Terrane (Wheeler *et al.*, 1991). To the west, a faulted contact, coinciding with the North Thompson

River valley, separates the Fennel Formation from the younger Nicola and Cache Creek groups. To the east, the Fennel Formation borders on the Eagle Bay Formation of the Kootenay terrane. The latter comprises metamorphosed clastic sedimentary rocks and subordinate volcanic rocks and limestones. Stratigraphic and age relationships of the two formations, as interpreted by various authors (*e.g.*, Campbell and Tipper, 1971; Campbell and Okulitch, 1976; Preto, 1979), are controversial. The latest study (Preto and Shiarizza, 1982), involving zircon age dating and paleontological evidence, suggests that the Fennel Formation is partly coeval with, and partly overlies the Eagle Bay Formation.

The Fennel Formation lithologically resembles and correlates with the Antler Formation of the Slide Mountain terrane, occurring about 100 km to the north and overlying Early Mississippian rocks. Both formations underlie Karnian shales and limestones. Thus, the inferred age of the Fennel Formation rocks is post-Early Mississippian and pre-early Triassic (Campbell and Tipper, 1971). Two large granitic bodies of Cretaceous age, the Baldy and Raft batholiths, intrude the Paleozoic rocks north of the Chu Chua deposit.

The upper (western) division of the Fennel Formation consists almost entirely of pillowed and massive basalt flows with minor amounts of bedded chert and gabbro. The intrusive and extrusive mafic igneous rocks have tholeiitic chemistry and locally contain microphenocrysts of kaersutite (Aggarwal *et al.* 1984). The same authors interpret these rocks to be oceanic island basalts. Both the Chinook Mountain prospect and the Chu Chua deposit are within the upper structural division of the Fennel Formation, not far above the transition zone.

A structurally lower division, occurring to the east, comprises a heterogeneous assemblage of bedded chert, gabbro, gabbroic dikes and sills, pillow basalt, clastic sediments, quartz-feldspar porphyritic rhyolite, and intraformational conglomerate. Rocks of this division are in direct contact with Eagle Bay rocks and are referred to as "transitional zone" by some authors (*e.g.*, McMillan, 1979). Field observations of pillow lavas and clast composition of intraformational conglomerates suggest the existence of a tight, antiformal fold, developed within the Fennel Formation.

### ***Local Geology***

In the vicinity of Chu Chua and Chinook mountains, bedrock consists of pillowed basalt flows interbedded with argillite and chert. Dioritic and gabbroic sills and dikes intrude the lowermost units in the area. The rocks are metamorphosed to greenschist grade based on the mineral assemblage. Basalts are pale to dark green, fine grained, with pillowed varieties occurring locally.

The primary minerals in the tholeiite basalts (Plate 3.2) are augite and plagioclase. Augite occurs most commonly as microphenocrysts, in some cases as larger phenocrysts (up to 1mm), typically making up about 25% of the rock volume. Plagioclase is almost entirely converted to albite and is saussuritised. The matrix is replaced by scattered epidote and zoisite, patches of carbonate and abundant chlorite. Titanomagnetite and kaersutite, although rare, also occur as porphyritic phases in the Fennel basalts. Olivine and orthopyroxene are not observed in this study and earlier were reported as “scarce or absent” (Aggarwal, 1982).

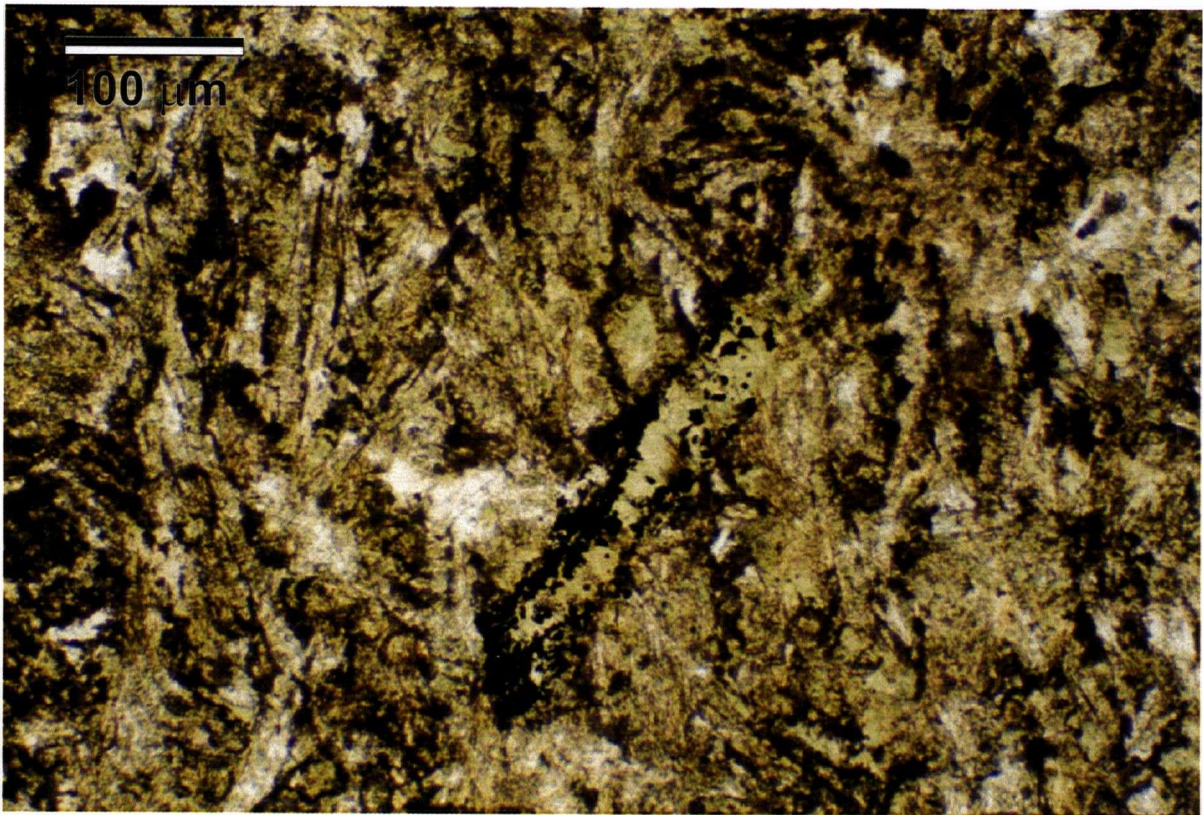


Plate 3.2. Photomicrograph of chloritised basalt from the host rocks to the Chu Chua VHMS showing (sample No. HS952035). Plane polarized light.

Greenschist metamorphism of the host rocks resulted in the alteration of augite to actinolite and chlorite. Plagioclase is albitized to a significant degree. Kaersutite and titanomagnetite are altered to rutile, titanite, and hematite. The groundmass is mostly replaced by actinolite, chlorite, albite, quartz and calcite. In some samples, sericite developed pervasively in the groundmass. These metamorphic phases overprint syn- or post-depositional hydrothermal alteration. Veins, although relatively thin (typically up to 3 mm) are common to very abundant (up to 10% of the rock volume) and are associated with brecciation and pillow margins. At least two generations of veins are observed, the first consisting of chlorite, zoisite, and quartz and the second of quartz and calcite.

Siliceous rocks are ubiquitous in the vicinity of the massive sulphide deposit. They occur as a wedge-shaped accumulation of significant thickness (Fig. 3.4), together with pillowed basalt flows and hyaloclastite. The morphology of the deposit is attributable to deposition in a graben depression, deepening to the north. An interpretation of these rocks as impure bedded chert is based on textural evidence (centimetre-scale bedding, Plate 3.4; peperitic textures, Plate 3.6) and on a comparison of their trace element signatures with those of other siliceous rocks, utilizing published data (Thurstun, 1972; Migdisov *et.al.*, 1983; Varentsov *et al.* 1983; Jarvis, 1985; MacLean and Kranidiotis, 1987; Barrett *et al.* 1991; Robinson *et al.* 1994; Barrie, pers. comm.). Alkali concentrations, attributable to a feldspar component, suggest the possibility that the impurities may be of tuffaceous origin. The rock is made up almost entirely of fine-grained quartz and minor sericite (Plate 3.3.a.), commonly defining weak schistosity. The unit displays rhythmic layering, defined by impurities and argillaceous partings (Plate 3.4). Euhedral pyrite and authigenic carbonate crystals occur locally in the siliceous rocks. Carbonate crystals have Ca-rich rhombic cores overgrown by ferromagnesian carbonate (Plate 3.5). The overgrowths occurred either as a typical diagenetic process (Hesse, 1986), or as a result of enhanced chemical activity of Fe and Mg in the vicinity of an actively venting hydrothermal system.

A monzonite porphyry dike cross-cuts the volcanic rocks and chert at the northern end of the deposit. It is feldspar and amphibole phyrlic and contains coarse, euhedral pyrite crystals.



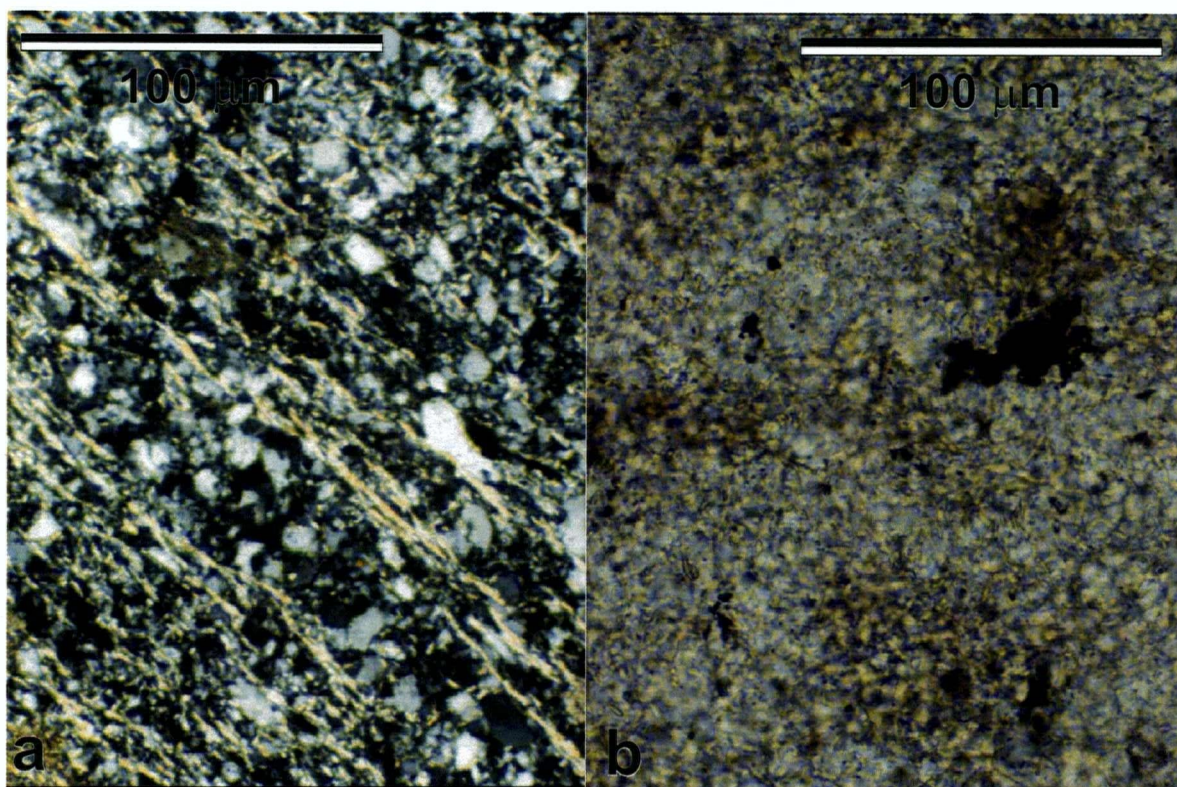


Plate 3.3. Photomicrograph of microcrystalline chert from the wall rocks of the Chu Chua VHMS showing (sample No. HS952025).

- a) Weak schistosity defined by muscovite. Cross polarised light
- b) Patchy chloritization. Plane polarised light



Plate 3.4. Polished slab of bedded chert with rhythmic layering defined by argillaceous partings with pyrite. Sample No. HS952086, hanging wall of the Chu Chua VHMS showing.



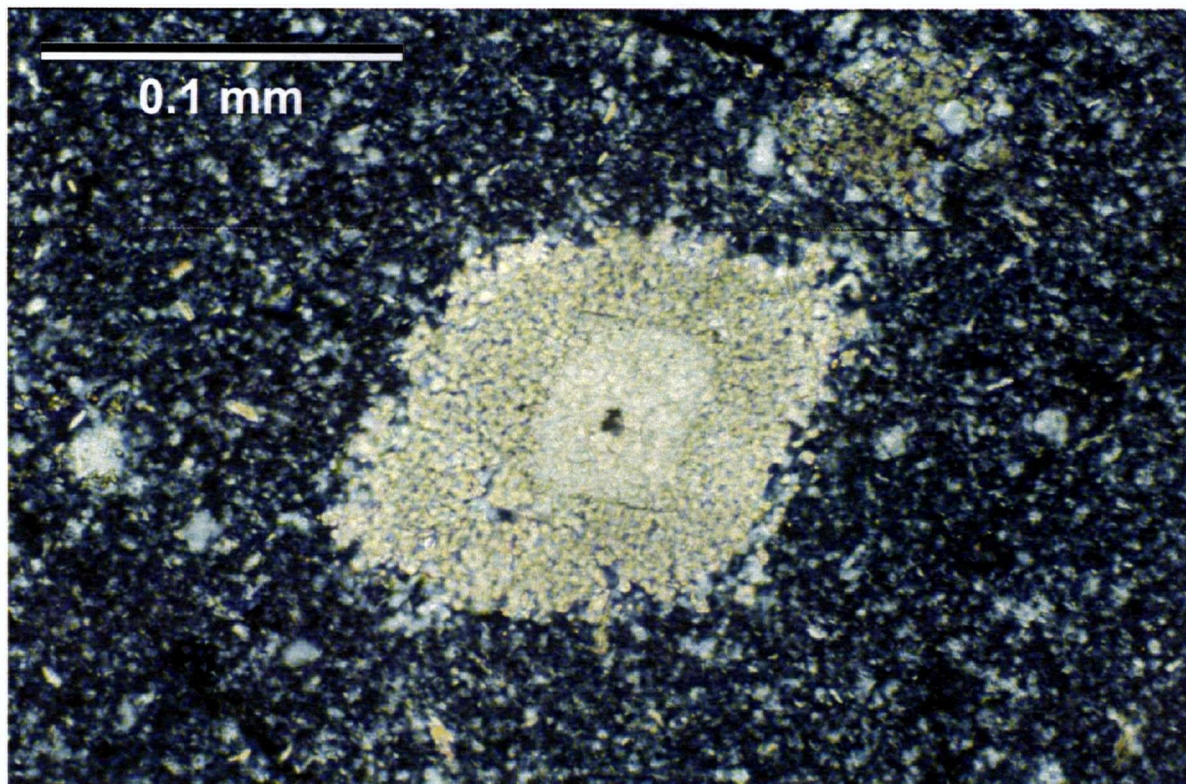


Plate 3.5. Photomicrograph of authigenic carbonate in chert from the hanging wall to the Chu Chua VHMS showing (sample No. HS952080). Cross polarised light. Diagenetic euhedral calcite is overgrown by Fe-Mg carbonate.

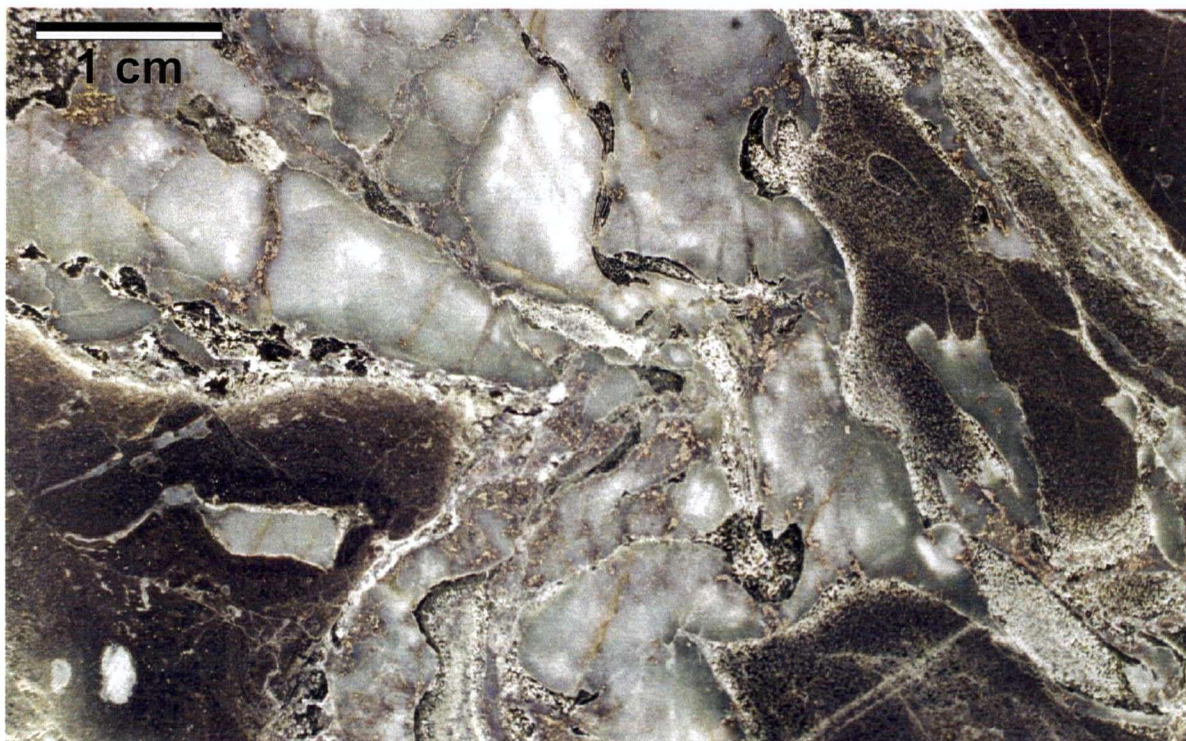


Plate 3.6. Polished slab of basalt disrupting soft siliceous sediment resulting in a peperitic texture (sample No. HS951071, hanging wall of the Chu Chua VHMS showing). Pyrrhotite mineralization occurs in the form of veinlets and disseminations.

## *Structure*

Very little structural information is available on the Fennel Formation, either with respect to its boundaries or its internal character. The large North Thompson River fault zone is the only well-established structure in the area, marking the upper boundary of the Fennel Formation with the younger Nicola and Cache Creek volcanic rocks. Little is known about the structural relations between the Fennel and the Eagle Bay formations. The boundary between them is either gradational or faulted.

Bedding of the basalt flows hosting the massive-sulphide deposit strikes approximately north-south and dips at  $60^{\circ}$ - $90^{\circ}$  to the west, so that the contemporary erosion surface represents an almost perfect cross section through the deposit. A tight anticline is considered to exist, just to the east of the Chu Chua deposit. Its recognition is based on opposing dips of the mostly volcanic stratigraphy. Stratigraphic tops were determined by means of pillow lava textures, as well as clast-size gradation in intraformational conglomerates (Preto, 1979). Thus, the Chu Chua deposit is hosted in the steeply to vertically dipping west limb of the anticline and the mineralised layer is structurally repeated a short distance to the east.

On a smaller scale, in the immediate vicinity of the deposit, the existence of a north-dipping normal fault is suggested (this study) by the spatial distribution of basalt and chert (Fig. 3.4.). The exact orientation of the fault plane could not be measured, because it has not been observed directly, but it dips generally to the north-west (Fig. 3.4). The reconstructed original dip direction of the fault at the time of deposition of the overlying lava flows was towards the north-east. The fault defines a half-graben (Fig. 3.4.) containing an accumulation of chert, basaltic flows, and hyaloclastite. The few extremely metasomatized samples were collected from the immediate hanging wall of the normal fault and the two sulphide lenses of the Chu Chua deposit extend from that location into the graben. This evidence is consistent with the interpretation of the fault as the main conduit for the mineralizing fluids.



## ***Metallogeny***

The volcanic and clastic metasedimentary rocks of the Eagle Bay and Fennel formations contain numerous hypogene, base- and precious metal deposits and showings of several types. Three volcanogenic massive-sulphide deposits occur at Chu Chua, Chinook Mountain (CM), and Harper Creek. The first two are located in greenstones of the Fennel Formation, whereas the Harper Creek deposit is hosted by the Eagle Bay Formation. All three are copper-rich, with subordinate zinc, silver, and low gold values. More massive-sulphide occurrences (several showings in the areas of Birk Creek and North Barriere Lake) are found in schists belonging to the Eagle Bay Formation. The deposits are stratabound and mostly Pb-Zn rich. However, relation to a volcanic or other igneous event has not been established.

High-grade gold mineralization associated with cross-cutting quartz veins and mineralized shear zones occur in the Fennel Formation, a few kilometres to the North of the Chu Chua deposit where the Windpass, Gold Hill and Sweet Home properties were mined briefly in the first half of the twentieth century. Skarns associated with the Cretaceous granitic intrusions, contain notable Cu, Pb, Zn, Ag, and Ni.

## ***Mineralization***

Although the sulphide mineralization is not the main focus of this study, some of its features are important in characterising the hydrothermal system responsible for the mineralization and alteration of host rocks. The description here is based on published data (McMillan, 1979), as well as on observation of drill core during sampling of the host rocks.

Chu Chua deposit consists of two large, parallel and elongate massive-sulphide lenses and a number of smaller sulphide zones. The two large zones, with strike lengths of approximately 400 and 200 m and up to 20 m thick, are apparently stratabound and arranged *en echelon*. They dip steeply to the west and, judging by the metal grades, their long axes plunge to the south. Two magnetite lenses of comparable size and similar geometry occur immediately adjacent to the sulphide lenses. The massive sulphides and magnetite are enclosed in an



asymmetric envelope of chert and volcanic rocks. Chert occurs more commonly in the hanging wall (to the west), whereas footwall alteration of host rocks is recognised at a distance of 5 to 25 m to the east. Visible alteration is defined by pervasive bleaching, silicification, and chloritization of basalt and by dense carbonate veining (up to 10%). Locally, talc occurs in extremely altered parts of the sequence.

The ore bodies consist of pyrite with several percent chalcopyrite and a minor amount of sphalerite. Chalcopyrite is interstitial to the pyrite grains or, together with quartz, carbonate, chlorite, pyrite, pyrrhotite, and sphalerite, occurs in veins cross-cutting altered volcanic rocks, chert, and massive-sulphide ore. Galena is rare and molybdenite is reported to occur in a single locality (McMillan, 1979). Layering of the sulphide is uncommon, but where it occurs, is defined either by thin chalcopyrite seams or variations in coarseness of pyrite grains. A crude pattern of distribution of the sulphides is recognised in the ore bodies (McMillan, 1979). Sphalerite is enriched in the stratigraphically higher portions of the ore bodies and in their peripheries. Increase in the Zn/Cu ratio of the main ore body with depth, as well as decrease of the overall ore grade and continuity suggests that deeper mineralization is further from the hydrothermal feeder zone.

## **Lithogeochemistry**

### ***Sampling and analytical quality control***

One hundred and fifteen samples, approximately 1 kg each, were collected from drill core in 1995 and 1997 from 25 drill holes at the Chu Chua copper massive sulphide deposit. Unfortunately, drilling was done mostly from the hanging wall and thus the presumably altered footwall is under-represented in the data set (Appendix 3). The sampled rocks consist of basalt and fine-grained gabbroic rocks, both altered to varying degrees and metamorphosed to greenschist grade, chert and a rhyolite dike (1 sample). Both unaltered rocks and all visibly distinguishable types of alteration were sampled so that alteration could be characterised taking into account the background variability of the host rocks.

Samples were analysed by X-Ray Fluorescence Spectrometry for the major oxides ( $\text{SiO}_2$ ,  $\text{TiO}_2$ ,  $\text{Al}_2\text{O}_3$ , total Fe as  $\text{Fe}_2\text{O}_3^T$ ,  $\text{MgO}$ ,  $\text{MnO}$ ,  $\text{CaO}$ ,  $\text{Na}_2\text{O}$ ,  $\text{K}_2\text{O}$  and  $\text{P}_2\text{O}_5$ ), a set of 6 trace elements (Ba, Rb, Sr, Y, Zr and Nb). Fused Li-tetraborate discs were used for the major oxides and pressed pellets for the trace element determinations. Wet chemistry, gravimetric and other methods were used for the determination of  $\text{H}_2\text{O}^+$ ,  $\text{CO}_2$ , total S, FeO and T.O.C. (total organic carbon). Sample preparation and analytical work was done by X-ray Assay Laboratories (XRAL) in Don Mills, Ontario. Details of the sample preparation and analysis are presented in Appendix 3.

The analytical quality control procedure accepted for the Lithogeochemical Exploration Research Project of MDRU (Sinclair and Stanley, 1995, Stanley, 1997a) was applied to the analytical results acquired for this study. The relative errors of the analyses are estimated based on replicate analyses of internal MDRU standards, submitted together with the lithogeochemical samples. Absolute and relative error terms and effective detection limits were determined using the THPLOT Matlab function (Stanley, 1997b; Appendix 4, Table A4.1). Analytical errors (precision) of the analyses is quoted as the departure (one standard deviation) from the accepted values of the internal MDRU standards (Appendix 4, Table A4.2; Stanley, 1997a). Because the MDRU reference materials were prepared for analysis separate from the samples, pulp duplicates were submitted with the analytical batch to assess any errors introduced in this phase (Table A4.3). It was established that analytical errors calculated for the pulp duplicates do not differ substantially from those for the MDRU reference materials.

Lithogeochemical analyses for an additional 533 samples, donated by Inmet Mining Corporation, were used to augment the original data, bringing the total number of chemically analysed samples from the Chu Chua deposit to 647 from 79 drillholes. The additional data were obtained also by X-ray fluorescence analysis, but information about the laboratory procedure and analytical precision was not available. However, based on a comparison between typical concentrations of potentially immobile oxide components ( $\text{TiO}_2$ ,  $\text{Al}_2\text{O}_3$ , Zr, and Y) in the Inmet and original data sets, the quality of the former is thought to be

comparable to the original data. Samples of the two donated data sets were not analysed for  $\text{H}_2\text{O}^+$ ,  $\text{CO}_2$ , total S, FeO and T.O.C., which limits their usefulness.

Lithogeochemical data from 221 samples from the neighbouring Chinook Mountain property were acquired from Inco Ltd. They were used in a comparative study of the two properties. No information was available concerning the analytical laboratory, where the analyses were performed, the analytical method or level of analytical precision of these data. The samples were analysed in three separate batches several years apart. Serious differences in average concentrations of some elements (e.g., Zr, Y) are apparent in the data set. For this reason, use of the Chinook Mountain data in this study was limited.

### ***Conserved elements and REE***

Identification of conserved elements involves examination of binary plots of potentially immobile elements and is a prerequisite for the application of PER analysis (see section “conserved elements” in Chapter 2). A conserved element must be identified for use as a denominator in the Pearce element ratios. Conserved elements are also used to test the cogenetic character of rocks and group them accordingly. The conserved elements used in this analysis are Al ( $\text{Al}_2\text{O}_3$ ), Ti ( $\text{TiO}_2$ ), Zr, and Y. The donated data set does not include analytical data for Zr and Y, which in the original data set display high analytical errors (Appendix 4). For these two reasons, higher significance is attached to Al and Ti.

The conserved element analysis of Chu Chua samples (Fig. 3.2 and Fig. 3.3a, b) identifies two large groups, representing the two prevalent types of rocks, occurring in the area of the deposit: impure chert and basalt. For most samples, corresponding data points lie within two standard deviations from lines passing through the origin. Thus the hypothesis that samples belonging to each group are cogenetic is not disproved, justifying the application of PER analysis separately for the cherty and basaltic samples. Similar logic leads to the assumption that the tested elements were conserved in all material transfer processes during the history of the rocks. Exceptions to this are a few basaltic samples, for which  $\text{TiO}_2/\text{Al}_2\text{O}_3$  ratios differ from the median ratio of the group by more than 2 standard deviations of analytical errors.

## Conserved element test on data from Chu Chua

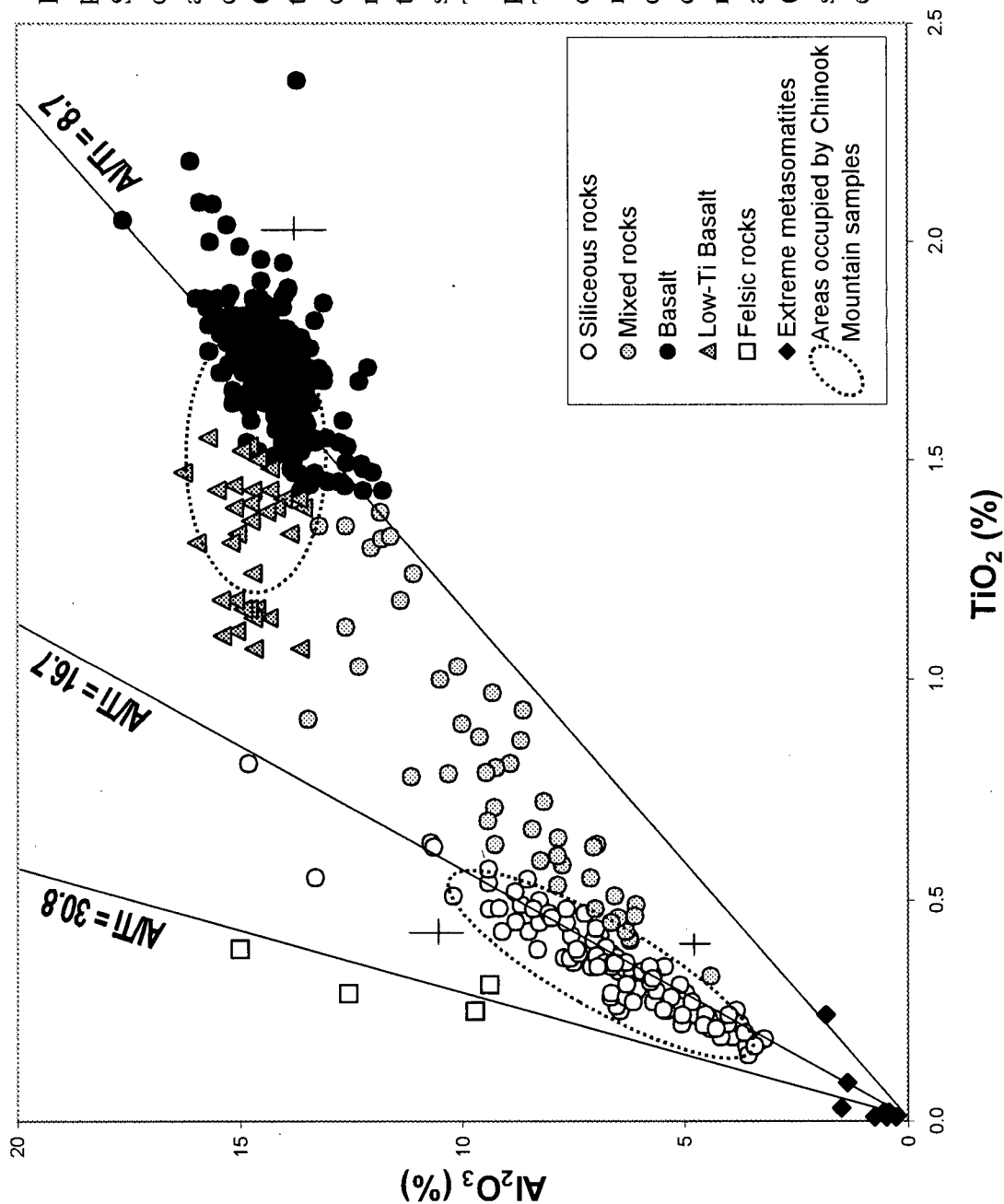


Fig. 3.2. Conserved element plot of  $\text{TiO}_2$  vs.  $\text{Al}_2\text{O}_3$ . Siliceous rocks of sedimentary or volcano-sedimentary origin and basalts plot as distinct clusters, identical to rocks from Chinook Mountain with respect to  $\text{Al}_2\text{O}_3$  and  $\text{TiO}_2$  concentrations. Physical mixtures between the two main types of rocks occur broadly. A spatially distinct (Fig. 3.4), low Ti basalt is distinguished on this plot. Felsic rocks have lower  $\text{TiO}_2$  and higher  $\text{Al}_2\text{O}_3$  concentrations than siliceous rocks. A group of samples display strong mass gain and correspond to the magnetite-talc metasomatites occurring in association with the ore bodies. Crosses correspond to two standard deviations of analytical errors (Appendix 4).

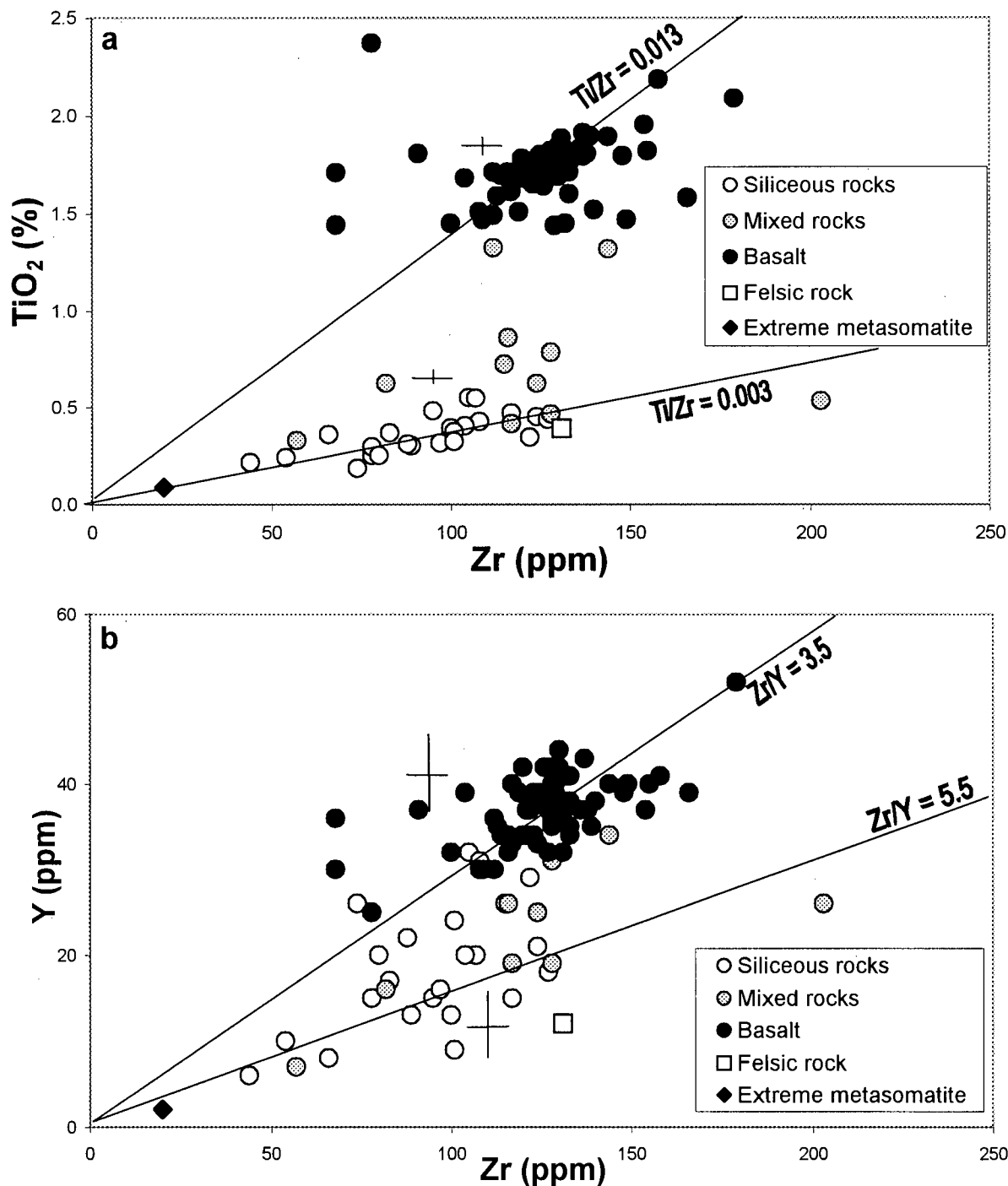


Fig. 3.3. Conserved element plots of (a) Zr vs. TiO<sub>2</sub> and (b) Zr vs. Y. Low-Ti basalt, and most of the extremely metasomatized samples and felsic rocks are not represented on these diagrams. The distinction between basalts and siliceous sedimentary or volcano-sedimentary rocks (Fig.3.2) is persistent. Zr/Y ratio of basalts is indicative of tholeiitic affinity. Crosses correspond to 2 standard deviations of analytical errors.

They all occur within a close distance of the deposit and alteration possibly has mobilized  $\text{Al}_2\text{O}_3$  and/or  $\text{TiO}_2$  or they represent a basalt of different composition. Because they do not fulfil the condition for a conserved element, they are excluded from the following PER analysis.

A subgroup of the basaltic rocks displays significantly lower Ti concentrations than the main group, whereas their aluminium concentrations are similar or slightly higher. They are further referred to as low-Ti basalt to distinguish them from the main group of basalt. Their spatial location is also distinct (Fig. 3.4), leading to the conclusion that they represent a chemically discrete stratigraphic level within the volcanic succession, having its base approximately 250 m stratigraphically above the mineralised layer. The low-Ti basalt is also slightly more siliceous and display a broader background variability of major-element concentrations (Fig. 3.2 and Fig. 3.5) compared with the more common basalt.

A relatively large group of samples lie on a mixing line between the two main groups and represents either physically mixed rocks or samples that include intervals of both basalt and chert. Physical mixing is commonly observed in hand specimens as hyaloclastite immersed in chert, siliceous rims around basaltic pillows and peperitic textures (Plate 3.6). Mixing is a specific type of physical mass transfer process in which proportions of elements depend on mixing ratios between end members and thus all elements are mobile. For that reason the mixed samples are not considered in PER analysis.

The majority of the basaltic rocks have constant immobile element ratios. The Zr/Y ratio for the main cluster of data points is approximately 3.5, which is characteristic of tholeiitic rocks (Barrett and MacLean, 1994), a conclusion about the Fennel Formation basalts consistent with other geochemical criteria (Aggarwal, 1982). Ti/V ratios between 20 and 50 suggest mid-ocean ridge (MORB) or backarc origin (Shervais, 1982).

Felsic igneous rocks are scarce at Chu Chua, represented by only 4 samples (less than 1%, Appendix 3). Their composition, apart from  $\text{SiO}_2$  concentration, is distinct from that of the

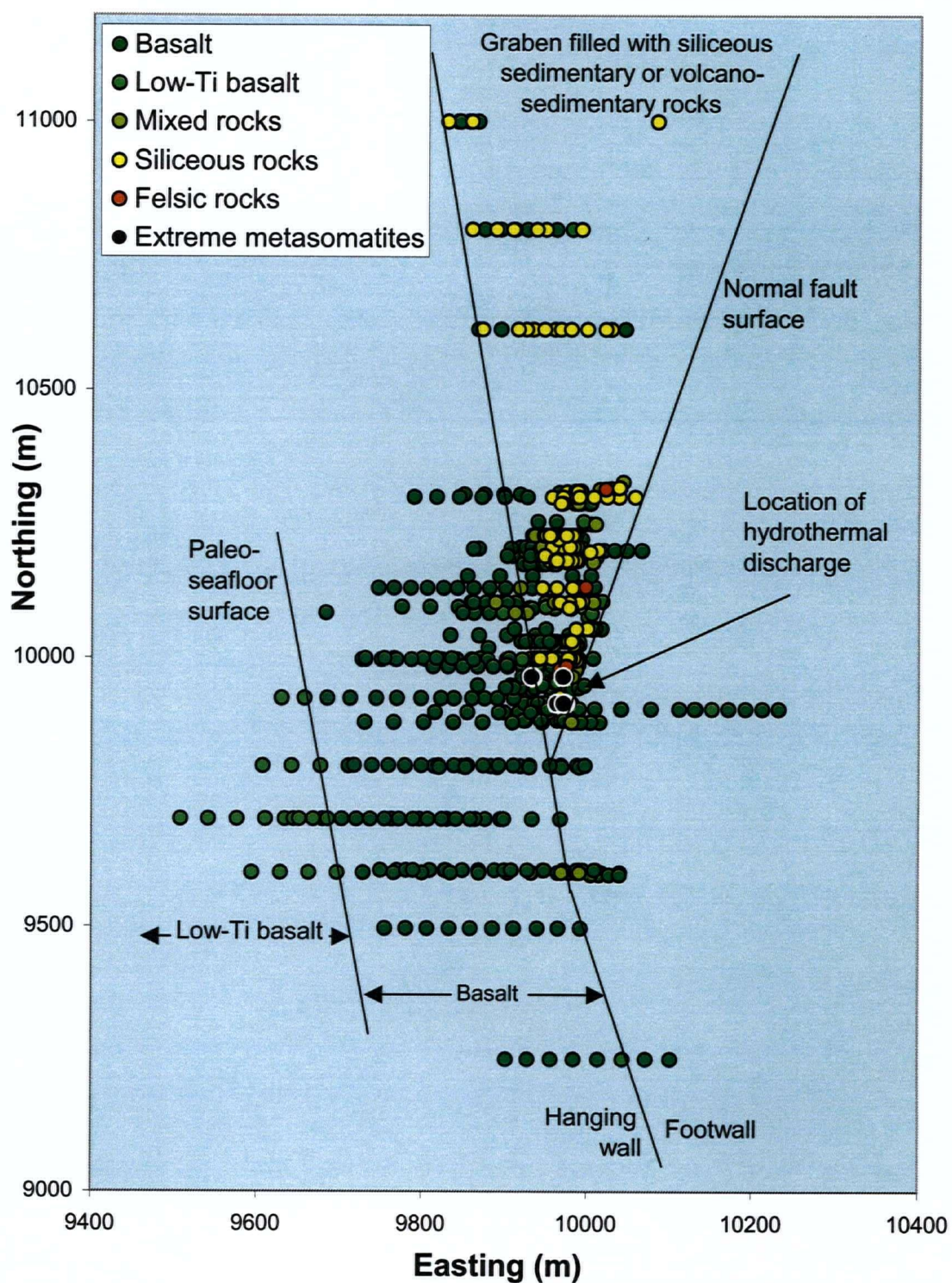


Fig. 3.4. Spatial position of the various sampled rock types and a geological interpretation. The geological boundaries are drawn according to geochemistry of samples as depicted by the  $\text{Al}_2\text{O}_3$  vs.  $\text{TiO}_2$  plot (Fig.3.2).



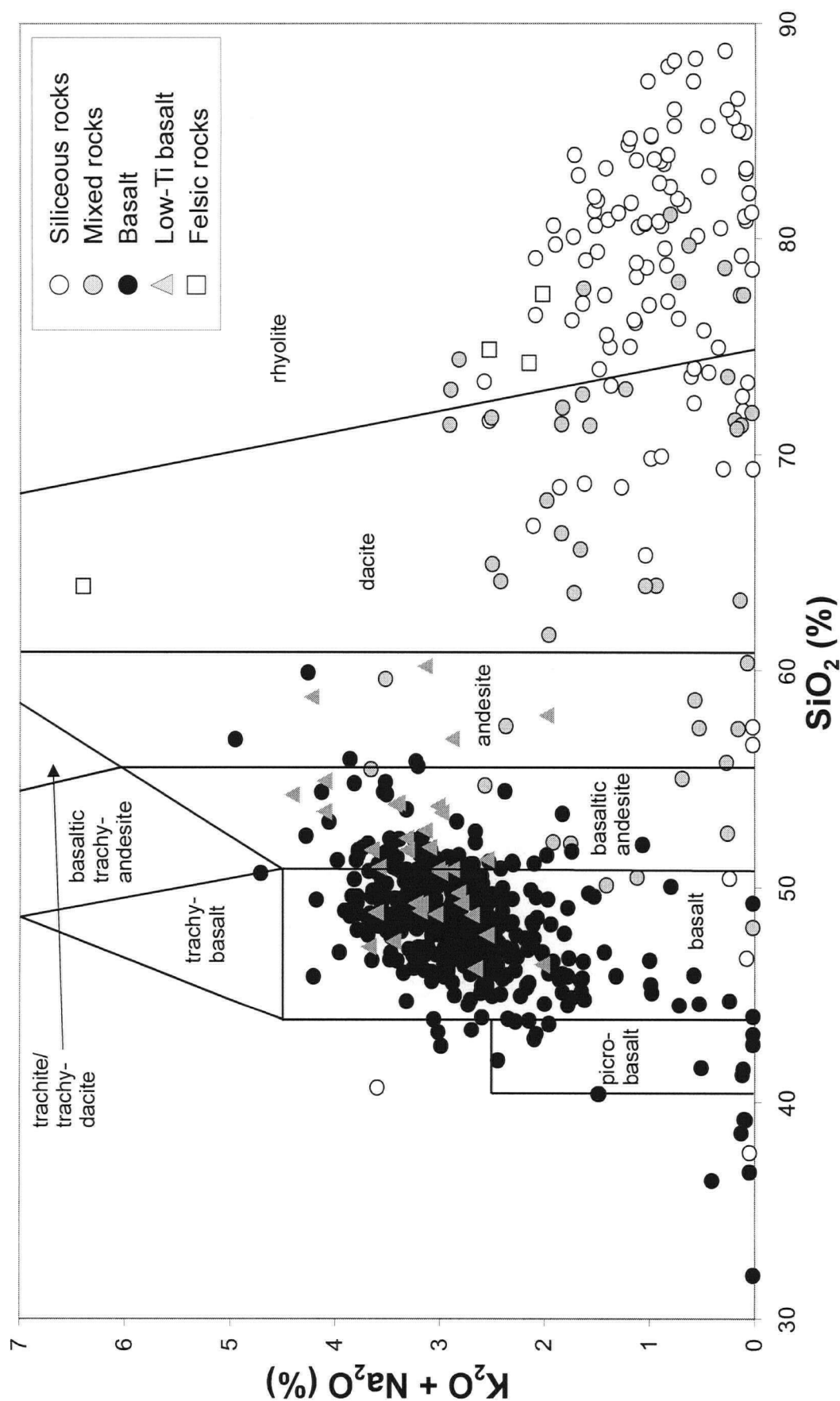


Fig. 3.5. Total alkalis vs. silica diagram (Le Maitre *et al.*, 1989): Basaltic rocks from Chu Chua truly fall in the field of basalts, while low-Ti basalts plot partially in the field of basaltic andesite and even andesite.

Felsic rocks are rhyolitic in composition and one sample is almost monzonitic. Siliceous rocks are sufficiently more siliceous than rhyolites. A number of samples, display significant to complete loss of alkalis.



banded chert, allowing for their discrimination purely on geochemical grounds. They have higher  $\text{Al}_2\text{O}_3/\text{TiO}_2$  ratio (Fig. 3.2) and Ca, Na and K concentrations than the chert and plot as rhyolite or dacite on the total alkalis versus  $\text{SiO}_2$  (TAS) diagram (Fig. 3.5). One of the samples, identified microscopically as a K-feldspar-phyric dacite, is significantly more alkalic than the remaining three. The latter belong to the donated data set and, thus, no samples were

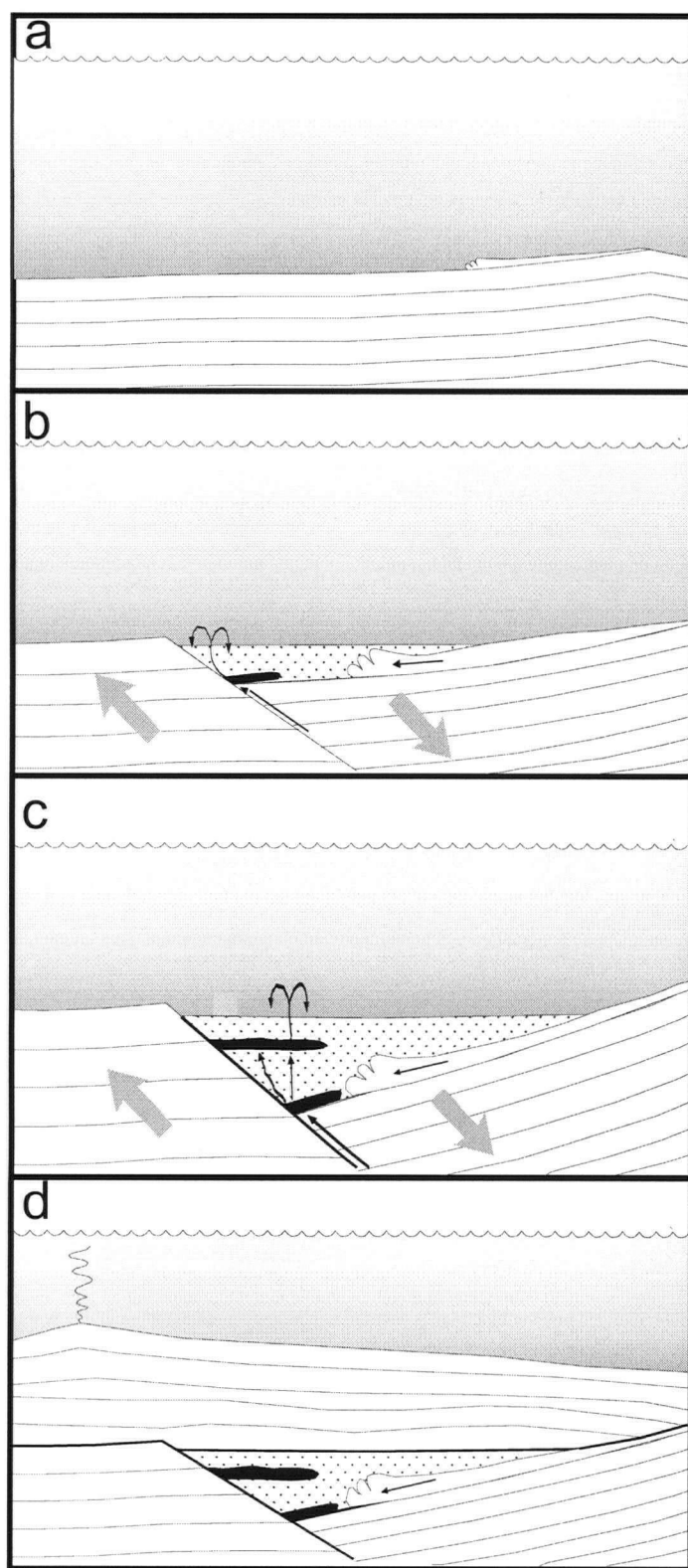
available to examine petrographically, but their chemical compositions are transitional between dacite and rhyolite. Judging by their sparse occurrence and the texture of the single sample available for examination, they represent small hypabyssal bodies such as dikes or sills. All felsic rocks occur close to the sulphide ore bodies and define a line parallel, or possibly coinciding with the sloping surface of the chert-filled paleo-graben depression.

Several strongly metasomatized samples display extreme mass gain (*i.e.*, plot close to the origin of Fig. 3.2). Judging by the ratios of the immobile elements, their protoliths belonged to different rock types, but current chemical compositions can be described largely by a set of four elements: Fe, Mg, Si, and S. The strongly metasomatized samples correspond to the magnetite-talc-pyrite “lodes” described above (MacMillan, 1979). They all occur in a small area in the immediate footwall of the sulphide bodies. With respect to structure, they are associated with the very edge of the paleo-graben defined above.

$\text{TiO}_2$  is used here as a denominator for the Pearce Element Ratios, because of its low analytical error (Appendix 4) and the fact that Ti analysis is available for all 647 samples from Chu Chua.

### **Interpretation of the property-scale geology based on geochemistry**

Distinction of rock types and subtypes based mostly on  $\text{Al}_2\text{O}_3$  and Zr concentrations allows for an interpretation of the immediate geological setting of the deposit. This is facilitated by the fact that lava beds dip steeply to vertically and thus, the erosion surface represents an almost perfect cross section of the stratigraphy. Two basaltic units are distinguished, based



a. Submarine deposition of tholeiitic basaltic flows in a MOR or back arc spreading environment.

b. Faulting of the volcanic pile as a result of extensional tectonics. Seafloor hydrothermal plume carries silica and metal sulphides into the graben. Peperite forms as a result of interaction of basaltic lava flows and the soft siliceous sediment filling the graben.

c. As the graben deepens, more siliceous sediment is deposited and new sulphide bodies of metal sulphides form at higher stratigraphic levels. New lava flows are intruded in the soft sediment, producing peperitic textures. Felsic magmatism taking place in the graben is not shown on the diagram.

d. A new volcanic centre spills basaltic lava flows of a similar but distinct (low Zr) composition, sealing the graben.

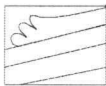
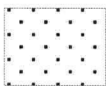

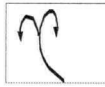
-  Submarine basaltic lava flows
-  Graben fill (impure banded chert, basalt, peperite)
-  Sulphide ore body
-  Hydrothermal solutions

Fig.3.6. Interpretation of the deposit scale geology, based on spatial distribution of rock types as defined by chemical composition.

on Zr and to a lesser extent on SiO<sub>2</sub> concentrations (Figs. 3.3 and 3.5). The boundary between the two units (Fig. 3.4) is to the west of the deposit and defines a relatively straight line on the erosion surface, coinciding with the lineations defined by the stratigraphy (lava flow surfaces). The low-Zr basaltic unit is interpreted to conformably overlie the sulphide-bearing basaltic unit and the boundary between the two basalts is, thus, a paleo-seafloor surface, subhorizontal at the time of lava deposition.

Further east, within the lower basaltic unit, lies the most prominent feature of the local geology: a normal fault, defining the edge of a graben (or half-graben). The graben itself has a wedge shape in cross section and is the site of all of the sampled siliceous sedimentary rocks. The sediments deposited and preserved in the graben were intruded by basaltic rocks, which is evidenced by the observed peperitic textures (Plate 3.6). Small felsic bodies also occur in the graben, indicating the bimodal nature of the magmatism in the area. The ore bodies are in the shape of two large and several small lenses subparallel to the paleo-seafloor. The ore bodies are situated *en echelon* down the normal fault, which can be attributed to their formation during distinct and successive time intervals and with intermittent movements along the normal fault. A group of extremely altered rocks (mass gain of Fe and Mg, mass loss of alkali and SiO<sub>2</sub>) occur at the edge of the graben and in the footwall of the sulphide bodies. The paleo-seafloor, away from the graben, is marked by several mixed (basalt and siliceous rocks) samples.

The deposition of siliceous exhalites in the graben is interpreted as an extensive manifestation of seafloor hydrothermal activity that was also responsible for the observed wall-rock alteration and the deposition of the sulphide bodies. The normal fault, defining the graben (or half-graben) depression was the focus of the hydrothermal activity and also of a small volume of felsic magmatism.

### **REE abundances**

Samples from the Chinook Mountain property (Appendix 3), approximately 10 km to the south in similar stratigraphy, show identical geochemical patterns with respect to the two

main rock types: chert and basalt (Fig. 3.2). Availability of rare-earth-element (REE) analytical data for these rocks allows the original tectonic setting of the Fennel Formation to be constrained. REE abundances in basalt and basaltic andesites vary between 103 and 158 ppm (Table A3.4) and vary more widely in the basalt compared to the basaltic andesites. Chondrite-normalised abundance patterns (Boynnton, 1984) of these mafic units are flat and even show some light rare earth element (LREE) deficit (typically  $\text{La} / \text{Lu} = 0.8 - 1.0$ ). They are more consistent for the elements from Sm to Lu, and somewhat more variable for the light rare earths. This difference in behaviour may be attributed to the easier mobilisation of the LREE in hydrothermal processes. Based on REE data, the tectonic setting of the Fennel Formation can be interpreted as an enriched, mid-ocean, spreading ridge (MOR) or a backarc basin. This conclusion is consistent with the observed abundances of other trace elements such as Ti, V, Zr and Y, as described both in this study and by (Aggarwal, 1982), although it contradicts conclusions made by Aggarwal, based on mineralogy.

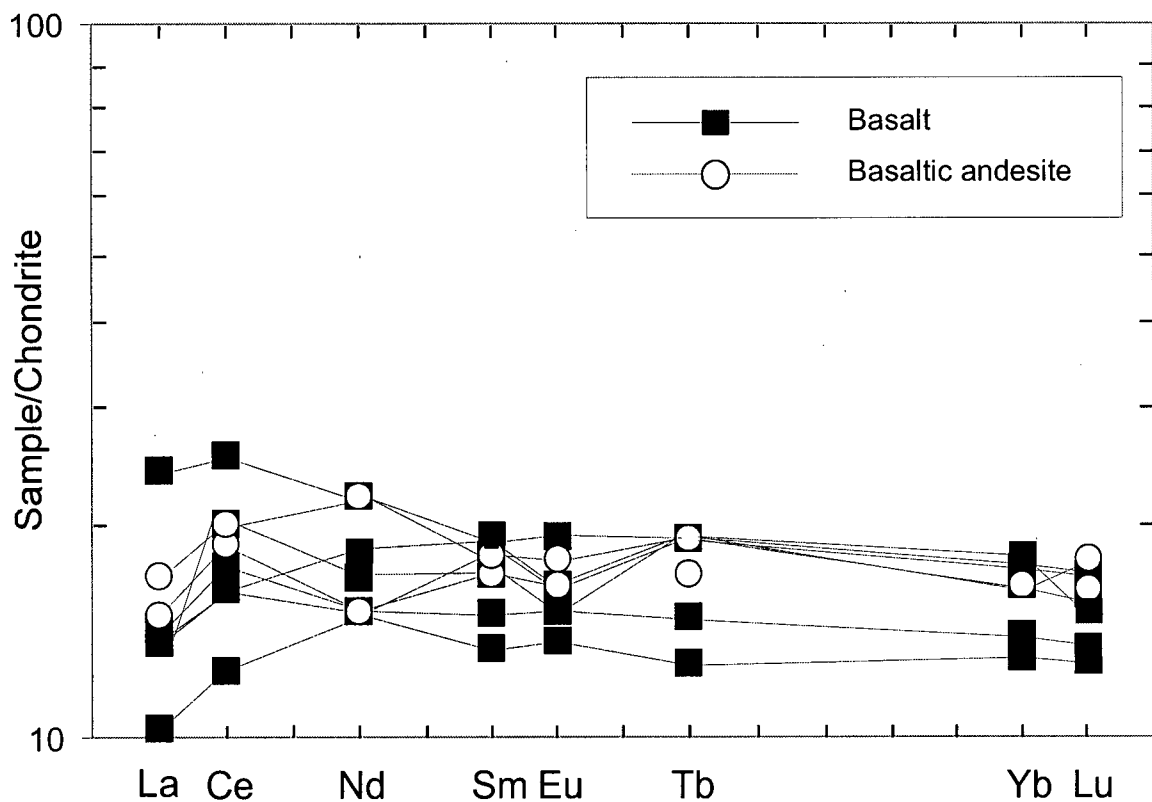


Fig.3.7. Chondrite-normalized (Boynnton, 1984) plot of REE abundances in basalts and basaltic andesites from the CM showing, measured by Neutron Activation Analysis, (Appendix 3, Table A3.4).

### ***PER analysis***

Various geological processes and artefacts are responsible for the compositional variability observed in the sampled rocks. If variations due to sampling errors, analytical errors, and closure are excluded from consideration, variability in volcanic rocks, such as those hosting the Chu Chua deposit, represents primarily igneous fractionation modified to variable degrees by hydrothermal alteration and metamorphism. Differentiating between these processes is essential, if the alteration effects on rock chemistry are to be identified and characterised. Because igneous fractionation in basaltic rocks involves a finite number of phases, it can be modelled by testing of various petrologic hypotheses. The Pearce Element Ratio Analysis used here (Pearce, 1968) is a methodology for graphical modelling of petrologic processes, which also eliminates the undesired effect of closure by utilising ratios of concentrations (Stanley, 1996). The validity of the model is judged by the correspondence between the positions of background samples data points and the model line. If the sampled rocks are cogenetic, deviation of data points from the model line indicates the effects of superimposed processes. The direction and magnitude of deviations characterise these processes.

### **Composition of fractionating phases**

Typical phases in basalt are olivine, ortho- and clinopyroxene and plagioclase, the latter expressed as a linear combination of albite and anorthite. Using simple, idealised mineral compositions for the purpose of the modelling (*i.e.*,  $\text{Ca(FeMg)Si}_2\text{O}_6$  for clinopyroxene) in most cases is sufficiently accurate. In the case of the Chu Chua basalt, however, clinopyroxene compositions differ significantly from idealised mineral stoichiometries. In order to identify the exact compositions of the fractionating phases, and thus refine the model, the rock-forming minerals were analysed by electron microprobe.

Compositions of pyroxenes from the Chu Chua basalt are centred on slightly magnesian augite (Fig. 3.8). Compositional variability of minerals can be conveniently expressed as a linear combination of a basic mineral species and a number of additive components (abstract chemical species) accounting for the element substitutions in

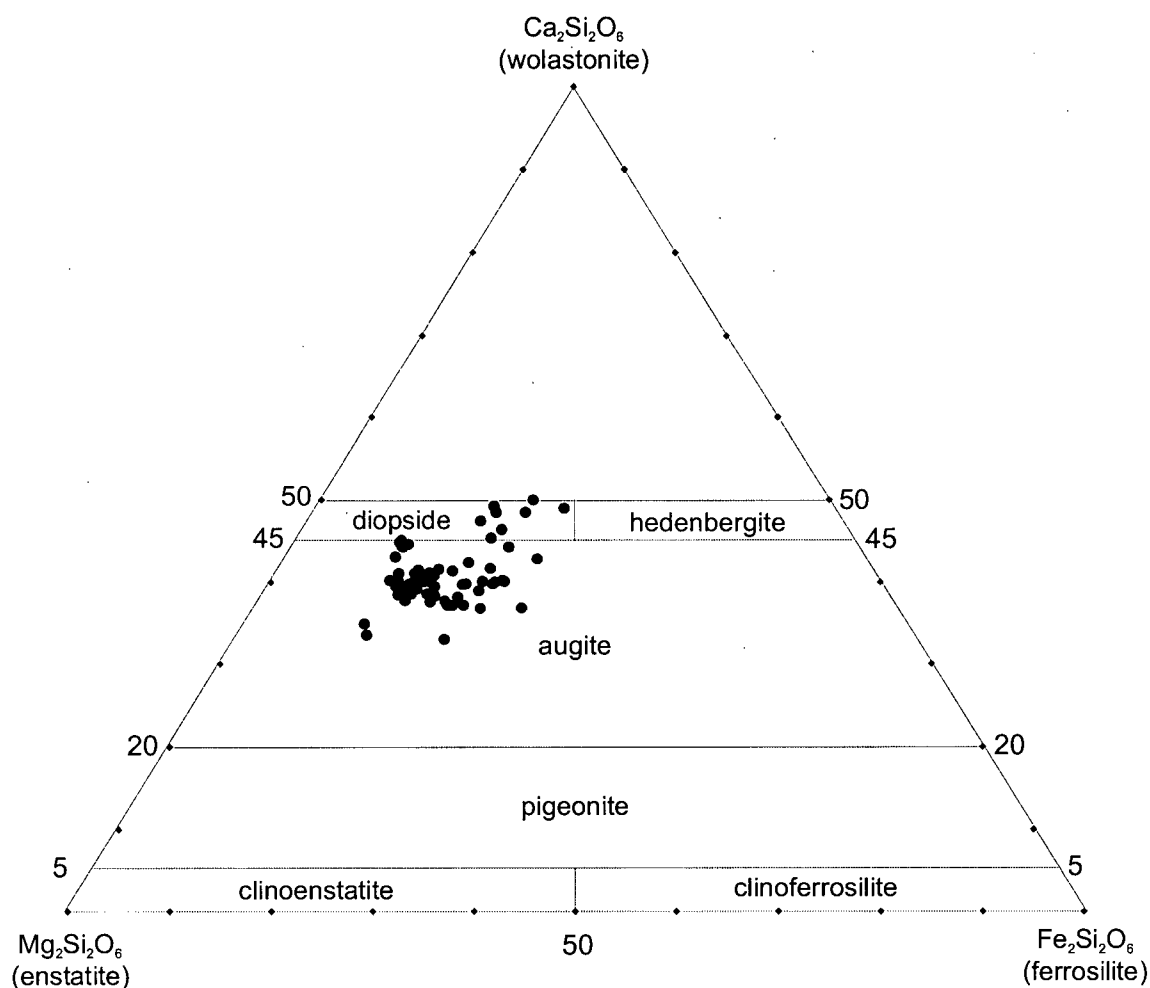


Fig.3.8. Compositions of pyroxenes from Chu Chua basalts (Composition ranges and accepted names from Morimoto, 1989).

the real mineral as compared to the idealised, basic mineral species. Major substitutions with respect to an idealised enstatite ( $\text{Mg}_2\text{Si}_2\text{O}_6$ ) formula are those of Ca and Fe for Mg. Average ratio of  $(\text{Fe}+\text{Mg})/\text{Ca}$  is approximately 5/3, deviating significantly from that of typical clinopyroxene. The pyroxenes also display a relatively high concentration of Al, which commonly substitutes for Fe (Dietrich and Skinner, 1979). For the purpose of PER diagram axes coefficient determination, the substitution of Fe for Mg is unimportant, because the two elements are considered as a sum. The remaining two substitutions allow the Chu Chua pyroxene to be expressed as a linear combination of two pyroxene phases with compositions as follows: (1)  $(\text{FeMg})_{1.95}\text{Ca}_{0.05}\text{Si}_2\text{O}_6$  and (2)  $(\text{FeMg})_{1.1}\text{Al}_{0.4}\text{Ca}_{0.7}\text{Si}_{1.8}\text{O}_6$ .

Variation in plagioclase compositions apart from the  $\text{NaSiCa}_{-1}\text{Al}_{-1}$  component is insignificant. All 38 probed plagioclase grains, except for two, are albite ( $\text{An}_0 - \text{An}_{12}$ ). Thus, the idealised formulas for anorthite ( $\text{CaAl}_2\text{Si}_2\text{O}_8$ ) and albite ( $\text{NaAlSi}_3\text{O}_8$ ) were used in the modelling. The two non-albite grains are correspondingly K-feldspar and andesine-labradorite ( $\text{An}_{50}$ ), the latter most likely representing a remnant of the original composition of plagioclase before spilitization.

### PER analysis applied to Chu Chua basalt

A matrix-algebraic procedure (Stanley and Madeisky, 1995) was used to determine the axes numerators ensuring that the hypothetical fractionation of plagioclase and pyroxene causes data points to plot along a line with a slope of unity. The procedure involves three matrices governed by the following equation:

Composition matrix						axes coefficient matrix			Displacement matrix		
C	Fe+Mg	Na	Ca	Al	Si	A	x	y	P	dX	dY
Anorthite (An)	0	0	1	2	2	Fe+Mg	0.6346	0	An	2	2
Albite (Ab)	0	1	0	1	3	Na	2.7019	0	Ab	3	3
Pyroxene 1 (P1)	1.95	0	1.05	0	2	Ca	1.4038	0	P1	2	2
Pyroxene 2 (P2)	1.1	0	0.7	0.4	1.8	Al	0.2980	0	P2	1.8	1.8
						Si	0	1			
(4 x 5)						(5 x 2)			(4 x 2)		

Table.3.1. Matrix equation for calculating axes coefficients for a PER diagram where the material transfer effects of plagioclase and Chu Chua pyroxene have slopes of unity.

Matrix **C** reflects the stoichiometries of the phases involved in the modelled material transfer. Matrix **P** contains numbers with the only constraint that the two columns are identical and consistent with **C** and column dY of **A**, which projects the matrix onto  $\text{SiO}_2$ . This condition ensures that the material transfer effects have slopes of unity. For calculation purposes it is

convenient to use the same numbers as in the column of the composition matrix, corresponding to the element to be balanced (in this case Si). Matrix **A** is calculated from matrices **P** and **C**, using the matrix equation:

$$\mathbf{A} = (\mathbf{C}^T \mathbf{C})^{-1} \mathbf{C}^T \mathbf{P}$$

TiO<sub>2</sub> concentrations were used as the denominators in accordance with the discussion in the previous section. The resulting plot (Fig. 3.9), showing only basaltic samples, represents the balance of the cations in plagioclase and pyroxene versus SiO<sub>2</sub>, with the assumption that all Al present in pyroxene substitutes for Fe. A few basaltic samples, for which Ti/Al ratios deviate from the median ratio of the group by more than 2 standard deviations of analytical errors (Fig. 3.2), suggesting possible mobility of one or both of these elements, are not taken into account. Low-Ti basalt, which also have varying Al/Ti ratios are shown on Fig. 3.9 but are not considered with regard to alteration, because they are proven not to be cogenetic with the main basalt group.

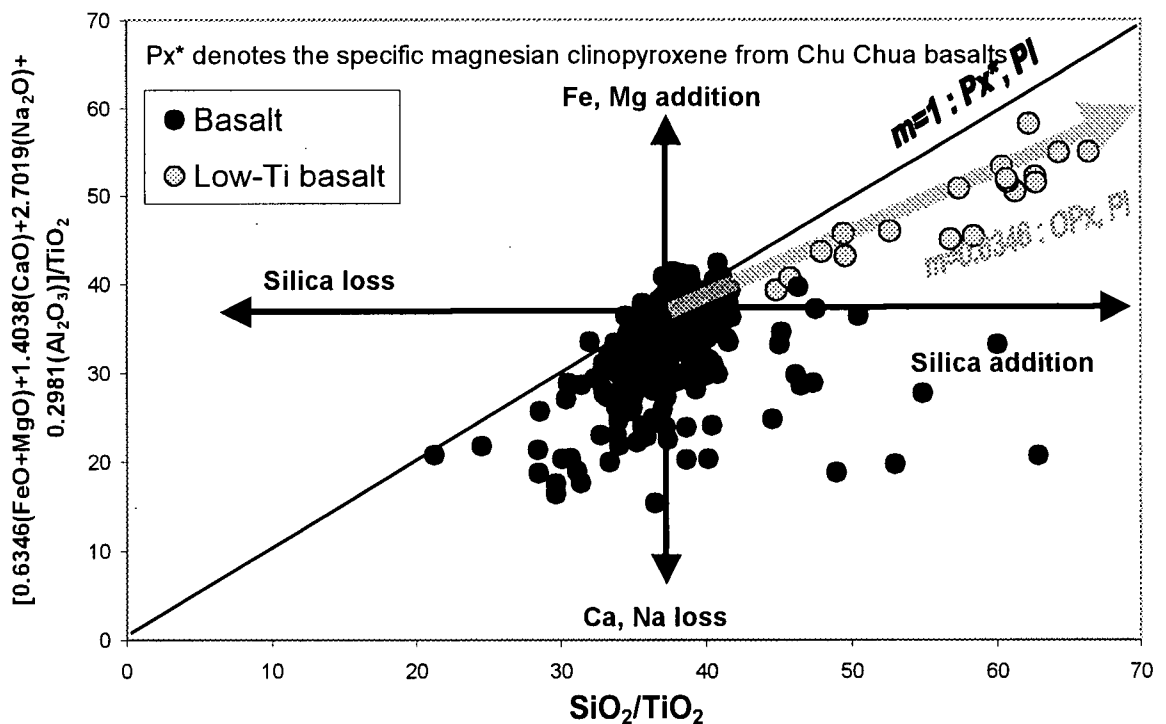


Fig. 3.9. PER plot of  $\text{SiO}_2/\text{TiO}_2$  vs.  $[0.6346(\text{FeO}+\text{MgO})+1.4038(\text{CaO})+2.7019(\text{Na}_2\text{O})+0.2981(\text{Al}_2\text{O}_3)]/\text{TiO}_2$ . Most samples are consistent with fractionation of plagioclase and magnesian clinopyroxene (Px\*). Low Ti basalts are consistent with fractionation of orthopyroxene. Many basaltic samples show silica mobility (both addition and loss) and/or loss of Ca and Na.



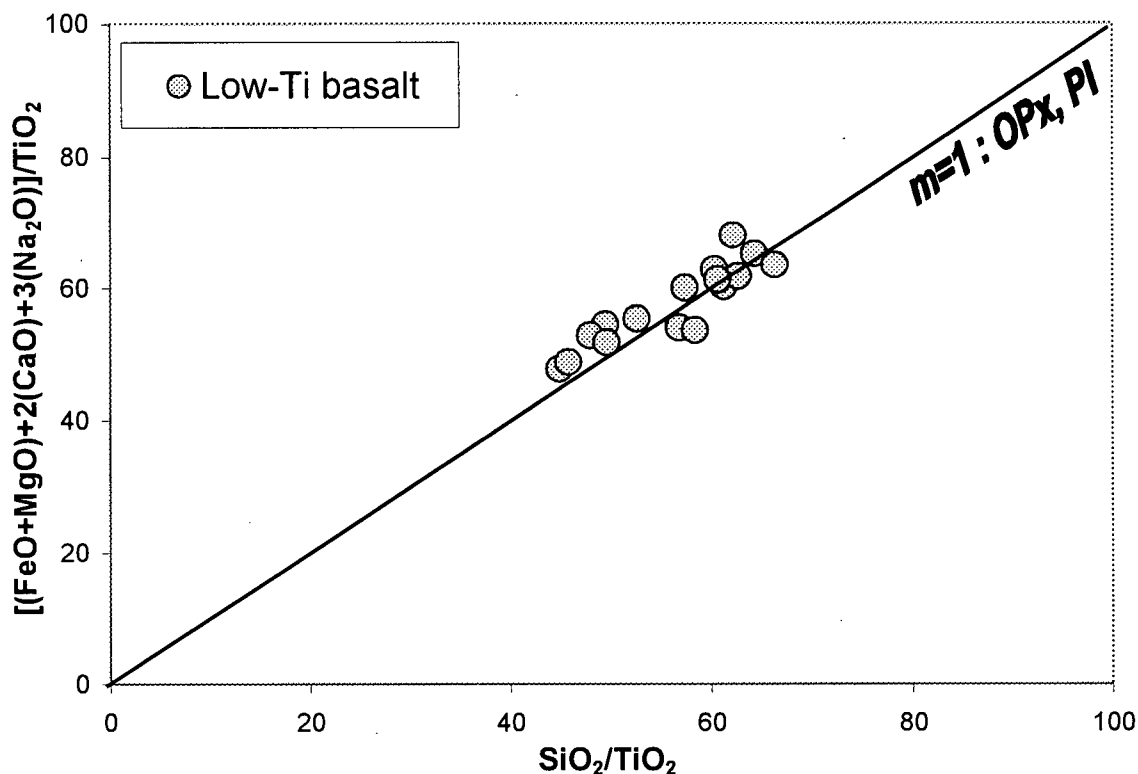


Fig. 3.10. PER plot of Si vs. cations, testing the hypothesis that chemical variation in low-Ti basalt samples are a result of fractionation of plagioclase and orthopyroxene.

The main cluster of data points, representing background variability in basalt, lie on a line with a slope of unity. This supports the hypothesis that fractionation of plagioclase and clinopyroxene is the primary cause of variability. Data points corresponding to low-Ti basalt define a more or less linear array with a slope of approximately 0.63, distinct from the rest of the basaltic samples. Their position is consistent with the fractionation of plagioclase and orthopyroxene (rather than the magnesian clinopyroxene in the case of the underlying basalt). A PER plot (Fig. 3.10) testing this hypothesis yields a positive result. The colinearity of the basalt data point cluster and the trend defined by low-Ti basalt (Fig. 3.9) can be interpreted to mean that the latter are an evolved derivative of the same initial melt from which the underlying basalt originated.

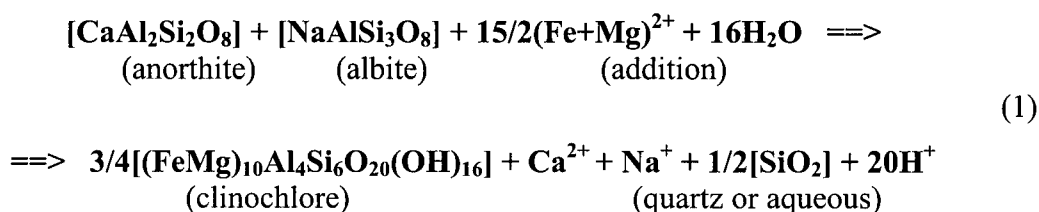
A number of basaltic samples, however, deviate from the main cluster (Fig. 3.9), which is interpreted to be a result of one or more superimposed mass-transfer processes. The known and inferred processes that influenced the Chu Chua rocks after their formation are: (1) metasomatism, related to the hydrothermal activity responsible for the deposit formation, and (2) regional metamorphism to greenschist grade. It is assumed that the greenschist metamorphism of the basaltic rocks was isochemical with respect to non-volatile components (*e.g.*, water and CO<sub>2</sub> were the only components involved in metamorphic mass transfer). This assumption is supported by the large number of background samples that show no significant chemical variation other than that introduced by the modelled magmatic fractionation process. Thus, variations distinct from those introduced by igneous fractionation characterise the processes of hydrothermal alteration. Furthermore, the residuals from the line with a slope of one are a quantitative measure in terms of moles of the metasomatic reactions that have modified the rocks.

Chloritization of plagioclase, for which abundant petrographic evidence exists in the studied rocks (Plate 3.2), can account for the observed deviations from the model line (Fig. 3.9).

Two logical presumptions help constrain the reaction:

1. As indicated by microprobe analysis (see discussion above), the initial composition of plagioclase corresponds to An<sub>50</sub>.
2. Based on the discussion in the previous section (see Fig. 3.2), aluminium is considered immobile and used for the balancing of the equation.

The reaction can be written as:

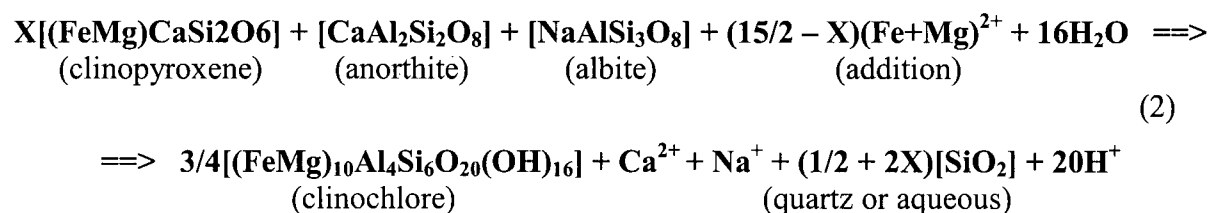


#### *Effect of Mg and Fe addition*

On the reactants side, the ferro-magnesian component is derived from the breakdown of pyroxene in the basalt. At least part of it originates in situ, which is supported by the

observation of intensive chloritization of pyroxenes in thin sections from the Chu Chua basalt (Plate 3.2). However, even if complete decomposition of pyroxene is assumed, for all of the required ferro-magnesian ions to be derived in situ, the pyroxene/feldspar volume ratio in the fresh basalt must not be less than 3/1, which is not consistent with the petrologic observations. This conclusion is based on (1) the 15/4 ratio of the ferromagnesian component on the product side of the reaction, (2) the approximately 3/4 ratio of molar volumes of clinopyroxene and andesine-labradorite feldspar, and (3) an assumption that Fe and Mg participate in equal molar proportions. Thus, it is clear that a significant portion of the Fe and Mg are introduced in the chloritized rocks. Seawater, from which the hydrothermal solutions are considered to originate (*e.g.*, Franklin, 1995), has a Mg concentration that may be significant when water/rock ratios are sufficiently high. Footwall alteration (*e.g.*, Morton and Franklin, 1987) is another possible mechanism of enrichment of the hydrothermal solutions in Fe and Mg.

The question about the ratio of introduced to in-situ-reprecipitated ferro-magnesian components is important with respect to the effect of metasomatism on the position of data points. In-situ reprecipitation of Fe and Mg causes no shift of data points, whereas introduction of these elements by hydrothermal solutions moves data-points up the ordinate of Fig. 3.9. However, this ratio is difficult and impractical to quantify, because it depends on (1) the pyroxene/plagioclase ratio, and (2) the degree of destruction of rock-forming pyroxene, parameters that can be determined only by extensive petrographic and microprobe studies. Following this discussion, reaction (1) can be appended to include the role of in-situ clinopyroxene as a source of Fe and Mg:



### *Effect of Na and Ca loss*

Among the products of reaction (2) are Na, Ca, and  $\text{SiO}_2$ . No secondary minerals containing Na are petrographically or otherwise observed in the altered rocks, which suggests that this element is flushed from the system and most likely released into sea water. Ca is ubiquitously precipitated in the vicinity of the deposit as calcite veins. However, because carbonate veins were carefully avoided during sampling, most of the Ca should have been mobile and considered lost by the system (the system is defined to have the size of the sample). The loss of these two elements is represented on the PER diagram (Fig. 3.9) as a negative residual down the ordinate. It balances and, as is seen in a number of data points, outweighs the opposite effect of Fe and Mg addition discussed in the previous paragraph. As a result, a significant number of data points are displaced towards the low end of the ordinate. However, due to the uncertainties associated with the quantification of the opposing effect of ferro-magnesian addition, the residuals along the ordinate can only be used as a qualitative measure of the degree of chloritization.

### *Dual nature and effect of $\text{SiO}_2$*

Another component present on the product side of equation (2) is  $\text{SiO}_2$ . Its influence on the data points is restricted to the direction parallel to the abscissa.  $\text{SiO}_2$  can be viewed as either a mineral or as an aqueous phase. Additional complexity is introduced by the fact that hydrolysis of plagioclase is coupled with in-situ destruction of pyroxene (reaction 2). Hence, an additional amount of  $\text{SiO}_2$  participates implicitly on the reactant side in the form of clinopyroxene. This has the effect of significantly increasing the amount of  $\text{SiO}_2$  resulting from the total reaction, as expressed in (2) by the non-quantifiable term "X". The magnitude of X is governed by the volume ratio of pyroxene/plagioclase. It is "0" when no pyroxene is present (then reactions 1 and 2 are identical) and approaches 15/2 when the volume ratio reaches approximately 3. When X exceeds 15/2, more ferro-magnesian component is released than is necessary for the in-situ formation of chlorite (clinochlore). Note that in this case, the addition of this component to the system becomes negative, meaning that it is lost by the system (reaction 2).

Two end-member scenarios are possible with respect to the behaviour of  $\text{SiO}_2$  and its influence on the data points (Fig. 3.11):

- (1)  $\text{SiO}_2$  is immobile: Quartz, in the amount of  $(1/2 + 2X)$  moles is precipitated in-situ per mole of reaction. Chloritization is accompanied by silicification. The vector, representing the reaction effect on the PER diagram (Fig. 3.9) is parallel to the ordinate (*i.e.*, no effect along the abscissa, Fig. 3.11).
- (2)  $\text{SiO}_2$  is mobile: The corresponding vector is directed towards the low end of both the abscissa and the ordinate and has a slope of approximately  $5/8$ , independent of  $X$  (Fig. 3.11).  $\text{SiO}_2$  leaves the system in the form of aqueous  $\text{SiO}_2$  ( $\text{SiOH}_4$  or  $\text{SiO}_2 \cdot n\text{H}_2\text{O}$ ) carried by the hydrothermal solutions. It may be reprecipitated (1) within the wall rocks to the deposit, further down the path of the mineralised fluids or (2) be flushed into the seawater. In the first case, it is recorded in the rock chemistry of that domain as pervasive or vein-related silicification caused by  $\text{SiO}_2$  addition (Fig. 3.11). In the second case, it is dispersed within the water column above the sea floor and likely precipitated in the form of thinly layered exhalative chert blanketing the hydrothermal discharge area, (*i.e.*, like the abundant siliceous rocks associated with the Chu Chua deposit). The abundant siliceous rocks associated with the Chu Chua deposit are interpreted to have originated in this way. In the rocks hosting the Chu Chua deposit,  $\text{SiO}_2$  addition outweighs  $\text{SiO}_2$  loss (Fig. 3.12), which means that the volume of basaltic rocks represented by the samples has registered a net gain of this component. It, however, is unrelated to the reaction of chloritization, because the reactant feldspars alone contain more than enough of this element to match the aluminium in chlorite (clinochlore).

An additional insight stemming from the reaction equation is that alteration of plagioclase to chlorite produces acidity at a rate of 20 moles per two moles of plagioclase destroyed.

The  $\text{SiO}_2$  balance PER diagram (Fig. 3.9) offers a good framework to comprehensively examine the effects of chloritization of the basaltic host rocks to the deposit. It is indispensable in comprehending and qualitatively characterising the behaviour of  $\text{SiO}_2$  in

each sample domain and in the deposit envelope as a whole. Fig. 3.14 is a version of this diagram, designed specifically to visualise the effects of SiO<sub>2</sub> mobility.

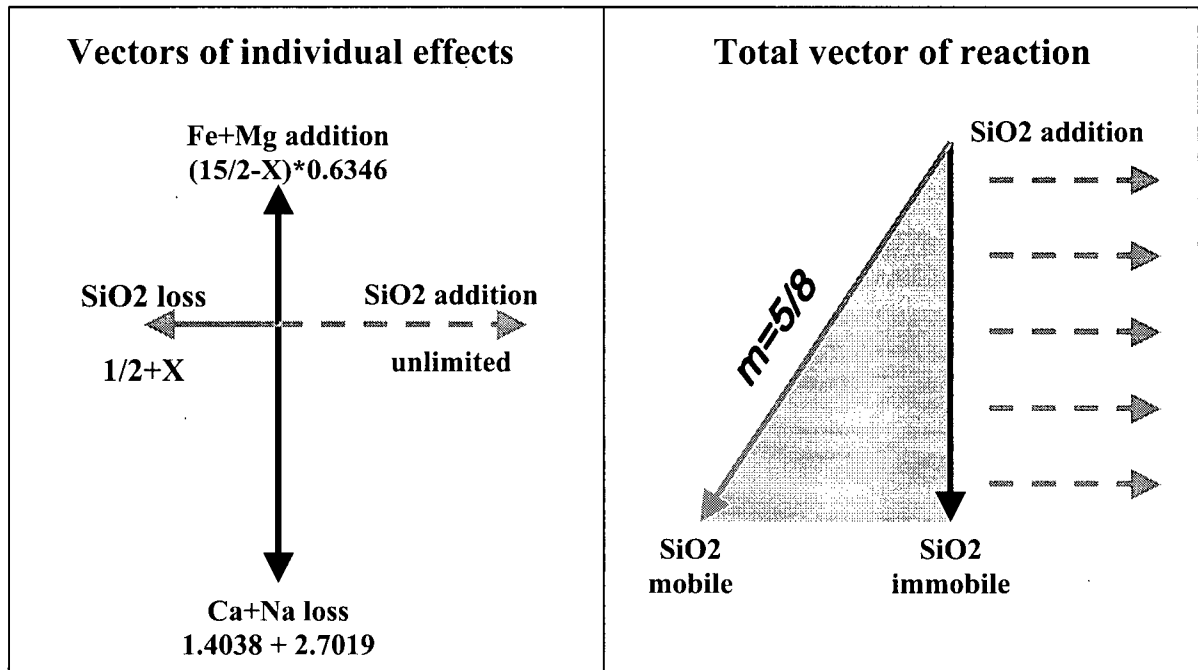


Fig. 3.11. Vectors of individual effects and total vector of reaction in the space of Fig. 3.9. Magnitude of individual vectors is the product of axes coefficients and number of moles of components as shown in the reaction (1). The shaded triangle corresponds to the possible range of the reaction vector in the case of partial mobility of SiO<sub>2</sub>.

Both figures 3.9 and 3.12, however, fail to adequately characterise the cation (Fe+Mg, Ca and Na) losses and additions, because of their opposing graphical effects. By rearranging the axes parameters, it is possible to isolate the effects of individual additions/losses, so that they can be quantified without interference. Figure 3.14 is a version of the SiO<sub>2</sub> balance plot, such that Ca and Na material transfer is the only effect moving data points with respect to the ordinate. Thus, the residuals along this axis quantitatively characterise destruction of feldspars in each sample. Residuals along the abscissa reflect the material transfer of both ferro-magnesian component and SiO<sub>2</sub>, which interfere and thus have no quantitative meaning. Similarly, Figure 3.13 quantifies the addition of Fe and Mg as the residual along the ordinate, when the rest of the effects are constrained to the abscissa.

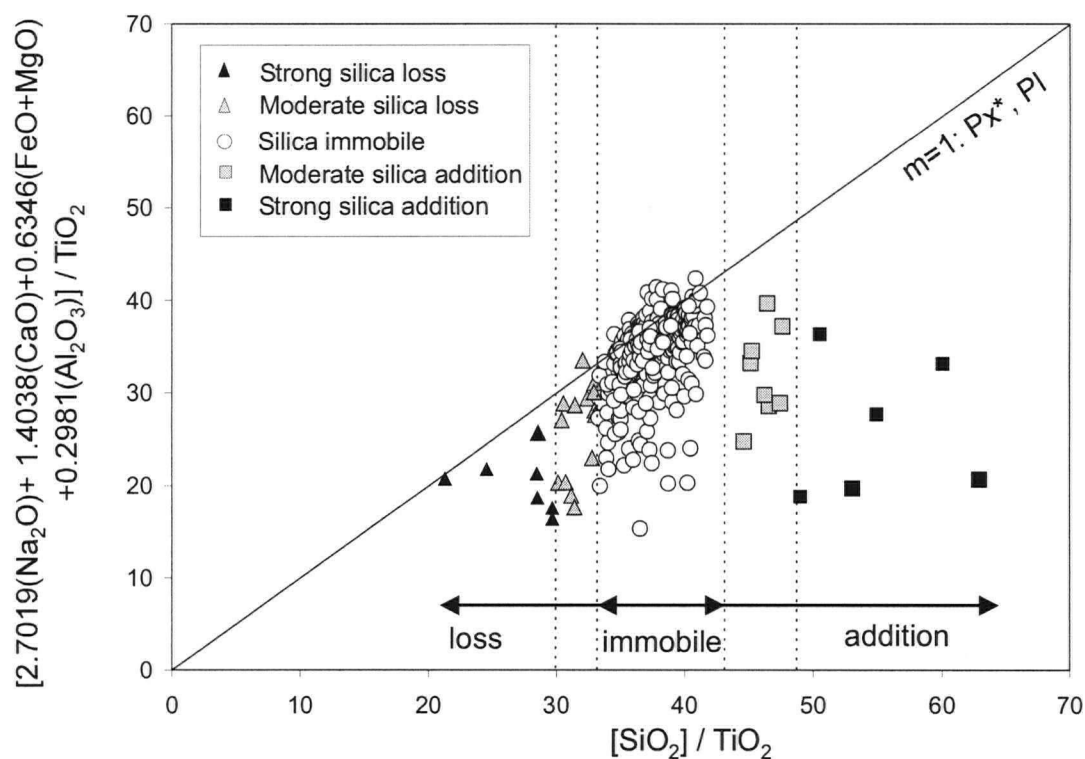


Fig. 3.12. PER diagram quantifying the mobility of silica as the abscissa of each data point. Axes parameters reflect the real stichiometry of the involved minerals.  $P^*$  denotes the average stoichiometry of pyroxene occurring in Chu Chua basalts.

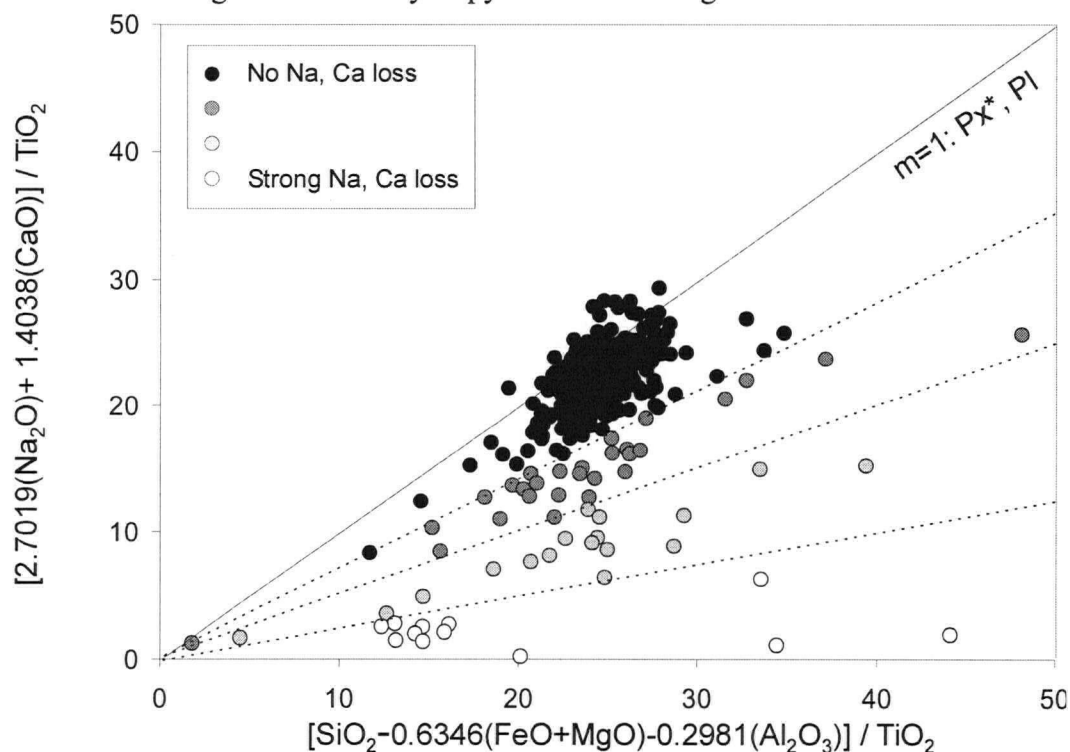


Fig. 3.13. PER diagram quantifying the loss of Ca and Na in the rocks hosting the Chu Chua deposit as the ordinate/abscissa ratio of each data point. Axes parameters reflect the real stichiometry of the involved minerals.  $P^*$  denotes the average stoichiometry of pyroxene occurring in Chu Chua basalts.

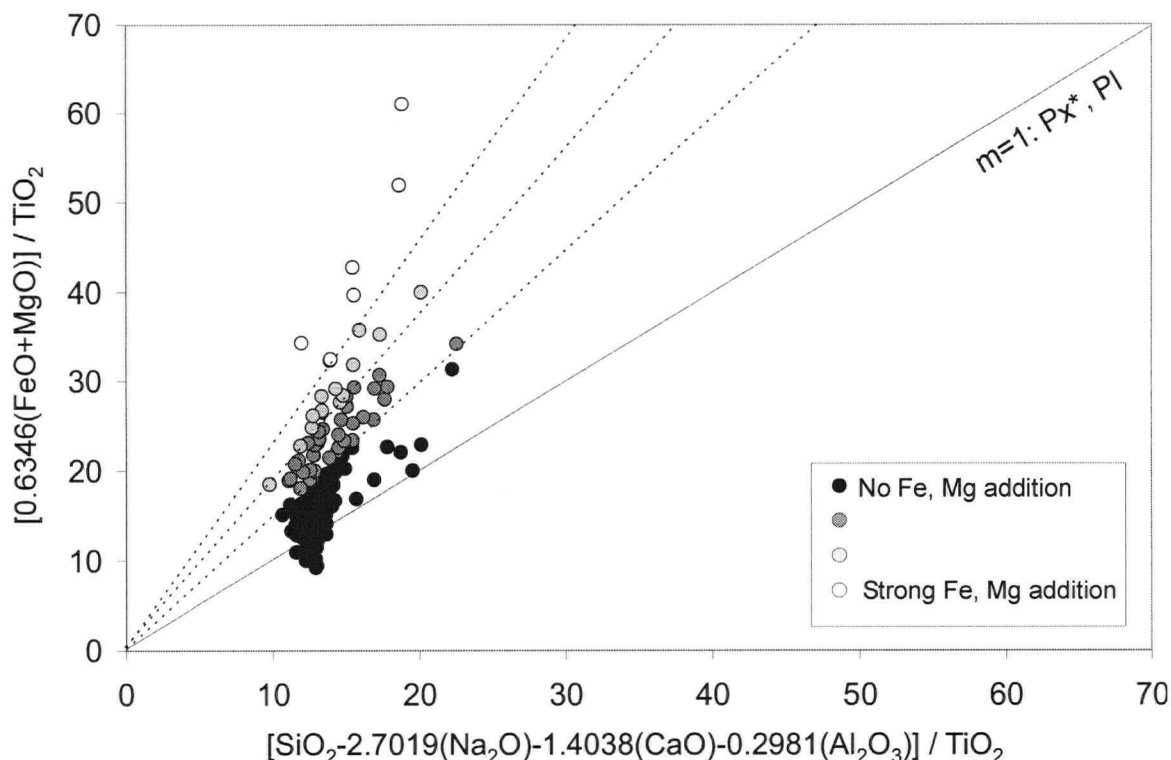


Fig. 3.14. PER diagram quantifying the addition of  $\text{Fe}_2\text{O}_3$  and  $\text{MgO}$  component as the ordinate/abscissa ratio of each data point. Axes coefficients reflect the real stoichiometry of the involved minerals.  $\text{P}^*$  denotes the average stoichiometry of pyroxene occurring in Chu Chua basalts. Dashed lines separate groups of samples with increasingly high degree of addition of ferromagnesian elements.

#### *Spatial patterns of basalt alteration*

The PER diagrams quantifying material transfer with respect to various components (Fig. 3.12, through Fig. 3.14) are used as a basis for describing the spatial aspects of the alteration. Basaltic samples with evidence of metasomatic alteration are plotted spatially (Fig. 3.15 through 3.17). It should be noted that extremely altered samples, which show signs of mobilisation of Al and/or Ti, are not represented on the diagrams.

The three individual effects of alteration have similar patterns and extent. They are restricted to the graben fill (Figs. 3.4 and 3.6) and are developed predominantly within 50 m (rarely 100 m) in the footwall to the ore lenses. Two clusters of altered samples are distinguished spatially. Alteration penetrates into the hanging wall, but is less obvious and



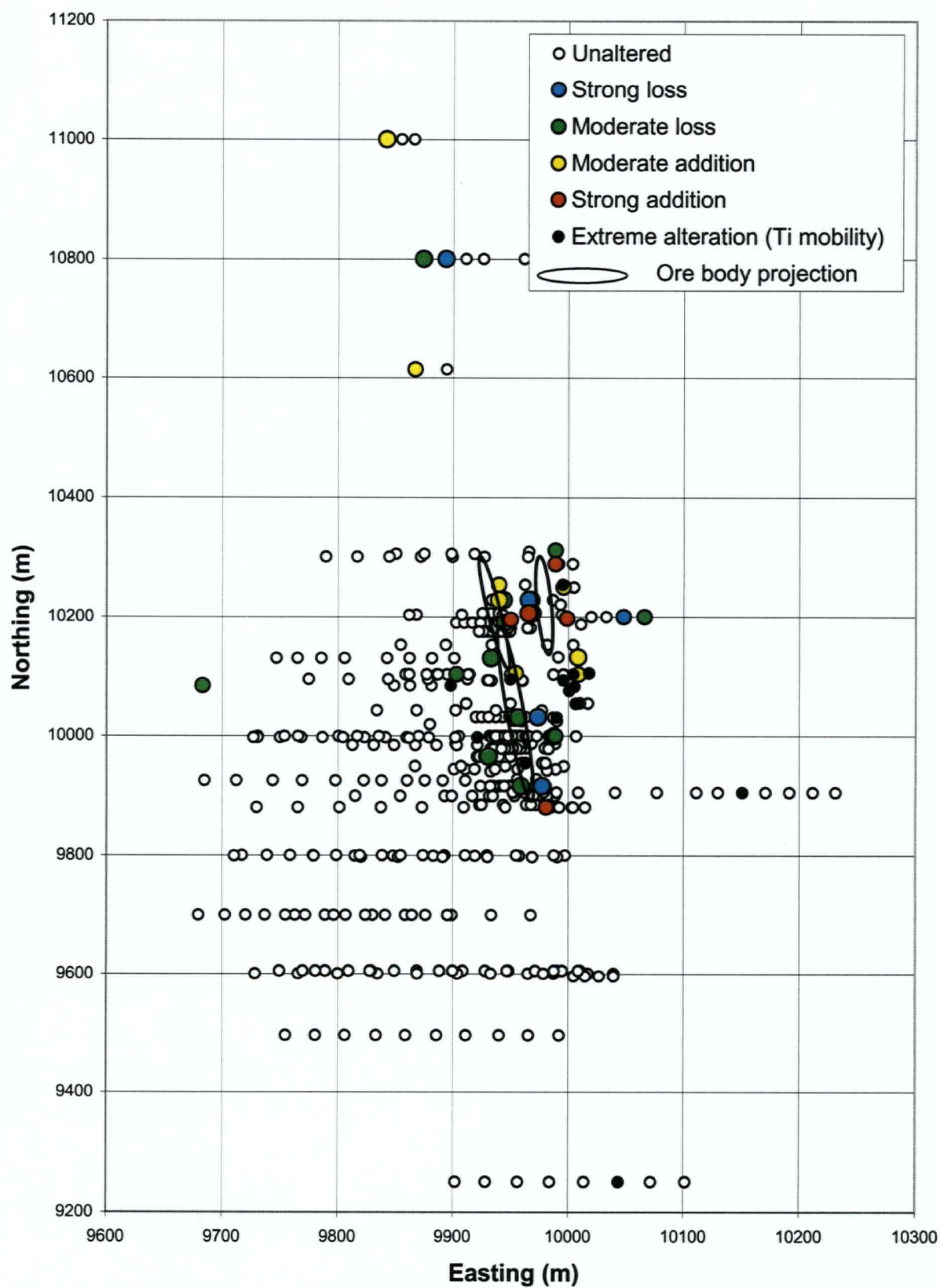


Fig. 3.15. Silica mobility in Chu Chua basalts based on PER analysis (Fig. 3.12)

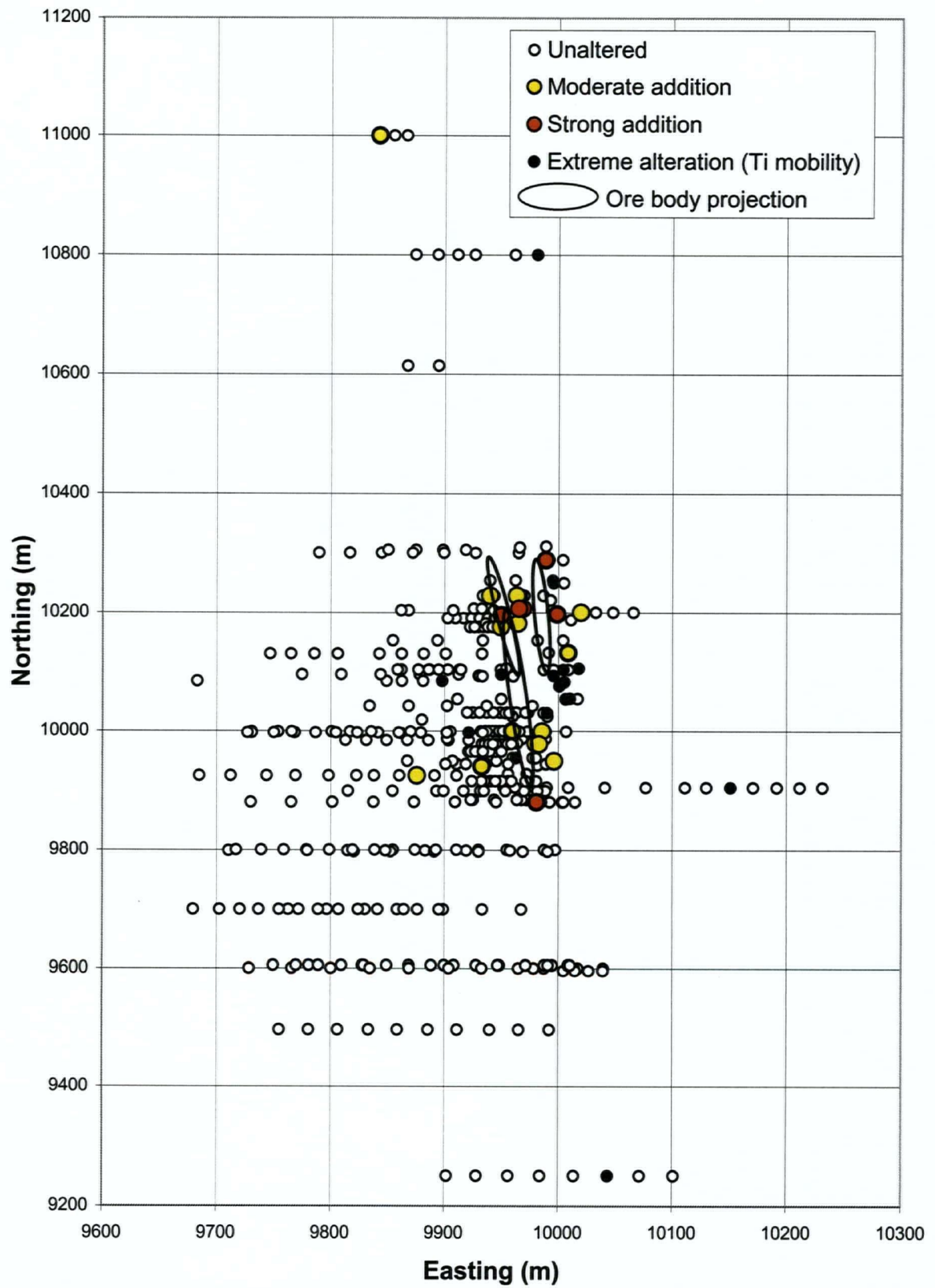


Fig. 3.16. Fe, Mg addition in Chu Chua basalts based on PER analysis (Fig. 3.14).

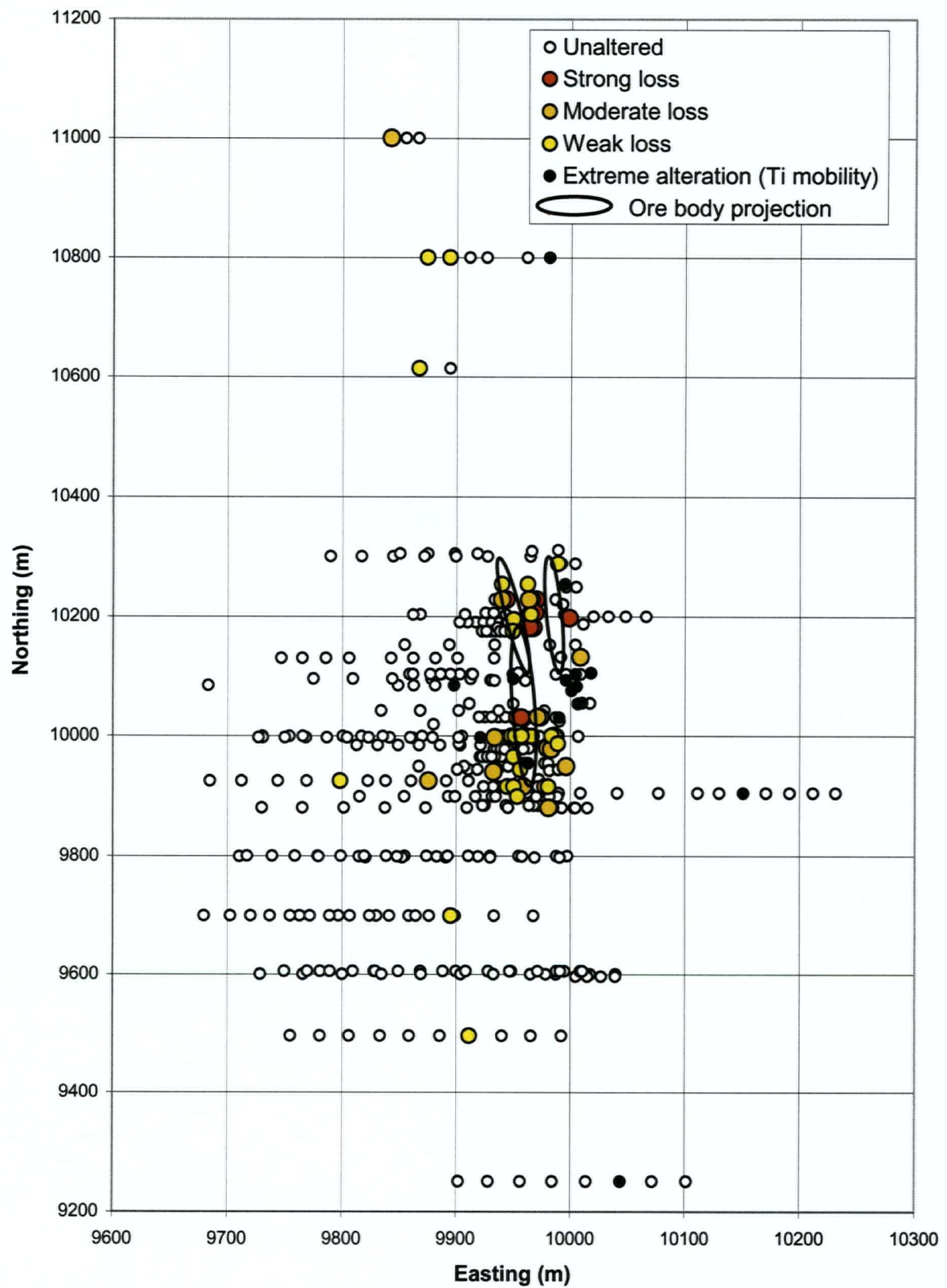


Fig.3.17. Ca, Na loss in Chu Chua basalts based on PER analysis (Fig. 3.13).

represented by a small number of scattered samples. Still, its presence in the hanging wall suggests that the hydrothermal activity in the Chu Chua area continued after the formation of the known ore bodies.

The most contrasting and well-defined alteration effect is loss of Ca and Na, which is not surprising, taking into account that it is essential to the process of chloritization of plagioclase (equation 1). Silicification is often associated with addition of Fe and Mg.  $\text{SiO}_2$  loss is mostly observed in the hanging wall and deeper into the footwall of the deposit. This material transfer pattern with regard to  $\text{SiO}_2$  may be interpreted to mean that  $\text{SiO}_2$  was mobilised from the bottoms of the volcanic units and concentrated toward the tops or exhaled onto the seafloor.

A group of samples were not taken into account in the PER analysis because of the non-conserved behaviour of Ti in them, presumably due to extreme alteration. These samples are plotted in space together with the ones subject to PER analysis. They plot within the altered halo of the deposit, most of them occupying its central footwall portions. This reinforces the earlier presumption about them being extremely altered and completes the picture of spatial pattern of alteration, by identifying a central zone of extreme metasomatism in the immediate footwall of the deposit, flanked by two areas of more moderate alteration facies.

The sample density proves to be inadequate to characterise the spatial effects in enough detail so that more meaningful zonation patterns are discerned. This is due to the discreet, vein-controlled character of chloritization and to the under-representation of the deposit footwall in the available drill core.

#### **PER analysis applied to Chu Chua siliceous rocks**

Siliceous rocks occurring in abundance in the wall rocks of the Chu Chua deposit were described as "cherty rocks" (McMillan, 1979) and are interpreted above as impure banded chert (Plates 3.3 through 3.5). They contain up to 90%  $\text{SiO}_2$  (Fig. 3.5), the rest comprising impurities of tuffaceous or sedimentary origin. Due to the simple composition of the major

component ( $\text{SiO}_2$ ), those impurities can be conveniently characterised by a PER diagram projecting from quartz. The aluminium balance plot (Fig. 3.18) represents the mineralogically controlled correspondence between aluminium from one side and Ca, Na and K from the other, allowing for conclusions to be drawn about the original and current mineralogy of the impurities.

The most likely aluminous phases that could have been included in the cherty rocks at the time of sedimentation are feldspar clasts of tuffaceous or terrigenous origin and pelagic, terrigenous or authigenic clay minerals. Typical examples of marine clays are illite and montmorillonite (Chamley, 1989). Secondary muscovite (sericite) and chlorite, which are observed in samples from the cherty rocks (Plate 3.3), need to be considered too.

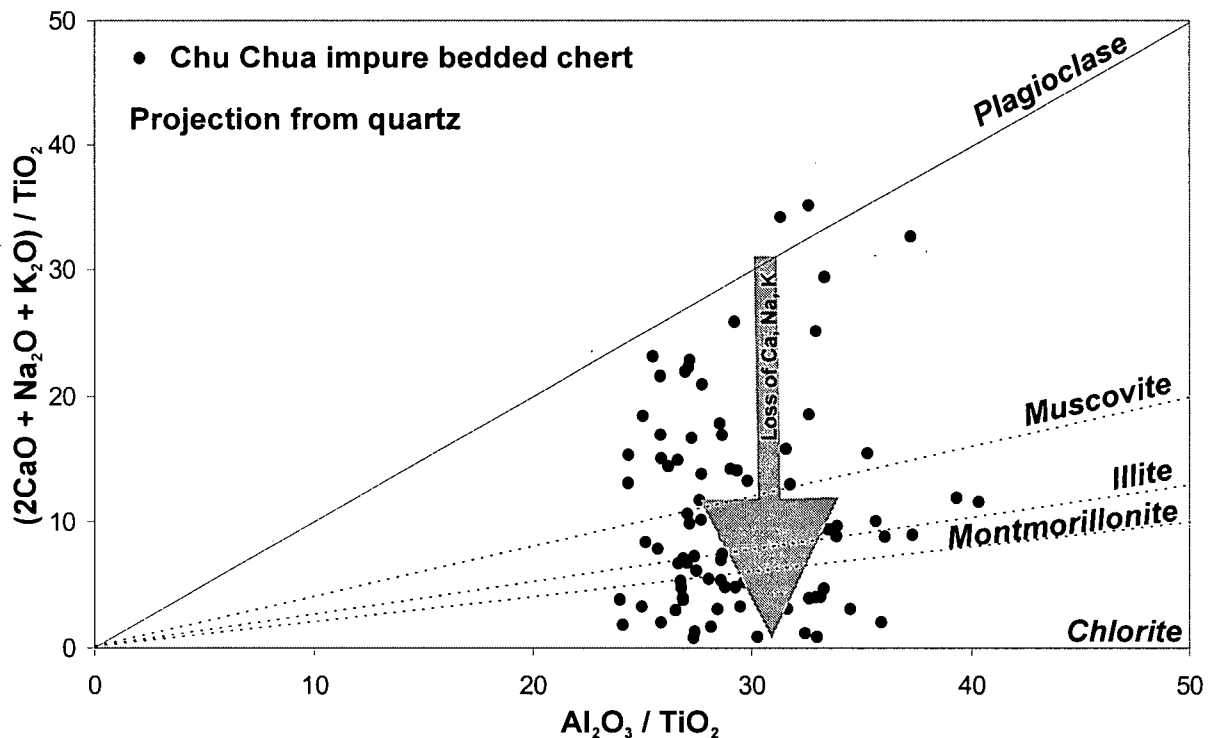


Fig.3.18. PER diagram using data for Chu Chua banded cherts. The main alteration effect represented and quantified in molar terms is loss of K, Na and Ca.

The position of several data points close to the plagioclase line (Fig. 3.18) suggests that at least part of the impurities were feldspar clasts. Participating in the graben fill, they were hydrolysed to form phyllosilicate minerals similar to the ones resulting from the processes observed in the underlying basalt (see discussion in the previous section). This process resulted in (1) the formation of chlorite and muscovite (sericite); and (2) loss of Ca, Na and K from the system. The latter effect is visualised on the diagram as a shift in data points towards the abscissa (arrow, Fig. 3.18). Its magnitude is inversely proportional to the angle defined by the line passing through the data point and the origin. The chemical composition of the strongly altered samples is consistent with intensive chloritization. The magnitude of Ca and Na loss can be used as a measure of the degree of alteration.

Because the lines corresponding to illite and montmorillonite (common sedimentary and diagenetic minerals) have slopes intermediate between those for muscovite and chlorite (Fig. 3.18), the presence of the former two minerals cannot be ruled out. However, another PER diagram (Fig. 3.19) involving structural water and cations, supports the observation that muscovite and chlorite make up the bulk of the impurities in the bedded chert. It also reveals that some samples contain talc (observed in hand specimens) or other ferro-magnesian minerals.

With muscovite and chlorite being the main phyllosilicate impurities in the Chu Chua banded chert, another PER diagram (Fig. 3.20a) is employed to assess the proportions of these two minerals. The diagram is based on molar ratios, but is modified to reflect volume ratios of the minerals, which makes its graphical representation compatible with petrographic observation. Because chloritization is associated with a more intensive loss of Ca and Na than sericitization (Fig. 3.18), it is assumed to be characteristic of a more advanced alteration and to be more proximal to the feeder zone. Distribution of phyllosilicates (Fig. 3.20b) follows a spatial pattern consistent with this assumption. Chloritic samples are restricted to the close vicinity of the normal fault defining the graben (or half-graben), while predominantly sericitic samples occur higher in the graben fill. Farther above and away from the feeder zone the proportions of the two minerals are about equal.

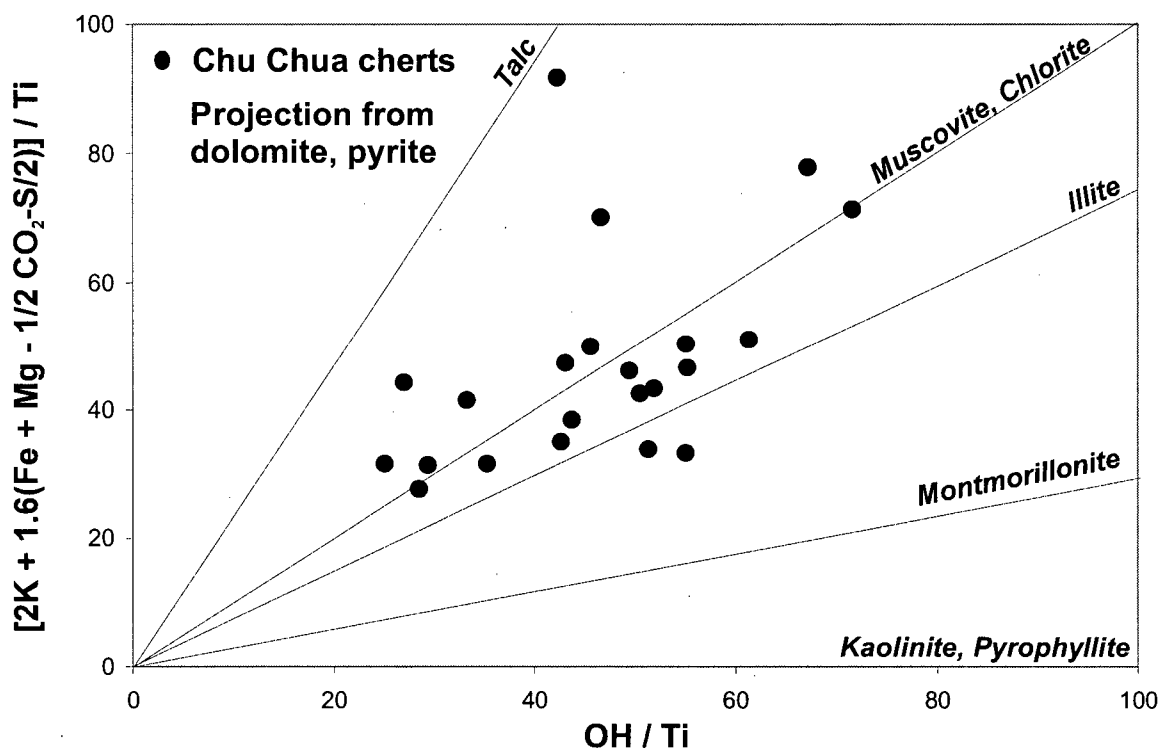


Fig.3.19. Phyllosilicate mineralogy of impurities in banded cherts from Chu Chua. The plot projects from dolomite and pyrite.

## Discussion

The Fennel Formation resulted from tholeiitic mafic volcanism in a MOR or back-arc tectonic environment (Fig. 3.6a). The section exposed by drilling in the vicinity of the Chu Chua deposit consists of two varieties of basalt distinguished mainly by their Ti concentrations (Fig. 3.2), the low-Ti variety being younger. The north-northwest striking interface between the two is marked by an extensional tectonic event, resulting in the formation of a graben or half graben, filled by intercalated sedimentary and volcanic rocks (Fig. 3.6b). The ore formation at Chu Chua was synchronous with this tectonic event and is spatially restricted to the interface between the two varieties of basaltic rocks. Intrusion of basaltic lavas into soft siliceous sediment resulted in peperitic textures. The normal fault defining the graben was the focus of heat and mass flow in the form of small volumes of felsic partial melts and presumably large volumes of hydrothermal solutions.

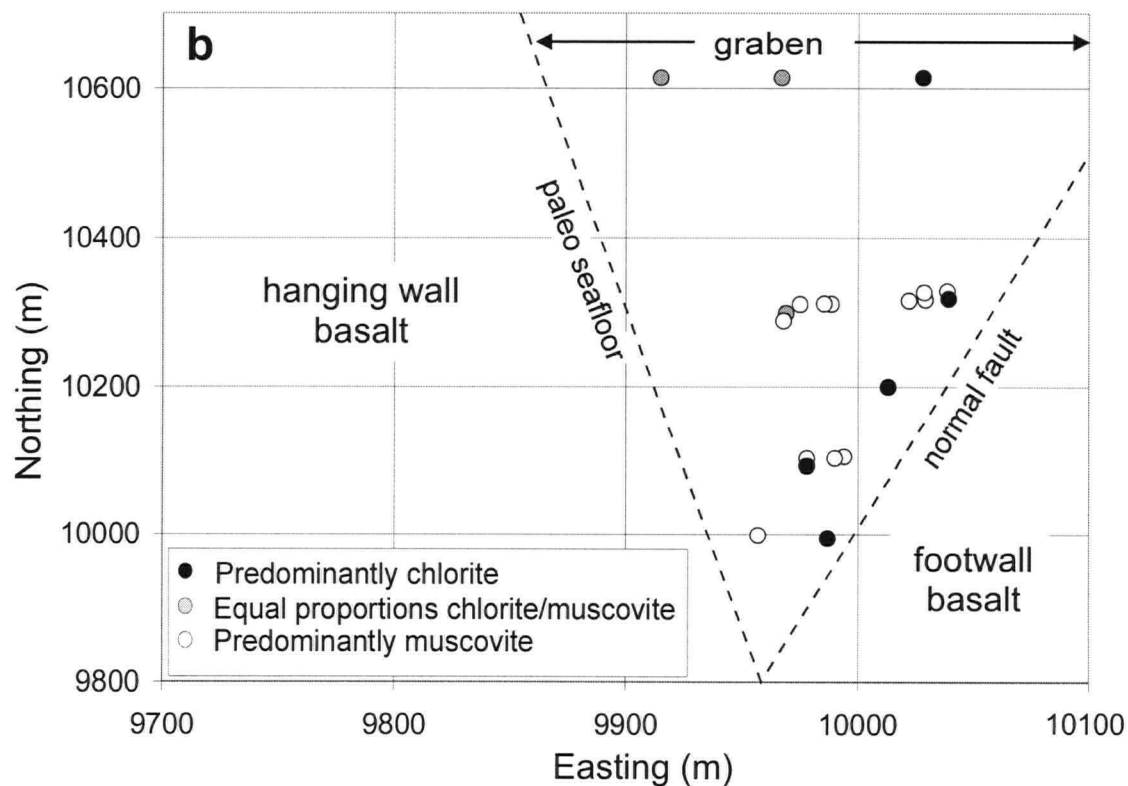
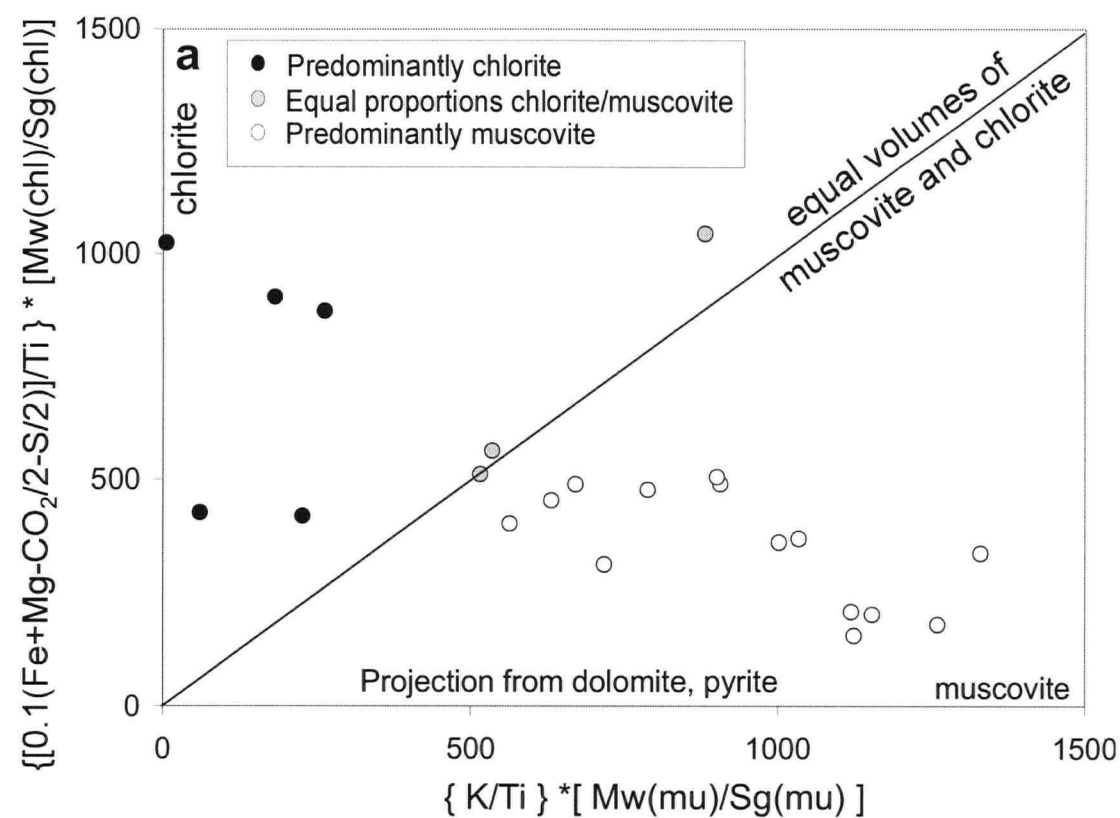


Fig. 3.20a. PER discrimination diagram, showing volume proportions of main phyllosilicate minerals in cherts. Mw = molecular weight; Sg = specific gravity.  
 Fig. 3.20b. Spatial distribution of secondary phyllosilicate minerals with respect to structural features.



As the graben grew deeper (Fig. 3.6c),  $\text{SiO}_2$ , exhaled by hydrothermal solutions precipitated biogenically and became one of the major constituents of the graben fill. The impurities to the siliceous rocks were supplied by pelagic and/or turbiditic sedimentation, and/or by volcanoclastic deposition. The latter source is very likely in view of the proven original feldspar content of the cherty rocks (Fig. 3.18). The sporadic banded appearance of the chert is due to the accumulation of pelagic clay material in times of quiescence in the hydrothermal activity or increased input of terrigenous or volcanoclastic material. Massive sulphides accumulated on the graben floor in at least two separate episodes, corresponding to the two vertically (in terms of stratigraphy) staggered sulphide lenses. The ore-controlling normal fault is not studied beyond a few tens of meters from the known ore bodies. This leaves open the possibility of more mineralization being present toward the north-northeast.

The hydrothermal activity altered both the basalt and the siliceous rocks along and in proximity to the normal fault. Mineralogically, the alteration is represented as chloritization of feldspar and pyroxene in basalt, as chloritization and sericitization in cherty rocks and as formation of Fe sulphides (pyrite and/or pyrrhotite). The most intensive chemical effect of alteration is the loss of Ca and Na, both from individual samples and from the system as a whole. Ca was partially redeposited within the seafloor rocks as calcite, whereas Na was released into seawater. Fe and Mg were introduced in the wall rocks of the deposit by the hydrothermal solutions, which contributed additional amounts of ferromagnesian component for the formation of chlorite. High chemical activity of Fe, Mg, and Ca in the solutions entering the graben may have caused the overgrowths of ferromagnesian carbonate on euhedral diagenetic carbonate.  $\text{SiO}_2$  was redistributed in the affected rocks, with some samples exhibiting loss, others enrichment, but the system as a whole gained  $\text{SiO}_2$  from the hydrothermal solutions leaching the underlying basaltic pile.

The extent of alteration as identified by this study is limited to 50 m in the footwall of the ore bodies and to about 200 m along their strike. It should be noted, however, that due to the drilling pattern applied, the footwall is under-represented in the data set. Zonation in the

altered envelope is not clear, which is attributed to the discrete, vein-controlled character of the alteration. Some crude patterns, however, are discernible:

1.  $\text{SiO}_2$  is lost from the deeper levels of the basaltic units and enriched in their upper levels.
2. In the siliceous rocks, chlorite is developed proximal to the feeder zone, with a more distal envelope of sericite alteration.

## Conclusions

1. Primary geochemical variability in the Chu Chua basalt is attributable to the fractionation of plagioclase and pyroxene. The plagioclase was originally andesine ( $\text{An}_{50}$ ), but subsequently was albitized to  $\text{An}_{0-12}$ . Two varieties of basalt are identified, differing in their  $\text{TiO}_2$  concentrations and in the type of pyroxene present. The basalt with higher concentration of  $\text{TiO}_2$  occur stratigraphically lower in the section and host the massive-sulphide deposit. The pyroxene in this basalt is slightly magnesian augite. The low-Ti basalt occur about 200 m to the west (stratigraphically higher) of the massive-sulphide ore bodies and contain orthopyroxene. The change in  $\text{TiO}_2$  concentrations in the basalt can be used as a local chemostratigraphic marker and to trace the mineralised horizon laterally.

Impure banded chert was deposited in a graben (or half-graben) depression as a result of hydrothermal  $\text{SiO}_2$  exhalation related to the sulphide ore formation. At least part of the aluminosilicate impurities in the chert is of volcanoclastic origin and contain plagioclase and phyllosilicates.

2. The PER methodology applied to data for the Chu Chua deposit has proven capable of distinguishing between the primary geochemical variability and that introduced by superimposed alteration processes. By selection of the axes parameters of the PER plot it is possible to visualise preferentially some aspects of the alteration signature (*e.g.*, Ca and Na loss, addition of ferromagnesian components or  $\text{SiO}_2$  mobility) and suppress the effect of other alteration processes on the diagram. This allows for more detailed and precise chemical characterization of the alteration. By measuring the residuals from the

fractionation model lines it is possible to quantify the alteration effects on a sample-by-sample basis and, thus, characterise alteration spatially. Phase discrimination PER diagrams are capable of distinguishing the chemical signature of even closely related minerals (e.g., phyllosilicates, Figs. 3.19 and 3.20a) and in this way can aid genetic interpretations.

3. Hydrothermal alteration was detected both in the basaltic rocks (the low-Ti basalt is not altered) and in the bedded chert (due to their minor but consistent volcanoclastic component).
  - a) Mineralogically, the alteration is manifested as hydrolysis of plagioclase and clinopyroxene and formation of chlorite and quartz.
  - b) In the course of the alteration process three groups of components, involved in the mineral reaction either as reactants or as products, experienced large scale mobility:
    - Ca and Na are released by the hydrolysis of plagioclase and, because they do not participate in any of the alteration product minerals, are flushed from the system in ionic form. Ca may precipitate as calcite in veins elsewhere down the path of the hydrothermal fluids, given sufficient concentrations of CO<sub>2</sub>, while Na is exhaled into the ocean.
    - Fe and Mg are consumed in the reaction of chloritization of plagioclase in the amount of 10 moles of ferromagnesian ions per mole of chlorite formed. Fe sulphides take up additional amounts of Fe. Part of the Fe and Mg necessary for the reaction originates *in situ* from the decomposition of clinopyroxene. However, additional quantities of Fe and Mg must be introduced by the hydrothermal solutions to account for the observed degree of chloritization.
    - SiO<sub>2</sub> participates on both sides of the alteration reaction. It is released in the course of hydrolysis of the primary silicate minerals in molar quantities 2-3 times larger than those of Ca and Na. On the product side, SiO<sub>2</sub> participates in the formation of chlorite and quartz, and as an aqueous phase, which leaves the system and either deposits pervasively or in veins, or is exhaled on the seafloor. Thus, on a sample scale, SiO<sub>2</sub> may exhibit either losses or additions. At Chu

Chua seafloor exhalation of  $\text{SiO}_2$  created thick accumulations of bedded chert. Their large volume indicates that  $\text{SiO}_2$  was leached not only from the immediate footwall of the deposit, which was characterized in this study, but also from deeper sections of the footwall.

- The alteration reaction releases 20 moles of acidity per mole of reaction. This may have additional implications about element mobility within the hydrothermal system.
4. Compared with other methods, PER analysis offers some fundamental advantages in studying the spatial expression of hydrothermal alteration (see Chapter 1). Two practical aspects of the problem are range (*i.e.*, the distance from the ore body at which alteration is still detectable) and resolution (*i.e.*, the ability to discern smaller features and zonation patterns).
- a) Geochemical anomalies of the three types (Ca and Na loss, Fe and Mg addition, and  $\text{SiO}_2$  mobility) were identified at distances of up to 50 m into the footwall and up to several hundred meters down the strike of the ore bodies (Figs. 3.15 through 3.17). Only two samples exhibit  $\text{SiO}_2$  loss at a distance of 100 m or more into the footwall. It must be noted, however, that sections of the footwall deeper than 50 m were rarely available for sampling. Hanging wall alteration of all three chemical types is developed at distance typically up to 50 m, but a few anomalous samples were identified at distances of up to 300 m.
  - b) The anomalous patterns observed in the wall rocks of the Chu Chua showing (Figs. 3.15 through 3.17) consist of two clusters of anomalous samples centered at the south end of the main ore body, and below and over the stratigraphically lower and smaller ore lens. More subtle details or zonation are not discernible, which reflects the vein-controlled nature of the alteration.
5. Based on spatial patterns of occurrence of basalt, chert, and massive sulphide lenses, it is suggested that a normal fault bounding a graben (or a half graben) depression exists in the footwall of the deposit. The structure is defined by the lower contact of the wedge of cherty rocks and its surface trace has a north-northeast trend. Hydrothermal activity, marked by chert exhalites, the massive sulphide ore bodies, rocks of anomalous

mineralogy (talc-magnetite) and chemistry (Na and Ca loss, Fe and Mg addition and SiO<sub>2</sub> mobility) is focused at the fault's intersection with the paleoseafloor indicating that the fault might have been the primary conduit for the hydrothermal solutions. Consequently, prospects for the occurrence of more ore bodies exist in a north-northeastern direction from the Chu Chua showing.

## References

- Aggarwal, P.K., (1982) Geochemistry of the Chu Chua Massive Sulfide Deposit, British Columbia: M.Sc. thesis, University of Alberta, Edmonton, AB, 70 p.
- Aggarwal, P.K., Toshitsugu, F. and Nesbitt, B.E., (1984) Magmatic Composition and Tectonic Setting of Altered Volcanic Rocks of the Fennel Formation, British Columbia: Canadian Journal of Earth Sciences, 21, p. 742-752.
- Barrett, T.J., MacLean, W.H., Cattalani, S., Hoy, L. and Riverin, G., (1991) Massive Sulphide Deposits of the Noranda Area, Quebec; III, The Ansil Mine: Canadian Journal of Earth Sciences, 28, p. 1699-1730.
- Barrett, T.J. and MacLean, W.H., (1994) Chemostratigraphy and Hydrothermal Alteration in Exploration for VHMS Deposits in Greenstones and Younger Volcanic Rocks. *In*: Lentz, D.R., (editor) Alteration and Alteration Processes Associated with Ore-forming Systems: Geological Association of Canada, Short Course Notes, 11, p. 433-467.
- Boynton, W.V., (1984) Geochemistry of the Rare Earth Elements: Meteorite Studies. *In*: Henderson P. (editor) Rare Earth Element Geochemistry: Elsevier, New York, p. 63-114.
- Campbell, R.B. and Tipper, H.W., (1971) Geology of Bonaparte Lake Map-area, British Columbia: Geological Survey of Canada, Memoir 363, 354 p.
- Campbell, R.B. and Okulitch, A. V., (1976) Stratigraphy and Structure of Mount Ida Group, Vernon (82L), Adams Lake (82MW1/2), and Bonaparte (92P) Map-areas: Report of Activities, Part A. Geological Survey of Canada, Paper 73-1A, p. 21-23.
- Chamley, H., (1989) Clay Sedimentology: Springer-Verlag, Berlin, Heidelberg, 623 p.
- Dietrich, R.V. and Skinner, B. J., (1979) Rocks and Rock Minerals: John Wiley & Sons, 319 p.
- Franklin, J.M., (1995) Volcanic Associated Massive Sulphide Base Metals: *In*: Eckstrand, O.R., Sinclair, W.D. and Thorpe, R.I., (editors) Geology of Canadian Mineral Deposit Types: Geological Survey of Canada, Geology of Canada, 8, p. 158-183.

- Jarvis, I., (1985) Geochemistry and Origin of Eocene-Oligocene Metalliferous Sediments from the Central Equatorial Pacific; Deep Sea Drilling Project sites 573 and 574. *In: Initial Reports of the Deep Sea Drilling Project Leg 85, Covering Cruises of the Drilling Vessel Glomar Challenger; Los Angeles, California to Honolulu, Hawaii, March-April 1982*, p. 781-804.
- Hesse, R., (1986) Diagenesis. Early Diagenetic Pore Water/Sediment Interaction: Modern Offshore Basins: *Geoscience Canada*, 13, p. 165-197.
- LeMaitre, R.W., (editor) Bateman, P., Dudek, A., Keller, J., Lemeyre, J., Le Bas, M.J., Sabine, P.A., Schmid, R., Sorensen, H., Streckeisen, A., Wooley, A.R., Zanettin, B., (1989) *A Classification of Igneous Rocks and Glossary of Terms: Blackwell Science Publications, Oxford, UK*, 193 p.
- MacLean, W.H. and Kranidiotis, P., (1987) Immobile Elements as Monitors of Mass Transfer in Hydrothermal Alteration; Phelps Dodge Massive Sulphide Deposit, Matagami, Quebec: *Economic Geology*, 82, p. 951-962.
- McMillan, W. J., (1979) CC Prospect, Chu Chua Mountain: Geological Fieldwork, 1979; a Summary of Field Activities, Ministry of Energy, Mines and Petroleum Resources, Paper 1980-1, p. 37-48.
- Migdisov, A.A., Gradusov, B.P., Bredanova, N.P., Bezrogova, E.V., Saveliev, B.V. and Smirnova, O.N., (1983) Major and Minor Elements in Hydrothermal and Pelagic Sediments of the Galapagos Mounds Area, Leg 70, Deep Sea Drilling Project. *In: Initial Reports of the Deep Sea Drilling Project Covering Leg 70 of the Cruises of the Drilling Vessel Glomar Challenger; Balboa, Panama to Callao, Peru, November-December, 1979*, p. 277-295.
- Morimoto, N., (1989) Nomenclature of Pyroxenes: *Canadian Mineralogist*, 27, p. 143-156.
- Morton, R.L. and Franklin, J.M., (1987) Two-fold Classification of Archean Volcanic-Associated Massive Sulphide Deposits: *Economic Geology*, 82, p.1057-1063.
- Pearce, T.H., (1968) A Contribution to the Theory of Variation Diagrams: *Contributions to Mineralogy and Petrology*, 19, p. 142-157.
- Preto, V.A., (1979) Barrier Lakes – Adams Plateau Area: British Columbia Department of Energy, Mines and Resources. Paper 1979-1C, p. 31-37.
- Preto, V. A. and Shiarizza, P., (1982) Geology and Mineral Deposits of the Eagle Bay and Fennel Formation from Adams Plateau and Clearwater, South-central B. C.: *Geological Association of Canada, Cordilleran Section, Program with Abstracts*, p. 22-24.
- Robinson, M., Godwin, C.I. and Juras, S.J., (1994) Major Lithologies of the Battle Zone, Buttle Lake Camp, Central Vancouver Island (92F/12E). *In: Geological Fieldwork 1993; a*

Summary of Field Activities and Current Research, Paper – Ministry of Energy, Mines and Petroleum Resources, p. 319-337.

Shervais, J.W., (1982) Ti-V Plots and the Petrogenesis of Modern and Ophiolitic Lavas. *Earth and Planetary Science Letters*, 59, p. 101-118.

Sinclair, A.J. and Stanley, C.R., (1995) Lithogeochemical Exploration for Metasomatic Alteration Zones Associated with Hydrothermal Mineral Deposits: University of British Columbia, MDRU Research Proposal, 7 p.

Stanley, C.R., (1996) Graphical Investigation of Lithogeochemical Variations Using Molar Element Ratio Diagrams: Theoretical Foundation. Lithogeochemical Exploration for Metasomatic Zones Associated with Hydrothermal Mineral Deposits, Mineral Deposits Research Unit, Lithogeochemical Research Project: Annual Technical Report Year 1, 40 p.

Stanley, C.R., (1997a) Analytical Quality Control and Assessment for the MDRU Lithogeochemical Exploration Research Project. Lithogeochemical Exploration for Metasomatic Zones Associated with Hydrothermal Mineral Deposits. Annual Technical Report, Years 1 and 2. Mineral Deposits Research Unit, Department of Geological Sciences, The University of British Columbia, Vancouver, B.C., 32 p.

Stanley, C.R., (1997b) THPLOT.M: A ATLAB Function to Implement Generalized Thompson-Howarth Error Analysis Using Replicate Data. Lithogeochemical Exploration for Metasomatic Zones Associated with Hydrothermal Mineral Deposits. Annual Technical Report, Years 1 and 2. Mineral Deposits Research Unit, Department of Geological Sciences, The University of British Columbia, Vancouver, B.C., 51 p.

Stanley, C.R. and Madeisky, H.E., (1995) Lithogeochemical Exploration for Metasomatic Zones Associated with Hydrothermal Mineral Deposits Using Pearce Element Ratio Analysis: 17<sup>th</sup> International Geochemical Exploration Symposium, Townsville, Queensland, Australia, Short Course #1 notes, May 13-14, 97 p.

Thurston, D.R., (1972) Studies on Bedded Cherts. *Contributions to Mineralogy and Petrology*, 36, p. 329-334.

Varentsov, I.M., Sakharov, B.A., Drits, V.A., Tsipursky, S.I., Choropov, D.Y. and Alexandrova, V.A., (1983) Hydrothermal Deposits of the Galapagos Rift Zone, Leg 70; Mineralogy and Geochemistry of Major Components. *In: Initial Reports of the Deep Sea Drilling Project Covering Leg 70 of the Cruises of the Drilling Vessel Glomar Challenger; Balboa, Panama to Callao, Peru, November-December, 1979*, p. 235-268.

Wheeler, J.O., Brookfield, A.J., Gabrielse, H., Monger, J.W.H., Tipper, H.W. and Woodsworth, G.J., (1991) Terrane Map of the Canadian Cordillera; Geological Survey of Canada, Map 1713A, 1:2 000 000.

## Chapter 4

### Molar Element Ratio Analysis of Major Element Lithogeochemical Data from the Konuto Lake Group Copper-zinc Volcanic Hosted Massive Sulphide Deposits, Flin Flon Mining Camp, Manitoba and Saskatchewan



Plate 4.1. The rocky banks of Konuto Lake.



## **Abstract**

Four, relatively small Cu-Zn VHMS deposits are hosted by mostly mafic rocks of the Birch Lake volcanic assemblage near Flin Flon, Manitoba. Mapping and drill-core sampling of the tholeiitic basalts and other rocks occurring in the area yielded 227 lithogeochemical samples. The primary and secondary lithogeochemical variability in the rocks was characterized and hydrothermal alteration was quantified using Molar Element Ratio (MER) methodology.

The rocks in the study area belong to two volcanic assemblages: Birch Lake and Sandy Bay assemblages. Using high-field-strength element concentrations, the Konuto Lake and Ruth Lake gabbroic sills are found to be chemically related to the volcanic rocks of the Birch Lake assemblage. Similarly, the gabbroic rocks of the Cable Lake sill are chemically related to the volcanic rocks of the Mosher Lake assemblage.

Hydrothermal alteration associated with the Konuto Lake, Birch Lake and Flexar deposits is subtle and, viewed on a property scale, discreet rather than pervasive. It is manifested as a combination of the following chemical effects: loss of Ca and Na, addition of  $\text{SiO}_2$  and addition of Fe and Mg. Low contrast and spotty lithogeochemical anomalies reflecting these losses and additions are outlined at distances of up to 250 m from the known ore bodies. The alteration patterns revealed by MER analysis are spatially correlated with the known sulphide ore bodies. The most useful alteration effect yielding the most intense anomalies was found to be Ca and Na loss. In the specific setting of the study area it was found that Generalized Element Ratio plots projected through  $\text{SiO}_2$  and, thus, removing the effect of this component of metasomatism, is the most useful in quantifying the ore-related alteration from an exploration perspective.

## **Introduction**

The Konuto Lake deposit is near the provincial boundary between Saskatchewan and Manitoba, approximately 16 km southwest of the mining town of Flin Flon and 1 km east of Denare Beach. The deposit contains approximately 1.5 million tonnes of ore grading over 5% copper and 1% zinc with significant gold and silver grades. The ore body was first

identified as an electromagnetic anomaly by a routine airborne survey, conducted by Hudson Bay Exploration and Development Co. (HBED). After follow-up drilling and development, underground production commenced in 1999.



Fig. 4.1. Location of the Konuto Lake deposit

Together with similar deposits such as Coronation (1.3 Mt), Flexar (0.31 Mt) and Birch Lake (0.28 Mt), the recently discovered Konuto Lake deposit represents the westward extension of the historic Flin Flon Mining Camp. Although small, the deposits have high copper grades (as high as 6% Cu) and together define a copper-rich region (Reilly, 1995). They all are hosted in a tholeiitic basalt-dominated sequence (Birch Lake assemblage; Slimmon, 1994), which distinguishes them from the rest of the deposits in the Flin Flon – Amisk area.

This work is part of a broader study of the lithogeochemistry of alteration zones associated with volcanic-hosted massive sulphide deposits. The study aims at testing the applicability of molar element ratio (MER) analysis as an exploration methodology, targeting alteration

halos of massive sulphide deposits. The goal is to separate the effects of metasomatism from those of other processes (*e.g.*, igneous fractionation, metamorphism) and quantitatively characterize alteration related to mineralization. The Konuto Lake deposit was chosen as a good example of a massive sulphide ore body, hosted by a predominantly mafic volcanic rock sequence.

## **Geologic Setting**

### ***Regional Geology***

The rocks hosting the Konuto Lake deposit are part of the Amisk Collage (Fig. 4.2c), a complex of distinct tectonostratigraphic assemblages (Lucas *et al.* 1996). The Amisk Collage together with the Snow Lake Arc assemblage and the Hanson Lake Block makes up the Flin Flon metavolcanic belt (Fig. 4.2b,c), a relatively low grade metamorphic domain within the Paleoproterozoic Trans-Hudson Orogen (Baird *et al.* 1996). The volcano-sedimentary assemblages making up the Amisk Collage were derived from a variety of tectonic environments: juvenile arc, mature arc, back arc and ocean floor. Amalgamation took place at a relatively early stage of the tectonic evolution of the region (1.88 – 1.87 Ga; Lucas *et al.* 1996). The volcanism is interpreted to have occurred in island arcs and back-arc basins ranging in age from 1.92 to 1.88 Ga (Gordon *et al.* 1990; David *et al.* 1993; Heaman *et al.* 1993; Stern *et al.* 1993; Syme *et al.* 1993). It was followed by convergent tectonic events leading to the terrane amalgamation and the formation of an intraoceanic accretionary complex at *ca.* 1.88 – 1.87 Ga (Lucas *et al.* 1996). Plutons and coeval volcanic rocks are imposed on the older volcanic terranes (Lucas and Stern, 1994) by a younger arc-trench system (or systems) propagating through the collage at *ca.* 1.87 – 1.84 Ga. Deposition of the molasse-type sediments of the Missi Group (Bruce, 1918) occurred approximately at the same time. This combination of tectonic and magmatic thickening of the crust eventually led to the stabilization of the Flin Flon Belt by 1.85 – 1.84 Ga (Lucas *et al.* 1996). Younger collisional thrusts (*ca.* 1.83 – 1.69 Ga.; Bickford *et al.* 1990; Gordon *et al.* 1990; Machado, 1990; Ashton *et al.* 1991; Stern and Lucas, 1994; Ansdel and Norman, 1995; Fedorowich *et al.* 1995; Heaman *et al.* 1995) bound the Flin Flon Belt on its west, north and east sides and structurally isolate it from the rest of the orogenic belt. Phanerozoic sedimentary rocks overly the belt to the south (Leclair *et al.* 1994a, 1994b).

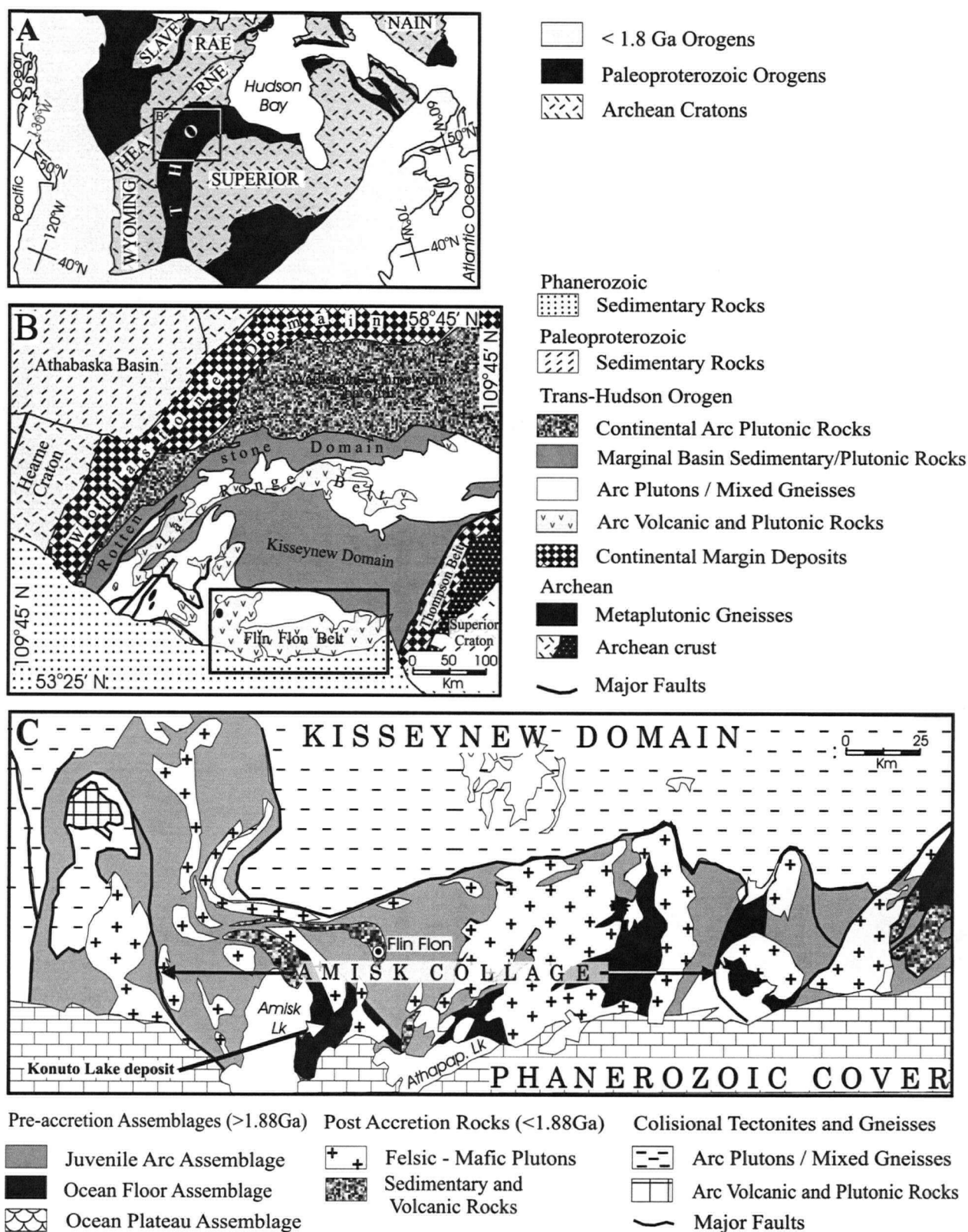


Fig. 4.2. Regional geologic setting of the Konuto Lake deposit area. (Modified from Lucas *et al.*, 1996)

A. Location of the Trans-Hudson Orogen (THO) relative to the Archean provinces of North America. (pre-Atlantic reconstruction), after Hoffman (1989). B. Major features of the THO, after Hoffman (1988).

C. Map of the Flin Flon Belt showing major tectono-stratigraphic assemblages and plutons.

Two volcanic assemblages, Birch Lake and Sandy Bay assemblages (Slimmon, 1991, 1993; Fig. 4.3), have been recognised in the area immediately east of Amisk Lake. These are distinguished based on their lithology, metamorphic grade and geochemical characteristics. It was previously believed that the rocks of the two assemblages were separated by the Mosher Lake Shear Zone, a north-south trending lineament (Slimmon, 1994). This study shows that:

(1) Sandy Bay assemblage volcanic rocks (here termed Mosher Lake volcanic rocks) occur on both sides of the Mosher Lake Shear Zone in its section north of Denare Beach.

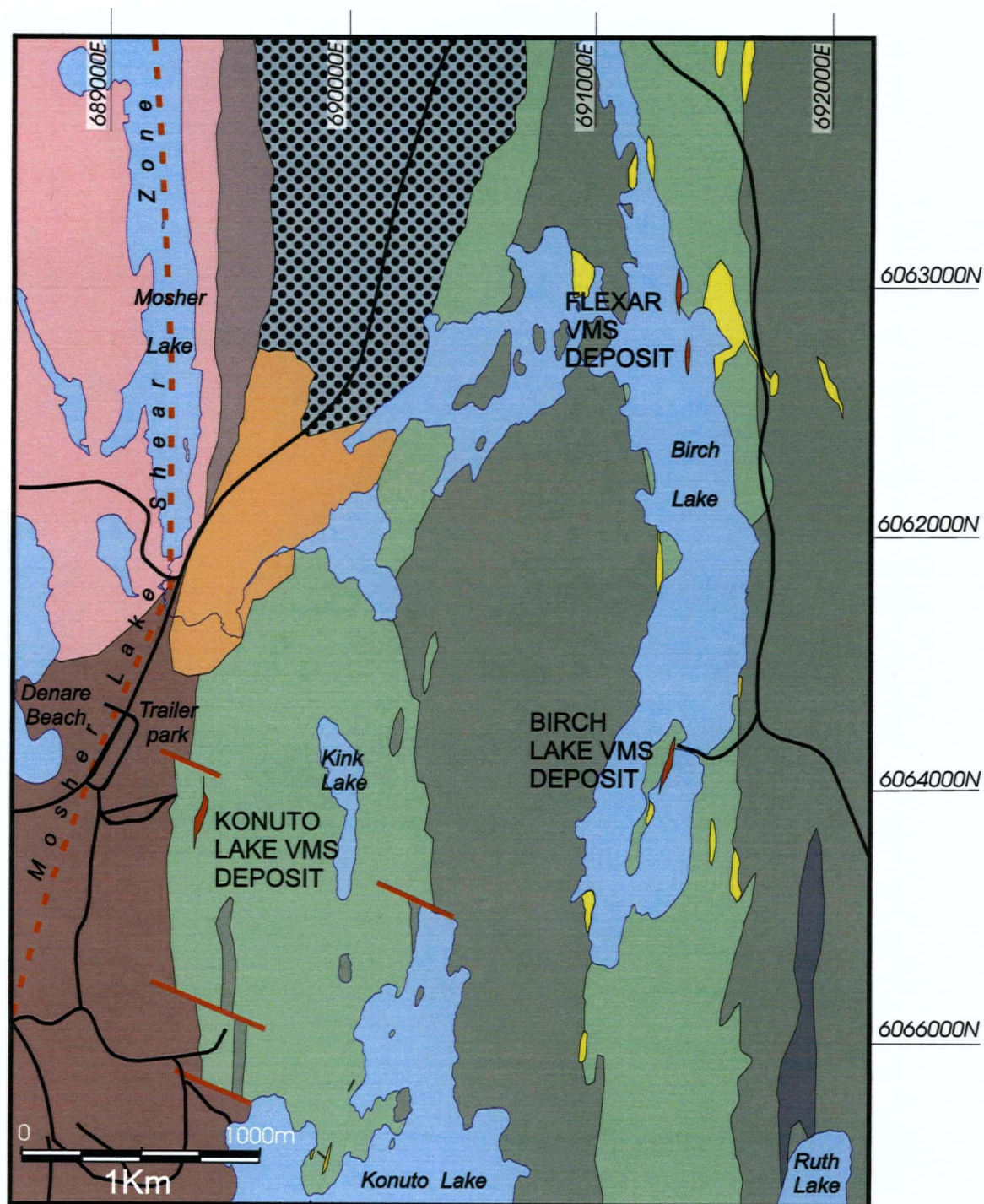
(2) The Cable Lake gabbroic sill is geochemically similar to the Mosher Lake volcanic rocks (Figs. 4.5 through 4.7) and, thus, belongs to the Sandy Bay assemblage.

Consequently, the boundary between the two assemblages does not coincide with the Mosher Lake Shear Zone, but rather lies to the east of it.

The Sandy Bay assemblage, lying west of the Mosher Lake Shear Zone, comprises primarily aphyric and feldspar-phyric pillowed mafic flows. Massive flows are less common and volcanoclastic deposits are rare. Primary volcanic structures are better displayed than in the adjacent Birch Lake assemblage. Pillowed flows, minor flow-breccia deposits and local, centimetre-scale interflow tuffaceous horizons were also described within this unit (*e.g.*, Slimmon, 1994). Based on their mineralogical composition (chlorite, albite, zoisite/clinozoisite, +/- quartz, +/- actinolite; Longiaru, 1980) the pale green rocks of the Sandy Bay assemblage belong to the greenschist metamorphic facies. Moderate to strong schistosity is typically present. Local shear zones are commonly carbonatized and silicified.

The Konuto Lake deposit is within the eastern Birch Lake assemblage. The host assemblage comprises a sequence of massive, feldspar phyric and amygdaloidal flows. Thin (less than 20 m) layers of ash and lapilli tuffs with felsic and mafic clasts in a mafic groundmass occur sporadically (Plate 4.2). The metamorphism is upper greenschist to lower amphibolite grade, as indicated by the present mineral paragenesis: hornblende, plagioclase, +/- epidote, +/- quartz (see also Robinson, 1996). A moderate to strong schistosity defines local high strain zones, where tectonic lamination gives the rocks a tuffaceous appearance.





### LEGEND:










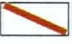

<u>Birch Lake assemblage</u>		<u>Sandy Bay assemblage</u>	
	Ruth Lake ultramafic sill (mela-olivine gabbro)		Cable Lake sill (gabbro)
	Konuto Lake and Birch Lake sills (gabbro)		Moshier Lake - West volcanic rocks (basalt)
	Birch Lake volcanic flows (basalt)		Moshier Lake - East volcanic rocks (basalt)
			Rhyolite
			Granodiorite and quartz-plagioclase porphyritic dacite
			Undivided rocks
			Fault
			Deposit

Fig. 4.3. General geology of Konuto Lake and Birch Lake area



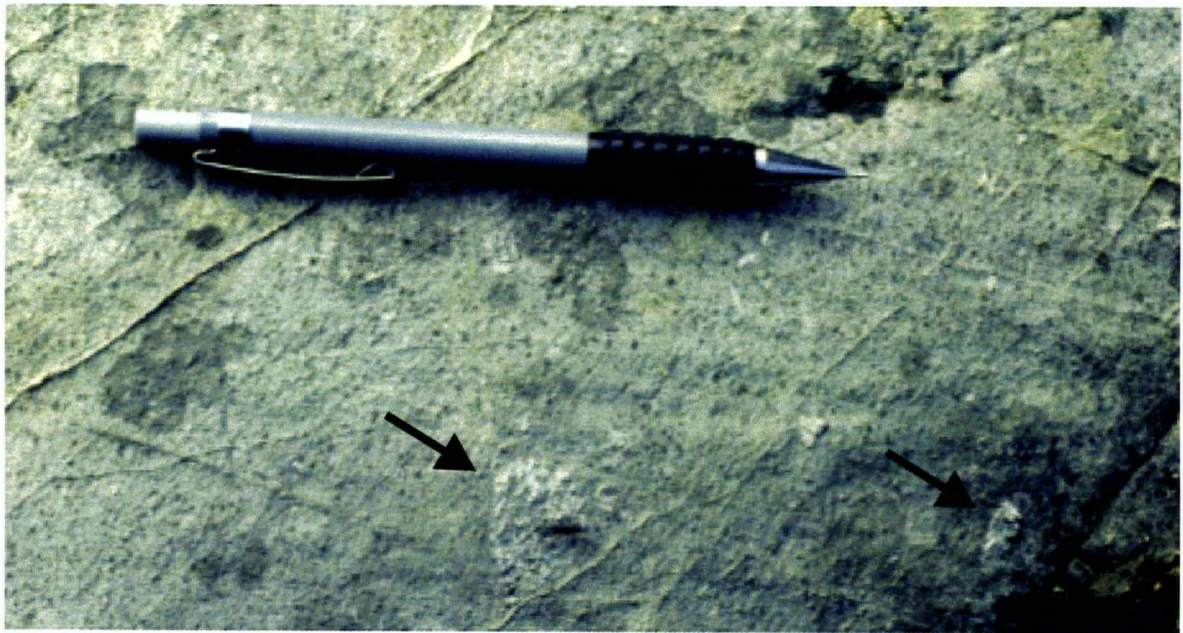


Plate 4.2. Felsic tuff lapilli (arrows) in a basaltic lava flow. Birch Lake Assemblage, Mapping point HS95M30 (Appendix 9).

### ***Local Geology***

The mapping program completed in June 1996 in the area of the Konuto Lake deposit (Fig. 4.3) offered ample opportunity for field observation of the rocks hosting the deposits. Three main types of rocks were identified (in order of decreasing age): (1) Birch Lake basalt flows; (2) Gabbroic sills and/or dykes; (3) Feldspar-porphyrific dacite/granodiorite. Variations within these rock types are responsible for the diversity of rocks occurring in the area.

#### **Birch Lake Assemblage Basalt Flows**

The volcanic rocks of the Birch Lake assemblage occupy most of the study area (Fig. 4.3) and host three VHMS deposits: Konuto Lake deposit and the more easterly situated Birch Lake and Flexar deposits. The basalt flows in this area have been previously described as "mafic volcanics" (Morgan, 1995) and "Birch Lake basaltic andesites" (Robinson, 1996). Here the term "basalt" is preferred because the chemical composition (Fig. 4.4) of the flows is closer to basalt than to andesites. The superficial andesitic character of the rocks is interpreted in part to be the result of superimposed processes.

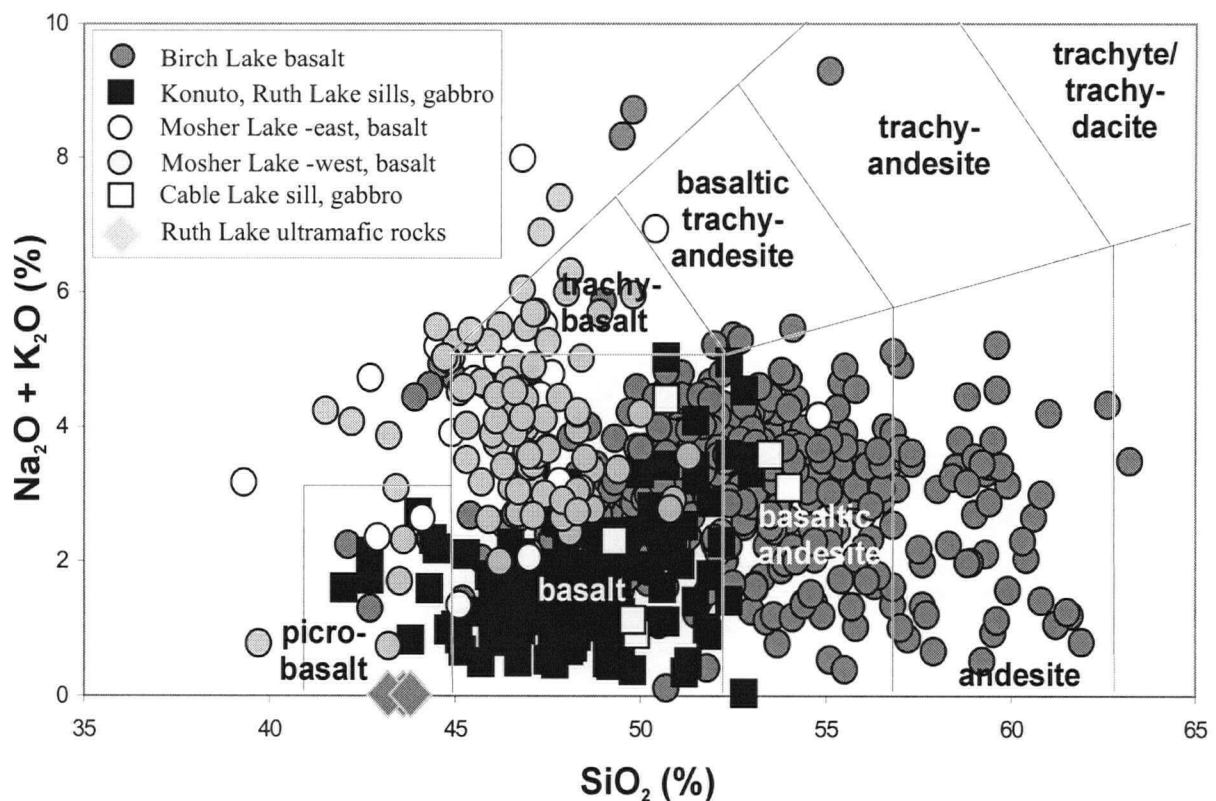


Fig. 4.4. Total alkalis vs. silica (TAS) diagram (Le Maitre *et al.*, 1989) for the mafic and ultramafic rocks of the Konuto Lake and Birch Lake areas. The diagram is devised for volcanic rocks, but plutonic rocks occurring in the study area are shown for comparison.

The basaltic flows occur in a broad north-south trending band between Konuto Lake and the west arm of Birch Lake. A second band occurs to the east of the mapped area and its western-most parts were mapped on the western shore of Birch Lake. The basaltic flows are flanked by gabbroic sills, the north-south trending contacts being of intrusive nature. Swarms of small dykes commonly cross-cut the volcanics in the vicinity of the contact and slivers and lenses of volcanic rocks penetrate into the gabbros. The immediate contact is commonly silicified and (to a lesser extent) epidotized, which in some cases (*e.g.*, mapping station No. HS96M315, Appendix 9) results in a several metres wide contact zone. Calcite and clinozoisite are also observed along the contacts and a few metres into the gabbros. Fault contacts are observed in the south-west portion of the area.



The volcanic rocks in the mapped area are invariably lava flows with thicknesses of several centimeters to more than 5 metres. On the TAS diagram (Fig. 4.4) many of them plot as basaltic andesite and even andesite. The more felsic character of some of the samples reflects epigenetic  $\text{SiO}_2$  deposition in voids (gas vesicles, contraction cracks *etc.*). The lava flows are vertical or very steeply dipping to the east or west, so that the erosion surface is a near-perfect perpendicular cross-section of the volcanic sequence. Separate lava flows are remarkably similar in colour and texture. As noted by Morgan (1995), "There were not enough features to permit breaking down the overall volcanic sequence in any convincing way". The combination of sparse and interrupted outcrops and monotonous character of the rocks with a lack of contrasting marker horizons makes lateral correlation of units impossible. However, careful observation of outcrops allowed three parts to be identified in each flow. Distinctions are based on colour in outcrop and hand sample, macroscopic and microscopic texture, mineralogy, sulphide abundance and morphology and distribution of amygdules, pipe vesicles and veinlets.

1. The flow bottoms (Plate. 4.3), distinguishable only in beds thicker than 0.5-1 m, have the following characteristics:
  - a) In outcrop, the flow bottoms are massive (as opposed to the foliated flow tops) and with very fine-grained granular texture. They are green-gray in colour, due to the presence of fine, but macroscopically distinguishable hornblende crystals. In thin section, they commonly exhibit a fully crystalline hypidiomorphic granular texture (Plate 4.4a), dominated by amphibole.
  - b) The size of the phenocrysts is on the order of 0.1 mm. Amphibole glomerocrysts are also present (Plate 4.4b).
  - c) The main leucocratic phase is granular plagioclase. No granular quartz is present.
  - d) The lower parts of the flow bottoms are cross-cut by quartz and epidote veinlets
  - e) The density and thickness of the veinlets increases strongly towards the interface with the underlying flow. They are predominantly oriented in parallel and perpendicular directions to the flow interface and are abruptly terminated by it.
  - f) Amygdules do not occur in this unit, whereas pipe amygdules are commonly observed (Plate 4.5), filled with quartz and epidote.

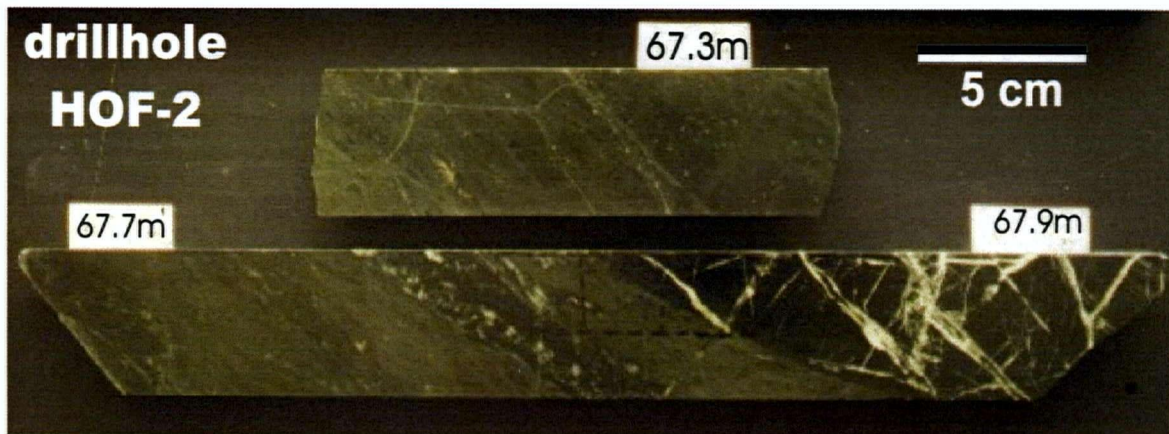


Plate 4.3. Interface between tops and bottoms of basalt flows in core from drill hole HOF-2, 67.2-67.9 m (Appendix 9). The tops are green, tectonized, containing fragments of amygdules, wisps of iron sulphides and abundant chlorite. The bottoms are massive, almost black, criss-crossed by abundant quartz-filled cracks. The majority of the cracks are orientated in two directions: roughly parallel and perpendicular to the interface surface.

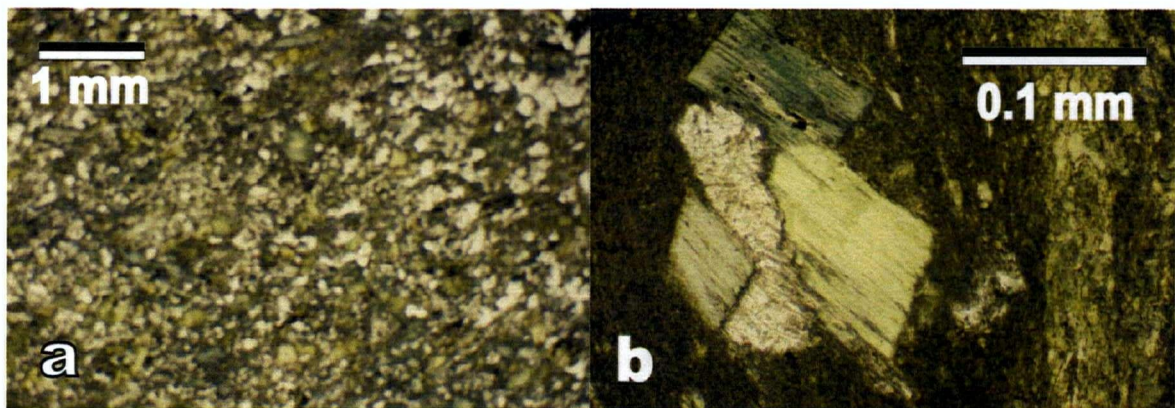


Plate 4.4. Basaltic flow bottoms, sample No. HS96M75-1 (Appendix 9).

- a. The rock is massive, composed of fine equigranular amphibole and plagioclase crystals (plane-polarized light).
- b. Amphibole replacing a glomerocryst of pyroxene (plane-polarized light).



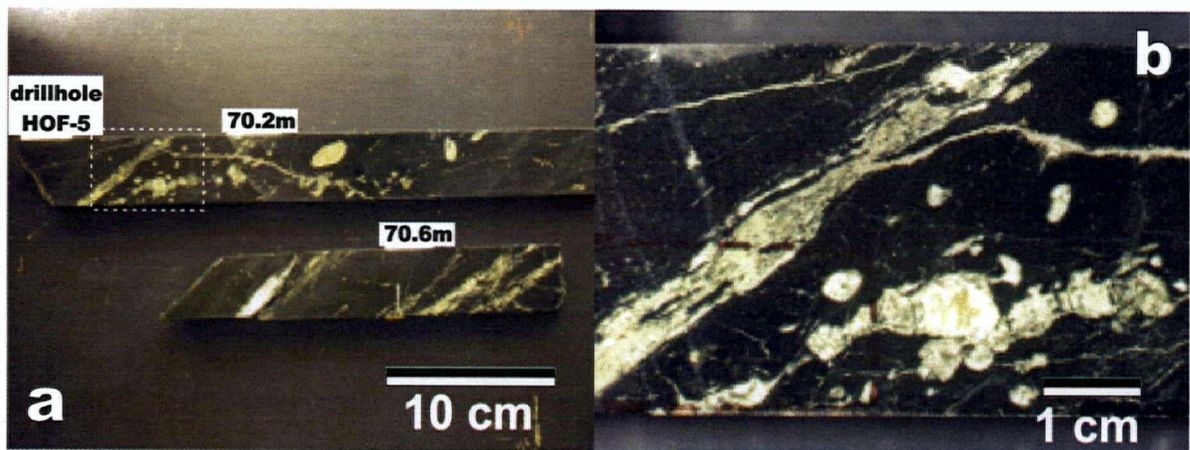


Plate 4.5. Pipe amygdules in basaltic flow bottoms in core from drill hole HOF-5, 70.1-70.7 m (Appendix 9).

- a. Pipe amygdules occur near the flow bottoms.
- b. A close-up photograph of a pipe vesicle.

2. The fine-grained, porphyritic, green flow-bottoms grade into aphyric, dark brown to black middle to upper portions of the flows, the interface being sharp (1-2 cm), but irregular in shape. Features that distinguish these parts of the flow from bottoms and tops are:
  - a) In outcrop these parts of the flows are finely fractured, which is a reflection of their increasingly foliated nature observed in thin sections.
  - b) In hand sample they are black, with slight brownish hue and aphanitic texture.
  - c) Irregular patches of amygdules up to 1 cm in size are characteristic of this part of the flows. Quartz amygdules occur more commonly towards the top of the flow, although their distribution is generally irregular. Only rarely the amygdaloidal domains can be traced laterally for distances of up to several meters, thus defining flow-planes. Pipe amygdules occur, but are uncommon and small in size.
  - d) The dominant leucocratic phase is quartz, present in the amygdules. Plagioclase microphenocrysts are present in the groundmass. Microscopic textures are aphanitic.
  - e) Cross-cutting veinlets are rarer and thinner in this part of the flows and exhibit random orientation.

3. The flow tops (Plate 4.6) are commonly 1 to 20 cm thick and exhibit the following characteristics:
- a) They are strongly foliated, having accommodated most of the flow-parallel shearing in the stratigraphic sequence section. Amygdules and pyrite grains are stretched into foliation acquiring a lenticular shape with high aspect ratio.
  - b) Colour in hand sample is green, due to intense chloritization, observable in thin section.
  - c) Amygdules are not visible in hand sample, due to being tectonized. However, in thin section stretched small amygdules are distinguishable and locally abundant. Larger ones are distorted to acquire the shape of lenses and veinlets, conformable to foliation.
- No pipe vesicles are observed in the flow tops.

The alternation of the units described above is obscure in most outcrops. At mapping station HS96M75 (Appendix 9) and in several drillholes, a relatively clear sequence is observed, indicating younging of the flow sequence to the west. The variations in the amygdule abundance in the basaltic rocks is ascribed to fractionation of gases within the individual flows, rather than to variability of gas exsolution from different flows.



Plate 4.6. Basaltic flow tops from drill hole HOF-5, 58 m (Appendix 9).

The rocks are intensively tectonized, with abundant quartz fragments, iron sulphide wisps (grains stretched into foliation) and chlorite.

a. Hand specimen; b. Thin section (plane polarized light)



Pillows and pillow-like epidosite domains of oval shape were observed within this unit or a small distance into the lower flow unit. Well defined pillows are rare and were observed only in a few locations. Invariably, they are isolated and not well preserved and cannot be used to draw conclusions about stratigraphic younging and flow directions. Where preserved, pillows exhibit typical spherulitic rinds (Plate 4.7). Epidosite domains vary in shape from almost globular to vein-like bodies. Their occurrence is restricted to the tops and the upper parts of the flows. They are diagenetic features that form at a later stage of the evolution of the rock. Cross-cutting relations show that at least some of the chlorite veining predated their formation.

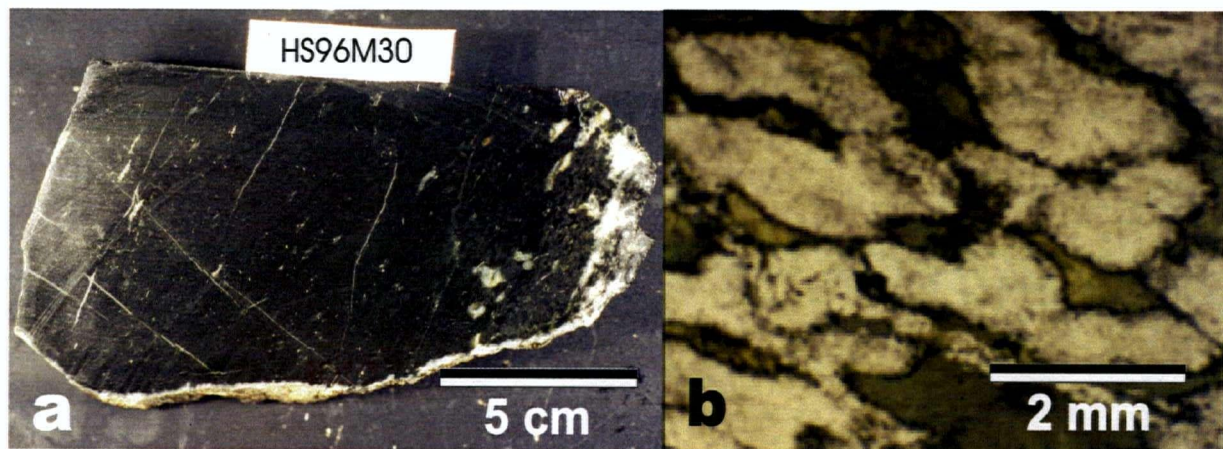


Plate 4.7. Pillow basalt, Birch Lake assemblage, sample HS96M30 (Appendix 9).

- a. A fragment of a basaltic pillow displaying typical spherulitic texture.
- b. Photomicrograph of spherulitic texture of a pillow rind, composed of felsic spherulites in a mafic groundmass (plane-polarized light).

### **Clinopyroxene Phyric Gabbro**

The Birch Lake basaltic flows are flanked on the east and west by two gabbroic intrusive bodies. Their exposed thicknesses are on the order of several hundred meters. The contacts with the volcanic rocks are clearly intrusive, which is indicated by the abundance of mafic volcanic xenoliths in the gabbros and gabbroic dykes and sills cross-cutting the volcanic rocks. Adjacent to the contacts, the gabbros are silicified and less intensely epidotized and carbonatized. In some outcrops the contacts can be mapped as gradational, which is

indicative of the large amount of assimilation that occurred. In some cases pyroxene is altered to serpentine. Plagioclase is only slightly sericitized.

The gabbros are typically clinopyroxene-phyric (Plate 4.8). They contain varying proportions of plagioclase and pyroxene, leading to modal compositions of plagioclase-rich gabbros to almost pyroxenite. Although they commonly have the appearance of a more felsic rock (Morgan, 1995, described them as "diorite or gabbro"), their chemical composition (Fig. 4.4) is typical of gabbros.

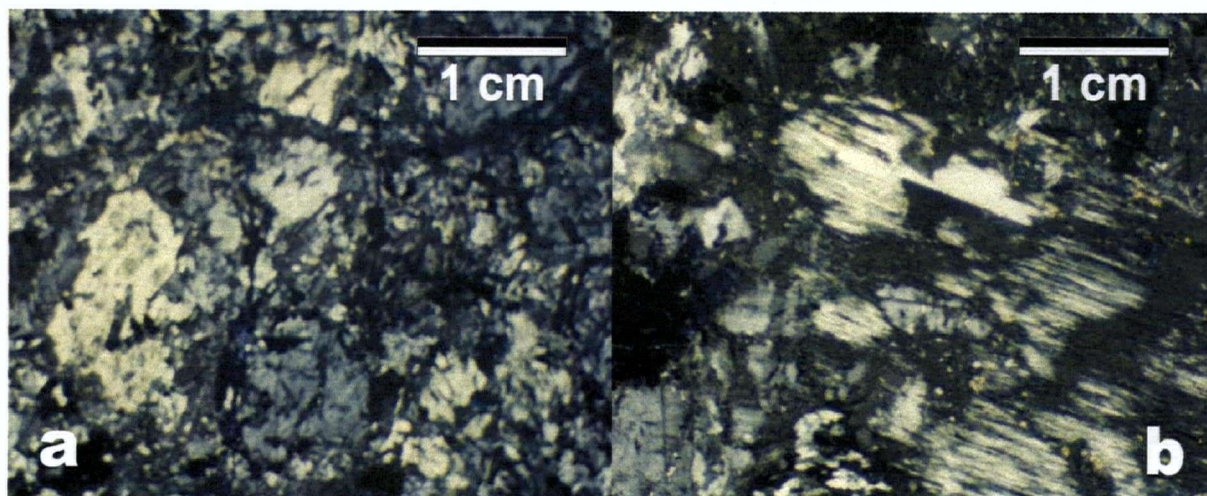


Plate 4.8. Gabbro, Konuto Lake sill, photomicrograph of sample No. HS96M240 (Appendix 9).  
a. Coarse grains of clinopyroxene in a Birch Lake gabbro (cross-polarized light), sample No. HS96M240 (Appendix 9).  
b. Serpentinized clinopyroxene grains in a coarse-grained Birch Lake gabbro (cross-polarized light), sample No. HS96M286 (Appendix 9).

#### **Ruth Lake Ultramafic Sill**

Ultramafic rocks in the vicinity of Birch Lake have been described previously (Reilly, 1995; Robinson, 1996) as pyroxenite or harzburgite. They occur in a narrow strip extending for several hundred meters north of Ruth Lake. The lithogeochemical data set contains four samples of these rocks, which have distinctive picritic chemistry and are practically devoid of K and Na (Fig. 4.4). They also have very low concentrations of the high-field-strength elements, such as Ti, Zr, Y, Nb and P. Petrographic specimens (hand samples or thin sections) were not available for observation and, thus, conclusions regarding their mineral



composition are drawn on the basis of their chemistry, using Pearce Element Ratio (PER) analysis (further in this text).

### **Granodiorite and Quartz-plagioclase Porphyritic Dacite**

Granodiorite occurs as a block in the north-western part of the map area, between the basalt to the east and south and a plutonic unit, containing mostly gabbro to the west and north. This is the youngest rock type in the study area as its associated dykes and aplites intrude both the gabbros and the basalt. The contacts of the granodiorite (and its related dykes and pegmatites) with the earlier intrusive rocks are sharp but irregular. North-south trending dykes of the same composition are present throughout the area. Their abundance increases with proximity to the gabbro-basalt contacts. Due to their nonplanar contacts, these dykes vary in thickness from centimeters to more than 10 m. Their margins commonly contain basaltic xenoliths.

The granodiorite and the quartz-plagioclase porphyritic dacite dykes (Plate 4.9) represent a series ranging from a plagioclase-phyric, fully crystalline rocks to porphyritic subvolcanic varieties (porphyritic dacite). Coarse plagioclase crystals are common in all varieties of

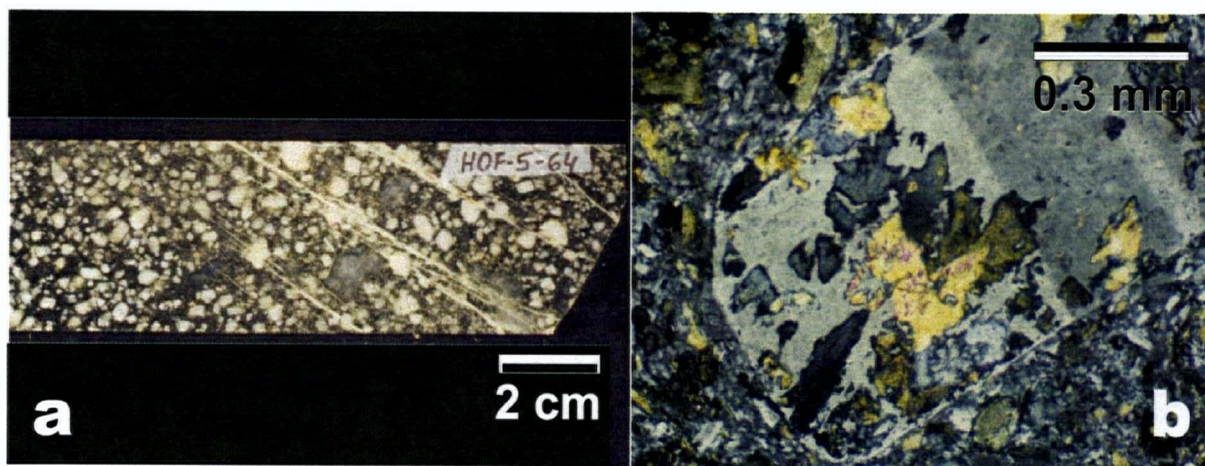


Plate 4.9. Quartz-plagioclase porphyritic dacite from drill hole HOF-5, 64 m (Appendix 9).

a. Hand specimen. Clearly seen are the plagioclase phenocrysts and the coarse and more rare quartz phenocrysts. The amphibole-rich groundmass is dark.

b. Photomicrograph, cross-polarized light. Plagioclase phenocryst including and immersed in a fine-grained groundmass of quartz, plagioclase, amphibole, and secondary epidote.

rocks of intermediate composition. In the dykes, they are commonly associated with coarse porphyritic quartz and finer porphyritic amphibole. Biotite phenocrysts are rare. Plagioclase and quartz phenocrysts display rounded (resorbed) edges and sometimes occur as skeletal crystals. Plagioclase also displays growth zones and is sericitized to a varying degree. Epidote is present in the samples only as infillings in the skeletal plagioclase crystals.

### **Mosher Lake Basalt Flows and Cable Lake Gabbro Sill**

The Mosher Lake basalt sequence (Fig. 4.3), belonging to the Sandy Bay assemblage, occurs approximately 2 km north and north-northwest of the study area. Unlike the mafic volcanic rocks of the Birch Lake assemblage, the Mosher Lake basalt displays well preserved pillow structures. Although these rocks are not related to the Konuto Lake deposit, analytical data donated by HBED were used for a comparison with the Birch Lake assemblage rocks.

According to previous studies (Slimmon, 1994), the north-trending Mosher Lake Tectonic Zone separates them from the basalt of the Birch Lake assemblage, hosting the Konuto Lake deposit. This study, however, found that samples collected by HBED east of Mosher Lake are chemically identical to the Mosher Lake basalt, occurring west of the lake. Thus, at least in the section north of Denare Beach, the Mosher Lake Zone is within the Sandy Bay assemblage. Furthermore, it was found that the gabbros of the Cable Lake sill (Fig. 4.3), occurring just west of the Konuto Lake deposit, have similar high-field-strength element ratios (Figures 4.4 through 4.7) and possibly are genetically related to the Mosher Lake basalt. Thus, it is possible that, the Cable Lake sill is part of the Sandy Bay assemblage.

### ***Structure***

Primary volcanic structures (*e.g.*, tuffaceous bedding, pillow structures, flow tops) are locally scarce or absent in the mapped area. Only a few pillows were positively recognized (Plate 4.7), but were not preserved well enough to positively determine the stratigraphic younging direction. No tuffaceous beds were observed. The only feature allowing interpretation of stratigraphic directions are the textures of different parts of the flows. Unfortunately, these features are much more conspicuous in the south-central part of the mapped area and not convincing in the northern part. According to the observed variation of textures of basaltic flows, the tops are to the west. This interpretation is consistent with the conclusion of earlier



workers in the area (Morgan, 1995), based on pillow tops. Although rarely and again restricted to the southern, HOF claim, alternation of textural features observed in core indicates the same direction of stratigraphic younging. At other locations within the area, however, the stratigraphic younging direction is determined to be to the east, based on one occurrence of an inch thick greywacke layer and metal zonation in the Konuto ore body (K.V. Gilmore and J.R. Pickell, pers. comm.). Folding was not identified in the area, possibly due to the scarcity of primary volcanic structures and other reliable stratigraphic indicators. The bedding is close to vertical, dipping to the east or west.

The most prominent and consistent structural feature in the area is the penetrative foliation, dipping steeply and trending northerly to north-northeasterly, subparallel to bedding. It is well developed in thin shear zones, coinciding in most cases with the basaltic flow tops. This foliation has significantly influenced the rock texture from only slight alignment of amphibole grains in the flow bottoms to development of mylonitic textures in the flow tops. The shape of amygdules is a good indicator of the extent of shearing associated with this foliation. Shapes and aspect ratios of amygdules vary from almost round (aspect ratio up to 1:2; Plate 4.10) to elongated, lenticular and even vein-like in the flow tops (Plate 4.6a). The most prominent tectonic feature in the region - the Mosher Lake Shear Zone is, at least in part of its extent, coplanar with the penetrative foliation in the basalt of the Konuto Lake area.

A number of shear zones striking at high angles to the stratigraphy were mapped within the area. The most prominent of them strikes northwest - southeast and is expressed as a series of photolineaments. It offsets lithologic contacts at distances of several hundred meters. The lithologic contact between the gabbros and the basalt along the western edge of the map are typically intrusive, but at two places, coinciding with big offsets, the contacts are sharp and seemingly tectonic in nature. One of these shear zones is responsible for the significant offset of the mineralized horizons to the north (red and blue zones of the Konuto Lake deposit) and to the south ("magenta" and "cyan" zones of the HOF claim).

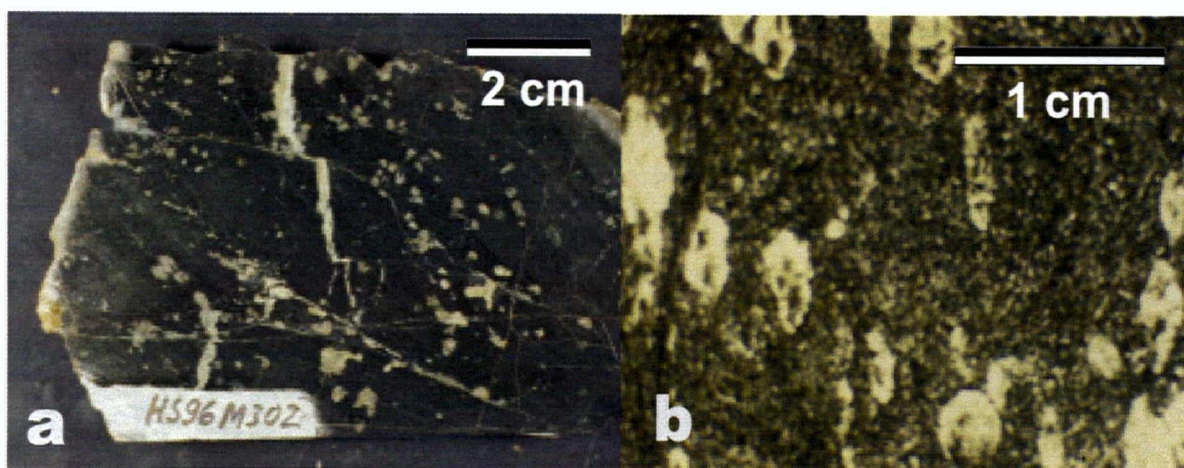


Plate 4.10. Amygdaloidal basalt from the Birch Lake assemblage, east of the Konuto Lake deposit and west of Kink Lake, sample No. HS96M302 (Appendix 9).

- a. Hand specimen showing quartz-epidote-filled amygdules of varying sizes and aspect ratios.
- b. Photomicrograph of quartz-epidote-filled amygdules (plane-polarized light).

### *Metamorphism*

The Birch Lake basalt is metamorphosed to amphibolite facies. The typical mineralogy consisting of amphibole and plagioclase is especially characteristic of the massive flow bottoms, which now are microamphibolites. Toward their tops, basalt flows become increasingly schistose, due to alignment of amphibole and plagioclase grains and stretching of amygdules. The flow tops are intensively sheared and fine-grained. Stretched quartz-filled amygdules and pyrite grains and aggregates emphasize schistosity.

Retrograde greenschist metamorphism is predominantly confined to the sheared portions of the sequence (the tops and upper parts) and is represented by growth of chlorite and epidote.

The gabbro and the granodiorite and porphyritic dacites in the area are metamorphosed only to a greenschist facies. This influence is stronger along permeable contacts with the rocks of the Birch Lake assemblage, where carbonate pods, as well as idiomorphic clinozoisite are developed. Plagioclase is sericitized moderately to intensely in different samples of these rocks and clinopyroxene is, in some cases, serpentized.

## ***Metallogeny***

The Early Proterozoic Flin Flon metavolcanic belt, occupying parts of northern Manitoba and Saskatchewan (Fig. 4.2c) is one of the most productive mineral regions in Canada. Twenty-five producing or past-producing Cu-Zn mines are located within the exposed portion of the belt covering an area of 250 by 50 Km. They are clustered in two mining camps: (1) the Flin Flon Mining Camp, encompassing the area within about 25 km from the town of Flin Flon and (2) the Snow Lake Mining Camp in the eastern portion of the belt. Production and reserves in these mines total over 110 Mt of ore (Syme and Bailes, 1993). The Flin Flon belt also hosts a number of gold mines.

### **Zn-Cu Basalt- and Rhyolite-hosted Deposits**

Large Zn-rich massive sulphide (VMS) deposits occur in the Flin Flon – Amisk Lake area (e.g., Flin Flon and Callinan mines), within tholeiitic island arc volcanic assemblages. These deposits typically occur in association with felsic volcanic units at major stratigraphic and compositional (major-element, trace-element and isotopic) breaks in the volcanic sequence. Most VMS deposits of this class are underlain by coarse volcanoclastic rocks, either mafic, intermediate or felsic, in which disconformable chloritic alteration zones are developed. Flin Flon (62.4 Mt) is the largest deposit of this type in the region.

### **Cu-rich, Predominantly Basalt-hosted Deposits**

The Birch Lake (0.28 Mt), Coronation (1.3 Mt), Flexar (0.31 Mt) and Konuto Lake (appr. 1.5 Mt) together define a Cu-rich trend on the western outskirts of the Flin Flon Mining Camp. They all are hosted by tholeiitic arc rocks. Metallogenic controls as described above for the Zn-rich deposits are unclear. Felsic volcanic rocks are present only in the wall rocks of the Birch Lake deposit.

Some VMS deposits present in the area do not conform to the above classification. The Fon deposit (5.1 Mt; Reilly, 1995) is hosted by calc-alkaline, dominantly felsic, volcanic and volcanoclastic rocks, while the West Arm deposit occurs in a pyritic, graphitic argillite.

## **Gold Deposits**

The Flin Flon – Amisk Lake area hosts numerous gold occurrences of which Newcor, Bootleg, Henning-Maloney, Rio, Monarch and Phantom have realized small amounts of production (Thomas, 1991). They are all shear zone-hosted, mesothermal type. The Laurel Lake gold–silver deposit has geological, structural, mineralogical and fluid inclusion characteristics resembling an epithermal system (Walker and McDougall, 1987; Ansdell and Kyser, 1991).

## **Porphyry Mineralization**

Porphyry-style copper-molybdenum-gold mineralization was documented on Missi Island (Kirkham, 1974). It is associated with a complex comprising felsic and intermediate porphyry dykes and lava flows and a polyphase pluton, interpreted as a subvolcanic vent structure (Chute and Ayres, 1977). The mineralization is characterized by extensive zones of pyritization, pervasive silicification and sericitization and a vein stockwork (quartz, carbonate, chlorite, epidote, hematite, pyrite) developed both in the porphyries and in the country rocks (Chute and Ayres, 1977).

## ***Konuto Lake Deposit***

The Konuto Lake deposit consists of two massive sulphide mineralized zones and one sulphide stringer zone that are crudely conformable with the stratigraphy and plunge steeply to the south. The west lens (Red #1) is the largest zone, while the central (Green #2) lens consists largely of sulphide stringers that often merge with somewhat banded and relatively Au- and Zn-rich eastern (Blue #3) lens. The sulphides consist of massive to disseminated chalcopyrite, pyrrhotite and pyrite, with lesser sphalerite and traces of arsenopyrite. Locally, bands of fine-grained magnetite, similar to those present at the nearby Birch Lake deposit occur in association with the sulphide zones. Bornite intergrown with chalcopyrite is microscopically observed in the ores. Present in trace amounts are cubanite, mackinawite, valleriite, tellurobismuthite, bismuthinite, molybdenite and native gold (K.V. Gilmore and J.R. Pickell, pers. comm.).

Hydrothermal alteration adjacent to the sulphide zones consists of chlorite, biotite, sericite, quartz and carbonate. This alteration dies out within a few metres of the sulphide zones. The host volcanic flows throughout the Konuto Lake area are extensively net-veined with fine epidote-quartz-carbonate-feldspar fracture-fill stringers (K.V. Gilmore and J.R. Pickell, pers. comm.).

## **Lithogeochemistry**

### ***Sampling and Analytical Quality Control***

The wall rocks of the Konuto Lake deposit and the adjacent Birch Lake, Flexar and Coronation deposits were sampled in 1995 and 1996. A total of 195 drill-core samples, approximately 1 kg each, representing the footwall and the hanging wall of the deposit, were taken from 20 drill holes (Appendix 5). They include both unaltered rocks and all visibly distinguishable types of alteration. The ore intervals were not available for sampling. Approximately 10% of these were duplicated in order to study the magnitude of analytical errors. The data set is augmented by 175 additional geochemical analyses of drill-core samples, supplied by Hudson Bay Exploration and Development (HBED).

In June 1996 a mapping project was implemented to constrain the structural setting of the deposit. Confident identification of the footwall and the hanging wall of the deposit was a necessary precondition for successful application of lithogeochemical methods of investigation. The mapping program yielded 32 samples collected from the surface and representing various lithologies occurring in the area. They, together with 539 local (Konuto Lake deposit) and regional surface samples, supplied by HBED were used to characterize the lithologic variability in the area, as well as to supplement the drill-core data set.

To justify mineralogical assumptions, made in the graphical investigation of lithogeochemical data, 83 thin sections of all visible varieties of rocks and alterations were prepared and partially studied (Appendix 7). The petrographic information was used as a control on the interpretations made using PER plots.

The Birch Lake and Flexar deposits, adjacent to Konuto Lake and occurring in a geologically similar environment were also sampled in 1995. A total of 38 samples were analyzed from these deposits and 53 thin sections were studied.

The samples from the main data set were analyzed for the major oxides ( $\text{SiO}_2$ ,  $\text{TiO}_2$ ,  $\text{Al}_2\text{O}_3$ , total iron as  $\text{Fe}_2\text{O}_3^T$ ,  $\text{MgO}$ ,  $\text{MnO}$ ,  $\text{CaO}$ ,  $\text{Na}_2\text{O}$ ,  $\text{K}_2\text{O}$  and  $\text{P}_2\text{O}_5$ ), a set of 6 trace elements (Ba, Rb, Sr, Y, Zr and Nb),  $\text{H}_2\text{O}^+$ ,  $\text{CO}_2$ , total S, FeO and T.O.C (total organic carbon). The analytical work was done by X-ray Assay Laboratories Ltd. (XRAL) in Don Mills, Ontario. The major oxides and trace elements were determined by X-Ray Fluorescence analysis (XRF). Fused Li-tetraborate discs were used for the major oxides and pressed pellets for the trace elements.

A quality control procedure was applied, which was standard for the Lithogeochemical Exploration Research Project of MDRU (Sinclair and Stanley, 1995, Stanley, 1997a). The analytical errors were estimated through replicate analysis of internal MDRU standards (Stanley, 1997a, Appendix 4). Absolute and relative error terms and effective detection limits (Appendix 6) were determined using the THPLOT Matlab function (Stanley, 1997b). Analytical precision is quoted as the departure (one standard deviation) from the accepted values of the internal MDRU standards as established by Stanley (1997a; Table A4.2). Pulp duplicates analyzed together with the samples are used as a control on the quality of sample preparation (Table A6.2)

Analytical data acquired from HBED, was obtained either by X-ray fluorescence analysis or ICP emission spectrometry. Most of these samples were not analyzed for  $\text{H}_2\text{O}^+$ ,  $\text{CO}_2$ , total S, FeO and T.O.C., which limited their usefulness in the lithogeochemical investigation. No information is available on the analytical quality of the donated data sets. However, samples from these data conform to the main data set, which is an indication that analytical errors are comparable between the two data sets.

### ***Conserved Elements***

Elements or oxide components that do not participate in material transfer processes (magmatic or sedimentary fractionation, metasomatism *etc.*) affecting the system are defined as ***conserved*** (Stanley and Russell, 1989). An X-Y plot of two such elements has a linear pattern. The concentrations of such elements are used as denominators in the Pearce Element Ratios (Pearce, 1968). Thus, their proper identification is a step towards the justifying use of the PER analysis of the lithogeochemical data. The conserved character of components cannot be strictly proven. A procedure is available, however, that can rigorously prove that the components involved ***are not*** conserved. In this study an element or oxide component is considered conserved if the test fails to prove the contrary (Stanley and Russell, 1989).

A set of potentially conserved elements or oxide components, involving  $\text{Al}_2\text{O}_3$ ,  $\text{TiO}_2$ , Zr, Nb, Y and P, are tested using binary scatterplots (Figs. 4.5 through 4.7). If both elements involved in the test are conserved and if the sampled rocks are cogenetic, the data should plot on a single line that passes through the origin (Russell and Stanley, 1990). If a linear trend exists, but has a non-zero intercept, the element on the axis, not containing the intercept, is likely to be more conserved (Stanley and Madeisky, 1995). Here data points are considered following a linear trend if they are within two standard deviations of analytical errors (Appendix 6) from the trend line.

### **Conserved Element Test Results:**

All mafic and ultramafic rocks, occurring in the general area of the Konuto Lake deposit are plotted together (Figs. 4.5 through 4.7), which allows for comparison and genetic interpretations. For each group of rocks (Birch Lake assemblage basalt flows, Birch Lake gabbro, Birch Lake ultramafic rocks, Mosher Lake basalt and Mosher Lake gabbro) the data points plot along straight lines passing through the origin. Thus, the two hypotheses (1) that the rocks are cogenetic within the groups and (2) that the elements or oxide components used for the test ( $\text{TiO}_2$ ,  $\text{P}_2\text{O}_5$ , Zr and Y) are conserved, are, not rejected. This validates the further application of PER analysis and the use of the above elements as denominators in Pearce element ratios.  $\text{Al}_2\text{O}_3$  is conserved in all groups, except the Mosher Lake basalts (not shown).

Clear distinction exists between the Birch Lake volcanic rocks, the Birch Lake gabbroic sills and the Birch Lake ultramafic rocks on one side and the Mosher Lake volcanic rocks and the Cable Lake gabbroic sill on the other. The second group is characterized by significantly higher Zr and Ti concentrations. The Zr/Y ratio (Fig. 4.6) of the Mosher Lake volcanic rocks is approximately 3.6 as opposed to 1.2 for the Birch Lake mafic rocks. Judged by their Zr/Y ratio alone, all mafic rocks in the area display a tholeiitic affinity, which is more pronounced for the Birch Lake gabbros and basaltic andesites (Barrett and MacLean, 1994). A ternary cation plot, projecting from Ca, Na and K (Jensen, 1976; Fig. 4.9), identifies the basaltic rocks as high-Fe tholeiites. It is deemed more appropriate for the mildly metamorphosed rocks under investigation, than the more commonly used AFM ternary plot (Irvine and Baragar, 1971), because it is insensitive to the possible mobility of K and Na.

Furthermore, the data distribution identifies two varieties of basalts within the Mosher Lake assemblage: one compositionally closer to the related gabbros and, another - characterized by higher concentrations of the tested (incompatible) elements, but with preserved ratios between them (Figs. 4.5 through 4.7).

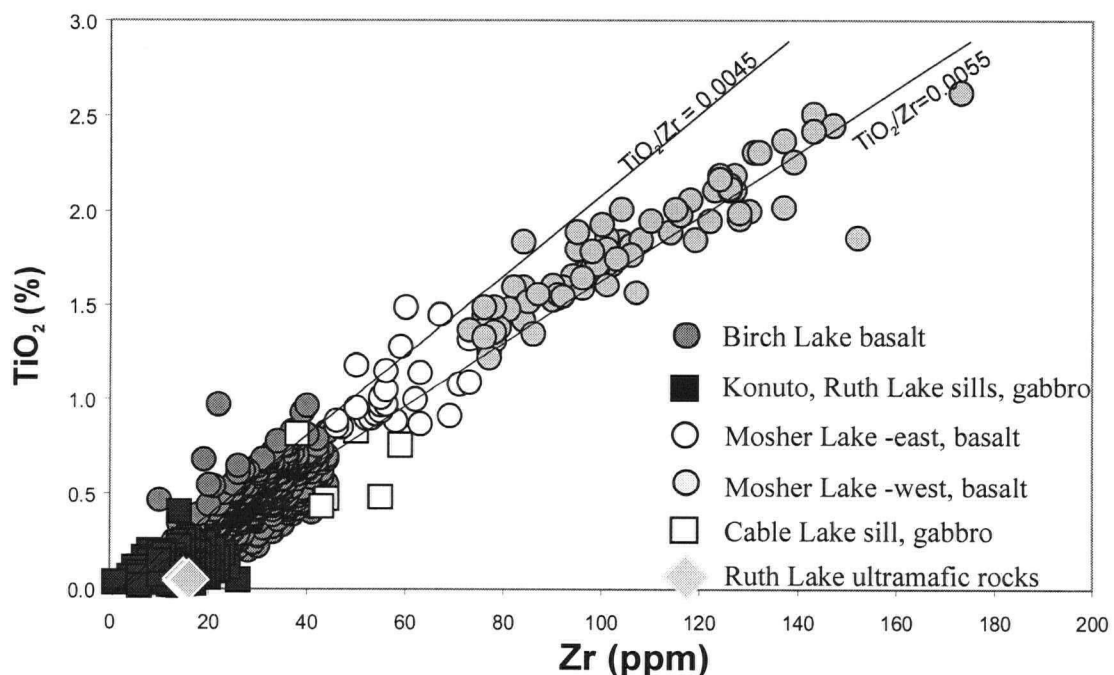


Fig.4.5.  $\text{TiO}_2$  vs. Zr scatterplot. Included are all mafic and ultramafic rocks from the Konuto Lake and Birch Lake area. The data points form linear arrays, passing through the origin. The slopes defined by the Birch Lake and the Mosher Lake basalts are slightly different.



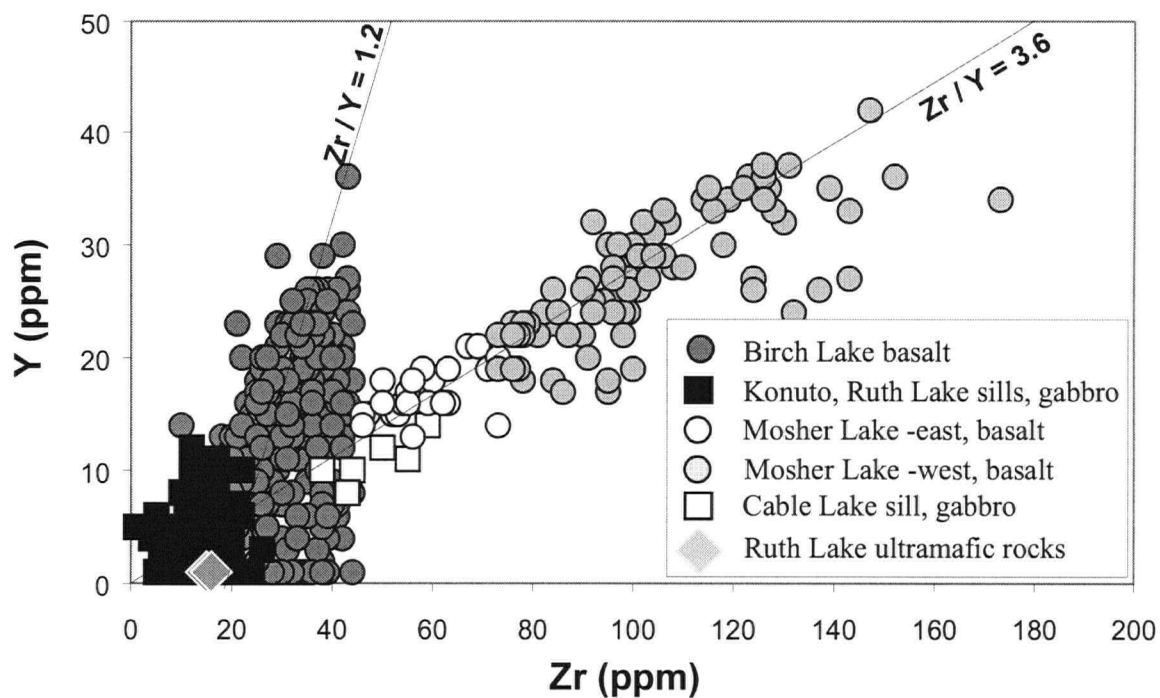


Fig.4.6. Y vs. Zr scatterplot. Data from mafic and ultramafic rocks from the Konuto Lake and Birch Lake area. The data points form linear arrays. The array for the Moshier Lake rocks passes through the origin. The array for the Birch Lake volcanic rocks intercepts the abscissa (Zr) at low values. The slopes for the two arrays are significantly different.

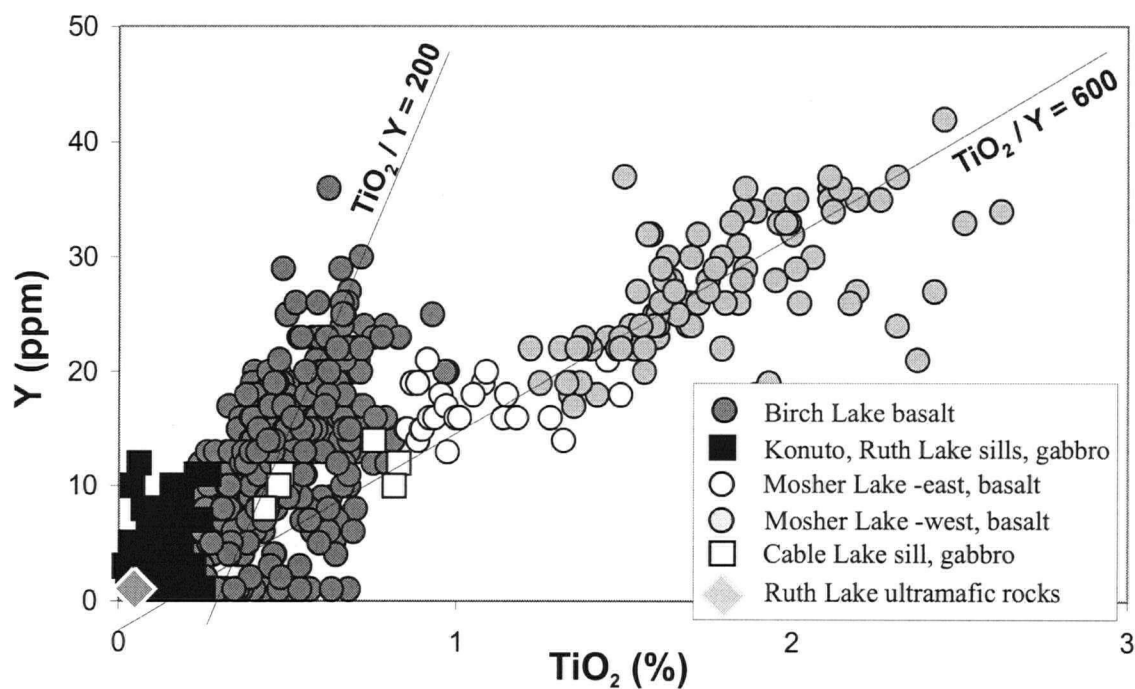


Fig.4.7. Y vs. TiO<sub>2</sub> scatterplot. Data for all mafic and ultramafic rocks from the Konuto Lake and Birch Lake area. The data points form linear arrays, passing through the origin. The slopes of the arrays are significantly different.

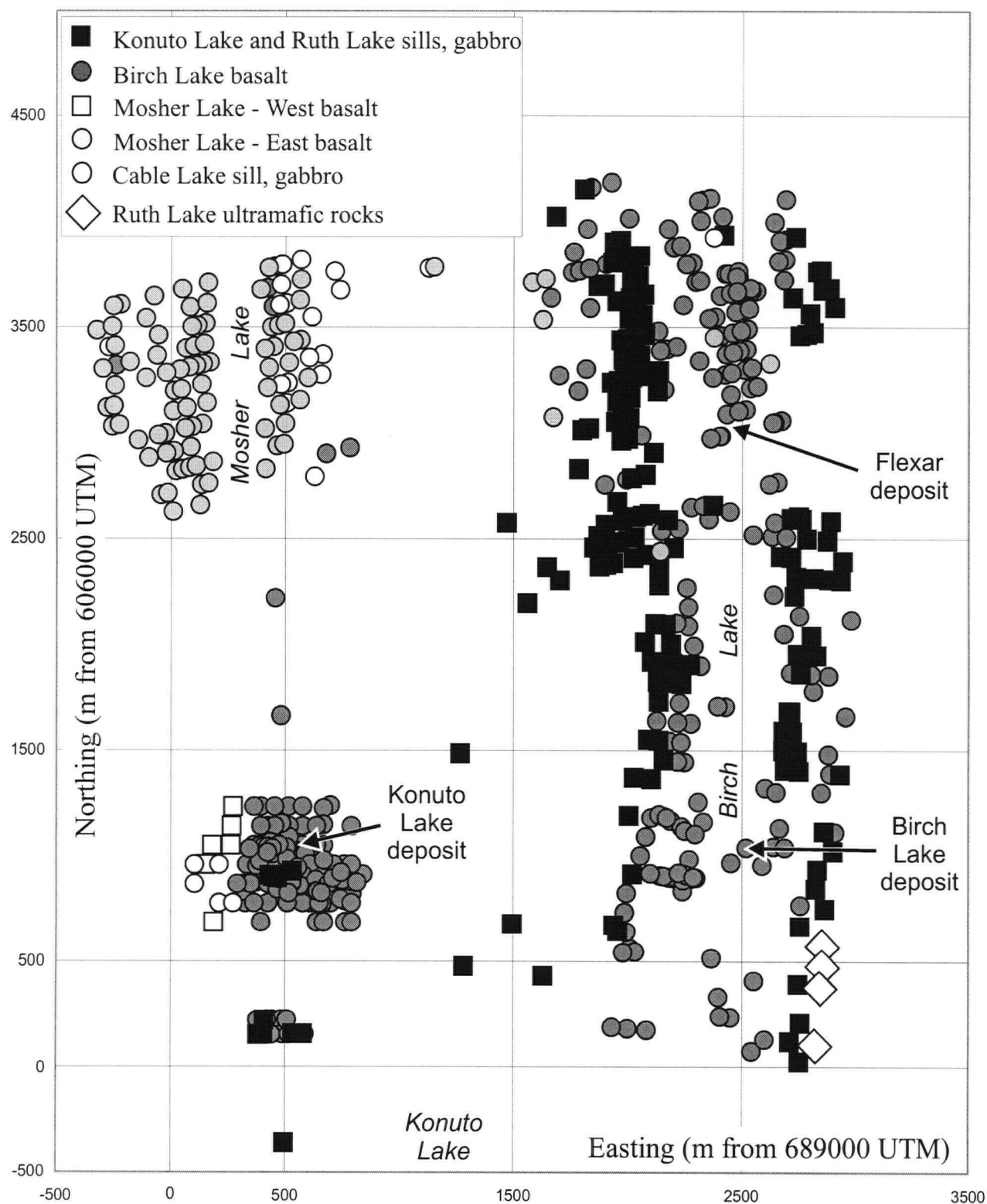


Fig. 4.8. Location of samples from mafic and ultramafic rocks, Konuto and Birch Lake areas

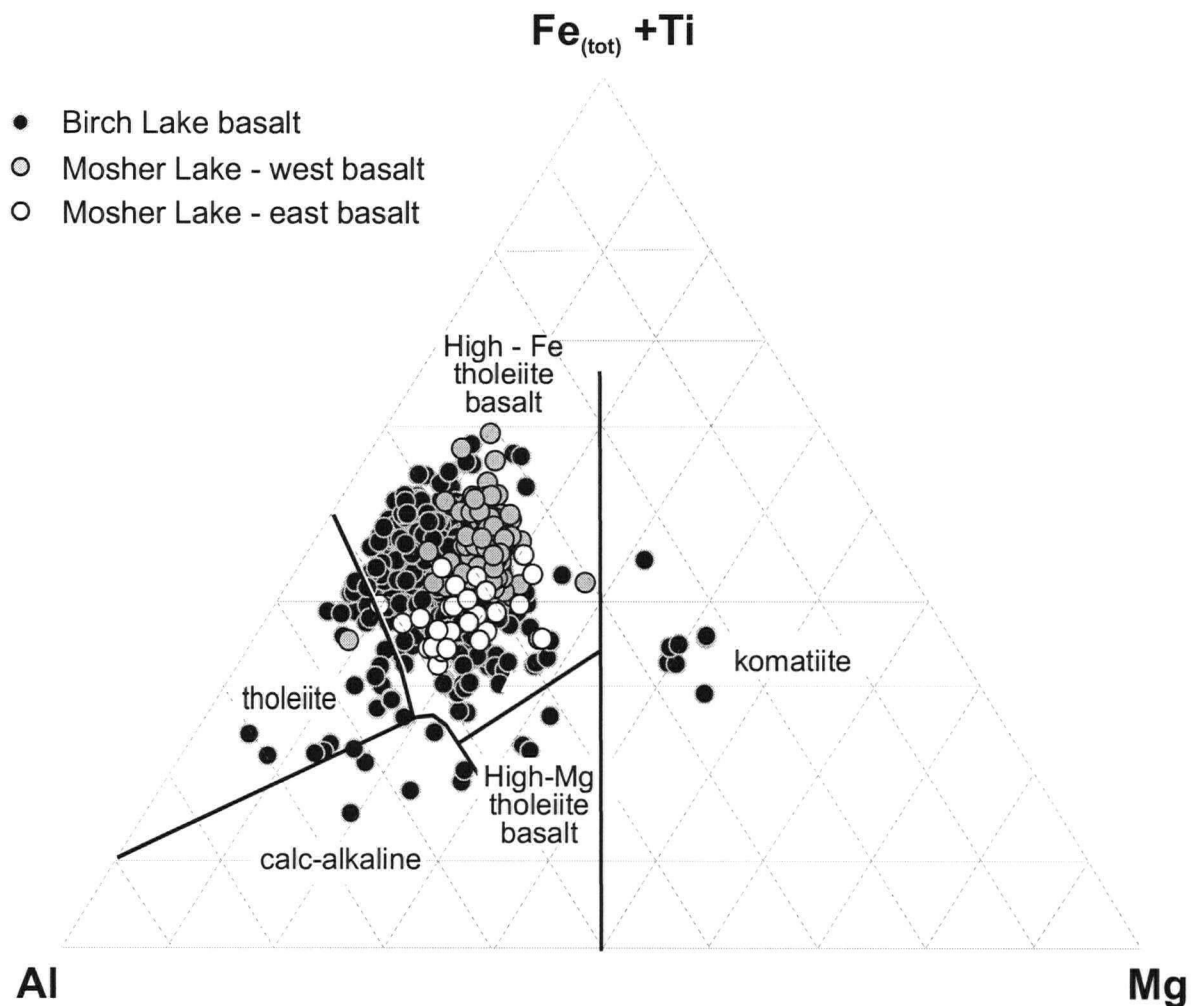


Fig. 4.9. Classification based on cation percentages of Al, (Fe(total) + Ti) and Mg (Jensen, 1976) for the basaltic rocks occurring in the area of the Konuto and Birch lakes.

The second group displays also higher  $\text{Fe}_{(\text{total})}$  concentrations (Fig. 4.9). These compositional differences can be explained either by fractionation and enrichment of the incompatible elements in later eruptive phases by contamination or by metasomatic mass loss/gain. The rocks of the first group occur in a restricted area east of Mosher Lake (Figs. 4.3 and 4.8) while those of the second group occur more broadly, both east and west of Mosher Lake. The two groups of rocks are further referred to as Mosher Lake – East basalts and the Mosher Lake – West basalts.

### ***Molar Element Ratio Analysis***

Chemical compositions of sampled rocks, are the result of a number of factors, including syngenetic and epigenetic geological processes, errors introduced during sampling and analysis and the effect of closure. While sampling and analytical errors cannot be completely avoided, their magnitude can be estimated and taken into account. Closure is an effect arising from the requirement that the sum of all components in an analyzed sample add up to 100%. Thus, true variation in one component would induce apparent variations in all other components. This effect is conveniently eliminated in MER analysis, by using ratios of components. In PER analysis, the denominator component is an immobile element, ensuring that unaltered samples plot along the fractionation model line. In this study,  $\text{TiO}_2$  is chosen as the denominator because its conserved character has been demonstrated and its relatively high analytical precision compared to other conserved components (Appendix 6). In Generalized Element Ratio (GER) analysis, any component can be chosen as a denominator, regardless of its mobility. In this case, the location of the data points is a function of the mineral composition of the sample. The data plot within a polygon with vertices corresponding to the chemical composition of the effectively participating minerals (either present, or original before any isochemical processes of phase transformation) in the coordinate system of the plot.

In order to quantify and study hydrothermal alteration, its effect needs to be extricated from those of other mass transfer processes. In volcanic rocks, such as those hosting the Konuto Lake deposit, mineral fractionation is the primary process introducing chemical variation. PER analysis is used to model this process and thus, account for the introduced variations. The method involves stating and then testing petrologic hypotheses, which is facilitated by the fact that the number of major phases participating in fractionation is limited. PER plots are designed by selecting axes parameters (linear combinations of oxide components) such that the minerals of the tested primary paragenesis would all plot along a model line with a prespecified slope, usually unity. At this stage of PER analysis it is already ascertained that the studied rocks are cogenetic. Therefore, if a sufficient proportion of background samples conform to the stated petrologic hypothesis (*i.e.*, plot along the fractionation model line) it is assumed that all samples had the same set of primary minerals and deviations are due to

secondary processes. Thus, the graphical approach utilized in PER analysis allows for the visual separation of fractionation effects from those of superimposed mass transfer processes.

This study assumes that the rocks underwent largely isochemical metamorphism, which did not involve the migration of components other than  $H_2O$  and  $CO_2$ . This assumption is tested simultaneously with the fractionation model, based on the understanding that metamorphism is affecting pervasively large volumes of rock. If a significant number of background samples conform to the model, then the mass transfer effect of metamorphism is negligible or non-existent, at least in the coordinates of the corresponding PER plot. Thus, variations distinct from those introduced by igneous fractionation characterise the processes of hydrothermal alteration. The residuals from the fractionation model line are interpreted in the context of the axes parameters of the plot and the chemical effects of hydrothermal metasomatism are identified. The magnitude of the residuals quantifies the intensity of the secondary process.

Similarly to PER, GER analysis represents the effects of primary and secondary mass transfer processes graphically, although the geometry of the two types of diagrams is different. On GER plots, the primary composition of the rock is represented as a node, situated inside a polygon defined by the primary fractionating minerals. Residuals caused by secondary mass transfer processes radiate from that node in a direction characteristic of the chemical effect of the process and towards nodes corresponding to the product minerals of that process. Another similarity of PER and GER plots is that the magnitude of the residual vectors is a quantitative measure of the intensity of the geochemical processes in terms of moles of reaction.

### **Birch Lake Assemblage Basalts and Gabbros**

Several hypotheses are tested, regarding the paragenesis of fractionating phases, leading to the formation of the basaltic and gabbroic rocks of the Birch Lake assemblage. They involve combinations of the major minerals typically present in mafic rocks: olivine, orthopyroxene, clinopyroxene and plagioclase. Analytical data from 424 basaltic and 165 gabbroic samples are used for this procedure.

A PER plot is constructed (Fig. 4.10) to test the hypothesis that one or more of the minerals orthopyroxene, clinopyroxene and plagioclase fractionated to produce the observed background geochemical variability. The majority of data points match very closely the model line with a slope of unity, confirming the validity of the hypothesis. A slight shift towards the olivine fractionation model line with a slope of 2, displayed by some gabbro samples, indicates the presence of small proportions of olivine in these rocks, negligible in the context of MER analysis. The plot, however, does not provide evidence whether some, or all three modeled phases participate in fractionation.

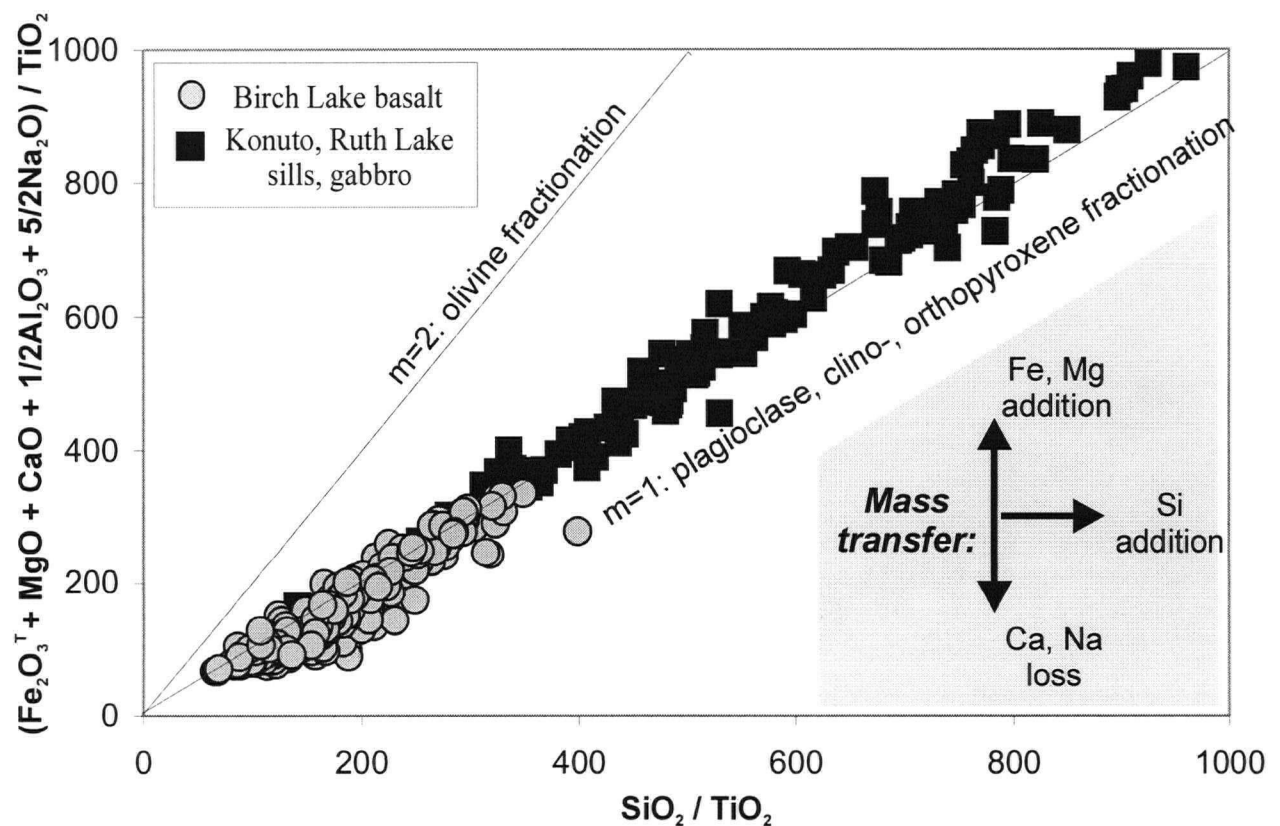


Fig. 4.10. PER plot for Birch Lake assemblage basalt and gabbro. The plot tests the hypothesis that all or any of the phases plagioclase, clinopyroxene, and orthopyroxene were involved in primary magmatic fractionation.

A similar plot (Fig. 4.11) is used to further study the data set by testing the hypothesis that olivine, clinopyroxene and plagioclase were involved in fractionation. In this case, the match to the model line with a slope of unity is poor. The data points plot between the model line with a slope of 1 (olivine, clinopyroxene and plagioclase fractionation) and a line with a slope of 1/2 (orthopyroxene fractionation). This indicates that orthopyroxene is involved in fractionation along with olivine, clinopyroxene and plagioclase. In both plots (Figs. 4.10 and 4.11), enrichment of the volcanic rocks in  $\text{TiO}_2$  (average of 0.56%  $\text{TiO}_2$ ) compared to the gabbroic rocks (average of 0.1%  $\text{TiO}_2$ ) causes the shift of basalt data points towards the origin.

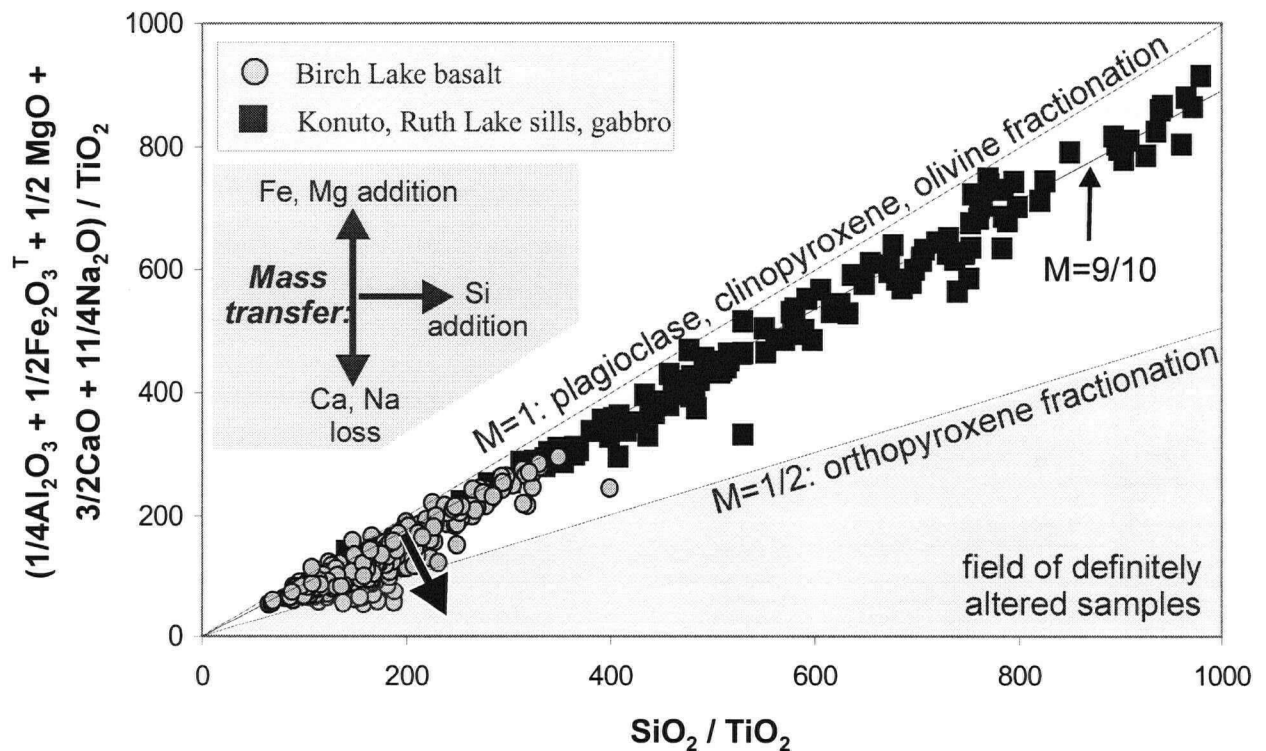


Fig. 4.11. PER fractionation model plot for Birch Lake basalt and gabbro with  $\text{TiO}_2$  as the conserved denominator. The plot tests the hypothesis that plagioclase, clinopyroxene, and olivine were the primary fractionating minerals and that orthopyroxene was not involved in fractionation.

On the plagioclase-clinopyroxene-orthopyroxene fractionation model (Fig. 4.10) and the plagioclase-clinopyroxene-olivine fractionation model (Fig. 4.11), background data points form linear arrays. For these samples igneous fractionation was the only geological source of variation. Deviation from the model lines, displayed by a relatively small proportion of the samples, as discussed above, is caused by another mass transfer process: hydrothermal alteration. On each particular diagram, the direction and magnitude of the effects of individual hydrothermal processes (*i.e.*, addition or loss of mobile elements) depend on the axes numerators. On figures 4.10 and 4.11, the displacements due to mobility of Ca, Na, Fe, Mg and Al are colinear and, therefore, cannot be distinguished. Based on general knowledge about alteration associated with VHMS deposits (*e.g.*, Franklin, 1993) it can be presumed that the most likely alteration processes involving these elements are loss of Ca and Na and/or addition of Fe and Mg. The effects of these processes displace data points in opposite directions and, thus, partially offset each other. Some data points on the two plots are displaced in a direction consistent with addition of SiO<sub>2</sub>, but the concurrent effect of Ca Na loss cannot be ruled out. Total displacement of data points from the fractionation model line can be used as an estimate of the overall intensity of alteration. The effect, however, is likely to be underestimated due to the counteraction of the effects of Fe and Mg addition and Ca and Na loss.

A plagioclase-clinopyroxene fractionation plot (Fig. 4.12) eliminates the interference of Fe and Mg addition by implicitly projecting from those components. In this case, however, the estimate of the combined effect of Si mobility and loss of Ca and Na is likely to be overestimated. This is due to unaccounted SiO<sub>2</sub> in olivine and orthopyroxene, which, although minor, is possibly present in the rocks.

As shown above, (Figs. 4.10 and 4.11), the Birch Lake assemblage rocks, both basalts and gabbros, are made up mostly of plagioclase and clinopyroxene. PER phase discrimination diagram (Fig. 4.13), allows the proportions of these minerals to be estimated for each individual sample. The estimates, however, are accurate only to the extent that the samples did not gain or lose any Ca, Na or Al through secondary geological, processes. Here a graphical approach is used (Fig. 4.13) in which the data points form an array represented by a



regression line with a slope of 1/3. This slope corresponds to the clinopyroxene/plagioclase ratio in the rocks, expressed in terms of moles. Given the molar weights and specific gravities of the two minerals, the average volume proportion is approximately 19/81.

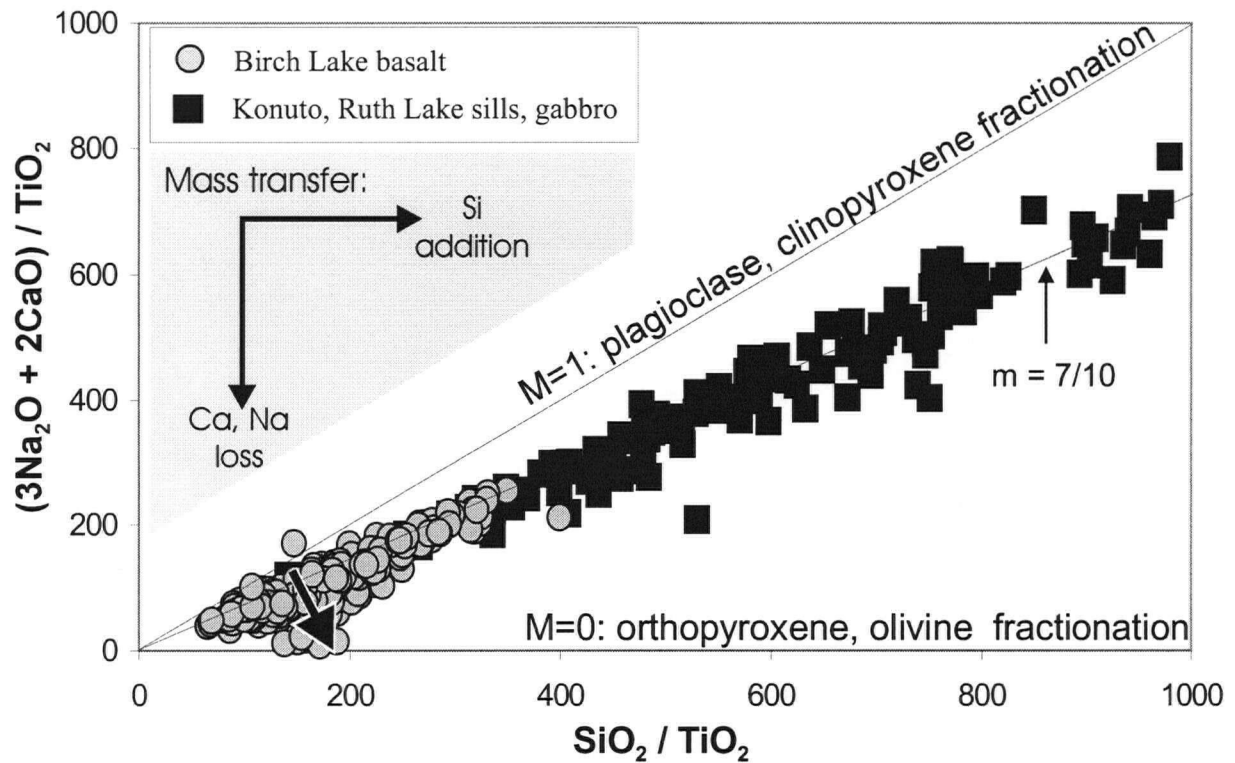


Fig. 4.12. PER diagram for Birch Lake assemblage basalt and gabbro rocks. The plot tests the hypothesis that plagioclase and clinopyroxene were the only minerals involved in primary (igneous) fractionation. It projects implicitly through  $\text{MgO}$  and  $\text{Fe}_2\text{O}_3^T$ .

The plagioclase-clinopyroxene phase discrimination diagram (Fig. 4.13) visualizes the effect of Ca and Na loss as well. Furthermore, because the plot projects from Si, Fe and Mg, the displacement of data points reflects Ca and Na loss, free of interference from Si, Fe and Mg mobility. Estimation of the magnitude of Ca and Na loss is not quantitative, because the primary concentrations of Ca and Na are inferred from the regression line only approximately. Some samples exhibit negative values for the sum  $2\text{CaO} + \text{Na}_2\text{O} - \text{Al}_2\text{O}_3$  (Fig. 4.13), which corresponds to the molar balance of Ca, Na and Al in plagioclase. Contingent on the assumption that all Al in the rocks was initially contained in plagioclase and given that  $\text{Al}_2\text{O}_3$  was earlier shown to be immobile, this fact indicates that those samples lost Ca and Na. This parameter represents a conservative estimate of the intensity of alteration, because

it does not account for Ca contained in clinopyroxene. It is further used to describe the spatial distribution of Ca and Na loss (Figs. 1 and 2, Appendix 5).

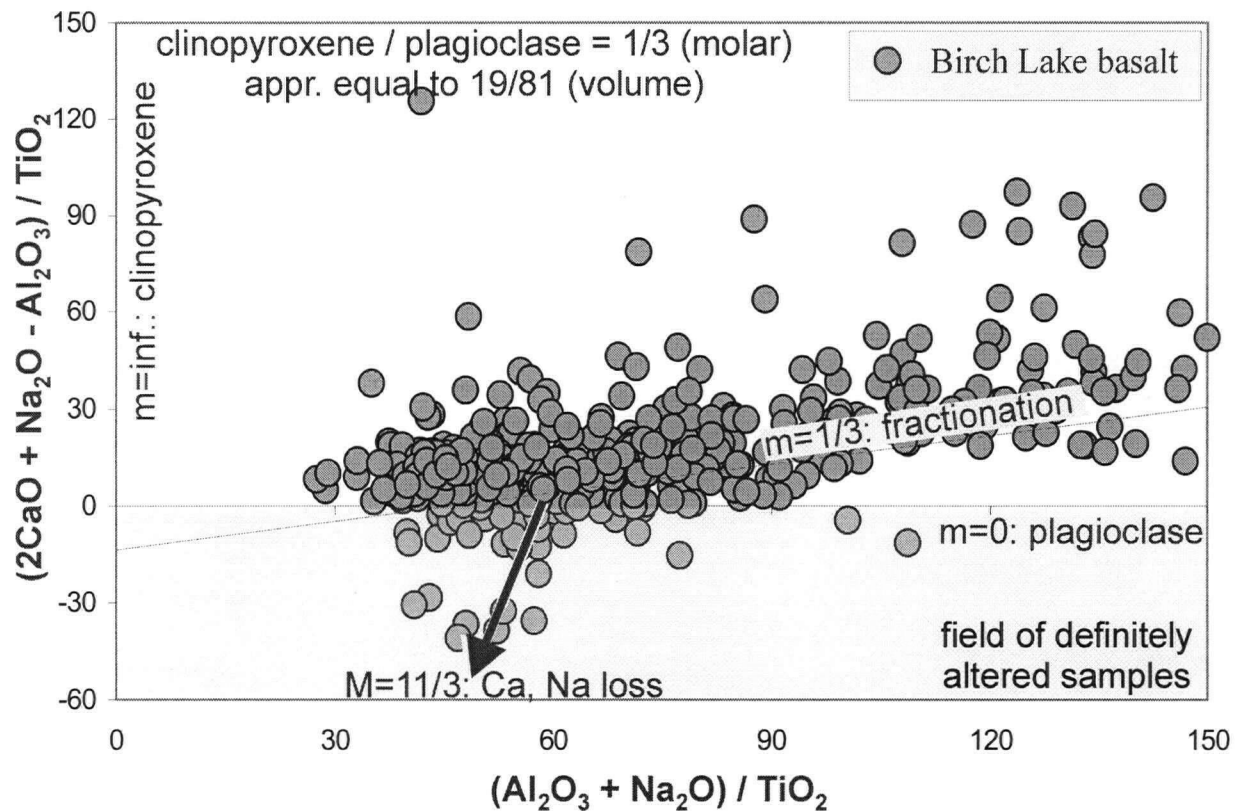


Fig. 4.13. PER phase discrimination diagram for Birch Lake assemblage basaltic rocks. The plot is designed to quantify the molar proportions of plagioclase and clinopyroxene in the primary mineral paragenesis.

Plotted on a GER diagram, the Birch Lake mafic rocks form a tight cluster centered in the tetragon defined by the primary mineral association (albite, anorthite, clinopyroxene and orthopyroxene, Fig. 4.14). However, a large number of data points, all of them corresponding to basaltic samples, are shifted towards the quartz node at the origin of the diagram. This reflects the epigenetic addition of  $\text{SiO}_2$ , infilling the abundant amygdules and contraction cracks in the lava flows (Plates 4.2, 4.6 and 4.9). This process masks any superimposed silicification, if present and obscures the signatures of Ca, Na, Fe and Mg mass transfer. Another group of samples exhibits a shift towards the ordinate and away from the abscissa. This negative slope shift reflects the combined effect of Fe and Mg addition and Ca

and Na loss through metasomatism. This process influenced particularly the basalts, but also the gabbros. Its magnitude is:

$$[(\text{Fe} + \text{Mg}) / (\text{Ca} + \text{Na})]_i - [(\text{Fe} + \text{Mg}) / (\text{Ca} + \text{Na})]_0,$$

where Fe, Mg, Ca and Na are the concentrations of the corresponding elements, “i” indicates any specific sample and “0” indicates the node of presumably unaltered background samples.

The above difference of ratios is a measure of hydrothermal alteration and, plotted in space, can be used to characterize spatial distribution of alteration (Appendix 8, Figs. A8.9 and A8.10). Finally, a few data points are shifted towards the high end of the abscissa. Those samples have, most likely, been impregnated by calcite.

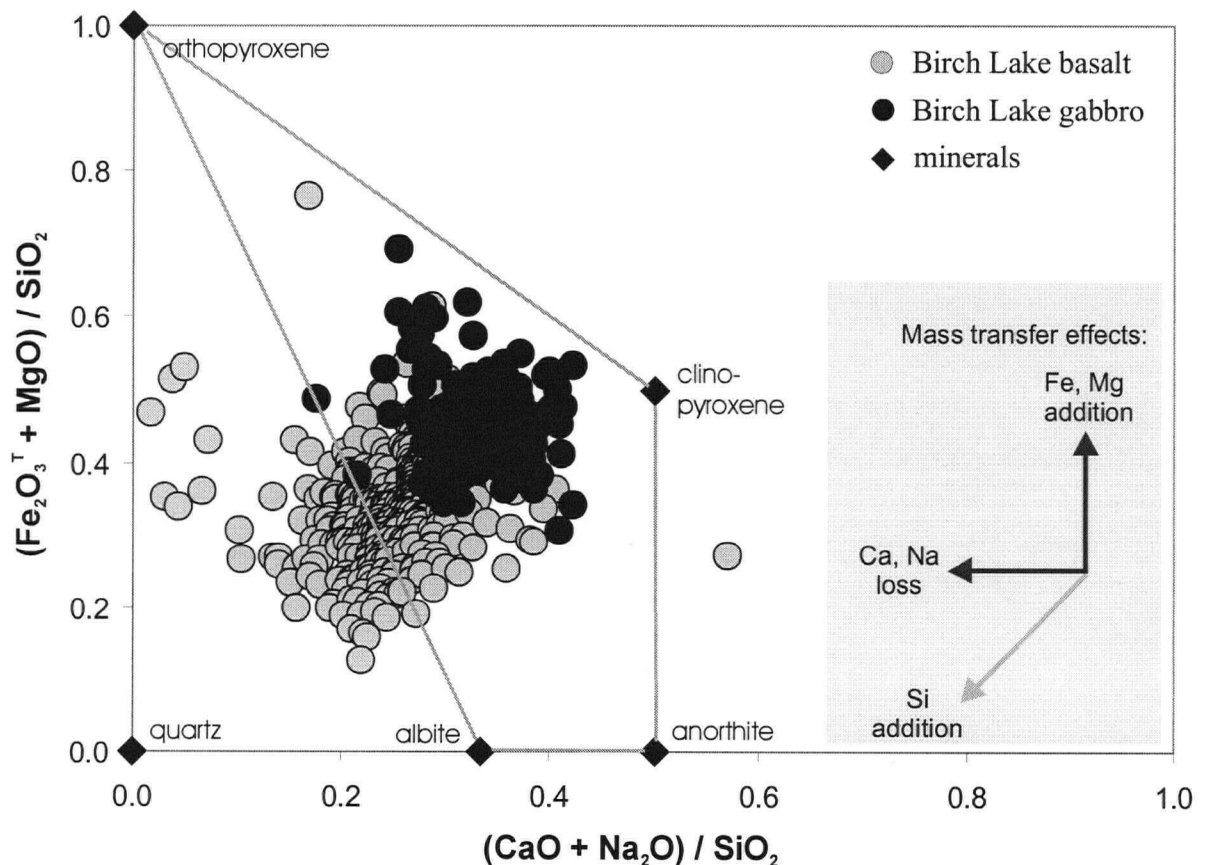


Fig. 4.14. GER diagram of Birch Lake basalt, basaltic andesite, and gabbro. The polygon in which most samples plot is defined by the minerals participating in primary (igneous) fractionation: orthopyroxene, clinopyroxene and plagioclase (albite and anorthite).

A GER diagram projecting from  $\text{SiO}_2$  (Fig. 4.15) allows for the representation of Ca, Na, Fe and Mg mass transfer free from interference due to  $\text{SiO}_2$  addition. Furthermore, on this plot, Ca and Na mass transfer is independent of Fe and Mg mass transfer, because their vectors are perpendicular to each other. Thus, the intensity of each of the two processes can be measured quantitatively in each sample. The Fe and Mg mobility is quantified by the parameter:  $(\text{Fe} + \text{Mg})_i - (\text{Fe} + \text{Mg})_0$ , and Ca and Na mobility is quantified by the similar parameter:  $(\text{Ca} + \text{Na})_i - (\text{Ca} + \text{Na})_0$ , where “i” denotes each individual sample and “0” denotes the main data cluster.

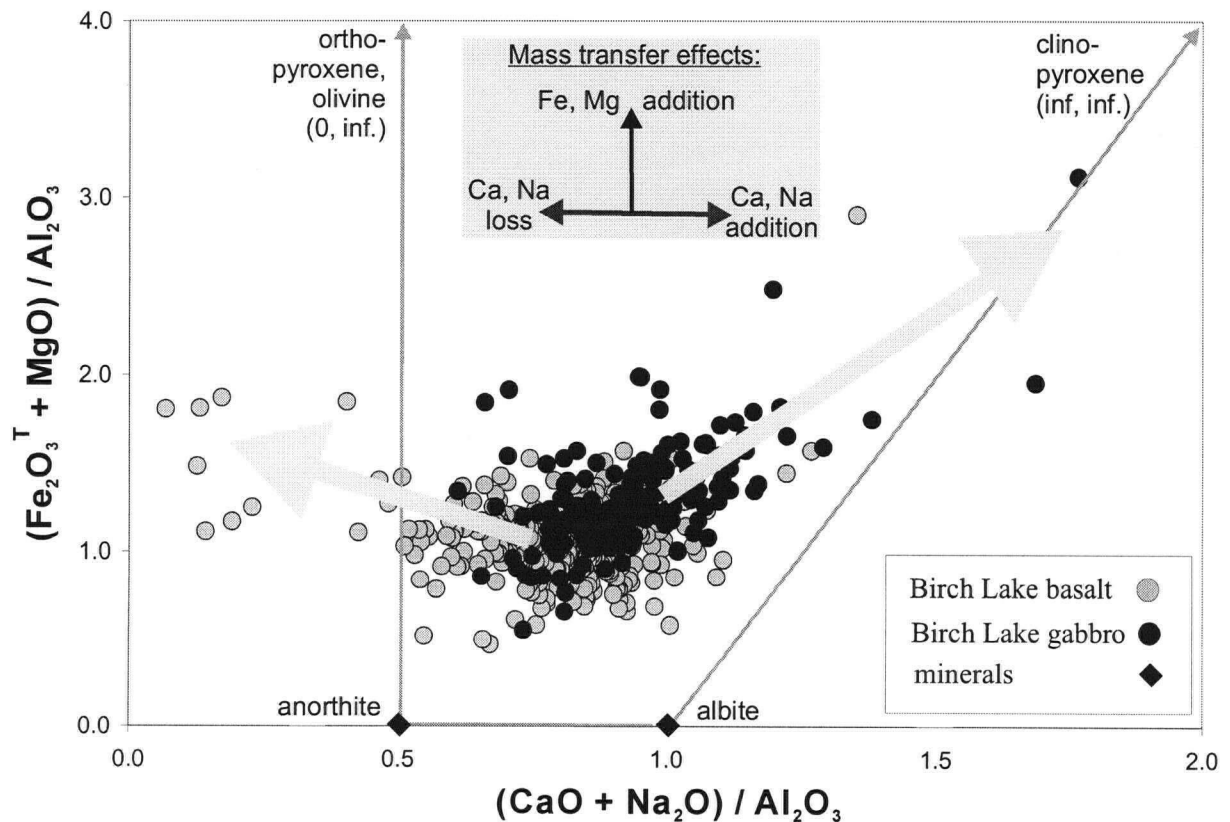


Fig. 4.15. GER plot of Birch Lake basalt, basaltic andesite, and gabbro, implicitly projecting from silica. The majority of the samples plot in the polygon defined by the fractionating phases: orthopyroxene, clinopyroxene and plagioclase (albite and anorthite). The ferro-magnesian end of the polygon extends into infinity due to the use of a denominator element ( $\text{Al}_2\text{O}_3$ ) which does not participate in the composition of the ferro-magnesian minerals.

Negative values indicate loss and positive ones – addition of the corresponding elements. For practical purposes, only the first members of the differences are used. The geographic coordinates of samples, with values higher than- (for addition) or lower than (for loss) an arbitrary threshold, are plotted to describe the spatial distribution of the processes.

According to the plot, a group of samples, almost exclusively basalts, have lost a significant proportion (up to 90%) of their Ca and Na. Because these elements are initially contained in plagioclase and clinopyroxene, the mass transfer effect indicates the destruction of these minerals and the extraction of the released Ca and Na from the sampled rock domain.

Another group of samples, mostly gabbros, have gained Ca and Na (Fig. 4.15). This process must be mineralogically expressed as a formation of Ca-rich and Na-rich minerals, such as calcite, albite and/or clay minerals. It is likely that the two processes are coupled so that the net effect within a larger volume of rock is nil. Both processes are associated with weak to moderate Fe and Mg addition (Fig. 4.15). Another possible sink for Ca and/or Na leached from the rocks may have been ocean water.

### ***Spatial patterns of alteration***

Hydrothermal material transfer effects visualized on MER diagrams (Figs. 4.10 through 4.14) are used as a basis for describing the distribution of hydrothermal alteration. Samples bearing evidence of metasomatic alteration are plotted in space (Figs. 4.16 and 4.17; Appendix 8). Clusters of altered samples form geochemical anomalies, which in an exploration context represent targets. In this study, the degree to which the identified anomalies match the location of known ore bodies is a criterion for the applicability of the methodology to exploration problems.

The four PER plots used in the study do not yield significantly different alteration patterns. This observation is not surprising for the three plots, which involve the same components, although viewed in different coordinate systems. This explanation, however, cannot be invoked with respect to the fourth plot, which projects through  $\text{Fe}_2\text{O}_3$ ,  $\text{MgO}$  and  $\text{SiO}_2$ . The similarity of alteration patterns (Figs. A8.1 through A8.8) in this case may be a sign that the methodology is robust enough not to be significantly influenced by the particular choice of axes parameters.

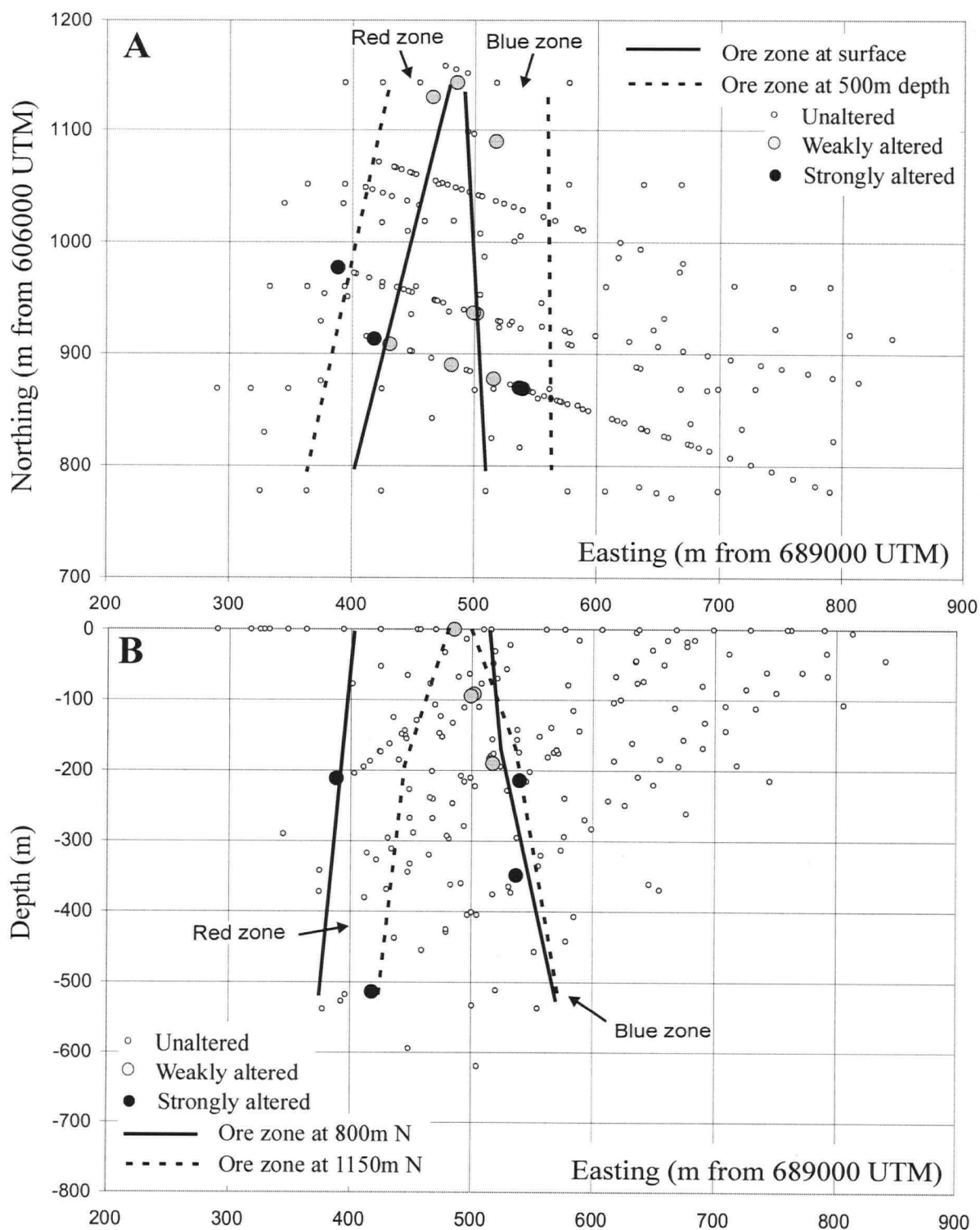


Fig. 4.16. Spatial distribution of hydrothermal alteration in the vicinity of the Konuto Lake deposit (NER claim), based on the GER plot (Fig. 4.14). A. Plan view; B. Combined cross section. The parameter used to classify the samples as strongly altered, weakly altered and unaltered is:  $(Ca + Na)_i - (Ca + Na)_0$ , where Fe, Mg, Ca and Na are the concentrations of the corresponding elements, "i" indicates any specific sample and "0" indicates the node of presumably unaltered background samples. Most altered samples occur within a short distance from the two mineralized zones.

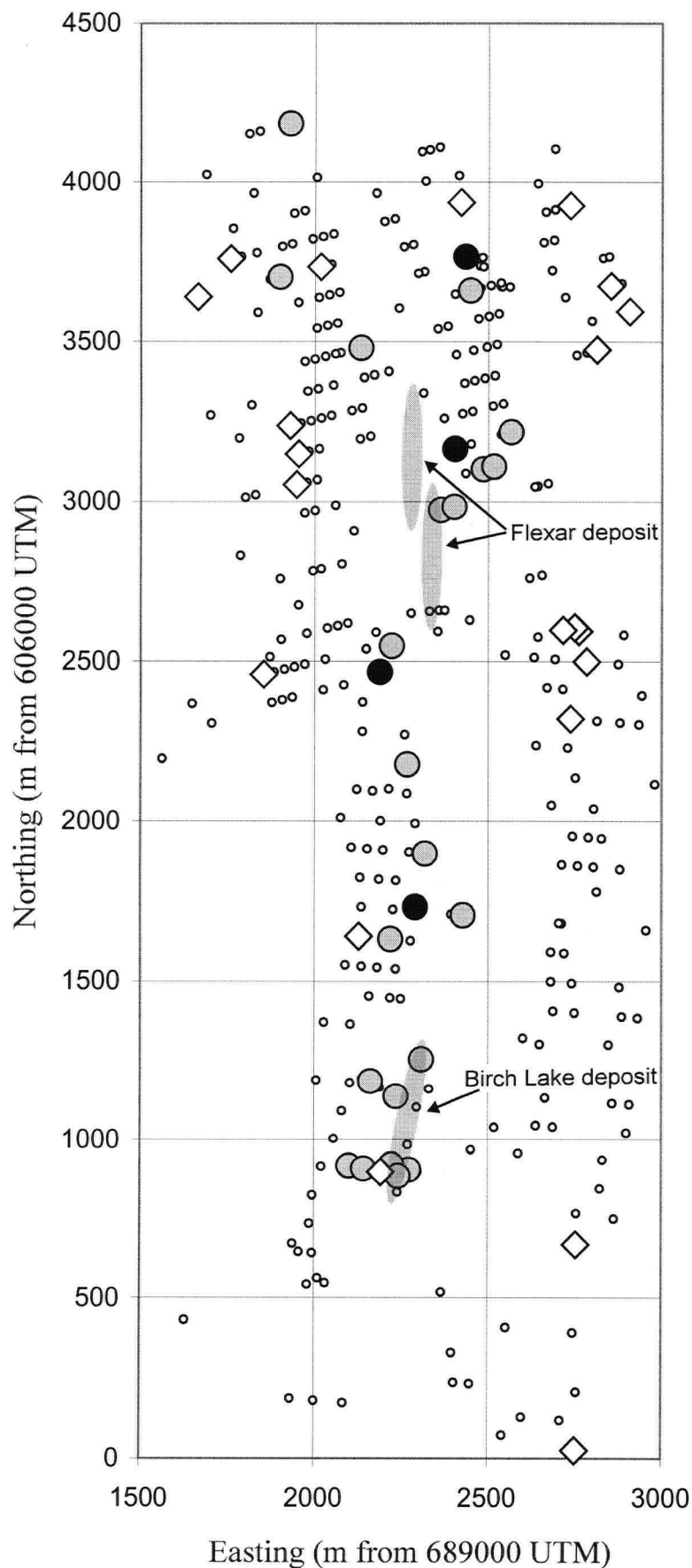


Fig. 4.17. Spatial distribution of hydrothermal alteration in the vicinity of the Birch Lake and Flexar deposits, based on the GER plot (Fig. 4.14). The parameter used to classify the samples according to their alteration is:

$$(\text{Ca} + \text{Na})_i - (\text{Ca} + \text{Na})_0,$$

where Fe, Mg, Ca, and Na are the concentrations of the corresponding elements, "i" indicates any specific sample and "0" indicates the node of presumably unaltered background samples.

Most samples influenced by Ca and Na loss occur in a band, within 250 m from the mineralized horizon.

Carbonatized samples (addition of Ca and Na) occur mostly in gabbros and form an outer halo around the deposit.

- Unaltered
- Moderate loss of Ca, Na
- Intensive loss of Ca, Na
- ◇ Carbonatization
- Ore body

The SiO<sub>2</sub>-present GER plot (Fig. 4.14) yields more concise anomalies than the PER plots. The reason for this is that on all PER plots used in this study, the effect of SiO<sub>2</sub> inevitably contains a vector component colinear with the effects of other components participating in mass transfer. Because quartz deposition is involved in processes unrelated to mineral deposition (*i.e.*, amygdale and vein infilling), it has an obscuring effect on mineralization-related alteration. On Fig. 4.14, on the other side, the effect of silicification is not colinear with any other mass transfer processes, allowing for their more accurate representation on the graphs.

The GER plot projecting from SiO<sub>2</sub> (Fig. 4.15) eliminates the interference of SiO<sub>2</sub> mass transfer altogether. Spatial alteration patterns based on it (Figs. 4.16 and 4.17) give well-defined anomalies. Anomalies cluster around the known ore occurrences, forming a halo around the Konuto Lake deposit and a band coinciding with the mineralized part of the stratigraphy at Birch Lake and Flexar deposits. The style of alteration at the Konuto Lake deposit is different than that at the Birch Lake and Flexar deposits. In the area of the Birch Lake and Flexar deposits, Ca and Na loss is identifiable at distances of up to 250 m from the mineralized horizon (Fig. 4.17). Carbonatization (appearing on the MER diagrams as addition of Ca) is distal to the ore body, influencing mostly the hanging wall gabbro. Alteration at the Konuto Lake deposit is weak and restricted to the close vicinity (within less than 50 m) of the ore zones (Fig. 4.16). Carbonatization is very weak to non-existent.

### **Ruth Lake Ultramafic Sill**

When applying PER analysis to the Ruth Lake sill rocks it is initially presumed that the rocks could be composed of any linear combination of the following major minerals: olivine, orthopyroxene, clinopyroxene and plagioclase (itself a linear combination of albite and anorthite). By stating a series of petrologic hypotheses and testing their validity, it is possible to determine the mineral composition of the rocks.

The hypothesis that the Ruth Lake ultramafic rocks originated by fractionation of plagioclase, clinopyroxene and olivine, is supported by the PER plot (Fig. 4.18). The plagioclase is extremely calcic, effectively anorthite, which is inferred from the low Na



concentrations of the rocks (Appendix 5). The hypothesis that olivine is absent from the rocks is tested as well, but it is not supported by the data. The plot (Fig. 4.19) shows that olivine participates in the mineral assemblage in a significant proportion. This is especially true for one of the samples, which differs in its overall chemical composition from the remaining three.

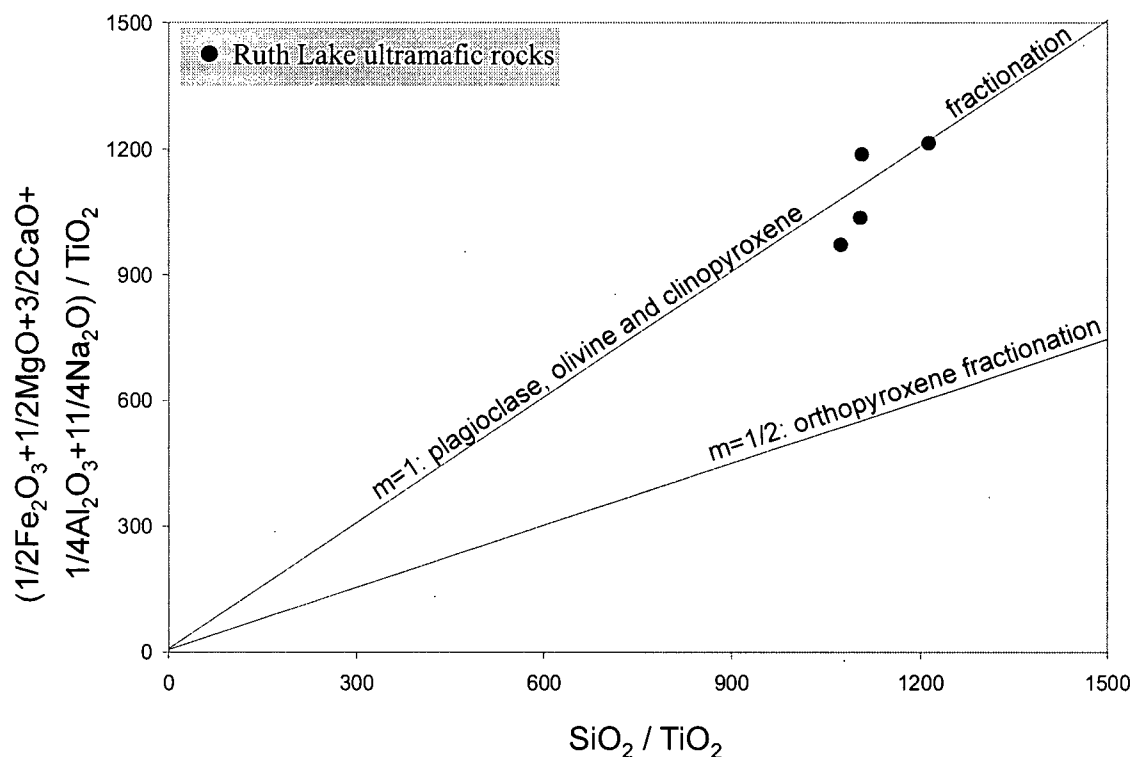


Fig. 4.18. PER fractionation model plot for the Ruth Lake ultramafic rocks. The plot tests the hypothesis that plagioclase, clinopyroxene and olivine were minerals participating in igneous fractionation.

After identifying the major phases present in the Ruth Lake ultramafic rocks as plagioclase (anorthite), clinopyroxene and olivine, PER phase discrimination plots (Figs. 4.20 and 4.21) are applied to determine their proportions. The rocks are transitional between wehrlite and mela-olivine gabbro (Philpotts, 1990). Three samples have wehrlite mineralogy: olivine 55.5%, clinopyroxene 36% and plagioclase, 9.5%. The fourth sample is more plagioclase-rich (13%) and plots in the field of mela-olivine gabbro. Calculation of the above mineral compositions involves the following assumptions:

1. The plagioclase is anorthite ( $An_{100}$ ), which is an approximation supported by the very low  $Na_2O$  concentrations in the rocks (0.01 to 0.05 wt.).
2. Orthopyroxene is present in negligible proportions as indicated by the olivine-clinopyroxene-plagioclase fractionation model plot (Fig. 4.18).
3. The ratio of  $Fe_2O_3$  (total) and  $MgO$  in olivine and clinopyroxene is equal to 85:15, which represents the bulk ratio of these components in the rocks.

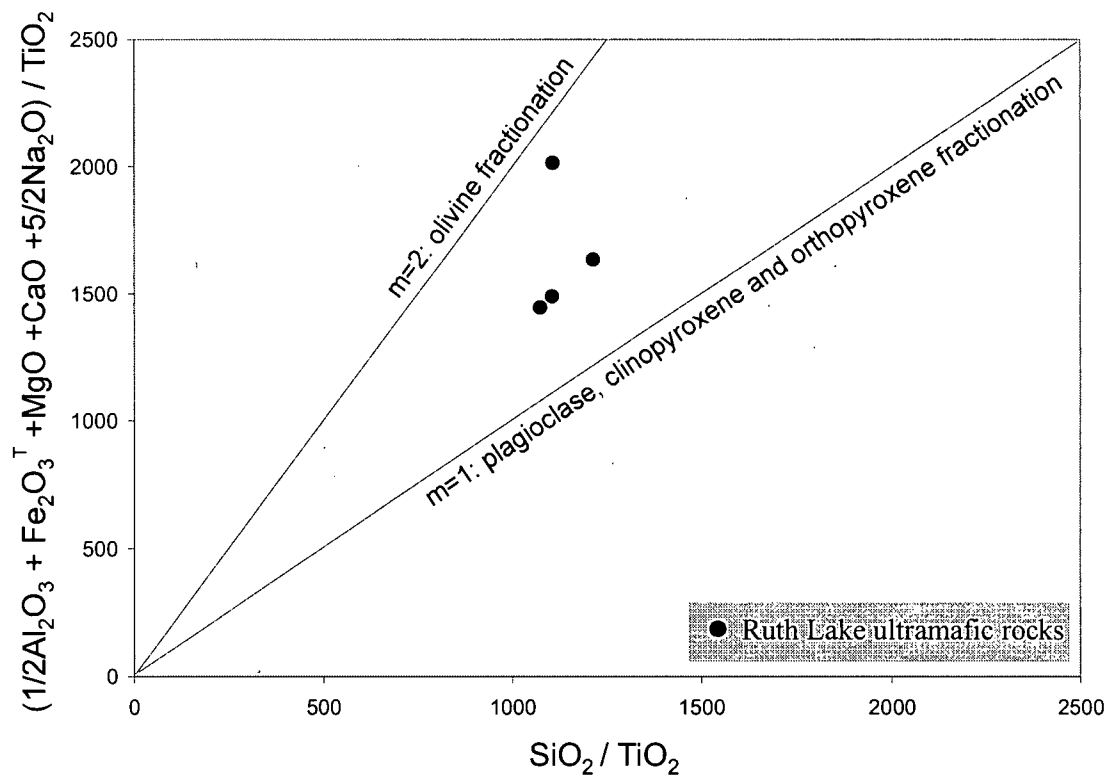


Fig. 4.19. Plagioclase, clinopyroxene and orthopyroxene PER fractionation model plot for the Ruth Lake ultramafic rocks with  $TiO_2$  as the conserved denominator.

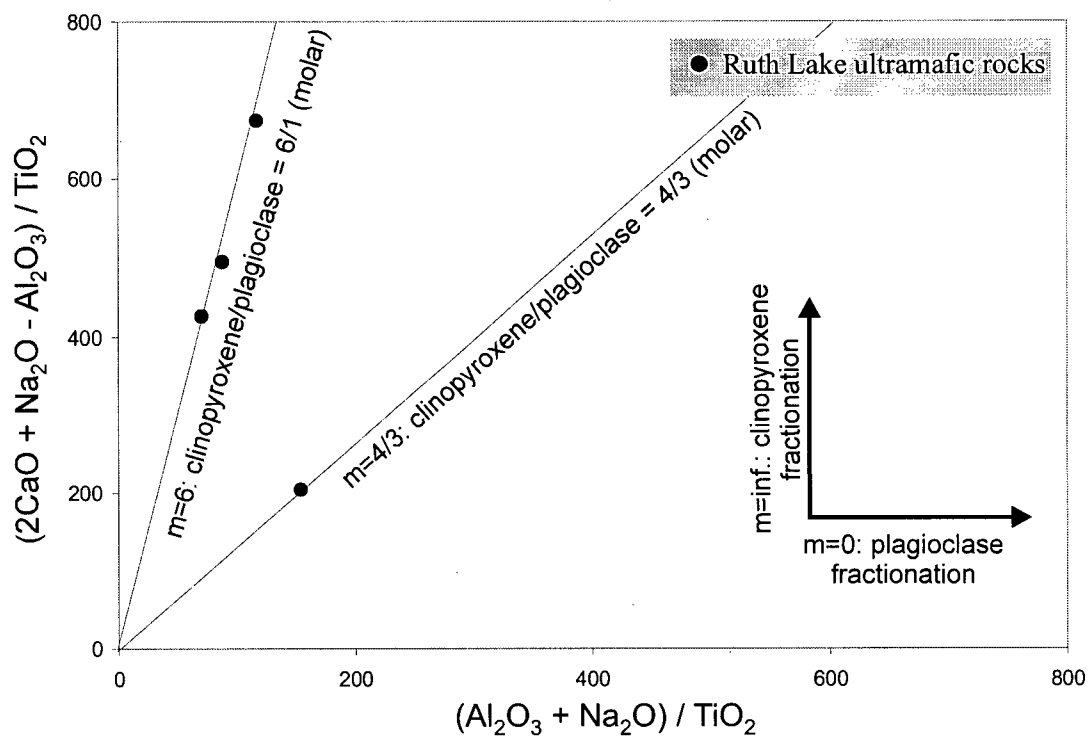


Fig. 4.20. Plagioclase and clinopyroxene PER phase discrimination plot with  $\text{TiO}_2$  as the conserved denominator for the Ruth Lake ultramafic rocks. Molar ratios of clinopyroxene to plagioclase vary between 6/1 and 4/3.

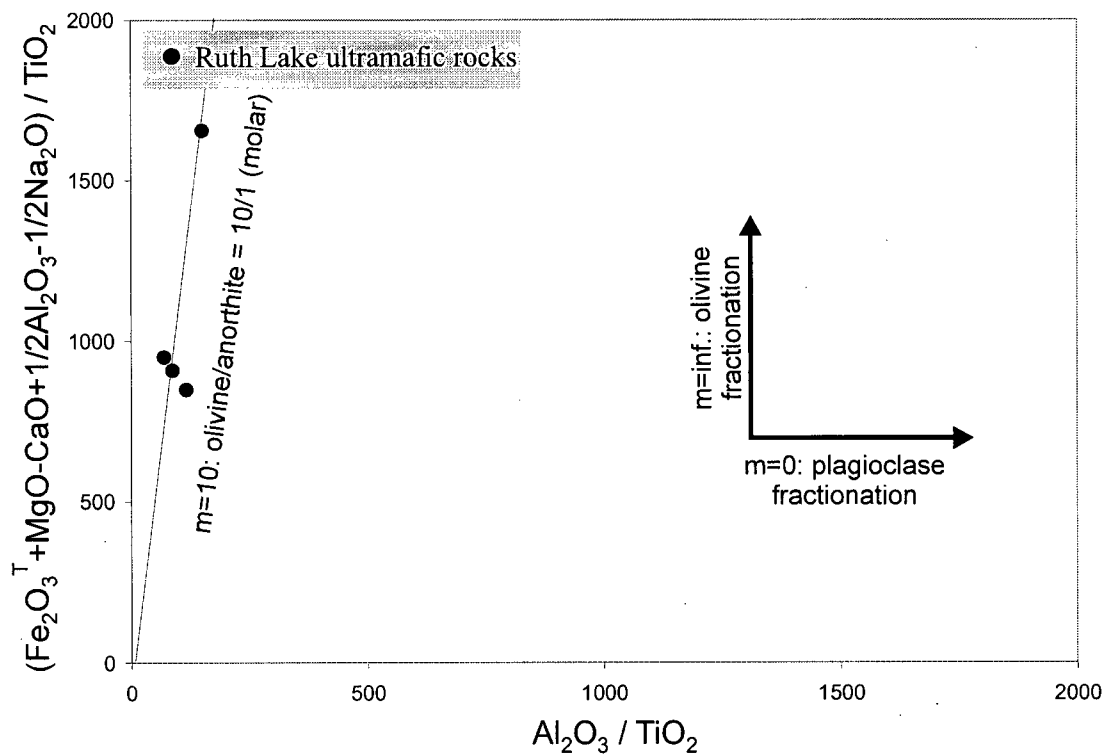


Fig. 4.21. Plagioclase and olivine PER phase discrimination plot with  $\text{TiO}_2$  as the conserved denominator for the Ruth Lake ultramafic rocks. Molar ratios of olivine to plagioclase (anorthite) are 10/1.

### Mosher Lake Basalts and Cable Lake Sill Gabbro

Conclusions about the original mineral composition of these volcanic rocks belonging to the Sandy Bay assemblage (Slimmon, 1994) are reached by means of PER analysis. The hypothesis that the rocks originated through fractionation of plagioclase, ortho- and clinopyroxene is confirmed by the PER analysis (Fig. 4.22). The same plot shows that participation of olivine in the igneous fractionation was minor to negligible. Another PER diagram (Fig. 4.23) tests the hypothesis that orthopyroxene is also absent from the fractionating mineral assemblage. Data points define two lines, both with slopes smaller than unity, indicating fractionation of orthopyroxene and, thus, the hypothesis is rejected. In most samples, including all basaltic rocks, the orthopyroxene proportion is low, whereas three gabbroic samples contain higher proportions of the mineral. The PER diagrams show no (Fig. 4.22), or very weak (Fig. 4.23) mass transfer effects that could be due either to Ca and Na loss or to the addition of  $\text{SiO}_2$ . Silicification could be either metasomatic or the result of vein and/or amygdale infilling.

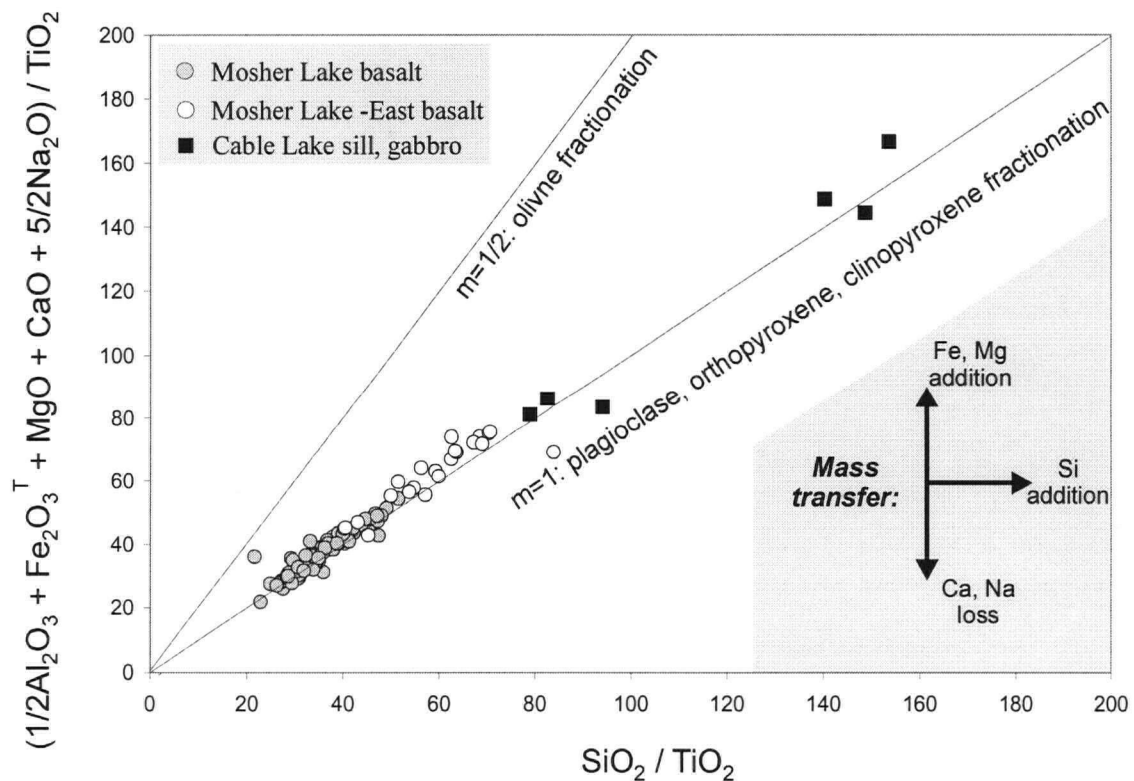


Fig. 4. 22. Plagioclase, orthopyroxene, and clinopyroxene PER fractionation model plot with  $\text{TiO}_2$  as the conserved denominator for the Sandy Bay assemblage rocks.

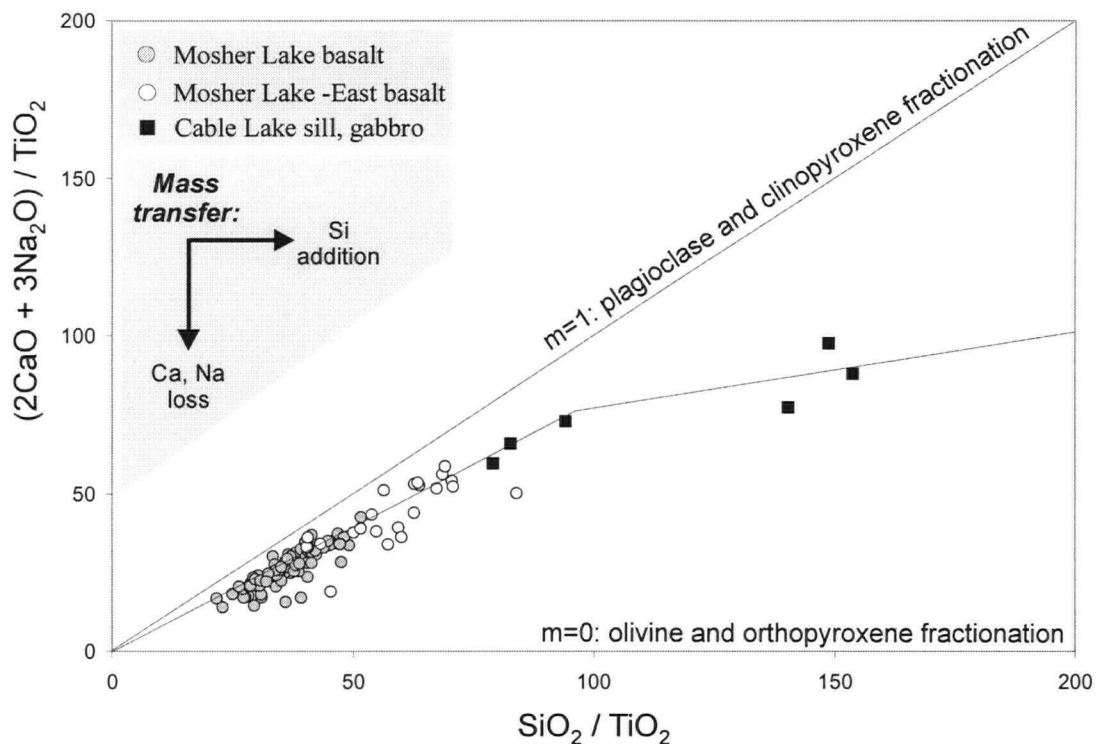


Fig. 4.23. Plagioclase and clinopyroxene PER fractionation model plot with  $\text{TiO}_2$  as the conserved denominator for the Sandy Bay rock assemblage.

As noted above, the Moshier Lake – east basalts are distinguished by their lower Ti, Zr, Y and P concentrations, which is the reason for their classification in a separate subgroup. The plagioclase fractionation model plot (Fig. 4.24) reveals differences in their major-element concentrations as well. The position of the data points below the background trend line for the Moshier Lake – West basalts can be interpreted in one of two ways:

1. The Moshier Lake – east basalts have higher proportion of plagioclase, indicating either fractionation peculiarities or compositional evolution of the magmas that produced the Moshier Lake lava flows, or
2. A metasomatic mass transfer process affected the Moshier Lake – East basalts, extracting Ca and Na from them. To account also for the lower concentrations of Ti, Zr, Y and P, this process has to occur with mass gain.

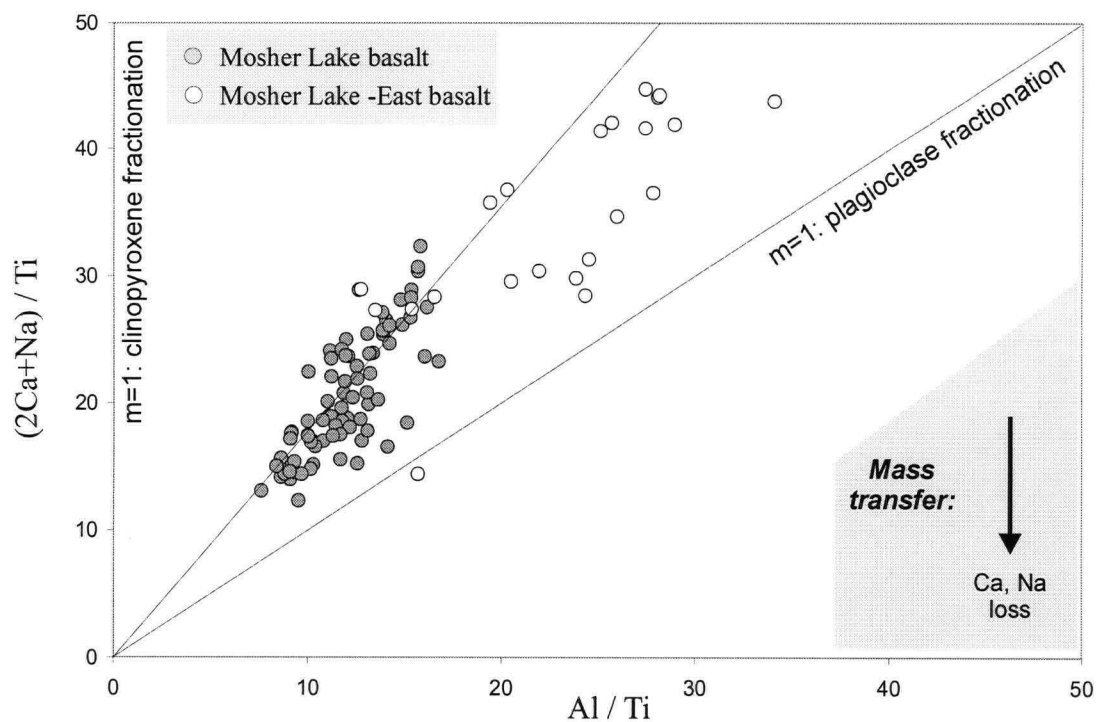


Fig. 4. 24. Plagioclase fractionation model plot for the Sandy Bay assemblage rocks.

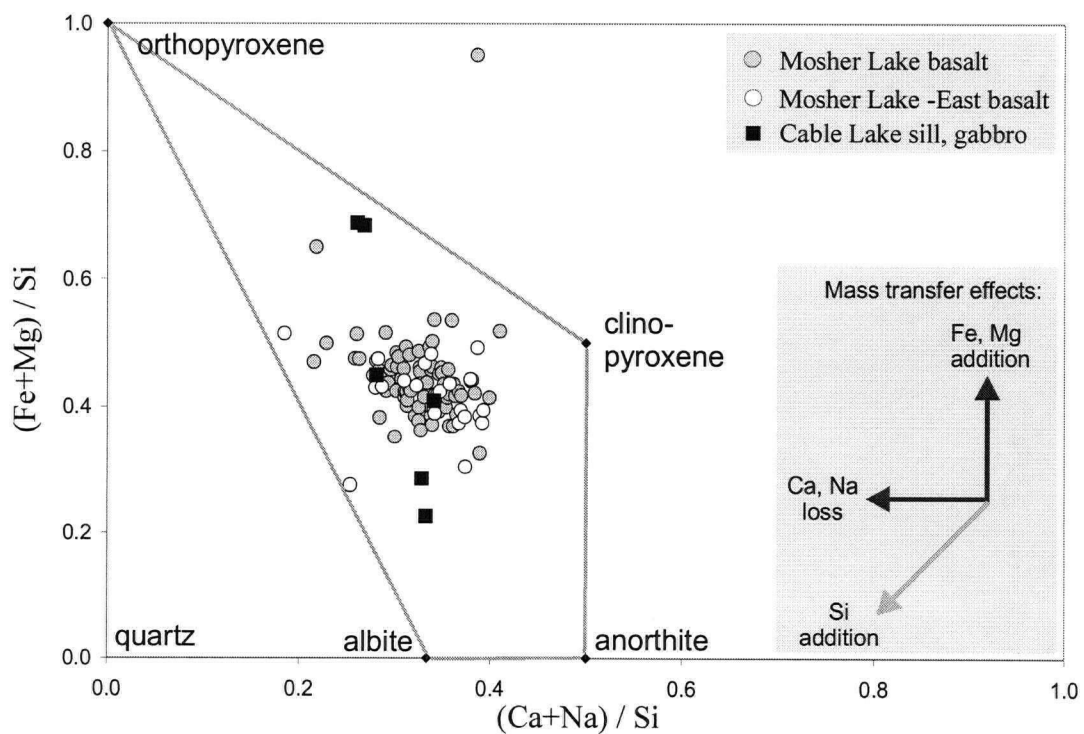


Fig. 4.25. GER plot for the Sandy Bay assemblage rocks. The data points form a tight cluster in the center of the field defined by the four minerals of the original paragenesis. Only one sample plots outside of the tetragon. Its position is most likely due to the presence of iron sulphide. Compared to the Birch Lake assemblage, the rocks are much less silicified and altered in any other way.

The GER plot constructed for the Mosher Lake basalts (Fig. 4.25) indicates a low degree of alteration, compared to the Birch Lake basalts (Fig. 4.14). Only a few Mosher Lake basalt samples display relatively weak alteration, represented by loss of Ca and Na and, to a lesser extent, by the addition of Fe and Mg. It is notable that the Mosher Lake – East basalt is not more intensively altered than the Mosher Lake – West basalt. This makes the first scenario above (variability in fractionation history and/or magmatic evolution within the Mosher Lake basalts) more probable. The few altered samples are erratically distributed in space and, thus, do not represent a geochemical signal useful in an exploration context.

## Conclusions

1. By devising PER ratios, the geochemical effect of hydrothermal mass transfer can be graphically visualized for each sample as the residual from the ascertained fractionation model line for a particular cogenetic suite of rocks. Relative mass transfer is numerically equal to the angle between the fractionation model line and the line defined by the sample data point and the origin of the plot. This angle is directly related to the degree of alteration of the sample.

Alteration, estimated in this way, is more pronounced in the Birch Lake volcanic rocks than in the Mosher Lake volcanic sequence. Various MER plots reflect metasomatism, but interference between the vectors of individual mass transfer effects and biases inherent to the plots allow only qualitative conclusions to be drawn about the intensity of alteration.

a) In the parameter:

$$| M - [(Fe_2O_3^T + MgO + CaO + 1/2 Al_2O_3 + 5/2 Na_2O) / SiO_2] |,$$

Fe, Mg, Ca, Al, Na and Si are the concentrations of the corresponding elements in the sample, divided by the concentration of a conserved element. M is the slope of the fractionation trend line (in the current case study the actual fractionation trend line coincides with the fractionation model line and, thus, M=1). The parameter is defined on the basis of the plagioclase – clinopyroxene - orthopyroxene fractionation model plot (Fig. 4.10). It is biased towards the Si addition component of alteration, because

Ca and Na loss and Fe and Mg addition components act in opposite directions to each other.

b) The same conclusion is valid for the parameter:

$$| M - (1/2 \text{Fe}_2\text{O}_3^T + 1/2 \text{MgO} + 3/2 \text{CaO} + 1/4 \text{Al}_2\text{O}_3 + 11/4 \text{Na}_2\text{O}) / \text{SiO}_2 |.$$

It is based on the plagioclase – clinopyroxene – olivine fractionation model plot (Fig. 4.11). For the data set used in this study,  $M = 9/10$ , which corresponds to the slope of the empirical fractionation trend line.

c) The parameter:

$$| M - [(2 \text{CaO} + 3 \text{Na}_2\text{O}) / \text{SiO}_2] |$$

is based on the plagioclase – clinopyroxene fractionation model plot (Fig. 4.12,  $M = 7/10$ ). By design, it is insensitive to mass transfer of Fe and Mg and, thus, equals the sum of Si addition and Ca and Na loss. Because one of the components of this sum, Si addition, can be either positive or negative (*e.g.*, either addition or loss of  $\text{SiO}_2$ , or neither can occur, depending on local conditions, Chapter 2 of this text), this parameter is not a satisfactory quantitative measure of alteration.

d) The parameter:

$$| M - [(2 \text{CaO} + \text{Na}_2\text{O} - \text{Al}_2\text{O}_3) / (\text{Al}_2\text{O}_3 + \text{Na}_2\text{O})] |$$

is derived from the plagioclase – clinopyroxene phase discrimination plot (Fig. 4.13,  $M = 1/3$ ). This parameter measures Ca and Na loss, free of the interference of any Fe, Mg and Si mobility. It falls short of being a useful quantitative measure of Ca and Na mobility, however, due to the uncertainty in the original plagioclase / clinopyroxene ratio ( $M$ ) for each individual sample.

2. GER plots represent mass transfer effects as residuals from nodes of background samples, considered to be unaltered.

a) The GER plot, with  $\text{SiO}_2$  at the origin visualizes Si addition, ferromagnesian addition and Ca and Na mobility. By means of this plot it is established that the Birch Lake basalts are intensively silicified, most likely through vein and amygdale infilling. Loss of Ca and Na and addition of Fe and Mg displace the data points at an angle



different from that of silicification. However, due to interference between the individual mass transfer effects quantitative characterization of alteration is not possible.

- b) The GER plot, projecting through  $\text{SiO}_2$  (Fig. 4.15), is the most useful in studying alteration, because it eliminates the interference of silicification. It visualizes two processes: Ca and Na mobility and Fe and Mg mobility. The representation of these processes on the plot is quantitative (in terms of moles of reaction), because their corresponding vectors are perpendicular and, thus, do not interfere with each other. The two processes are quantified by the following parameters:

$$[(\text{CaO} + \text{Na}_2\text{O}) / \text{Al}_2\text{O}_3]_i - [(\text{CaO} + \text{Na}_2\text{O}) / \text{Al}_2\text{O}_3]_0$$

- c) quantifies Ca and Na mobility. Negative values indicate loss, whereas positive values indicate addition of these elements. The samples used in this study represent both processes. Loss of Ca and Na is restricted to basaltic rocks, whereas addition is mostly identified in gabbroic rocks.

Fe and Mg mobility is quantified by the parameter:

$$(\text{Fe}_2\text{O}_3^T + \text{MgO}) / \text{Al}_2\text{O}_3]_i - [(\text{Fe}_2\text{O}_3^T + \text{MgO}) / \text{Al}_2\text{O}_3]_0.$$

- d) In the Birch Lake assemblage rocks ferromagnesian addition typically accompanies the process of Ca and Na mobility.
3. Alteration at Konuto Lake, Birch Lake and Flexar deposits is subtle and, viewed on a property scale, discrete, rather than pervasive. The delineated anomalies are of low contrast. Nonetheless, in the test case, anomalies cluster around the known ore occurrences, forming a halo around the Konuto Lake deposit and a band coinciding with the mineralized part of the stratigraphy at Birch Lake and Flexar deposits, supporting the validity of the methodology as an exploration tool. Some differences exist in the style of alteration between the areas of the Konuto Lake deposit on one side and the Birch Lake and Flexar deposits on the other:
- a) In the area of the Birch Lake and Flexar deposits the strongest geochemical signal of alteration is that of Ca and Na loss. It can be detected at distances of up to 250 m from the mineralized horizon (Fig. 4.17). Carbonatization is present in the host rocks, most

notably in the hanging wall gabbros. It occurs at larger distances from the ore body and forms an outer alteration halo.

- b) Alteration at Konuto Lake is represented by Ca and Na loss and Fe and Mg addition. It is weak and spatially restricted to within less than 50 m from the ore bodies (Fig. 4.16). Carbonatization is very weak to non-existent. Thus, zonation cannot be discerned in this area.
4. The MER methodology of processing lithogeochemical data is capable of identifying even subtle manifestations of hydrothermal alteration. With the selection of appropriate projections, interference between the individual mass transfer effects constituting the overall alteration can be minimized (*e.g.* Fig. 4.14) or eliminated altogether (*e.g.* Fig. 4.15). In this way it is possible to quantify processes such as silicification, Ca and Na loss, Fe and Mg addition *etc.* Because these processes also have mineralogical effects, the lithogeochemical information, acquired by means of MER analysis, can be integrated and validated with petrographic and field data. This underscores the applicability of MER analysis to exploration tasks.
5. PER analysis can be used to determine the mineral composition of rocks, based on their chemical composition. Especially when major-element lithogeochemical data are available, the methodology allows for statistically sound, quick and cost-efficient classification of rocks. Using this methodology, the Ruth Lake ultramafic sill samples were identified as intermediate between wehrlite and mela-olivine gabbro.
6. Apart from the study of alteration, the lithogeochemical study of the rocks in the vicinity of the Konuto Lake deposit yielded some information pertaining to the geologic setting of the area:
  - a) The gabbros of the Cable Lake sill are possibly cogenetic with the Sandy Bay assemblage volcanic rocks, whereas the Konuto and Ruth Lake Lake sills are possibly cogenetic with the Birch Lake assemblage basalts (Figs. 4.6 and 4.7). Thus, south of Mosher Lake, the boundary between the Sandy Bay assemblage and the Birch Lake assemblage must be drawn along the eastern margin of the Cable Lake sill, rather than along the Mosher Lake Zone.

- b) The volcanic rocks cropping out on the eastern shore of Mosher Lake belong to the Sandy Bay assemblage (Figs. 4.3, 4.6 and 4.7). Thus, north of the Denare Beach mobile home park, the Mosher Lake Zone lies within the Sandy Bay assemblage.
- c) Two compositionally distinct groups of volcanic rocks, belonging to the Sandy Bay assemblage, are identified in the study area, termed here "Mosher Lake – East basalt" and "Mosher Lake – West basalt". The Mosher Lake – East basalt is characterized by lower concentrations of  $\text{Fe}_2\text{O}_3^T$  and incompatible elements: Ti, Y, Zr and P (Figs. 4.5 through 4.7), higher proportion of plagioclase (Fig 4.23) and significant presence of orthopyroxene. It occurs near the eastern margin of the Sandy Bay assemblage.

## References

- Ansdell, K.M. and Kyser, T.K., (1991) The Geochemistry and Fluid History of the Proterozoic Laurel Lake Au-Ag deposit, Flin Flon Greenstone belt: Canadian Journal of Earth Science, 28, p. 155-171.
- Ansdell, K.M. and Norman, A.R., (1995) U-Pb Geochronology and Tectonic Development of the Southern Flank of the Kiseeynew Domain, Trans-Hudson Orogen, Canada: Precambrian Research, 72, p. 147-167.
- Ashton, K.E., Hunt, P.A. and Froese, E., (1991) Age Constraints on the Evolution of the Flin Flon Volcanic Belt and Kiseeynew Gneiss Belt, Saskatchewan and Manitoba. *In*: Radiogenic Age and Isotopic Studies Report 5: Geological Survey of Canada Paper 91-2, p. 55-69.
- Baird, D.J., Nelson, K.D., Knapp, J.H., Walters, J.J. and Brown, L.D., (1996) Crustal Structure and Evolution of the Trans-Hudson Orogen: Results from Seismic Reflection Profiling: Tectonics, 15; p. 416-426.
- Barrett, T.J. and MacLean, W.H., (1994) Chemostratigraphy and Hydrothermal Alteration in Exploration for VHMS Deposits in Greenstones and Younger Volcanic Rocks. *In*: Lentz, D.R., (editor), Alteration and Alteration Processes Associated with Ore-forming Systems: Geological Association of Canada, Short Course Notes, 11, p. 433-467.
- Bates, R.L. and Jackson, J.A., (editors) (1987) Glossary of Geology: American Geological Institute, Washington, DC, 788 p.
- Bickford, M.E., Collerson, K.D., Lewry, J.F., Van Schmus, W.R. and Chiarenzelli, J.R., (1990) Proterozoic Collisional Tectonism in the Trans-Hudson Orogen, Saskatchewan: Geology, v.18, p. 14-18.
- Bruce, E.L., (1918) Amisk – Athapapuskow Lake District: Geological Survey of Canada, Memoir 105, 91 p.

Chute, M.E. and Ayres, L.D., (1977) Missy Island Volcanic Centre, Saskatchewan: Geological Survey of Canada, Paper 84-1, 134 p.

David, J., Machado, N., Bailes, A. and Syme, E., (1993) U-Pb Geochronology of the Flin Flon-Snow Lake Belt: New results. *In*: Hajnal, Z. and Lewry, J. (editors), LITHOPROBE, Trans-Hudson Orogen Transect, Report 34, p. 84-87.

Fedorowich, J.S., Kerrich, R. and Stauffer, M.R., (1995) Geodynamic Evolution and Thermal History of the Central Flin Flon Domain, Trans-Hudson orogen: Constraints from Structural Development,  $^{40}\text{Ar}/^{39}\text{Ar}$  and Stable Isotope Geothermometry: *Tectonics*, 14, p. 472-573.

Franklin, J.M., (1993). Volcanic-associated Massive Sulphide Deposits. *In*: Kirkham, R.V., Sinclair, W.D., Thorpe, R.I. and Duke J.M., (editors) Mineral Deposit Modeling: Geological Association of Canada Special Paper, 40, p. 315-334.

Gilmore, K.V. and Pickell, J.R. (2000). The Konuto Lake VMS Deposit: Hudson Bay Exploration and Development Co. Limited Report, 44 p.

Gordon, T.M., Hunt, P.A. and Syme, E.C., (1990) U-Pb Ages from the Flin Flon and Kiseeynew belts, Manitoba: Chronology of Crust Formation at an Early Proterozoic Accretionary Margin; *In* Lewry, J.F. and Stauffer, M.R., (eds.), The Early Proterozoic Trans-Hudson Orogen of North America: Geological Association of Canada Special Paper 37, p. 177-200.

Heaman, L.M., Ashton, K.E., Reilly, B.A., Sibbald, T.I.I., Slimmon, W.L. and Thomas, D.J., (1993) 1992-93 U-Pb Geochronological Investigations in the Trans-Hudson Orogen, Saskatchewan. *In*: Summary of Investigations 1993: Saskatchewan Geological Survey, Saskatchewan Ministry of Energy & Mines, Miscellaneous Report 93-4, p. 109-111.

Heaman, L.M., Lewry, J.F. and Ashton, K.E., (1995) U-Pb Geochronology of the Pelican Window: Preliminary Results: Trans-Hudson Orogen Transect Workshop, LITHOPROBE Report 48, p. 143-147.

Hoffman, P.F., (1988) United Plates of America, the Birth of a Craton: Early Proterozoic Assembly and Growth of Laurentia: *Annual Reviews of Earth and Planetary Science*, 16, p. 543-603.

Irvine, T.N. and Baragar, W.R.A., (1971) A Guide to the Chemical Classification of the Common Volcanic Rocks: *Canadian Journal of Earth Sciences*, 8, p. 523-548.

Jensen, L.S., (1976) A New Cation Plot for Classifying Subalkalic Volcanic Rocks. Ontario Division of Mines Miscellaneous Paper 66, p. 1-22.

Kirkham, R.V., (1974) Geology of Copper and Molybdenum Deposits in Canada: Report of Activities, Part A, Geological Survey of Canada, Paper 74-1A, p. 377-379.

Leclair, A.D., Lucas, S.B. and Stern, R.A., (1994a) Significance of Buried Lithotectonic Domains for the Tectonic Evolution of the Trans-Hudson Orogen (Canada): Geological Society of America, Abstracts with Programs, 26, p. A-404.

Leclair, A.D., Lucas, S.B. and Stern, R.A., (1994b) Tectonics of the Flin Flon – Snow Lake Belt: View from Below the Phanerozoic Cover: Trans-Hudson Orogen Transect Workshop, LITHOPROBE Report 38, p. 123 – 134.

LeMaitre, R.W., (editor) Bateman, P., Dudek, A., Keller, J., Lemeyre, J., Le Bas, M.J., Sabine, P.A., Schmid, R., Sorensen, H., Streckeisen, A., Wooley, A.R., Zanettin, B., (1989) A Classification of Igneous Rocks and Glossary of Terms: Blackwell Science Publications, Oxford, UK, 193 p.

Longiaru, S.J., Structure and Metamorphism of the Northeast Amisk Lake Area: M.Sc. thesis, University of Saskatchewan, Saskatoon, Saskatchewan, 119 p.

Lucas, S.B. and Stern, R.A., (1994) Significance of Accretion and Melting Processes for the Development of the Paleoproterozoic Continental Lithosphere: Geological Association of Canada, Program with Abstracts, 19, p. A-67.

Lucas, S. B., Stern, R. A., Syme, E. C., Reilly, B. A. and Thomas, D. J., (1996) Intraoceanic Tectonics and the Development of Continental Crust; 1.92-1.84 Ga Evolution of the Flin Flon Belt, Canada: Geological Society of America Bulletin, 108, p. 602-629.

Machado, N., (1990) Timing of Collisional Events in the Trans-Hudson Orogen: Evidence from U-Pb Geochronology from the New Quebec Orogen, the Thompson Belt and the Reindeer Zone (Manitoba and Saskatchewan). *In*: Lewry, J.F. and Stauffer, M.R., (editors), The Early Proterozoic Trans-Hudson Orogen of North America: Geological Association of Canada Special Paper 37, p. 433-441.

Morgan, J., (1995) Geological Mapping of the Area of Denare Beach - Konuto Lake - Birch Lake. Hudson Bay Exploration and Development Co. Limited, 42 p.

Pearce, T.H., (1968). A Contribution to the Theory of Variation Diagrams: Contributions to Mineralogy and Petrology, 19, p. 142-157.

Philpotts, A. R., (1990). Principles of Igneous and Metamorphic Petrology: Prentice Hall, Englewood Cliffs, New Jersey, 498 p.

Reilly, B.A. (1995) The Geological Setting of Mineral Deposits of the Flin Flon - Amisk Lake area. *In*: Summary of Investigations 1995: Saskatchewan Geological Survey, Saskatchewan Ministry of Energy & Mines Miscellaneous Report 95-4, p. 3-12.

Robinson, M., (1996) Birch Lake Assemblage, Spring and Fall 1995. Hudson Bay Exploration and Development Co., Report, 57 p.

Rollinson, H.R., (1993) Using Geochemical Data: Evaluation, Presentation, Interpretation. John Wiley & Sons, New York, 352 p.

Russell, J.K. and Stanley, C.R., (1990). Material Transfer Equations and Chemical Variation Diagrams. *In*: Russell, J.K. and Stanley, C.R. (editors), Theory and Application of Pearce Element Ratios to Geochemical Data Analysis, Geological Association of Canada, Short Course Notes, 8, p. 23-54.

Sinclair, A.J. and Stanley, C.R., (1995) Lithogeochemical Exploration for Metasomatic Alteration Zones Associated with Hydrothermal Mineral Deposits: University of British Columbia, MDRU Research Proposal, 7 p.

Slimmon, W.L., (1991) Revision Bedrock Geology, Table Lake Area (part of NTS 63L-9), Sheet 1: North; 1:12 500 Scale Map. *In*: Summary of Investigations 1991: Saskatchewan Geological Survey, Saskatchewan Ministry of Energy & Mines, Misc. Rep. 91-4, p. 16-20.

Slimmon, W.L., (1993) Bedrock Geology of the Comeback Bay Area, Amisc Lake (Part of NTS 63L-6 and 16). *In*: Summary of Investigations 1993: Saskatchewan Geological Survey, Saskatchewan Ministry of Energy & Mines, Miscellaneous Report, 93-4, p. 21-29.

Slimmon, W.L. (1994) Bedrock Geology of the Konuto Lake Area (part of NTS 63-9). *In*: Summary of Investigations 1994: Saskatchewan Geological Survey, Saskatchewan Ministry of Energy & Mines, Miscellaneous Report, 94-4, p. 18-26.

Stanley, C.R., (1996) Graphical Investigation of Lithogeochemical Variations Using Molar Element Ratio Diagrams: Theoretical Foundation. Lithogeochemical Exploration for Metasomatic Zones Associated with Hydrothermal Mineral Deposits, Mineral Deposits Research Unit, Lithogeochemical Research Project, Annual Technical Report Year 1., 40 p.

Stanley, C.R., (1997a) Analytical Quality Control and Assessment for the MDRU Lithogeochemical Exploration Research Project. Lithogeochemical Exploration for Metasomatic Zones Associated with Hydrothermal Mineral Deposits. Annual Technical Report, Years 1 and 2. Mineral Deposits Research Unit, Department of Geological Sciences, The University of British Columbia, Vancouver, B.C., 32 p.

Stanley, C.R., (1997b) THPLOT.MATLAB Function to Implement Generalized Thompson-Howarth Error Analysis Using Replicate Data. Lithogeochemical Exploration for Metasomatic Zones Associated with Hydrothermal Mineral Deposits. Annual Technical Report, Years 1 and 2. Mineral Deposits Research Unit, Department of Geological Sciences, The University of British Columbia, Vancouver, B.C., 51 p.

Stanley, C.R. and Russell, J.K., (1989) Petrologic Hypothesis Testing with Pearce Element Ratio Diagrams: Derivation of Diagram Axes: Contributions to Mineralogy and Petrology 103, p. 78-89.

Stanley, C.R. and Madejsky, H.E., (1995). Lithogeochemical Exploration for Metasomatic Zones Associated with Hydrothermal Mineral Deposits Using Pearce Element Ratio Analysis: 17<sup>th</sup> International Geochemical Exploration Symposium, Townsville, Queensland, Australia, Short Course Notes, 97 p.

Stern, R.A., Lucas, S.B., Syme, E.C., Bailes, A.H., Thomas, D.J., Leclair, A.D. and Hulbert, L. (1993) Geochronological Studies in the Flin Flon Domain, Manitoba-Saskatchewan, NATMAP Schield Margin Project Area: Results for 1992-1993: Radiogenic Age and Isotopic Studies, Report 7, Geological Survey of Canada, Paper 93-2, p. 59-70.

Stern, R.A. and Lucas, S.B., (1994) U-Pb Zircon Constraints on the Early Tectonic History of the Flin Flon Accretionary Collage, Saskatchewan: Radiogenic Age and Isotopic Studies Report 8. Geological Survey of Canada Current Research 1994F, p. 75-86.

Syme, E.C., Thomas, D.J., Bailes, A.H., Reilly, B.A. and Slimmon, W.L. (1993) Geology of the Flin Flon area, Manitoba and Saskatchewan (parts of NTS 63K and 63L); 1 Sheet, 1:50,000 Scale Map, Geological Survey of Canada, Open File 2658.

Syme, E.C. and Bailes, A.H., (1993) Stratigraphic and Tectonic Setting of Early Proterozoic Volcanogenic Massive Sulphide Deposits, Flin Flon, Manitoba: Economic Geology, 88, p. 566-589.

Thomas, D.J., (1991) Revision Bedrock Geological Mapping: Bootleg Birch Lake Area (Parts of NTS 63K-12 and 63L-9). *In*: Summary of investigations 1991: Saskatchewan Geological Survey, Saskatchewan Ministry of Energy & Mines, Miscellaneous Report, 91-4, p. 2-8.

Walker, T. and McDougall, F., (1987) Geology of the Laurel Lake Gold-silver Deposit. *In*: Gilboy, C.F. and Vigrass, L.W., (editors), Economic Minerals of Saskatchewan, Saskatchewan Geological Society, Special Publication 8, p. 44-53.

## **Chapter 5**

### **Conclusions**

The studies of the Goldstream, Chu Chua, and Konuto Lake deposits (Chapters 2, 3, and 4) show that Molar Element Ratio (MER) analysis provides deterministic insight into the sources of observed geochemical variability. In comparison, other known methodologies are less informative. MER techniques can help distinguish variations in rock chemistry due to both syngenetic and epigenetic processes. Implementation of MER does not require any unusual sampling or analytical procedures, dedicated software or hardware, or extensive training of geology professionals. Thus, the MER analysis can be conveniently and successfully applied at various stages in exploration practice, as well as more generally in the study of mineral deposit genesis.

### **MER Analysis: Modus Operandi**

#### ***Conditions***

Pearce element ratio (PER) analysis is subject to two significant preconditions concerning the rocks under investigation:

1. In order to be considered together, the rocks have to be cogenetic - the result of the same primary fractionation processes acting on a common parent material that was at one time homogenous.
2. At least one conserved element, which was not influenced by epigenetic processes, must be present in the rocks.

To ensure that the two conditions are met, the data are tested, by plotting pairs of elements together and searching for linear correlations. These are usually found to exist between elements incompatible in mafic igneous systems (*e.g.*, Zr, Ti, Nb, Y, and P). Linear correlation existing between any pair of elements is an indication (although strict proof that the conditions are met is impossible) that the data are not inconsistent with the two conditions. When applied to a diverse set of samples, this test is itself a useful tool for



distinguishing stratigraphic units. This test, for example, helped distinguish the otherwise identical varieties of basalts occurring in the wall rocks of the Chu Chua deposit (Chapter 3, Fig. 3.2). Another example is the distinction between metapelites of turbiditic and pelagic origin hosting the Goldstream deposit (Chapter 2, Fig. 2.10.a).

If the test yields negative results (*i.e.*, no linear correlation is observed between any two elements), the application of the PER technique is not warranted. The Generalized Element Ratio (GER) technique, which does not require a conserved denominator, can be applied in this case. The condition that the rocks are cogenetic, however, is still required for meaningful interpretation of the plots.

### ***Formation of Molar Element Ratios (MER)***

Pearce element ratios (PER) and generalized element ratios (GER) are formed by the same two-step procedure. The first step involves the conversion of the lithogeochemical data from weight concentration format, as are typically reported by labs, to molar concentrations. This is achieved through division by the corresponding oxide molar weights.

The second step involves the division of the molar concentrations of all elements by the corresponding sample's molar concentration of an element chosen for a denominator. If the element chosen for a denominator is conserved, the resulting ratio is a PER. Where more than one element is identified as conserved, the choice of a conserved denominator element in PER is not critical and the only issue of concern is minimization of the propagated analytical error. Thus the logical choice is an element with highest analytical precision. In all three case studies presented here, titanium was chosen as denominator according to the above criterion.

If the denominator element is not conserved, the result is GER. In this case, unlike the PER technique, the choice of a denominator element has fundamental impact on the diagram's geometry. Thus, in order to fully utilize the data, it may be prudent to construct GER diagrams with different denominator elements.

Pearce element ratio analysis and general element ratio analysis are two varieties of MER analysis techniques, which supplement each other in the study of mass transfer processes. The PER variety can be further subdivided into several functional types (Stanley, 1998) offering different perspectives on the same data set and allowing for exhaustive study of the data.

### ***Construction of MER Diagrams***

The axis parameters of MER diagrams are formed as linear combinations of molar element ratios. While this step is procedurally simple, the selection of the components and coefficients participating in the linear combination is the critical and most conceptually involved step in the MER analysis. The choice of axis parameters sets the composition-space in which the data are viewed, and by that, the diagram's functional type, ultimately determining the analytical power of the diagram. The choice of appropriate axis parameters is aided by prior knowledge about the host rocks and the mineralogy of the alteration. This places the MER technique among the few known deterministic methodologies for processing of lithogeochemical data. The diagrams tie mineral and chemical compositions of the rocks through the chemical effects of minerals involved in material transfer processes.

The following types of MER diagrams are distinguished (Stanley, 1998):

1. PER Assemblage Test Diagram (*e.g.*, Figs. 3.9, 3.10, 3.12 through 3.14, 4.10 through 4.12, 4.18, 4.19, 4.22, 4.23): The material transfer effects of the constraining minerals displace rock compositions along a line of a predetermined (typically 1) slope.
2. PER Phase Discrimination Diagram (*e.g.*, Figs. 3.18 through 3.20a, 4.13, 4.20, 4.21, 4.24): The material transfer effects of the constraining minerals displace rock compositions at equal distances along the horizontal or vertical axes on the diagram. This diagram is most useful when the constraining minerals are two and the diagram projects from all other participating phases.
3. Specialized PER Diagrams: The material transfer effects of the constraining minerals displace rock compositions in directions and at distances specific for the given diagram.

This diagram has no standard format (*e.g.*, Figs. 2.13 through 2.15.a, 2.16 through 2.18, 4.18, 4.19, 4.22 through 4.24).

4. GER Diagrams: The material transfer effects of the constraining minerals displace rock compositions toward or away from the locations where the constraining minerals plot on the diagram. This diagram, unlike PER diagrams does not require a conserved element for the formation of the axes parameter ratios. Thus, it not only provides an additional perspective on the data (*e.g.*, Figs. 2.12, 2.19, 4.14, 4.15, 4.25), but is the only type of MER diagram available for use when the conserved element condition is not met.

In most cases the MER diagrams are constructed (*i.e.*, axes parameters are selected) by inspection, taking into account two factors: (1) the primary mineral composition (observed or probable) of the rocks; and, (2) the desired displacements of rock compositions on the diagram. A rigorous matrix algebraic procedure exists, allowing for the construction of PER diagrams under more complicated circumstances, such as:

1. When the number and combination of minerals prevents an easy, "by-inspection" construction of the PER diagram.
2. When a specific displacement of rock compositions is sought, for which there is no obvious set of axes parameters.
3. When non-ideal mineral stoichiometries are used (*e.g.*, in the case study presented in Chapter 3, where stoichiometries acquired by microprobe analysis were used for the rock-forming minerals).

The matrix algebraic procedure is based on the matrix equation:

$$\mathbf{C} \mathbf{A} = \mathbf{P} \quad (5.1)$$

Where:  $\mathbf{C}$  is a matrix ( $m \times e$ ) with row vectors describing the compositions of the minerals under consideration and columns representing chemical components (elements);

$\mathbf{A}$  is an ( $e \times d$ ) matrix ( $e \times d$ ) where column vectors correspond to the set of chemical component coefficients for the two axes ( $d = 2$ ) in PER diagrams or to the two axes and common denominator ( $d = 3$ ) in GER diagrams;  $\mathbf{P}$  is a matrix ( $m \times d$ ) with row vectors

describing the displacements of rock compositions due to material transfer of each mineral. Two of the column vectors represent the displacements along the two diagram axes. The third column vector, present only in relation to GER diagrams and corresponding to the common denominator scales the first two by equal proportions; and **m** is the number of constraining minerals for the MER diagram, **e** is the number of measured components (elements) and **d** is the number of axes variables (numerators and denominators).

Matrix **C** in the above equation is fully determined by the mineral phases under consideration and the set of measured elements. Matrix **P** consists of the desired displacements and is, thus, also known. The equation is solved for the matrix **A**, which tabulates the coefficients in the linear combinations (and in the case of GER diagrams – common denominators) representing the axes parameters. The matrix equation that gives the array of values for **A** is:

$$\mathbf{A} = (\mathbf{C}^T \mathbf{C})^{-1} \mathbf{C}^T \mathbf{P} \quad (5.2)$$

More in-depth descriptions of the theory and procedures leading to construction of MER plots are available in Stanley and Russell, 1989; Stanley, 1996. A detailed example of the matrix algebraic procedure, applied in order to accommodate non-ideal mineral compositions is presented in Chapter 1. However, the method was found robust enough to accommodate typical departures from the ideal mineral compositions.

### ***Interpretation of MER Diagrams***

1. PER Assemblage Test Diagrams serve two purposes: (1) test a fractionation model; and, (2) characterize secondary processes through residuals from the fractionation model line. In order to achieve both goals, a data set has to include both background and altered samples. The fractionation model test is positive (*i.e.*, the fractionation model adequately describes the rocks under investigation) when background samples plot within a confidence interval from the model line, set in relation to measurement error. Samples plotting away from the model line have undergone mass transfer processes inconsistent with, and (because all samples are cogenetic) superimposed on primary variability.

2. The residuals from each of the data points to the model line characterize the secondary process both qualitatively (direction of displacement) and quantitatively in terms of moles of reaction (angle of displacement). The qualitative information allows the additions and losses of chemical components to be identified and thus for the alteration process to be typified (*e.g.*, two-way mobility of silica and loss of Ca and Na in Fig. 3.9). Angular magnitudes of residuals quantitatively (in terms of moles of reaction) correspond to the intensity of alteration. The mineralogical effects of the process can be inferred (*i.e.*, destruction of plagioclase accompanied in some samples by silicification, Fig. 3.9) from the starting (background) composition and the nature of material transfer. Mineral compositions are represented on the PER diagrams as lines emanating from the origin.
3. PER Phase Discrimination Diagrams are constructed to visualize the proportions of two minerals in the sampled rocks. If the two minerals under consideration are primary minerals, the diagram carries information about the primary paragenesis (*e.g.*, Fig. 4.21 indicating that the olivine/plagioclase ratio in the Ruth Lake ultramafic rocks is 10/1). If the minerals under consideration are metasomatic alteration phases, the diagram can be used to outline two different types of alteration (*e.g.*, chlorite vs. sericite alteration, Fig. 3.20a). If the minerals are a reactant/product pair, the diagram can be used to spatially characterize the intensity of the alteration process.
4. Specialized PER Diagrams (Figs. 2.13 through 2.15a and 2.16 through 2.18) do not have a standard format. Their axes parameters are not set up with any particular mineral in mind. This particular use of PER diagrams is practical when the primary mineralogy is complex and a fractionation model cannot be easily proposed as is the case with the Goldstream metapelitic host rocks. Instead, chemical components that are likely to have significant participation in the primary minerals are chosen as PER axes numerators (in Goldstream rocks these are Al, K, Na, Fe, Mg). If the data points form a linear array, the slope of the line corresponds to the proportions of the diagram numerator components in the background (primary) bulk rock chemistry. In this way conclusions can be made about

the primary mineral paragenesis. Residuals from the background linear trend are interpreted in the same way as the residuals on PER assemblage test diagrams (see above).

5. In GER Diagrams mineral compositions are represented as nodes with specific coordinates (unlike PER diagrams where they are represented as lines with specific slopes). Clusters of data points (typically isometric) represent background rock compositions. They plot within polygons defined by the minerals of the primary paragenesis (*e.g.*, Figs. 2.12, 4.14, 4.15 and 4.25). Deviations from the background cluster indicate secondary mass transfer processes. The direction of the deviation points to the product mineral(s) of the mass transfer process, whereas the magnitude characterizes its intensity (*e.g.*, Figs. 2.19, 4.14 and 4.15). Thus, GER diagrams allow conclusions to be drawn regarding: (1) the primary mineral paragenesis, (2) the chemical and mineralogical nature of the alteration processes and (3) the intensity of alteration of the samples.

MER analysis, applied in any of its varieties outlined above, has the capacity to determine the type and quantify the degree of alteration in each sample. This allows alteration anomalies to be characterized spatially and, thus, has direct application in the search for mineral deposits. The following approach was applied in this study and was found to be practical: Samples exhibiting the same type of alteration are ranked according to the magnitude of angular displacement from the model line (PER analysis), or according to the distance of displacement from the primary composition node (GER analysis). Then, the samples are arbitrarily classified in a few (2 to 4) categories (*e.g.*, unaltered, weakly altered, moderately altered, strongly altered). The categories are colour-coded and the samples are plotted in space to reveal the spatial distribution of alteration. The anomaly contrast can be adjusted by varying the classification thresholds.

## **Applicability of MER Analysis to Mineral Exploration Problems**

### ***Chemostratigraphy***

As outlined above, PER assemblage test diagrams are used to determine the primary mineral paragenesis formed through processes such as igneous fractionation and sedimentary sorting.

This offers valuable insight into rock genesis, especially where primary phases, transformed through epigenetic processes (e.g., diagenesis and metamorphism), are not available for direct identification. While normative analysis is a well-established technique applicable to igneous rocks, no alternative method exists for the determination of primary mineral compositions of fine-grained sedimentary and metasedimentary rocks. Furthermore, the ability of PER to handle sample sets containing some proportion of altered rocks is an advantage over normative analysis. Even where the primary paragenesis is preserved and the rocks are coarse-grained, allowing modal mineral compositions to be determined through standard petrographic methods, the PER analysis alternative offers the benefit of cost-, and time-efficiency. In the practice of mineral exploration, studying primary compositional variations can be used to delineate geological units with distinct histories of rock formation (chemostratigraphy).

### ***Characterization of Hydrothermal Metasomatism***

PER analysis is superior to other existing methods in studying lithogeochemical variability due to secondary mass transfer processes. Integration of geochemical data with mineralogical and petrological insight gives PER analysis the conceptual strength of a deterministic, rather than a statistical, method. Although the complexity of the procedures involved is relatively high, the results are easily comprehensible. This is due to two factors: (1) the method underscores the relationship between chemical mass transfer and observable mineralogical transformations; and (2) the output is in a graphical format, visualizing not only sample compositions (as coordinates in two dimensions) but also mineral compositions (as lines with characteristic slopes emanating from the origin) and processes (as vectors).

The sensitivity of a method can be defined as its capacity to suppress background variability and concentrate on the desired signal. In exploration for alteration zones associated with mineral deposits, the useful signal is due to secondary mass transfer processes (hydrothermal metasomatism). The background signal typically comprises: (1) primary variability, (2) errors, including sampling and analytical, and (3) the closure effect (a mathematical effect inherent to compositional data). MER (including its PER variety) analysis neutralizes two of

the sources of background noise: The effect of closure is eliminated entirely by the use of molar ratios; primary variability is accounted for by the design of the MER diagrams, which restrict it to a line (the fractionation model line in PER) or a region (the background composition region in GER). Sampling errors are minimized through sound sampling practices, including ensuring sufficient sample size and homogeneity of subsamples (*e.g.*, Gy, 1979; Cheng, 1995).

The geochemical anomalies identified by this study in the three studied areas were found to extend at distances from 50m (Chu Chua, Chapter 3) to 200m (Birch Lake, Chapter 4) across the stratigraphy. Often, as was the case at Chu Chua and Birch Lake, the anomalies are traced along the stratigraphy at much larger distances relative to the extent of the ore bodies themselves. Thus, the method is capable of providing much larger targets for the intermediate stages of mineral exploration.

The contrast of the identified anomalies using MER analysis is directly related to: (1) the nature of the anomaly (pervasive vs. vein-controlled); and, (2) the density of sampling. This study showed that with a typical sampling density (core from existing exploration drill holes were resampled for the purposes of the study) the contrast of the anomalies outlined in the basaltic host rocks was insufficient to identify clear zonation with respect to type and intensity of alteration. This is attributed to the discrete nature of the alteration associated with the studied type of deposits. Crude zonation pattern was noted only at the Chu Chua deposit (Chapter 3, Figs. 3.15, 3.16 and 3.17).

### ***Contribution to the Genetic/Deposit Model***

The studies of the Goldstream (Chapter 2) Chu Chua (Chapter 3) and Konuto Lake (Chapter 4) deposits identified common characteristics of the associated alteration as well as differences. Naturally, more similarities exist between Chu Chua and Konuto Lake, which are both of the mafic-hosted type of VHMS deposit, whereas Goldstream is a Besshi-type deposit.



The alteration was found to comprise several chemical mass-transfer effects having different spatial distribution and intensity:

- 1) Fe-Mg addition occurred in all of the studied deposits. It is restricted to the footwall. Mineralogically, addition of Fe and Mg is represented as chloritization. At the Chu Chua deposit its extreme form resulted in a talc-magnetite paragenesis, developed in the immediate vicinity (up to a few tens of meters) of the ore bodies. At the Goldstream deposit, the ferromagnesian paragenesis possibly included clay minerals such as saponite and nontronite, forming at, or a short distance under, the seafloor.
- 2) Ca-Na loss is mineralogically expressed as destruction of plagioclase and pyroxene. It is widespread, and influences both the footwall and the hanging wall (best documented at the Chu Chua deposit). This is an indication that the hydrothermal activity continued until after the capping of the ore bodies by the hanging-wall lava flows.
- 3) Potassium is mobilized probably from the deeper zones of the footwall (up to 100m) and is introduced in the immediate (up to 20 m from the ore body) footwall. This conclusion is based exclusively on the Goldstream (Besshy-type) deposit. Background concentrations of K in the mafic host rocks to the Chu Chua and Konuto Lake deposits are very low (0.2 – 0.4 %). However, elevated concentrations of K and microscopically visible sericite in the cherts indicate possible participation of that element in the exhaled solutions.
- 4) Si mobility is also the result of destruction of plagioclase and pyroxene. Silica, released in the process is redistributed in the following manner:
  - a) net loss from the foot-wall and part of the hanging wall;
  - b) net addition in relatively small volumes of rock in the immediate footwall of the deposit where quartz forms metasomatically and through vein filling;
  - c) the balance of the silica leached from the footwall is released onto the seafloor, forming chert accumulations ranging from laterally extensive, thin sheets (*e.g.* Goldstream deposit) to thick graben-fill deposits (*e.g.* Chu Chua deposit).
- 5) Aluminum generally behaves as immobile and participates only in *in-situ* transformations between primary and metasomatic minerals.

## References

Cheng, X., (1995) Mass Changes During Hydrothermal Alteration, Silver Queen Epithermal Deposit, Owen Lake, Central British Columbia: PhD thesis, University of British Columbia, Vancouver, BC, 297 p.

Gy, P.M., (1979) Sampling of Particulate Materials, Theory and Practice: Elsevier, Amsterdam, The Netherlands, 431 p.

Stanley, C.R., (1996) Graphical Investigation of Lithogeochemical Variations Using Molar Element Ratio Diagrams: Theoretical Foundation. Lithogeochemical Exploration for Metasomatic Zones Associated with Hydrothermal Mineral Deposits: Mineral Deposits Research Unit, Lithogeochemical Research Project, Annual Technical Report Year 1., 40 p.

Stanley, C.R., (1998) Lithogeochemical Exploration for Metasomatic Zones Associated with Hydrothermal Mineral Deposits Using Molar Element Ratio Analysis: Advanced Topics: Mineral Deposits Research Unit, University of British Columbia, Short Course Notes, 168 p.

Stanley, C.R. and Russell, J.K., (1989) Petrologic Hypothesis Testing with Pearce Element Ratio Diagrams: Derivation of Diagram Axes: Contributions to Mineralogy and Petrology, 103, p. 78-89.

## **Appendix 1**

### **Samples and analytical data used in the study of the Goldstream deposit.**

The data set used in the study of the Goldstream deposit is built around 180 original samples of drill core and outcrops, taken in 1995. The original samples represent the lithologies hosting the ore body both in its immediate vicinity and farther to the west, where another mineralized zone was drill-tested. Regional samples were taken from outcrops along Highway 23, approximately 14 km to the west of the Goldstream mine, and Trans-Canada Highway 1, more than 50 km to the southeast. The latter location was suggested (Jim Logan pers. comm.) as distal stratigraphic equivalent to the studied area. Location coordinates for these distal samples are not provided in Table A1.1.

An additional 123 samples from surface exposure, drill core and underground workings donated by T. Hoy and J. Logan augment the original data set. Exact locations of some of these donated samples were not available. The donated samples were not analyzed for the same set of components and not all were analyzed by the same analytical methods as the original samples.

Abbreviations used in Table1 include:

M	=	marble	DGBP	=	dark grey banded phyllite
GZ	=	garnet zone	HW-1	=	Trans Canada Highway 1
VOLC	=	volcanic rocks	HW-23	=	Highway 23
QTZ	=	quartzite	OP	=	Open pit of the Goldstream mine
GGP	=	green grey phyllite			

The samples are referenced on the Goldstream mine grid, which is rotated at 20° East of true North. The grid has its origin on the west bank of the Revelstoke dam. On this grid the center of the main mine building has coordinates 15330m E and 2705m N and the point where the Goldstream mine road forks off highway 23 has coordinates 2225m E and 1275m N.

### **Sampling and sample preparation**

The samples used in the lithogeochemical study of the Goldstream deposit were collected from drill core stored at the mine site as well as from the open mine-pit. The samples represent all five visual varieties of rock units that were sampled at various stratigraphic

levels. The intention was to characterize three cross sections through the deposit in its western, central and eastern part as well as a long section connecting the Goldstream deposit and the neighbouring C zone. This goal was achieved only in part due to problems with core availability and distribution of the drilling sites. Any excessively thick marble layers were avoided. When collecting the few samples from the open pit, care was taken to discard any weathered material. Any remaining weathering crusts were subsequently removed using a diamond saw. Recognizing the fine-grained nature of the rocks and the lack of visible accessory minerals, it was assumed that a sample size of 1 kg would adequately characterize their chemical composition.

The samples were prepared for analysis at the Chemex Laboratory facility in Vancouver, BC by laboratory staff. The standard preparation procedure was followed, which involved crushing the entire sample to better than 70% of the sample passing through a 2 mm sieve (Chemex crushing method code: CRU-31). A 200 to 250 g split was then taken, using a stainless steel riffle splitter. The split was pulverized in a tungsten carbide bowl to better than 85% of the sample passing 75 microns (Chemex crushing method code: PUL-33).

#### **Analytical procedure**

The major elements were analyzed in fused lithium tetraborate discs. A prepared sample (1.000 g) is added to lithium tetraborate flux (9.000 g), mixed well and fused in a furnace at 1100°C. A flat glass disc is prepared from the resulting melt. Trace elements (Ba, Rb, Sr, Zr, Y and Nb) are analyzed in pressed powder pellets in order to avoid dilution by flux. The discs or pellets are then analyzed by X-Ray fluorescence spectrometry (Chemex code: ME-XRF06). Oxide concentration is calculated from the determined elemental concentration and the result is reported in that format.

To determine loss on ignition (L.O.I.), a porcelain crucible is dried in an oven at 105°C, cooled and the weight is recorded. A prepared sample (3.00 g) is added to the crucible and then ashed at 1000°C for 1 hour. The sample is then cooled in a desiccator, weighed and the loss on ignition is calculated as a percent of the initial sample weight. The recording limits for the major elements are 0.01% (lower) and 100% (upper). Analytical data reported as "below detection" are assigned values of ½ of the detection limit. The samples were also analyzed for total carbon by Leco furnace (Chemex code: C-IR07) ferrous iron by HCl – HF acid digestion and titrimetric finish (Chemex code: Fe-VOL05) and total sulphur by Leco furnace and infrared spectroscopy (Chemex code: S-IR08).

Table A1.1. Sample location and field identification

Sample#	Lithology	Drill hole/ location	Depth (m)	Source	Northing (m)	Easting (m)	Elevation (m)
HS951001	M	G-94-9	634.95	This study	3416	16120	1579
HS951002	GGP	G-94-9	629.93	This study	3417	16121	1583
HS951003	GGP	G-94-9	623.65	This study	3418	16123	1588
HS951004	GZ	G-94-9	613.1	This study	3421	16125	1598
HS951005	DGBP	G-94-9	593.25	This study	3426	16130	1615
HS951006	M	G-94-8	502.55	This study	3263	16088	1557
HS951007	GGP	G-94-8	497.15	This study	3264	16088	1563
HS951008	GGP	G-94-8	485.5	This study	3265	16088	1574
HS951009	GZ	G-94-8	480.95	This study	3265	16088	1579
HS951010	DGBP	G-94-8	465.8	This study	3267	16088	1593
HS951011	M	G-94-2	390.1	This study	3106	15924	1639
HS951012	GGP	G-94-2	375.9	This study	3107	15924	1653
HS951013	GGP	G-94-2	372.1	This study	3107	15924	1657
HS951014	GZ	G-94-2	357.55	This study	3108	15924	1671
HS951015	DGBP	G-94-2	343.9	This study	3110	15924	1685
HS951016	M	G-93-3	309.3	This study	2929	15785	1845
HS951017	GGP	G-93-3	303.8	This study	2931	15785	1850
HS951018	GGP	G-93-3	286.95	This study	2936	15785	1866
HS951019	GZ	G-93-3	273.95	This study	2940	15785	1878
HS951020	DGBP	G-93-3	278	This study	2939	15785	1874
HS951021	M	GR-93-4	85.05	This study	1470	17036	3077
HS951022	GGP	GR-93-4	96.785	This study	1462	17041	3071
HS951024	GZ	GR-93-4	102.45	This study	1458	17043	3068
HS951025	DGBP	GR-93-4	116.3	This study	1448	17049	3060
HS951028	GGP	NG-60	130.5	This study	1641	9194	2079
HS951030	DGBP	NG-60	31.5	This study	1698	9194	2159
HS951033	GGP	NG-54	53.5	This study	2469	12197	2106
HS951035	DGBP	NG-54	35.05	This study	2480	12197	2121
HS951038	GGP	NG-52	88.4	This study	2200	11800	2328
HS951040	DGBP	NG-52	36.4	This study	2229	11800	2371
HS951043	GGP	GR-93-6	97.4	This study	2352	9571	1870
HS951045	DGBP	GR-93-6	182	This study	2309	9582	1797
HS951046	M	GR-93-5	120.7	This study	2659	13715	2032
HS951048	GGP	GR-93-5	133.3	This study	2652	13715	2022
HS951049	GZ	GR-93-5	115.25	This study	2663	13715	2037
HS951050	DGBP	GR-93-5	111.3	This study	2665	13715	2040
HS951052	GGP	GR-93-1	113.8	This study	1069	16121	3935
HS951054	GZ	GR-93-1	112.65	This study	1070	16121	3936
HS951055	DGBP	GR-93-1	186.4	This study	1024	16146	3886
HS951056	M	U-92-2	60.55	This study	2429	15	2033
HS951057	GGP	U-92-2	58.2	This study	2426	15407	1983
HS951058	GGP	U-92-2	51	This study	2429	15406	1989
HS951059	GZ	U-92-2	46.6	This study	2431	15405	1992
HS951060	DGBP	U-92-2	31.5	This study	2438	15404	2005
HS951062	GGP	GR-94-4	39.95	This study	-178	5287	3457
HS951063	GGP	GR-94-4	26	This study	-170	5285	3469
HS951066	M	GR-94-3	124.5	This study	-511	4336	3098
HS951067	GGP	GR-94-3	119.65	This study	-509	4335	3101
HS951070	DGBP	GR-94-3	119	This study	-508	4335	3102

Sample#	Lithology	Drill hole/ location	Depth (m)	Source	Northing (m)	Easting (m)	Elevation (m)
HS951072	GGP	NG-6	48.95	This study	2074	14800	2593
HS951075	DGBP	NG-6	20.2	This study	2091	14800	2617
HS951080	DGBP	NG-56	42.95	This study	2504	16198	2515
HS951082	GGP	NG-46	497.5	This study			
HS951086	M	NG-56	63.8	This study	2492	16198	2498
HS951087	GGP	NG-56	59.3	This study	2495	16198	2502
HS951089	GZ	NG-56	52.6	This study	2499	16198	2507
HS951090	DGBP	NG-56	44.4	This study	2504	16198	2514
HS951091	M	BG-4	56.9	This study	2069	15030	2574
HS951092	GGP	BG-4	56.25	This study	2070	15030	2575
HS951093	GGP	BG-4	48.4	This study	2074	15030	2582
HS951094	GZ	BG-4	45.7	This study	2076	15030	2583
HS951095	DGBP	BG-4	28.7	This study	2085	15030	2597
HS951096	M	BG-2	67.25	This study	2055	15030	2574
HS951098	GGP	BG-2	49.4	This study	2067	15030	2586
HS951099	GZ	BG-2	41.6	This study	2072	15030	2591
HS951100	DGBP	BG-2	32.2	This study	2079	15030	2598
HS951101	M	GS-91-c35	35.6	This study	-3	5601	3473
HS951102	GGP	GS-91-c35	31	This study	-2	5599	3477
HS951103	GGP	GS-91-c35	22.05	This study	2	5595	3484
HS951105	DGBP	GS-91-c35	18.85	This study	3	5593	3486
HS951106	M	GS-91-b27	49.35	This study	1289	7894	1956
HS951107	GGP	GS-91-b27	44.3	This study	1291	7893	1960
HS951110	DGBP	GS-91-b27	33.7	This study	1297	7891	1968
HS951111	M	GS-91-c25	51.75	This study	1096	7471	2092
HS951113	GGP	GS-91-c25	19.95	This study	1109	7459	2118
HS951115	DGBP	GS-91-c25	18.45	This study	1110	7458	2119
HS951116	M	GS-91-c23	89.1	This study	639	6545	2695
HS951120	DGBP	GS-91-c23	75.65	This study	643	6539	2705
HS951121	M	GS-91-A-31	167.35	This study	2474	16267	2011
HS951122	GGP	GS-91-A-31	165.5	This study	2474	16267	2012
HS951123	GGP	GS-91-A-31	155.6	This study	2480	16268	2020
HS951124	GZ	GS-91-A-31	154.15	This study	2481	16268	2022
HS951125	DGBP	GS-91-A-31	146.8	This study	2485	16268	2028
HS951127	GGP	GS-91-34	211.7	This study	2571	16469	2022
HS951128	GGP	GS-91-34	203.5	This study	2575	16469	2029
HS951129	GZ	GS-91-34	198.6	This study	2522	16469	2033
HS951130	DGBP	GS-91-34	195.85	This study	2580	16469	2036
HS951131	M	GR-94-2	86.5	This study	-96	5402	3373
HS951132	GGP	GR-94-2	89.5	This study	-98	5403	3370
HS951133	GGP	GR-94-2	69.1	This study	-87	5399	3387
HS951135	DGBP	GR-94-2	67.75	This study	-86	5399	3388
HS951136	M	GS-91-a29	48.75	This study	2412	15968	2178
HS951137	GGP	GS-91-a29	48.45	This study	2413	15968	2179
HS951139	GZ	GS-91-a29	42.675	This study	2416	15968	2183
HS951140	DGBP	GS-91-a29	36.6	This study	2419	15969	2188
HS951142	GGP	GS-91-c39	27.75	This study	20	4500	3513
HS951143	GGP	GS-91-c39	23.7	This study	21	5498	3516
HS951144	GZ	GS-91-c39	20.95	This study	22	4497	3519
HS951148	GGP	GS-91-c22	51.45	This study	126	6046	3311
HS951150	DGBP	GS-91-c22	43.85	This study	128	6044	3317

Sample#	Lithology	Drill hole/ location	Depth (m)	Source	Northing (m)	Easting (m)	Elevation (m)
HS951151	M	GS-91-c9	59.55	This study	327	6198	3060
HS951152	GGP	GS-91-c9	65.4	This study	325	6200	3056
HS951155	DGBP	GS-91-c9	70.55	This study	323	6203	3051
HS951156	M	GS-91-c14	43.25	This study	109	5823	3424
HS951158	GGP	GS-91-c14	42.685	This study	109	5823	3424
HS951159	GZ	GS-91-c14	36.2	This study	111	5820	3430
HS951160	DGBP	GS-91-c14	29.7	This study	114	5818	3434
HS951161	M	GS-91-d3a	22.75	This study	2407	15769	2213
HS951162	GGP	GS-91-d3a	22.55	This study	2407	15769	2213
HS951164	GZ	GS-91-d3a	15.65	This study	2411	15769	2219
HS951165	DGBP	GS-91-d3a	9.6	This study	2414	15770	2224
HS951166	M	GS-91-d4	278.4	This study	2702	14763	1832
HS951167	GGP	GS-91-d4	276.95	This study	2703	14763	1833
HS951169	GZ	GS-91-d4	272.6	This study	2705	14763	1836
HS951170	DGBP	GS-91-d4	265.8	This study	2709	14763	1842
HS951171	M	D-02-91	275.5	This study	2648	15420	1897
HS951172	GGP	D-02-91	269.4	This study	2651	15420	1903
HS951173	GGP	D-02-91	264.1	This study	2654	15420	1908
HS951174	GZ	D-02-91	249.25	This study	2662	15421	1921
HS951175	DGBP	D-02-91	239.9	This study	2666	15421	1929
HS951176	M	D-01-91	265.35	This study	2926	15876	1798
HS951177	GGP	D-01-91	263.1	This study	2839	15870	1799
HS951178	GGP	D-01-91	255.6	This study	2843	15870	1806
HS951179	GZ	D-01-91	251.3	This study	2845	15871	1810
HS951181	M	OP	0	This study	2000	15130	2950
HS951182	GGP	OP	0	This study	2000	15140	2950
HS951183	GGP	OP	0	This study	2000	15150	2950
HS951184	GZ	OP	0	This study	2000	15160	2950
HS951185	DGBP	OP	0	This study	2000	15170	2950
HS951901	DGBP	G-94-8	427.3	This study	3269	16089	1631
HS951902	M	G-94-2	371.3	This study	3107	15924	1658
HS951903	DGBP	G-94-2	302.7	This study	3113	15925	1725
HS951904	M	G-93-3	309.3	This study	2929	15785	1845
HS951905	DGBP	NG-60	69.5	This study	1676	9194	2128
HS951906	DGBP	NG-54	58.2	This study	2467	12197	2102
HS951907	GGP	NG-52	?	This study	2221	11800	2358
HS951908	DGBP	GR-93-5	70.55	This study	2688	13717	2072
HS951909	DGBP	GR-93-1	186.4	This study	1024	16146	3886
HS951910	M	GR-93-1	?	This study	1039	16138	3902
HS951911	CMZ	GR-93-1	44.7	This study	1112	16098	3983
HS951912	M	U-92-2	54.5	This study	2428	15406	1986
HS951913	DGBP	U-92-2	5.54	This study	2451	15401	2028
HS951914	DGBP	GR-94-4	18.75	This study	-166	5284	3474
HS951915	M	NG-6	47	This study	2075	14800	2595
HS951916	DGBP	NG56	20.75	This study	2517	16198	2533
HS951917	DGBP	BG-4	15.6	This study	2093	15030	2608
HS951918	DGBP	BG-2	21	This study	2087	15030	2606
HS951920	M	GS-91-b27	31.35	This study	1298	7890	1971
HS951921	M	GS-91-c25	17.35	This study	1110	7457	2120
HS951922	DGBP	GS-91-c23	133.975	This study	624	6565	2657
HS951924	DGBP	GS-91-34	147	This study	2607	16468	2077

Sample#	Lithology	Drill hole/ location	Depth (m)	Source	Northing (m)	Easting (m)	Elevation (m)
HS951925	DGBP	GR-94-2	91.7	This study	-99	5404	3368
HS951926	M	GR-94-2	93.55	This study	-100	5404	3367
HS951927	DGBP	GR-94-2	47.05	This study	-75	5396	3405
HS951928	DGBP	GS-91-a29	14.35	This study	2432	15969	2207
HS951929	DGBP	GS-91-c39	30	This study	17	4503	3508
HS951930	M	GS-91-c22	28.7	This study	134	6037	3329
HS951931	DGBP	GS-91-c22	11	This study	141	6030	3344
HS951932	M	GS-91-c9	36.55	This study	336	6189	3079
HS951933	DGBP	GS-91-d4	243.7	This study	2720	14763	1861
HS951934	GGP	D-02-91	271.6	This study	2650	15420	1901
HS951935	GGP	D-02-91	255.4	This study	2658	15420	1916
HS951936	DGBP	D-02-91	202.8	This study	2685	15422	1961
HS951937	DGBP	D-02-91	165.15	This study	2705	15423	1994
HS951938	M	D-01-91	251.5	This study	2844	15870	1809
HS951939	DGBP	D-01-91	187.3	This study	2874	15872	1867
HS951941	P	HW-1	0	This study			
HS951942	P	HW-1	0	This study			
HS951943	R	HW-1	0	This study			
HS951944	R	HW-1	0	This study			
HS951945	R	HW-1	0	This study			
HS951946	R	HW-1	0	This study			
HS951948	R	HW-1	0	This study			
HS951949	R	HW-1	0	This study			
HS951950	R	HW-1	0	This study			
HS951951	R	HW-1	0	This study			
HS951952	DGBP-A	HW-23	0	This study	1280	2275	2230
HS951953	DGBP-A	HW-23	0	This study	1300	2275	2230
HS951954	M	HW-23	0	This study	1320	2275	2230
HS951955	DGBP-A	HW-23	0	This study	1340	2275	2230
17302	GZ	N/A	0	T. Hoy			
17303	GZ	N/A	0	T. Hoy			
17304	DGBP	N/A	0	T. Hoy			
17305	DGBP	N/A	0	T. Hoy			
17310	VOLC	N/A	0	T. Hoy			
26591	GZ	N/A	0	T. Hoy			
26593	GZ	N/A	0	T. Hoy			
26594		N/A	0	T. Hoy			
26595	GGP	N/A	0	T. Hoy			
26596		N/A	0	T. Hoy			
26597	GZ	N/A	0	T. Hoy			
26598	GGP	N/A	0	T. Hoy			
26599	GZ	N/A	0	T. Hoy			
26600	?	N/A	0	T. Hoy			
26601	GGP	N/A	0	T. Hoy			
26602	QTZT	N/A	0	T. Hoy			
26604	M	N/A	0	T. Hoy			
26605	M	N/A	0	T. Hoy			
26606	GZ	N/A	0	T. Hoy			
26607	GZ	N/A	0	T. Hoy			
26608	GZ	N/A	0	T. Hoy			
26609	GZ	N/A	0	T. Hoy			



Sample#	Lithology	Drill hole/ location	Depth (m)	Source	Northing (m)	Easting (m)	Elevation (m)
26610	GGP	N/A	0	T. Hoy			
26611	QTZT	N/A	0	T. Hoy			
26612	GGP	N/A	0	T. Hoy			
26613	M	N/A	0	T. Hoy			
26615	GZ	N/A	0	T. Hoy			
26616	GZ	N/A	0	T. Hoy			
48519	VOLC	N/A	0	J. Logan	1535	16215	3450
49142	GZ	N/A	0	J. Logan	1155	16090	4000
49146	VOLC	N/A	0	J. Logan	1334	16050	3700
49155	VOLC	N/A	0	J. Logan	3748	14150	3000
49460	GZ	N/A	0	J. Logan	2095	15235	2870
49461	GZ	N/A	0	J. Logan	2095	15240	2870
49462	GZ	N/A	0	J. Logan	2095	15245	2870
49479	DGBP	N/A	0	J. Logan	2005	15245	2870
49480	GGP	N/A	0	J. Logan	2075	15230	2880
49481	GGP	N/A	0	J. Logan	2095	15230	2870
49848	M	N/A	0	J. Logan	3100	16020	810
49860	GGP	N/A	0	J. Logan	3100	16000	810
49863	M	N/A	0	J. Logan	3100	16010	810
49865	GGP	N/A	0	J. Logan	3100	15980	810
49866	GGP	N/A	0	J. Logan	3100	15990	810
49875	M	N/A	0	J. Logan	1965	14980	3070
49876	GGP	N/A	0	J. Logan	2025	15210	2945
49877	DGBP	N/A	0	J. Logan	2000	14972	2980
49878	GGP	N/A	0	J. Logan	1670	18540	3000
49879	GZ	N/A	0	J. Logan	1155	16090	4000
49880	GGP	N/A	0	J. Logan	1170	15960	4000
49885	M	N/A	0	J. Logan	1030	15020	4300
49905	VOLC	N/A	0	J. Logan	2607	13711	1961
49909	GZ	GR93-5	107.5	J. Logan	2660	13715	2045
49919	DGBP	N/A	0	J. Logan	2790	16530	751
49929	DGBP	N/A	0	J. Logan	2553	15972	2193
103051	DGBP	700 HAUL		T. Hoy	2210	15220	2134
103052	M	700 HAUL		T. Hoy	2210	15230	2134
103053	M	700 HAUL		T. Hoy	2210	15240	2134
103054	M	700 HAUL		T. Hoy	2210	15250	2134
103055	M	700 HAUL		T. Hoy	2210	15260	2134
103056	GGP	700 HAUL		T. Hoy	2210	15270	2134
103057	M	NG-56	63.11	T. Hoy	2493	16198	2499
103058	M	NG-56	73.20	T. Hoy	2487	16198	2490
103059	DGBP	NG-56	80.20	T. Hoy	2483	16198	2484
103060	DGBP	NG-56	93.80	T. Hoy	2476	16198	2474
103061	M	NG-56	104.80	T. Hoy	2469	16198	2465
103062	QTZT	NG-56	115.80	T. Hoy	2463	16198	2456
103063	GZ	NG-56	52.30	T. Hoy	2499	16198	2507
103064	DGBP	NG-56	42.20	T. Hoy	2505	16198	2516
103065	DGBP	NG-56	32.20	T. Hoy	2511	16198	2524
103066	DGBP	NG-56	22.20	T. Hoy	2516	16198	2532
103067	DGBP	NG-56	12.20	T. Hoy	2522	16198	2540
103068	GZ	NG-56	49.39	T. Hoy	2501	16198	2511
103069	GZ	NG-56	51.24	T. Hoy	2500	16198	2509

Sample#	Lithology	Drill hole/ location	Depth (m)	Source	Northing (m)	Easting (m)	Elevation (m)
103070	GZ	NG-47	84.00	T. Hoy	2522	15910	2261
103071	DGBP	NG-47	66.00	T. Hoy	2532	15910	2276
103072	GZ	NG-22	168.90	T. Hoy	2509	15400	2023
103073	M	NG-22	193.00	T. Hoy	2495	15400	2003
103074	GZ	NG-40	191.00	T. Hoy	2691	15700	1904
103075	GGP	NG-40	207.00	T. Hoy	2682	15700	1891
103076	M	NG-40	211.00	T. Hoy	2680	15700	1888
103077	DGBP	NG-27	204.66	T. Hoy	2708	15610	1875
103078	GZ	NG-27	216.55	T. Hoy	2701	15610	1865
103079	M	NG-27	237.89	T. Hoy	2689	15610	1848
103080	M	GS91-DO2	269.90	T. Hoy	2650	15424	1904
103081	DGBP	GS91-DO2	268.00	T. Hoy	2651	15424	1905
103082	DGBP	GS91-DO2	267.40	T. Hoy	2652	15424	1906
103083	GZ	GS91-DO2	250.40	T. Hoy	2661	15424	1921
103084	M	700 HAUL		T. Hoy	2210	15280	2134
103085	GGP	700 HAUL		T. Hoy	2210	15290	2134
103086	GZ	700 HAUL		T. Hoy	2210	15300	2134
103087	GZ	700 HAUL		T. Hoy	2210	15310	2134
103090	DGBP	770 XCUT		T. Hoy	2130	15240	2347
103091	DGBP	770 XCUT		T. Hoy	2130	15250	2347
103092	GGP	770 XCUT		T. Hoy	2130	15260	2347
103094	GZ	770 XCUT		T. Hoy	2130	15270	2347
103095	DGBP	770 XCUT		T. Hoy	2130	15280	2347
103096	GGP	830 XCUT		T. Hoy	2045	15100	2530
103097	GGP	830 XCUT		T. Hoy	2045	15110	2530
103098	GZ	830 XCUT		T. Hoy	2045	15120	2530
103099	M	550.6 VA		T. Hoy	2500	15500	1676
103100	DGBP	550.6 VA		T. Hoy	2500	15510	1676
103101	DGBP	550.6 VA		T. Hoy	2500	15520	1676
103102	M	550.6 VA		T. Hoy	2500	15530	1676
103103	M	550.6 VA		T. Hoy	2500	15540	1676
103104	DGBP	550.6 VA		T. Hoy	2500	15550	1676
103120	DGBP	G93-1	302.22	T. Hoy	2979	15821	1844
103121	M	G93-1	309.95	T. Hoy	2977	15821	1836
103122	DGBP	G93-1	297.50	T. Hoy	2979	15821	1848
103123	GGP	G93-1	295.40	T. Hoy	2980	15822	1851
103124	DGBP	G93-1	275.61	T. Hoy	2983	15823	1869
103125	GZ	G93-1	287.91	T. Hoy	2981	15822	1857
103126	GGP	G93-2	308.75	T. Hoy	2985	15890	1753
103127	M	G93-2	312.09	T. Hoy	2985	15890	1749
103128	DGBP	G93-2	307.66	T. Hoy	2984	15890	1741
103129	DGBP	G93-2	282.60	T. Hoy	2984	15890	1728
103130	M	G93-2	294.70	T. Hoy	2984	15890	1727
103131	GZ	G93-2	287.04	T. Hoy	2983	15890	1724
103132	DGBP	G93-3	271.15	T. Hoy	2941	15785	1881
103133	GZ	G93-3	277.67	T. Hoy	2939	15785	1874
103134	GGP	G93-3	291.29	T. Hoy	2935	15785	1862
103135	M	G93-3	299.90	T. Hoy	2932	15785	1854
103136	DGBP	G93-3	303.90	T. Hoy	2931	15785	1850
103137	M	G93-3	307.90	T. Hoy	2930	15785	1846

Table A1.2. Major element concentrations

Sample#	Al <sub>2</sub> O <sub>3</sub> (%)	CaO (%)	Cr <sub>2</sub> O <sub>3</sub> (%)	Fe(tot) (%)	K <sub>2</sub> O (%)	MgO (%)	MnO (%)	Na <sub>2</sub> O (%)	P <sub>2</sub> O <sub>5</sub> (%)	SiO <sub>2</sub> (%)	TiO <sub>2</sub> (%)
HS951001	10.03	26.65	0.04	4.31	2.02	1.87	0.06	1.02	0.11	34.72	0.59
HS951002	17.81	2.5	0.04	7.61	3.95	2.44	0.08	1.4	0.19	58.54	1.09
HS951003	19.53	1.23	0.04	8.11	4.83	2.7	0.08	1.16	0.11	57.7	0.97
HS951004	9.4	4.37	0.08	6.86	2.05	1.55	0.92	0.5	0.12	69.56	0.3
HS951005	13.97	14.39	0.09	5.87	2.7	4.15	0.07	0.86	0.17	46.65	0.69
HS951006	8.3	32.22	0.12	3.34	1.8	1.51	0.04	0.64	0.1	26.68	0.33
HS951007	12.15	14.23	0.17	5.27	2.31	2.08	0.07	1.43	0.12	50.75	0.77
HS951008	21	7.36	0.07	8.93	3.93	2.96	0.18	0.66	0.1	49.54	0.94
HS951009	5.94	5.57	0.02	24.29	0.12	2.43	5.21	0.005	0.58	52.61	0.24
HS951010	15.46	8.72	0.03	6.5	2.8	3.98	0.08	1.46	0.15	54.51	0.86
HS951011	6.2	36.7	0.03	2.43	1.97	1.14	0.04	0.43	0.1	21.87	0.27
HS951012	14.44	13.93	0.02	10.21	2.37	2.53	0.14	0.94	0.08	46.25	0.63
HS951013	12.84	18.57	0.02	4.66	3.43	2.11	0.1	0.55	0.07	41.69	0.53
HS951014	11.08	3.66	0.04	11.7	2.22	1.55	0.46	0.77	0.36	63.07	0.67
HS951015	6.48	34.29	0.04	2.84	1.31	3.44	0.05	0.6	0.13	22.84	0.36
HS951016	13.84	17.11	0.05	6.25	3.35	2.95	0.17	1.05	0.13	43.33	0.79
HS951017	15.91	1.8	0.05	7.6	3.09	2.24	0.09	1.61	0.23	63.39	1.08
HS951018	20.46	2.64	0.02	6.06	5.24	2.46	0.05	0.97	0.07	57.3	1.01
HS951019	9.72	3.23	0.01	5.48	2.28	1.49	0.48	0.86	0.11	72.09	0.35
HS951020	15.24	11.7	0.02	5.99	2.88	4.09	0.07	0.89	0.1	50.77	0.66
HS951021	10.44	22.17	0.03	4.5	2.46	1.77	0.11	1.18	0.13	43.95	0.69
HS951022	19.39	4.06	0.02	7.84	4.31	3.27	0.1	1.67	0.15	53.66	0.96
HS951024	9.95	2.66	0.02	4.72	1.93	1.43	0.23	1.14	0.12	73.8	0.33
HS951025	13	11.04	0.04	6.4	2.79	4.34	0.16	0.65	0.22	56	0.81
HS951028	14.85	1.64	0.03	6.72	3.17	2.23	0.06	1.5	0.18	64.88	1.11
HS951030	9.12	10.29	0.04	4.62	1.9	2.45	0.09	0.84	0.25	60.23	0.56
HS951033	18.73	1.56	0.04	8.03	4.14	2.58	0.09	1.38	0.18	58.22	1.11
HS951035	8.73	2.03	0.02	3.22	1.29	1.03	0.02	0.65	0.73	74.23	0.32
HS951038	17.58	0.67	0.02	6.95	3.96	2.71	0.08	1.06	0.13	62.57	0.72
HS951040	19.52	6.05	0.03	7.51	2.14	2.15	0.07	1.63	0.29	54.62	0.83
HS951043	18.49	1.19	0.02	9.74	4.13	2.76	0.15	1.12	0.12	56.98	1.29
HS951045	2.41	0.51	0.01	2.04	0.58	0.54	0.04	0.005	0.09	91.04	0.32
HS951046	8.63	17.54	0.04	3.02	1.8	1.99	0.03	0.87	0.09	51.63	0.45
HS951048	16.46	0.96	0.02	8.26	4.29	2.45	0.09	1.33	0.16	61.12	1.47
HS951049	8.29	7.33	0.03	11.01	2.23	1.98	0.87	0.27	0.27	59.38	0.43
HS951050	9.76	23.93	0.03	4.34	1.99	3.99	0.08	0.68	0.12	36.32	0.48
HS951052	11.43	21.34	0.04	4.77	2.53	3.32	0.09	0.77	0.11	39.54	0.52
HS951054	9.72	2.95	0.05	12.85	1.68	2.55	1.31	0.1	0.9	61.87	0.39
HS951055	13.84	14.82	0.02	5.98	2.77	4.16	0.1	0.94	0.17	46.9	0.67
HS951056	13.11	17.89	0.03	5.49	2.92	2.19	0.08	1.04	0.09	43.63	0.61
HS951057	18.29	1.03	0.03	7.99	4.13	2.49	0.07	1.37	0.19	59.43	1.13
HS951058	19.47	1.81	0.04	9	4.54	2.88	0.07	1.13	0.08	56.22	1
HS951059	7.26	7.95	0.07	20.9	0.55	1.55	0.84	0.11	0.57	52.97	0.41
HS951060	11.16	21.63	0.02	4.69	2.02	3.97	0.08	0.72	0.11	37.97	0.53
HS951062	21.82	0.75	0.06	8.75	4.38	2.16	0.07	0.86	0.23	55.17	1.33
HS951063	16.52	2.95	0.03	8.46	2.95	2.83	0.12	1.56	0.14	56.55	1.01
HS951066	8.25	26.05	0.01	3.76	1.82	1.57	0.1	0.49	0.1	36.07	0.48
HS951067	14.15	0.82	0.03	6.22	2.52	2.14	0.05	1.83	0.14	67.04	1.17
HS951070	12.56	2.32	0.03	5.46	2.86	1.42	0.08	0.7	0.36	66.2	0.54

Sample#	Al <sub>2</sub> O <sub>3</sub> (%)	CaO (%)	Cr <sub>2</sub> O <sub>3</sub> (%)	Fe(tot) (%)	K <sub>2</sub> O (%)	MgO (%)	MnO (%)	Na <sub>2</sub> O (%)	P <sub>2</sub> O <sub>5</sub> (%)	SiO <sub>2</sub> (%)	TiO <sub>2</sub> (%)
HS951072	13.98	1.93	0.02	6.26	2.35	2.12	0.07	2.39	0.17	66.33	1.08
HS951075	8.33	26.84	0.02	4.22	1.45	3.82	0.08	0.56	0.2	33.42	0.53
HS951080	13.96	2.58	0.03	5.69	3.22	1.68	0.07	1.51	0.13	65.63	0.72
HS951082	15.31	2.89	0.04	6.34	3.51	2.09	0.08	0.97	0.09	65.43	0.77
HS951086	3.14	46.29	0.01	1.23	0.78	1.08	0.02	0.18	0.08	11.27	0.14
HS951087	11.99	1.95	0.03	4.8	2.35	1.59	0.06	2.27	0.22	72.04	0.8
HS951089	4.23	10.41	0.03	23.16	0.18	1.56	1.07	0.005	0.91	47.45	0.22
HS951090	15.15	9.86	0.03	6.58	2.88	4.13	0.08	1.14	0.14	52.67	0.74
HS951091	11.69	24.1	0.03	4.53	2.84	1.85	0.08	0.86	0.09	34.85	0.54
HS951092	16.11	5.38	0.03	6.99	3.38	2.23	0.06	0.98	0.14	59.05	1
HS951093	20.13	1.07	0.02	8.46	5.43	2.32	0.1	0.63	0.07	56.51	1
HS951094	4.7	7.07	0.03	34.36	0.19	2.17	3.98	0.005	0.81	40.9	0.19
HS951095	12.01	9.35	0.03	7.28	2.2	2.58	0.37	1.08	0.24	55.96	0.49
HS951096	9.08	28.93	0.01	3.55	2.25	1.3	0.04	0.62	0.09	31.79	0.38
HS951098	18.12	1.33	0.03	7.88	4.1	2.2	0.07	1.16	0.08	61.05	0.87
HS951099	5.11	13.45	0.04	23.01	0.18	2.2	3.58	0.005	0.92	43.06	0.21
HS951100	7.76	7.62	0.03	15.51	1.59	2.06	1.89	0.54	0.43	55.82	0.29
HS951101	8.41	21.07	0.1	8.88	1.72	3.59	0.44	0.42	0.3	34.14	1.36
HS951102	19.26	5.19	0.08	8.31	3.1	1	0.4	2.39	0.11	49.57	1.5
HS951103	16.29	2.54	0.03	6.19	2.99	1.94	0.14	0.9	0.14	62.13	1.03
HS951105	9.45	2.24	0.04	7.43	1.75	0.79	0.26	0.38	0.66	69.81	0.64
HS951106	1.22	8.55	0.01	0.47	0.32	0.17	0.01	0.005	0.05	81.96	0.07
HS951107	15.44	2.12	0.03	7.06	2.87	2.41	0.07	1.48	0.18	62.34	1.1
HS951110	14.4	3.52	0.03	7.46	3.4	2.04	0.07	0.75	0.29	61.72	0.96
HS951111	3.69	10.88	0.01	1.45	1.03	0.53	0.02	0.07	0.12	73.26	0.21
HS951113	18.93	1.23	0.02	8.11	4.01	2.55	0.07	1.05	0.1	58.36	1.01
HS951115	7.58	16.11	0.02	3.78	1.9	1.68	0.06	0.25	0.11	53.8	0.55
HS951116	7.73	22.33	0.13	8.24	0.48	8.05	0.17	0.005	0.46	30.98	1.64
HS951120	10.22	4.63	0.02	5.83	2.39	2.15	0.24	0.37	0.56	64.99	0.48
HS951121	11.01	23.75	0.03	4.7	2.65	1.71	0.07	0.95	0.1	37.69	0.51
HS951122	13.31	2.75	0.04	7.1	2.47	1.74	0.1	2.24	0.26	65.76	1.29
HS951123	17.04	2.75	0.07	7.91	4.33	2.37	0.13	1.44	0.15	58.75	1.16
HS951124	4.96	5.14	0.03	24.27	0.18	2.18	2.37	0.01	0.68	55.92	0.21
HS951125	15.67	10.81	0.02	6.56	3.21	4.2	0.11	1.16	0.19	50.57	0.78
HS951127	18.47	1.02	0.06	9.86	3.42	2.62	0.11	1.57	0.16	57.2	1.44
HS951128	13.12	3.24	0.03	7.23	3.82	2.17	0.24	0.33	0.26	64.65	1.14
HS951129	14.6	13.55	0.02	6.07	3.03	5.02	0.09	1.16	0.14	45.66	0.72
HS951130	8.51	3.19	0.03	9.98	1.96	1.95	0.72	0.49	0.31	68.18	0.35
HS951131	12.88	11.83	0.06	13.21	0.35	9	0.12	0.36	0.52	35.95	2.33
HS951132	9.89	13.59	0.06	9.72	0.99	7.52	0.13	0.17	0.42	38.97	1.75
HS951133	10.63	13	0.04	9.59	2.53	5.69	0.15	0.44	0.39	38.17	1.91
HS951135	3.79	27.83	0.03	2.68	1.24	1.31	0.08	0.06	0.16	39.38	0.46
HS951136	9.55	28.66	0.02	3.62	2.48	1.41	0.04	0.69	0.09	31.76	0.41
HS951137	15.77	1.82	0.04	6.9	3.78	1.57	0.08	1.81	0.26	63.17	1.39
HS951139	4.9	5.23	0.02	32.98	0.14	2.88	4.42	0.02	0.78	43.57	0.19
HS951140	13.69	15.16	0.02	5.91	3.28	4.15	0.11	1.28	0.12	43.83	0.65
HS951142	12.98	4.71	0.02	6.75	3.11	1.46	0.26	0.95	0.19	63.45	0.95
HS951143	18.97	8.05	0.07	7.58	3.5	3.72	0.25	2.84	0.09	41.15	0.96
HS951144	9.87	5.74	0.03	12.96	2.35	1.98	1.01	0.23	0.56	55.44	0.55
HS951148	14.16	1.95	0.06	7.04	3.09	2.12	0.07	1.59	0.16	64.46	1.11
HS951150	16.12	1.66	0.06	7.66	3.7	2.34	0.08	1.04	0.32	61.22	1.16

Sample#	Al <sub>2</sub> O <sub>3</sub> (%)	CaO (%)	Cr <sub>2</sub> O <sub>3</sub> (%)	Fe(tot) (%)	K <sub>2</sub> O (%)	MgO (%)	MnO (%)	Na <sub>2</sub> O (%)	P <sub>2</sub> O <sub>5</sub> (%)	SiO <sub>2</sub> (%)	TiO <sub>2</sub> (%)
HS951151	7.32	26.72	0.2	9.19	0.27	8	0.18	0.005	0.52	24.31	1.57
HS951152	16.44	1.13	0.07	8.58	3.2	2.45	0.09	1.89	0.15	59.74	1.44
HS951155	5.51	11.92	0.01	2.1	1.71	0.86	0.04	0.09	0.28	66.94	0.31
HS951156	9.12	21.93	0.07	8.01	1.52	5.43	0.14	0.3	0.37	31.71	1.41
HS951158	15.61	3.05	0.06	16.77	1.74	1.16	0.63	0.62	0.31	52.47	1.2
HS951159	5.37	7.31	0.03	32.38	0.27	1.17	1.09	0.16	2.09	38.01	0.2
HS951160	10.78	10.65	0.02	6.45	2.51	2.49	0.21	0.42	0.32	53.96	0.94
HS951161	8.28	30.73	0.02	3.29	2.32	1.2	0.06	0.41	0.08	29.91	0.35
HS951162	15.33	1.79	0.01	6.66	3.62	1.73	0.06	1.75	0.18	64.43	1.25
HS951164	6.26	6.74	0.02	23.05	0.58	2.32	4.02	0.06	0.65	52.48	0.21
HS951165	13.74	12.64	0.02	5.76	2.3	3.58	0.1	1.09	0.12	50.17	0.61
HS951166	5.32	38.98	0.01	2.87	1.16	1.82	0.04	0.5	0.08	19.58	0.33
HS951167	12.7	5.95	0.03	6.89	2.73	3.2	0.14	1.26	0.23	60.03	1.13
HS951169	11.8	2.98	0.02	5.39	2.86	1.57	0.45	1.16	0.12	70.28	0.37
HS951170	11.38	5.97	0.02	5.66	2.41	2.32	0.24	0.88	0.24	64.22	0.46
HS951171	7.32	33.98	0.06	2.86	1.4	1.99	0.04	0.59	0.1	26.29	0.29
HS951172	16.45	2.4	0.04	7.64	3.53	2.68	0.09	1.57	0.18	60.14	1.2
HS951173	20.59	0.45	0.03	8.54	4.76	2.77	0.06	0.85	0.08	56.67	0.99
HS951174	9.04	2.76	0.03	8.19	1.87	1.5	0.5	0.57	0.18	71.33	0.36
HS951175	14.78	4.73	0.02	6.89	3.43	3.56	0.1	0.94	0.24	60.14	0.64
HS951176	8.3	27.81	0.03	3.76	1.72	2.06	0.05	0.86	0.12	33.89	0.56
HS951177	14.77	1.76	0.04	5.52	3.89	1.78	0.08	1.39	0.18	64.91	1.16
HS951178	18.25	3.98	0.07	9.39	4.15	3.71	0.16	0.75	0.15	54.29	1.35
HS951179	4.93	5.98	0.06	29.4	0.17	2.02	3.23	0.04	0.61	47.27	0.21
HS951181	14.24	11.8	0.02	6.23	2.88	4.6	0.09	1.06	0.15	49.05	0.69
HS951182	16.23	1.67	0.02	6.73	3.99	2.07	0.07	0.89	0.18	63.76	1.01
HS951183	18.88	1.28	0.02	7.65	4.84	2.28	0.08	1.06	0.08	58.83	0.95
HS951184	4.89	7.74	0.02	27.35	0.07	2.19	4.09	0.01	0.77	48.72	0.23
HS951185	15.61	3.88	0.02	6.02	2.84	4.27	0.04	2.41	0.23	61.08	0.66
HS951901	7.31	14.3	0.02	5.32	1.54	2.42	0.08	0.84	0.36	54.91	0.86
HS951902	8.3	29.28	0.01	3.22	2.62	1.61	0.11	0.33	0.08	30.64	0.35
HS951903	8.71	15.47	0.03	6.21	1.82	3.54	0.11	1.25	0.38	50.07	1.33
HS951904	9.26	12.92	0.02	5.84	2	3.08	0.12	0.62	0.3	53.73	0.76
HS951905	2.1	48.31	0.005	0.97	0.64	0.56	0.1	0.04	0.07	8.26	0.1
HS951906	9.8	17.69	0.02	4.86	2.46	1.58	0.09	0.79	0.07	47.67	0.5
HS951907	15.99	7.61	0.02	6.83	3.75	2.29	0.08	1.52	0.13	53.95	0.9
HS951908	5.76	9.42	0.02	4.82	1.27	1.47	0.05	0.87	0.34	67.51	0.49
HS951909	6.73	10.87	0.01	4.83	1.61	2.9	0.06	1.07	0.36	64.28	0.7
HS951910	0.03	53.9	0.005	0.21	0.01	0.22	0.05	0.1	0.005	0.19	0.005
HS951911	20.83	0.92	0.02	9.22	4.42	2.52	0.1	1.46	0.11	55.11	1.26
HS951912	8.48	32.86	0.01	3.14	2.73	1.22	0.1	0.61	0.1	25.79	0.37
HS951913	13.86	17.7	0.02	5.57	2.83	4.07	0.11	1.06	0.12	42.14	0.65
HS951914	11.13	20.03	0.04	9.35	2.73	1.91	0.18	0.35	0.49	31.66	1.88
HS951915	0.47	50.98	0.005	0.78	0.12	0.47	0.09	0.14	0.005	4.61	0.02
HS951916	13.47	11.22	0.03	6.57	2.96	4.23	0.15	0.91	0.22	52	0.87
HS951917	16.53	7.18	0.02	6.83	3.23	4.19	0.07	1.51	0.17	55.14	0.86
HS951918	12.9	10.19	0.02	5.74	2.79	3.93	0.11	0.86	0.18	55.09	0.63
HS951920	13.71	9.85	0.07	9.05	0.1	7.25	0.16	2.66	0.12	44.53	1.2
HS951921	6.61	25.27	0.09	6.1	0.85	5.86	0.1	0.005	0.31	31.64	1.16
HS951922	13.71	15.5	0.06	5.78	2.76	4.25	0.07	1.18	0.13	45.07	0.64
HS951924	14.35	14.08	0.04	5.69	3.45	3.79	0.12	0.83	0.13	46.03	0.74

Sample#	Al <sub>2</sub> O <sub>3</sub> (%)	CaO (%)	Cr <sub>2</sub> O <sub>3</sub> (%)	Fe(tot) (%)	K <sub>2</sub> O (%)	MgO (%)	MnO (%)	Na <sub>2</sub> O (%)	P <sub>2</sub> O <sub>5</sub> (%)	SiO <sub>2</sub> (%)	TiO <sub>2</sub> (%)
HS951925	8.31	4.95	0.02	3.32	1.82	1.15	0.02	0.25	0.05	72.45	0.34
HS951926	0.1	52.88	0.005	0.59	0.04	0.42	0.03	0.07	0.005	1.31	0.01
HS951927	19.27	3.68	0.03	6.37	5.57	2.33	0.05	0.52	0.25	53.55	0.8
HS951928	12.78	11.36	0.02	5.5	2.76	3.59	0.13	0.95	0.22	53.66	0.75
HS951929	13.51	5.78	0.02	6.58	3.21	1.7	0.12	0.47	0.16	58.57	0.74
HS951930	8.99	19.3	0.06	7.78	0.83	5.85	0.12	0.61	0.3	36.66	1.24
HS951931	13.28	2.59	0.03	6.09	2.5	1.8	0.17	0.73	0.21	64.89	0.78
HS951932	9.67	20.77	0.07	8.45	0.21	6.2	0.18	1.8	0.4	31.49	1.39
HS951933	11.32	6.44	0.02	7.02	2.21	3.06	0.06	1.1	0.43	60.86	1.29
HS951934	12.54	20.25	0.02	5.5	2.86	2.13	0.08	1.2	0.12	39.59	0.74
HS951935	19.4	1.43	0.03	8.64	4.54	2.89	0.14	1.69	0.11	56.2	1.04
HS951936	7.46	9.5	0.01	5.19	1.77	2.31	0.12	0.77	0.38	63.75	0.58
HS951937	8.29	7.92	0.02	5.77	2.12	1.19	0.06	1.07	0.39	66.27	0.85
HS951938	2.55	45.18	0.02	1.82	0.82	1.14	0.2	0.01	0.08	10.76	0.14
HS951939	6.7	16.24	0.03	5.22	1.54	1.36	0.07	0.64	0.33	56.95	0.75
HS951941	20.18	0.96	0.04	9.73	3.53	4.19	0.03	1.71	0.44	50.71	2.14
HS951942	16.06	0.49	0.03	8.75	2.66	2.92	0.03	2.12	0.47	58.54	1.85
HS951943	6.86	18.66	0.02	4.4	1.79	0.91	0.1	0.61	0.26	46.59	0.66
HS951944	15.23	7.6	0.02	5.32	2.92	3.26	0.06	1.38	0.12	53.48	0.64
HS951945	18.31	0.83	0.04	6.22	3.73	3.94	0.03	1.59	0.13	59.69	0.71
HS951946	12.19	14.4	0.02	4.54	1.82	5.34	0.07	1.08	0.08	43.71	0.44
HS951948	13.65	10.35	0.02	4.58	2.73	3.58	0.06	1.01	0.14	51.87	0.53
HS951949	15.1	7.84	0.01	5.27	2.8	3.63	0.05	1.34	0.13	53.17	0.59
HS951950	8.61	9.31	0.01	2.47	2.52	6.71	0.02	1.24	0.1	53.66	0.43
HS951951	15.74	7.15	0.02	5.87	3.58	3.53	0.07	1.2	0.13	53.36	0.72
HS951952	6.76	13.61	0.02	5.36	1.62	1.48	0.11	0.85	0.33	57.46	0.76
HS951953	9.97	11.95	0.03	5.74	2.28	2.16	0.15	1.12	0.28	54.18	0.7
HS951954	7.17	32.16	0.01	2.84	2.1	1.14	0.1	0.5	0.08	26.32	0.3
HS951955	14.94	6.59	0.03	6.91	3.09	4.44	0.08	0.66	0.17	52.35	0.82
17302	4.06	12.21	0.02	27.34	0.06	2.24	3.9	0.21	0.95	43.25	0.17
17303	1.57	3.61	0.01	15.23	0.09	1.35	1.63	0.16	0.46	73.22	0.07
17304	11.3	12.52	0.03	7.58	2.2	4.45	0.14	0.99	0.42	51	1.66
17305	11.33	11.07	0.02	7.04	2.25	4.17	0.07	1.61	0.41	53.29	1.53
17310	13.14	8.66	0.01	13.18	0.13	8.89	0.18	3.62	0.13	44.77	1.37
26591	10.49	1.97	0.04	6.66	3.34	1.76	0.28	1.15	0.11	69.96	0.57
26593	5.49	3.93	0.04	13.93	0.72	1.04	1.62	0.12	0.24	67.8	0.17
26594	8.83	14.56	0.07	9.17	2.55	2.56	0.87	0.33	0.25	48.86	1.03
26595	15.28	1.86	0.04	8.33	3.91	1.98	0.1	0.85	0.16	61.38	1.11
26596	6.53	2.92	0.02	10.22	1.25	1.9	0.16	0.26	0.27	68.4	0.36
26597	7.05	3.11	0.03	9.32	1.75	1.65	0.75	0.75	0.18	69.66	0.26
26598	5.34	0.83	0.04	4.8	1.36	1.74	0.04	0.64	0.11	81.54	0.5
26599	8.23	4.26	0.03	9.39	1.43	1.96	1.67	0.47	0.35	67.4	0.28
26600	9.9	6.24	0.03	13.48	2.04	2.46	0.75	0.4	0.43	56.42	0.56
26601	10.24	0.78	0.06	6.8	3.09	0.73	0.04	0.12	0.22	73.25	0.71
26602	2.9	7.6	0.01	15.38	0.3	2.26	0.31	0.58	0.44	58.7	0.12
26604	16.71	2.3	0.04	7.06	4.02	1.77	0.1	0.75	0.25	61.27	1.21
26605	3.49	23.46	0.005	2.11	0.55	1.95	0.18	0.72	0.07	47.9	0.15
26606	7.18	2.1	0.04	13.55	1.74	1.14	0.48	0.4	0.36	68.09	0.21
26607	8.02	5.44	0.03	4.76	2.18	1.14	0.34	0.54	0.14	70.05	0.27
26608	9.12	6.25	0.04	3.66	1.74	1.38	0.14	1.21	0.17	68.17	0.3
26609	3.89	4.44	0.03	17.76	0.08	1.08	1.44	0.005	0.58	64.98	0.15

Sample#	Al <sub>2</sub> O <sub>3</sub> (%)	CaO (%)	Cr <sub>2</sub> O <sub>3</sub> (%)	Fe(tot) (%)	K <sub>2</sub> O (%)	MgO (%)	MnO (%)	Na <sub>2</sub> O (%)	P <sub>2</sub> O <sub>5</sub> (%)	SiO <sub>2</sub> (%)	TiO <sub>2</sub> (%)
26610	7.04	7.13	0.06	16.73	1.21	1.97	0.33	0.47	0.52	56.28	0.36
26611	1.61	2	0.05	23.77	0.42	0.26	0.09	0.03	0.45	65.5	0.09
26612	16.16	5.1	0.04	8.17	2.27	12.97	0.28	0.52	0.07	46.46	0.65
26613	18.18	5.1	0.09	7.68	4.74	2.75	0.11	1.13	0.12	51.51	1
26615	12.57	6.79	0.07	16.04	3.01	1.67	0.63	0.8	0.23	48.97	0.63
26616	6.17	9.47	0.08	6.14	1.13	1.25	0.48	0.55	0.19	66.87	0.27
48519	12.7	8.76	0.01	17.8	0.09	5.61	0.28	3.04	0.24	47.8	2.5
49142	14.44	1.71	0.01	2.8	3.69	1.89	0.02	1.32	0.06	66.84	0.5
49146	13.14	9.78	0.04	14.31	0.33	6.5	0.21	2.85	0.17	50.19	1.81
49155	14.11	8.71	0.01	16.08	0.28	7.18	0.25	3.35	0.2	47.45	2.09
49460	3.72	6.04	0.02	33.95	0.08	2.51	4.72	0.31	0.58	44.19	0.17
49461	3.5	7.27	0.01	34.32	0.08	2.52	4.77	0.27	0.63	42.81	0.15
49462	4.33	10.08	0.03	28.24	0.14	2.4	3.22	0.2	0.84	44.63	0.2
49479	10.28	5	0.005	4.78	2.39	1.54	0.16	1.35	0.26	66.11	0.36
49480	18.4	6.4	0.01	7.99	3.9	3.71	0.2	0.7	0.09	54.64	0.9
49481	6.17	0.85	0.01	3.73	0.98	1.11	0.06	1.12	0.07	82.67	0.5
49848	19.33	0.93	0.01	8.2	4.29	2.25	0.09	1.52	0.22	58.54	1.33
49860	14.14	1.93	0.01	6.31	3.51	2.15	0.08	0.8	0.19	66.49	0.98
49863	11.02	25.55	0.01	3.86	1.86	2.25	0.09	1.29	0.09	36.35	0.55
49865	10.61	26.07	0.01	3.86	2.82	1.6	0.04	0.82	0.08	35.05	0.45
49866	0.24	40.57	0.005	2.8	0.06	2.63	1.3	0.12	0.02	23.83	0.02
49875	13.67	18.11	0.01	5.47	2.71	2.01	0.05	1.57	0.09	45.99	0.59
49876	3.21	1.24	0.005	5.12	0.25	1.12	0.02	1.21	0.44	85.04	0.21
49877	14.19	6.31	0.01	5.8	2.6	4.45	0.12	1.18	0.12	60.67	0.57
49878	23.9	0.46	0.03	7.47	5.5	2.83	0.04	0.92	0.12	53.58	1.06
49879	14.43	1.77	0.01	2.78	3.66	1.92	0.02	1.31	0.06	66.76	0.5
49880	20.74	0.48	0.02	9.18	3.48	3.19	0.12	3.06	0.09	53.95	1.01
49885	5.65	41.38	0.005	2.6	1.29	1.14	0.06	0.39	0.08	20.07	0.23
49905	14.44	10.47	0.01	13.52	0.23	6.56	0.23	3.65	0.14	49.69	1.63
49909	11.67	2.47	0.01	6.03	2.73	1.2	0.28	0.93	0.27	70.24	0.42
49919	8.63	6.87	0.01	8.31	2.24	2.72	0.02	1.02	0.28	61.46	0.97
49929	6.71	33.18	0.01	2.72	1.6	3.23	0.03	0.84	0.1	25.1	0.39
103051	16.80	1.95	0.03	7.09	3.85	2.22	0.06	1.20	0.19	61.40	0.95
103052	9.71	23.40	0.01	4.49	2.13	2.48	0.04	0.90	0.16	37.70	0.61
103053	5.24	41.30	0.00	1.94	1.19	1.10	0.04	0.32	0.10	18.10	0.17
103054	7.42	34.40	0.00	2.80	1.99	1.44	0.03	0.36	0.11	24.40	0.25
103055	14.40	2.24	0.03	6.45	3.21	1.94	0.06	1.59	0.15	64.50	1.16
103056	12.30	5.23	0.02	4.56	2.14	1.51	0.05	1.04	0.11	66.90	0.63
103057	8.54	26.40	0.00	3.69	2.33	2.29	0.05	0.69	0.12	34.80	0.47
103058	12.70	25.00	0.00	4.28	3.41	1.87	0.07	0.63	0.11	31.70	0.50
103059	12.50	1.63	0.02	6.10	3.00	1.94	0.08	1.29	0.19	68.90	0.95
103060	16.70	1.52	0.02	8.01	3.26	1.90	0.09	1.59	0.21	62.00	1.16
103061	12.30	15.30	0.00	4.14	2.80	1.74	0.06	1.63	0.08	50.30	0.55
103062	14.60	4.06	0.02	5.86	3.34	2.16	0.07	1.58	0.12	64.10	0.75
103063	4.50	14.70	0.02	15.20	0.38	1.82	1.30	0.09	0.69	50.10	0.25
103064	12.20	11.40	0.02	7.19	2.58	4.27	0.12	0.60	0.39	52.40	1.25
103065	10.60	21.60	0.00	4.93	2.37	4.20	0.09	0.62	0.18	37.90	0.52
103066	15.70	11.40	0.01	6.35	3.09	4.35	0.08	1.00	0.13	50.40	0.69
103067	10.60	11.20	0.01	6.42	2.38	3.97	0.23	0.67	0.32	54.30	0.73
103068	6.13	6.46	0.03	21.30	1.17	1.79	1.34	0.31	0.64	53.60	0.37
103069	9.30	4.82	0.02	18.30	1.93	1.74	0.82	0.34	0.45	55.50	0.62

Sample#	Al <sub>2</sub> O <sub>3</sub> (%)	CaO (%)	Cr <sub>2</sub> O <sub>3</sub> (%)	Fe(tot) (%)	K <sub>2</sub> O (%)	MgO (%)	MnO (%)	Na <sub>2</sub> O (%)	P <sub>2</sub> O <sub>5</sub> (%)	SiO <sub>2</sub> (%)	TiO <sub>2</sub> (%)
103070	3.92	7.45	0.02	29.00	0.05	2.12	3.14	0.00	0.78	47.70	0.20
103071	13.60	15.20	0.00	5.58	2.71	3.92	0.08	0.96	0.16	45.90	0.64
103072	8.48	3.56	0.02	6.09	1.82	1.44	0.46	0.73	0.14	72.60	0.38
103073	12.30	23.70	0.00	4.70	2.76	1.83	0.06	0.77	0.10	36.80	0.46
103074	8.62	3.65	0.01	8.50	2.05	1.74	0.80	0.57	0.21	69.60	0.36
103075	9.85	27.10	0.00	3.90	2.65	1.83	0.06	0.51	0.10	32.30	0.40
103076	6.24	38.00	0.00	2.42	1.57	1.43	0.02	0.35	0.10	19.60	0.24
103077	14.30	14.50	0.00	5.96	2.87	3.85	0.10	1.06	0.14	46.20	0.63
103078	9.48	3.92	0.00	7.86	2.16	1.61	0.68	0.74	0.21	68.90	0.33
103079	10.40	26.50	0.00	3.82	2.31	1.73	0.05	0.74	0.10	34.00	0.40
103080	14.20	6.22	0.02	6.61	2.44	2.43	0.09	1.82	0.17	59.10	0.95
103081	14.50	2.51	0.02	8.36	4.40	1.79	0.10	0.29	0.21	60.70	0.78
103082	15.80	5.12	0.02	7.76	4.64	2.69	0.21	0.21	0.11	54.40	0.75
103083	8.81	4.79	0.02	8.84	2.00	1.61	0.65	0.27	0.21	68.90	0.29
103084	7.55	7.86	0.02	5.68	0.88	5.69	0.28	1.87	0.10	61.90	0.37
103085	12.60	20.50	0.00	6.45	3.28	2.43	0.14	0.33	0.13	37.50	0.57
103086	4.25	6.78	0.02	32.40	0.04	2.78	5.12	0.00	0.70	45.20	0.21
103087	6.82	15.10	0.02	13.50	1.04	2.29	2.00	0.12	0.39	44.20	0.36
103090	18.10	0.54	0.02	7.16	5.24	2.03	0.06	0.26	0.09	59.90	0.86
103091	8.29	6.16	0.02	24.80	1.34	2.06	1.96	0.25	0.72	47.30	0.50
103092	11.10	9.94	0.06	16.10	2.52	3.50	0.88	0.37	0.50	42.40	1.28
103094	7.62	4.70	0.02	14.40	0.75	2.00	1.30	0.17	0.41	62.40	0.34
103095	19.00	4.30	0.02	7.34	3.93	4.58	0.06	1.17	0.11	54.60	0.78
103096	5.55	1.37	0.05	5.12	1.23	1.00	0.05	0.61	0.16	81.50	0.64
103097	8.56	4.53	0.02	7.35	1.67	1.95	0.80	0.46	0.23	69.00	0.34
103098	3.62	5.57	0.03	17.00	0.10	1.58	2.14	0.00	0.37	63.90	0.17
103099	12.00	1.25	0.02	5.24	2.84	1.79	0.06	1.36	0.22	72.30	0.99
103100	16.60	0.96	0.02	7.86	4.02	2.54	0.08	1.60	0.17	61.80	1.39
103101	14.80	1.14	0.02	6.16	3.32	1.90	0.07	2.31	0.18	67.20	1.15
103102	7.75	33.00	0.00	3.03	2.12	1.60	0.03	0.48	0.12	25.60	0.28
103103	6.55	36.60	0.00	2.44	1.69	1.81	0.03	0.49	0.11	21.30	0.23
103104	12.40	8.88	0.02	5.31	3.18	1.72	0.05	0.72	0.16	57.30	0.86
103120	15.20	2.49	0.02	6.26	3.59	1.68	0.08	1.10	0.18	62.50	0.68
103121	9.92	27.90	0.00	3.74	2.18	1.73	0.05	0.79	0.10	30.80	0.38
103122	8.38	2.84	0.02	9.91	2.15	6.61	0.21	1.03	0.11	61.50	0.41
103123	11.30	25.20	0.00	4.68	2.83	1.96	0.09	0.45	0.10	36.00	0.43
103124	12.50	7.04	0.02	6.25	2.70	2.50	0.17	1.04	0.27	61.10	0.49
103125	3.80	9.75	0.01	29.10	0.01	2.16	2.75	0.00	1.12	44.30	0.17
103126	15.50	10.50	0.04	9.54	1.54	7.58	0.18	1.93	0.11	48.80	1.06
103127	10.20	26.30	0.00	4.33	2.20	1.88	0.09	0.79	0.11	35.50	0.44
103128	17.40	2.13	0.01	6.26	4.14	1.99	0.06	1.38	0.24	61.10	0.89
103129	12.70	5.50	0.01	6.37	2.48	3.13	0.21	1.01	0.27	63.90	0.53
103130	15.80	12.70	0.00	6.72	3.10	4.29	0.16	1.27	0.10	47.70	0.64
103131	4.21	5.34	0.02	12.70	0.25	1.18	0.71	0.03	0.20	68.80	0.19
103132	8.97	7.67	0.01	5.06	2.04	1.44	0.31	1.06	0.23	65.60	0.33
103133	7.33	7.14	0.01	19.30	0.57	2.70	1.95	0.07	0.51	55.00	0.42
103134	18.10	20.50	0.00	5.73	2.71	2.00	0.10	0.62	0.08	41.00	0.55
103135	11.60	10.90	0.00	5.98	2.55	11.00	0.31	0.64	0.13	47.90	0.57
103136	14.20	11.00	0.01	6.60	2.81	2.34	0.09	1.15	0.17	52.60	0.77
103137	6.60	35.90	0.00	3.28	1.58	1.87	0.06	0.37	0.15	22.60	0.41



Table A1.3. Concentrations of various additional components

Sample#	CO <sub>2</sub> (%)	H <sub>2</sub> O(+) (%)	H <sub>2</sub> O(-) (%)	S % (%)	LOI % (%)	TOTAL	T.O.C. (%)	FeO (%)
HS951001	17.7	1.09	0.18	0.52	18.02	99.44	0.55	3.34
HS951002	1.6	2.96	0.22	0.87	3.61	99.26	0.025	6.16
HS951003	0.9	2.59	0.11	0.41	3.08	99.54	0.025	6.62
HS951004	3	1.24	0.1	0.69	4.32	100.03	0.5	4.56
HS951005	8.7	1.42	0.18	0.45	9.66	99.27	0.8	4.61
HS951006	24.4	0.91	0.13	0.34	23.95	99.03	0.2	2.32
HS951007	10.2	1.29	0.17	0.44	9.85	99.2	0.05	3.95
HS951008	1.6	3.54	0.23	0.73	3.78	99.45	0.15	6.7
HS951009	3.1	1.06	0.32	2.86	2.48	99.49	0.9	17.6
HS951010	4.1	0.91	0.14	0.8	4.55	99.1	0.45	5.31
HS951011	28.2	0.79	0.2	0.34	27.59	98.77	0.35	1.8
HS951012	7.5	1.85	0.19	2.17	7.51	99.05	0.35	7.98
HS951013	12.8	2.1	0.21	0.2	14.5	99.07	0.5	3.64
HS951014	0.9	1.74	0.15	2.42	4.06	99.64	1.3	9.62
HS951015	25.7	0.66	0.14	0.31	26.7	99.08	1.3	2.24
HS951016	10.8	1.57	0.26	1.91	9.89	98.91	0.25	4.91
HS951017	0.1	2.19	0.12	0.66	2.35	99.44	0.1	6.08
HS951018	0.1	2.56	0.17	0.89	2.98	99.26	0.1	4.62
HS951019	1.1	1.68	0.17	0.23	3.22	99.32	0.5	4.53
HS951020	5.3	1.2	0.15	0.2	6.71	99.12	0.55	4.51
HS951021	11.8	0.24	0.1	0.55	11.64	99.07	0.3	3.4
HS951022	0.9	3.11	0.27	0.57	4.03	99.46	0.25	6.02
HS951024	0.9	1.14	0.13	0.14	3	99.33	0.45	3.74
HS951025	1.6	0.07	0.09	0.97	3.7	99.15	1.1	5.12
HS951028	0.7	2.06	0.05	0.38	2.69	99.06	0.2	5.43
HS951030	7.5	1.24	0.08	0.9	8.19	98.58	1.2	3.78
HS951033	0.4	2.7	0.11	0.35	3.26	99.32	0.15	6.47
HS951035	0.1	1	0.18	0.95	6.84	99.11	4.7	2.21
HS951038	0.1	2.51	0.08	0.11	3.12	99.57	0.05	5.79
HS951040	1.2	1.84	0.12	1.16	4.28	99.12	1.3	6.18
HS951043	0.7	2.95	0.11	0.76	3.65	99.64	0.15	7.76
HS951045	0.4	0.19	0.03	0.07	1.55	99.13	0.8	1.55
HS951046	11.8	0.66	0.16	0.34	12.95	99.04	0.4	2.16
HS951048	0.1	2.38	0.11	0.64	2.83	99.44	0.05	6.24
HS951049	4.6	1.3	0.28	3.14	7.99	100.08	1.15	7.26
HS951050	16.8	1.26	0.2	0.2	16.98	98.7	0.75	3.27
HS951052	13	1.21	0.3	0.24	14.66	99.12	0.7	3.2
HS951054	0.1	2.05	0.72	1.55	5.19	99.56	1.75	5.93
HS951055	6.1	1.58	0.23	0.47	9.02	99.39	0.95	3.75
HS951056	10.8	0.86	0.13	0.36	12.53	99.61	0.4	4.09
HS951057	0.1	2.6	0.07	1.09	3.2	99.35	0.15	6.59
HS951058	0.1	2.71	0.17	0.68	3.05	99.29	0.1	7.23
HS951059	5.2	1.09	0.08	4.27	6.2	99.38	1.05	15.7
HS951060	14.5	0.99	0.17	0.31	16.21	99.11	1.2	3.59
HS951062	0.7	4.04	0.13	0.59	4.47	100.05	0.1	6.84
HS951063	3.3	3.07	0.15	0.71	6.21	99.33	0.2	6.08
HS951066	20.2	1.06	0.14	0.58	20.37	99.07	0.6	2.68
HS951067	0.7	2.34	0.07	0.22	3.09	99.2	0.025	4.78
HS951070	2	1.64	0.17	1.61	7.07	99.6	2.45	2.53

Sample#	CO <sub>2</sub> (%)	H <sub>2</sub> O(+) (%)	H <sub>2</sub> O(-) (%)	S % (%)	LOI % (%)	TOTAL	T.O.C. (%)	FeO (%)
HS951072	0.5	1.83	0.18	0.33	2.22	98.92	0.025	4.85
HS951075	19.1	0.97	0.13	0.36	19.63	99.1	0.95	3.38
HS951080	1.2	1.18	0.15	0.58	3.97	99.19	1.18	4.41
HS951082	0.1	1.74	0.14	0.27	1.85	99.37	0.1	4.69
HS951086	37.6	0.18	0.19	0.21	34.99	99.21	0.025	0.89
HS951087	0.9	1.08	0.21	0.19	1.72	99.82	0.025	3.31
HS951089	7.8	0.96	0.25	7.3	9.78	99	1.75	18.4
HS951090	5.8	0.95	0.1	0.58	5.64	99.04	0.4	4.96
HS951091	17.6	0.68	0.15	0.35	17.56	99.02	0.3	3.28
HS951092	3.1	1.87	0.18	0.65	3.95	99.3	0.025	4.99
HS951093	0.5	3.21	0.08	0.23	3.27	99.01	0.025	5.91
HS951094	4.7	0.71	0.73	3.61	5.26	99.66	1.6	23.8
HS951095	5.7	0.87	0.23	1.21	8.3	99.89	1.11	4.63
HS951096	20.5	0.59	0.13	0.37	20.99	99.03	0.45	2.44
HS951098	0.1	2.83	0.2	0.25	2.77	99.66	0.1	5.71
HS951099	8.9	1.03	0.22	3.36	7.87	99.63	2.15	16.5
HS951100	5.2	1.2	0.18	2.57	6.44	99.98	1.5	11
HS951101	21	0.97	0.15	1.55	18.47	98.9	0.35	6.27
HS951102	6.9	1.85	0.14	0.8	8.02	98.93	0.3	5.6
HS951103	4	2.75	0.09	0.41	4.79	99.11	0.2	4.39
HS951105	2.4	1.82	0.19	1.8	6.23	99.68	2.45	4.47
HS951106	6.1	0.005	0.06	0.14	6.4	99.23	0.5	0.13
HS951107	1.4	2.99	0.16	0.42	4	99.1	0.25	5.2
HS951110	2.6	2	0.11	2.43	4.33	98.97	0.65	5.5
HS951111	8.5	0.17	0.04	0.37	8.06	99.33	0.5	0.81
HS951113	1.2	3.1	0.05	0.66	3.82	99.26	0.25	6.12
HS951115	12.6	0.64	0.06	0.79	13.32	99.16	1.35	2.48
HS951116	19.2	3.21	0.03	0.89	19.05	99.26	0.025	6.67
HS951120	5.9	1.37	0.07	1.1	7.53	99.41	1.85	3.99
HS951121	16.9	0.66	0.08	0.4	15.88	99.05	0.15	3.56
HS951122	0.4	1.83	0.21	0.6	2.15	99.21	0.05	5.47
HS951123	0.6	2.81	0.26	0.19	3.42	99.52	0.2	5.78
HS951124	1.9	0.57	0.25	4.71	3.52	99.47	1.3	18.4
HS951125	4.7	0.81	0.09	0.4	5.72	99	0.7	4.97
HS951127	0.1	3.26	0.17	0.4	3.35	99.28	0.1	7.81
HS951128	0.9	2.26	0.16	0.04	3.32	99.55	0.15	5.33
HS951129	7.8	1.51	0.17	0.29	9.12	99.18	0.7	4.62
HS951130	1.1	1.81	0.33	1.49	4.36	100.03	0.85	7.04
HS951131	10	5.75	0.15	0.64	12.91	99.52	0.05	10.6
HS951132	14.8	2.97	0.06	0.35	15.9	99.11	0.15	7.77
HS951133	17.3	1.72	0.1	0.19	16.62	99.16	0.025	7.47
HS951135	21.8	0.25	0.11	0.43	22.05	99.07	1.15	1.5
HS951136	20.4	1.02	0.09	0.34	20.41	99.14	0.7	2.67
HS951137	0.9	2.36	0.22	0.39	2.64	99.23	0.025	8.05
HS951139	3.2	1.33	0.89	4.23	4.51	99.64	1.2	23.8
HS951140	9.6	1.93	0.41	0.15	10.85	99.05	0.5	4.34
HS951142	5.5	1.62	0.12	2.21	3.73	98.56	0.025	4.75
HS951143	11.6	2.31	0.14	0.22	11.99	99.17	0.025	5.59
HS951144	8.3	1.62	0.11	2.82	8.24	98.96	1	7.38
HS951148	1.5	2.36	0.15	0.26	3.23	99.04	0.1	5.29
HS951150	1.6	2.87	0.11	0.5	4.01	99.37	0.45	5.57

Sample#	CO <sub>2</sub> (%)	H <sub>2</sub> O(+) (%)	H <sub>2</sub> O(-) (%)	S % (%)	LOI % (%)	TOTAL	T.O.C. (%)	FeO (%)
HS951151	20.9	3.28	0.07	1.54	20.27	98.55	0.025	6.76
HS951152	1.4	2.72	0.08	0.32	3.87	99.05	0.025	6.56
HS951155	9.8	0.09	0.01	0.46	9.45	99.22	0.8	1.29
HS951156	18.8	2.45	0.07	1.03	19.07	99.08	0.05	5.55
HS951158	4.3	3.05	0.06	1.64	5.73	99.35	0.5	12.3
HS951159	8.1	1.47	0.1	10.7	11.45	99.53	1.5	25.7
HS951160	11.9	1.4	0.05	1.02	10.55	99.3	0.35	4.61
HS951161	23.6	0.45	0.04	0.005	22.67	99.32	0.025	2.27
HS951162	0.4	1.75	0.05	0.61	2.46	99.27	0.1	5.18
HS951164	4.3	0.88	0.57	3.19	3.26	99.65	0.9	14.2
HS951165	7.5	0.53	0.04	0.4	8.96	99.09	0.4	4.36
HS951166	29.3	0.49	0.08	0.33	28.41	99.1	0.3	2.12
HS951167	3.3	2.08	0.15	0.25	5.36	99.65	0.05	4.97
HS951169	0.7	1.5	0.11	0.19	2.91	99.91	0.4	3.38
HS951170	3	1.93	0.17	0.81	6.11	99.91	1.1	4.25
HS951171	25.7	0.46	0.05	0.27	24	98.92	0.25	2
HS951172	0.9	2.55	0.09	0.58	3.27	99.19	0.025	6.06
HS951173	0.4	3.57	0.05	0.21	3.61	99.4	0.025	6.5
HS951174	1.3	1.34	0.07	0.83	3.53	99.86	0.55	5.69
HS951175	1.2	0.98	0.11	1.08	3.87	99.34	1.25	5.2
HS951176	20.8	1.13	0.08	0.49	19.84	99	0.2	2.83
HS951177	0.8	1.85	0.11	1.02	3.7	99.18	0.35	3.57
HS951178	1.2	2.25	0.04	0.62	3.37	99.62	0.05	7.22
HS951179	3.6	0.85	0.04	5.08	5.77	99.69	2.2	20.8
HS951181	7.2	0.96	0.12	0.57	8.5	99.31	0.55	5.04
HS951182	0.4	1.75	0.07	0.91	3.04	99.66	0.1	4.59
HS951183	1.3	3.1	2.13	0.41	3.05	99	0.025	5.71
HS951184	5.1	0.5	0.12	2.3	3.42	99.5	1	19.1
HS951185	0.5	0.93	0.07	0.5	2.57	99.63	0.6	4.64
HS951901	10.6	0.46	0.04	1.85	10.85	98.81	1	4.25
HS951902	23	1.44	0.07	0.21	22.75	99.3	0.1	2.35
HS951903	10.9	0.28	0.02	1.66	9.63	98.55	0.7	5.1
HS951904	10.5	1.46	0.06	1.34	10.41	99.06	0.95	4.63
HS951905	37.2	0.005	0.02	0.21	37.75	98.9	0.4	0.78
HS951906	13.3	1.29	0.08	0.37	13.1	98.63	0.025	3.93
HS951907	5.5	2.7	0.1	0.55	6.25	99.32	0.025	5.54
HS951908	6.8	0.27	0.04	2.19	7.1	99.12	1.3	2.99
HS951909	4.3	0.44	0.15	1.5	5.86	99.28	1.3	2.86
HS951910	42.3	0.005	0.01	0.005	43.13	97.84	0.3	0.1
HS951911	0.3	3.75	0.05	0.47	3.5	99.47	0.025	7.5
HS951912	23.2	0.18	0.07	0.87	23.34	98.75	0.35	2.33
HS951913	11.1	0.42	0.07	0.32	11.47	99.6	0.4	4.53
HS951914	16.6	2.39	0.43	0.07	19.68	99.43	0.2	1.98
HS951915	40.9	0.02	0.06	0.16	40.58	98.26	0.1	0.34
HS951916	6.3	1.17	0.13	0.88	6.82	99.45	0.85	5.29
HS951917	2.6	1.22	0.15	0.6	3.27	99	0.45	5.41
HS951918	5.9	1.75	0.2	0.59	7.04	99.48	0.5	4.15
HS951920	8.2	4.53	0.08	0.05	11.11	99.81	0.025	7.65
HS951921	21.1	2.17	0.05	1.46	21.12	99.11	0.4	4.35
HS951922	9.7	0.89	0.07	0.37	10.2	99.35	0.4	4.39
HS951924	8.7	1.82	0.15	0.4	9.8	99.05	0.3	4.29

Sample#	CO <sub>2</sub> (%)	H <sub>2</sub> O(+) (%)	H <sub>2</sub> O(-) (%)	S % (%)	LOI % (%)	TOTAL	T.O.C. (%)	FeO (%)
HS951925	4	1.13	0.06	0.63	6.42	99.1	1.65	1.85
HS951926	42.3	0.005	0.03	0.07	42.66	98.11	0.6	0.4
HS951927	5.3	2.61	0.07	0.39	7.3	99.72	0.35	4.66
HS951928	7.3	0.92	0.11	0.69	7.5	99.22	0.55	4.32
HS951929	7.1	1.89	0.11	1.21	8.35	99.21	0.7	3.85
HS951930	15.3	3.14	0.06	0.67	17.4	99.14	0.3	6.35
HS951931	3.2	2.1	0.06	0.9	6.5	99.57	1.9	3.83
HS951932	16.1	3.79	0.19	0.24	19.27	99.9	0.35	6.72
HS951933	3.1	0.87	0.05	2.36	5.64	99.45	1.25	5.63
HS951934	13.1	0.93	0.1	0.6	14.01	99.04	0.4	4.26
HS951935	0.3	2.97	0.08	0.43	3.09	99.2	0.1	6.96
HS951936	5.5	0.36	0.09	1.7	7.47	99.31	2.2	4.12
HS951937	4.5	0.3	0.12	2.21	5.13	99.08	1.3	4.33
HS951938	35.3	0.36	0.1	0.18	36.02	98.74	0.65	1.26
HS951939	10.4	0.12	0.08	1.94	9.17	99	1.3	4.02
HS951941	0.3	5.21	0.77	0.11	6.36	100.02	0.75	4.38
HS951942	0.1	3.69	0.72	0.17	5.33	99.25	0.95	3.14
HS951943	13.8	1.2	0.39	0.03	18.37	99.23	2.25	0.32
HS951944	5.3	3.37	0.2	0.07	8.96	98.99	0.6	3.19
HS951945	0.1	4.22	0.15	0.04	4.58	99.8	0.55	3.29
HS951946	12.2	2.74	0.13	0.07	15.76	99.45	0.7	3.54
HS951948	7.8	3.11	0.18	0.18	11.07	99.59	0.95	3.28
HS951949	4.9	3.13	0.16	0.005	9.09	99.02	0.8	3.54
HS951950	12.6	0.85	0.09	0.61	13.95	99.03	0.8	1.5
HS951951	5.2	3.22	0.31	0.98	8.02	99.39	0.65	3.62
HS951952	10.6	0.54	0.14	1.75	10.69	99.05	1.15	3.44
HS951953	8.5	1.54	0.19	1.38	10.02	98.58	0.95	3.52
HS951954	24.3	1.03	0.09	0.04	26.54	99.26	0.5	1.65
HS951955	5.9	3.54	0.21	0.17	9.11	99.19	0.9	4.45
17302	7.9	0.77		1.49	4.66	99.07	1.1	21.7
17303	3.6	0.42		1.84	1.2	98.6	0.5	11.2
17304	7	0.98		1.52	5.98	98.54	0.9	6.5
17305	6.4	0.64		1.41	5.45	98.24	0.9	5.82
17310	2.5	3.72		0.05	5.1	99.18	0.15	10.6
26591	0.8	2.14	0.42	0.18	3.1	99.43	0.3	4.89
26593	2	1.08	0.24	3.17	4.71	99.81	1.2	10.8
26594	10.4	0.89	0.18	0.54	10.17	99.25	0.7	6.91
26595	0.6	1.96	0.2	2.87	4.13	99.13	0.025	6.08
26596	1.3	1.29	0.26	4.91	5.21	97.5	0.1	8.45
26597	1.5	1.82	0.3	1.67	4.84	99.35	1.15	7.3
26598	0.3	0.63	0.11	1.08	1.75	98.69	0.15	3.76
26599	1.9	1.27	0.2	1.75	4.32	99.79	1	7.48
26600	3.3	1.14	0.22	5.92	6.38	99.09	0.025	11.7
26601	0.6	1.12	0.2	2.92	2.91	98.95	0.025	5.83
26602	5.3	0.33	0.19	9.09	8.91	97.51	0.05	14.1
26604	0.4	1.8	0.11	2.05	3.97	99.45	0.7	5.95
26605	18.4	0.15	0.06	0.68	17.19	97.77	0.55	1.9
26606	0.9	1.26	0.14	3.86	4.42	99.71	1.2	11
26607	3.1	1.48	0.28	0.69	6.03	98.94	1.3	3.34
26608	3.2	2.3	0.58	0.56	6.99	99.17	1.55	2.04
26609	1.7	1.02	0.37	3.88	5.37	99.8	1.3	14.3

Sample#	CO <sub>2</sub> (%)	H <sub>2</sub> O(+) (%)	H <sub>2</sub> O(-) (%)	S % (%)	LOI % (%)	TOTAL	T.O.C. (%)	FeO (%)
26610	3.9	1.19	0.21	6.99	7.58	99.68	0.2	14.9
26611	0.7	0.26	0.13	10.4	5.28	99.55	0.2	20.9
26612	1.6	5.69	0.44	0.76	6.86	99.55	0.15	6.79
26613	1.7	3.51	0.54	1.61	6.67	99.08	0.8	5.51
26615	4.2	2.8	0.52	2.5	7.87	99.28	1.75	11.9
26616	6.3	1.43	0.24	0.51	6.11	98.71	0.9	4.11
48519					0.52	99.35		
49142					5.39	98.67		
49146					0.4	99.73		
49155					0.82	100.53		
49460					3	99.29		
49461					3.5	99.83		
49462					6.01	100.32		
49479					6.93	99.16		
49480					2.93	99.87		
49481					1.17	98.44		
49848					3.06	99.77		
49860					3.33	99.92		
49863					16.38	99.3		
49865					17.21	98.62		
49866					27.83	99.42		
49875					7.93	98.2		
49876					1.53	99.39		
49877					3.5	99.52		
49878					4.42	100.33		
49879					5.34	98.56		
49880					3.65	98.97		
49885					27.28	100.17		
49905					0.34	100.91		
49909					3.36	99.61		
49919					5.63	98.16		
49929					24.65	98.56		
103051					4.05	99.80		
103052					17.30	98.90		
103053					30.20	99.70		
103054					26.70	99.90		
103055					2.45	98.20		
103056					5.30	99.80		
103057					20.50	99.90		
103058					18.60	98.90		
103059					1.70	98.30		
103060					2.90	99.40		
103061					9.75	98.60		
103062					2.30	99.00		
103063					3.75	92.80		
103064					5.80	98.20		
103065					15.70	98.70		
103066					5.85	99.10		
103067					7.35	98.20		
103068					4.35	97.50		
103069					4.30	98.10		

Sample#	CO <sub>2</sub> (%)	H <sub>2</sub> O(+) (%)	H <sub>2</sub> O(-) (%)	S % (%)	LOI % (%)	TOTAL	T.O.C. (%)	FeO (%)
103070					5.25	99.60		
103071					10.00	98.80		
103072					2.80	98.50		
103073					16.10	99.60		
103074					2.75	98.90		
103075					20.50	99.20		
103076					28.30	98.30		
103077					8.40	98.00		
103078					2.75	98.60		
103079					18.70	98.80		
103080					4.45	98.50		
103081					5.45	99.10		
103082					3.35	95.10		
103083					2.90	99.30		
103084					3.65	95.80		
103085					14.20	98.10		
103086					2.90	100.40		
103087					10.80	96.60		
103090					4.30	98.60		
103091					4.70	98.10		
103092					7.35	96.00		
103094					3.30	97.40		
103095					2.50	98.40		
103096					1.65	98.90		
103097					2.95	97.90		
103098					3.70	98.20		
103099					1.90	100.00		
103100					2.50	99.50		
103101					1.90	100.20		
103102					24.70	98.70		
103103					28.20	99.40		
103104					4.90	95.50		
103120					5.45	99.20		
103121					21.30	98.90		
103122					2.45	95.60		
103123					16.80	99.80		
103124					3.85	97.90		
103125					2.65	95.80		
103126					1.95	98.70		
103127					17.80	99.60		
103128					3.75	99.30		
103129					2.85	99.00		
103130					4.50	97.00		
103131					2.90	96.50		
103132					4.30	97.00		
103133					2.60	97.60		
103134					8.70	100.10		
103135					6.70	98.30		
103136					6.50	98.20		
103137					26.80	99.60		

Table A1.4. Trace element concentrations

Sample#	Ba (ppm)	Rb (ppm)	Sr (ppm)	Nb (ppm)	Zr (ppm)	Y (ppm)
HS951001	260	66	870	12	111	20
HS951002	670	136	286	26	231	38
HS951003	320	146	150	20	150	34
HS951004	810	78	80	16	144	30
HS951005	725	98	384	16	111	20
HS951006	185	54	1305	8	69	18
HS951007	465	76	718	20	216	24
HS951008	310	120	360	18	141	32
HS951009	160	8	66	2	69	24
HS951010	1585	102	404	24	135	22
HS951011	135	54	1360	4	51	14
HS951012	185	90	382	12	99	24
HS951013	350	110	360	16	117	24
HS951014	640	82	120	14	219	28
HS951015	665	44	584	8	51	12
HS951016	405	108	526	22	126	30
HS951017	440	106	114	22	267	38
HS951018	385	162	224	22	147	30
HS951019	790	96	126	14	132	28
HS951020	875	112	378	16	102	22
HS951021	185	70	418	16	138	20
HS951022	720	154	288	22	153	30
HS951024	670	88	144	16	156	28
HS951025	1175	94	404	24	135	22
HS951028	995	130	134	26	354	32
HS951030	2580	66	426	20	105	22
HS951033	850	138	138	20	222	34
HS951035	5280	64	174	8	60	26
HS951038	850	124	68	12	174	26
HS951040	2010	96	590	18	138	32
HS951043	445	154	106	20	231	34
HS951045	350	24	22	8	309	14
HS951046	190	72	602	18	165	22
HS951048	995	134	92	26	243	34
HS951049	1130	76	160	10	117	30
HS951050	700	74	466	12	69	18
HS951052	595	100	686	12	84	18
HS951054	545	72	152	6	84	38
HS951055	890	106	476	18	105	22
HS951056	400	96	754	16	111	26
HS951057	610	142	130	26	246	42
HS951058	310	146	124	18	141	30
HS951059	50	24	100	4	117	36
HS951060	745	82	538	14	81	20
HS951062	1120	160	122	28	228	46
HS951063	475	92	160	24	180	28
HS951066	410	60	690	10	99	18
HS951067	1040	92	90	26	450	32
HS951070	1730	114	152	14	114	30

Sample#	Ba (ppm)	Rb (ppm)	Sr (ppm)	Nb (ppm)	Zr (ppm)	Y (ppm)
HS951072	785	80	200	24	381	34
HS951075	535	56	546	14	72	16
HS951080	1940	104	126	16	159	26
HS951082	490	124	196	12	207	24
HS951086	140	24	1140	2	33	6
HS951087	545	86	282	16	450	32
HS951089	30	10	70	2	63	28
HS951090	1115	110	356	20	117	22
HS951091	350	82	1020	16	105	22
HS951092	535	114	400	20	204	32
HS951093	315	170	78	20	144	30
HS951094	35	14	92	1	57	22
HS951095	490	96	220	14	117	26
HS951096	215	68	1160	8	78	18
HS951098	215	134	100	24	141	28
HS951099	15	10	136	1	54	38
HS951100	385	54	138	6	87	28
HS951101	725	56	254	32	96	18
HS951102	1190	100	356	10	108	30
HS951103	665	104	202	20	324	32
HS951105	820	64	106	8	210	28
HS951106	170	12	134	4	66	6
HS951107	895	100	130	28	300	30
HS951110	1195	114	198	28	177	26
HS951111	590	36	204	6	138	12
HS951113	535	130	188	24	189	30
HS951115	630	58	240	16	99	18
HS951116	340	16	312	52	147	16
HS951120	1060	90	132	12	93	26
HS951121	295	76	1105	16	99	24
HS951122	590	88	248	26	450	40
HS951123	525	136	140	24	267	36
HS951124	105	12	28	1	60	28
HS951125	1025	120	364	20	129	24
HS951127	580	142	156	28	216	32
HS951128	450	132	98	36	405	34
HS951129	920	108	414	18	108	22
HS951130	1245	66	88	12	135	32
HS951131	235	14	250	78	192	18
HS951132	540	36	202	66	165	18
HS951133	1140	60	282	58	168	20
HS951135	385	28	608	14	57	12
HS951136	340	68	1390	12	87	22
HS951137	805	120	178	24	423	46
HS951139	30	8	54	1	60	26
HS951140	1045	122	610	14	96	20
HS951142	995	98	168	16	198	26
HS951143	805	98	250	4	66	16
HS951144	940	60	110	8	90	24
HS951148	785	106	114	22	288	28
HS951150	950	128	104	22	246	38



Sample#	Ba (ppm)	Rb (ppm)	Sr (ppm)	Nb (ppm)	Zr (ppm)	Y (ppm)
HS951151	180	8	376	48	126	14
HS951152	875	120	118	26	279	30
HS951155	745	56	300	6	174	14
HS951156	705	36	350	34	87	16
HS951158	1025	56	168	6	96	22
HS951159	75	18	92	1	45	24
HS951160	675	84	216	34	150	22
HS951161	275	64	1220	8	78	18
HS951162	620	114	260	24	342	38
HS951164	255	20	66	2	63	30
HS951165	860	98	438	14	96	20
HS951166	210	38	736	4	75	14
HS951167	790	96	154	28	291	28
HS951169	665	104	152	16	147	32
HS951170	805	102	180	18	144	28
HS951171	185	48	1295	6	66	18
HS951172	805	108	246	32	318	32
HS951173	350	154	82	18	141	32
HS951174	620	72	76	12	138	34
HS951175	880	136	190	18	132	24
HS951176	200	50	834	14	99	16
HS951177	560	136	278	20	315	38
HS951178	245	150	82	26	150	30
HS951179	35	10	42	1	63	26
HS951181	1030	118	428	16	108	20
HS951182	715	144	160	22	276	38
HS951183	320	142	128	20	141	30
HS951184	10	8	76	1	54	28
HS951185	780	128	434	18	108	16
HS951901	1200	56	448	32	120	24
HS951902	290	82	452	8	72	20
HS951903	1130	64	418	42	159	22
HS951904	1190	68	420	28	120	22
HS951905	50	20	1240	2	24	6
HS951906	385	70	388	6	135	20
HS951907	655	120	262	20	180	34
HS951908	2130	46	336	18	84	18
HS951909	950	52	418	26	114	20
HS951910	5	2	928	1	6	1
HS951911	715	138	206	20	168	32
HS951912	170	68	780	6	63	18
HS951913	910	84	456	16	99	22
HS951914	805	64	156	68	168	20
HS951915	20	4	846	1	9	2
HS951916	1125	106	358	26	138	22
HS951917	1365	122	404	24	141	22
HS951918	850	110	334	18	105	22
HS951920	55	2	242	6	78	18
HS951921	540	26	302	42	108	16
HS951922	715	102	448	14	96	18
HS951924	870	100	350	18	120	22

Sample#	Ba (ppm)	Rb (ppm)	Sr (ppm)	Nb (ppm)	Zr (ppm)	Y (ppm)
HS951925	565	66	138	6	69	16
HS951926	150	2	324	1	9	6
HS951927	875	188	330	16	123	28
HS951928	1580	92	460	20	108	20
HS951929	3180	114	148	18	135	22
HS951930	595	22	314	36	117	18
HS951931	720	94	156	12	99	18
HS951932	125	12	376	66	150	18
HS951933	2430	76	370	48	201	28
HS951934	445	80	1010	16	141	28
HS951935	320	150	96	22	141	30
HS951936	1860	56	448	22	108	24
HS951937	655	74	248	36	150	22
HS951938	55	20	686	1	27	8
HS951939	520	50	362	28	108	20
HS951941	4370	120	208	140	633	38
HS951942	3190	96	174	72	318	28
HS951943	1890	50	628	22	105	20
HS951944	1170	104	336	14	114	18
HS951945	1330	142	142	16	123	16
HS951946	2140	72	350	8	63	14
HS951948	2710	88	356	14	96	16
HS951949	1875	94	348	14	123	16
HS951950	2090	68	152	8	204	22
HS951951	2530	138	222	16	120	16
HS951952	585	54	346	30	120	22
HS951953	500	72	262	24	120	20
HS951954	210	52	1010	8	69	20
HS951955	845	122	318	22	120	18
17302	10	6	128	1	48	30
17303	15	8	58	2	27	24
17304	1270	80	376	56	216	26
17305	1520	80	412	56	210	24
17310	35	4	116	4	87	26
26591	610	118	118	16	372	34
26593	1310	22	44	4	51	30
26594	435	72	142	42	117	24
26595	1350	132	104	20	234	32
26596	250	50	40	6	84	16
26597	2960	58	70	6	96	22
26598	220	64	58	16	117	14
26599	2490	42	70	8	81	26
26600	325	64	92	10	150	32
26601	720	100	26	14	219	26
26602	105	10	48	2	30	6
26604	620	134	126	26	276	44
26605	50	20	686	4	36	10
26606	645	68	52	8	108	32
26607	795	92	116	12	120	24
26608	350	70	234	14	135	24
26609	40	6	38	2	45	30

Sample#	Ba (ppm)	Rb (ppm)	Sr (ppm)	Nb (ppm)	Zr (ppm)	Y (ppm)
26610	180	38	68	4	69	32
26611	105	18	2 1		30	22
26612	335	90	98	22	141	28
26613	650	162	246	10	123	30
26615	420	80	164	12	111	28
26616	845	48	198	8	117	22
48519	213	4	109	10	162	54
49142	1500	160	236	11	75	16
49146	239	21	167	9	119	46
49155	191	15	125	7	138	53
49460	77	2	61	5	52	50
49461	79	7	72	2	50	48
49462	66	1	111	8	62	55
49479	711	93	200	15	150	29
49480	251	169	168	17	141	30
49481	208	43	95	12	417	23
49848	948	152	160	22	283	48
49860	449	148	135	18	278	40
49863	276	72	1270	16	121	23
49865	210	99	1720	16	115	23
49866	56	3	333	1	17	5
49875	247	106	1180	18	141	29
49876	85	5	29	7	90	12
49877	478	126	215	14	88	21
49878	843	186	235	16	196	36
49879	1460	160	231	12	77	13
49880	753	103	162	19	140	32
49885	144	32	1950	8	67	15
49905	157	5	184	7	93	38
49909	1830	106	164	16	135	30
49919	1350	77	325	26	134	14
49929	551	67	841	12	61	9
103051	516	118	245	17	255	46
103052	256	66	760	17	134	18
103053	151	33	1350	5	64	7
103054	235	52	1230	8	82	14
103055	744	91	239	16	324	30
103056	537	65	387	17	277	24
103057	394	68	686	10	166	20
103058	452	104	1270	13	125	27
103059	838	96	188	21	354	32
103060	662	123	178	22	261	46
103061	439	91	548	14	210	23
103062	568	118	243	15	255	37
103063	152	16	134	7	74	43
103064	1530	99	387	37	176	24
103065	825	80	490	14	74	18
103066	785	109	397	14	103	22
103067	1090	81	495	20	134	25
103068	399	38	97	9	161	39
103069	323	53	105	12	226	33

Sample#	Ba (ppm)	Rb (ppm)	Sr (ppm)	Nb (ppm)	Zr (ppm)	Y (ppm)
103070	193	20	100	7	68	32
103071	780	90	451	15	95	22
103072	706	73	110	11	130	30
103073	340	83	1290	13	111	24
103074	1230	80	99	9	120	26
103075	343	78	1030	13	96	22
103076	212	44	1420	6	67	8
103077	1030	94	456	13	96	26
103078	2310	80	140	12	122	33
103079	278	66	1310	12	101	21
103080	483	92	358	22	252	36
103081	509	157	181	14	144	34
103082	469	153	143	17	120	33
103083	579	84	91	12	122	31
103084	153	30	118	14	79	15
103085	203	94	409	15	98	28
103086	84	8	85	5	75	28
103087	1010	33	265	7	105	43
103090	317	159	106	17	119	32
103091	257	37	97	13	122	35
103092	2700	66	148	50	204	24
103094	383	28	76	13	130	31
103095	1410	135	321	17	126	26
103096	319	43	111	16	127	27
103097	2140	62	86	12	116	29
103098	337	5	56	5	48	25
103099	861	97	170	19	467	42
103100	1010	116	157	24	299	37
103101	931	109	168	14	353	39
103102	266	57	1610	9	88	16
103103	185	47	1460	8	76	11
103104	731	98	368	14	244	32
103120	456	133	148	11	181	35
103121	312	61	1080	12	91	18
103122	332	88	117	13	95	17
103123	246	79	726	10	93	23
103124	819	109	222	13	131	27
103125	97	7	89	6	62	35
103126	185	69	364	4	71	20
103127	318	77	1110	10	106	17
103128	543	133	175	15	206	34
103129	826	109	196	19	122	24
103130	433	114	349	19	128	27
103131	222	12	56	4	48	19
103132	944	78	151	11	116	24
103133	872	24	107	10	134	30
103134	176	83	147	13	109	10
103135	237	94	251	16	121	14
103136	398	96	371	15	187	20
103137	188	54	1550	15	130	1

## Appendix 2

### Estimates of analytical precision of the geochemical analyses performed at Chemex Laboratories Ltd.

Samples, included in the Goldstream data set, were analyzed by Chemex Laboratories Ltd. in North Vancouver, BC. Analytical errors are estimated by replicate analyses of internal MDRU standards (Table 1). Seven internal MDRU standards were used: ALB-1 (Ajax albitite), CHI-1 (Chilliwack Limestone), CUL-1 (Cultus Lake Shale), MBX-1 (MBX stock, Afton), P-1 (Porteau Cove granodiorite), QUA-1 (Quadra Island sandstone) and WP-1 (Watts Point Dacite). Each of the standards was submitted four times, in random order, in the same batch as the actual samples. The analytical results and statistical values are provided in table A2.1. Analytical errors were graphically estimated using a modified weighed Thompson-Howarth (Thompson and Howarth, 1978) replicate error analysis (Figs. A2.1 through A2.11). A dedicated computer code (Stanley, 1997b) was used for the graphical estimation. Analytical errors (precision) are expressed (Figs. A2.1 through A2.11) as the sum of an absolute error term (Y-intercept) and a relative error term (slope).

The concentrations of Cr, Rb, Y and Nb are close to, or below the detection limit of the analytical method. Their analyses, as well as those for Mn,  $\text{H}_2\text{O}^{(+)}$ ,  $\text{H}_2\text{O}^{(-)}$  and T.O.C., have very high relative standard deviations (Table A2.1) and, therefore, are of low precision. The analyses of most of the major elements are of high precision, having relative standard deviations within 1% (Table A2.1). Ti and P were analyzed with acceptable precision (relative standard deviation within a few percent, Table A2.1), given their lower concentrations in the samples and in the internal standards.

To address concerns about errors introduced during sample preparation, pulp duplicates were included randomly in the analytical batch. Precision of these analyses (Table A2.3) is similar to that of the internal standards and confirms the conclusion that, with the exception of the elements mentioned above, the analytical quality is satisfactory.

No quality control data were available for the data donated by T. Hoy and J. Logan. The data were assumed to be compatible with the main data set because the analytical sums are sufficiently close to 100% and because no unusual dispersion of the data was noticed in comparison to the data obtained specifically for this study.

In accordance with the practice established for the Lithogeochemical Exploration Research Project (Sinclair and Stanley, 1995), an additional measure of the analytical precision is provided by a comparison of the author's analytical results with the accepted values of element concentrations in the internal (MDRU) standards as reported by Stanley (1997a). A database of replicate analyses of the standards was accumulated as a result of an initial round-robin "accepted value determinations at three reputable Canadian laboratories: (1) Bondar-Clegg and Co. Ltd., North Vancouver, B.C.; (2) Chemex Laboratories Ltd., North Vancouver, B.C.; and, (3) X-ray Assay Laboratories Ltd., Don Mills, Ontario. Following the initial determination, the standards were submitted with every analytical batch of project research samples. These data are summarized in Table A2.2.

## References

Sinclair, A.J. and Stanley, C.R., (1995) Lithogeochemical Exploration for Metasomatic Alteration Zones Associated with Hydrothermal Mineral Deposits: University of British Columbia, MDRU Research Proposal, 7 p.

Stanley, C.R., (1997a) Analytical Quality Control and Assessment for the MDRU Lithogeochemical Exploration Research Project. Lithogeochemical Exploration for Metasomatic Zones Associated with Hydrothermal Mineral Deposits. Annual Technical Report, Years 1 and 2. Mineral Deposits Research Unit, Department of Geological Sciences, The University of British Columbia, Vancouver, B.C., 32 p.

Stanley, C.R., (1997b) THPLOT.MATLAB Function to Implement Generalized Thompson-Howarth Error Analysis Using Replicate Data. Lithogeochemical Exploration for Metasomatic Zones Associated with Hydrothermal Mineral Deposits. Annual Technical Report, Years 1 and 2. Mineral Deposits Research Unit, Department of Geological Sciences, The University of British Columbia, Vancouver, B.C., 51 p.

Thompson, M., and Howarth, R.J., (1978) A New Approach to the Estimation of Analytical Precision. *Journal of Geochemical Exploration*, 9, pp. 23-30.

**Table A2.1. Replicate analyses and precision of internal (MDRU) reference materials analyzed by Chemex labs with Goldstream samples**

STD = Standard deviation, RSTD% = Relative standard deviation in percent, P = precision

Internal standard	Al <sub>2</sub> O <sub>3</sub>	CaO	Cr <sub>2</sub> O <sub>3</sub>	Fe(tot)	K <sub>2</sub> O	MgO	MnO	Na <sub>2</sub> O	P <sub>2</sub> O <sub>5</sub>	SiO <sub>2</sub>	TiO <sub>2</sub>	LOI	TOTAL
	%	%	%	%	%	%	%	%	%	%	%	%	
ALB-1	18.32	10.03	0.01	1.62	0.88	2.79	0.03	5.74	0.26	54.92	0.61	3.59	98.80
ALB-1	18.52	10.06	0.01	1.64	0.87	2.79	0.03	5.73	0.27	55.18	0.60	3.61	99.31
ALB-1	18.38	10.01	<0.01	1.63	0.89	2.76	0.03	5.75	0.26	54.93	0.61	3.59	98.84
ALB-1	18.39	9.98	0.01	1.63	0.88	2.79	0.03	5.72	0.28	55.08	0.61	3.42	98.82
Mean	<b>18.40</b>	<b>10.02</b>	<b>0.01</b>	<b>1.63</b>	<b>0.88</b>	<b>2.78</b>	<b>0.03</b>	<b>5.74</b>	<b>0.27</b>	<b>55.03</b>	<b>0.61</b>	<b>3.55</b>	<b>98.94</b>
STD	<b>0.08</b>	<b>0.03</b>	<b>0.00</b>	<b>0.01</b>	<b>0.01</b>	<b>0.02</b>	<b>0.00</b>	<b>0.01</b>	<b>0.01</b>	<b>0.13</b>	<b>0.01</b>	<b>0.09</b>	<b>0.25</b>
RSTD(%)	<b>0.46</b>	<b>0.34</b>	<b>0.00</b>	<b>0.50</b>	<b>0.93</b>	<b>0.54</b>	<b>0.00</b>	<b>0.23</b>	<b>3.58</b>	<b>0.23</b>	<b>0.82</b>	<b>2.50</b>	<b>0.25</b>
P	<b>0.92</b>	<b>0.67</b>	<b>0.00</b>	<b>1.00</b>	<b>1.86</b>	<b>1.08</b>	<b>0.00</b>	<b>0.45</b>	<b>7.16</b>	<b>0.46</b>	<b>1.65</b>	<b>5.00</b>	<b>0.50</b>
CHI-1	1.29	37.77	0.02	1.01	0.12	4.73	0.03	0.07	0.07	21.73	0.12	31.76	98.72
CHI-1	1.29	37.75	0.01	1.02	0.12	4.75	0.03	0.08	0.07	21.65	0.12	31.63	98.52
CHI-1	1.30	37.72	0.02	1.01	0.12	4.77	0.03	0.09	0.07	21.80	0.12	31.74	98.79
CHI-1	1.28	37.61	0.01	1.01	0.12	4.72	0.03	0.08	0.08	21.64	0.13	32.60	99.31
Mean	<b>1.29</b>	<b>37.71</b>	<b>0.02</b>	<b>1.01</b>	<b>0.12</b>	<b>4.74</b>	<b>0.03</b>	<b>0.08</b>	<b>0.07</b>	<b>21.71</b>	<b>0.12</b>	<b>31.93</b>	<b>98.84</b>
STD	<b>0.01</b>	<b>0.07</b>	<b>0.01</b>	<b>0.01</b>	<b>0.00</b>	<b>0.02</b>	<b>0.00</b>	<b>0.01</b>	<b>0.00</b>	<b>0.08</b>	<b>0.01</b>	<b>0.45</b>	<b>0.34</b>
RSTD(%)	<b>0.63</b>	<b>0.19</b>	<b>38.49</b>	<b>0.49</b>	<b>0.00</b>	<b>0.47</b>	<b>0.00</b>	<b>10.21</b>	<b>6.90</b>	<b>0.35</b>	<b>4.08</b>	<b>1.41</b>	<b>0.34</b>
P	<b>1.27</b>	<b>0.38</b>	<b>76.98</b>	<b>0.99</b>	<b>0.00</b>	<b>0.94</b>	<b>0.00</b>	<b>20.41</b>	<b>13.79</b>	<b>0.69</b>	<b>8.16</b>	<b>2.81</b>	<b>0.68</b>
CUL-1	13.91	6.78	0.01	9.91	0.77	2.07	0.14	2.51	0.15	51.60	0.89	10.33	99.07
CUL-1	13.88	6.78	0.02	9.83	0.78	2.06	0.14	2.51	0.15	51.73	0.89	10.41	99.18
CUL-1	13.89	6.75	0.01	9.86	0.79	2.07	0.14	2.50	0.15	51.68	0.89	10.25	98.98
CUL-1	14.03	6.84	0.01	9.89	0.77	2.06	0.14	2.49	0.15	51.96	0.89	9.88	99.11
Mean	<b>13.93</b>	<b>6.79</b>	<b>0.01</b>	<b>9.87</b>	<b>0.78</b>	<b>2.07</b>	<b>0.14</b>	<b>2.50</b>	<b>0.15</b>	<b>51.74</b>	<b>0.89</b>	<b>10.22</b>	<b>99.09</b>
STD	<b>0.07</b>	<b>0.04</b>	<b>0.01</b>	<b>0.03</b>	<b>0.01</b>	<b>0.01</b>	<b>0.00</b>	<b>0.01</b>	<b>0.00</b>	<b>0.15</b>	<b>0.00</b>	<b>0.23</b>	<b>0.08</b>
RSTD(%)	<b>0.50</b>	<b>0.56</b>	<b>40.00</b>	<b>0.35</b>	<b>1.23</b>	<b>0.28</b>	<b>0.00</b>	<b>0.38</b>	<b>0.00</b>	<b>0.30</b>	<b>0.00</b>	<b>2.29</b>	<b>0.08</b>
P	<b>1.00</b>	<b>1.11</b>	<b>80.00</b>	<b>0.71</b>	<b>2.46</b>	<b>0.56</b>	<b>0.00</b>	<b>0.77</b>	<b>0.00</b>	<b>0.60</b>	<b>0.00</b>	<b>4.59</b>	<b>0.17</b>
MBX-1	17.11	3.73	0.02	4.02	5.01	2.10	0.07	5.20	0.23	57.07	0.48	3.94	98.98
MBX-1	16.99	3.74	0.02	4.00	4.91	2.10	0.07	5.20	0.23	57.04	0.47	3.98	98.75
MBX-1	17.12	3.74	0.01	3.97	5.00	2.11	0.07	5.28	0.23	57.63	0.49	3.99	99.64
MBX-1	17.28	3.79	0.01	3.99	4.98	2.03	0.07	5.21	0.23	57.79	0.48	3.81	99.67
Mean	<b>17.13</b>	<b>3.75</b>	<b>0.02</b>	<b>4.00</b>	<b>4.98</b>	<b>2.09</b>	<b>0.07</b>	<b>5.22</b>	<b>0.23</b>	<b>57.38</b>	<b>0.48</b>	<b>3.93</b>	<b>99.26</b>
STD	<b>0.12</b>	<b>0.03</b>	<b>0.01</b>	<b>0.02</b>	<b>0.05</b>	<b>0.04</b>	<b>0.00</b>	<b>0.04</b>	<b>0.00</b>	<b>0.38</b>	<b>0.01</b>	<b>0.08</b>	<b>0.47</b>
RSTD(%)	<b>0.70</b>	<b>0.72</b>	<b>38.49</b>	<b>0.52</b>	<b>0.91</b>	<b>1.77</b>	<b>0.00</b>	<b>0.74</b>	<b>0.00</b>	<b>0.67</b>	<b>1.70</b>	<b>2.11</b>	<b>0.47</b>
P	<b>1.39</b>	<b>1.44</b>	<b>76.98</b>	<b>1.04</b>	<b>1.81</b>	<b>3.55</b>	<b>0.00</b>	<b>1.48</b>	<b>0.00</b>	<b>1.34</b>	<b>3.40</b>	<b>4.22</b>	<b>0.94</b>

Internal	Al <sub>2</sub> O <sub>3</sub>	CaO	Cr <sub>2</sub> O <sub>3</sub>	Fe(tot)	K <sub>2</sub> O	MgO	MnO	Na <sub>2</sub> O	P <sub>2</sub> O <sub>5</sub>	SiO <sub>2</sub>	TiO <sub>2</sub>	LOI	TOTAL
standard	%	%	%	%	%	%	%	%	%	%	%	%	
P-1	13.91	3.44	0.02	3.81	2.21	1.12	0.07	3.78	0.08	69.64	0.39	0.42	98.89
P-1	13.84	3.45	0.02	3.81	2.20	1.10	0.07	3.82	0.07	69.58	0.39	0.43	98.78
P-1	13.78	3.49	0.02	3.84	2.19	1.12	0.07	3.79	0.08	69.91	0.38	0.45	99.12
P-1	13.94	3.46	0.02	3.80	2.18	1.12	0.07	3.79	0.07	69.59	0.38	0.42	98.84
Mean	<b>13.87</b>	<b>3.46</b>	<b>0.02</b>	<b>3.82</b>	<b>2.20</b>	<b>1.12</b>	<b>0.07</b>	<b>3.80</b>	<b>0.08</b>	<b>69.68</b>	<b>0.39</b>	<b>0.43</b>	<b>98.91</b>
STD	<b>0.07</b>	<b>0.02</b>	<b>0.00</b>	<b>0.02</b>	<b>0.01</b>	<b>0.01</b>	<b>0.00</b>	<b>0.02</b>	<b>0.01</b>	<b>0.16</b>	<b>0.01</b>	<b>0.01</b>	<b>0.15</b>
RSTD(%)	<b>0.52</b>	<b>0.62</b>	<b>0.00</b>	<b>0.45</b>	<b>0.59</b>	<b>0.90</b>	<b>0.00</b>	<b>0.46</b>	<b>7.70</b>	<b>0.22</b>	<b>1.50</b>	<b>3.29</b>	<b>0.15</b>
P	<b>1.04</b>	<b>1.25</b>	<b>0.00</b>	<b>0.91</b>	<b>1.18</b>	<b>1.79</b>	<b>0.00</b>	<b>0.91</b>	<b>15.40</b>	<b>0.45</b>	<b>3.00</b>	<b>6.58</b>	<b>0.30</b>
QUA-1	15.17	4.09	0.02	4.45	1.49	2.54	0.08	4.04	0.13	65.58	0.46	1.39	99.44
QUA-1	15.00	4.10	0.03	4.50	1.49	2.54	0.08	4.02	0.13	65.45	0.46	1.40	99.20
QUA-1	14.98	4.09	0.02	4.44	1.50	2.54	0.08	4.09	0.12	65.34	0.47	1.41	99.08
QUA-1	15.20	4.10	0.01	4.44	1.50	2.50	0.08	4.09	0.13	65.77	0.46	1.34	99.61
Mean	<b>15.09</b>	<b>4.10</b>	<b>0.02</b>	<b>4.46</b>	<b>1.50</b>	<b>2.53</b>	<b>0.08</b>	<b>4.06</b>	<b>0.13</b>	<b>65.54</b>	<b>0.46</b>	<b>1.39</b>	<b>99.33</b>
STD	<b>0.11</b>	<b>0.01</b>	<b>0.01</b>	<b>0.03</b>	<b>0.01</b>	<b>0.02</b>	<b>0.00</b>	<b>0.04</b>	<b>0.01</b>	<b>0.18</b>	<b>0.00</b>	<b>0.03</b>	<b>0.24</b>
RSTD(%)	<b>0.75</b>	<b>0.14</b>	<b>54.97</b>	<b>0.64</b>	<b>0.39</b>	<b>0.79</b>	<b>0.00</b>	<b>0.88</b>	<b>3.92</b>	<b>0.28</b>	<b>1.08</b>	<b>2.24</b>	<b>0.24</b>
P	<b>1.51</b>	<b>0.28</b>	<b>109.95</b>	<b>1.29</b>	<b>0.77</b>	<b>1.58</b>	<b>0.00</b>	<b>1.75</b>	<b>7.84</b>	<b>0.56</b>	<b>2.16</b>	<b>4.49</b>	<b>0.48</b>
WP-1	16.19	5.00	0.02	4.45	1.66	2.67	0.08	4.27	0.16	63.86	0.51	0.10	98.97
WP-1	16.20	5.00	0.02	4.43	1.67	2.68	0.07	4.28	0.17	64.02	0.50	0.14	99.18
WP-1	16.27	4.98	0.01	4.41	1.67	2.67	0.07	4.31	0.17	64.03	0.50	0.14	99.23
WP-1	16.21	4.92	0.01	4.39	1.69	2.69	0.08	4.33	0.16	63.92	0.51	0.13	99.04
Mean	<b>16.22</b>	<b>4.98</b>	<b>0.02</b>	<b>4.42</b>	<b>1.67</b>	<b>2.68</b>	<b>0.08</b>	<b>4.30</b>	<b>0.17</b>	<b>63.96</b>	<b>0.51</b>	<b>0.13</b>	<b>99.11</b>
STD	<b>0.04</b>	<b>0.04</b>	<b>0.01</b>	<b>0.03</b>	<b>0.01</b>	<b>0.01</b>	<b>0.01</b>	<b>0.03</b>	<b>0.01</b>	<b>0.08</b>	<b>0.01</b>	<b>0.02</b>	<b>0.12</b>
RSTD(%)	<b>0.22</b>	<b>0.76</b>	<b>38.49</b>	<b>0.58</b>	<b>0.75</b>	<b>0.36</b>	<b>7.70</b>	<b>0.64</b>	<b>3.50</b>	<b>0.13</b>	<b>1.14</b>	<b>14.85</b>	<b>0.12</b>
P	<b>0.44</b>	<b>1.52</b>	<b>76.98</b>	<b>1.17</b>	<b>1.50</b>	<b>0.72</b>	<b>15.40</b>	<b>1.28</b>	<b>7.00</b>	<b>0.26</b>	<b>2.29</b>	<b>29.69</b>	<b>0.24</b>



Internal	Ba	Rb	Sr	Nb	Zr	Y	H <sub>2</sub> O(+)	H <sub>2</sub> O(-)	CO <sub>2</sub>	T.O.C.	FeO	S
standard	ppm	ppm	ppm	ppm	ppm	ppm	%	%	%	%	%	%
ALB-1	250	22	702	2	69	20	1.38	0.41	1.1	0.15	1.05	0.23
ALB-1	255	20	704	2	66	22	1.07	0.27	1.3	0.1	1.16	0.22
ALB-1	250	22	706	2	66	22	1.19	0.32	1.2	0.1	1.25	0.21
ALB-1	255	20	702	4	66	20	1.47	0.4	1.3	0.1	1.22	0.23
Mean	<b>252.5</b>	<b>21</b>	<b>703.5</b>	<b>2.5</b>	<b>66.75</b>	<b>21</b>	<b>1.2775</b>	<b>0.35</b>	<b>1.225</b>	<b>0.1125</b>	<b>1.17</b>	<b>0.223</b>
STD	<b>2.89</b>	<b>1.15</b>	<b>1.91</b>	<b>1.00</b>	<b>1.50</b>	<b>1.15</b>	<b>0.18</b>	<b>0.07</b>	<b>0.10</b>	<b>0.03</b>	<b>0.09</b>	<b>0.01</b>
RSTD(%)	<b>1.14</b>	<b>5.50</b>	<b>0.27</b>	<b>40.00</b>	<b>2.25</b>	<b>5.50</b>	<b>14.17</b>	<b>19.10</b>	<b>7.82</b>	<b>22.22</b>	<b>7.55</b>	<b>4.30</b>
P	<b>3.33</b>	<b>1.33</b>	<b>2.21</b>	<b>1.15</b>	<b>1.73</b>	<b>1.33</b>	<b>0.21</b>	<b>0.08</b>	<b>0.11</b>	<b>0.03</b>	<b>0.10</b>	<b>0.01</b>
CHI-1	35	4	154	2	27	18	0.46	0.38	29.5	1.4	0.09	0.55
CHI-1	40	4	150	2	24	18	0.44	0.32	30.2	1.2	0.16	0.55
CHI-1	40	4	150	2	24	18	0.53	0.43	29.3	1.4	0.18	0.53
CHI-1	40	4	152	2	24	16	0.3	0.33	30.2	1.15	0.11	0.54
Mean	<b>38.75</b>	<b>4</b>	<b>151.5</b>	<b>2</b>	<b>24.75</b>	<b>17.5</b>	<b>0.4325</b>	<b>0.365</b>	<b>29.8</b>	<b>1.2875</b>	<b>0.135</b>	<b>0.543</b>
STD	<b>2.50</b>	<b>0.00</b>	<b>1.91</b>	<b>0.00</b>	<b>1.50</b>	<b>1.00</b>	<b>0.10</b>	<b>0.05</b>	<b>0.47</b>	<b>0.13</b>	<b>0.04</b>	<b>0.01</b>
RSTD(%)	<b>6.45</b>	<b>0.00</b>	<b>1.26</b>	<b>0.00</b>	<b>6.06</b>	<b>5.71</b>	<b>22.29</b>	<b>13.88</b>	<b>1.57</b>	<b>10.21</b>	<b>31.13</b>	<b>1.76</b>
P	<b>12.90</b>	<b>0.00</b>	<b>2.53</b>	<b>0.00</b>	<b>12.12</b>	<b>11.43</b>	<b>44.57</b>	<b>27.76</b>	<b>3.15</b>	<b>20.43</b>	<b>62.27</b>	<b>3.53</b>
CUL-1	655	14	244	<2	54	18	4.2	1.44	3.8	1.2	5.09	2.1
CUL-1	655	16	244	2	54	18	4.01	1.22	3.8	1.2	4.94	2.1
CUL-1	650	16	246	<2	51	18	4.87	1.56	3.7	1.25	4.89	2.09
CUL-1	655	14	246	2	54	20	4.1	1.33	3.8	1.25	4.86	2.09
Mean	<b>653.8</b>	<b>15</b>	<b>245</b>	<b>2</b>	<b>53.25</b>	<b>18.5</b>	<b>4.295</b>	<b>1.388</b>	<b>3.775</b>	<b>1.225</b>	<b>4.945</b>	<b>2.095</b>
STD	<b>2.50</b>	<b>1.15</b>	<b>1.15</b>	<b>0.00</b>	<b>1.50</b>	<b>1.00</b>	<b>0.39</b>	<b>0.15</b>	<b>0.05</b>	<b>0.03</b>	<b>0.10</b>	<b>0.01</b>
RSTD(%)	<b>0.38</b>	<b>7.70</b>	<b>0.47</b>	<b>0.00</b>	<b>2.82</b>	<b>5.41</b>	<b>9.11</b>	<b>10.52</b>	<b>1.32</b>	<b>2.36</b>	<b>2.07</b>	<b>0.28</b>
P	<b>0.76</b>	<b>15.40</b>	<b>0.94</b>	<b>0.00</b>	<b>5.63</b>	<b>10.81</b>	<b>18.21</b>	<b>21.03</b>	<b>2.65</b>	<b>4.71</b>	<b>4.13</b>	<b>0.55</b>
MBX-1	705	84	482	12	96	18	0.78	0.2	2.2	0.2	1.84	0.22
MBX-1	700	84	478	12	99	18	0.67	0.11	2.2	0.2	1.69	0.22
MBX-1	705	80	480	12	99	18	1.31	0.19	2.3	0.2	1.81	0.23
MBX-1	695	82	478	12	99	16	1.28	0.2	2.2	0.2	1.84	0.24
Mean	<b>701.3</b>	<b>82.5</b>	<b>479.5</b>	<b>12</b>	<b>98.25</b>	<b>17.5</b>	<b>1.01</b>	<b>0.175</b>	<b>2.225</b>	<b>0.2</b>	<b>1.795</b>	<b>0.228</b>
STD	<b>4.79</b>	<b>1.91</b>	<b>1.91</b>	<b>0.00</b>	<b>1.50</b>	<b>1.00</b>	<b>0.33</b>	<b>0.04</b>	<b>0.05</b>	<b>0.00</b>	<b>0.07</b>	<b>0.01</b>
RSTD(%)	<b>0.68</b>	<b>2.32</b>	<b>0.40</b>	<b>0.00</b>	<b>1.53</b>	<b>5.71</b>	<b>32.91</b>	<b>24.91</b>	<b>2.25</b>	<b>0.00</b>	<b>3.98</b>	<b>4.21</b>
P	<b>1.37</b>	<b>4.64</b>	<b>0.80</b>	<b>0.00</b>	<b>3.05</b>	<b>11.43</b>	<b>65.81</b>	<b>49.82</b>	<b>4.49</b>	<b>0.00</b>	<b>7.96</b>	<b>8.42</b>

Internal	Ba	Rb	Sr	Nb	Zr	Y	H <sub>2</sub> O(+)	H <sub>2</sub> O(-)	CO <sub>2</sub>	T.O.C.	FeO	S
standard	ppm	ppm	ppm	ppm	ppm	ppm	%	%	%	%	%	%
P-1	770	52	208	2	123	20	0.25	0.12	0.1	0.01	1.85	<0.01
P-1	765	52	210	2	123	20	0.1	0.05	0.1	0.01	1.82	<0.01
P-1	760	48	210	4	123	22	0.3	0.08	0.1	0.01	1.82	<0.01
P-1	760	48	206	2	126	22	0.51	0.12	0.1	0.01	1.83	<0.01
Mean	<b>763.8</b>	<b>50</b>	<b>208.5</b>	<b>2.5</b>	<b>123.8</b>	<b>21</b>	<b>0.29</b>	<b>0.093</b>	<b>0.1</b>	<b>0.01</b>	<b>1.83</b>	<b>0.005</b>
STD	<b>4.79</b>	<b>2.31</b>	<b>1.91</b>	<b>1.00</b>	<b>1.50</b>	<b>1.15</b>	<b>0.17</b>	<b>0.03</b>	<b>0.00</b>	<b>0.00</b>	<b>0.01</b>	<b>0.00</b>
RSTD(%)	<b>0.63</b>	<b>4.62</b>	<b>0.92</b>	<b>40.00</b>	<b>1.21</b>	<b>5.50</b>	<b>58.45</b>	<b>36.79</b>	<b>0.00</b>	<b>0.00</b>	<b>0.77</b>	<b>0.00</b>
P	<b>1.25</b>	<b>9.24</b>	<b>1.84</b>	<b>80.00</b>	<b>2.42</b>	<b>11.00</b>	<b>116.90</b>	<b>73.59</b>	<b>0.00</b>	<b>0.00</b>	<b>1.55</b>	<b>0.00</b>
QUA-1	710	28	602	6	102	14	0.81	0.37	0.1	0.05	1.37	0.06
QUA-1	715	26	598	6	102	14	0.77	0.36	0.1	0.01	1.5	0.06
QUA-1	720	26	600	6	102	14	0.82	0.41	0.1	0.05	1.56	0.06
QUA-1	720	26	596	6	99	14	0.78	0.42	0.1	0.1	1.68	0.06
Mean	<b>716.3</b>	<b>26.5</b>	<b>599</b>	<b>6</b>	<b>101.3</b>	<b>14</b>	<b>0.795</b>	<b>0.39</b>	<b>0.1</b>	<b>0.0525</b>	<b>1.528</b>	<b>0.06</b>
STD	<b>4.79</b>	<b>1.00</b>	<b>2.58</b>	<b>0.00</b>	<b>1.50</b>	<b>0.00</b>	<b>0.02</b>	<b>0.03</b>	<b>0.00</b>	<b>0.04</b>	<b>0.13</b>	<b>0.00</b>
RSTD(%)	<b>0.67</b>	<b>3.77</b>	<b>0.43</b>	<b>0.00</b>	<b>1.48</b>	<b>0.00</b>	<b>2.99</b>	<b>7.55</b>	<b>0.00</b>	<b>70.20</b>	<b>8.44</b>	<b>0.00</b>
P	<b>1.34</b>	<b>7.55</b>	<b>0.86</b>	<b>0.00</b>	<b>2.96</b>	<b>0.00</b>	<b>5.99</b>	<b>15.10</b>	<b>0.00</b>	<b>140.40</b>	<b>16.88</b>	<b>0.00</b>
WP-1	650	26	700	4	126	16	0.07	0.1	0.1	0.01	2.21	<0.01
WP-1	650	24	700	4	126	14	0.12	0.07	0.1	0.01	2.19	<0.01
WP-1	655	24	706	4	126	14	0.07	0.06	0.1	0.01	2.15	<0.01
WP-1	645	26	706	4	126	14	0.19	0.13	0.1	0.01	2.21	<0.01
Mean	<b>650</b>	<b>25</b>	<b>703</b>	<b>4</b>	<b>126</b>	<b>14.5</b>	<b>0.1125</b>	<b>0.09</b>	<b>0.1</b>	<b>0.01</b>	<b>2.19</b>	<b>0.005</b>
STD	<b>4.08</b>	<b>1.15</b>	<b>3.46</b>	<b>0.00</b>	<b>0.00</b>	<b>1.00</b>	<b>0.06</b>	<b>0.03</b>	<b>0.00</b>	<b>0.00</b>	<b>0.03</b>	<b>0.00</b>
RSTD(%)	<b>0.63</b>	<b>4.62</b>	<b>0.49</b>	<b>0.00</b>	<b>0.00</b>	<b>6.90</b>	<b>50.48</b>	<b>35.14</b>	<b>0.00</b>	<b>0.00</b>	<b>1.29</b>	<b>0.00</b>
P	<b>1.26</b>	<b>9.24</b>	<b>0.99</b>	<b>0.00</b>	<b>0.00</b>	<b>13.79</b>	<b>100.96</b>	<b>70.27</b>	<b>0.00</b>	<b>0.00</b>	<b>2.58</b>	<b>0.00</b>

**Table A2.2. Precision (relative error) of accepted values for internal  
(MDRU) reference materials, analyzed by Chemex**

Internal standard	Al <sub>2</sub> O <sub>3</sub> %	CaO %	Cr <sub>2</sub> O <sub>3</sub> %	Fe <sub>2</sub> O <sub>3</sub> %	K <sub>2</sub> O %	MgO %	MnO %	Na <sub>2</sub> O %	P <sub>2</sub> O <sub>5</sub> %	SiO <sub>2</sub> %	TiO <sub>2</sub> %
<b>ALB-1</b>											
Mean	18.615	10.362	0.007	1.599	0.863	2.846	0.025	5.959	0.294	55.140	0.613
StdDev	0.269	0.342	0.003	0.029	0.035	0.060	0.005	0.188	0.027	0.324	0.017
RelErr(%)	1.45	3.30	35.90	1.84	4.02	2.09	20.52	3.15	9.30	0.59	2.74
Number	11	11	11	11	11	11	11	11	11	11	11
<b>CHI-1</b>											
Mean	1.282	37.681	0.021	1.013	0.126	4.824	0.033	0.083	0.074	21.715	0.127
StdDev	0.010	0.144	0.009	0.008	0.007	0.076	0.005	0.007	0.005	0.077	0.005
RelErr(%)	0.81	0.38	41.70	0.81	5.55	1.57	14.64	8.13	6.98	0.35	3.80
Number	11	11	11	11	11	11	11	11	11	11	11
<b>CUL-1</b>											
Mean	14.018	6.795	0.014	9.946	0.796	2.073	0.139	2.486	0.149	52.033	0.127
StdDev	0.105	0.043	0.007	0.074	0.014	0.043	0.003	0.032	0.004	0.243	0.005
RelErr(%)	0.75	0.63	52.28	0.74	1.72	2.05	1.79	1.31	2.96	0.47	3.80
Number	16	16	16	16	16	16	16	16	16	16	10
<b>MBX-1</b>											
Mean	17.243	3.889	0.015	3.986	4.893	2.115	0.066	5.348	0.251	57.351	0.900
StdDev	0.269	0.121	0.019	0.064	0.233	0.038	0.005	0.118	0.038	0.570	0.011
RelErr(%)	1.56	3.10	127.37	1.62	4.75	1.79	7.60	2.20	14.96	0.99	1.22
Number	11	11	11	11	11	11	11	11	11	11	16
<b>P-1</b>											
Mean	14.084	3.550	0.017	3.811	2.161	1.124	0.072	3.935	0.091	69.705	0.489
StdDev	0.349	0.093	0.006	0.051	0.102	0.028	0.004	0.116	0.029	0.696	0.014
RelErr(%)	2.47	2.59	37.44	1.34	4.71	2.49	5.63	2.96	32.43	1.00	2.96
Number	11	11	11	11	11	11	11	11	11	11	11
<b>QGRM-100</b>											
Mean	14.767	2.243	0.040	3.777	5.245	1.005	0.033	4.308	0.168	66.815	0.383
StdDev	0.306	0.018	0.017	0.078	0.190	0.048	0.005	0.038	0.037	0.922	0.011
RelErr(%)	2.07	0.78	41.83	2.06	3.62	4.82	15.49	0.87	21.72	1.38	2.88
Number	6	6	6	6	6	6	6	6	6	6	11
<b>QGRM-101</b>											
Mean	15.778	8.712	0.008	14.616	1.066	5.746	0.174	3.196	0.208	48.158	0.490
StdDev	0.094	0.407	0.003	0.070	0.038	0.082	0.005	0.156	0.025	0.690	0.017
RelErr(%)	0.60	4.67	34.23	0.48	3.61	1.42	3.15	4.88	11.97	1.43	3.41
Number	5	5	5	5	5	5	5	5	5	5	6
<b>QUA-1</b>											
Mean	15.124	4.084	0.016	4.434	1.488	2.497	0.080	4.051	0.125	65.558	2.028
StdDev	0.083	0.029	0.007	0.033	0.015	0.047	0.000	0.047	0.005	0.199	0.031
RelErr(%)	0.55	0.72	44.23	0.74	0.99	1.89	0.00	1.15	4.13	0.30	1.54
Number	16	16	16	16	16	16	16	16	16	16	5
<b>WP-1</b>											
Mean	16.444	5.128	0.015	4.403	1.635	2.724	0.074	4.431	0.186	64.342	0.465
StdDev	0.266	0.154	0.013	0.066	0.045	0.047	0.005	0.11	0.029	0.483	0.006
RelErr(%)	1.62	3	82.43	1.5	2.74	1.71	6.85	2.49	15.42	0.75	1.36
Number	11	11	11	11	11	11	11	11	11	11	16

Internal standard	LOI %	Ba ppm	Rb ppm	Sr ppm	Nb ppm	Zr ppm	Y ppm	H <sub>2</sub> O(+) %	CO <sub>2</sub> % C(inorg) %	T.O.C. %	
<b>ALB-1</b>											
Mean	3.425	251.5	21.7	750.5	4.5	70.6	20.7	1.399	1.264		
StdDev	0.129	5.3	1.7	47.1	2.7	4.5	1.3	0.182	0.103		
RelErr(%)	3.78	2.12	7.65	6.28	60.14	6.34	6.14	13.04	8.13		
Number	11	11	9	11	11	11	11	13	11		
<b>CHI-1</b>											
Mean	32.191	39	3	151.6	2.0	24.3	17.2	0.409	31.523	9.083	
StdDev	0.364	3.2	1.1	1.6	0.0	0.9	1	0.081	1.279	0.015	
RelErr(%)	1.13	8.11	35.14	1.04	0.00	3.90	6.00	19.75	4.06	0.17	
Number	10	10	10	10	10	10	10	16	13	3	
<b>CUL-1</b>											
Mean	9.806	648.8	15.6	246	2.1	53.1	19.5	4.03	3.823	1.048	2.073
StdDev	0.442	12.4	1.8	1.9	0.5	1.4	1.4	0.308	0.274	0.049	0.025
RelErr(%)	4.51	1.92	11.66	0.79	23.53	2.71	7.01	7.64	7.18	4.72	1.21
Number	16	16	16	16	16	16	16	22	13	6	3
<b>MBX-1</b>											
Mean	3.831	660	83	496.3	12.3	97.3	16.9	1.080	2.327		
StdDev	0.128	56.3	2.8	18.2	1.2	4.4	1.8	0.262	0.142		
RelErr(%)	3.35	8.53	3.36	3.67	9.70	4.55	10.73	24.25	6.10		
Number	11	11	11	11	11	11	11	15	11		
<b>P-1</b>											
Mean	0.453	726.4	47.8	217.6	5.1	125	20.9	0.345	0.136		
StdDev	0.074	43.4	4.9	8.7	2.6	3.2	1.4	0.188	0.05		
RelErr(%)	16.35	5.98	10.24	3.98	51.56	2.53	6.58	54.55	37.00		
Number	11	11	11	11	11	11	11	15	11		
<b>QGRM-100</b>											
Mean	1.207	869	134.8	464.2	16.7	403.3	47.7	0.473	0.483		
StdDev	0.036	71.2	6	12.9	2.7	25.4	3	0.099	0.133		
RelErr(%)	2.95	8.19	4.44	2.77	15.95	6.31	6.32	20.93	27.50		
Number	6	6	6	6	6	6	6	10	6		
<b>QGRM-101</b>											
Mean	0.142	270.6	30	272	9	141.8	36.6	0.249	0.28		
StdDev	0.121	64.9	3	12	1.2	4.0	7.8	0.131	0.11		
RelErr(%)	85.00	23.98	10.00	4.42	13.61	2.84	21.30	52.58	39.12		
Number	5	5	5	5	5	5	5	9	5		
<b>QUA-1</b>											
Mean	1.339	721.6	25.8	598.3	6.4	101.6	14.6	0.894	0.246	0.050	0.075
StdDev	0.035	9.1	1	3.6	0.8	1.5	1.0	0.107	0.088	0.000	0.021
RelErr(%)	2.64	1.26	3.88	0.61	12.65	1.48	6.55	12.03	35.63	19.11	28.28
Number	16	16	16	16	16	16	16	21	13	6	2
<b>WP-1</b>											
Mean	0.135	614.6	25.4	719.3	5.9	126.1	14.9	0.12	0.136		
StdDev	0.049	35.5	1.4	21	2.1	4.5	1.1	0.052	0.05		
RelErr(%)	36.62	5.77	5.60	2.92	35.06	3.61	7.62	43.30	37.00		
Number	11	11	9	11	11	11	11	15	11		

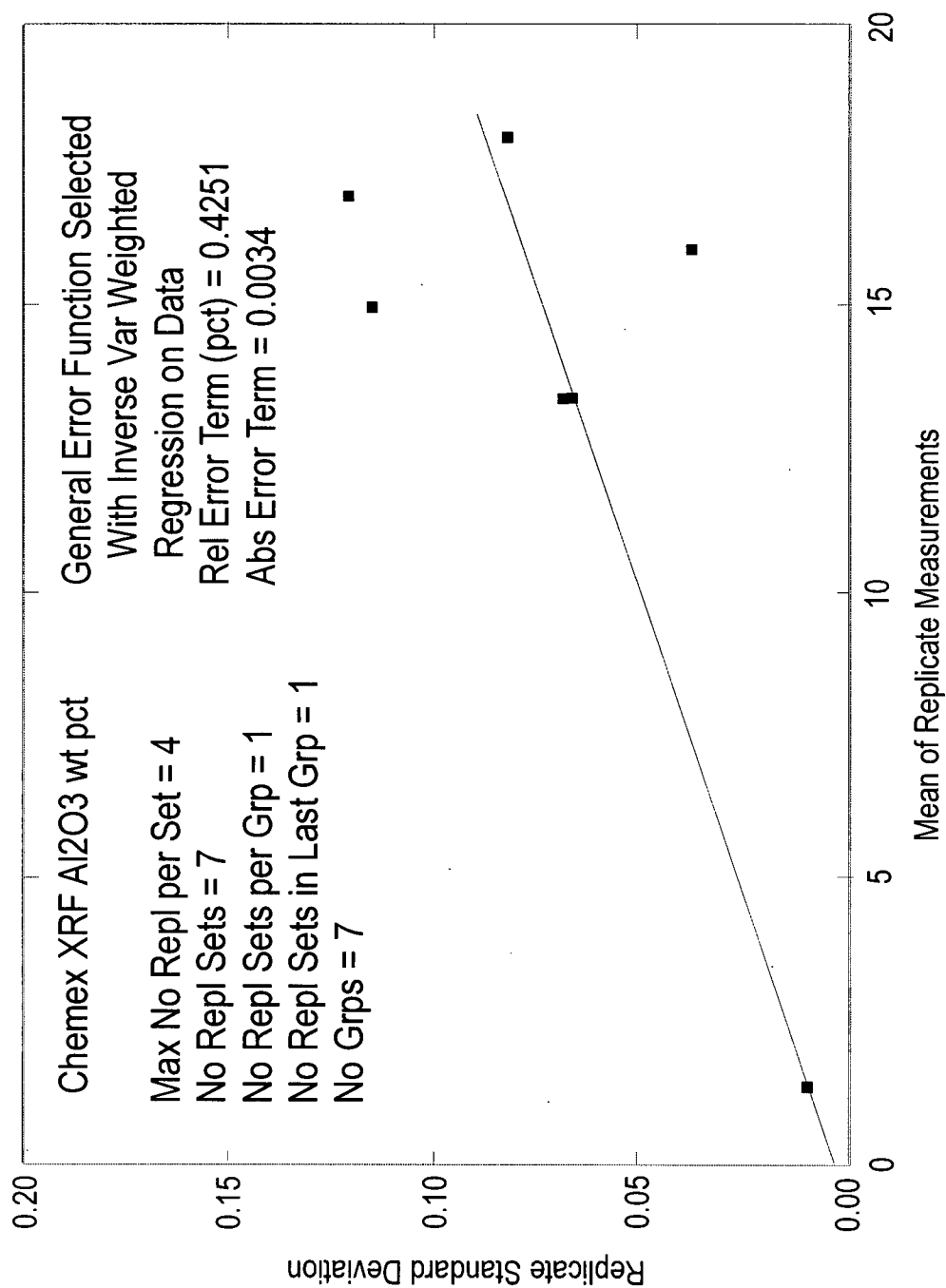


Fig. A2.1. Modified Thompson-Howarth Replicate Error AnalysisF

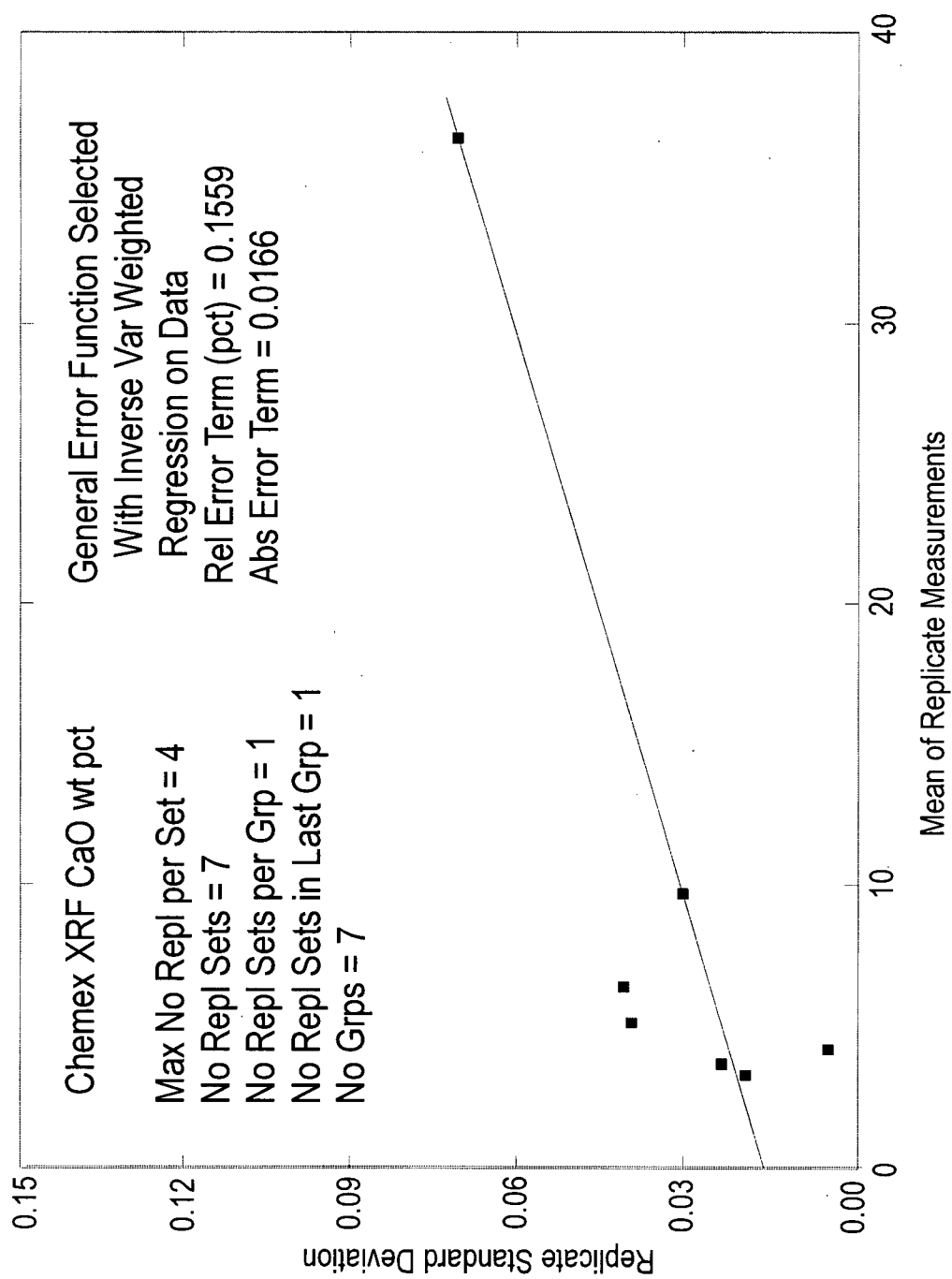


Fig. A2.2. Modified Thompson-Howarth Replicate Error Analysis

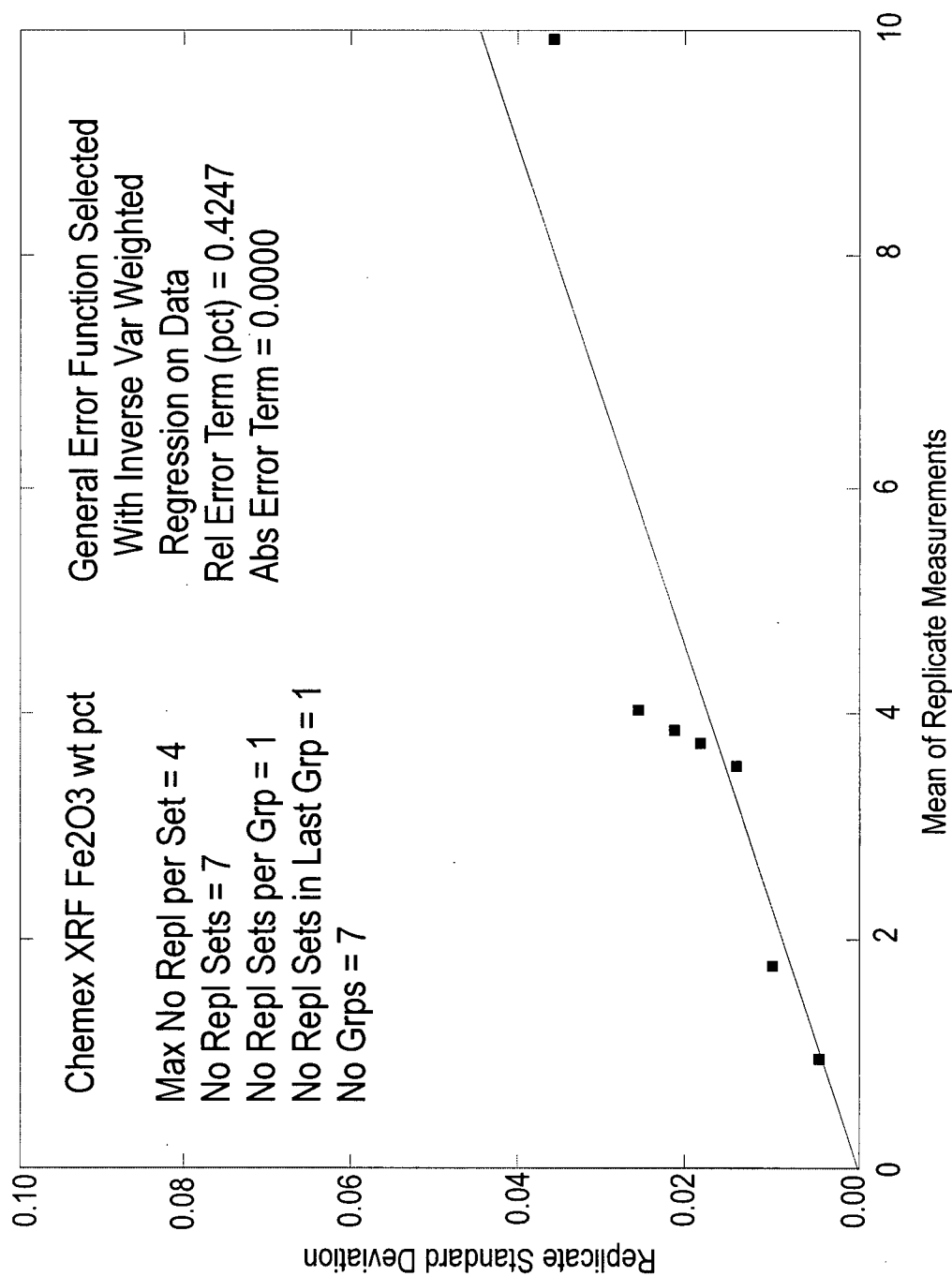


Fig. A2.3. Modified Thompson-Howarth Replicate Error Analysis

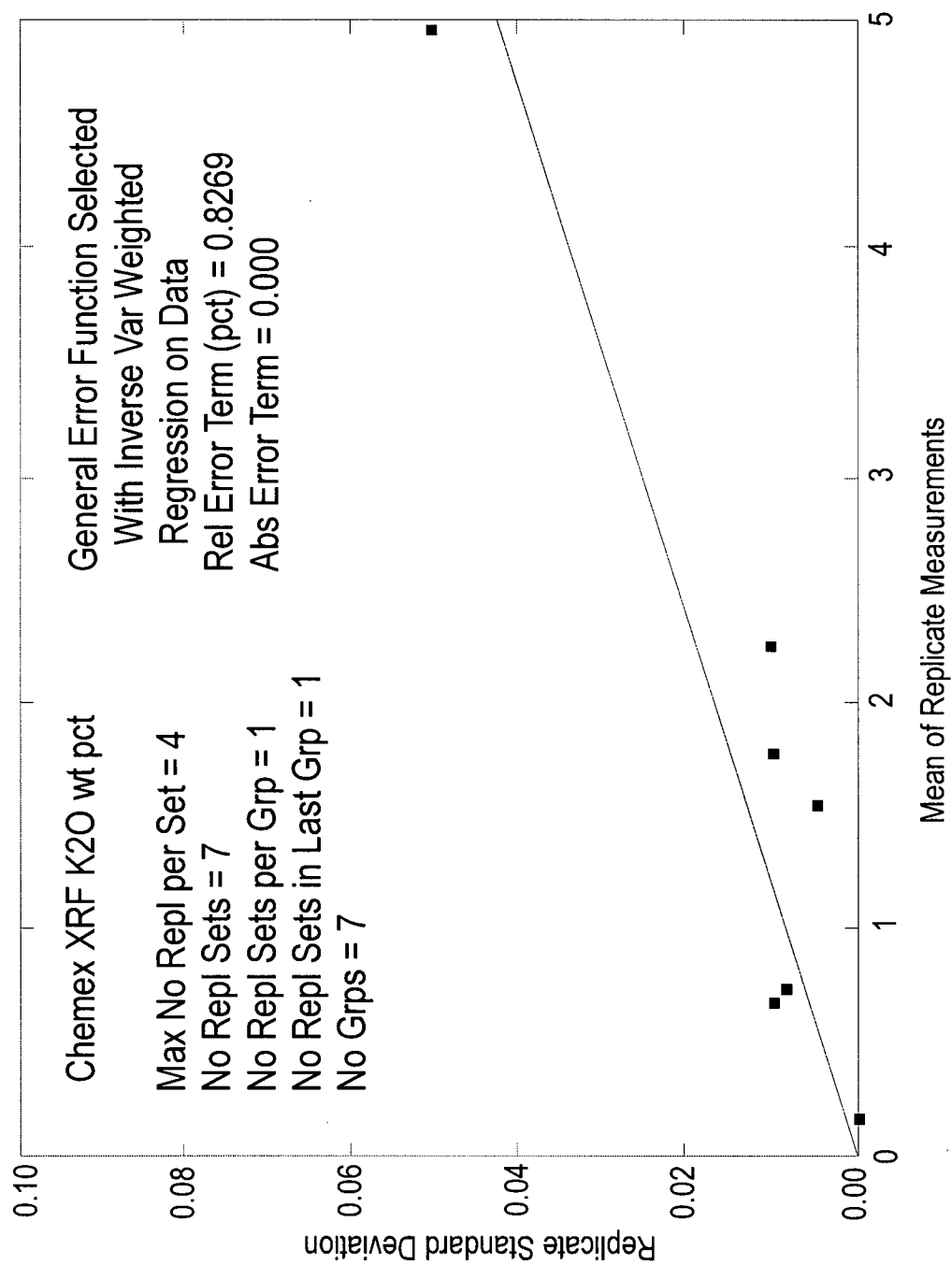


Fig. A2.4. Modified Thompson-Howarth Replicate Error Analysis



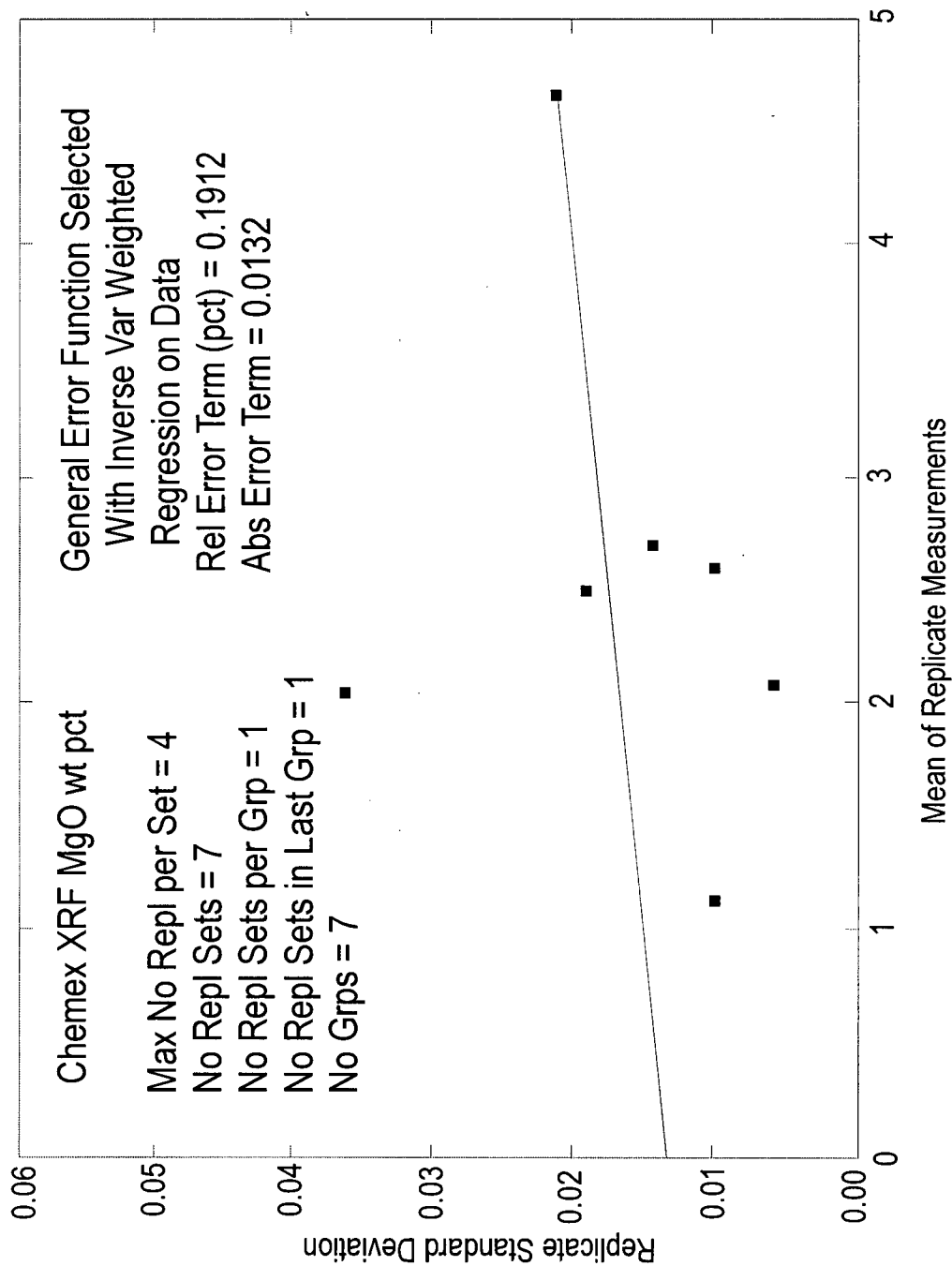


Fig. A2.5. Modified Thompson-Howarth Replicate Error Analysis

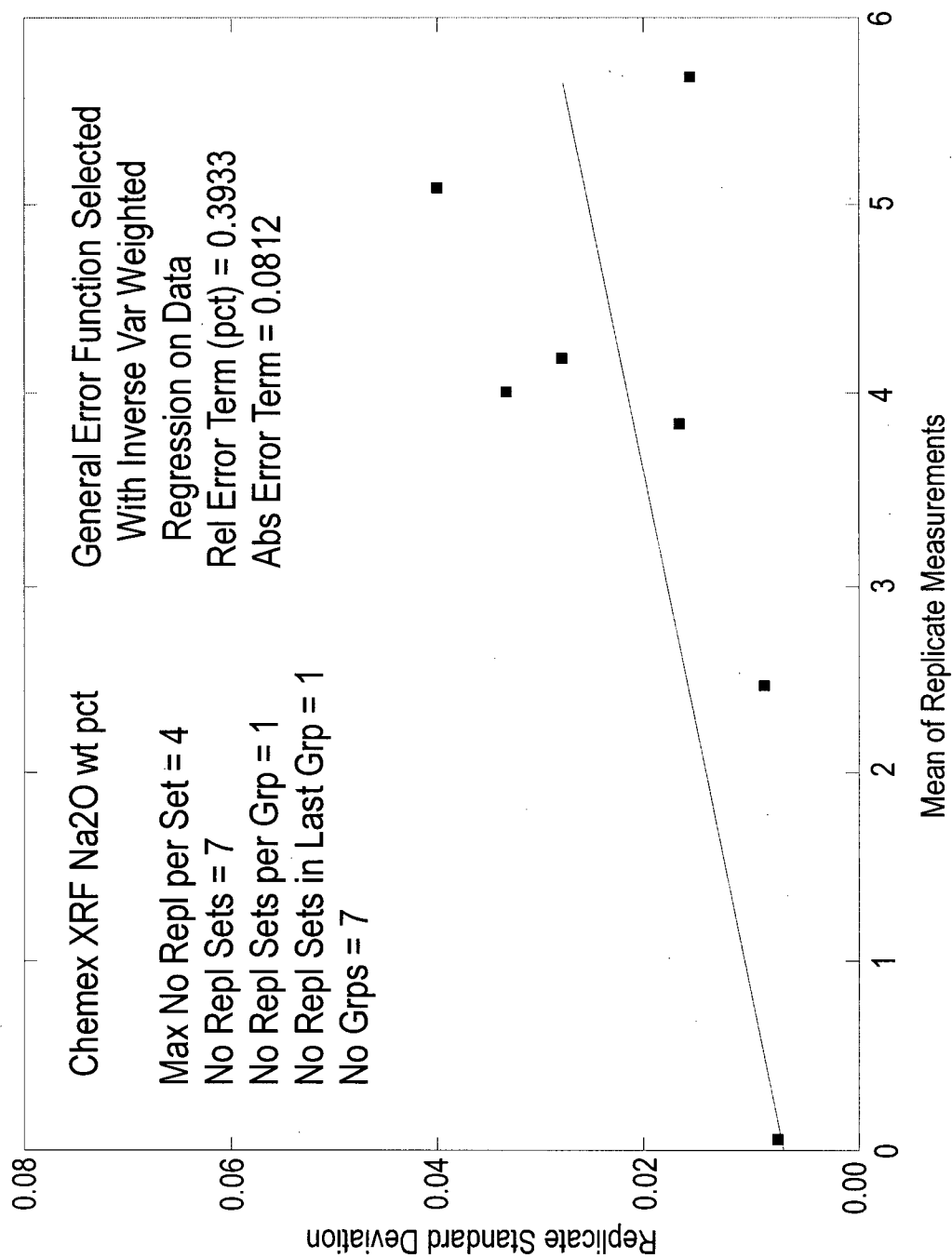


Fig. A2.6. Modified Thompson-Howarth Replicate Error Analysis

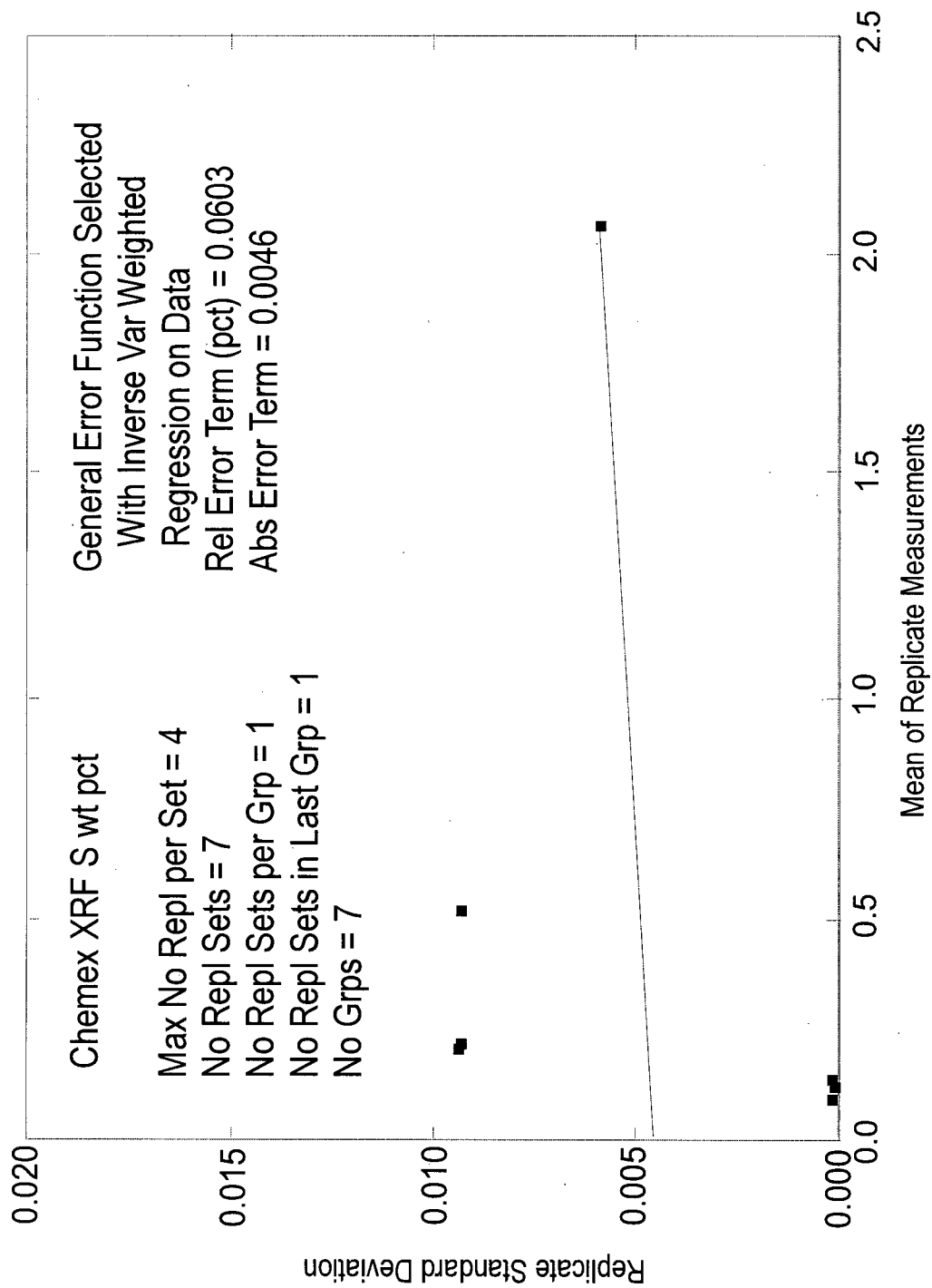


Fig. A2.7. Modified Thompson-Howarth Replicate Error Analysis

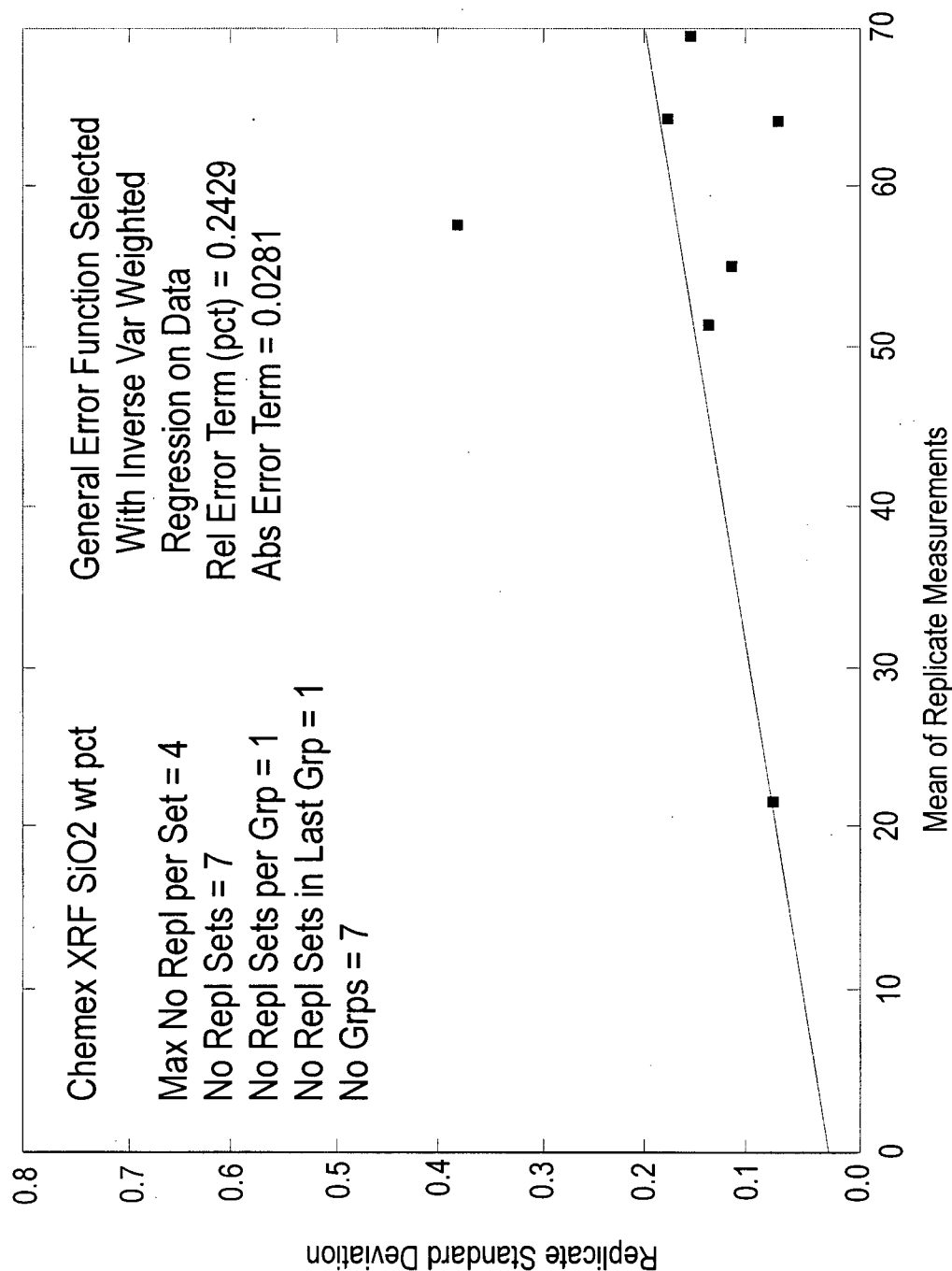


Fig. A2.8. Modified Thompson-Howarth Replicate Error Analysis

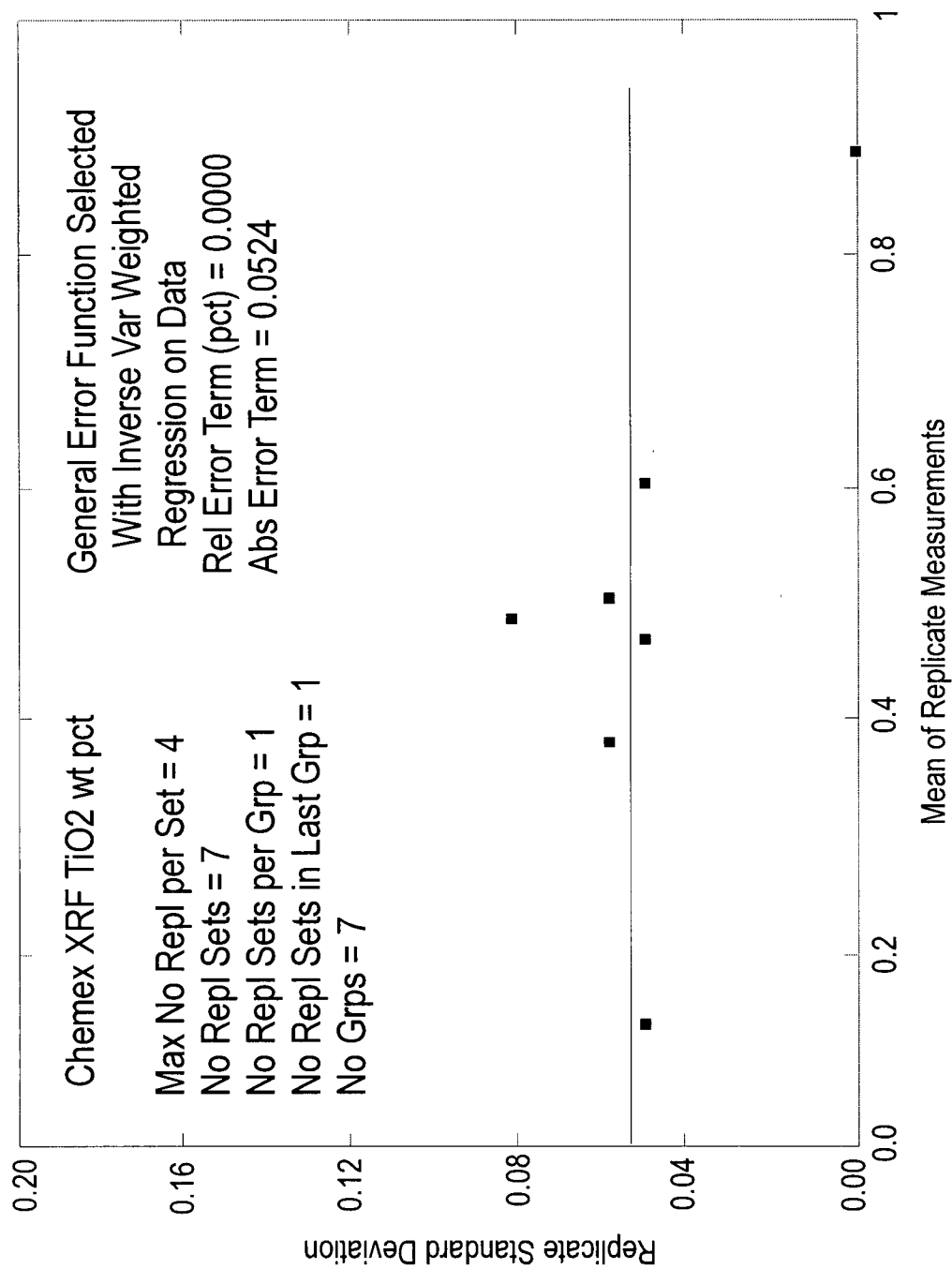


Fig. A2.9. Modified Thompson-Howarth Replicate Error Analysis

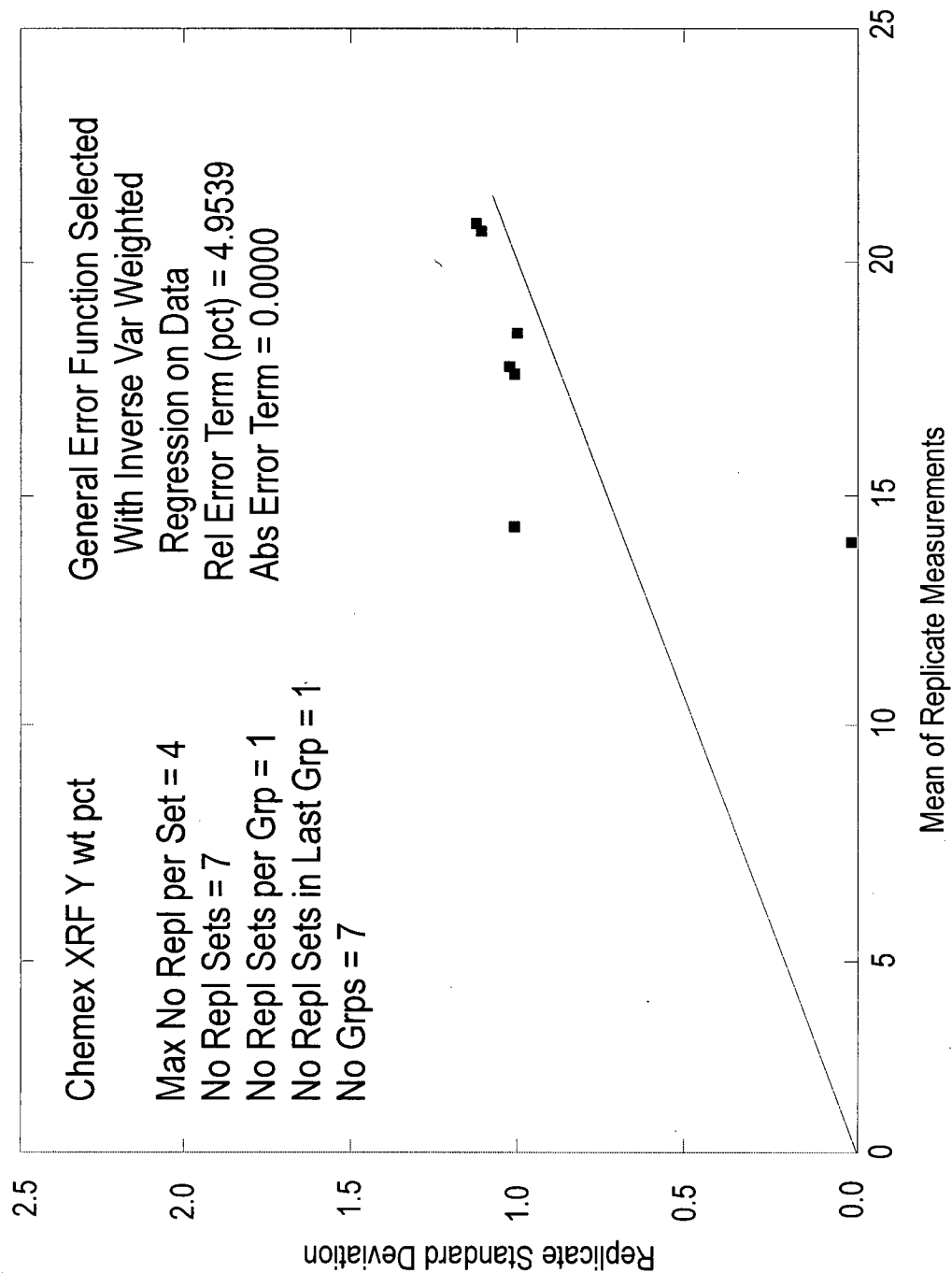


Fig. A2.10. Modified Thompson-Howarth Replicate Error Analysis

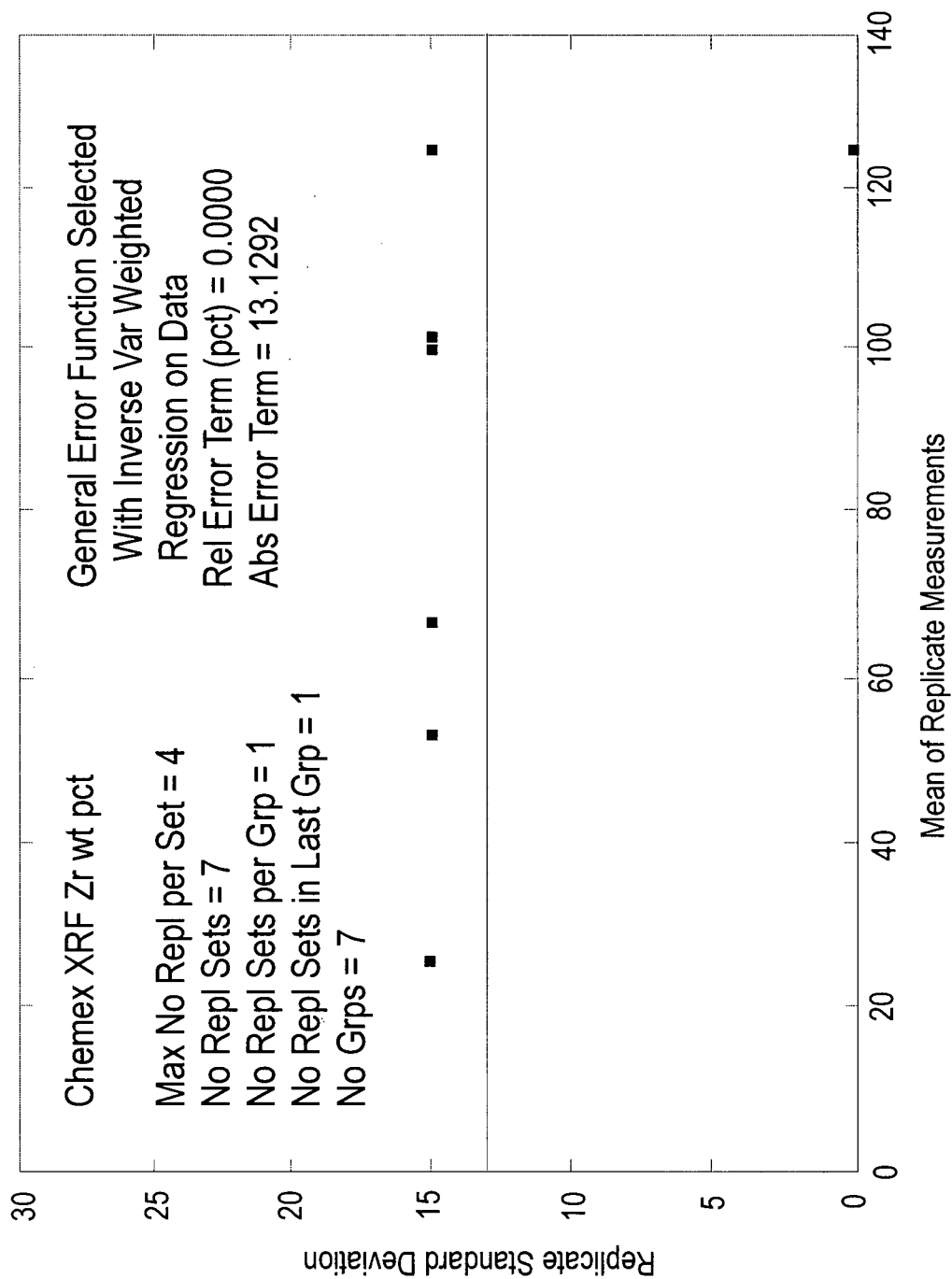


Fig. A2.11. Modified Thompson-Howarth Replicate Error Analysis

Table A2.3. Analytical precision based on duplicate pulps of Goldstream  
deposit samples analyzed by Chemex Laboratories Inc.

Sample#	Al <sub>2</sub> O <sub>3</sub> (%)	CaO (%)	Cr <sub>2</sub> O <sub>3</sub> (%)	Fe(tot) (%)	K <sub>2</sub> O (%)	MgO (%)	MnO (%)	Na <sub>2</sub> O (%)	P <sub>2</sub> O <sub>5</sub> (%)	SiO <sub>2</sub> (%)	TiO <sub>2</sub> (%)
<b>Phyllites</b>											
HS951030	9.12	10.29	0.04	4.62	1.90	2.45	0.09	0.84	0.25	60.23	0.56
HS959030	9.03	10.25	0.04	4.55	1.92	2.51	0.07	0.85	0.26	60.33	0.55
HS951090	15.15	9.86	0.03	6.58	2.88	4.13	0.08	1.14	0.14	52.67	0.74
HS959090	15.21	9.88	0.02	6.54	2.79	4.14	0.07	1.16	0.17	52.66	0.75
HS951095	12.01	9.35	0.03	7.28	2.20	2.58	0.37	1.08	0.24	55.96	0.49
HS959095	12.13	9.29	0.03	7.33	2.23	2.57	0.35	1.09	0.22	55.91	0.51
HS951160	10.78	10.65	0.02	6.45	2.51	2.49	0.21	0.42	0.32	53.96	0.94
HS959160	10.85	10.65	0.02	6.51	2.55	2.44	0.24	0.44	0.31	54.02	0.94
HS951916	13.47	11.22	0.03	6.57	2.96	4.23	0.15	0.91	0.22	52.00	0.87
HS959916	13.45	11.31	0.03	6.63	2.85	4.22	0.15	0.95	0.24	51.89	0.88
HS951953	9.97	11.95	0.03	5.74	2.28	2.16	0.15	1.12	0.28	54.18	0.70
HS959953	9.97	12.02	0.04	5.75	2.28	2.13	0.17	1.16	0.26	54.19	0.70
HS951038	17.58	0.67	0.02	6.95	3.96	2.71	0.08	1.06	0.13	62.57	0.72
HS959038	17.56	0.62	0.02	6.88	3.95	2.75	0.09	1.01	0.10	62.61	0.72
HS951087	11.99	1.95	0.03	4.80	2.35	1.59	0.06	2.27	0.22	72.04	0.80
HS959087	11.88	1.99	0.03	4.87	2.41	1.66	0.06	2.29	0.26	72.05	0.81
HS951128	13.12	3.24	0.03	7.23	3.82	2.17	0.24	0.33	0.26	64.65	1.14
HS959128	13.20	3.32	0.03	7.15	3.79	2.19	0.25	0.34	0.26	64.68	1.15
HS951935	19.40	1.43	0.03	8.64	4.54	2.89	0.14	1.69	0.11	56.20	1.04
HS959935	19.42	1.48	0.03	8.51	4.51	2.84	0.16	1.71	0.11	56.41	1.03
<b>Average</b>	<b>13.265</b>	<b>7.071</b>	<b>0.029</b>	<b>6.479</b>	<b>2.934</b>	<b>2.743</b>	<b>0.159</b>	<b>1.093</b>	<b>0.218</b>	<b>58.461</b>	<b>0.802</b>
<b>Error variance</b>	<b>0.0025</b>	<b>0.0016</b>	<b>1E-05</b>	<b>0.0025</b>	<b>0.0014</b>	<b>0.0008</b>	<b>0.0001</b>	<b>0.0004</b>	<b>0.0002</b>	<b>0.0038</b>	<b>5E-05</b>
<b>Precision (%)</b>	<b>0.76</b>	<b>1.12</b>	<b>21.81</b>	<b>1.53</b>	<b>2.58</b>	<b>2.11</b>	<b>14.88</b>	<b>3.57</b>	<b>14.21</b>	<b>0.21</b>	<b>1.76</b>
<b>Garnet zone</b>											
HS951009	5.94	5.57	0.02	24.29	0.12	2.43	5.21	0.01	0.58	52.61	0.24
HS959009	6.06	5.49	0.02	24.36	0.13	2.38	5.24	0.01	0.61	52.65	0.25
HS951059	7.26	7.95	0.07	20.90	0.55	1.55	0.84	0.11	0.57	52.97	0.41
HS959059	7.09	8.02	0.06	21.02	0.58	1.54	0.88	0.12	0.62	53.11	0.41
HS951139	4.90	5.23	0.02	32.98	0.14	2.88	4.42	0.02	0.78	43.57	0.19
HS959139	4.83	5.22	0.02	33.05	0.16	2.86	4.39	0.02	0.77	43.91	0.18



HS951169	11.80	2.98	0.02	5.39	2.86	1.57	0.45	1.16	0.12	70.28	0.37
HS959169	11.72	2.89	0.02	5.33	2.87	1.59	0.41	1.19	0.11	69.93	0.36
HS951169	4.89	7.74	0.02	27.35	0.07	2.19	4.09	0.01	0.77	48.72	0.23
HS959169	5.06	7.70	0.02	27.20	0.07	2.22	4.11	0.01	0.79	48.56	0.23
<b>Average</b>	<b>6.955</b>	<b>5.879</b>	<b>0.029</b>	<b>22.187</b>	<b>0.755</b>	<b>2.121</b>	<b>3.004</b>	<b>0.266</b>	<b>0.572</b>	<b>53.631</b>	<b>0.287</b>
<b>Error variance</b>	<b>0.0042</b>	<b>0.0011</b>	<b>5E-06</b>	<b>0.0025</b>	<b>8E-05</b>	<b>0.0002</b>	<b>0.0003</b>	<b>5E-05</b>	<b>0.0002</b>	<b>0.0142</b>	<b>2E-05</b>
<b>Precision (%)</b>	<b>1.86</b>	<b>1.10</b>	<b>15.42</b>	<b>0.45</b>	<b>2.29</b>	<b>1.38</b>	<b>1.09</b>	<b>5.39</b>	<b>4.94</b>	<b>0.45</b>	<b>2.70</b>
<b>Marble</b>											
HS951011	6.20	36.70	0.03	2.43	1.97	1.14	0.04	0.43	0.10	21.87	0.27
HS959011	6.33	36.75	0.02	2.45	1.99	1.16	0.04	0.45	0.08	20.98	0.29
HS951096	9.08	28.93	0.01	3.55	2.25	1.30	0.04	0.62	0.09	31.79	0.38
HS959096	9.15	28.99	0.01	3.48	2.19	1.28	0.04	0.62	0.11	31.42	0.41
HS951136	9.55	28.66	0.02	3.62	2.48	1.41	0.04	0.69	0.09	31.76	0.41
HS959136	9.67	28.61	0.02	3.58	2.52	1.42	0.05	0.77	0.10	32.01	0.40
HS951181	14.24	11.80	0.02	6.23	2.88	4.60	0.09	1.06	0.15	49.05	0.69
HS959181	14.18	11.76	0.02	6.29	2.89	4.62	0.10	1.09	0.15	48.91	0.68
HS951932	9.67	20.77	0.07	8.45	0.21	6.20	0.18	1.80	0.40	31.49	1.39
HS959932	9.76	20.75	0.07	8.41	0.26	6.10	0.19	1.82	0.41	31.55	1.39
<b>Average</b>	<b>9.783</b>	<b>25.372</b>	<b>0.029</b>	<b>4.849</b>	<b>1.964</b>	<b>2.92</b>	<b>0.081</b>	<b>0.935</b>	<b>0.168</b>	<b>33.1</b>	<b>0.6</b>
<b>Error variance</b>	<b>0.0048</b>	<b>0.0011</b>	<b>1E-05</b>	<b>0.0012</b>	<b>0.0008</b>	<b>0.0011</b>	<b>3E-05</b>	<b>0.001</b>	<b>0.000</b>	<b>0.101</b>	<b>0.000</b>
<b>Precision (%)</b>	<b>1.41</b>	<b>0.26</b>	<b>21.81</b>	<b>1.43</b>	<b>2.92</b>	<b>2.30</b>	<b>13.52</b>	<b>6.09</b>	<b>11.90</b>	<b>1.93</b>	<b>3.88</b>

	LOI % (%)	TOTAL	CO <sub>2</sub> (%)	H <sub>2</sub> O(+) (%)	S % (%)	Ba (ppm)	Nb (ppm)	Zr (ppm)	Y (ppm)
<b>Phyllites</b>									
HS951030	8.19	98.58	7.50	1.24	0.90	2580	20	105	22
HS959030	8.23	100.56	7.80	1.26	0.91	2590	20	105	23
HS951090	5.64	99.04	5.80	0.95	0.58	1115	20	117	22
HS959090	5.55	101.12	5.90	1.01	0.55	1120	22	118	22
HS951095	8.30	99.89	5.70	0.87	1.21	490	14	117	26
HS959095	8.22	99.58	5.70	0.89	1.22	495	16	115	25
HS951160	10.55	99.30	11.90	1.40	1.02	675	34	150	22
HS959160	10.54	103.31	11.60	1.33	1.05	679	33	148	22
HS951916	6.82	99.45	6.30	1.17	0.88	1125	26	138	22
HS959916	6.62	101.10	6.10	1.17	0.92	1131	25	135	23
HS951953	10.02	98.58	8.50	1.54	1.38	500	24	120	20
HS959953	10.12	99.94	8.20	1.52	1.32	510	25	122	22
HS951038	3.12	99.57	0.10	2.51	0.11	850	12	174	26
HS959038	3.18	99.28	0.20	2.55	0.14	854	12	175	24
HS951087	1.72	99.82	0.90	1.08	0.19	545	16	450	32
HS959087	1.81	99.85	0.60	1.09	0.25	545	15	455	32
HS951128	3.32	99.55	0.90	2.26	0.49	450	36	405	34
HS959128	3.32	99.31	0.80	2.29	0.42	460	35	406	33
HS951935	3.09	99.20	0.30	2.97	0.43	320	22	141	30
HS959935	3.11	99.78	0.50	3.02	0.49	326	22	141	33
<b>Average</b>	<b>6.074</b>	<b>99.841</b>	<b>4.77</b>	<b>1.606</b>	<b>0.723</b>	<b>868.0</b>	<b>22.5</b>	<b>191.9</b>	<b>25.8</b>
<b>Error variance</b>	<b>0.004</b>	<b>1.473</b>	<b>0.024</b>	<b>0.001</b>	<b>0.001</b>	<b>22.7</b>	<b>0.65</b>	<b>2.45</b>	<b>1.05</b>
<b>Precision (%)</b>	<b>2.06</b>	<b>2.43</b>	<b>6.43</b>	<b>3.39</b>	<b>8.79</b>	<b>1.10</b>	<b>7.18</b>	<b>1.63</b>	<b>7.96</b>
<b>Garnet zone</b>									
HS951009	2.48	99.49	3.10	1.06	2.86	160	2	69	24
HS959009	2.45	104.39	3.30	1.11	2.99	162	2	71	25
HS951059	6.20	99.38	5.20	1.09	4.27	50	4	117	36
HS959059	6.23	99.45	5.40	1.12	4.22	52	4	118	35
HS951139	4.51	99.64	3.20	1.33	4.23	30	1	60	26
HS959139	4.49	99.98	3.50	1.34	4.29	33	1	60	27

HS951169	2.91	99.91	0.70	1.50	0.19	665	16	147	32
HS959169	2.90	99.01	0.50	1.52	0.25	667	15	149	33
HS951169	3.42	99.50	5.10	0.50	2.30	10	1	54	28
HS959169	3.38	98.89	5.30	0.55	2.45	11	1	55	29
<b>Average</b>	<b>3.897</b>	<b>99.965</b>	<b>3.53</b>	<b>1.112</b>	<b>2.805</b>	<b>184.0</b>	<b>4.7</b>	<b>90.0</b>	<b>29.5</b>
<b>Error variance</b>	<b>0.0002</b>	<b>1.27</b>	<b>0.0125</b>	<b>0.0003</b>	<b>0.0025</b>	<b>1.10</b>	<b>0.05</b>	<b>0.50</b>	<b>0.25</b>
<b>Precision (%)</b>	<b>0.72</b>	<b>2.25</b>	<b>6.33</b>	<b>3.22</b>	<b>3.53</b>	<b>1.14</b>	<b>9.52</b>	<b>1.57</b>	<b>3.39</b>
<b>Marble</b>									
HS951011	27.59	98.77	28.20	0.79	0.34	135	4	51	14
HS959011	27.23	100.02	26.00	0.82	0.29	136	4	50	16
HS951096	20.99	99.03	20.50	0.59	0.37	215	8	78	18
HS959096	20.89	100.32	20.90	0.55	0.33	218	9	77	17
HS951136	20.41	99.14	20.40	1.02	0.34	340	12	87	22
HS959136	20.33	102.51	20.70	1.09	0.30	345	11	85	22
HS951181	8.50	99.31	7.20	0.96	0.57	1030	16	108	20
HS959181	8.46	100.75	7.50	0.99	0.52	1030	18	110	21
HS951932	19.27	99.90	16.10	3.79	0.24	125	66	150	18
HS959932	19.36	100.76	15.80	3.75	0.27	128	64	152	17
<b>Average</b>	<b>19.303</b>	<b>99.72</b>	<b>18.33</b>	<b>1.44</b>	<b>0.357</b>	<b>370.2</b>	<b>21.2</b>	<b>94.8</b>	<b>18.5</b>
<b>Error variance</b>	<b>0.0156</b>	<b>1.50341</b>	<b>0.53</b>	<b>0.00</b>	<b>0.0009</b>	<b>4.4</b>	<b>1</b>	<b>1.4</b>	<b>0.7</b>
<b>Precision (%)</b>	<b>1.2929</b>	<b>2.459</b>	<b>7.92</b>	<b>4.39</b>	<b>16.9</b>	<b>1.13323</b>	<b>9.434</b>	<b>2.4962</b>	<b>9.045</b>

## **Appendix 3**

### **Samples and analytical data used in the study of the Chu Chua deposit.**

The Chu Chua deposit data set (Table 1 through Table 3) consists of 115 original samples of drill core, taken from 25 drillholes in 1995 and 1997. The original samples represent the lithologies hosting the ore bodies at distance of up to 500m. The mineralized horizon and the hanging wall are better represented, due to the drilling pattern. An attempt was made during sampling to make full use of the limited drillholes penetrating the footwall. Additional 533 drill core samples donated by INMET Inc. augment the original data set. They were not analyzed for carbonate, Zr, Y and some other components, which was a slight impediment in their utilization. Eight samples analyzed for Rare Earth elements (Table 4) were donated by INCO Ltd. The samples are referenced on the Minnova exploration grid, which is parallel to true North and has the center of the deposit at approximately 10000m east and 10000m north of the origin.

#### **Sampling and sample preparation**

The samples used in the lithogeochemical study of the Goldstream deposit were collected from drill core. All visual varieties of rocks and alteration were sampled. Recognizing the fine-grained nature of the rocks and the lack of visible accessory minerals, it was assumed that a sample size of 1 kg would adequately characterize their chemical composition.

The samples were prepared for analysis at the X-ray Assay Laboratories Ltd. (XRAL) in Don Mills, Ontario by laboratory staff. The standard preparation procedure was followed, which involved crushing the entire sample in a jaw crusher to better than 70% of the sample passing through a 2 mm sieve. A 200 to 250 g split was then taken, using a Jones riffle splitter. The split was pulverized in a hardened chrome steel ring and puck mill. Theoretically, the mill can be a source of contamination with Cr and Fe, however this contamination is usually not detectable (less than 100 ppm) when normal silicate rocks are processed (Walter Grondin, pers. comm.).

#### **Analytical procedure**

The major elements were analyzed in fused Li-tetraborate discs. A prepared sample (2 g) is added to lithium tetraborate flux (7.7 g), mixed well and fused in a furnace at 1100°C. A flat

glass disc is prepared from the resulting melt. Trace elements (Ba, Rb, Sr, Zr, Y and Nb are analyzed in pressed powder pellets (3 g of powdered sample) in order to avoid dilution by flux. The discs or pellets are then analyzed by X-Ray fluorescence spectrometry (XRAL code: XRF-103) using a Siemens SRS3000 sequential wavelength dispersive XRF spectrometer (fused discs) and Philips PW1400 sequential wavelength dispersive X-ray spectrometer (pressed pellets). Oxide concentration is calculated from the determined elemental concentration and the result is reported in that format.

Loss on ignition (L.O.I.) is determined by heating in a furnace and then gravimetrically determining the loss as percent of the initial weight. Total organic carbon (T.O.C.) and sulphur are analyzed by Leco furnace and ferric iron by wet chemistry (acid digestion with titrimetric finish).

Analytical data reported as "below detection" are assigned values of  $\frac{1}{2}$  of the detection limit.

Table A3.1. Sample location and identification							
Sample#	Lithology	Drill hole/ location	Depth (m)	Source	Northing (m)	Easting (m)	Elevation (m)
HS952001	Basalt	CC-2	63.50	This study	9995.0	9987.0	1743.4
HS952002	Basalt	CC-2	21.00	This study	9995.0	9962.0	1777.9
HS952003	Basalt	CC-5	85.00	This study	10195.0	9981.0	1759.4
HS952004	Basalt	CC-5	16.00	This study	10195.0	9950.0	1811.8
HS952005	Basalt	CC-6	17.50	This study	10197.0	9999.0	1810.7
HS952006	Chert	CC-1	98.00	This study	10093.0	9978.0	1720.7
HS952007	<Ti basalt	CC-1	127.25	This study	10093.0	9996.0	1696.8
HS952008	Basalt	CC-1	0.07	This study	10093.0	9960.0	1747.8
HS952009	Basalt	CC-1	14.00	This study	10093.0	9930.0	1789.5
HS952010	Basalt	CC-1	15.50	This study	10093.0	9931.0	1788.3
HS952011	Chert	CC-7	14.00	This study	10288.0	9968.0	1812.3
HS952012	Basalt	CC-7	46.00	This study	10288.0	9989.0	1788.0
HS952013	Basalt	CC-7	52.50	This study	10288.0	9992.0	1783.0
HS952014	Basalt	CC-7	71.15	This study	10288.0	10004.0	1768.8
HS952015	Basalt	CC-9	81.50	This study	9884.0	9972.0	1721.1
HS952016	Basalt	CC-9	85.40	This study	9884.0	9975.0	1718.5
HS952017	Basalt	CC-9	97.50	This study	9884.0	9984.0	1709.6
HS952018	Basalt	CC-9	79.50	This study	9884.0	9968.0	1722.6
HS952019	Basalt	CC-9	9.00	This study	9884.0	9925.0	1768.4
HS952020	Chert	CC-7	16.00	This study	10288.0	9969.0	1810.8
HS952021	Mixed	CC-12	62.65	This study	10103.0	9889.0	1749.1
HS952022	Basalt	CC-12	60.50	This study	10103.0	9888.0	1750.8
HS952023	Basalt	CC-12	259.50	This study	10103.0	10009.0	1592.2
HS952024	Basalt	CC-12	236.65	This study	10103.0	9996.0	1610.4
HS952025	Chert	CC-12	227.50	This study	10103.0	9990.0	1617.7
HS952026	Basalt	CC-12	221.50	This study	10103.0	9886.0	1622.5
HS952027	Chert	CC-12	207.50	This study	10103.0	9978.0	1633.6
HS952028	Chert	CC-12	187.50	This study	10103.0	9967.0	1649.2
HS952029	Basalt	CC-12	84.00	This study	10103.0	9903.0	1732.0
HS952030	Basalt	CC-12	222.50	This study	10103.0	9887.0	1621.7
HS952031	Basalt	CC-12	16.00	This study	10103.0	9862.0	1786.2
HS952032	Basalt	CC-21	8.15	This study	9905.0	10130.0	1779.7
HS952033	Basalt	CC-21	46.60	This study	9905.0	10077.0	1758.9
HS952034	Basalt	CC-21	99.50	This study	9905.0	10041.0	1720.3
HS952035	Basalt	CC-21	147.00	This study	9905.0	10009.0	1685.5
HS952036	Basalt	CC-21	174.00	This study	9905.0	9990.0	1665.8
HS952037	Basalt	CC-21	190.65	This study	9905.0	9979.0	1654.0
HS952038	Basalt	CC-21	215.00	This study	9905.0	9962.0	1635.8
HS952039	Basalt	CC-21	230.40	This study	9905.0	9953.0	1624.6
HS952040	Basalt	CC-21	231.45	This study	9905.0	9952.0	1624.1
HS952041	Outlier	CCF-64	232.55	This study	10614.0	10045.0	1551.5
HS952042	Chert	CCF-64	303.50	This study	10614.0	10028.0	1575.4
HS952043	Mixed	CCF-64	250.75	This study	10614.0	9999.0	1618.8
HS952044	Chert	CCF-64	195.30	This study	10614.0	9967.0	1664.4
HS952045	Chert	CCF-64	104.55	This study	10614.0	9915.0	1739.4
HS952046	Basalt	CCF-64	19.40	This study	10614.0	9867.0	1809.1
HS952047	Basalt	CCF-69	348.55	This study	9996.0	9862.0	1459.4
HS952048	Basalt	CC-46	419.50	This study	9605.0	10009.0	1387.5
HS952049	Basalt	CC-46	395.65	This study	9605.0	9995.0	1405.8
HS952050	Basalt	CCF-64	19.40	This study	10614.0	9867.0	1809.1

Sample#	Lithology	Drill hole/ location	Depth (m)	Source	Northing (m)	Easting (m)	Elevation (m)
HS952051	Basalt	CC-46	385.65	This study	9605.0	9988.0	1413.8
HS952052	Basalt	CC-46	320.50	This study	9605.0	9947.0	1464.3
HS952053	Basalt	CC-46	245.65	This study	9605.0	9900.0	1522.4
HS952054	Basalt	CC-46	0.13	This study	9605.0	9828.0	1611.4
HS952055	Basalt	CC-46	55.65	This study	9605.0	9781.0	1669.8
HS952056	Basalt	CC-40	51.50	This study	10249.0	9996.0	1780.9
HS952057	Basalt	CC-40	39.60	This study	10249.0	10005.0	1789.9
HS952058	Mixed	CC-40	26.50	This study	10249.0	10010.0	1799.9
HS952059	Basalt	CC-55	470.75	This study	9999.0	10007.0	1406.2
HS952060	Basalt	CC-46	418.50	This study	9605.0	10009.0	1388.3
HS952061	Basalt	CC-55	441.60	This study	9999.0	9989.0	1429.4
HS952063	Basalt	CC-55	415.65	This study	9999.0	9973.0	1450.0
HS952064	Basalt	CC-55	403.75	This study	9999.0	9966.0	1459.4
HS952065	Chert	CC-55	391.00	This study	9999.0	9957.0	1469.6
HS952066	Basalt	CC-55	374.90	This study	9999.0	9948.0	1482.7
HS952067	Basalt	CC-55	233.80	This study	9999.0	9964.0	1594.4
HS952068	Basalt	CC-55	155.60	This study	9999.0	9817.0	1556.5
HS952069	Basalt	CC-55	50.60	This study	9999.0	9754.0	1739.8
HS971070	Chert	CCF-61	75.00	This study	10200.0	10013.0	1756
HS971071	Mixed	CCF-61	76.00	This study	10200.0	10014.0	1755
HS971072	Basalt	CCF-61	88.00	This study	10200.0	10020.0	1744.8
HS971073	Basalt	CCF-61	115.00	This study	10200.0	10033.0	1724.8
HS971074	Basalt	CCF-61	148.00	This study	10200.0	10066.0	1692.8
HS971075	Basalt	CCF-61	175.00	This study	10200.0	10048.0	1699.5
HS971076	Basalt	CCF-63	320.00	This study	10300.0	9965.0	1541.6
HS971077	Basalt	CCF-63	321.00	This study	10309.0	9966.0	1540.8
HS971078	Chert	CCF-63	331.00	This study	10310.0	9975.0	1532.2
HS971079	Chert	CCF-63	348.00	This study	10311.0	9985.5	1517.9
HS971080	Chert	CCF-63	335.00	This study	10310.5	9988.5	1528.9
HS971081	Basalt	CCF-63	357.00	This study	10311.0	9989.0	1510.2
HS971082	Mixed	CCF-63	363.00	This study	10311.5	9992.0	1505.2
HS971083	Mixed	CCF-63	303.00	This study	10314.5	10015.0	1471.2
HS971084	Chert	CCF-63	409.00	This study	10315.0	10022.0	1466.1
HS971085	Chert	CCF-63	420.00	This study	10316.0	10028.5	1456.8
HS971086	Chert	CCF-63	422.00	This study	10316.2	10029.0	1455.1
HS971087	Chert	CCF-63	437.00	This study	10317.5	10038.5	1442.4
HS971088	Chert	CCF-63	438.00	This study	10317.7	10039.0	1441.6
HS971089	Chert	CCF-63	439.00	This study	10317.9	10039.5	1440.7
HS971090	Mixed	CCF-63	445.00	This study	10328.0	10043.0	1435.6
HS971091	Basalt	CCF-69	396.00	This study	9997.0	9727.0	1780
HS971092	Basalt	CCF-71	700.00	This study	10084.0	9683.0	1785
HS971093	Basalt	CC-17	76.00	This study	10105.2	9954.4	1802.7
HS971094	Basalt	CC-18	77.00	This study	10253.6	9940.0	1824.8
HS971095	Basalt	CC-19	214.00	This study	10203.0	9861.9	1811.4
HS971096	Chert	CC-22	20.00	This study	10105.0	9994.0	1796.2
HS971097	Basalt	CC-22	36.00	This study	10105.0	10005.0	1783.9
HS971098	Basalt	CC-22	56.00	This study	10105.0	10018.0	1768.6
HS971099	Mt-tlc altrd	?	?	This study			
HS971100	Basalt	CC-39	100.00	This study	11000.0	9844.3	1683.4
HS971101	Basalt	CC-39	?	This study	11000.0	9855.0	1670
HS971102	Basalt	CC-39	134.00	This study	11000.0	9866.1	1657.35

Sample#	Lithology	Drill hole/ location	Depth (m)	Source	Northing (m)	Easting (m)	Elevation (m)
HS971103	Mixed	?	182.00	This study			
HS971104	Basalt	?	272.50	This study			
HS971105	Basalt	CC-42	45.00	This study	9596.0	10005.0	1698.5
HS971106	Basalt	CC-42	61.50	This study	9596.0	10015.0	1685.5
HS971107	Basalt	CC-42	80.00	This study	9596.0	10027.0	1671.6
HS971108	Basalt	CC-42	100.00	This study	9596.0	10039.5	1656.3
HS971109	Chert	CC-43	97.00	This study	9800.0	11255.0	1759.7
HS971110	Basalt	?	317.00	This study			
HS971111	Basalt	CC-49	451.00	This study	9880.0	9992.5	1390.3
HS971112	Mixed	CC-49	429.00	This study	9880.0	9980.5	1408.3
HS971113	Basalt	CC-49	430.00	This study	9880.0	9981.0	1408
HS971114	Basalt	CC-49	472.00	This study	9880.0	10004.5	1373
HS971115	Basalt	CC-49	495.50	This study	10019.0	9880.0	1353.8
HS971125	Chert	CCF-63	416.00	This study	10315.0	10022.0	1467.7
BCD20701	Basalt	CCF-32	29.95	Inmet	10030.5	9953.6	1775.4
BCD20702	Basalt	CCF-32	35.45	Inmet	10030.5	9956.9	1771.0
BCD20705	Chert	CCF-32	75.40	Inmet	10030.5	9981.0	1739.1
BCD20706	Mixed	CCF-32	80.50	Inmet	10030.5	9984.0	1735.0
BCD20707	Basalt	CCF-32	85.50	Inmet	10030.5	9987.1	1731.0
BCD20708	<Ti basalt	CCF-32	90.65	Inmet	10030.5	9990.2	1726.9
BCD20709	Basalt	CCF-33	7.50	Inmet	10024.4	9959.7	1794.1
BCD20711	Chert	CCF-33	41.00	Inmet	10024.4	9983.4	1770.4
BCD20712	Mixed	CCF-33	46.00	Inmet	10024.4	9986.9	1766.9
BCD20713	Basalt	CCF-33	50.90	Inmet	10024.4	9990.4	1763.4
BCD20714	Basalt	CCF-34	5.78	Inmet	9977.8	9933.0	1786.7
BCD20715	Basalt	CCF-34	11.45	Inmet	9977.8	9935.8	1781.8
BCD20716	Basalt	CCF-34	18.35	Inmet	9977.8	9939.3	1775.8
BCD20717	Basalt	CCF-34	24.30	Inmet	9977.8	9942.3	1770.7
BCD20718	Basalt	CCF-34	30.25	Inmet	9977.8	9945.2	1765.5
BCD20719	Basalt	CCF-34	36.85	Inmet	9977.8	9948.5	1759.8
BCD20720	Basalt	CCF-34	43.85	Inmet	9977.8	9952.0	1753.7
BCD20721	Basalt	CCF-34	50.90	Inmet	9977.8	9955.6	1747.6
BCD20722	Basalt	CCF-34	57.80	Inmet	9977.8	9959.0	1741.6
BCD20723	Mixed	CCF-34	113.30	Inmet	9977.8	9986.8	1693.6
BCD20724	Basalt	CCF-35	5.58	Inmet	9977.4	9935.5	1787.8
BCD20725	Basalt	CCF-35	10.60	Inmet	9977.4	9939.1	1784.2
BCD20879	Basalt	CCF-35	15.45	Inmet	9977.4	9942.5	1780.8
BCD20880	Basalt	CCF-35	72.95	Inmet	9977.4	9983.2	1740.1
BCD20881	Basalt	CCF-36	7.60	Inmet	9978.8	9963.9	1787.7
BCD20882	?	CCF-36	11.70	Inmet	9978.8	9966.8	1784.8
BCD20883	Basalt	CCF-36	30.35	Inmet	9978.8	9980.0	1771.6
BCD20884	Basalt	CCF-37	5.08	Inmet	9954.0	9960.1	1786.4
BCD20885	<Ti basalt	CCF-37	9.15	Inmet	9954.0	9963.0	1783.5
BCD20886	Basalt	CCF-37	29.85	Inmet	9954.0	9977.6	1768.9
BCD20887	Basalt	CCF-37	34.00	Inmet	9954.0	9980.5	1766.0
BCD20888	Basalt	CCF-37	38.25	Inmet	9954.0	9983.5	1763.0
BCD20889	Basalt	CCF-38	7.45	Inmet	10131.6	9991.5	1808.6
BCD20891	?	CCF-38	17.00	Inmet	10131.6	9998.2	1801.9
BCD20892	Basalt	CCF-38	31.70	Inmet	10131.6	10008.6	1791.5
BCD21862	Basalt	CCF-48	51.70	Inmet	9915.4	9956.3	1745.6
BCD21863	Basalt	CCF-48	73.30	Inmet	9915.4	9971.5	1730.4



Sample#	Lithology	Drill hole/ location	Depth (m)	Source	Northing (m)	Easting (m)	Elevation (m)
BCD21864	Basalt	CCF-49	35.00	Inmet	9915.5	9935.4	1751.3
BCD21865	Basalt	CCF-49	45.00	Inmet	9915.5	9940.1	1742.5
BCD21866	Basalt	CCF-49	54.80	Inmet	9915.5	9944.7	1733.8
BCD21867	Basalt	CCF-49	66.70	Inmet	9915.5	9950.3	1723.3
BCD21868	Basalt	CCF-49	85.10	Inmet	9915.5	9959.0	1707.1
BCD21869	Mt-tlc altrd	CCF-49	94.75	Inmet	9915.5	9963.5	1698.5
BCD21870	Mt-tlc altrd	CCF-49	101.00	Inmet	9915.5	9966.4	1693.0
BCD21871	Mt-tlc altrd	CCF-49	110.75	Inmet	9915.5	9971.0	1684.4
BCD21872	Mt-tlc altrd	CCF-49	114.10	Inmet	9915.5	9972.6	1681.5
BCD21873	Mt-tlc altrd	CCF-49	116.60	Inmet	9915.5	9973.7	1679.2
BCD21874	Basalt	CCF-49	124.70	Inmet	9915.5	9977.5	1672.1
BCD21875	Basalt	CCF-49	131.40	Inmet	9915.5	9980.7	1666.2
BCD21876	Basalt	CCF-39	5.05	Inmet	10228.0	9933.6	1813.8
BCD21877	Mixed	CCF-39	8.70	Inmet	10228.0	9936.2	1811.2
BCD21878	Basalt	CCF-39	11.65	Inmet	10228.0	9938.2	1809.2
BCD21879	Basalt	CCF-39	14.15	Inmet	10228.0	9940.0	1807.4
BCD21880	Basalt	CCF-39	16.65	Inmet	10228.0	9941.8	1805.6
BCD21881	Basalt	CCF-39	19.40	Inmet	10228.0	9943.7	1803.7
BCD21882	Mixed	CCF-39	22.30	Inmet	10228.0	9945.8	1801.6
BCD21883	Chert	CCF-39	25.35	Inmet	10228.0	9947.9	1799.5
BCD21884	Chert	CCF-39	28.50	Inmet	10228.0	9950.2	1797.2
BCD21885	Chert	CCF-39	31.50	Inmet	10228.0	9952.3	1795.1
BCD21886	Chert	CCF-39	34.50	Inmet	10228.0	9954.4	1793.0
BCD21887	Chert	CCF-39	37.60	Inmet	10228.0	9956.6	1790.8
BCD21888	Mixed	CCF-39	40.85	Inmet	10228.0	9958.9	1788.5
BCD21889	Mixed	CCF-39	44.15	Inmet	10228.0	9961.2	1786.2
BCD21890	Basalt	CCF-39	47.40	Inmet	10228.0	9963.5	1783.9
BCD21891	Basalt	CCF-39	50.50	Inmet	10228.0	9965.7	1781.7
BCD21892	Basalt	CCF-39	53.50	Inmet	10228.0	9967.8	1779.6
BCD21893	Basalt	CCF-39	56.65	Inmet	10228.0	9970.1	1777.3
BCD21894	Chert	CCF-39	59.90	Inmet	10228.0	9972.4	1775.0
BCD21895	Chert	CCF-39	63.25	Inmet	10228.0	9974.7	1772.7
BCD21896	Chert	CCF-39	66.75	Inmet	10228.0	9977.2	1770.2
BCD21897	Chert	CCF-39	70.25	Inmet	10228.0	9979.7	1767.7
BCD21898	Chert	CCF-39	73.55	Inmet	10228.0	9982.0	1765.4
BCD21899	Chert	CCF-39	75.35	Inmet	10228.0	9983.3	1764.1
BCD21900	Chert	CCF-39	76.55	Inmet	10228.0	9984.1	1763.3
BCD21901	Mixed	CCF-39	78.20	Inmet	10228.0	9985.3	1762.1
BCD21902	Basalt	CCF-39	80.40	Inmet	10228.0	9986.9	1760.5
BCD21903	Basalt	CCF-39	82.55	Inmet	10228.0	9988.4	1759.0
BCD21904	Basalt	CCF-40	6.10	Inmet	10181.0	9936.0	1808.8
BCD21905	Basalt	CCF-40	12.10	Inmet	10181.0	9940.2	1804.5
BCD21906	Basalt	CCF-40	17.75	Inmet	10181.0	9944.1	1800.4
BCD21907	Basalt	CCF-40	20.70	Inmet	10181.0	9946.2	1798.3
BCD21908	Basalt	CCF-40	22.85	Inmet	10181.0	9947.7	1796.8
BCD21909	Basalt	CCF-40	26.20	Inmet	10181.0	9950.0	1794.4
BCD21910	Chert	CCF-40	32.20	Inmet	10181.0	9954.2	1790.0
BCD21911	Mixed	CCF-40	38.05	Inmet	10181.0	9958.2	1785.8
BCD21912	Chert	CCF-40	41.95	Inmet	10181.0	9960.9	1783.0
BCD21913	Chert	CCF-40	43.40	Inmet	10181.0	9961.9	1782.0
BCD21914	Chert	CCF-40	45.30	Inmet	10181.0	9963.3	1780.6

Sample#	Lithology	Drill hole/ location	Depth (m)	Source	Northing (m)	Easting (m)	Elevation (m)
BCD21915	Basalt	CCF-40	47.20	Inmet	10181.0	9964.6	1779.2
BCD21916	Chert	CCF-40	49.15	Inmet	10181.0	9965.9	1777.8
BCD21917	Basalt	CCF-40	51.05	Inmet	10181.0	9967.3	1776.5
BCD21918	Chert	CCF-40	54.10	Inmet	10181.0	9969.4	1774.3
BCD21919	Chert	CCF-40	58.90	Inmet	10181.0	9972.7	1770.8
BCD21920	Chert	CCF-40	62.25	Inmet	10181.0	9975.0	1768.4
BCD21921	Mixed	CCF-40	65.10	Inmet	10181.0	9977.0	1766.4
BCD21922	Mixed	CCF-40	67.20	Inmet	10181.0	9978.5	1764.9
BCD21923	Chert	CCF-40	71.00	Inmet	10181.0	9981.1	1762.1
BCD21924	Chert	CCF-40	78.05	Inmet	10181.0	9986.0	1757.1
BCD21925	Chert	CCF-40	82.10	Inmet	10181.0	9988.8	1754.1
BCD21926	Basalt	CCF-41	5.85	Inmet	10175.0	9922.4	1804.4
BCD21927	Basalt	CCF-41	11.25	Inmet	10175.0	9926.3	1800.5
BCD21928	Basalt	CCF-41	16.75	Inmet	10175.0	9930.1	1796.7
BCD21929	Basalt	CCF-41	22.25	Inmet	10175.0	9934.0	1792.8
BCD21930	Basalt	CCF-41	28.00	Inmet	10175.0	9938.1	1788.7
BCD21931	Basalt	CCF-41	33.75	Inmet	10175.0	9942.2	1784.6
BCD21932	Basalt	CCF-41	39.00	Inmet	10175.0	9945.9	1780.9
BCD21933	Basalt	CCF-41	44.00	Inmet	10175.0	9949.4	1777.4
BCD21934	Mixed	CCF-41	56.95	Inmet	10175.0	9958.6	1768.2
BCD21935	Chert	CCF-41	62.05	Inmet	10175.0	9962.2	1764.6
BCD21936	Basalt	CCF-42	5.45	Inmet	10190.0	9902.9	1805.1
BCD21937	Basalt	CCF-42	15.00	Inmet	10190.0	9909.6	1798.4
BCD21938	Basalt	CCF-42	25.00	Inmet	10190.0	9916.7	1791.3
BCD21939	Basalt	CCF-42	35.00	Inmet	10190.0	9923.7	1784.3
BCD21940	Basalt	CCF-42	45.00	Inmet	10190.0	9930.8	1777.2
BCD21941	Basalt	CCF-42	55.00	Inmet	10190.0	9937.9	1770.1
BCD21942	Basalt	CCF-42	64.30	Inmet	10190.0	9944.5	1763.5
BCD21943	Basalt	CCF-42	64.95	Inmet	10190.0	9944.9	1763.1
BCD21944	Chert	CCF-42	73.10	Inmet	10190.0	9950.7	1757.3
BCD21945	Chert	CCF-42	81.00	Inmet	10190.0	9956.3	1751.7
BCD21964	Basalt	CCF-43	5.75	Inmet	10206.0	9919.1	1808.8
BCD21965	Basalt	CCF-43	15.00	Inmet	10206.0	9925.6	1802.3
BCD21966	Basalt	CCF-43	25.00	Inmet	10206.0	9932.7	1795.2
BCD21967	Basalt	CCF-43	35.00	Inmet	10206.0	9939.7	1788.2
BCD21968	Basalt	CCF-43	42.55	Inmet	10206.0	9945.1	1782.8
BCD21969	Mixed	CCF-43	48.55	Inmet	10206.0	9949.3	1778.6
BCD21970	Basalt	CCF-43	55.25	Inmet	10206.0	9954.1	1773.8
BCD21971	Chert	CCF-43	60.25	Inmet	10206.0	9957.6	1770.3
BCD21972	Chert	CCF-43	66.35	Inmet	10206.0	9961.9	1766.0
BCD21973	Basalt	CCF-43	71.35	Inmet	10206.0	9965.5	1762.4
BCD21974	Mixed	CCF-43	73.85	Inmet	10206.0	9967.2	1760.7
BCD21975	Basalt	CCF-43	76.25	Inmet	10206.0	9968.9	1759.0
BCD21976	Chert	CCF-43	78.50	Inmet	10206.0	9970.5	1757.4
BCD21977	Mixed	CCF-43	82.30	Inmet	10206.0	9973.2	1754.7
BCD21978	Chert	CCF-43	90.35	Inmet	10206.0	9978.9	1749.0
BCD21979	Basalt	CCF-43	97.20	Inmet	10206.0	9983.7	1744.2
BCD21980	Mixed	CCF-43	102.70	Inmet	10206.0	9987.6	1740.3
BCD21981	Basalt	CCF-44	6.55	Inmet	10031.1	9919.9	1792.7
BCD21982	Basalt	CCF-44	15.00	Inmet	10031.1	9925.0	1785.9
BCD21983	Basalt	CCF-44	25.00	Inmet	10031.1	9931.0	1777.9

Sample#	Lithology	Drill hole/ location	Depth (m)	Source	Northing (m)	Easting (m)	Elevation (m)
BCD21984	Basalt	CCF-44	35.00	Inmet	10031.1	9937.1	1769.9
BCD21985	Basalt	CCF-44	45.00	Inmet	10031.1	9943.1	1762.0
BCD21986	Basalt	CCF-44	55.00	Inmet	10031.1	9949.1	1754.0
BCD21987	Basalt	CCF-44	65.00	Inmet	10031.1	9955.1	1746.0
BCD21988	Basalt	CCF-44	73.00	Inmet	10031.1	9959.9	1739.6
BCD21989	Basalt	CCF-44	78.60	Inmet	10031.1	9963.3	1735.1
BCD21990	Basalt	CCF-44	91.95	Inmet	10031.1	9971.3	1724.5
BCD21991	Basalt	CCF-44	95.90	Inmet	10031.1	9973.7	1721.3
BCD21992	Chert	CCF-44	101.40	Inmet	10031.1	9977.0	1716.9
BCD21993	Chert	CCF-44	108.30	Inmet	10031.1	9981.2	1711.4
BCD22351	Basalt	CCF-31	5.50	Inmet	9999.7	9936.0	1790.3
BCD22352	Basalt	CCF-31	10.50	Inmet	9999.7	9939.1	1786.3
BCD22353	Basalt	CCF-31	15.50	Inmet	9999.7	9942.1	1782.4
BCD22354	Basalt	CCF-31	20.50	Inmet	9999.7	9945.2	1778.4
BCD22355	Basalt	CCF-31	25.50	Inmet	9999.7	9948.3	1774.5
BCD22356	Basalt	CCF-31	30.50	Inmet	9999.7	9951.4	1770.6
BCD22357	Basalt	CCF-31	35.50	Inmet	9999.7	9954.5	1766.6
BCD22358	Basalt	CCF-31	40.00	Inmet	9999.7	9957.2	1763.1
BCD22359	Basalt	CCF-31	43.75	Inmet	9999.7	9959.5	1760.1
BCD22362	Mixed	CCF-31	77.50	Inmet	9999.7	9980.3	1733.5
BCD22363	Basalt	CCF-31	82.50	Inmet	9999.7	9983.4	1729.6
BCD22364	Basalt	CCF-31	87.30	Inmet	9999.7	9986.3	1725.8
BCD22514	Basalt	CCF-45	17.30	Inmet	9999.4	9932.0	1780.1
BCD22515	Basalt	CCF-45	57.30	Inmet	9999.4	9953.2	1746.2
BCD22516	Basalt	CCF-45	67.30	Inmet	9999.4	9958.5	1737.7
BCD22517	Basalt	CCF-45	77.30	Inmet	9999.4	9963.8	1729.2
BCD22518	Chert	CCF-45	101.65	Inmet	9999.4	9976.7	1708.6
BCD22519	Chert	CCF-45	106.25	Inmet	9999.4	9979.1	1704.7
BCD22520	Chert	CCF-45	110.80	Inmet	9999.4	9981.5	1700.8
BCD22521	Chert	CCF-45	115.00	Inmet	9999.4	9983.7	1697.3
BCD22522	Basalt	CCF-45	118.65	Inmet	9999.4	9985.7	1694.2
BCD22524	Basalt	CCF-46	6.60	Inmet	9964.9	9921.0	1783.9
BCD22525	Basalt	CCF-46	11.65	Inmet	9964.9	9923.9	1779.8
BCD22558	Basalt	CCF-47	7.65	Inmet	9964.8	9922.9	1783.7
BCD22559	Mixed	CCF-47	14.85	Inmet	9964.8	9927.8	1778.4
BCD22560	Basalt	CCF-47	17.90	Inmet	9964.8	9929.9	1776.2
BCD22561	Mt-tlc altrd	CCF-47	21.50	Inmet	9964.8	9932.4	1773.6
BCD22562	Mt-tlc altrd	CCF-47	24.25	Inmet	9964.8	9934.2	1771.6
BCD22563	Basalt	CCF-47	32.40	Inmet	9964.8	9939.8	1765.6
BCD22564	Basalt	CCF-47	40.00	Inmet	9964.8	9945.0	1760.0
BCD22565	Basalt	CCF-47	47.55	Inmet	9964.8	9950.1	1754.5
BCD22566	Mt-tlc altrd	CCF-47	77.75	Inmet	9964.8	9970.7	1732.4
BCD22567	Chert	CCF-47	81.55	Inmet	9964.8	9973.3	1729.7
BCD22568	Chert	CCF-47	84.70	Inmet	9964.8	9975.5	1727.4
BCD22569	Mixed	CCF-47	94.20	Inmet	9964.8	9981.9	1720.4
BCD22570	Basalt	CCF-46	17.60	Inmet	9964.9	9927.3	1774.9
BCD22571	Basalt	CCF-46	24.15	Inmet	9964.9	9931.1	1769.5
BCD22572	Chert	CCF-46	25.15	Inmet	9964.9	9931.6	1768.7
BCD22573	Basalt	CCF-46	29.15	Inmet	9964.9	9933.9	1765.4
BCD22574	Basalt	CCF-46	36.30	Inmet	9964.9	9938.0	1759.6
BCD22575	Basalt	CCF-48	6.25	Inmet	9915.4	9924.1	1777.8

Sample#	Lithology	Drill hole/ location	Depth (m)	Source	Northing (m)	Easting (m)	Elevation (m)
BCD22576	Basalt	CCF-48	18.00	Inmet	9915.4	9932.4	1769.5
BCD22577	Basalt	CCF-48	30.00	Inmet	9915.4	9940.9	1761.0
BCD22578	Basalt	CCF-48	41.00	Inmet	9915.4	9948.7	1753.2
BCD22877	Basalt	CCF-50	12.85	Inmet	9927.4	9956.0	1776.9
BCD22878	Chert	CCF-50	24.30	Inmet	9927.4	9964.1	1768.8
BCD22879	Chert	CCF-50	28.75	Inmet	9927.4	9967.2	1765.7
BCD22880	Basalt	CCF-50	36.05	Inmet	9927.4	9972.4	1760.5
BCD22882	Basalt	CCF-51	71.10	Inmet	10190.0	9939.8	1750.8
BCD22883	Basalt	CCF-51	78.40	Inmet	10190.0	9944.0	1744.8
BCD22884	Chert	CCF-51	85.95	Inmet	10190.0	9948.3	1738.6
6501	Basalt	CC-48	5.00	Inmet	9800.0	9717.2	1736.9
6502	Basalt	CC-48	39.00	Inmet	9800.0	9739.1	1710.9
6503	Basalt	CC-48	70.00	Inmet	9800.0	9759.0	1687.1
6504	Basalt	CC-48	101.00	Inmet	9800.0	9778.9	1663.4
6505	Basalt	CC-48	132.00	Inmet	9800.0	9798.8	1639.6
6506	Basalt	CC-48	164.00	Inmet	9800.0	9819.4	1615.1
6507	Basalt	CC-48	194.00	Inmet	9800.0	9838.7	1592.1
6508	Basalt	CC-48	219.00	Inmet	9800.0	9854.8	1573.0
6509	Basalt	CC-48	249.00	Inmet	9800.0	9874.1	1550.0
6510	Basalt	CC-48	278.00	Inmet	9800.0	9892.7	1527.8
6511	Basalt	CC-48	306.00	Inmet	9800.0	9910.7	1506.3
6512	Basalt	CC-48	336.00	Inmet	9800.0	9930.0	1483.3
6513	Basalt	CC-48	375.00	Inmet	9800.0	9955.0	1453.5
6514	Basalt	CC-48	396.00	Inmet	9800.0	9968.5	1437.4
6515	Basalt	CC-48	426.00	Inmet	9800.0	9987.8	1414.4
6516	Basalt	CC-48	441.00	Inmet	9800.0	9997.5	1402.9
6517	Basalt	CC-28	9.00	Inmet	9899.0	9899.2	1770.1
6518	Basalt	CC-28	40.00	Inmet	9899.0	9916.9	1744.7
6519	Basalt	CC-28	71.00	Inmet	9899.0	9934.7	1719.3
6520	Basalt	CC-28	104.00	Inmet	9899.0	9953.7	1692.3
6521	Basalt	CC-28	153.00	Inmet	9899.0	9981.8	1652.2
6526	Basalt	CC-49	5.00	Inmet	9880.0	9729.9	1755.6
6527	Basalt	CC-49	67.00	Inmet	9880.0	9765.4	1704.8
6528	Basalt	CC-49	130.00	Inmet	9880.0	9801.6	1653.2
6529	Basalt	CC-49	193.00	Inmet	9880.0	9837.7	1601.6
6530	Basalt	CC-49	255.00	Inmet	9880.0	9873.3	1550.8
6531	Basalt	CC-49	318.00	Inmet	9880.0	9909.4	1499.2
6532	Basalt	CC-49	381.00	Inmet	9880.0	9945.5	1447.6
6533	Basalt	CC-49	450.00	Inmet	9880.0	9985.1	1391.1
6534	Basalt	CC-49	482.00	Inmet	9880.0	10003.5	1364.9
6535	Basalt	CC-49	502.00	Inmet	9880.0	10014.9	1348.5
6536	Basalt	CC-21	5.00	Inmet	9905.0	10111.2	1789.4
6537	Basalt	CC-21	36.00	Inmet	9905.0	10131.1	1765.6
6538	<Ti basalt	CC-21	67.00	Inmet	9905.0	10151.1	1741.9
6539	Basalt	CC-21	98.00	Inmet	9905.0	10171.0	1718.1
6540	Basalt	CC-21	130.00	Inmet	9905.0	10191.6	1693.6
6541	Basalt	CC-21	161.50	Inmet	9905.0	10211.8	1669.5
6542	Basalt	CC-21	192.00	Inmet	9905.0	10231.4	1646.1
6543	Basalt	CC-17	68.00	Inmet	10105.2	9998.1	1750.6
6544	<Ti basalt	CC-17	99.00	Inmet	10105.2	10018.0	1726.9
6545	Basalt	CC-23	50.00	Inmet	10054.3	10017.1	1770.0

Sample#	Lithology	Drill hole/ location	Depth (m)	Source	Northing (m)	Easting (m)	Elevation (m)
6547	Basalt	CC-18	35.00	Inmet	10253.6	9962.5	1798.0
6548	<Ti basalt	CC-18	86.00	Inmet	10253.6	9995.3	1758.9
6549	Basalt	CC-19	10.00	Inmet	10203.3	9868.3	1803.7
6550	Basalt	CC-19	71.00	Inmet	10203.3	9907.5	1757.0
6551	Basalt	CC-19	126.50	Inmet	10203.3	9943.2	1714.5
6552	Basalt	CC-19	161.00	Inmet	10203.3	9965.4	1688.1
6553	Basalt	CC-19	206.00	Inmet	10203.3	9994.3	1653.6
6554	Basalt	CC-29	10.00	Inmet	10152.4	9854.5	1796.0
6555	Basalt	CC-29	71.00	Inmet	10152.4	9893.7	1749.3
6556	Basalt	CC-29	133.00	Inmet	10152.4	9933.6	1701.8
6557	Basalt	CC-29	208.00	Inmet	10152.4	9981.8	1644.4
6558	Basalt	CC-29	243.00	Inmet	10152.4	10004.3	1617.6
6559	Basalt	CC-30	5.00	Inmet	9899.0	9815.2	1765.5
6560	Basalt	CC-30	66.00	Inmet	9899.0	9854.4	1718.7
6561	Basalt	CC-30	126.00	Inmet	9899.0	9893.0	1672.8
6562	Basalt	CC-30	186.00	Inmet	9899.0	9931.6	1626.8
6563	Basalt	CC-30	246.00	Inmet	9899.0	9970.1	1580.9
6564	Basalt	CC-30	275.00	Inmet	9899.0	9988.8	1558.6
6565	Basalt	CC-32	10.00	Inmet	10305.0	9850.4	1810.3
6566	Basalt	CC-32	48.00	Inmet	10305.0	9874.9	1781.2
6567	Basalt	CC-32	85.00	Inmet	10305.0	9898.6	1752.9
6568	Basalt	CC-32	116.00	Inmet	10305.0	9918.6	1729.1
6577	Basalt	CC-38	21.00	Inmet	9797.0	9820.5	1738.3
6578	Basalt	CC-38	71.00	Inmet	9797.0	9852.6	1700.0
6579	Basalt	CC-38	131.00	Inmet	9797.0	9891.2	1654.0
6580	Basalt	CC-38	191.50	Inmet	9797.0	9930.1	1607.7
6581	Basalt	CC-38	252.00	Inmet	9797.0	9969.0	1561.4
6582	Basalt	CC-38	286.00	Inmet	9797.0	9990.8	1535.3
6588	Basalt	CC-55	10.00	Inmet	9999.0	9730.7	1771.9
6589	Basalt	CC-55	71.00	Inmet	9999.0	9765.7	1722.0
6590	Basalt	CC-55	132.00	Inmet	9999.0	9800.7	1672.0
6591	Basalt	CC-55	193.00	Inmet	9999.0	9835.7	1622.0
6592	Basalt	CC-55	253.00	Inmet	9999.0	9870.1	1572.9
6593	Basalt	CC-55	314.00	Inmet	9999.0	9905.1	1522.9
6594	Basalt	CC-55	370.00	Inmet	9999.0	9937.2	1477.0
6595	Basalt	CC-55	415.00	Inmet	9999.0	9963.0	1440.2
6596	Basalt	CC-55	456.00	Inmet	9999.0	9986.6	1406.6
6597	Basalt	CC-56	14.00	Inmet	9700.0	9763.0	1717.7
6598	Basalt	CC-56	73.00	Inmet	9700.0	9796.9	1669.4
6599	Basalt	CC-56	131.00	Inmet	9700.0	9830.1	1621.9
6600	Basalt	CC-56	191.00	Inmet	9700.0	9864.6	1572.7
6651	Basalt	CC-56	251.00	Inmet	9700.0	9899.0	1523.6
6652	Basalt	CC-56	311.00	Inmet	9700.0	9933.4	1474.4
6653	Basalt	CC-56	371.00	Inmet	9700.0	9967.8	1425.3
6654	Basalt	CC-24	5.00	Inmet	9984.0	9812.9	1772.6
6655	Basalt	CC-24	37.00	Inmet	9984.0	9831.2	1746.4
6656	Basalt	CC-24	68.00	Inmet	9984.0	9849.0	1721.0
6657	Basalt	CC-24	100.00	Inmet	9984.0	9867.4	1694.8
6658	Basalt	CC-24	132.00	Inmet	9984.0	9885.7	1668.6
6659	Basalt	CC-24	163.00	Inmet	9984.0	9903.5	1643.2
6660	Basalt	CC-24	194.00	Inmet	9984.0	9921.3	1617.8

Sample#	Lithology	Drill hole/ location	Depth (m)	Source	Northing (m)	Easting (m)	Elevation (m)
6661	Basalt	CC-24	225.00	Inmet	9984.0	9939.1	1592.4
6662	Basalt	CC-24	257.00	Inmet	9984.0	9957.4	1566.2
6663	Basalt	CC-24	301.00	Inmet	9984.0	9982.6	1530.1
6664	Basalt	CC-25	3.00	Inmet	9944.0	9901.0	1781.7
6665	Basalt	CC-25	34.00	Inmet	9944.0	9918.8	1756.3
6666	Basalt	CC-25	65.00	Inmet	9944.0	9936.6	1731.0
6667	Basalt	CC-25	99.00	Inmet	9944.0	9956.1	1703.1
6668	Basalt	CC-25	157.00	Inmet	9944.0	9989.4	1655.6
6669	Basalt	CC-26	20.00	Inmet	9944.0	9910.8	1767.8
6670	Basalt	CC-26	78.00	Inmet	9942.0	9981.7	1723.1
6671	Basalt	CC-27	5.00	Inmet	10042.1	9834.0	1787.4
6672	Basalt	CC-27	65.00	Inmet	10042.1	9868.4	1738.3
6673	Basalt	CC-27	124.00	Inmet	10042.1	9902.2	1689.9
6674	Basalt	CC-27	185.00	Inmet	10042.1	9937.2	1640.0
6675	Basalt	CC-27	255.00	Inmet	10042.1	9977.4	1582.6
6676	Basalt	CC-45	5.00	Inmet	10095.0	9774.9	1787.9
6677	Basalt	CC-45	65.00	Inmet	10095.0	9809.3	1738.8
6678	Basalt	CC-45	125.00	Inmet	10095.0	9843.7	1689.6
6679	Basalt	CC-45	185.00	Inmet	10095.0	9878.1	1640.5
6680	Basalt	CC-45	245.00	Inmet	10095.0	9912.5	1591.3
6681	<Ti basalt	CC-45	310.00	Inmet	10095.0	9949.8	1538.1
6682	Basalt	CC-46	5.00	Inmet	9605.0	9749.7	1725.1
6683	Basalt	CC-46	37.00	Inmet	9605.0	9769.8	1700.3
6684	Basalt	CC-46	68.00	Inmet	9605.0	9789.4	1676.2
6685	Basalt	CC-46	100.00	Inmet	9605.0	9809.6	1651.4
6686	Basalt	CC-46	131.00	Inmet	9605.0	9829.1	1627.3
6687	Basalt	CC-46	163.00	Inmet	9605.0	9849.3	1602.5
6688	Basalt	CC-46	194.00	Inmet	9605.0	9868.9	1578.4
6689	Basalt	CC-46	225.00	Inmet	9605.0	9888.4	1554.4
6690	Basalt	CC-46	257.00	Inmet	9605.0	9908.6	1529.6
6691	Basalt	CC-46	288.00	Inmet	9605.0	9928.1	1505.5
6692	Basalt	CC-46	320.00	Inmet	9605.0	9948.3	1480.7
6693	Basalt	CC-46	357.00	Inmet	9605.0	9971.7	1452.0
6694	Basalt	CC-46	388.00	Inmet	9605.0	9991.2	1427.9
6695	Basalt	CC-46	419.00	Inmet	9605.0	10010.8	1403.8
6696	<Ti basalt	CC-54	10.00	Inmet	9799.0	9606.7	1722.6
6697	<Ti basalt	CC-54	71.00	Inmet	9799.0	9641.7	1672.6
6698	<Ti basalt	CC-54	132.00	Inmet	9799.0	9676.7	1622.7
6699	Basalt	CC-54	191.00	Inmet	9799.0	9710.6	1574.3
6701	Basalt	CC-54	311.00	Inmet	9799.0	9779.4	1476.0
6702	<Ti basalt	CC-15	101.00	Inmet	10054.7	10010.2	1717.9
6703	Basalt	CC-14	5.00	Inmet	9949.0	9867.2	1777.2
6704	Basalt	CC-14	67.00	Inmet	9949.0	9907.1	1729.7
6705	Basalt	CC-14	127.00	Inmet	9949.0	9945.6	1683.7
6706	Basalt	CC-14	206.00	Inmet	9949.0	9996.4	1623.2
6707	Basalt	CC-13	6.00	Inmet	10053.8	9911.4	1794.0
6708	Basalt	CC-13	66.00	Inmet	10053.8	9949.9	1748.0
6709	Chert	CC-13	123.00	Inmet	10053.8	9986.6	1704.4
6710	<Ti basalt	CC-13	154.00	Inmet	10053.8	10006.5	1680.6
6711	Basalt	CC-12	10.00	Inmet	10103.0	9858.7	1790.8
6712	Basalt	CC-12	42.00	Inmet	10103.0	9877.1	1764.6

Sample#	Lithology	Drill hole/ location	Depth (m)	Source	Northing (m)	Easting (m)	Elevation (m)
6713	Basalt	CC-12	73.00	Inmet	10103.0	9894.9	1739.2
6714	Basalt	CC-12	105.00	Inmet	10103.0	9913.2	1713.0
6715	Basalt	CC-12	107.00	Inmet	10103.0	9914.4	1711.4
6716	Basalt	CC-12	168.00	Inmet	10103.0	9949.4	1661.4
6717	Mixed	CC-12	187.00	Inmet	10103.0	9960.3	1645.8
6718	Basalt	CC-12	234.00	Inmet	10103.0	9987.2	1607.3
6719	<Ti basalt	CC-12	264.00	Inmet	10103.0	10004.4	1582.7
6720	Basalt	CC-11	38.00	Inmet	9940.0	9932.7	1755.5
6721	Basalt	CC-9	5.00	Inmet	9884.0	9923.2	1772.2
6722	Basalt	CC-9	37.00	Inmet	9884.0	9943.8	1747.7
6723	Basalt	CC-9	68.00	Inmet	9884.0	9963.7	1723.9
6724	Basalt	CC-9	100.00	Inmet	9884.0	9984.3	1699.4
6725	Basalt	CC-7	40.00	Inmet	10288.0	9984.7	1796.8
6726	Basalt	CC-7	66.00	Inmet	10288.0	10001.4	1776.8
6735	Basalt	CC-3	5.00	Inmet	9986.5	9902.4	1785.9
6736	Basalt	CC-3	65.00	Inmet	9986.5	9936.8	1736.8
6737	Basalt	CC-3	120.00	Inmet	9986.5	9968.3	1691.7
6738	Basalt	CC-3	156.00	Inmet	9986.5	9989.0	1662.2
6739	Basalt	CC-1	20.00	Inmet	10092.2	9933.5	1783.7
6740	Basalt	CC-1	67.00	Inmet	10092.2	9960.4	1745.2
6741	Basalt	CC-54	373.00	Inmet	9799.0	9814.9	1425.3
6742	Basalt	CC-54	431.00	Inmet	9799.0	9848.2	1377.7
6743	Basalt	CC-54	492.00	Inmet	9799.0	9883.2	1327.8
6744	Basalt	CC-54	555.00	Inmet	9799.0	9919.3	1276.2
6745	Basalt	CC-54	622.00	Inmet	9799.0	9957.8	1221.3
6746	Basalt	CC-54	683.00	Inmet	9799.0	9992.8	1171.3
6747	<Ti basalt	CC-57	10.00	Inmet	9700.0	9633.7	1712.5
6748	<Ti basalt	CC-57	40.00	Inmet	9700.0	9650.9	1688.0
6749	<Ti basalt	CC-57	70.00	Inmet	9700.0	9668.2	1663.4
6750	<Ti basalt	CC-57	100.00	Inmet	9700.0	9685.4	1638.8
6767	Chert	CC-7	18.00	Inmet	10288.0	9970.6	1813.6
6768	Chert	CC-12	198.00	Inmet	10103.0	9966.6	1636.8
6769	Mixed	CC-12	269.00	Inmet	10103.0	10007.3	1578.6
6773	Chert	CC-15	85.00	Inmet	10054.7	9999.9	1730.2
6800	Basalt	CC-57	130.00	Inmet	9700.0	9702.6	1614.2
6801	Basalt	CC-57	161.00	Inmet	9700.0	9720.3	1588.8
6802	Basalt	CC-57	190.00	Inmet	9700.0	9737.0	1565.1
6803	Basalt	CC-57	221.00	Inmet	9700.0	9754.8	1539.7
6804	Basalt	CC-57	251.00	Inmet	9700.0	9772.0	1515.1
6805	Basalt	CC-57	281.00	Inmet	9700.0	9789.2	1490.5
6806	Basalt	CC-57	312.00	Inmet	9700.0	9807.0	1465.1
6807	Basalt	CC-57	342.00	Inmet	9700.0	9824.2	1440.6
6808	Basalt	CC-57	372.00	Inmet	9700.0	9841.4	1416.0
6809	Basalt	CC-57	402.00	Inmet	9700.0	9858.6	1391.4
6810	Basalt	CC-57	433.00	Inmet	9700.0	9876.4	1366.0
6811	Basalt	CC-57	466.00	Inmet	9700.0	9895.3	1339.0
6812	<Ti basalt	CC-58	6.00	Inmet	9700.0	9507.4	1699.8
6813	<Ti basalt	CC-58	65.00	Inmet	9700.0	9541.3	1651.5
6814	<Ti basalt	CC-58	125.00	Inmet	9700.0	9575.7	1602.3
6815	<Ti basalt	CC-58	185.00	Inmet	9700.0	9610.1	1553.2
6816	<Ti basalt	CC-58	245.00	Inmet	9700.0	9644.5	1504.0

Sample#	Lithology	Drill hole/ location	Depth (m)	Source	Northing (m)	Easting (m)	Elevation (m)
6817	Basalt	CC-58	306.00	Inmet	9700.0	9679.5	1454.1
6818	<Ti basalt	CC-59	5.00	Inmet	9600.0	9593.9	1686.9
6819	<Ti basalt	CC-59	65.00	Inmet	9600.0	9628.3	1637.8
6820	<Ti basalt	CC-59	125.00	Inmet	9600.0	9662.7	1588.6
6821	<Ti basalt	CC-59	185.00	Inmet	9600.0	9697.1	1539.5
6822	Basalt	CC-59	240.00	Inmet	9600.0	9728.7	1494.4
6823	Basalt	CC-59	305.00	Inmet	9600.0	9765.9	1441.2
6824	Basalt	CC-59	365.00	Inmet	9600.0	9800.4	1392.0
6825	Basalt	CC-59	425.00	Inmet	9600.0	9834.8	1342.9
6826	Basalt	CC-59	485.00	Inmet	9600.0	9869.2	1293.7
6827	Basalt	CC-59	546.00	Inmet	9600.0	9904.2	1243.7
6828	Basalt	CC-59	596.00	Inmet	9600.0	9932.9	1202.8
10281	Chert	CC-37	49.50	Inmet	10800.0	9908.8	1773.1
10282	Chert	CC-37	111.50	Inmet	10800.0	9948.7	1725.6
10288	Chert	CC-39	76.50	Inmet	11000.0	9829.2	1701.4
10289	Basalt	CC-39	96.50	Inmet	11000.0	9842.0	1686.1
10290	Chert	CC-39	121.50	Inmet	11000.0	9858.1	1666.9
10293	Chert	CC-1	101.50	Inmet	10092.2	9980.2	1717.0
10294	Chert	CC-6	33.50	Inmet	10196.5	10003.5	1798.2
10295	Mixed	CC-6	71.50	Inmet	10196.5	9979.0	1769.1
10298	?	CC-24	287.25	Inmet	9984.0	9974.8	1541.4
10299	Chert	CC-55	379.50	Inmet	9999.0	9942.7	1469.2
10300	Basalt	CC-55	458.50	Inmet	9999.0	9988.0	1404.5
10301	Chert	CC-39	472.50	Inmet	11000.0	10083.7	1398.0
17525	<Ti basalt	CCF-19	78.50	Inmet	10082.3	10005.4	1746.1
18003	Basalt	CCF-25	45.50	Inmet	10187.1	10011.1	1787.4
18004	Mixed	CCF-26	19.50	Inmet	10177.7	9976.2	1801.7
18017	Mixed	CCF-26	67.50	Inmet	10177.7	10007.1	1764.9
18051	Chert	CCF-24	20.50	Inmet	10220.4	9965.0	1804.7
18052	Basalt	CCF-24	29.50	Inmet	10220.4	9970.8	1797.8
18067	Basalt	CCF-24	64.50	Inmet	10220.4	9993.3	1771.0
18087	<Ti basalt	CCF-20	104.95	Inmet	10075.4	10001.0	1725.1
24928	Basalt	CCF-62	695.80	Inmet	9600.0	9965.3	1152.0
24929	Mixed	CCF-62	702.15	Inmet	9600.0	9969.3	1147.1
24941	Basalt	CCF-62	716.70	Inmet	9600.0	9978.7	1136.0
24942	Basalt	CCF-62	730.70	Inmet	9600.0	9987.7	1125.3
24947	Basalt	CCF-62	735.85	Inmet	9600.0	9991.0	1121.3
24948	Basalt	CCF-62	771.80	Inmet	9600.0	10014.1	1093.8
24951	Basalt	CCF-62	777.10	Inmet	9600.0	10017.5	1089.7
24952	Basalt	CCF-62	811.60	Inmet	9600.0	10039.7	1063.3
34751	Chert	CCF-63	384.73	Inmet	10300.0	9986.9	1486.7
34755	Chert	CCF-63	390.95	Inmet	10300.0	9990.2	1481.5
34768	Chert	CCF-64	182.70	Inmet	10614.0	9960.0	1674.8
34779	Mixed	CCF-66	475.25	Inmet	10130.0	9919.0	1352.4
35076	Basalt	CCF-69	551.65	Inmet	9997.0	9933.7	1268.5
35077	Chert	CCF-69	567.80	Inmet	9997.0	9939.7	1253.5
35078	<Ti basalt	CCF-70	64.60	Inmet	9925.0	9629.3	1692.4
35079	<Ti basalt	CCF-70	125.58	Inmet	9925.0	9657.0	1638.1
35080	Basalt	CCF-70	186.50	Inmet	9925.0	9684.7	1583.8
35081	Basalt	CCF-70	247.50	Inmet	9925.0	9712.4	1529.5
35082	Basalt	CCF-70	316.83	Inmet	9925.0	9743.8	1467.7



Sample#	Lithology	Drill hole/ location	Depth (m)	Source	Northing (m)	Easting (m)	Elevation (m)
35083	Basalt	CCF-70	372.50	Inmet	9925.0	9769.1	1418.1
35084	Basalt	CCF-70	436.50	Inmet	9925.0	9798.2	1361.1
35085	Basalt	CCF-70	490.50	Inmet	9925.0	9822.7	1313.0
35086	Basalt	CCF-70	524.50	Inmet	9925.0	9838.1	1282.7
35087	Basalt	CCF-70	573.30	Inmet	9925.0	9860.3	1239.2
35088	Basalt	CCF-70	607.25	Inmet	9925.0	9875.7	1208.9
35089	Basalt	CCF-70	641.55	Inmet	9925.0	9891.3	1178.4
35090	Basalt	CCF-70	684.55	Inmet	9925.0	9910.8	1140.1
35091	Basalt	CCF-71	485.20	Inmet	10084.0	9848.9	1329.1
35092	Basalt	CCF-71	524.80	Inmet	10084.0	9862.5	1291.8
35093	Basalt	CCF-71	579.70	Inmet	10084.0	9881.3	1240.3
35094	<Ti basalt	CCF-71	628.50	Inmet	10084.0	9898.0	1194.4
35095	Mixed	CCF-71	671.10	Inmet	10084.0	9912.5	1154.4
35096	Mixed	CCF-71	713.80	Inmet	10084.0	9927.1	1114.2
35201	Basalt	CCF-63	12.50	Inmet	10300.0	9789.6	1802.4
35202	Basalt	CCF-63	63.70	Inmet	10300.0	9816.8	1759.0
35203	Basalt	CCF-63	116.15	Inmet	10300.0	9844.6	1714.5
35204	Basalt	CCF-63	167.90	Inmet	10300.0	9872.0	1670.6
35205	Basalt	CCF-63	219.70	Inmet	10300.0	9899.4	1626.7
35206	Basalt	CCF-63	272.20	Inmet	10300.0	9927.2	1582.2
35207	Chert	CCF-63	329.15	Inmet	10300.0	9957.4	1533.9
35208	Chert	CCF-63	353.80	Inmet	10300.0	9970.5	1513.0
35209	Chert	CCF-63	424.00	Inmet	10300.0	10007.7	1453.4
35210	Chert	CCF-63	454.50	Inmet	10300.0	10023.8	1427.6
35211	Chert	CCF-63	481.90	Inmet	10300.0	10038.4	1404.3
35212	Chert	CCF-63	518.50	Inmet	10300.0	10057.8	1373.3
35213	Chert	CCF-64	27.70	Inmet	10614.0	9871.8	1802.2
35214	Basalt	CCF-64	67.30	Inmet	10614.0	9894.3	1769.7
35215	Chert	CCF-64	121.50	Inmet	10614.0	9925.1	1725.1
35216	Chert	CCF-64	136.50	Inmet	10614.0	9933.7	1712.8
35217	Chert	CCF-64	216.70	Inmet	10614.0	9979.3	1646.8
35218	Chert	CCF-64	251.70	Inmet	10614.0	9999.2	1618.0
35219	Chert	CCF-64	290.50	Inmet	10614.0	10021.3	1586.1
35220	Chert	CCF-65	24.70	Inmet	10800.0	9858.9	1787.9
35221	Basalt	CCF-65	67.30	Inmet	10800.0	9874.1	1748.2
35222	Chert	CCF-64	103.95	Inmet	10614.0	9915.1	1739.5
35223	Chert	CCF-64	160.15	Inmet	10614.0	9947.1	1693.3
35224	Chert	CCF-65	107.00	Inmet	10800.0	9888.3	1711.1
35225	Basalt	CCF-65	122.05	Inmet	10800.0	9893.7	1697.1
35226	Basalt	CCF-65	170.55	Inmet	10800.0	9911.1	1651.8
35227	Basalt	CCF-65	212.90	Inmet	10800.0	9926.3	1612.2
35228	Chert	CCF-65	244.15	Inmet	10800.0	9937.5	1583.1
35229	Basalt	CCF-65	311.20	Inmet	10800.0	9961.5	1520.5
35230	<Ti basalt	CCF-65	366.00	Inmet	10800.0	9981.2	1469.3
35231	Chert	CCF-65	396.70	Inmet	10800.0	9992.2	1440.6
35232	Basalt	CCF-66	15.50	Inmet	10130.0	9746.8	1778.6
35233	Basalt	CCF-66	64.50	Inmet	10130.0	9765.2	1733.2
35234	Basalt	CCF-66	119.20	Inmet	10130.0	9785.7	1682.5
35235	Basalt	CCF-66	173.50	Inmet	10130.0	9806.0	1632.1
35236	Basalt	CCF-66	225.50	Inmet	10130.0	9825.5	1583.9
35237	Basalt	CCF-66	271.50	Inmet	10130.0	9842.7	1541.3

Sample#	Lithology	Drill hole/ location	Depth (m)	Source	Northing (m)	Easting (m)	Elevation (m)
35238	Basalt	CCF-66	323.50	Inmet	10130.0	9862.2	1493.1
35239	Basalt	CCF-66	375.50	Inmet	10130.0	9881.7	1444.8
35240	Basalt	CCF-66	427.00	Inmet	10130.0	9901.0	1397.1
35241	Basalt	CCF-66	512.50	Inmet	10130.0	9933.0	1317.8
35242	Chert	CCF-66	545.90	Inmet	10130.0	9945.5	1286.9
35243	Chert	CCF-66	592.50	Inmet	10130.0	9963.0	1243.6
35244	Chert	CCF-66	643.50	Inmet	10130.0	9982.1	1196.4
35245	Chert	CCF-66	686.10	Inmet	10130.0	9998.0	1156.9
35246	Basalt	CCF-67	15.20	Inmet	9496.0	9754.9	1677.0
35247	Basalt	CCF-67	64.60	Inmet	9496.0	9780.8	1634.9
35248	Basalt	CCF-67	113.50	Inmet	9496.0	9806.3	1593.2
35249	Basalt	CCF-67	165.20	Inmet	9496.0	9833.3	1549.1
35250	Basalt	CCF-67	214.00	Inmet	9496.0	9858.8	1507.5
35251	Basalt	CCF-67	265.80	Inmet	9496.0	9885.9	1463.4
35252	Basalt	CCF-67	314.50	Inmet	9496.0	9911.3	1421.8
35253	Basalt	CCF-67	369.50	Inmet	9496.0	9940.1	1374.9
35254	Basalt	CCF-67	418.20	Inmet	9496.0	9965.5	1333.4
35255	Basalt	CCF-67	469.50	Inmet	9496.0	9992.3	1289.7
35257	Basalt	CCF-68	34.15	Inmet	9250.0	10101.4	1667.0
35258	Basalt	CCF-68	85.95	Inmet	9250.0	10071.7	1624.6
35259	<Ti basalt	CCF-68	134.70	Inmet	9250.0	10043.7	1584.7
35260	Basalt	CCF-68	186.50	Inmet	9250.0	10014.0	1542.2
35261	Basalt	CCF-68	238.35	Inmet	9250.0	9984.3	1499.8
35262	Basalt	CCF-68	287.10	Inmet	9250.0	9956.3	1459.8
35263	Basalt	CCF-68	335.90	Inmet	9250.0	9928.3	1419.8
35264	Basalt	CCF-68	381.50	Inmet	9250.0	9902.2	1382.5
35265	Basalt	CCF-69	10.00	Inmet	9997.0	9730.7	1770.7
35266	Basalt	CCF-69	61.88	Inmet	9997.0	9750.2	1722.6
35267	Basalt	CCF-69	110.65	Inmet	9997.0	9768.5	1677.4
35268	Basalt	CCF-69	159.35	Inmet	9997.0	9786.7	1632.3
35269	Basalt	CCF-69	206.90	Inmet	9997.0	9804.5	1588.2
35270	Basalt	CCF-69	256.90	Inmet	9997.0	9823.2	1541.8
35271	Basalt	CCF-69	305.70	Inmet	9997.0	9841.5	1496.6
35272	Basalt	CCF-69	354.50	Inmet	9997.0	9859.8	1451.3
35273	Basalt	CCF-69	406.20	Inmet	9997.0	9879.2	1403.4
35274	Basalt	CCF-69	467.55	Inmet	9997.0	9902.1	1346.5
35275	<Ti basalt	CCF-69	518.45	Inmet	9997.0	9921.2	1299.3

Sample#	Table A3.2. Major element concentrations										
	Al <sub>2</sub> O <sub>3</sub> (%)	CaO (%)	Cr <sub>2</sub> O <sub>3</sub> (%)	Fe(tot) (%)	K <sub>2</sub> O (%)	MgO (%)	MnO (%)	Na <sub>2</sub> O (%)	P <sub>2</sub> O <sub>5</sub> (%)	SiO <sub>2</sub> (%)	TiO <sub>2</sub> (%)
HS952001	13.30	8.01	0.01	11.60	0.60	6.10	0.18	3.00	0.16	40.70	0.55
HS952002	13.90	6.90	0.02	11.10	1.54	6.41	0.17	2.67	0.17	45.90	1.51
HS952003	13.50	9.55	0.01	11.20	1.97	7.33	0.17	0.48	0.13	42.00	1.45
HS952004	13.30	6.82	0.01	10.40	0.17	5.39	0.15	3.06	0.19	55.80	1.47
HS952005	13.00	3.31	0.01	12.80	1.48	6.49	0.25	0.35	0.17	53.40	1.45
HS952006	3.21	0.33	0.01	4.07	0.14	3.04	0.01	0.03	0.13	86.50	0.19
HS952007	14.70	9.05	0.02	10.70	0.43	6.63	0.17	3.01	0.15	47.50	1.43
HS952008	14.40	6.94	0.02	12.80	0.59	7.82	0.19	2.56	0.18	46.20	1.76
HS952009	14.20	9.85	0.02	12.10	0.24	6.57	0.19	2.98	0.18	47.20	1.79
HS952010	14.20	10.20	0.02	12.20	0.13	6.57	0.19	2.64	0.18	48.00	1.75
HS952011	5.47	0.23	0.01	1.42	0.95	2.34	0.01	0.07	0.06	87.30	0.25
HS952012	11.80	5.39	0.01	8.24	0.19	3.98	0.13	3.33	0.18	59.60	1.32
HS952013	12.30	11.40	0.04	11.40	0.10	7.91	0.19	2.21	0.13	48.40	1.68
HS952014	14.50	9.60	0.02	12.40	0.12	7.30	0.20	2.35	0.18	47.90	1.78
HS952015	14.00	9.81	0.02	11.90	0.38	6.60	0.19	2.59	0.18	46.60	1.75
HS952016	13.70	11.00	0.02	12.50	0.29	5.81	0.20	1.99	0.17	43.80	1.69
HS952017	13.90	11.90	0.02	11.90	0.08	6.28	0.19	2.25	0.17	46.80	1.76
HS952018	14.10	10.20	0.02	12.20	0.44	6.28	0.19	2.52	0.17	47.20	1.72
HS952019	14.00	10.60	0.02	12.10	0.14	6.38	0.19	2.54	0.17	47.50	1.74
HS952020	5.76	0.10	0.01	12.12	1.15	2.15	0.01	0.04	0.05	84.60	0.32
HS952021	8.67	3.65	0.01	6.73	0.68	3.29	0.13	1.83	0.15	71.70	0.86
HS952022	13.50	8.27	0.01	10.10	0.23	4.28	0.18	3.28	0.15	54.30	1.44
HS952023	14.20	6.38	0.01	10.10	0.34	4.25	0.17	3.79	0.17	54.40	1.60
HS952024	13.60	9.23	0.01	11.50	0.12	6.58	0.20	3.67	0.20	48.80	1.61
HS952025	6.32	1.26	0.01	5.16	1.44	1.90	0.11	0.06	0.28	79.40	0.35
HS952026	13.20	8.44	0.02	11.70	0.24	7.24	0.25	2.26	0.16	45.00	1.71
HS952027	5.63	0.36	0.01	3.19	1.63	1.87	0.18	0.05	0.08	82.90	0.30
HS952028	5.10	0.92	0.01	4.04	1.01	2.02	0.06	0.12	0.13	83.60	0.31
HS952029	14.50	10.10	0.02	12.70	0.09	7.31	0.20	2.97	0.19	46.00	1.91
HS952030	13.60	9.20	0.02	11.60	0.05	7.09	0.22	3.03	0.17	46.10	1.73
HS952031	14.00	10.70	0.02	12.00	0.15	6.68	0.19	2.12	0.18	47.80	1.80
HS952032	14.70	9.33	0.01	11.60	0.09	6.65	0.19	3.42	0.18	48.00	1.75
HS952033	14.40	10.20	0.01	11.30	0.10	6.64	0.18	2.89	0.17	48.30	1.65
HS952034	13.50	10.50	0.03	11.80	0.02	7.68	0.19	2.00	0.16	47.00	1.65
HS952035	14.40	9.15	0.02	12.20	0.03	6.87	0.19	3.08	0.17	47.20	1.82
HS952036	14.00	8.94	0.84	12.80	0.05	6.33	0.20	3.03	0.17	45.70	1.79
HS952037	13.60	7.78	0.41	12.60	0.81	6.28	0.20	2.25	0.17	43.90	1.69
HS952038	14.20	9.05	0.02	12.30	0.94	7.39	0.18	1.21	0.18	45.60	1.64
HS952039	14.20	10.10	0.02	11.90	0.16	6.92	0.19	2.86	0.17	48.80	1.75
HS952040	14.40	9.52	0.02	12.10	0.18	6.98	0.20	3.11	0.17	49.10	1.75
HS952041	13.70	8.94	0.01	16.00	0.05	6.39	0.25	2.12	0.09	45.50	2.37
HS952042	3.84	0.31	0.01	8.08	0.01	3.14	0.06	0.03	0.04	81.20	0.25
HS952043	7.85	0.21	0.01	5.77	0.55	3.83	0.03	0.18	0.10	78.00	0.54
HS952044	8.79	0.89	0.01	5.48	1.00	3.80	0.02	0.14	0.06	76.10	0.45
HS952045	5.71	1.08	0.01	1.74	0.69	3.13	0.01	0.08	0.02	85.20	0.32
HS952046	13.90	9.36	0.02	12.70	0.04	7.26	0.15	2.78	0.20	47.40	1.89
HS952047	14.70	10.70	0.02	12.40	0.12	6.62	0.19	2.61	0.18	47.50	1.82
HS952048	14.20	10.40	0.02	11.30	0.08	6.66	0.19	3.02	0.17	49.30	1.70
HS952049	14.40	10.30	0.02	12.00	0.19	6.85	0.19	2.80	0.17	48.70	1.77
HS952050	13.50	7.52	0.01	10.30	0.48	5.33	0.13	2.84	0.17	53.60	1.58

Sample#	Al <sub>2</sub> O <sub>3</sub> (%)	CaO (%)	Cr <sub>2</sub> O <sub>3</sub> (%)	Fe(tot) (%)	K <sub>2</sub> O (%)	MgO (%)	MnO (%)	Na <sub>2</sub> O (%)	P <sub>2</sub> O <sub>5</sub> (%)	SiO <sub>2</sub> (%)	TiO <sub>2</sub> (%)
HS952051	14.40	8.70	0.02	11.80	0.14	6.76	0.19	3.51	0.18	49.60	1.77
HS952052	13.70	13.20	0.02	10.70	0.02	5.99	0.18	1.92	0.15	48.30	1.59
HS952053	14.40	10.80	0.03	12.00	0.14	6.49	0.19	2.73	0.18	48.10	1.79
HS952054	14.10	8.94	0.02	11.90	0.08	6.62	0.19	3.76	0.18	49.60	1.77
HS952055	14.50	10.60	0.02	12.20	0.22	6.65	0.19	2.40	0.18	47.90	1.82
HS952056	13.60	7.80	0.01	9.89	0.14	5.38	0.17	3.40	0.18	54.40	1.52
HS952057	13.60	9.67	0.02	12.20	0.13	6.96	0.20	2.93	0.15	48.20	1.78
HS952058	10.30	4.16	0.01	8.09	1.09	4.33	0.33	0.63	0.22	63.60	0.79
HS952059	14.70	9.26	0.02	14.10	0.02	7.02	0.17	2.01	0.18	47.00	1.82
HS952060	14.50	8.71	0.02	12.40	0.07	7.44	0.20	3.43	0.19	48.40	1.84
HS952061	13.40	6.36	0.02	21.00	0.26	7.37	0.14	1.22	0.17	40.40	1.71
HS952063	14.40	11.20	0.02	12.10	0.06	6.42	0.19	2.31	0.17	47.20	1.72
HS952064	13.40	6.33	0.02	16.30	0.31	7.35	0.23	1.52	0.17	46.00	1.68
HS952065	6.91	2.17	0.01	12.20	2.03	1.84	0.07	0.08	0.30	66.70	0.43
HS952066	14.30	9.90	0.02	12.00	0.37	6.74	0.19	2.51	0.18	47.20	1.76
HS952067	14.40	9.26	0.02	12.00	0.18	6.66	0.19	3.22	0.18	48.90	1.80
HS952068	14.60	10.60	0.02	12.10	0.25	6.83	0.20	2.68	0.17	48.40	1.77
HS952069	14.20	10.40	0.02	12.60	0.21	6.51	0.19	2.47	0.17	47.10	1.79
HS971070	6.98	1.57	0.03	3.88	0.41	2.53	0.06	1.12	0.11	81.30	0.44
HS971071	6.96	2.00	0.03	5.55	0.05	3.43	0.08	1.58	0.10	77.70	0.63
HS971072	13.30	7.09	0.01	10.60	0.06	3.83	0.16	3.80	0.20	55.90	1.82
HS971073	15.20	6.39	-0.01	12.30	0.05	5.82	0.15	3.47	0.18	49.60	1.88
HS971074	15.60	5.94	-0.01	13.10	0.07	7.60	0.18	3.41	0.21	47.90	2.09
HS971075	16.10	5.97	-0.01	14.10	0.07	6.45	0.15	3.07	0.19	46.90	2.19
HS971076	13.10	9.84	0.04	10.90	0.04	6.79	0.27	2.51	0.16	45.50	1.68
HS971077	13.10	8.67	0.04	11.10	0.43	6.69	0.25	2.27	0.16	43.40	1.70
HS971078	8.52	2.10	0.02	7.17	1.28	2.62	0.29	0.09	0.35	73.20	0.55
HS971079	6.28	2.70	0.02	3.88	1.40	1.20	0.64	0.21	0.09	79.00	0.30
HS971080	6.97	2.20	0.02	3.17	1.74	1.26	0.10	0.18	0.06	80.60	0.37
HS971081	13.10	8.72	0.03	11.80	0.05	8.18	0.27	1.59	0.17	45.80	1.86
HS971082	8.15	5.04	0.04	5.55	0.02	3.25	0.12	1.82	0.12	71.40	0.72
HS971083	6.11	2.65	0.03	5.55	0.24	6.20	0.11	0.02	0.12	73.60	0.46
HS971084	4.57	0.21	0.03	2.63	0.81	1.93	-0.01	0.02	-0.01	88.00	0.22
HS971085	9.16	0.48	0.02	3.16	1.34	4.36	0.03	0.09	0.01	77.40	0.48
HS971086	6.55	0.07	0.02	2.14	0.94	3.03	0.01	0.05	0.01	84.70	0.36
HS971087	4.53	0.72	0.03	3.58	0.72	1.50	0.02	0.05	0.01	86.00	0.24
HS971088	6.97	2.52	0.03	6.51	0.10	2.16	0.51	0.63	0.26	76.30	0.40
HS971089	8.04	0.14	0.03	7.55	1.10	3.12	0.03	0.09	0.04	75.00	0.47
HS971090	6.23	0.21	0.02	5.08	0.75	3.09	0.03	0.06	0.01	81.10	0.41
HS971091	13.70	9.00	0.04	11.60	1.18	6.63	0.17	2.07	0.16	46.30	1.71
HS971092	14.00	10.10	0.04	12.40	0.02	6.91	0.20	2.31	0.19	48.30	1.95
HS971093	12.60	10.90	0.04	10.30	0.01	6.35	0.17	2.65	0.17	52.10	1.49
HS971094	12.00	7.61	0.03	10.80	0.15	7.21	0.18	2.15	0.15	51.10	1.47
HS971095	14.00	9.00	0.02	11.20	0.13	5.10	0.18	2.53	0.20	52.60	1.79
HS971096	7.56	0.41	0.03	6.64	1.58	1.67	0.40	0.06	0.14	77.00	0.37
HS971097	13.40	8.60	0.04	9.70	1.88	6.30	0.19	1.14	0.13	43.30	1.44
HS971098	14.20	9.97	0.03	10.60	0.06	5.90	0.17	3.28	0.15	50.30	1.51
HS971099	1.35	0.78	-0.01	3.33	-0.01	29.70	-0.01	0.11	0.03	58.60	0.09
HS971100	13.90	10.70	0.03	11.90	0.25	6.27	0.18	3.14	0.19	48.10	1.90
HS971101	13.80	9.85	0.04	11.50	0.31	6.91	0.20	1.92	0.17	45.00	1.77
HS971102	14.30	10.50	0.04	11.40	0.02	6.82	0.18	2.93	0.17	47.60	1.77

Sample#	Al <sub>2</sub> O <sub>3</sub> (%)	CaO (%)	Cr <sub>2</sub> O <sub>3</sub> (%)	Fe(tot) (%)	K <sub>2</sub> O (%)	MgO (%)	MnO (%)	Na <sub>2</sub> O (%)	P <sub>2</sub> O <sub>5</sub> (%)	SiO <sub>2</sub> (%)	TiO <sub>2</sub> (%)
HS971103	4.40	2.99	0.03	5.91	0.09	4.98	0.06	0.02	0.04	77.40	0.33
HS971104	14.20	8.72	0.03	11.50	0.57	6.88	0.18	3.39	0.17	47.00	1.81
HS971105	14.20	10.60	0.04	11.90	0.14	6.29	0.19	3.06	0.17	48.40	1.78
HS971106	13.80	10.90	0.04	11.40	0.23	6.63	0.19	2.70	0.16	48.10	1.72
HS971107	13.40	10.90	0.04	11.60	0.06	6.53	0.18	2.62	0.17	48.50	1.76
HS971108	14.30	9.89	0.04	12.10	0.31	6.64	0.19	2.73	0.17	48.10	1.83
HS971109	6.76	1.77	0.02	2.81	2.05	2.16	0.04	0.04	0.06	79.10	0.39
HS971110	12.10	5.49	0.03	11.10	1.01	10.00	0.16	0.42	0.17	47.00	1.71
HS971111	14.30	9.33	0.04	11.90	0.05	6.53	0.20	3.64	0.17	48.60	1.81
HS971112	9.25	2.64	0.03	5.76	0.44	2.48	0.20	2.46	0.18	73.00	0.63
HS971113	11.60	3.33	0.03	14.10	0.63	4.91	0.34	1.94	0.15	54.70	1.33
HS971114	14.30	8.83	0.04	11.80	0.04	6.68	0.24	2.72	0.17	49.90	1.77
HS971115	14.00	8.55	0.04	12.60	0.03	7.39	0.17	2.95	0.18	48.90	1.70
HS971125	15.00	2.86	0.01	4.35	2.62	1.43	0.07	3.78	0.20	63.90	0.39
BCD20701	15.45	2.23		13.93	0.12	10.34	0.17	0.01	0.19	38.57	1.80
BCD20702	15.67	1.79		12.66	0.11	9.39	0.16	0.01	0.22	41.30	1.75
BCD20705	8.49	0.01		5.72	0.88	3.53	0.84	0.01	0.02	69.91	0.43
BCD20706	10.49	4.78		8.43	0.62	4.05	0.40	1.34	0.04	61.64	1.00
BCD20707	13.98	11.67		11.05	0.07	6.37	0.24	2.90	0.14	46.10	1.72
BCD20708	14.79	14.05		10.04	0.06	5.43	0.19	1.96	0.12	46.43	1.53
BCD20709	14.95	8.79		11.61	1.03	6.04	0.18	2.05	0.13	47.78	1.73
BCD20711	8.25	0.01		4.82	0.57	2.21	0.72	0.01	0.04	73.98	0.50
BCD20712	8.41	2.82		5.30	0.98	2.47	0.38	0.85	0.01	72.17	0.66
BCD20713	14.41	11.52		10.69	0.20	5.38	0.20	2.47	0.14	48.40	1.67
BCD20714	14.57	11.21		11.78	0.25	6.16	0.19	2.20	0.11	46.37	1.77
BCD20715	14.61	10.32		10.77	0.26	6.12	0.19	2.87	0.13	47.23	1.72
BCD20716	14.55	9.75		10.86	0.36	6.33	0.19	2.41	0.13	48.16	1.70
BCD20717	14.02	10.37		10.22	0.30	5.78	0.19	2.68	0.11	48.51	1.60
BCD20718	14.24	11.67		10.85	0.18	5.98	0.19	2.39	0.11	47.80	1.63
BCD20719	14.59	11.80		11.05	0.23	6.12	0.19	2.53	0.12	47.95	1.69
BCD20720	14.50	11.58		10.97	0.24	6.14	0.20	2.48	0.12	47.76	1.69
BCD20721	14.48	11.21		11.15	0.23	6.08	0.19	2.21	0.10	47.46	1.69
BCD20722	14.52	10.27		11.44	0.44	6.55	0.19	1.33	0.13	46.72	1.69
BCD20723	6.55	2.13		15.57	0.01	18.27	0.06	0.01	0.08	48.14	0.51
BCD20724	13.93	12.23		10.45	0.59	5.81	0.18	2.04	0.10	46.74	1.64
BCD20725	13.78	10.74		10.35	0.64	5.73	0.18	1.97	0.12	45.16	1.60
BCD20879	14.20	9.24		11.25	0.88	6.15	0.18	1.54	0.13	45.09	1.68
BCD20880	13.51	8.83		10.06	0.71	5.98	0.18	0.01	0.12	44.55	1.59
BCD20881	14.76	10.29		11.78	0.38	6.13	0.21	2.42	0.12	47.46	1.74
BCD20882	9.70	0.03		1.62	1.97	0.78	0.01	0.05	0.01	77.45	0.25
BCD20883	14.15	8.88		10.84	1.51	6.07	0.20	0.27	0.12	45.90	1.67
BCD20884	14.89	9.12		11.34	0.27	6.61	0.21	2.93	0.14	47.24	1.75
BCD20885	13.64	7.69		7.20	0.56	4.05	0.14	1.42	0.01	57.91	1.07
BCD20886	13.76	8.88		10.87	0.23	6.16	0.19	2.73	0.12	45.89	1.68
BCD20887	12.19	13.01		9.13	1.03	5.20	0.18	1.57	0.09	44.00	1.48
BCD20888	13.76	10.76		0.35	0.52	5.83	0.18	2.67	0.12	46.64	1.64
BCD20889	14.34	9.42		11.23	0.38	5.89	0.20	2.97	0.10	49.52	1.66
BCD20891	12.55	1.94		2.36	1.94	0.80	0.03	0.59	0.01	74.87	0.29
BCD20892	12.75	6.97		10.52	0.63	5.99	0.19	1.11	0.09	51.69	1.45
BCD21862	14.28	10.70		10.79	0.42	5.98	0.20	2.43	0.08	48.32	1.63
BCD21863	14.14	8.49		11.32	1.00	7.02	0.18	1.60	0.13	45.47	1.71

Sample#	Al <sub>2</sub> O <sub>3</sub> (%)	CaO (%)	Cr <sub>2</sub> O <sub>3</sub> (%)	Fe(tot) (%)	K <sub>2</sub> O (%)	MgO (%)	MnO (%)	Na <sub>2</sub> O (%)	P <sub>2</sub> O <sub>5</sub> (%)	SiO <sub>2</sub> (%)	TiO <sub>2</sub> (%)
BCD21864	14.33	12.55		10.86	0.13	6.26	0.20	2.34	0.12	47.26	1.70
BCD21865	14.41	11.83		11.31	0.13	6.22	0.20	2.36	0.12	46.34	1.72
BCD21866	12.57	9.28		13.19	0.30	6.28	0.18	1.51	0.12	47.87	1.53
BCD21867	13.65	8.41		12.75	0.38	8.22	0.18	0.13	0.14	41.63	1.61
BCD21868	13.83	4.16		14.19	0.08	8.95	0.16	0.01	0.16	39.18	1.73
BCD21869	0.53	0.01		53.56	0.03	11.44	0.03	0.04	0.17	29.12	0.02
BCD21870	0.53	0.01		51.56	0.02	10.69	0.07	0.02	0.14	30.47	0.02
BCD21871	1.83	0.01		48.39	0.05	11.78	0.03	0.01	0.14	31.72	0.24
BCD21872	0.43	0.01		51.79	0.03	12.21	0.03	0.02	0.14	31.88	0.02
BCD21873	0.48	0.01		85.17	0.03	3.26	0.04	0.01	0.20	9.62	0.01
BCD21874	15.66	1.20		26.73	0.01	11.70	0.20	0.01	0.25	31.99	2.00
BCD21875	13.54	9.49		10.31	1.35	6.11	0.18	0.75	0.12	42.99	1.64
BCD21876	15.24	10.20		11.24	0.10	6.13	0.21	2.80	0.13	46.74	1.79
BCD21877	9.59	6.14		6.10	0.39	2.57	0.19	1.59	0.01	67.89	0.87
BCD21878	13.63	7.20		10.41	0.06	5.13	0.23	4.00	0.18	53.05	1.74
BCD21879	11.77	5.46		15.54	0.05	7.43	0.12	0.75	0.12	50.05	1.43
BCD21880	14.02	2.53		19.23	0.01	11.26	0.10	0.01	0.19	43.18	1.87
BCD21881	13.96	1.81		18.58	0.01	10.72	0.10	0.01	0.22	44.02	1.88
BCD21882	7.03	0.01		13.46	0.93	3.31	0.03	0.01	0.01	63.94	0.62
BCD21883	6.62	0.01		4.60	1.04	3.28	0.02	0.01	0.01	80.69	0.35
BCD21884	6.77	0.01		3.30	0.67	4.62	0.02	0.01	0.01	81.53	0.36
BCD21885	6.64	0.01		4.38	0.32	5.56	0.03	0.01	0.01	80.48	0.29
BCD21886	4.41	0.20		3.44	0.15	3.79	0.02	0.01	0.07	84.98	0.21
BCD21887	4.44	0.01		3.63	0.09	4.30	0.02	0.01	0.01	84.91	0.23
BCD21888	6.31	0.01		4.11	0.28	6.05	0.04	0.01	0.01	78.66	0.43
BCD21889	6.08	0.66		4.09	0.62	4.69	0.08	0.01	0.01	79.70	0.49
BCD21890	13.46	3.73		10.27	0.71	9.09	0.22	1.26	0.15	49.46	1.70
BCD21891	15.88	1.40		7.74	0.99	15.12	0.11	0.01	0.22	46.62	2.09
BCD21892	15.28	1.86		12.25	0.79	12.50	0.15	0.20	0.18	45.50	2.04
BCD21893	14.51	2.29		9.51	0.53	14.93	0.10	0.05	0.20	45.94	1.83
BCD21894	6.30	0.62		3.81	1.49	2.22	0.03	0.01	0.20	81.74	0.28
BCD21895	5.30	0.01		4.03	1.20	1.75	0.03	0.01	0.01	84.33	0.28
BCD21896	6.31	0.24		2.61	0.88	4.96	0.05	0.01	0.01	80.58	0.36
BCD21897	6.52	0.57		2.82	0.85	5.14	0.03	0.01	0.08	79.54	0.26
BCD21898	4.73	1.11		3.59	0.08	5.18	0.02	0.01	0.53	80.84	0.24
BCD21899	6.43	1.00		8.97	0.01	6.89	0.04	0.01	0.01	69.34	0.25
BCD21900	5.70	0.62		9.03	0.60	4.25	0.03	0.01	0.01	73.63	0.27
BCD21901	9.45	2.67		8.21	1.83	3.35	0.16	0.01	0.01	66.36	0.79
BCD21902	14.44	8.76		11.34	1.07	4.91	0.19	2.58	0.11	46.64	1.68
BCD21903	13.84	6.51		8.42	0.17	4.00	0.14	4.78	0.10	56.81	1.48
BCD21904	14.40	11.70		10.98	0.13	6.38	0.19	2.82	0.12	48.42	1.72
BCD21905	14.60	12.51		11.12	0.08	6.43	0.21	2.78	0.14	47.93	1.71
BCD21906	14.58	12.51		11.14	0.10	6.39	0.20	2.22	0.12	46.88	1.70
BCD21907	14.86	12.31		9.84	0.17	5.29	0.17	1.83	0.93	44.63	1.71
BCD21908	15.36	10.57		10.59	0.23	6.31	0.20	1.79	0.91	46.92	1.70
BCD21909	15.22	7.87		12.67	0.53	7.73	0.21	1.33	0.90	45.77	1.83
BCD21910	6.11	0.63		11.24	1.56	0.58	0.02	0.06	0.35	68.66	0.31
BCD21911	6.99	0.37		8.21	1.58	1.78	0.02	0.06	0.31	72.78	0.48
BCD21912	4.26	1.08		2.69	0.08	6.12	0.03	0.02	0.36	81.02	0.23
BCD21913	10.19	6.07		5.42	0.07	16.97	0.22	0.01	0.88	46.73	0.51
BCD21914	4.18	0.15		3.02	0.08	5.66	0.01	0.01	0.32	83.02	0.19

Sample#	Al <sub>2</sub> O <sub>3</sub> (%)	CaO (%)	Cr <sub>2</sub> O <sub>3</sub> (%)	Fe(tot) (%)	K <sub>2</sub> O (%)	MgO (%)	MnO (%)	Na <sub>2</sub> O (%)	P <sub>2</sub> O <sub>5</sub> (%)	SiO <sub>2</sub> (%)	TiO <sub>2</sub> (%)
BCD21915	14.34	0.15		8.42	0.01	16.45	0.03	0.01	0.64	49.28	1.63
BCD21916	3.76	0.33		4.70	0.05	5.14	0.02	0.01	0.35	82.09	0.22
BCD21917	13.79	0.89		14.19	0.04	15.46	0.05	0.07	0.80	41.56	1.55
BCD21918	6.63	0.02		5.84	0.12	5.31	0.03	0.02	0.32	77.39	0.38
BCD21919	6.89	0.83		8.67	0.23	4.07	0.06	0.21	0.41	73.80	0.42
BCD21920	3.34	0.38		5.87	0.43	2.52	0.03	0.01	0.29	82.87	0.18
BCD21921	6.21	1.28		5.06	0.18	9.14	0.06	0.01	0.50	71.58	0.41
BCD21922	8.91	2.65		5.27	0.06	12.53	0.11	0.01	0.66	60.35	0.81
BCD21923	6.27	0.25		2.89	0.79	3.64	0.04	0.02	0.28	82.37	0.31
BCD21924	7.42	0.08		2.08	1.27	3.80	0.02	0.03	0.24	81.19	0.39
BCD21925	7.54	0.07		7.57	0.29	8.01	0.05	0.01	0.43	69.34	0.42
BCD21926	14.96	10.28		10.72	0.17	6.34	0.20	2.65	0.91	48.76	1.71
BCD21927	14.62	11.43		10.43	0.11	6.29	0.20	2.24	0.90	48.34	1.70
BCD21928	14.88	10.09		10.76	0.18	6.59	0.20	3.19	0.89	47.98	1.74
BCD21929	14.85	10.60		10.63	0.15	6.50	0.20	3.08	0.87	48.13	1.73
BCD21930	15.44	10.28		10.89	0.04	6.14	0.19	2.79	0.86	47.55	1.70
BCD21931	14.40	11.19		10.34	0.21	6.10	0.19	2.30	0.90	48.36	1.68
BCD21932	15.20	9.83		10.77	0.17	6.21	0.20	2.50	0.89	47.81	1.78
BCD21933	15.96	4.78		11.64	0.57	5.84	0.17	1.62	0.68	47.65	1.87
BCD21934	8.23	0.50		6.97	0.15	6.49	0.05	0.02	0.44	71.19	0.59
BCD21935	7.03	0.48		4.67	0.72	3.43	0.04	0.12	0.28	78.76	0.41
BCD21936	14.92	10.11		10.99	0.12	6.36	0.21	3.17	0.86	48.36	1.77
BCD21937	14.28	12.80		10.92	0.08	5.98	0.20	2.61	0.09	47.02	1.69
BCD21938	14.38	12.33		10.69	0.07	6.52	0.19	3.19	0.12	46.87	1.68
BCD21939	14.56	12.42		10.76	0.07	5.99	0.19	2.85	0.10	46.18	1.64
BCD21940	14.85	11.54		11.05	0.10	6.07	0.20	2.67	0.13	46.45	1.75
BCD21941	14.58	11.54		11.07	0.11	6.20	0.20	2.83	0.12	47.40	1.72
BCD21942	12.21	13.89		9.32	0.31	5.52	0.20	2.04	0.11	43.93	1.43
BCD21943	15.46	9.55		11.76	0.29	7.61	0.21	1.49	0.18	44.56	1.83
BCD21944	7.65	0.38		3.12	1.12	4.62	0.02	0.01	0.01	78.23	0.45
BCD21945	6.96	0.39		3.55	0.52	5.20	0.03	0.51	0.01	78.67	0.37
BCD21964	14.73	13.17		10.50	0.15	6.60	0.20	2.37	0.09	47.00	1.59
BCD21965	14.44	12.17		11.20	0.06	6.34	0.19	2.61	0.13	46.73	1.69
BCD21966	14.82	12.46		11.36	0.07	6.00	0.19	2.10	0.14	45.40	1.72
BCD21967	14.31	12.68		10.87	0.05	6.28	0.19	2.23	0.14	46.18	1.68
BCD21968	12.61	8.67		11.53	0.18	5.52	0.17	1.74	0.09	52.10	1.35
BCD21969	6.63	0.51		10.14	0.12	5.82	0.03	0.01	0.01	71.36	0.45
BCD21970	12.04	0.31		8.95	0.15	12.51	0.05	0.01	0.12	57.32	1.30
BCD21971	7.36	0.06		3.02	1.04	3.70	0.02	0.01	0.01	80.74	0.38
BCD21972	7.23	0.26		7.59	0.06	6.43	0.05	0.01	0.01	73.34	0.47
BCD21973	11.08	1.13		10.64	0.56	9.04	0.12	0.01	0.05	58.64	1.24
BCD21974	7.74	1.63		6.15	1.22	4.38	0.14	0.01	0.04	73.02	0.58
BCD21975	11.82	0.72		12.22	0.68	9.84	0.13	0.01	0.16	55.01	1.38
BCD21976	8.26	0.51		4.10	1.47	5.51	0.05	0.01	0.01	73.95	0.45
BCD21977	7.83	3.18		6.41	0.13	10.86	0.12	0.01	0.01	63.26	0.64
BCD21978	5.94	0.16		4.26	1.17	2.37	0.08	0.01	0.01	81.64	0.34
BCD21979	8.61	0.81		13.23	0.26	9.95	0.10	0.01	0.06	55.76	0.93
BCD21980	10.00	5.39		7.98	0.72	4.07	0.14	1.70	0.04	64.14	0.90
BCD21981	14.37	12.01		11.36	0.18	5.88	0.20	2.44	0.14	46.57	1.74
BCD21982	14.61	11.69		11.52	0.14	6.22	0.20	2.81	0.12	47.25	1.76
BCD21983	14.38	12.31		10.88	0.17	6.30	0.19	2.57	0.11	47.31	1.71

Sample#	Al <sub>2</sub> O <sub>3</sub> (%)	CaO (%)	Cr <sub>2</sub> O <sub>3</sub> (%)	Fe(tot) (%)	K <sub>2</sub> O (%)	MgO (%)	MnO (%)	Na <sub>2</sub> O (%)	P <sub>2</sub> O <sub>5</sub> (%)	SiO <sub>2</sub> (%)	TiO <sub>2</sub> (%)
BCD21984	14.41	12.23		11.09	0.16	6.41	0.20	2.55	0.13	46.74	1.71
BCD21985	14.50	12.26		11.08	0.15	6.32	0.20	2.32	0.16	46.85	1.73
BCD21986	14.49	11.86		10.85	0.17	6.44	0.19	2.56	0.14	47.33	1.71
BCD21987	14.50	11.85		11.20	0.31	6.31	0.20	2.38	0.10	46.71	1.71
BCD21988	14.46	11.46		10.87	0.26	6.23	0.19	2.32	0.12	47.09	1.69
BCD21989	14.15	11.01		12.25	0.40	6.38	0.19	1.70	0.10	47.63	1.59
BCD21990	13.38	2.83		5.25	0.01	21.18	0.08	0.01	0.12	42.72	1.63
BCD21991	14.98	1.61		6.11	0.04	23.15	0.13	0.01	0.14	36.73	1.99
BCD21992	6.52	0.84		3.70	1.10	2.94	0.30	0.03	0.01	78.88	0.37
BCD21993	6.04	0.76		2.82	1.24	1.55	0.19	0.18	0.01	83.24	0.30
BCD22351	14.34	10.46		10.83	0.11	6.04	0.19	2.55	0.14	47.78	1.66
BCD22352	14.76	10.80		10.61	0.15	5.95	0.18	2.88	0.13	48.05	1.70
BCD22353	14.53	12.98		10.70	0.16	5.94	0.19	2.00	0.11	47.12	1.68
BCD22354	12.62	13.45		9.48	0.52	5.20	0.17	1.56	0.12	43.22	1.44
BCD22355	14.65	8.64		11.80	0.86	6.64	0.19	1.10	0.13	43.68	1.71
BCD22356	14.42	8.98		11.09	0.75	6.17	0.19	1.36	0.14	48.28	1.69
BCD22357	14.47	9.56		10.85	1.06	6.16	0.19	1.64	0.10	46.17	1.70
BCD22358	13.87	8.59		10.69	1.01	6.14	0.18	0.82	0.11	45.17	1.61
BCD22359	13.82	7.22		10.53	0.23	6.37	0.17	0.01	0.13	44.75	1.59
BCD22362	9.41	1.09		10.75	0.52	10.94	0.15	0.01	0.08	57.34	0.68
BCD22363	13.29	9.53		9.88	0.81	5.77	0.21	0.84	0.13	45.21	1.54
BCD22364	14.25	9.49		11.27	0.40	6.08	0.20	2.48	0.14	45.62	1.67
BCD22514	14.58	10.71		11.61	0.18	6.27	0.19	2.67	0.24	47.32	1.74
BCD22515	14.39	10.51		11.59	0.23	6.41	0.20	2.37	0.26	46.63	1.70
BCD22516	14.57	10.80		11.59	0.18	6.48	0.20	2.34	0.24	47.32	1.73
BCD22517	14.27	9.37		12.02	0.43	6.34	0.19	1.83	0.22	46.78	1.68
BCD22518	4.79	0.01		9.54	0.50	0.41	0.01	0.08	0.10	72.39	0.24
BCD22519	3.93	0.01		10.27	0.10	4.26	0.01	0.01	0.10	72.01	0.19
BCD22520	7.49	2.33		8.36	0.01	12.81	0.10	0.01	0.12	56.58	0.36
BCD22521	6.90	0.64		11.95	1.02	3.83	0.12	0.02	0.40	65.35	0.43
BCD22522	13.51	7.26		11.35	1.57	6.85	0.33	0.17	0.23	44.90	1.66
BCD22524	14.50	9.65		11.72	0.08	6.54	0.21	3.40	0.28	46.68	1.80
BCD22525	13.77	12.68		10.55	0.19	5.42	0.19	1.44	0.22	46.58	1.50
BCD22558	14.73	10.07		11.88	0.17	6.33	0.20	2.98	0.24	47.15	1.75
BCD22559	13.46	15.58		8.03	0.24	3.00	0.14	1.17	0.16	50.12	0.91
BCD22560	13.87	8.08		11.16	1.12	6.16	0.18	1.87	0.19	42.66	1.66
BCD22561	1.49	1.37		15.23	0.01	19.74	0.01	0.07	0.16	50.82	0.03
BCD22562	0.74	0.69		42.63	0.01	14.79	0.01	0.07	0.13	35.45	0.01
BCD22563	14.02	9.63		11.86	0.46	6.41	0.18	2.03	0.22	46.76	1.65
BCD22564	14.34	9.51		11.37	0.69	6.29	0.19	2.78	0.21	46.99	1.69
BCD22565	14.11	7.62		11.37	0.85	6.12	0.19	0.81	0.21	45.72	1.64
BCD22566	0.27	0.01		64.86	0.01	9.60	0.01	0.04	0.15	23.42	0.01
BCD22567	4.97	0.34		28.06	0.08	15.93	0.03	0.02	0.14	39.22	0.29
BCD22568	7.70	0.50		7.88	0.01	17.64	0.03	0.01	0.17	57.39	0.37
BCD22569	10.09	1.07		15.69	0.22	9.23	0.08	0.04	0.20	52.52	1.03
BCD22570	14.06	7.72		12.49	0.61	6.52	0.18	2.34	0.23	46.16	1.61
BCD22571	12.66	6.48		15.31	0.37	11.21	0.14	0.04	0.29	36.34	1.59
BCD22572	3.79	3.70		24.77	0.01	12.61	0.07	0.04	0.17	37.65	0.20
BCD22573	13.95	8.78		11.79	0.79	6.87	0.18	1.92	0.26	46.02	1.62
BCD22574	14.63	10.97		11.66	0.21	6.30	0.20	2.51	0.26	47.38	1.69
BCD22575	14.59	10.41		11.60	0.11	6.27	0.21	2.62	0.26	46.82	1.69



Sample#	Al <sub>2</sub> O <sub>3</sub> (%)	CaO (%)	Cr <sub>2</sub> O <sub>3</sub> (%)	Fe(tot) (%)	K <sub>2</sub> O (%)	MgO (%)	MnO (%)	Na <sub>2</sub> O (%)	P <sub>2</sub> O <sub>5</sub> (%)	SiO <sub>2</sub> (%)	TiO <sub>2</sub> (%)
BCD22576	14.53	10.28		11.57	0.11	6.36	0.20	2.72	0.24	47.12	1.69
BCD22577	14.45	10.69		11.31	0.25	6.33	0.19	2.46	0.25	44.82	1.66
BCD22578	14.31	10.84		11.35	0.14	6.29	0.20	2.45	0.24	46.32	1.67
BCD22877	13.74	11.01		11.18	0.28	6.21	0.19	2.57	0.12	46.70	1.65
BCD22878	14.80	17.84		7.65	0.23	2.20	0.12	0.01	0.20	50.43	0.81
BCD22879	9.39	2.04		7.57	1.83	3.03	0.14	0.03	0.04	68.50	0.54
BCD22880	14.22	9.79		10.63	0.58	5.99	0.20	2.56	0.10	48.34	1.67
BCD22882	13.86	12.41		10.46	0.04	5.92	0.19	2.82	0.11	47.58	1.62
BCD22883	14.03	11.45		10.16	0.51	5.69	0.19	2.29	0.13	47.11	1.54
BCD22884	5.83	0.34		4.79	1.39	1.36	0.05	0.01	0.01	80.87	0.33
6501	13.91	8.53		11.30	0.21	6.32	0.28	3.57		51.73	1.77
6502	14.53	10.00		11.94	0.16	6.08	0.27	2.94		49.82	1.74
6503	15.10	10.57		12.85	0.34	6.46	0.28	2.54		50.06	1.79
6504	14.00	10.87		12.16	0.30	6.96	0.28	2.48		48.37	1.77
6505	14.92	9.33		14.35	0.43	6.56	0.28	2.41		53.06	1.83
6506	14.62	10.33		12.01	0.26	6.16	0.27	2.50		50.45	1.75
6507	14.80	10.50		12.76	0.22	6.16	0.27	2.33		49.18	1.77
6508	14.96	9.30		12.55	0.15	6.27	0.28	3.53		50.78	1.79
6509	14.69	9.28		11.80	0.19	6.32	0.26	3.40		51.09	1.72
6510	14.78	11.01		12.55	0.15	6.24	0.27	2.25		49.98	1.75
6511	14.83	10.53		12.26	0.30	6.23	0.27	2.83		51.21	1.72
6512	14.44	10.12		11.75	0.13	6.08	0.27	3.17		50.09	1.70
6513	14.92	10.25		12.23	0.15	6.14	0.27	2.79		50.67	1.72
6514	15.01	9.53		11.89	0.27	6.22	0.26	2.92		50.20	1.64
6515	14.78	10.55		12.39	0.11	6.64	0.28	2.90		50.50	1.70
6516	15.28	8.35		12.41	0.14	6.41	0.28	3.84		51.28	1.77
6517	14.87	9.66		12.85	0.23	6.01	0.28	2.79		50.09	1.75
6518	14.50	9.48		11.96	0.10	6.08	0.27	3.50		50.85	1.66
6519	15.07	10.01		11.16	0.07	5.99	0.25	3.32		52.25	1.75
6520	14.71	8.55		11.80	0.48	6.46	0.23	1.10		49.73	1.68
6521	14.46	10.30		11.91	0.25	5.80	0.27	2.61		50.98	1.70
6526	13.85	9.14		11.51	0.28	5.75	0.23	2.12		48.90	1.68
6527	14.30	9.19		11.42	0.16	5.96	0.25	2.92		50.14	1.66
6528	14.66	10.01		12.39	0.15	6.09	0.28	2.88		51.32	1.75
6529	14.48	9.35		11.92	0.23	5.99	0.27	3.41		49.87	1.68
6530	14.00	6.92		11.32	0.11	6.01	0.25	3.75		48.70	1.64
6531	14.85	8.83		12.39	0.36	6.19	0.26	2.86		51.75	1.81
6532	14.82	8.76		12.21	0.10	6.22	0.27	3.41		51.65	1.72
6533	15.37	8.42		12.37	0.25	6.47	0.35	3.04		49.89	1.79
6534	15.10	9.19		12.55	0.05	6.19	0.35	3.75		51.29	1.75
6535	13.73	8.07		12.44	0.10	6.35	0.21	2.44		48.70	1.58
6536	14.32	9.44		11.30	0.05	5.59	0.25	3.17		50.84	1.68
6537	14.57	9.46		11.03	0.21	6.11	0.23	2.94		50.06	1.52
6538	14.17	8.23		10.46	0.15	6.25	0.22	3.46		48.84	1.39
6539	14.19	11.19		12.01	0.01	7.17	0.28	1.97		51.51	1.64
6540	14.01	7.80		11.60	0.11	6.16	0.31	3.80		48.93	1.66
6541	15.07	8.94		12.35	0.03	6.14	0.27	3.45		52.26	1.75
6542	14.23	7.97		11.76	0.71	5.57	0.26	4.00		50.68	1.68
6543	13.76	7.96		10.76	0.68	5.73	0.22	2.62		48.62	1.47
6544	14.58	9.28		11.62	0.08	5.71	0.25	2.91		50.70	1.50
6545	14.19	6.89		12.30	0.15	5.99	0.30	4.03		49.43	1.72

Sample#	Al <sub>2</sub> O <sub>3</sub> (%)	CaO (%)	Cr <sub>2</sub> O <sub>3</sub> (%)	Fe(tot) (%)	K <sub>2</sub> O (%)	MgO (%)	MnO (%)	Na <sub>2</sub> O (%)	P <sub>2</sub> O <sub>5</sub> (%)	SiO <sub>2</sub> (%)	TiO <sub>2</sub> (%)
6547	13.60	6.19		13.35	0.05	9.10	0.33	2.05		51.12	1.77
6548	13.57	7.51		9.19	0.10	4.23	0.21	3.04		60.18	1.39
6549	14.21	9.67		11.91	0.20	6.25	0.29	3.00		51.98	1.79
6550	15.08	11.03		12.35	0.26	6.06	0.26	2.16		50.90	1.75
6551	14.26	9.89		12.03	0.17	6.93	0.29	2.65		51.50	1.79
6552	14.26	4.83		13.03	0.41	9.78	0.21	2.16		48.70	1.85
6553	14.66	7.41		12.21	0.15	4.50	0.29	3.37		54.84	1.83
6554	14.37	9.80		11.80	0.21	6.46	0.27	3.22		50.93	1.70
6555	14.62	9.76		12.50	0.10	6.73	0.28	2.83		50.64	1.75
6556	15.12	10.67		12.60	0.21	6.66	0.28	2.57		49.79	1.79
6557	14.55	8.69		13.44	0.43	7.52	0.31	3.36		49.31	1.85
6558	14.55	10.55		12.62	0.03	7.13	0.38	2.66		50.54	1.72
6559	14.39	10.07		12.01	0.16	6.33	0.26	2.88		51.25	1.64
6560	14.96	10.26		12.92	0.14	7.18	0.29	2.55		49.85	1.81
6561	15.42	10.46		12.92	0.25	6.49	0.28	2.84		49.12	1.79
6562	15.39	11.42		12.89	0.10	6.85	0.28	2.36		48.40	1.79
6563	14.80	9.98		12.58	0.13	6.47	0.27	2.75		50.20	1.72
6564	14.19	7.60		11.98	0.57	6.34	0.25	3.12		47.81	1.68
6565	13.91	9.41		11.69	0.43	7.00	0.26	1.93		45.95	1.70
6566	14.26	10.42		11.85	0.20	6.02	0.26	2.75		48.68	1.66
6567	13.92	10.58		11.30	0.15	5.99	0.26	2.32		48.39	1.60
6568	13.87	9.19		12.26	0.20	5.61	0.26	2.84		49.48	1.75
6577	15.19	10.30		12.85	0.23	6.22	0.29	2.67		50.50	1.81
6578	15.17	9.78		12.57	0.21	6.28	0.28	2.98		50.76	1.79
6579	14.51	9.89		12.00	0.14	6.01	0.28	3.33		51.85	1.70
6580	14.44	9.80		11.89	0.14	6.24	0.27	2.95		51.75	1.70
6581	14.92	10.19		12.23	0.07	6.39	0.28	3.08		51.09	1.72
6582	14.82	10.80		12.14	0.07	5.98	0.27	2.62		51.06	1.75
6588	15.05	9.28		12.62	0.44	6.67	0.28	3.12		50.32	1.79
6589	14.33	10.14		11.96	0.14	5.88	0.25	2.41		48.51	1.68
6590	14.25	9.58		11.82	0.25	5.67	0.23	2.79		47.87	1.66
6591	14.80	10.30		12.73	0.21	6.32	0.28	2.57		50.75	1.77
6592	14.42	10.03		12.08	0.16	6.31	0.27	3.07		50.60	1.72
6593	14.91	9.07		12.28	0.05	6.08	0.27	2.95		47.82	1.70
6594	14.00	10.03		11.98	0.21	5.56	0.25	2.32		48.34	1.64
6595	14.73	7.74		12.39	0.21	6.81	0.59	2.57		50.31	1.70
6596	14.42	6.32		12.28	0.14	7.75	0.27	2.17		51.20	1.68
6597	14.82	10.35		12.60	0.27	5.83	0.28	2.88		50.70	1.75
6598	14.07	11.48		11.85	0.21	5.89	0.27	2.58		48.29	1.64
6599	14.89	10.05		12.48	0.21	6.33	0.28	3.20		51.40	1.75
6600	15.23	10.32		12.87	0.21	5.97	0.28	2.66		50.93	1.79
6651	15.26	11.23		12.85	0.21	6.22	0.28	2.57		49.18	1.87
6652	15.17	9.48		13.30	0.26	6.83	0.28	3.12		49.43	1.77
6653	14.75	8.96		12.23	0.07	6.55	0.28	3.67		51.85	1.72
6654	14.42	10.14		12.12	0.28	6.31	0.27	2.95		50.56	1.72
6655	14.57	9.69		12.28	0.10	6.50	0.28	3.07		51.09	1.72
6656	15.30	9.42		12.94	0.21	6.55	0.28	3.58		49.59	1.81
6657	15.10	10.62		12.23	0.27	6.64	0.27	2.66		50.21	1.79
6658	14.98	9.55		12.64	0.19	6.31	0.28	3.15		50.81	1.79
6659	15.10	9.07		13.01	0.15	6.41	0.28	3.36		50.18	1.77
6660	14.98	10.55		12.53	0.23	6.13	0.27	2.51		50.81	1.75

Sample#	Al <sub>2</sub> O <sub>3</sub> (%)	CaO (%)	Cr <sub>2</sub> O <sub>3</sub> (%)	Fe(tot) (%)	K <sub>2</sub> O (%)	MgO (%)	MnO (%)	Na <sub>2</sub> O (%)	P <sub>2</sub> O <sub>5</sub> (%)	SiO <sub>2</sub> (%)	TiO <sub>2</sub> (%)
6661	15.48	10.55		12.96	0.03	6.34	0.27	2.54		49.78	1.87
6662	14.94	10.39		12.73	0.10	5.77	0.27	2.69		49.04	1.75
6663	14.73	8.03		12.67	0.39	6.25	0.35	2.53		45.85	1.75
6664	15.76	7.42		13.37	0.20	6.16	0.28	2.99		51.54	1.87
6665	14.66	8.85		12.73	0.28	5.91	0.27	2.79		50.18	1.74
6666	14.42	10.03		12.17	0.70	6.26	0.26	2.50		49.43	1.66
6667	14.78	8.48		12.10	1.10	6.18	0.25	1.58		51.09	1.70
6668	15.07	10.92		12.87	0.27	6.34	0.29	1.81		49.56	1.81
6669	15.69	9.51		12.96	0.42	6.60	0.30	2.91		49.23	1.81
6670	14.83	10.14		12.82	0.40	6.16	0.28	2.78		50.21	1.81
6671	15.05	11.08		12.60	0.21	6.25	0.27	2.49		50.00	1.81
6672	14.53	11.12		13.37	0.25	6.21	0.28	2.25		49.71	1.87
6673	14.25	8.62		11.76	0.16	6.06	0.26	3.29		51.31	1.66
6674	14.53	10.03		11.94	0.15	6.22	0.26	2.83		50.76	1.70
6675	14.14	8.98		11.60	0.52	6.72	0.51	2.08		50.54	1.62
6676	14.75	9.25		12.66	0.22	6.41	0.27	2.95		52.37	1.77
6677	14.94	9.03		13.25	0.20	6.13	0.28	2.71		51.40	1.79
6678	13.55	9.23		11.23	0.22	5.59	0.23	2.76		48.84	1.56
6679	14.44	9.41		12.23	0.13	6.11	0.27	3.11		49.57	1.72
6680	13.71	9.17		11.37	0.07	5.96	0.23	2.70		47.18	1.60
6681	15.51	8.21		12.96	0.15	6.33	0.34	3.03		49.25	1.43
6682	14.69	9.26		12.82	0.14	6.21	0.27	2.79		48.00	1.81
6683	14.78	10.30		12.55	0.17	6.85	0.28	2.42		50.18	1.70
6684	15.08	8.78		13.01	0.61	6.44	0.27	2.25		49.04	1.83
6685	14.21	10.46		12.14	0.23	6.08	0.27	2.46		49.76	1.70
6686	14.94	9.57		12.60	0.19	6.32	0.27	3.63		50.40	1.77
6687	14.14	10.37		12.58	0.08	6.01	0.27	3.09		51.84	1.72
6688	14.92	10.73		12.66	0.25	6.33	0.28	3.11		49.50	1.79
6689	14.01	9.39		11.51	0.19	5.82	0.25	3.03		48.09	1.64
6690	15.08	10.01		12.82	0.21	6.32	0.28	2.95		50.50	1.81
6691	14.94	9.32		12.23	0.23	6.22	0.27	3.46		52.03	1.79
6692	14.75	9.64		12.07	0.07	6.10	0.27	3.71		51.65	1.72
6693	14.67	8.51		12.17	0.14	6.03	0.27	4.14		52.40	1.74
6694	13.78	8.37		11.44	0.26	6.01	0.25	3.25		48.76	1.60
6695	14.82	10.08		11.96	0.26	6.19	0.26	2.98		52.18	1.70
6696	14.92	9.62		10.42	0.36	5.91	0.22	2.62		53.45	1.16
6697	15.10	8.66		11.03	0.33	6.40	0.22	3.07		53.90	1.18
6698	15.39	6.50		10.51	0.31	5.76	0.21	3.79		54.89	1.10
6699	15.05	10.96		12.30	0.21	5.78	0.27	2.63		50.65	1.72
6701	14.51	9.98		12.21	0.13	6.00	0.26	2.65		49.48	1.70
6702	15.19	9.85		10.21	0.17	6.00	0.22	2.62		49.29	1.31
6703	14.94	10.39		12.53	0.10	6.08	0.28	2.54		50.26	1.79
6704	14.87	9.89		12.03	0.25	6.11	0.26	3.13		50.79	1.72
6705	15.30	9.50		12.62	0.19	6.57	0.27	3.12		49.79	1.81
6706	15.73	5.03		14.75	1.20	8.14	0.23	0.58		49.06	1.85
6707	14.35	8.76		11.96	0.22	5.85	0.26	3.20		47.98	1.70
6708	15.37	10.64		12.44	0.14	6.47	0.28	2.75		49.79	1.79
6709	7.09	0.55		4.00	1.72	1.60	0.22	0.02		76.22	0.35
6710	16.27	10.89		11.51	0.16	6.47	0.25	2.66		49.76	1.47
6711	15.17	10.51		12.60	0.17	5.92	0.27	2.62		50.29	1.79
6712	14.94	10.03		12.19	0.28	5.86	0.27	2.65		51.43	1.75

Sample#	Al <sub>2</sub> O <sub>3</sub> (%)	CaO (%)	Cr <sub>2</sub> O <sub>3</sub> (%)	Fe(tot) (%)	K <sub>2</sub> O (%)	MgO (%)	MnO (%)	Na <sub>2</sub> O (%)	P <sub>2</sub> O <sub>5</sub> (%)	SiO <sub>2</sub> (%)	TiO <sub>2</sub> (%)
6713	13.98	9.60		11.87	0.17	5.73	0.27	2.58		47.43	1.70
6714	14.46	10.01		11.89	0.08	6.16	0.27	3.37		50.98	1.72
6715	14.50	10.78		11.94	0.14	5.83	0.25	1.93		48.59	1.70
6716	15.19	10.30		12.51	0.26	6.40	0.28	2.45		50.39	1.77
6717	7.10	4.93		4.74	1.24	2.78	0.10	0.33		71.34	0.55
6718	14.01	10.30		11.17	0.03	6.32	0.25	2.57		48.84	1.62
6719	14.01	6.83		9.53	0.27	4.08	0.25	3.95		58.75	1.41
6720	12.76	4.56		12.26	1.52	6.06	0.19	0.10		44.82	1.54
6721	14.46	9.85		12.12	0.14	6.02	0.27	2.44		49.09	1.74
6722	15.17	10.14		12.37	0.10	6.32	0.27	2.94		51.10	1.77
6723	13.73	7.73		10.92	0.76	6.08	0.26	2.71		47.73	1.64
6724	14.73	8.85		12.62	0.07	6.47	0.28	3.26		50.40	1.75
6725	13.62	5.05		9.08	0.23	4.01	0.21	4.03		59.89	1.43
6726	13.67	6.74		10.42	0.13	5.27	0.22	3.08		55.59	1.47
6735	15.26	11.89		12.00	0.20	5.64	0.28	2.51		49.31	1.87
6736	14.10	11.44		11.23	0.17	5.68	0.27	2.36		46.65	1.74
6737	14.03	8.89		11.17	0.34	5.83	0.27	3.45		48.03	1.72
6738	13.83	6.41		11.26	0.93	5.91	0.28	1.47		45.79	1.79
6739	14.91	10.58		11.58	0.15	5.48	0.26	2.71		49.17	1.79
6740	14.87	6.16		12.46	0.46	6.82	0.27	2.74		46.62	1.81
6741	14.01	9.64		10.80	0.29	5.57	0.25	2.75		47.93	1.70
6742	13.78	9.60		10.55	0.17	5.31	0.25	2.69		47.21	1.70
6743	14.16	10.76		11.23	0.08	5.76	0.29	2.87		48.06	1.72
6744	13.55	11.23		10.44	0.10	5.46	0.28	3.25		46.07	1.62
6745	13.58	6.52		10.48	0.32	6.40	0.45	2.41		44.59	1.66
6746	14.83	9.03		10.73	0.42	5.16	0.25	2.78		48.67	1.54
6747	14.32	10.23		10.37	0.72	5.49	0.26	2.51		49.26	1.43
6748	14.69	8.78		9.67	0.32	5.57	0.23	3.33		51.73	1.14
6749	14.62	8.41		9.69	1.29	5.43	0.21	2.29		50.95	1.16
6750	15.42	9.57		9.89	0.31	5.49	0.23	3.12		53.84	1.18
6767	6.16	0.05		2.92	1.10	2.90	0.01	0.01		80.53	0.31
6768	5.09	0.30		2.50	0.36	4.42	0.15	0.56		80.78	0.26
6769	9.23	2.33		6.36	1.08	3.29	0.16	1.74		74.40	0.80
6773	8.32	3.07		4.28	1.20	2.84	0.13	0.07		68.49	0.48
6800	15.19	10.48		11.14	0.02	5.80	0.26	3.53		51.17	1.79
6801	14.85	9.71		12.23	0.65	7.18	0.30	2.92		49.82	1.81
6802	15.01	10.58		11.50	0.27	6.06	0.28	3.05		50.84	1.83
6803	14.89	10.33		11.48	0.21	6.11	0.29	3.61		54.79	1.81
6804	14.82	11.30		11.57	0.21	5.66	0.28	2.63		50.40	1.81
6805	14.66	10.69		11.51	0.34	5.50	0.27	2.94		50.64	1.83
6806	15.23	10.94		10.96	0.26	6.24	0.27	2.62		49.95	1.72
6807	15.10	11.89		11.55	0.15	5.82	0.26	2.23		54.43	1.83
6808	15.03	11.67		11.28	0.16	5.63	0.27	2.62		50.98	1.75
6809	15.12	10.71		12.07	0.21	6.01	0.29	2.96		50.54	1.83
6810	14.82	10.32		11.51	0.14	6.27	0.28	3.45		50.90	1.79
6811	14.57	4.43		13.94	1.47	7.00	0.23	1.85		44.75	1.70
6812	15.05	10.03		10.62	0.31	6.43	0.26	2.57		56.84	1.33
6813	15.96	10.23		10.96	0.20	6.05	0.23	2.49		48.73	1.31
6814	14.71	9.07		10.28	0.61	5.64	0.23	3.49		53.51	1.24
6815	13.87	10.48		10.28	0.27	5.69	0.25	2.87		52.65	1.33
6816	14.35	10.23		10.01	0.45	5.72	0.23	2.57		53.76	1.14

Sample#	Al <sub>2</sub> O <sub>3</sub> (%)	CaO (%)	Cr <sub>2</sub> O <sub>3</sub> (%)	Fe(tot) (%)	K <sub>2</sub> O (%)	MgO (%)	MnO (%)	Na <sub>2</sub> O (%)	P <sub>2</sub> O <sub>5</sub> (%)	SiO <sub>2</sub> (%)	TiO <sub>2</sub> (%)
6817	14.32	11.55		11.55	0.20	5.74	0.28	2.51		51.09	1.83
6818	13.67	11.08		10.37	0.23	5.52	0.26	2.79		50.85	1.41
6819	14.96	11.94		11.26	0.43	5.52	0.26	2.12		51.31	1.52
6820	15.12	10.28		11.12	0.56	6.03	0.25	2.54		51.87	1.39
6821	14.80	8.89		9.80	0.16	5.52	0.23	4.25		54.26	1.16
6822	14.39	10.55		11.62	0.26	6.33	0.29	3.34		50.71	1.81
6823	14.01	10.94		11.35	0.17	6.16	0.28	2.71		49.40	1.79
6824	14.32	11.92		11.73	0.17	5.61	0.27	2.36		51.20	1.83
6825	14.41	10.10		11.69	0.16	5.53	0.28	3.40		51.54	1.85
6826	14.26	10.94		11.51	0.17	6.24	0.27	2.79		51.26	1.81
6827	13.12	10.12		10.83	0.20	5.68	0.27	3.58		51.54	1.70
6828	14.78	12.01		10.85	0.29	6.31	0.26	2.57		50.85	1.62
10281	4.29	0.43		1.50	0.53	2.05	0.01	0.04	0.01	88.37	0.21
10282	6.14	0.36		3.02	0.98	1.71	0.09	0.01	0.01	84.76	0.27
10288	7.97	0.56		4.26	1.72	1.69	0.05	0.01	0.01	80.09	0.46
10289	13.03	4.15		15.83	0.29	6.75	0.16	0.78	0.09	51.98	1.55
10290	6.58	1.22		3.14	1.52	1.85	0.03	0.01	0.01	81.92	0.36
10293	3.65	0.36		3.66	0.20	3.13	0.01	0.01	0.03	85.59	0.20
10294	5.04	1.62		2.45	0.82	1.20	0.14	0.01	0.01	83.84	0.24
10295	6.48	1.25		5.18	0.02	9.26	0.03	0.01	0.01	71.93	0.46
10298	9.37	3.36		3.92	2.14	1.55	0.16	0.01	0.01	74.25	0.31
10299	5.44	1.53		2.49	0.11	11.70	0.03	0.01	0.01	72.69	0.35
10300	14.14	4.96		18.97	0.50	8.22	0.19	0.99	0.11	40.40	1.63
10301	5.06	0.66		3.46	0.02	7.41	0.01	0.01	0.01	78.59	0.22
17525	15.13	10.14		10.48	0.21	6.26	0.56	2.45	0.20	46.24	1.44
18003	14.47	6.90		11.03	0.16	6.72	0.61	2.61	0.20	46.39	1.76
18004	7.84	1.66		9.93	0.97	2.01	0.17	0.69	0.11	65.62	0.60
18017	13.21	6.13		8.46	0.30	4.21	0.30	3.36	0.20	55.45	1.35
18051	5.40	0.19		3.04	0.91	1.81	0.04	0.05	0.11	83.65	0.25
18052	9.30	0.80		8.06	0.09	6.36	0.27	0.95	0.15	63.93	0.97
18067	14.23	7.72		10.93	0.23	6.19	0.34	2.44	0.20	47.13	1.67
18087	14.74	10.06		9.53	0.32	5.76	0.35	2.23	0.18	47.80	1.36
24928	14.06	12.63		10.34	0.38	5.82	0.21	2.92	0.08	47.16	1.61
24929	12.61	12.80		10.12	0.15	4.83	0.23	1.60	0.10	52.04	1.12
24941	13.99	13.12		11.07	0.29	5.55	0.20	2.30	0.08	47.69	1.54
24942	13.87	11.64		10.65	0.14	6.27	0.21	2.77	0.08	46.75	1.63
24947	11.38	9.20		7.81	0.36	4.66	0.21	2.01	0.06	57.43	1.18
24948	13.47	10.66		10.20	0.28	6.36	0.19	2.58	0.09	45.03	1.58
24951	13.70	11.10		10.47	0.02	6.21	0.19	3.39	0.04	46.63	1.62
24952	14.08	13.10		10.75	0.08	6.41	0.18	2.96	0.08	46.91	1.65
34751	6.20	0.01		4.89	1.39	1.16	0.06	0.13	0.01	80.60	0.29
34755	3.57	0.01		3.49	0.76	0.13	0.01	0.01	0.01	88.27	0.15
34768	3.36	0.01		10.41	0.48	1.50	0.01	0.01	0.01	75.75	0.18
34779	12.32	4.63		14.44	0.65	6.38	0.20	0.47	0.08	50.48	1.03
35076	13.97	4.41		14.03	0.15	10.79	0.14	0.38	0.14	44.62	1.63
35077	9.39	2.09		5.27	0.19	3.98	0.11	2.34	0.06	71.56	0.57
35078	15.07	8.46		9.88	0.52	6.48	0.17	2.80	0.02	52.29	1.11
35079	14.68	8.94		9.52	0.42	6.25	0.17	2.89	0.02	51.73	1.07
35080	14.27	9.06		10.82	0.20	6.07	0.19	3.45	0.08	49.57	1.71
35081	14.36	9.45		11.11	0.23	6.32	0.19	2.82	0.08	49.29	1.70
35082	14.72	9.01		11.65	0.21	6.48	0.19	3.37	0.14	48.86	1.79

Sample#	Al <sub>2</sub> O <sub>3</sub> (%)	CaO (%)	Cr <sub>2</sub> O <sub>3</sub> (%)	Fe(tot) (%)	K <sub>2</sub> O (%)	MgO (%)	MnO (%)	Na <sub>2</sub> O (%)	P <sub>2</sub> O <sub>5</sub> (%)	SiO <sub>2</sub> (%)	TiO <sub>2</sub> (%)
35083	14.57	9.24		11.43	0.33	6.47	0.19	2.16	0.08	49.44	1.75
35084	15.13	10.62		11.38	0.16	5.59	0.19	1.37	0.08	49.58	1.77
35085	14.78	7.93		11.15	0.50	6.40	0.19	2.82	0.08	49.11	1.74
35086	14.74	10.42		10.99	0.19	6.00	0.19	2.12	0.07	49.47	1.66
35087	14.50	9.36		11.49	0.11	6.78	0.20	2.32	0.09	49.49	1.72
35088	13.34	6.62		7.23	2.30	10.45	0.14	0.01	0.09	47.14	1.55
35089	14.32	9.15		11.01	0.16	6.66	0.21	2.66	0.10	49.93	1.70
35090	13.92	7.25		12.01	0.05	6.89	0.14	2.60	0.14	50.55	1.80
35091	14.60	9.21		11.13	0.31	6.26	0.19	2.77	0.10	49.79	1.71
35092	14.45	9.50		11.00	0.16	6.59	0.20	2.46	0.09	49.60	1.67
35093	15.02	9.04		11.53	0.23	6.14	0.20	2.59	0.09	49.09	1.78
35094	14.76	8.98		10.38	0.27	6.43	0.30	2.61	0.08	50.85	1.40
35095	11.13	6.30		7.26	0.06	3.26	0.15	2.44	0.06	64.93	0.78
35096	9.27	5.04		5.79	0.07	2.31	0.09	2.84	0.01	71.38	0.71
35201	14.83	9.36		11.19	0.20	6.46	0.19	2.66	0.09	49.93	1.77
35202	14.87	9.52		11.62	0.16	6.40	0.21	2.94	0.08	49.24	1.77
35203	14.86	8.94		11.60	0.32	6.53	0.20	3.11	0.06	49.51	1.72
35204	15.03	10.37		11.42	0.17	6.29	0.19	1.96	0.06	49.88	1.76
35205	14.68	9.49		11.83	0.14	6.32	0.19	2.34	0.09	49.58	1.87
35206	14.44	8.98		12.59	0.28	6.71	0.20	2.95	0.09	49.10	1.86
35207	8.67	3.01		8.80	0.98	2.65	0.27	0.01	0.17	69.81	0.49
35208	8.29	2.73		3.30	1.92	1.34	0.12	0.17	0.01	76.47	0.39
35209	9.38	0.01		3.02	1.14	4.60	0.04	0.01	0.01	76.23	0.48
35210	3.61	0.01		5.05	0.44	1.17	0.02	0.01	0.01	85.21	0.17
35211	9.09	0.01		3.66	1.00	3.89	0.15	0.01	0.01	76.93	0.43
35212	4.04	0.21		3.15	0.26	2.86	0.03	0.01	0.01	85.98	0.22
35213	5.70	0.71		3.40	0.86	2.80	0.03	0.01	0.01	83.44	0.33
35214	14.28	8.13		12.82	0.06	7.53	0.14	1.90	0.11	46.05	1.80
35215	4.83	0.46		3.51	0.08	4.54	0.02	0.01	0.01	83.21	0.27
35216	6.46	0.48		8.65	1.32	0.79	0.02	0.09	0.01	75.54	0.34
35217	3.43	0.01		2.81	0.28	1.63	0.01	0.01	0.01	88.72	0.17
35218	8.80	0.04		5.42	0.78	3.45	0.03	0.05	0.01	77.10	0.52
35219	6.94	0.67		2.39	0.64	3.55	0.05	0.10	0.01	81.82	0.35
35220	10.70	1.47		3.27	1.65	2.59	0.02	0.93	0.01	73.38	0.63
35221	14.02	7.38		12.93	0.06	10.16	0.20	1.26	0.09	45.91	1.85
35222	10.63	0.01		2.86	1.37	5.01	0.02	0.01	0.01	74.98	0.62
35223	6.17	0.04		4.54	0.54	3.67	0.01	0.01	0.01	80.12	0.34
35224	5.77	0.58		2.34	0.19	2.14	0.02	1.53	0.01	83.84	0.35
35225	17.61	4.41		6.07	0.93	11.29	0.08	1.22	0.17	43.85	2.05
35226	15.30	8.62		10.85	0.11	4.22	0.19	3.08	0.10	49.77	1.82
35227	13.80	10.73		11.34	0.14	6.11	0.18	1.78	0.05	46.57	1.73
35228	4.01	0.78		1.91	0.33	2.47	0.03	0.26	0.01	87.30	0.24
35229	15.69	8.29		10.09	0.10	5.13	0.15	3.69	0.08	49.60	1.75
35230	15.71	8.57		11.07	0.09	6.57	0.21	2.95	0.05	48.76	1.55
35231	6.65	1.54		4.20	0.17	2.98	0.06	1.73	0.01	79.73	0.28
35232	14.19	9.12		11.02	0.16	6.22	0.20	3.11	0.10	50.06	1.65
35233	14.71	10.01		11.57	0.15	6.38	0.20	1.97	0.11	48.40	1.80
35234	14.48	9.98		11.19	0.23	6.22	0.20	3.03	0.09	49.28	1.70
35235	14.69	9.07		11.56	0.38	6.47	0.20	2.75	0.11	48.87	1.84
35236	15.14	9.46		10.73	0.20	7.05	0.18	2.82	0.09	48.25	1.63
35237	14.60	8.71		11.21	0.11	6.53	0.19	3.74	0.12	48.93	1.76

Sample#	Al <sub>2</sub> O <sub>3</sub> (%)	CaO (%)	Cr <sub>2</sub> O <sub>3</sub> (%)	Fe(tot) (%)	K <sub>2</sub> O (%)	MgO (%)	MnO (%)	Na <sub>2</sub> O (%)	P <sub>2</sub> O <sub>5</sub> (%)	SiO <sub>2</sub> (%)	TiO <sub>2</sub> (%)
35238	14.82	9.60		11.07	0.16	6.35	0.19	2.57	0.09	49.71	1.74
35239	14.29	9.97		11.07	0.32	6.70	0.20	2.11	0.09	48.22	1.64
35240	14.61	9.37		11.13	0.21	6.62	0.20	2.96	0.10	49.59	1.72
35241	14.51	9.21		11.93	0.05	6.74	0.23	2.81	0.14	48.53	1.96
35242	6.29	0.01		2.66	0.89	2.92	0.02	0.01	0.01	83.56	0.31
35243	6.10	0.01		3.52	0.12	5.36	0.02	0.01	0.01	79.22	0.29
35244	7.65	0.01		2.14	0.89	2.76	0.01	0.02	0.01	82.56	0.48
35245	8.39	0.01		4.26	0.34	6.18	0.01	0.01	0.01	74.97	0.48
35246	14.49	9.72		10.91	0.23	6.03	0.19	2.58	0.09	49.71	1.70
35247	13.68	8.77		11.79	0.09	9.03	0.20	2.36	0.10	46.01	1.61
35248	14.38	9.04		11.22	0.16	6.21	0.19	3.24	0.09	48.83	1.72
35249	14.15	8.95		11.25	0.10	6.17	0.19	3.10	0.10	48.23	1.74
35250	14.68	8.88		11.60	0.20	6.42	0.20	2.49	0.09	48.44	1.77
35251	14.54	9.90		11.25	0.28	6.43	0.19	2.27	0.09	48.08	1.66
35252	12.25	8.18		11.85	0.21	9.43	0.20	0.77	0.07	45.14	1.49
35253	14.90	8.86		11.84	0.24	6.55	0.20	3.16	0.09	49.18	1.80
35254	13.82	9.32		10.46	0.22	6.03	0.19	3.37	0.08	48.23	1.57
35255	14.81	8.98		11.37	0.28	6.61	0.19	2.71	0.09	48.78	1.75
35257	14.17	9.06		10.06	0.15	6.07	0.18	3.54	0.07	47.93	1.57
35258	14.63	9.40		10.64	0.16	5.87	0.18	2.28	0.09	49.52	1.64
35259	14.30	9.85		10.04	0.22	6.30	0.19	2.97	0.06	48.91	1.48
35260	15.14	8.43		11.04	0.05	6.33	0.19	3.57	0.09	48.74	1.66
35261	13.92	9.63		10.53	0.65	5.86	0.18	1.93	0.10	45.93	1.63
35262	14.52	8.69		10.94	0.22	6.12	0.19	3.45	0.10	48.80	1.73
35263	14.69	8.82		10.92	0.32	6.53	0.19	3.04	0.09	48.81	1.66
35264	14.52	8.88		11.03	0.21	6.44	0.19	2.64	0.10	48.40	1.71
35265	14.29	9.91		11.20	0.41	6.22	0.20	2.54	0.09	48.90	1.69
35266	14.45	10.03		11.10	0.27	5.97	0.19	2.61	0.08	48.49	1.74
35267	14.24	9.06		11.55	0.28	6.34	0.19	2.84	0.10	48.37	1.73
35268	14.80	9.18		11.13	0.29	6.31	0.20	3.27	0.11	49.23	1.76
35269	14.43	10.10		10.37	0.38	6.55	0.19	2.26	0.08	47.69	1.63
35270	14.46	8.87		10.95	0.14	6.14	0.19	3.26	0.11	48.20	1.69
35271	14.72	9.21		11.45	0.21	6.62	0.20	2.82	0.09	48.97	1.75
35272	14.82	9.12		10.96	0.19	6.38	0.19	3.38	0.09	49.41	1.72
35273	14.66	9.23		11.35	0.45	6.20	0.19	2.45	0.08	49.15	1.73
35274	14.20	9.19		10.73	0.21	6.25	0.19	3.11	0.08	48.36	1.66
35275	14.39	9.92		9.92	0.22	6.88	0.32	3.46	0.05	47.25	1.38

Sample#	Table A3.3. Trace element and additional components concentrations											
	CO <sub>2</sub> (%)	H <sub>2</sub> O(+) (%)	S % (%)	LOI % (%)	TOTAL	FeO (%)	Ba (ppm)	Rb (ppm)	Sr (ppm)	Nb (ppm)	Zr (ppm)	Y (ppm)
HS952001	0.69	2.90	0.11	2.95	90.90	9.30	32900	198	252	7	105	32
HS952002	2.35	3.20	0.15	4.90	98.80	7.90	32400	22	135	3	119	39
HS952003	9.08	4.50	0.27	12.30	100.30	8.40	1130	43	139	4	100	32
HS952004	0.60	2.80	0.66	2.35	99.50	8.10	3200	2	158	5	149	40
HS952005	2.29	4.40	2.22	4.95	98.40	7.50	6380	39	54	5	132	41
HS952006	0.29	1.50	1.47	2.45	100.20	1.70	626	8	51	3	74	26
HS952007	1.65	3.20	0.14	3.95	98.30	8.20	4420	1	141	4	107	30
HS952008	1.14	3.90	0.15	4.50	99.60	9.30	14000	1	130	4	128	39
HS952009	0.79	2.80	0.13	2.90	98.60	8.70	3320	1	144	5	125	39
HS952010	0.44	2.80	0.14	2.50	98.80	8.70	1910	1	153	5	129	38
HS952011	0.03	1.30	0.11	1.70	100.30	0.60	4010	27	42	23	80	20
HS952012	3.28	2.80	0.13	5.35	99.70	6.50	1020	1	108	6	144	34
HS952013	0.87	2.70	0.21	2.65	98.50	8.60	334	1	147	18	104	39
HS952014	1.00	3.30	0.28	3.60	100.00	8.80	390	1	204	5	130	42
HS952015	1.06	3.20	0.14	3.60	98.20	9.00	4960	1	129	5	128	40
HS952016	4.54	4.20	0.40	8.00	99.80	8.60	5090	1	164	6	128	38
HS952017	1.74	3.00	0.13	4.00	99.40	8.80	745	1	127	4	124	39
HS952018	1.07	3.00	0.35	3.10	98.80	9.20	5480	1	132	6	124	38
HS952019	2.00	3.00	0.17	4.35	99.80	8.20	126	1	163	16	123	39
HS952020	0.01	1.50	0.60	1.80	98.60	0.90	4080	21	36	5	97	16
HS952021	0.71	2.00	0.80	1.90	99.70	4.50	1090	8	76	5	116	26
HS952022	1.63	2.40	0.15	3.30	99.20	6.70	730	3	205	10	129	39
HS952023	1.27	2.60	0.14	3.25	98.80	7.20	1210	1	162	6	133	34
HS952024	1.39	2.40	0.26	3.05	98.70	8.90	1190	1	100	8	117	33
HS952025	1.48	1.30	1.31	2.85	99.60	2.60	3850	45	59	11	122	29
HS952026	5.97	4.70	0.02	9.70	100.10	9.10	1580	1	103	6	116	34
HS952027	2.17	0.90	0.15	3.00	99.60	2.30	3320	45	45	9	78	15
HS952028	1.00	1.50	0.10	2.15	100.00	2.70	4280	30	59	4	88	22
HS952029	0.51	3.20	0.12	3.00	99.00	8.50	73	1	142	6	137	43
HS952030	3.53	4.00	0.03	6.80	99.70	8.70	741	1	111	8	121	37
HS952031	0.87	3.10	0.11	3.50	99.20	8.00	74	1	132	10	125	39
HS952032	0.55	3.00	0.06	2.80	98.80	8.30	251	1	197	5	131	38
HS952033	0.74	2.70	0.16	2.80	98.70	8.30	121	1	157	4	123	34
HS952034	0.60	3.60	0.03	3.60	98.20	9.00	91	1	96	7	117	40
HS952035	1.44	3.50	0.07	4.05	99.20	9.40	177	1	118	4	129	42
HS952036	3.49	3.50	0.16	6.20	100.60	9.20	1680	9	146	2410	137	43
HS952037	5.68	4.20	0.13	8.70	100.40	9.30	17100	23	164	685	130	44
HS952038	1.62	3.70	0.14	4.70	99.60	8.00	19600	16	184	12	126	42
HS952039	0.21	2.60	0.15	2.35	99.60	8.50	1270	2	219	9	133	41
HS952040	0.39	2.70	0.19	2.55	100.30	8.50	1480	4	189	3	128	40
HS952041	2.15	3.70	0.73	3.90	99.40	12.40	176	1	150	1	78	25
HS952042	1.68	1.90	0.46	3.20	100.20	6.30	26	1	35	3	78	15
HS952043	0.04	2.80	0.58	3.10	100.40	4.00	1620	15	57	21	203	26
HS952044	0.03	2.80	0.72	3.00	100.20	3.60	3500	17	56	10	124	21
HS952045	0.05	1.80	0.03	1.95	100.20	1.20	2440	21	50	7	101	24
HS952046	0.87	3.10	0.10	2.90	98.70	8.50	238	5	172	5	144	40
HS952047	0.10	2.50	0.17	2.45	99.40	7.70	66	2	152	7	128	35
HS952048	0.54	2.60	0.16	2.25	99.30	8.60	69	4	99	6	122	38
HS952049	0.18	2.40	0.15	2.00	99.40	8.40	75	10	191	5	129	40
HS952050	1.05	2.50	0.09	2.70	98.40	7.10	1580	15	149	7	166	39



Sample#	CO <sub>2</sub> (%)	H <sub>2</sub> O(+) (%)	S % (%)	LOI % (%)	TOTAL	FeO (%)	Ba (ppm)	Rb (ppm)	Sr (ppm)	Nb (ppm)	Zr (ppm)	Y (ppm)
HS952051	1.22	2.90	0.16	3.05	100.20	8.80	114	4	118	3	128	42
HS952052	1.42	2.50	0.13	2.90	98.70	7.30	40	1	99	3	113	35
HS952053	1.13	2.90	0.10	2.35	99.20	8.80	36	2	143	15	128	42
HS952054	0.57	3.40	0.10	2.20	99.40	9.20	21	1	97	6	126	38
HS952055	0.29	2.90	0.19	2.60	99.30	8.60	35	6	152	6	129	38
HS952056	1.18	2.80	0.08	3.20	99.80	7.40	900	1	151	6	140	38
HS952057	1.69	4.00	0.27	3.40	99.50	9.00	2000	3	134	9	120	42
HS952058	3.20	3.90	0.37	4.40	98.90	5.90	8450	34	71	7	128	31
HS952059	0.28	3.50	0.65	3.30	99.70	8.00	123	1	188	8	131	37
HS952060	0.77	3.50	0.13	2.60	99.80	9.50	55	1	110	6	130	41
HS952061	0.61	4.40	7.43	8.20	100.40	7.10	546	11	207	9	133	38
HS952063	0.48	2.50	0.11	2.50	98.40	7.40	484	1	150	6	122	37
HS952064	1.15	4.20	3.93	5.35	99.00	7.50	2430	4	119	5	120	34
HS952065	1.90	1.20	8.06	6.90	100.40	0.80	6350	54	43	6	108	31
HS952066	0.74	3.00	0.17	2.90	98.60	7.50	4320	1	224	5	130	41
HS952067	0.34	2.80	0.16	2.20	99.10	8.60	68	3	120	5	127	37
HS952068	0.37	2.50	0.12	2.25	99.90	7.70	71	7	180	3	128	36
HS952069	1.36	3.10	0.28	3.30	99.00	9.00	45	1	123	5	127	38
HS971070	0.13	2.10	0.06	1.65	100.20	3.10	929	16	42	8	127	18
HS971071	0.24	2.10	0.51	1.90	100.20	5.00	1630	4	33	5	82	16
HS971072	2.26	2.90	0.17	2.35	99.30	8.30	1070	5	122	6	155	40
HS971073	1.73	4.30	0.98	3.55	98.60	9.70	196	4	74	2	131	38
HS971074	0.35	4.50	0.94	3.80	100.00	10.40	149	5	139	5	179	52
HS971075	1.02	5.00	0.44	3.90	99.10	11.30	177	5	122	4	158	41
HS971076	6.06	4.60	0.07	9.45	100.30	8.10	388	3	128	3	116	32
HS971077	9.81	4.00	0.02	12.50	100.40	9.00	986	13	108	4	114	34
HS971078	2.06	2.70	0.02	3.85	100.40	5.90	2460	40	24	6	107	20
HS971079	3.54	1.20	0.04	4.15	100.40	2.60	4530	53	65	5	89	13
HS971080	2.85	1.20	0.25	3.30	100.50	2.00	4220	60	44	7	101	9
HS971081	5.33	5.10	0.06	8.70	100.40	9.20	409	5	177	4	131	32
HS971082	2.57	2.40	0.12	3.70	100.00	4.10	420	3	107	6	115	26
HS971083	2.77	3.30	0.02	4.90	100.10	4.50	390	10	21	7	128	19
HS971084	0.23	1.50	0.83	1.70	100.30	1.20	1950	23	15	5	44	6
HS971085	0.60	3.00	0.03	2.95	100.10	2.60	5390	33	27	9	95	15
HS971086	0.05	2.10	0.29	1.90	100.30	1.50	4300	25	12	9	66	8
HS971087	0.91	1.40	1.71	2.40	100.30	1.40	4080	16	30	5	54	10
HS971088	2.86	2.50	0.02	3.90	100.30	5.40	306	6	56	5	104	20
HS971089	-0.01	2.60	3.72	4.20	100.40	2.80	5190	25	18	9	117	15
HS971090	0.26	2.30	2.00	2.95	100.30	2.40	3320	18	19	8	117	19
HS971091	1.52	3.70	0.12	4.00	98.60	8.00	18160	20	201	3	68	36
HS971092	0.42	3.80	0.02	3.15	99.70	6.90	288	2	269	4	154	37
HS971093	0.80	3.00	0.13	2.65	99.50	8.00	265	2	73	3	112	30
HS971094	4.38	4.70	0.45	7.15	100.00	8.40	921	6	82	4	109	30
HS971095	0.52	3.20	0.16	2.50	99.40	7.60	817	5	191	4	148	39
HS971096	1.78	2.10	1.50	3.85	100.40	3.80	5740	47	10	5	83	17
HS971097	11.10	3.50	0.17	12.90	100.40	7.90	11660	43	73	4	68	30
HS971098	1.45	3.20	0.11	3.20	99.40	8.20	455	3	109	4	108	30
HS971099	0.90	3.50	0.01	5.80	99.70	2.50	-20	3	9	3	20	2
HS971100	1.14	3.00	0.02	3.35	100.00	6.60	266	10	123	6	139	35
HS971101	5.10	4.80	0.06	8.75	100.40	9.00	917	12	101	3	121	34
HS971102	1.55	3.60	0.04	3.80	99.70	8.30	164	3	130	4	131	36

Sample#	CO <sub>2</sub> (%)	H <sub>2</sub> O(+) (%)	S % (%)	LOI % (%)	TOTAL	FeO (%)	Ba (ppm)	Rb (ppm)	Sr (ppm)	Nb (ppm)	Zr (ppm)	Y (ppm)
HS971103	3.39	2.60	0.57	4.10	100.40	4.30	349	4	33	3	57	7
HS971104	0.99	3.30	0.12	3.05	98.80	9.20	10820	10	143	3	91	37
HS971105	0.64	3.20	0.06	2.75	99.50	9.40	81	2	104	4	133	35
HS971106	1.86	3.50	0.16	4.00	99.80	8.70	89	8	98	3	124	33
HS971107	1.75	3.40	0.11	4.05	99.80	9.10	-20	4	83	3	128	36
HS971108	0.97	3.50	0.05	3.35	99.70	9.60	121	7	127	4	136	37
HS971109	3.98	1.30	0.09	4.45	100.40	2.00	6040	81	118	8	100	13
HS971110	7.12	4.90	0.61	10.40	100.30	8.60	5770	27	69	3	112	36
HS971111	1.03	3.00	0.02	3.05	99.70	8.80	175	2	108	3	138	37
HS971112	1.55	2.40	0.07	3.10	100.40	4.80	1820	15	45	6	124	25
HS971113	2.24	3.80	4.09	5.30	98.70	7.40	3220	20	43	4	112	30
HS971114	0.73	3.70	0.14	3.10	99.60	7.80	118	4	146	3	128	35
HS971115	0.49	3.70	0.09	2.90	99.40	8.20	107	4	95	4	127	32
HS971125	3.58	1.80	0.81	4.05	99.00	2.30	2630	68		11	131	12
BCD20701			1.46		90.60		63420					
BCD20702			1.99		92.03		69880					
BCD20705			0.77		93.31		27200					
BCD20706			1.10		94.72		8340					
BCD20707			0.08		94.53		2110					
BCD20708			0.01		94.83		2360					
BCD20709			1.01		96.91		16110					
BCD20711			2.84		97.94		40070					
BCD20712			0.37		94.97		5570					
BCD20713			0.28		95.73		3820					
BCD20714			0.11		94.86		1160					
BCD20715			0.13		94.54		1900					
BCD20716			0.40		95.44		5980					
BCD20717			0.25		94.41		3810					
BCD20718			0.22		95.55		2950					
BCD20719			0.26		96.86		3370					
BCD20720			0.29		96.41		4390					
BCD20721			0.45		95.84		5790					
BCD20722			1.07		95.83		14750					
BCD20723			4.70		96.07		500					
BCD20724			0.33		94.60		5540					
BCD20725			0.22		90.83		3330					
BCD20879			0.66		91.96		9560					
BCD20880			3.03		93.20		46250					
BCD20881			0.29		96.04		4700					
BCD20882			2.77		98.98		43280					
BCD20883			0.60		91.05		8400					
BCD20884			0.12		84.00		2370					
BCD20885			1.14		96.50		16850					
BCD20886			0.31		91.26		4350					
BCD20887			0.15		88.24		2020					
BCD20888			0.22		92.98		2980					
BCD20889			0.12		96.02		1770					
BCD20891			1.07		98.07		16360					
BCD20892			0.74		93.07		9420					
BCD21862			0.49		96.02		7010					
BCD21863			1.44		94.46		19520					

Sample#	CO <sub>2</sub> (%)	H <sub>2</sub> O(+) (%)	S % (%)	LOI % (%)	TOTAL	FeO (%)	Ba (ppm)	Rb (ppm)	Sr (ppm)	Nb (ppm)	Zr (ppm)	Y (ppm)
BCD21864			0.06		95.89		870					
BCD21865			0.10		94.90		1500					
BCD21866			1.76		95.35		7580					
BCD21867			3.94		96.78		57340					
BCD21868			4.21		92.69		60220					
BCD21869			1.09		96.10		760					
BCD21870			3.72		97.34		960					
BCD21871			3.64		98.03		2090					
BCD21872			0.39		96.97		400					
BCD21873			0.02		98.86		350					
BCD21874			0.04		89.77		60					
BCD21875			1.19		89.32		16680					
BCD21876			0.06		94.70		630					
BCD21877			0.03		95.49		1340					
BCD21878			0.02		95.76		1110					
BCD21879			0.47		93.33		1490					
BCD21880			0.02		92.44		200					
BCD21881			0.53		91.84		110					
BCD21882			9.20		98.90		3530					
BCD21883			1.05		97.97		3170					
BCD21884			0.02		97.49		2080					
BCD21885			0.01		97.79		820					
BCD21886			0.01		97.31		350					
BCD21887			0.01		97.65		260					
BCD21888			0.02		95.99		940					
BCD21889			0.03		96.62		1870					
BCD21890			0.39		90.71		2810					
BCD21891			0.24		90.70		2930					
BCD21892			0.42		91.38		2180					
BCD21893			0.30		90.35		1640					
BCD21894			1.10		98.11		3080					
BCD21895			1.75		98.94		2670					
BCD21896			0.40		96.59		2030					
BCD21897			0.56		96.57		2030					
BCD21898			0.47		96.82		270					
BCD21899			3.10		96.04		70					
BCD21900			3.55		97.81		1230					
BCD21901			1.26		94.57		4750					
BCD21902			1.14		93.21		3420					
BCD21903			0.08		96.49		1750					
BCD21904			0.06		97.01		880					
BCD21905			0.02		97.60		800					
BCD21906			0.13		96.16		1890					
BCD21907			0.04		92.07		2770					
BCD21908			0.07		95.16		5210					
BCD21909			0.79		95.94		10960					
BCD21910			8.20		98.67		9570					
BCD21911			5.75		98.78		4420					
BCD21912			0.46		96.36		90					
BCD21913			0.43		87.51		110					
BCD21914			0.71		97.35		50					

Sample#	CO <sub>2</sub> (%)	H <sub>2</sub> O(+) (%)	S % (%)	LOI % (%)	TOTAL	FeO (%)	Ba (ppm)	Rb (ppm)	Sr (ppm)	Nb (ppm)	Zr (ppm)	Y (ppm)
BCD21915			1.58		92.56		50					
BCD21916			1.54		98.21		50					
BCD21917			4.80		93.21		80					
BCD21918			0.12		96.27		790					
BCD21919			1.02		96.69		940					
BCD21920			3.10		99.22		2080					
BCD21921			1.48		96.06		1560					
BCD21922			0.56		92.13		2350					
BCD21923			0.63		98.47		9740					
BCD21924			0.28		97.28		4790					
BCD21925			0.08		93.90		1020					
BCD21926			0.06		96.81		530					
BCD21927			0.03		96.22		400					
BCD21928			0.07		96.63		730					
BCD21929			0.04		96.84		530					
BCD21930			0.06		96.00		710					
BCD21931			0.10		95.92		1450					
BCD21932			0.17		95.78		2430					
BCD21933			0.89		92.41		9400					
BCD21934			0.56		95.81		6150					
BCD21935			0.28		96.52		2900					
BCD21936			0.04		96.92		150					
BCD21937			0.04		95.72		160					
BCD21938			0.02		96.09		190					
BCD21939			0.02		94.83		380					
BCD21940			0.03		94.93		880					
BCD21941			0.07		95.95		1070					
BCD21942			0.06		89.41		3940					
BCD21943			0.14		93.59		5160					
BCD21944			0.53		96.46		3390					
BCD21945			0.12		96.43		1150					
BCD21964			0.09		96.53		330					
BCD21965			0.13		95.73		270					
BCD21966			0.17		94.48		480					
BCD21967			0.06		94.71		420					
BCD21968			1.49		95.58		1270					
BCD21969			1.17		96.28		390					
BCD21970			0.01		92.77		260					
BCD21971			0.02		96.67		3140					
BCD21972			0.24		95.69		180					
BCD21973			0.40		93.04		1430					
BCD21974			0.75		95.95		3160					
BCD21975			2.86		94.99		1760					
BCD21976			1.35		95.96		3310					
BCD21977			1.74		94.22		410					
BCD21978			1.12		97.32		2460					
BCD21979			1.24		90.98		310					
BCD21980			0.60		95.89		2110					
BCD21981			0.04		94.98		520					
BCD21982			0.05		96.43		530					
BCD21983			0.03		96.05		800					

Sample#	CO <sub>2</sub> (%)	H <sub>2</sub> O(+) (%)	S % (%)	LOI % (%)	TOTAL	FeO (%)	Ba (ppm)	Rb (ppm)	Sr (ppm)	Nb (ppm)	Zr (ppm)	Y (ppm)
BCD21984			0.07		95.80		1050					
BCD21985			0.05		95.76		1330					
BCD21986			0.04		95.95		1780					
BCD21987			0.08		95.73		3670					
BCD21988			0.06		95.15		3920					
BCD21989			0.39		96.58		7790					
BCD21990			0.52		87.73		200					
BCD21991			0.02		84.93		260					
BCD21992			0.69		96.53		11500					
BCD21993			0.64		97.44		4750					
BCD22351			0.08		94.22		490					
BCD22352			0.06		95.36		760					
BCD22353			0.06		95.59		1070					
BCD22354			0.19		88.20		2380					
BCD22355			0.34		90.28		5260					
BCD22356			0.67		94.99		12520					
BCD22357			1.61		95.72		22150					
BCD22358			2.68		95.45		45810					
BCD22359			3.06		94.29		63970					
BCD22362			2.20		93.88		7160					
BCD22363			1.06		90.18		18980					
BCD22364			0.39		92.69		7050					
BCD22514			0.12		95.67		500					
BCD22515			0.16		94.66		2150					
BCD22516			0.23		95.96		2750					
BCD22517			0.69		94.64		8150					
BCD22518			7.50		98.73		31800					
BCD22519			7.25		98.43		3300					
BCD22520			1.49		89.66		100					
BCD22521			7.60		98.73		4800					
BCD22522			0.51		89.10		7650					
BCD22524			0.09		94.96		200					
BCD22525			0.03		92.60		300					
BCD22558			0.06		95.63		700					
BCD22559			0.12		93.09		1600					
BCD22560			1.33		90.18		18900					
BCD22561			2.10		91.09		6000					
BCD22562			1.54		96.08		200					
BCD22563			0.55		94.52		7500					
BCD22564			0.64		95.58		8750					
BCD22565			3.02		96.18		45250					
BCD22566			0.13		98.51		150					
BCD22567			4.56		93.84		2050					
BCD22568			0.42		92.13		100					
BCD22569			3.58		94.50		7450					
BCD22570			0.72		93.61		9700					
BCD22571			1.76		88.44		22550					
BCD22572			13.50		96.59		900					
BCD22573			0.94		94.31		11850					
BCD22574			0.16		96.17		2000					
BCD22575			0.04		94.62		170					

Sample#	CO <sub>2</sub> (%)	H <sub>2</sub> O(+) (%)	S % (%)	LOI % (%)	TOTAL	FeO (%)	Ba (ppm)	Rb (ppm)	Sr (ppm)	Nb (ppm)	Zr (ppm)	Y (ppm)
BCD22576			0.05		94.90		320					
BCD22577			0.09		92.56		700					
BCD22578			0.17		94.08		1020					
BCD22877			0.43		94.31		2280					
BCD22878			3.46		97.87		1230					
BCD22879			0.67		94.72		9370					
BCD22880			0.56		95.30		6850					
BCD22882			0.21		95.26		400					
BCD22883			1.69		94.95		1700					
BCD22884			0.48		95.71		2690					
6501					97.63		50					
6502					97.49		50					
6503					100.00		50					
6504					97.20		50					
6505					103.18		80					
6506					98.36		50					
6507					98.00		50					
6508					99.62		50					
6509					98.76		50					
6510					98.99		50					
6511					100.19		50					
6512					97.76		50					
6513					99.15		100					
6514					98.03		920					
6515					99.92		650					
6516					99.84		760					
6517					98.54		80					
6518					98.41		80					
6519					99.90		290					
6520					95.55		8100					
6521					98.29		80					
6526					93.47		50					
6527					96.01		50					
6528					99.54		50					
6529					97.21		50					
6530					92.71		60					
6531					99.31		120					
6532					99.17		140					
6533					98.11		1630					
6534					100.23		80					
6535					93.63		130					
6536					96.65		80					
6537					96.14		140					
6538					93.18		120					
6539					99.98		50					
6540					94.39		100					
6541					100.28		160					
6542					97.60		7360					
6543					92.19		3690					
6544					96.66		330					
6545					95.57		5730					

Sample#	CO <sub>2</sub> (%)	H <sub>2</sub> O(+) (%)	S % (%)	LOI % (%)	TOTAL	FeO (%)	Ba (ppm)	Rb (ppm)	Sr (ppm)	Nb (ppm)	Zr (ppm)	Y (ppm)
6547					97.87		3100					
6548					99.50		810					
6549					99.31		100					
6550					99.86		140					
6551					99.69		1750					
6552					95.28		540					
6553					99.35		860					
6554					98.75		50					
6555					99.22		80					
6556					99.74		510					
6557					99.77		3090					
6558					100.20		160					
6559					99.00		50					
6560					99.97		50					
6561					99.58		50					
6562					99.49		80					
6563					98.98		810					
6564					94.09		5540					
6565					92.29		60					
6566					96.11		80					
6567					94.52		80					
6568					95.48		210					
6577					100.07		50					
6578					99.83		50					
6579					99.72		50					
6580					99.19		50					
6581					99.99		190					
6582					99.53		230					
6588					99.59		170					
6589					95.30		50					
6590					94.13		50					
6591					99.74		50					
6592					98.67		50					
6593					95.14		60					
6594					94.49		1560					
6595					97.21		1630					
6596					96.25		210					
6597					99.49		50					
6598					96.29		50					
6599					100.60		50					
6600					100.27		50					
6651					99.68		120					
6652					99.65		110					
6653					100.09		50					
6654					98.78		50					
6655					99.31		50					
6656					99.69		50					
6657					99.80		50					
6658					99.71		60					
6659					99.34		50					
6660					99.77		100					

Sample#	CO <sub>2</sub> (%)	H <sub>2</sub> O(+) (%)	S % (%)	LOI % (%)	TOTAL	FeO (%)	Ba (ppm)	Rb (ppm)	Sr (ppm)	Nb (ppm)	Zr (ppm)	Y (ppm)
6661					99.83		50					
6662					97.70		160					
6663					92.99		4440					
6664					99.62		310					
6665					97.49		760					
6666					98.13		6950					
6667					99.28		20190					
6668					99.60		6580					
6669					99.81		3810					
6670					99.93		5030					
6671					99.77		60					
6672					99.60		80					
6673					97.38		60					
6674					98.44		190					
6675					97.01		2950					
6676					100.67		170					
6677					99.74		80					
6678					93.22		50					
6679					97.00		50					
6680					92.00		80					
6681					97.37		1620					
6682					96.00		50					
6683					99.24		50					
6684					97.32		50					
6685					97.32		50					
6686					99.70		50					
6687					100.11		50					
6688					99.58		50					
6689					93.94		50					
6690					99.99		50					
6691					100.50		50					
6692					99.99		50					
6693					100.08		100					
6694					93.73		50					
6695					100.44		50					
6696					98.69		50					
6697					99.90		50					
6698					98.47		50					
6699					99.58		50					
6701					96.93		50					
6702					95.08		2180					
6703					98.91		50					
6704					99.07		230					
6705					99.25		840					
6706					98.09		15180					
6707					94.38		1000					
6708					99.83		1570					
6709					92.34		5710					
6710					99.77		3320					
6711					99.35		50					
6712					99.41		80					



Sample#	CO <sub>2</sub> (%)	H <sub>2</sub> O(+) (%)	S % (%)	LOI % (%)	TOTAL	FeO (%)	Ba (ppm)	Rb (ppm)	Sr (ppm)	Nb (ppm)	Zr (ppm)	Y (ppm)
6713					93.34		90					
6714					98.95		80					
6715					95.69		310					
6716					99.71		1570					
6717					93.51		4030					
6718					95.15		360					
6719					99.13		510					
6720					88.88		50730					
6721					96.15		160					
6722					100.34		1560					
6723					92.51		9490					
6724					98.48		470					
6725					97.82		2660					
6726					96.62		320					
6735					98.97		80					
6736					93.71		670					
6737					94.19		4590					
6738					88.68		10070					
6739					96.85		2220					
6740					93.01		8000					
6741					92.95		80					
6742					91.27		90					
6743					94.94		50					
6744					92.01		80					
6745					86.52		1090					
6746					93.44		270					
6747					94.60		80					
6748					95.47		80					
6749					94.06		80					
6750					99.06		80					
6767					94.30		3070					
6768					94.59		1740					
6769					99.49		1020					
6773					89.52		6380					
6800					99.39		50					
6801					99.48		80					
6802					99.43		50					
6803					103.53		50					
6804					98.69		50					
6805					98.39		50					
6806					98.20		50					
6807					103.27		50					
6808					99.40		50					
6809					99.75		60					
6810					99.50		230					
6811					91.23		12880					
6812					103.46		160					
6813					96.16		50					
6814					98.79		80					
6815					97.70		50					
6816					98.47		60					

Sample#	CO <sub>2</sub> (%)	H <sub>2</sub> O(+) (%)	S % (%)	LOI % (%)	TOTAL	FeO (%)	Ba (ppm)	Rb (ppm)	Sr (ppm)	Nb (ppm)	Zr (ppm)	Y (ppm)
6817					99.08		50					
6818					96.19		50					
6819					99.33		50					
6820					99.17		80					
6821					99.08		50					
6822					99.31		50					
6823					96.82		50					
6824					99.42		50					
6825					98.97		50					
6826					99.26		50					
6827					97.05		50					
6828					99.55		110					
10281			0.09		97.73		2050					
10282			0.22		98.17		6200					
10288			0.60		97.68		2850					
10289			1.18		95.79		50					
10290			1.11		98.25		5050					
10293			1.12		97.94		50					
10294			0.19		97.61		20700					
10295			1.41		96.01		50					
10298			0.25		96.46		11500					
10299			0.12		94.47		50					
10300			6.97		97.08		50					
10301			0.60		96.03		50					
17525			0.19		93.73		4070					
18003			0.88		92.49		7360					
18004			5.80		95.96		5650					
18017			0.66		94.10		4480					
18051			0.75		96.53		3280					
18052			1.29		93.51		13300					
18067			0.56		92.03		3660					
18087			0.43		93.22		4310					
24928			0.28		95.52		450					
24929			0.14		95.84		1000					
24941			0.07		96.10		1950					
24942			0.20		94.33		1200					
24947			0.19		94.56		750					
24948			0.13		90.59		250					
24951			0.04		93.43		150					
24952			0.15		96.36		150					
34751			2.61		97.70		3750					
34755			2.45		99.20		3700					
34768			7.55		99.31		700					
34779			4.82		95.91		4150					
35076			1.16		91.41		50					
35077			0.12		95.73		450					
35078			0.27		97.07		50					
35079			0.21		95.91		50					
35080			0.27		95.70		50					
35081			0.26		95.81		50					
35082			0.20		96.62		50					

Sample#	CO <sub>2</sub> (%)	H <sub>2</sub> O(+) (%)	S % (%)	LOI % (%)	TOTAL	FeO (%)	Ba (ppm)	Rb (ppm)	Sr (ppm)	Nb (ppm)	Zr (ppm)	Y (ppm)
35083			0.31		95.97		50					
35084			0.24		96.12		50					
35085			0.24		94.94		50					
35086			0.23		96.09		50					
35087			0.25		96.31		50					
35088			0.26		89.16		650					
35089			0.19		96.09		50					
35090			0.21		95.53		50					
35091			0.23		96.29		50					
35092			0.19		95.91		50					
35093			0.26		95.96		50					
35094			0.14		96.21		50					
35095			0.17		96.66		1150					
35096			0.14		97.66		100					
35201			0.19		96.89		50					
35202			0.22		97.04		50					
35203			0.22		97.07		50					
35204			0.18		97.32		50					
35205			0.10		96.62		50					
35206			0.09		97.31		50					
35207			0.09		95.03		900					
35208			0.26		95.72		7250					
35209			0.41		96.05		7500					
35210			2.83		98.52		100					
35211			0.55		96.43		7450					
35212			0.56		97.38		750					
35213			0.04		97.38		800					
35214			0.11		92.94		50					
35215			0.32		97.25		50					
35216			4.84		99.27		7350					
35217			0.41		97.46		50					
35218			0.65		96.95		950					
35219			0.09		96.84		2400					
35220			0.17		95.77		9550					
35221			0.25		94.11		50					
35222			0.07		96.41		8450					
35223			1.93		97.56		1950					
35224			0.16		96.92		50					
35225			0.11		88.97		11700					
35226			0.18		94.23		50					
35227			0.12		92.55		50					
35228			0.11		97.44		50					
35229			0.13		94.69		50					
35230			0.27		95.80		50					
35231			0.08		97.41		50					
35232			0.30		96.12		50					
35233			0.23		95.52		50					
35234			0.26		96.66		50					
35235			0.26		96.19		50					
35236			0.21		95.77		50					
35237			0.30		96.20		50					

Sample#	CO <sub>2</sub> (%)	H <sub>2</sub> O(+) (%)	S % (%)	LOI % (%)	TOTAL	FeO (%)	Ba (ppm)	Rb (ppm)	Sr (ppm)	Nb (ppm)	Zr (ppm)	Y (ppm)
35238			0.21		96.50		50					
35239			0.29		94.91		50					
35240			0.19		96.70		50					
35241			0.15		96.25		50					
35242			0.12		97.14		3850					
35243			0.66		95.29		50					
35244			0.17		97.20		5000					
35245			1.16		95.89		950					
35246			0.19		95.85		50					
35247			0.21		93.85		50					
35248			0.33		95.42		50					
35249			0.37		94.34		50					
35250			0.28		95.07		50					
35251			0.34		95.02		50					
35252			0.23		89.81		50					
35253			0.25		97.08		50					
35254			0.25		93.52		50					
35255			0.23		95.80		50					
35257			0.22		93.01		50					
35258			0.28		94.70		50					
35259			0.22		94.55		50					
35260			0.23		95.46		50					
35261			0.20		90.56		50					
35262			0.28		95.04		50					
35263			0.20		95.27		50					
35264			0.22		94.34		50					
35265			0.28		95.74		50					
35266			0.24		95.16		50					
35267			0.22		94.93		50					
35268			0.18		96.46		50					
35269			0.14		93.82		50					
35270			0.30		94.32		50					
35271			0.18		96.21		50					
35272			0.17		96.43		50					
35273			0.19		96.00		3100					
35274			0.37		94.35		150					
35275			0.23		91.81		50					

## **Appendix 4**

### **Estimates of analytical precision of the geochemical analyses performed at X-RAL Laboratories on samples from the Chu Chua deposit**

Samples, included in the Chu Chua data set were analyzed by X-ray Assay Laboratories Ltd. (XRAL) in Don Mills, Ontario. Analytical errors are estimated by replicate analyses (Table A4.1). Three internal MDRU standards were used: ALB-1 (Ajax albitite), CUL-1 (Cultus Lake Shale) and MBX-1 (MBX stock, Afton). Reported data for laboratory standards as well as analytical duplicates were also used. Each of the standards was submitted up to ten times, in random order, together with samples from the Chu Chua (Chapter 3), Konuto Lake (Chapter 4) and Anderson Lake (not used in this work) data sets. The estimation involved a computer code, THPLOT, embedded as a function in Matlab (Stanley, 1997b). It performs a weighed Thompson-Howarth (Thompson and Howarth, 1978) replicate error analysis. Analytical errors (precision) is expressed as the sum of an absolute error term and a relative error term (Table A4.2).

It was recognized that the MDRU reference materials were prepared for analysis (crushed, pulverized and homogenized) separately from the samples. If the samples included in the Chu Chua data set were not prepared as carefully, an error could be introduced during the preparation phase. To study that possibility, duplicate pulps were prepared and analyzed within the same batch. Data from these duplicate analyses are presented in Table A4.3. Comparison of these data with those for the MDRU standards show that the quality of analysis was not compromised during the sample preparation process.

No quality control data was available for the data donated by INMET (included in the Chu Chua data set), INCO Ltd. (Chinook Mountain property). The data were assumed to be compatible with the main data sets, after significant and systematic differences between this data and the main data set were not observed.

In accordance with the practice established for the Lithogeochemical Exploration Research Project (Sinclair and Stanley, 1995), a measure of the analytical precision is provided by a comparison of the author's analytical results with the accepted values of element concentrations in the internal (MDRU) standards as reported by Stanley (1997a). A database of replicate analyses of the standards was compiled from an initial round-robin "accepted value" determinations at three laboratories: (1) Bondar-Clegg and Co. Ltd., North Vancouver, B.C.; (2) Chemex Laboratories Ltd., North Vancouver, B.C.; and, (3) X-ray Assay Laboratories Ltd., Don Mills, Ontario. Following the initial determination, the standards were submitted with every analytical batch of project research samples. Thus, a considerable database (Table A4.2) was accumulated allowing the accepted values of the internal MDRU standards to be considered statistically sound for the purposes of this study. Most of the elements were analyzed with sufficient precision (typically less than a few percent relative error). Problematic are the elements Cr, Mn, Rb, Nb and Y which are present in the samples at levels close to or below the effective detection limits.

## References

Sinclair, A.J. and Stanley, C.R., (1995) Lithogeochemical Exploration for Metasomatic Alteration Zones Associated with Hydrothermal Mineral Deposits: University of British Columbia, MDRU Research Proposal, 7 p.

Stanley, C.R., (1997a) Analytical Quality Control and Assessment for the MDRU Lithogeochemical Exploration Research Project. Lithogeochemical Exploration for Metasomatic Zones Associated with Hydrothermal Mineral Deposits. Annual Technical Report, Years 1 and 2. Mineral Deposits Research Unit, Department of Geological Sciences, The University of British Columbia, Vancouver, B.C., 32 p.

Stanley, C.R., (1997b) THPLOT.MATLAB Function to Implement Generalized Thompson-Howarth Error Analysis Using Replicate Data. Lithogeochemical Exploration for Metasomatic Zones Associated with Hydrothermal Mineral Deposits. Annual Technical Report, Years 1 and 2. Mineral Deposits Research Unit, Department of Geological Sciences, The University of British Columbia, Vancouver, B.C., 51 p.

Thompson, M., and Howarth, R.J., (1978) A New Approach to the Estimation of Analytical Precision. *Journal of Geochemical Exploration*, 9, pp. 23-30.

**Table A4.1. Replicate analyses and precision of internal (MDRU) reference materials  
analyzed by X-RAL labs with Chu Chua area samples**

**STD = Standard deviation, RSTD% = Relative standard deviation in percent, P = precision**

Internal	SiO <sub>2</sub>	TiO <sub>2</sub>	Al <sub>2</sub> O <sub>3</sub>	Cr <sub>2</sub> O <sub>3</sub>	Fe <sub>2</sub> O <sub>3</sub>	MnO	MgO	CaO	Na <sub>2</sub> O	K <sub>2</sub> O	P <sub>2</sub> O <sub>5</sub>	LOI	SUM
standard	%	%	%	%	%	%	%	%	%	%	%	%	
MBX-1	57.50	0.48	17.40	0.01	4.18	0.07	2.07	3.93	4.95	4.50	0.24	3.00	98.50
MBX-1	58.50	0.49	17.70	0.01	4.09	0.07	2.11	4.01	4.99	4.40	0.24	3.20	100.00
MBX-1	57.70	0.48	17.50	0.01	4.12	0.07	2.03	3.89	5.01	4.70	0.24	3.40	99.30
MBX-1	57.00	0.49	17.20	0.01	4.13	0.07	2.00	3.85	4.94	4.71	0.23	3.55	98.30
MBX-1	56.50	0.48	17.20	0.01	4.18	0.07	2.00	3.86	5.02	4.83	0.23	3.55	98.10
MBX-1	57.30	0.47	17.10	0.01	4.18	0.07	1.95	3.84	4.89	4.75	0.23	3.50	98.40
MBX-1	57.90	0.50	17.50	0.01	4.18	0.07	2.10	3.96	5.28	5.00	0.24	3.55	100.40
MBX-1	57.60	0.51	17.40	0.01	4.08	0.07	2.02	3.97	5.15	4.82	0.24		
MBX-1	57.60	0.51	17.40	0.01	3.96	0.06	2.02	3.81	5.14	4.90	0.24		
MBX-1	58.00	0.50	17.40	0.01	3.93	0.06	1.96	3.86	5.18	4.84	0.24		
<b>Mean</b>	<b>57.56</b>	<b>0.49</b>	<b>17.38</b>	<b>0.01</b>	<b>4.10</b>	<b>0.07</b>	<b>2.03</b>	<b>3.90</b>	<b>5.06</b>	<b>4.75</b>	<b>0.24</b>	<b>3.39</b>	<b>99.00</b>
<b>STD</b>	<b>0.55</b>	<b>0.01</b>	<b>0.18</b>	<b>0.00</b>	<b>0.09</b>	<b>0.00</b>	<b>0.05</b>	<b>0.07</b>	<b>0.13</b>	<b>0.18</b>	<b>0.00</b>	<b>0.21</b>	<b>0.91</b>
<b>RSTD(%)</b>	<b>0.96</b>	<b>2.98</b>	<b>1.01</b>	<b>0.00</b>	<b>2.24</b>	<b>6.20</b>	<b>2.65</b>	<b>1.69</b>	<b>2.48</b>	<b>3.80</b>	<b>2.04</b>	<b>6.33</b>	<b>0.92</b>
<b>P</b>	<b>1.91</b>	<b>5.96</b>	<b>2.02</b>	<b>0.00</b>	<b>4.47</b>	<b>12.40</b>	<b>5.31</b>	<b>3.38</b>	<b>4.96</b>	<b>7.61</b>	<b>4.08</b>	<b>12.67</b>	<b>1.84</b>
CUL-1	52.20	0.90	14.10	0.01	11.30	0.14	2.06	7.11	2.44	0.70	0.15	7.55	98.80
CUL-1	52.20	0.90	14.10	0.01	10.70	0.14	2.06	7.16	2.39	0.71	0.15	7.25	97.90
CUL-1	52.40	0.89	14.20	0.01	10.80	0.14	2.08	7.21	2.42	0.70	0.15	7.35	98.50
CUL-1	52.30	0.91	14.20	0.01	10.80	0.14	2.07	7.23	2.39	0.68	0.15	7.22	98.20
CUL-1	52.70	0.92	14.20	0.01	10.20	0.14	2.05	7.10	2.48	0.73	0.16		
CUL-1	53.20	0.92	14.30	0.01	10.20	0.14	2.02	7.17	2.45	0.72	0.16		
CUL-1	52.40	0.91	14.10	0.01	10.20	0.14	2.01	7.16	2.45	0.73	0.15		
CUL-1	52.80	0.89	14.20	0.01	10.50	0.14	2.03	7.09	2.41	0.71	0.15	7.70	98.70
CUL-1	52.10	0.90	14.10	0.01	10.70	0.14	2.03	7.12	2.44	0.74	0.15	7.80	98.30
CUL-1	52.60	0.90	14.20	0.01	11.10	0.14	2.05	7.16	2.42	0.72	0.15	7.40	99.00
<b>Mean</b>	<b>52.49</b>	<b>0.90</b>	<b>14.17</b>	<b>0.01</b>	<b>10.65</b>	<b>0.14</b>	<b>2.05</b>	<b>7.15</b>	<b>2.43</b>	<b>0.71</b>	<b>0.15</b>	<b>7.47</b>	<b>98.49</b>
<b>STD</b>	<b>0.34</b>	<b>0.01</b>	<b>0.07</b>	<b>0.00</b>	<b>0.38</b>	<b>0.00</b>	<b>0.02</b>	<b>0.05</b>	<b>0.03</b>	<b>0.02</b>	<b>0.00</b>	<b>0.22</b>	<b>0.38</b>
<b>RSTD(%)</b>	<b>0.64</b>	<b>1.13</b>	<b>0.48</b>	<b>0.00</b>	<b>3.58</b>	<b>0.00</b>	<b>1.11</b>	<b>0.65</b>	<b>1.17</b>	<b>2.49</b>	<b>2.77</b>	<b>2.99</b>	<b>0.39</b>
<b>P</b>	<b>1.29</b>	<b>2.26</b>	<b>0.95</b>	<b>0.00</b>	<b>7.15</b>	<b>0.00</b>	<b>2.22</b>	<b>1.29</b>	<b>2.34</b>	<b>4.98</b>	<b>5.55</b>	<b>5.97</b>	<b>0.77</b>
ALB-1	54.70	0.61	18.80	0.01	1.74	0.04	2.83	10.00	5.62	0.74	0.29	2.90	98.40
ALB-1	55.00	0.61	18.90	0.01	1.76	0.04	2.79	10.00	5.57	0.77	0.29	3.05	98.90
ALB-1	54.50	0.60	18.70	0.01	1.79	0.03	2.75	9.99	5.62	0.81	0.29	3.00	98.20
ALB-1	53.40	0.60	18.50	0.01	1.63	0.03	2.70	9.90	5.62	0.81	0.28	3.15	96.80
ALB-1	53.80	0.60	18.40	0.01	2.01	0.04	2.70	9.80	5.53	0.80	0.28	2.95	97.00
ALB-1	54.00	0.60	18.70	0.01	1.63	0.03	2.77	10.10	5.67	0.78	0.29	3.10	97.80
ALB-1	53.70	0.60	18.60	0.01	1.62	0.03	2.76	10.00	5.59	0.78	0.29	3.35	97.50
ALB-1	55.00	0.63	18.80	0.01	1.56	0.03	2.66	10.00	5.79	0.81	0.29		
ALB-1	54.40	0.61	18.60	0.01	1.67	0.03	2.70	10.00	5.71	0.79	0.28		
ALB-1	54.70	0.60	18.80	0.01	1.60	0.03	2.71	10.10	5.72	0.78	0.29		
<b>Mean</b>	<b>54.32</b>	<b>0.61</b>	<b>18.68</b>	<b>0.01</b>	<b>1.70</b>	<b>0.03</b>	<b>2.74</b>	<b>9.99</b>	<b>5.64</b>	<b>0.79</b>	<b>0.29</b>	<b>3.07</b>	<b>97.80</b>
<b>STD</b>	<b>0.56</b>	<b>0.01</b>	<b>0.15</b>	<b>0.00</b>	<b>0.13</b>	<b>0.00</b>	<b>0.05</b>	<b>0.09</b>	<b>0.08</b>	<b>0.02</b>	<b>0.00</b>	<b>0.15</b>	<b>0.76</b>
<b>RSTD(%)</b>	<b>1.04</b>	<b>1.66</b>	<b>0.83</b>	<b>0.00</b>	<b>7.74</b>	<b>14.64</b>	<b>1.89</b>	<b>0.88</b>	<b>1.39</b>	<b>2.81</b>	<b>1.68</b>	<b>4.87</b>	<b>0.78</b>
<b>P</b>	<b>2.07</b>	<b>3.32</b>	<b>1.66</b>	<b>0.00</b>	<b>15.48</b>	<b>29.28</b>	<b>3.77</b>	<b>1.75</b>	<b>2.78</b>	<b>5.63</b>	<b>3.37</b>	<b>9.74</b>	<b>1.55</b>

Internal	Ba	Rb	Sr	Nb	Zr	Y	H2O+	S	CO2	FeO	
standard	ppm	ppm	ppm	ppm	ppm	ppm	%	%	%	%	
MBX-1	709	85	516	10	101	24	1.2	0.24	2.82		
MBX-1	718	84	509	10	100	21	1.1	0.24	2.81	1.05	
MBX-1	719	90	507	10	98	19	1.1	0.23	2.83	1.16	
MBX-1	725				100	16	1.00	0.24	2.83	1.25	
MBX-1	735				98	18	1.10	0.23	2.80	1.22	
MBX-1	711				97	18	1.10	0.23	2.82		
MBX-1	695				103	18	1.10	0.24	2.77		
MBX-1	705	79	505	9	101	7		0.24	2.73		
MBX-1	703	80	510	9	100	8		0.23	2.74		
MBX-1	697	80	511	9	99	9		0.23	2.83		
Mean	711.7	83	509.7	9.5	99.7	15.8	1.1	0.235	2.798	1.17	
STD	12.63	4.195	3.777	0.548	1.767	5.808	0.0577	0.005	0.038	0.088	
RSTD(%)	1.775	5.055	0.741	5.766	1.772	36.76	5.2486	2.243	1.356	7.549	
P	3.55	10.11	1.482	11.53	3.545	73.52	10.497	4.486	2.712	15.1	
CUL-1	673				53	30	4.10	2.02	4.09	1.84	
CUL-1	677				53	18	4.30	2.06	4.04	1.69	
CUL-1	707				54	23	4.40	2.05	3.98	1.81	
CUL-1	710				54	16	4.20	2.03	4.02	1.84	
CUL-1	619	3	235	1	52	13		2.06	3.94		
CUL-1	590	8	240	1	53	11		2.02	3.86	1.85	
CUL-1	613	26	250	4	58	16		2.06	3.86	1.82	
CUL-1							4.2	2.02	3.97	1.82	
CUL-1							4.3	2.04	4	1.83	
CUL-1							4.1	2.03	3.93		
Mean	655.6	12.33	241.7	2	53.86	18.14	4.2286	2.039	3.969	1.813	
STD	47.99	12.1	7.638	1.732	1.952	6.466	0.1113	0.017	0.074	0.051	
RSTD(%)	7.321	98.08	3.16	86.6	3.624	35.64	2.6314	0.848	1.868	2.825	
P	14.64	196.2	6.321	173.2	7.248	71.28	5.2628	1.696	3.737	5.65	
Alb-1	255	25	783	10	75	27	1.6	0.23	1.61	2.21	
Alb-1	263	28	792	2	77	31	1.6	0.24	1.6	2.19	
Alb-1	249	25	789	16	73	32	1.5	0.22	1.59	2.15	
ALB-1	267				74	24	1.60	0.23	1.59	2.21	
ALB-1	274				74	24	1.40	0.23	1.61		
ALB-1	265				74	24	1.50	0.23	1.59		
ALB-1	253				74	22	1.60	0.23	1.59		
ALB-1											
ALB-1											
ALB-1											
Mean	260.9	26	788	9.333	74.43	26.29	1.5429	0.23	1.597	2.19	
STD	8.84	1.732	4.583	7.024	1.272	3.861	0.0787	0.006	0.01	0.028	
RSTD(%)	3.389	6.662	0.582	75.25	1.71	14.69	5.0996	2.51	0.596	1.292	
P	6.778	13.32	1.163	150.5	3.419	29.37	10.199	5.02	1.191	2.583	



**Table A4.2. Precision (relative error) of accepted values for internal  
(MDRU) reference materials, analyzed by X-RAL**

Internal standard	Al <sub>2</sub> O <sub>3</sub> %	CaO %	Cr <sub>2</sub> O <sub>3</sub> %	Fe <sub>2</sub> O <sub>3</sub> %	K <sub>2</sub> O %	MgO %	MnO %	Na <sub>2</sub> O %	P <sub>2</sub> O <sub>5</sub> %	SiO <sub>2</sub> %	TiO <sub>2</sub> %
<b>ALB-1</b>											
Mean	18.707	10.077	0.005	1.719	0.783	2.774	0.032	5.618	0.335	54.293	0.600
StdDev	0.219	0.291	0.000	0.127	0.023	0.058	0.004	0.092	0.126	0.673	0.009
RelErr(%)	1.17	2.88	0.00	7.36	3.00	2.09	12.94	1.64	37.69	1.94	1.42
Number	15	15	15	15	15	15	15	15	15	15	15
<b>CHI-1</b>											
Mean	1.228	36.517	0.005	1.163	0.110	5.025	0.050	0.195	0.070	22.583	0.132
StdDev	0.016	0.117	0.000	0.048	0.000	0.031	0.000	0.008	0.000	0.098	0.003
RelErr(%)	1.30	0.32	0.00	4.09	0.00	0.61	0.00	4.29	0.00	0.44	2.11
Number	6	6	6	6	6	6	6	6	6	6	6
<b>CUL-1</b>											
Mean	14.272	7.147	0.005	10.789	0.714	2.058	0.140	2.434	0.152	52.611	0.895
StdDev	0.132	0.049	0.000	0.181	0.015	0.015	0.000	0.030	0.004	0.322	0.008
RelErr(%)	0.92	0.68	0.00	1.68	2.16	0.74	0.00	1.21	2.53	0.61	0.85
Number	18	18	18	18	18	18	18	18	18	18	18
<b>MBX-1</b>											
Mean	17.363	3.924	0.005	4.119	4.709	2.034	2.070	5.033	0.253	57.369	0.483
StdDev	0.203	0.209	0.000	0.049	0.144	0.049	0.000	0.109	0.069	0.520	0.012
RelErr(%)	1.17	5.34	0.00	1.19	3.05	2.41	0.00	2.17	27.13	0.91	2.39
Number	16	16	16	16	16	16	16	16	16	16	16
<b>P-1</b>											
Mean	14.167	3.540	0.005	3.794	2.002	1.067	0.072	3.723	0.075	69.900	0.372
StdDev	0.123	0.030	0.001	0.060	0.043	0.030	0.004	0.039	0.005	0.785	0.011
RelErr(%)	0.87	0.84	24.21	1.58	2.17	2.85	5.75	1.04	6.92	1.12	2.84
Number	15	15	15	15	15	15	15	15	15	15	15
<b>QGRM-100</b>											
Mean	14.840	2.170	0.022	3.798	4.932	0.966	0.040	4.016	0.146	67.100	0.473
StdDev	0.114	0.037	0.004	0.054	0.125	0.031	0.000	0.050	0.013	0.485	0.017
RelErr(%)	0.77	1.72	2.33	1.42	2.53	3.24	0.00	1.24	9.19	0.72	3.59
Number	5	5	5	5	5	5	5	5	5	5	5
<b>QGRM-101</b>											
Mean	15.825	8.283	0.005	15.025	1.020	5.743	0.185	3.003	0.188	48.500	1.948
StdDev	0.050	0.048	0.000	0.050	0.024	0.043	0.006	0.013	0.005	0.337	0.010
RelErr(%)	0.32	0.58	0.00	0.33	2.40	0.76	3.12	0.42	2.67	0.69	0.49
Number	4	4	4	4	4	4	4	4	4	4	4
<b>QUA-1</b>											
Mean	15.342	4.108	0.005	4.383	1.383	2.411	0.080	3.911	0.125	65.700	0.442
StdDev	0.138	0.035	0.000	0.066	0.021	0.024	0.000	0.056	0.005	0.395	0.006
RelErr(%)	0.90	0.84	0.00	1.51	1.55	0.99	0.00	1.42	4.18	0.60	1.25
Number	12	12	12	12	12	12	12	12	12	12	12
<b>WP-1</b>											
Mean	16.525	5.002	0.006	4.416	1.539	2.629	0.078	4.183	0.169	64.000	0.489
StdDev	0.142	0.061	0.004	0.099	0.032	0.034	0.004	0.072	0.003	0.346	0.006
RelErr(%)	0.86	1.21	69.28	2.24	2.10	1.30	4.97	1.79	1.71	0.54	1.24
Number	12	12	12	12	12	12	12	12	12	12	12

Internal standard	LOI %	Ba ppm	Rb ppm	Sr ppm	Nb ppm	Zr ppm	Y ppm	H <sub>2</sub> O(+) %	CO <sub>2</sub> % %	C(inorg) %	T.O.C. %
<b>ALB-1</b>											
Mean	3.127	268.9	21.8	771.4	4.9	73.9	25.9	1.579	1.565	0.225	0.950
StdDev	0.125	18.3	5.1	17.3	4.2	1.6	4.2	0.080	0.155	0.009	0.151
RelErr(%)	4.00	6.80	23.47	2.25	85.82	2.22	16.26	5.08	9.93	3.80	15.89
Number	15	15	15	15	15	15	15	14	14	14	14
<b>CHI-1</b>											
Mean	32.583	205.2	1	257.3	1.0	30.3	25.9	0.550	33.283	0.510	0.200
StdDev	0.098	16.9	0	2.7	0.0	1.2	0.8	0.105	0.098	0.006	0.000
RelErr(%)	0.30	8.26	0.00	1.03	0.00	3.99	5.00	19.07	0.30	1.24	0.00
Number	6	6	6	6	6	6	6	6	6	6	6
<b>CUL-1</b>											
Mean	7.584	681.3	6.7	251.8	1.8	53.3	21	4.194	3.991	2.008	4.864
StdDev	0.261	14.4	5.7	5.6	1.2	1.1	3.5	0.166	0.036	0.027	0.103
RelErr(%)	3.44	2.12	84.43	2.23	65.59	2.03	16.82	3.96	0.90	1.35	2.11
Number	18	18	18	18	18	18	18	18	18	18	11
<b>MBX-1</b>											
Mean	3.504	716.4	80.1	494	9.3	99.1	17.7	1.114	2.683	0.231	1.870
StdDev	0.209	14.6	5.3	15.5	1.0	1.5	3.5	0.066	0.468	0.009	0.048
RelErr(%)	5.97	2.04	6.57	3.14	10.81	1.54	19.55	5.95	17.43	3.97	2.58
Number	16	16	16	16	16	16	16	14	14	14	10
<b>P-1</b>											
Mean	0.393	684.4	42.3	230.1	4.0	130.1	21.3	0.520	0.023	0.006	1.962
StdDev	0.112	15.4	4.3	5.7	1.9	3.6	2.4	0.068	0.015	0.002	0.051
RelErr(%)	28.37	2.24	10.25	2.48	48.18	2.77	11.31	13.00	67.15	36.14	2.58
Number	15	15	15	15	15	15	15	15	15	15	13
<b>QGRM-100</b>											
Mean	1.024	896	122.4	442.8	16.0	413.6	49.0	0.600	0.598	0.118	1.720
StdDev	0.056	14.8	2.1	5.6	0.0	5.7	1.6	0.000	0.019	0.004	0.045
RelErr(%)	5.46	1.65	1.69	1.27	0.00	1.38	3.23	0.00	3.22	3.79	2.60
Number	5	5	5	5	5	5	5	5	5	5	5
<b>QGRM-101</b>											
Mean	0.085	205.8	19.5	250.5	7.3	156.8	30.8	0.533	0.417	0.177	10.800
StdDev	0.054	18.6	1.7	5.9	1.9	1.0	1.0	0.058	0.012	0.006	0.000
RelErr(%)	64.08	9.05	8.88	2.36	26.11	0.61	3.11	10.83	2.77	3.27	0.00
Number	4	4	4	4	4	4	4	3	3	3	3
<b>QUA-1</b>											
Mean	1.225	646.1	17.3	579	1.8	100	14.7	1.033	0.203	0.058	1.760
StdDev	0.087	10.8	2.5	5.6	1.0	1.0	2.1	0.065	0.021	0.011	0.052
RelErr(%)	7.07	1.67	14.62	0.97	55.16	1.00	14.04	6.30	10.34	19.11	2.93
Number	12	12	12	12	12	12	12	12	12	12	10
<b>WP-1</b>											
Mean	0.146	554.8	21.5	688.9	5.0	123.3	16.8	0.275	0.014	0.006	2.30
StdDev	0.086	11.3	6.1	18.2	3.5	1.2	3.9	0.045	0.018	0.002	0.043
RelErr(%)	59.31	2.04	28.36	2.65	70.84	0.94	23.19	16.45	127.55	36.18	1.85
Number	12	12	12	12	12	12	12	12	12	12	12

**Table A4.3. Analytical precision based on duplicate pulps of Chu Chua samples  
analyzed by X-Ray Laboratories Inc.**

SAMPLE	SiO <sub>2</sub> %	TiO <sub>2</sub> %	Al <sub>2</sub> O <sub>3</sub> %	Cr <sub>2</sub> O <sub>3</sub> %	Fe <sub>2</sub> O <sub>3</sub> %	MnO %	MgO %	CaO %	Na <sub>2</sub> O %	K <sub>2</sub> O %	P <sub>2</sub> O <sub>5</sub> %	LOI %
<b>Basalt</b>												
HS-95-2001	40.70	0.552	13.30	<0.01	11.60	0.18	6.10	8.01	3.00	0.60	0.16	2.95
HS-95-9001	41.10	0.547	13.40	<0.01	11.60	0.18	6.09	8.08	2.96	0.58	0.16	2.60
HS-95-2014	47.90	1.780	14.50	0.02	12.40	0.20	7.30	9.60	2.35	0.12	0.18	3.60
HS-95-9014	48.30	1.780	14.70	0.02	12.30	0.19	7.32	9.63	2.33	0.12	0.18	3.48
HS-95-2069	47.10	1.790	14.20	0.02	12.60	0.19	6.51	10.40	2.47	0.21	0.17	3.30
HS-95-9069	47.30	1.790	14.30	0.02	12.70	0.19	6.57	10.50	2.50	0.20	0.17	3.50
HS952056	54.50	1.530	13.60	0.01	9.94	0.17	5.40	7.79	3.42	0.13	0.19	3.35
HS959056	54.40	1.520	13.60	0.01	9.89	0.17	5.38	7.80	3.40	0.14	0.18	3.20
HS-99-2008	46.20	1.760	14.40	0.02	12.80	0.19	7.82	6.94	2.56	0.59	0.18	4.50
HS-95-9008	45.80	1.770	14.43	0.02	12.86	0.20	7.85	6.90	2.55	0.60	0.18	4.26
HS-95-2017	46.80	1.760	13.90	0.02	11.90	0.19	6.28	11.90	2.25	0.08	0.17	4.00
HS-95-9017	46.90	1.760	13.82	0.02	11.88	0.21	6.33	11.87	2.28	0.08	0.18	4.12
HS-95-2039	48.80	1.750	14.20	0.02	11.90	0.19	6.92	10.10	2.86	0.16	0.17	2.35
HS-95-9039	48.60	1.740	14.01	0.02	11.86	0.19	6.85	10.12	2.87	0.15	0.17	2.33
HS-95-2053	48.10	1.790	14.40	0.03	12.00	0.19	6.49	10.80	2.73	0.14	0.18	2.35
HS-95-9053	48.40	1.790	14.51	0.03	12.30	0.18	6.52	10.77	2.70	0.15	0.18	2.19
HS-95-2066	47.20	1.760	14.30	0.02	12.00	0.19	6.74	9.90	2.51	0.37	0.18	2.90
HS-95-9066	47.11	1.750	14.33	0.02	12.30	0.19	6.78	9.95	2.48	0.36	0.08	2.82
<b>Average</b>	<b>47.512</b>	<b>1.607</b>	<b>14.106</b>	<b>0.017</b>	<b>11.935</b>	<b>0.188</b>	<b>6.625</b>	<b>9.503</b>	<b>2.679</b>	<b>0.266</b>	<b>0.170</b>	<b>3.211</b>
<b>Error variance</b>	<b>0.038</b>	<b>0.00002</b>	<b>0.006</b>	<b>0.000</b>	<b>0.012</b>	<b>0.00004</b>	<b>0.0009</b>	<b>0.0012</b>	<b>0.0003</b>	<b>0.0001</b>	<b>0.0006</b>	<b>0.02</b>
<b>Precision (%)</b>	<b>0.82</b>	<b>0.60</b>	<b>1.14</b>	<b>0.00</b>	<b>1.80</b>	<b>6.62</b>	<b>0.88</b>	<b>0.74</b>	<b>1.39</b>	<b>5.61</b>	<b>28.01</b>	<b>8.09</b>
<b>Silicic rocks</b>												
HS952028	83.90	0.287	5.09	0.01	4.02	0.05	2.01	0.92	0.10	1.02	0.13	2.15
HS959028	83.70	0.309	5.10	0.01	4.04	0.06	2.02	0.92	0.12	1.01	0.13	2.15
HS952042	80.90	0.241	3.86	0.01	8.10	0.05	3.15	0.30	0.02	0.01	0.04	3.55
HS959042	81.20	0.251	3.84	0.01	8.08	0.06	3.14	0.31	0.03	0.01	0.04	3.20
HS-95-2028	83.60	0.309	5.10	<0.01	4.04	0.06	2.02	0.92	0.12	1.01	0.13	2.15
HS-95-9028	83.35	0.312	5.12	<0.01	4.03	0.05	2.02	0.91	0.11	0.99	0.14	2.02
HS-95-2045	85.20	0.323	5.71	<0.01	1.74	0.01	3.13	1.08	0.08	0.69	0.02	1.95
HS-95-9045	84.80	0.321	5.75	<0.01	1.77	0.01	3.09	1.09	0.09	0.67	0.02	2.05
<b>Average</b>	<b>83.331</b>	<b>0.294</b>	<b>4.946</b>	<b>0.000</b>	<b>4.478</b>	<b>0.044</b>	<b>2.573</b>	<b>0.806</b>	<b>0.084</b>	<b>0.806</b>	<b>0.081</b>	<b>2.403</b>
<b>Error variance</b>	<b>0.044</b>	<b>0.000</b>	<b>0.000</b>	<b>0.000</b>	<b>0.000</b>	<b>0.000</b>	<b>0.000</b>	<b>0.000</b>	<b>0.000</b>	<b>0.000</b>	<b>0.000</b>	<b>0.019</b>
<b>Precision (%)</b>	<b>0.50</b>	<b>5.87</b>	<b>0.71</b>	<b>0.00</b>	<b>0.67</b>	<b>27.99</b>	<b>1.17</b>	<b>1.52</b>	<b>22.34</b>	<b>1.52</b>	<b>8.70</b>	<b>11.38</b>

SAMPLE	Ba PPM	Rb PPM	Sr PPM	Nb PPM	Zr PPM	Y PPM	SAMPLE	H <sub>2</sub> O+ %	S %	CO <sub>2</sub> %	FEO %
<b>Basalt</b>											
HS-95-2001	32900	198	252	7	105	32	HS-95-2001		0.11		9.30
HS-95-9001	32700	199	252	7	106	31	HS-95-9001		0.11		9.20
HS-95-2014	390	-2	204	5	130	42	HS952056	1.50	1.32	1.54	
HS-95-9014	373	-2	204	5	129	41	HS959056	1.30	1.31	1.48	
HS-95-2069	45	-2	123	5	127	38	HS952028	1.00	0.14		
HS-95-9069	42	6	124	4	129	37	HS959028	0.90	0.15		
HS952056	877	1	153	6	139	38	HS952042	2.60	0.21	0.88	
HS959056	900	1	151	6	140	38	HS959042	2.70	0.21	0.87	
HS-99-2008	14000	2	130	4	128	39	HS-95-2025	1.30	1.31	1.48	2.60
HS-95-9008	13900	2	132	4	127	38	HS-95-9025	1.50	1.32	1.54	2.50
HS-95-2017	745	-2	127	4	124	39	HS-95-2037	4.20	0.13	5.68	9.30
HS-95-9017	755	-2	128	4	126	39	HS-95-9037	4.20	0.14	5.71	9.20
HS-95-2039	1270	2	219	9	133	41	HS-95-2047	2.50	0.17	0.10	7.70
HS-95-9039	1255	2	221	10	130	40	HS-95-9047	2.40	0.17	0.10	7.50
HS-95-2053	36	2	143	15	128	42	HS-95-2059	3.50	0.65	0.28	8.00
HS-95-9053	33	2	145	16	129	43	HS-95-9059	3.60	0.64	0.29	7.90
HS-95-2066	4320	-2	224	5	130	41	HS-95-2071	0.60	0.01	0.01	1.90
HS-95-9066	4335	-2	222	5	128	40	HS-95-9071	0.60	0.01	0.01	2.00
<b>Average</b>	<b>6048.7</b>	<b>22.4</b>	<b>175.2</b>	<b>6.7</b>	<b>127.1</b>	<b>38.8</b>	<b>Average</b>	<b>2.15</b>	<b>0.451</b>	<b>1.426</b>	<b>6.43</b>
<b>Error varianc</b>	<b>2854.8</b>	<b>3.611</b>	<b>1.222</b>	<b>0.167</b>	<b>1.444</b>	<b>0.389</b>	<b>Error varianc</b>	<b>0.00</b>	<b>0.000</b>	<b>0.000</b>	<b>0.006</b>
<b>Precision (%)</b>	<b>1.77</b>	<b>16.98</b>	<b>1.26</b>	<b>12.15</b>	<b>1.89</b>	<b>3.21</b>	<b>Precision (%)</b>	<b>3.29</b>	<b>1.48</b>	<b>1.18</b>	<b>2.38</b>
<b>Silicic rocks</b>											
HS952028	4300	30	58	3	89	22					
HS959028	4280	30	59	4	88	22					
HS952042	29	1	36	4	79	17					
HS959042	26	1	35	3	78	15					
HS-95-2028	4280	30	59	4	88	22					
HS-95-9028	4255	30	60	4	89	23					
HS-95-2045	2440	21	50	7	101	24					
HS-95-9045	2445	21	51	6	101	22					
<b>Average</b>	<b>2756.9</b>	<b>20.5</b>	<b>51.0</b>	<b>4.4</b>	<b>89.1</b>	<b>20.9</b>					
<b>Error varianc</b>	<b>132.375</b>	<b>0.000</b>	<b>0.500</b>	<b>0.375</b>	<b>0.375</b>	<b>1.125</b>					
<b>Precision (%)</b>	<b>0.83</b>	<b>0.00</b>	<b>2.77</b>	<b>27.99</b>	<b>1.37</b>	<b>10.16</b>					

## **Appendix 5**

### **Samples and analytical data from the areas of the Konuto Lake, Birch Lake, Flexar and Coronation deposits**

The Konuto Lake, Birch Lake, Flexar and Coronation deposits data set (Table 1 through Table 3) consists of 227 original samples of drill core and outcropping rocks. A total of 29 drillholes were sampled in 1996 and a mapping program yielded an additional 32 samples of various lithologies. The original samples represent the lithologies hosting the ore bodies at distance of up to 500m. The presumed footwall was sampled more heavily, which was facilitated by the drilling pattern on the NER and HOF claims (Konuto Lake deposit) and the B and FX (Birch Lake and Flexar deposits) drilling programs.

The samples were analyzed at XRAL (X-Ray Analytical Laboratories) in Don Mills, Ontario. The set of analyses and analytical techniques are identical to those applied on samples from the Chu Chua VHMS showing (Chapter 3) and described in Appendix 3.

The lithology of the samples is listed as described in the field. No corrections are introduced following thin section study and the acquisition of the analytical data.

The samples supplied by HBED and used in the lithogeochemical investigation are not included in this appendix, due to their large number (over 800).

Table A5.1. Sample location and identification

Sample#	Lithology	Drill hole/ location	Depth (DH) (m)	Northing (UTM)	Easting (UTM)	Depth (vert) (m)
HOF2-119	Basalt	HOF-2	119	6060222	689446	84
HOF2-15	Basalt	HOF-2	15	6060223	689519	11
HOF2-156	Basalt	HOF-2	156	6060221	689420	110
HOF-2-173	Basalt	HOF-2	173	6060221	689408	122
HOF2-197	Basalt	HOF-2	197	6060221	689391	139
HOF2-214	Basalt	HOF-2	214	6060221	689379	151
HOF-2-290	Diorite	HOF-2	290	6060220	689325	205
HOF-2-32	Basalt	HOF-2	32	6060223	689507	23
HOF-2-33	Basalt	HOF-2	33	6060223	689507	23
HOF2-40	Basalt	HOF-2	40	6060223	689502	28
HOF2-68	Basalt	HOF-2	68	6060223	689482	48
HOF-5-127	Basalt	HOF-5	127	6060155	689537	91
HOF-5-130	Basalt	HOF-5	130	6060155	689535	94
HOF-5-131	Basalt	HOF-5	131	6060155	689534	94
HOF-5-154	Basalt	HOF-5	154	6060155	689518	111
HOF-5-156	Basalt	HOF-5	156	6060155	689517	112
HOF-5-196	Basalt	HOF-5	196	6060155	689489	141
HOF-5-224	Basalt	HOF-5	224	6060154	689469	161
HOF-5-268	Basalt	HOF-5	268	6060154	689439	193
HOF-5-272	Diorite	HOF-5	272	6060154	689436	196
HOF-5-297	Basalt	HOF-5	297	6060154	689418	214
HOF-5-320	Basalt	HOF-5	320	6060153	689403	230
HOF-5-348	Diorite	HOF-5	348	6060153	689383	250
HOF-5-353	Diorite	HOF-5	353	6060153	689380	254
HOF-5-58	Basalt	HOF-5	58	6060156	689585	42
HOF-5-64	Quartz porphyry	HOF-5	64	6060156	689578	47
HOF-5-67	Basalt	HOF-5	67	6060156	689578	48
HOF-5-67.7	Basalt	HOF-5	68	6060156	689578	49
HOF-5-67.9	Basalt	HOF-5	68	6060156	689578	49
HOF-5-68	Basalt	HOF-5	68	6060156	689578	49
HOF-5-71	Basalt	HOF-5	71	6060156	689576	51
HOF-5-75	Basalt, amygdaloidal	HOF-5	75	6060156	689573	54
HOF-5-87	Basalt	HOF-5	87	6060156	689564	63
NER-102-104	Basalt	NER-102	104	6060961	689712	34
NER-102-204	Basalt, amygdaloidal	NER-102	204	6060974	689667	111
NER-102-303	Basalt, amygdaloidal	NER-102	303	6060986	689617	187
NER-102-450	Basalt	NER-102	450	6061006	689537	295
NER-102-543	Basalt	NER-102	543	6061019	689483	362
NER-105-224	Basalt, amygdaloidal	NER-105	224	6060833	689718	193
NER-105-305	Basalt chloritized	NER-105	305	6060838	689676	261
NER-105-390	Basalt, amygdaloidal	NER-105	390	6060845	689632	332
NER-105-481	Basalt, amygdaloidal	NER-105	481	6060854	689584	407
NER-105-542	Basalt, amygdaloidal	NER-105	542	6060860	689552	457
NER-105-637	Basalt, silicified	NER-105	637	6060868	689500	533
NER-105-724	Basalt	NER-105	724	6060872	689453	604
NER-105-76	Basalt, amygdaloidal	NER-105	76	6060823	689793	66
NER-107-1002	Basalt, silicified	NER-107	1002	6060973	689358	856
NER-107-122	Basalt	NER-107	122	6060917	689806	106
NER-107-246	Basalt amygdaloidal	NER-107	246	6060923	689745	214
NER-107-427	Basalt	NER-107	427	6060932	689654	369

Sample#	Lithology	Drill hole/ location	Depth (DH) (m)	Northing (UTM)	Easting (UTM)	Depth (vert) (m)
NER-107-50	Basalt	NER-107	50	6060914	689841	44
NER-107-624	Basalt	NER-107	624	6060946	689555	537
NER-107-722	Basalt	NER-107	722	6060953	689504	619
NER-107-823	Basalt	NER-107	823	6060960	689452	704
NER-107W1-43	Basalt	NER-107W1	436	6060922	689646	361
NER-107W1-55	Basalt	NER-107W1	550	6060919	689578	442
NER-107W1-64	Basalt	NER-107W1	646	6060924	689520	511
NER-107W1-76	Basalt, amygdaloidal	NER-107W1	764	6060936	689448	594
NER-111-157	Basalt	NER-111	157	6061033	689454	129
NER-111-175	Gabbro	NER-111	175	6061037	689445	143
NER-111-198	Basalt	NER-111	198	6061041	689432	162
NER-111-212	Gabbro	NER-111	212	6061044	689425	174
NER-111-228	Gabbro	NER-111	228	6061047	689416	187
NER-111-238	Basalt	NER-111	238	6061049	689411	195
NER-116-389	Basalt	NER-116	389	6061035	689345	290
NER-116-493	Gabbro	NER-116	493	6061076	689280	368
NER-122-135	Rhyolite	NER-122	135	6060931	689329	xxx
NER-122-141	Gabbro	NER-122	141	6060933	689236	xxx
NER-122-150	Basalt	NER-122	150	6060934	689231	xxx
NER-122-173	Gabbro	NER-122	173	6060939	689218	xxx
NER-69-19	Basalt	NER-69	19	6061045	689495	13
NER-69-46	Basalt	NER-69	46	6061051	689477	33
NER-69-92	Basalt	NER-69	92	6061062	689447	65
NER-71-176	Basalt	NER-71	176	6061067	689435	124
NER-71-31	Basalt	NER-71	31	6061032	689532	22
NER-71-62	Basalt	NER-71	62	6061039	689511	44
NER-71-95	Basalt	NER-71	95	6061047	689489	67
NER-73-109	Basalt, QEC-veined	NER-73	109	6060973	689401	77
NER-73-28	Basalt, QEC-veined	NER-73	28	6060953	689455	20
NER-73-74	Basalt, QEC-veined	NER-73	74	6060964	689425	52
NER-75-130	Basalt, QEC-veined	NER-75	130	6060948	689469	106
NER-75-181	Basalt, QEC-veined	NER-75	181	6060958	689442	148
NER-75-38	Basalt	NER-75	38	6060930	689519	31
NER-75-77	Basalt	NER-75	77	6060937	689498	63
NER-78-125	Basalt	NER-78	125	6060936	689502	91
NER-78-129	Basalt, chloritized	NER-78	129	6060937	689499	94
NER-78-168	Basalt, QEC-veined	NER-78	168	6060946	689474	123
NER-78-212	Basalt, QEC-veined	NER-78	212	6060956	689446	155
NER-78-279	Basalt, silicified	NER-78	279	6060972	689403	204
NER-78-95	Basalt, QEC-veined	NER-78	95	6060929	689521	69
NER-80-150	Basalt	NER-80	150	6061041	689506	110
NER-80-201	Basalt	NER-80	201	6061053	689473	147
NER-80-21	Basalt	NER-80	21	6061011	689588	15
NER-80-253	Basalt	NER-80	253	6061065	689440	185
NER-80-75	Basalt, amygdaloidal	NER-80	75	6061023	689554	55
NER-82-122	Basalt	NER-82	122	6061152	689494	111
NER-82-146	Basalt, chloritized	NER-82	146	6061155	689484	132
NER-82-168	Basalt	NER-82	168	6061158	689475	152
NER-82-50	Basalt	NER-82	50	6061141	689522	45

Sample#	Lithology	Drill hole/ location	Depth (DH) (m)	Northing (UTM)	Easting (UTM)	Depth (vert) (m)
NER-84-301	Basalt, QEC-veined	NER-84	301	6060948	689468	240
NER-84-178	Basalt	NER-84	178	6060923	689538	142
NER-84-260	Basalt, QEC-veined	NER-84	260	6060940	689491	208
NER-84-335	Basalt	NER-84	335	6060955	689449	268
NER-84-397	Basalt, QEC-veined	NER-84	397	6060968	689414	317
NER-84-5	Basalt	NER-84	5	6060887	689635	4
NER-84-98	Basalt	NER-84	98	6060907	689583	78
NER-86-143	Basalt, amygdaloidal	NER-86	143	6060800	689583	105
NER-86-168	Basalt, amygdaloidal	NER-86	168	6060806	689567	123
NER-86-21	Basalt	NER-86	21	6060772	689661	15
NER-86-214	Basalt	NER-86	214	6060817	689537	157
NER-86-250	Basalt	NER-86	250	6060825	689514	183
NER-86-326	Basalt	NER-86	326	6060843	689466	238
NER-86-40	Basalt	NER-86	40	6060776	689649	29
NER-86-468	Basalt	NER-86	468	6060876	689375	342
NER-86-62	Basalt	NER-86	62	6060781	689635	45
NER-98-100	Basalt	NER-98	100	6060868	689690	80
NER-98-202	Basalt, QEC-veined	NER-98	202	6060889	689632	161
NER-98-300	Basalt, QEC-veined	NER-98	300	6060909	689577	240
NER-98-451	Basalt, QEC-veined	NER-98	451	6060940	689491	360
NER-98-548	Basalt, QEC-veined	NER-98	548	6060960	689436	438
NER-99-489	Basalt, amygdaloidal	NER-99	489	6061001	689532	373
NER-99-532	Basalt	NER-99	532	6061008	689504	405
NER-99-602	Basalt	NER-99	602	6061019	689459	455
NER-99-704	Basalt	NER-99	704	6061034	689393	527
HS95M123A	Quartz porphyry	Map	0	6059489	689969	0
HS95M123AA	Quartz porphyry	Map	0	6059489	689969	0
HS95M157	Quartz porphyry	Map	0	6060192	689206	0
HS95M161-1	Basalt	Map	0	6060830	689329	0
HS95M161-2	Basalt	Map	0	6060843	689306	0
HS95M240-1	Gabbro	Map	0	6061486	690267	0
HS95M260	Gabbro	Map	0	6060476	690281	0
HS95M285	Basalt/microgabbro	Map	0	6062219	689457	0
HS95M286	Gabbro/diorite	Map	0	6062195	690562	0
HS95M291-2	Quartz-Chlorite schist	Map	0	6062367	690648	0
HS95M292	Gabbro	Map	0	6062305	690705	0
HS95M293	Gabbro	Map	0	6062514	690871	0
HS95M294	Altered gabbro	Map	0	6062590	691176	0
HS95M295	Gabbro/diorite	Map	0	6061371	689243	0
HS95M315-1	Basalt	Map	0	6060542	690980	0
HS95M315-2	Rhyolite	Map	0	6060542	690980	0
HS95M326	Gabbro	Map	0	6060671	690938	0
HS95M69-1	Gabbro	Map	0	6059962	689343	0
HS96M170	Mafic tuff	Map	0	6061125	689306	0
HS96M298	Gabbro	Map	0	6061662	689481	0
HS96M308-1	Basalt	Map	0	6061354	689397	0
HS96M309	Gabbro/diorite	Map	0	6062176	689924	0
HS96M315-3	Gabbro	Map	0	6060562	691010	0
HS96M320	Gabbro	Map	0	6060432	690629	0
HS96M322	Gabbro	Map	0	6060595	690511	0
HS96M323	Gabbro	Map	0	6060676	690495	0



Sample#	Lithology	Drill hole/ location	Depth (DH) (m)	Northing (UTM)	Easting (UTM)	Depth (vert) (m)
HS96M75-3	Basalt	Map	0	6059788	689824	0
HS96M328	Gabbro	Map	0	6062576	690471	0
HS96M67	Gabbro	Map	0	6059638	689495	0
HS96M75-1	Basalt	Map	0	6059755	689829	0
HS96M75-2	Basalt, amygdaloidal	Map	0	6059758	689824	0
HS96M76	Quartz porphyry	Map	0	6059882	689848	0
B-87-116	lapilli tuff	B-87	35	6060916	691237	27
B-87-154	Diorite	B-87	47	6060914	691245	36
B-87-176	Basalt, amygdaloidal	B-87	54	6060912	691249	41
B-87-220	Andesite tuff	B-87	67	6060910	691257	51
B-87-259	Altered rock	B-87	79	6060908	691260	60
B-87-302	Andesite flow	B-87	92	6060905	691272	70
B-87-37	Andesite flow	B-87	11	6060921	691223	8
B-87-381	Diorite	B-87	116	6060900	691287	89
B-87-435	Andesite lapilli tuff	B-87	133	6060897	691297	102
B-87-489	Diorite	B-87	149	6060893	691307	114
B-87-57	Andesite lapilli tuff	B-87	17	6060920	691226	13
B-87-621	Basalt, amygdaloidal	B-87	189	6060885	691332	145
B-87-649	Andesite lapilli tuff	B-87	198	6060884	691337	152
B-87-680	Rhyolite tuff	B-87	207	6060883	691342	158
B-87-746	Andesite flow	B-87	228	6060882	691351	175
B-88-1038	Basalt flow	B-88	317	6060880	691380	223
B-88-1296	Basalt flow	B-88	395	6060900	691177	382
B-88-1497	Mafic tuff	B-88	456	6060896	691192	440
B-88-1773	Basalt flow	B-88	540	6060892	691213	522
B-88-2044	Basalt flow	B-88	623	6060888	691233	600
B-88-2145	Felsic tuff	B-88	654	6060885	691242	632
B-88-297	Basalt flow	B-88	91	6060918	691100	88
B-88-653	Basalt flow	B-88	230	6060911	691128	303
B-88-847	Basalt flow	B-88	258	6060908	691142	249
B-89-1000	Basalt flow	B-89	305	6061197	691138	298
B-89-1125	Mafic tuff/flow	B-89	343	6061187	691161	336
B-89-1242	Basalt, amygdaloidal	B-89	379	6061182	691170	371
B-89-1424	Basalt, chloritized	B-89	434	6061168	691188	425
B-89-1814	Basalt, amygdaloidal	B-89	553	6061139	691235	541
B-89-1958	Gabbro-diorite	B-89	597	6061120	691250	584
FX-30-144	Andesite tuff	FX-30	144	6062629	691446	
FX-34-W1-1048	Gabbro-diorite	FX-34-W1	1048	6063747	691448	
FX-34-W1-1176	Gabbro-diorite	FX-34-W1	1176	6063753	691428	
FX-34-W1-812	Basalt	FX-34-W1	812	6063735	691485	
FX-34-W1-872	Basalt flow	FX-34-W1	872	6063738	691475	
FX-35-147	Basalt flow	FX-35	147	6063671	691561	
FX-35-304	Mafic tuff	FX-35	304	6063671	691550	
FX-35-420	Basalt	FX-35	420	6063672	691540	

Sample#	Lithology	Drill hole/ location	Depth (DH) (m)	Northing (UTM)	Easting (UTM)	Depth (vert) (m)
FX-36-931	Mafic tuff	FX-36	931	6062650	691277	
CN-90-1-1061	Basalt	CN-90-1	1061			
FX-35-456	Basalt, pillowed	FX-35	456	6063673	691536	
FX-35-61	Gabbro-diorite	FX-35	61	6063672	691566	
FX-36-129	Andesite tuff	FX-36	129	6062668	691458	
FX-36-313	Basalt flow	FX-36	313	6062664	691419	
FX-36-486	Mafic dike	FX-36	486	6062659	691374	
FX-36-560	Mafic tuff	FX-36	560	6062659	691358	
FX-36-694	Mafic tuff	FX-36	694	6062656	691330	
CN-90-1-1128	Basalt, amygdaloidal	CN-90-1	1128			
CN-90-1-270	Diorite dike	CN-90-1	270			
CN-90-1-457	Metabasalt, Ant-bearing	CN-90-1	457			
CN-90-1-692	Biotite gneiss	CN-90-1	692			
CN-90-1-701	Tr-Ant-gneiss	CN-90-1	701			
CN-90-1-715	Gt-Bi-Tr-gneiss	CN-90-1	715			
CN-90-1-761	Basalt	CN-90-1	761			
CN-90-1-843	Basalt, amygdaloidal	CN-90-1	841			
CN-90-1-964	Basalt	CN-90-1	964			
CN-90-2-163	Basalt	CN-90-2	163			
CN-90-2-281	Basalt, veined	CN-90-2	281			
CN-90-2-291	Metabasalt, Tr-bearing	CN-90-2	291			
CN-90-2-444	Basalt	CN-90-2	444			
CN-90-2-523	Metabasalt, Tr-bearing	CN-90-2	523			
CN-90-2-650	Basalt	CN-90-2	650			
CN-90-2-722	Basalt	CN-90-2	722			
CN-90-2-848	Basalt	CN-90-2	848			
CN-90-2-880	MaficBasalt	CN-90-2	880			
CN-90-3-178	Basalt	CN-90-3	178			
CN-90-3-225	Basalt	CN-90-3	225			
CN-90-3-437	Basalt, amygdaloidal	CN-90-3	437			
CN-90-3-514	Metabasalt, Ant-bearing	CN-90-3	514			
CN-90-3-633	Basalt, amygdaloidal	CN-90-3	633			
CN-90-3-725	Basalt	CN-90-3	725			

Table A5.2. Major element concentrations

Sample#	SiO <sub>2</sub> (%)	Al <sub>2</sub> O <sub>3</sub> (%)	TiO <sub>2</sub> (%)	Fe(tot) (%)	Cr <sub>2</sub> O <sub>3</sub> (%)	MnO (%)	MgO (%)	CaO (%)	Na <sub>2</sub> O (%)	K <sub>2</sub> O (%)	P <sub>2</sub> O <sub>5</sub> (%)
HOF2-119	52.80	13.90	0.24	10.90	0.01	0.17	7.37	7.33	3.61	0.22	0.03
HOF2-15	56.40	13.20	0.43	13.30	0.01	0.12	4.18	2.28	3.12	1.67	0.06
HOF2-156	52.00	13.30	0.49	17.30	0.01	0.33	4.43	6.13	2.08	0.26	0.04
HOF-2-173	49.30	14.60	0.09	7.47	0.04	0.14	10.30	11.60	1.45	0.83	0.01
HOF2-197	63.20	11.70	0.42	11.50	0.01	0.13	2.03	4.65	2.83	0.07	0.08
HOF2-214	52.70	13.90	0.42	15.20	0.01	0.24	5.56	5.42	3.14	0.20	0.04
HOF-2-290	49.10	15.20	0.12	9.40	0.01	0.16	6.67	10.30	2.69	0.86	0.02
HOF-2-32	51.10	13.30	0.35	13.60	0.01	0.16	4.56	4.52	3.67	1.12	0.04
HOF-2-33	52.60	14.40	0.28	11.50	0.01	0.18	6.76	7.99	3.09	1.24	0.02
HOF2-40	53.80	13.80	0.44	14.00	0.01	0.21	5.96	4.95	3.00	0.27	0.06
HOF2-68	51.60	14.90	0.24	11.90	0.01	0.19	7.23	6.62	3.53	0.26	0.03
HOF-5-127	49.20	14.40	0.35	14.10	0.01	0.17	9.13	6.17	2.64	0.10	0.04
HOF-5-130	54.80	14.30	0.43	15.30	0.01	0.16	6.00	3.21	3.01	0.12	0.05
HOF-5-131	52.40	13.90	0.14	9.81	0.04	0.17	8.27	8.70	3.24	0.34	0.01
HOF-5-154	54.50	14.10	0.38	14.70	0.01	0.20	5.41	5.58	3.52	0.12	0.04
HOF-5-156	51.10	13.80	0.28	10.60	0.04	0.18	8.63	9.07	2.89	0.37	0.02
HOF-5-196	51.30	13.90	0.23	12.20	0.01	0.22	6.84	8.06	3.65	0.42	0.02
HOF-5-224	52.60	14.00	0.50	15.20	0.01	0.24	5.54	3.91	4.50	0.12	0.06
HOF-5-268	51.90	13.40	0.40	16.00	0.01	0.23	4.28	4.69	2.97	0.09	0.04
HOF-5-272	49.30	14.10	0.33	19.60	<0.01	0.24	5.49	4.15	1.74	0.06	0.03
HOF-5-297	46.40	14.90	0.38	17.60	<0.01	0.33	6.52	6.80	2.79	0.07	0.03
HOF-5-320	42.00	14.10	0.08	8.24	0.02	0.13	9.88	11.10	1.01	0.59	0.01
HOF-5-348	44.00	15.10	0.18	9.81	0.01	0.16	10.00	7.35	2.20	0.51	0.01
HOF-5-353	48.60	15.40	0.20	10.80	0.01	0.18	8.63	10.20	2.04	0.37	0.01
HOF-5-58	50.40	15.70	0.56	13.20	0.01	0.15	6.68	5.05	4.12	0.32	0.07
HOF-5-64	65.10	16.30	0.36	3.90	0.03	0.05	1.56	4.24	5.38	0.87	0.10
HOF-5-67	55.00	14.40	0.52	12.90	0.01	0.15	5.08	4.64	4.20	0.34	0.07
HOF-5-67.7	51.10	15.30	0.51	12.90	0.03	0.16	5.83	4.87	4.04	0.32	0.06
HOF-5-67.9	53.00	12.70	0.15	10.40	0.06	0.18	7.90	9.34	2.94	0.38	0.01
HOF-5-68	50.70	14.50	0.19	10.10	0.04	0.18	8.38	9.37	2.62	0.80	0.02
HOF-5-71	57.30	13.40	0.36	13.60	0.01	0.19	3.55	6.46	3.37	0.22	0.04
HOF-5-75	51.20	14.40	0.37	13.70	0.01	0.19	6.91	6.34	3.56	0.25	0.05
HOF-5-87	51.20	13.90	0.45	12.70	0.01	0.20	6.78	6.32	3.96	0.22	0.05
NER-102-104	53.10	13.10	0.54	14.70	0.01	0.20	5.46	8.02	2.88	0.15	0.04
NER-102-204	54.60	13.60	0.32	13.40	0.01	0.20	4.39	8.58	2.24	0.26	0.04
NER-102-303	58.60	13.30	0.48	13.10	0.01	0.19	2.62	5.64	3.47	0.33	0.05
NER-102-450	54.20	14.50	0.61	12.90	0.01	0.16	3.60	7.35	3.03	0.43	0.07
NER-102-543	52.60	13.30	0.31	10.70	0.03	0.18	6.92	9.02	3.13	1.09	0.03
NER-105-224	52.80	14.50	0.28	12.70	0.01	0.21	5.57	8.15	2.46	0.16	0.03
NER-105-305	48.80	12.70	0.26	12.00	0.01	0.18	5.12	7.21	3.34	0.09	0.02
NER-105-390	52.00	14.50	0.19	11.50	0.01	0.19	6.44	9.00	3.21	0.10	0.02
NER-105-481	54.00	13.40	0.43	15.10	0.01	0.22	3.70	6.63	3.45	0.20	0.04
NER-105-542	45.40	12.30	0.32	11.20	0.01	0.18	5.47	10.40	2.00	0.68	0.03
NER-105-637	54.60	11.70	0.40	18.00	0.01	0.27	3.79	5.45	1.99	0.12	0.05
NER-105-724	63.30	12.00	0.43	10.10	0.01	0.17	2.50	4.61	3.26	0.10	0.08
NER-105-76	52.10	12.80	0.72	17.10	0.01	0.23	3.90	7.19	3.19	0.12	0.06
NER-107-1002	46.60	13.90	1.43	13.80	0.01	0.20	7.45	9.61	2.40	0.19	0.12
NER-107-122	54.80	13.30	0.44	15.10	0.01	0.22	3.73	5.81	3.23	0.30	0.04
NER-107-246	49.30	13.10	0.67	16.70	0.01	0.22	5.16	7.67	3.07	0.12	0.05
NER-107-427	46.60	14.90	0.47	16.50	0.01	0.26	4.78	6.77	2.57	0.13	0.04

Sample#	SiO <sub>2</sub> (%)	Al <sub>2</sub> O <sub>3</sub> (%)	TiO <sub>2</sub> (%)	Fe(tot) (%)	Cr <sub>2</sub> O <sub>3</sub> (%)	MnO (%)	MgO (%)	CaO (%)	Na <sub>2</sub> O (%)	K <sub>2</sub> O (%)	P <sub>2</sub> O <sub>5</sub> (%)
NER-107-50	52.20	13.80	0.51	14.50	0.01	0.22	4.98	7.65	3.01	0.19	0.04
NER-107-624	51.40	13.60	0.54	15.60	0.01	0.22	4.23	7.80	2.53	0.14	0.04
NER-107-722	51.90	13.90	0.38	15.00	0.01	0.23	5.22	7.37	3.50	0.48	0.03
NER-107-823	52.10	14.70	0.32	13.20	0.01	0.19	5.51	6.37	3.55	0.55	0.03
NER-107W1-43	50.50	14.50	0.29	14.20	0.01	0.20	6.23	6.88	3.52	0.13	0.03
NER-107W1-55	52.60	14.30	0.29	12.20	0.01	0.20	6.38	8.05	3.46	0.43	0.02
NER-107W1-64	51.30	14.40	0.39	14.40	0.01	0.22	4.88	8.63	1.93	0.44	0.03
NER-107W1-76	57.10	12.50	0.44	13.90	0.01	0.21	3.12	6.47	3.08	0.46	0.05
NER-111-157	56.20	13.60	0.67	14.10	0.01	0.20	3.08	6.10	2.88	0.32	0.07
NER-111-175	48.10	13.80	0.39	12.90	0.01	0.19	4.79	8.05	3.17	0.68	0.04
NER-111-198	53.10	13.60	0.44	13.20	0.01	0.17	5.63	6.72	2.65	0.35	0.05
NER-111-212	52.10	14.20	0.44	13.50	0.01	0.22	5.40	7.30	2.92	0.76	0.04
NER-111-228	52.10	13.70	0.24	12.20	0.01	0.19	7.00	7.47	3.11	1.05	0.02
NER-111-238	53.20	13.90	0.25	12.40	0.01	0.19	6.58	7.48	3.33	1.27	0.02
NER-116-389	52.90	13.30	0.61	14.20	0.01	0.19	4.69	8.11	2.60	0.82	0.05
NER-116-493	51.00	15.00	0.89	9.44	0.03	0.15	6.32	9.12	4.24	0.47	0.32
NER-122-135	60.30	16.10	0.68	5.36	<0.01	0.06	2.91	5.16	4.48	0.50	0.23
NER-122-141	64.50	13.90	0.42	8.61	<0.01	0.05	2.95	2.63	3.51	0.76	0.11
NER-122-150	47.10	13.50	1.94	14.70	<0.01	0.21	6.72	10.80	0.95	0.14	0.16
NER-122-173	48.90	12.80	0.57	7.14	0.04	0.11	7.14	7.14	2.97	1.44	0.07
NER-69-19	51.90	14.10	0.30	12.20	0.01	0.18	6.16	7.82	3.09	0.51	0.03
NER-69-46	51.80	13.70	0.41	15.40	0.01	0.21	4.05	5.55	4.05	0.46	0.04
NER-69-92	51.50	12.90	0.55	14.70	0.01	0.24	5.50	7.43	2.95	0.54	0.04
NER-71-176	52.90	13.20	0.33	14.80	0.01	0.20	4.27	7.67	2.95	0.63	0.03
NER-71-31	55.60	13.20	0.40	15.90	0.01	0.22	2.91	5.87	3.06	0.42	0.05
NER-71-62	61.50	13.20	0.45	11.00	0.01	0.16	2.24	4.69	3.50	0.35	0.07
NER-71-95	53.20	13.90	0.46	14.70	0.01	0.21	5.20	6.32	3.21	0.24	0.04
NER-73-109	55.40	14.10	0.23	11.30	0.01	0.17	5.54	5.86	3.81	0.85	0.04
NER-73-28	54.50	14.20	0.47	11.20	0.01	0.16	3.83	6.76	2.60	0.17	0.06
NER-73-74	53.10	13.70	0.28	12.40	0.01	0.19	5.52	7.02	3.18	0.69	0.03
NER-75-130	59.40	12.40	0.20	8.96	0.01	0.13	4.22	7.19	2.77	0.66	0.05
NER-75-181	55.30	13.40	0.33	14.50	0.01	0.22	3.50	5.91	3.87	0.40	0.03
NER-75-38	54.50	13.60	0.45	14.00	0.01	0.21	4.35	7.34	2.65	0.40	0.05
NER-75-77	53.20	13.60	0.42	14.50	0.01	0.13	6.53	4.93	2.96	0.11	0.04
NER-78-125	51.40	11.90	0.41	13.70	0.01	0.16	4.14	5.64	1.19	1.72	0.05
NER-78-129	51.10	13.20	0.34	14.80	0.01	0.18	7.35	3.53	2.12	0.13	0.04
NER-78-168	53.00	14.00	0.27	14.00	0.01	0.25	4.65	6.60	3.79	0.40	0.03
NER-78-212	55.50	11.90	0.24	11.10	0.01	0.16	3.87	8.27	2.81	0.37	0.03
NER-78-279	53.70	13.90	0.38	13.60	0.01	0.23	4.88	6.48	3.61	0.62	0.04
NER-78-95	53.00	13.00	0.48	13.60	0.01	0.17	3.73	7.12	2.58	0.25	0.05
NER-80-150	54.10	13.90	0.41	13.90	0.01	0.17	4.46	7.38	3.31	0.17	0.04
NER-80-201	50.20	14.40	0.62	15.60	0.01	0.22	4.67	7.72	2.75	0.23	0.05
NER-80-21	55.00	13.30	0.52	15.30	0.01	0.20	3.61	4.51	3.26	0.25	0.07
NER-80-253	49.40	13.20	0.66	15.70	0.01	0.25	5.69	8.37	2.71	0.46	0.05
NER-80-75	60.20	12.80	0.45	12.90	0.01	0.19	1.86	5.53	3.20	0.28	0.07
NER-82-122	51.30	14.50	0.25	10.50	0.01	0.18	6.76	9.04	3.21	0.86	0.02
NER-82-146	48.80	13.10	0.41	13.70	0.01	0.21	4.51	8.03	2.13	0.75	0.04
NER-82-168	51.00	14.70	0.37	15.80	0.01	0.21	5.20	5.72	3.81	0.20	0.03
NER-82-50	57.70	13.40	0.44	15.40	0.01	0.19	1.28	6.23	3.00	0.39	0.08

Sample#	SiO <sub>2</sub> (%)	Al <sub>2</sub> O <sub>3</sub> (%)	TiO <sub>2</sub> (%)	Fe(tot) (%)	Cr <sub>2</sub> O <sub>3</sub> (%)	MnO (%)	MgO (%)	CaO (%)	Na <sub>2</sub> O (%)	K <sub>2</sub> O (%)	P <sub>2</sub> O <sub>5</sub> (%)
NER-84-301	52.00	14.20	0.26	12.30	0.01	0.17	6.45	7.95	2.80	0.82	0.02
NER-84-178	55.10	13.30	0.43	14.90	0.01	0.22	3.56	5.89	3.22	0.24	0.04
NER-84-260	53.40	11.50	0.49	15.20	0.01	0.16	2.47	10.10	1.05	0.07	0.06
NER-84-335	50.70	14.20	0.56	14.80	0.01	0.23	5.60	7.49	3.27	0.30	0.05
NER-84-397	53.40	13.60	0.28	13.00	0.01	0.20	4.40	6.87	3.80	0.45	0.03
NER-84-5	49.20	12.80	0.61	15.20	0.01	0.24	6.31	8.23	2.51	0.55	0.05
NER-84-98	60.10	13.20	0.51	12.40	0.01	0.18	2.48	5.61	3.58	0.25	0.06
NER-86-143	56.70	13.00	0.50	15.00	0.01	0.22	2.27	5.91	3.20	0.23	0.06
NER-86-168	63.50	11.90	0.41	11.70	0.01	0.18	0.83	4.81	3.62	0.30	0.07
NER-86-21	49.30	14.30	0.66	16.90	0.01	0.23	5.46	5.88	3.32	0.51	0.05
NER-86-214	53.10	13.80	0.38	15.40	0.01	0.25	5.40	4.78	3.24	0.09	0.04
NER-86-250	50.00	12.50	0.97	18.80	0.01	0.25	4.09	7.35	3.27	0.41	0.06
NER-86-326	52.70	13.80	0.45	13.80	0.01	0.19	3.40	6.22	2.98	0.12	0.04
NER-86-40	51.00	13.20	0.68	16.80	0.01	0.23	4.84	7.57	2.86	0.56	0.05
NER-86-468	49.70	14.10	0.34	13.20	0.01	0.22	6.56	7.63	3.49	0.73	0.03
NER-86-62	49.80	13.10	0.71	16.00	0.01	0.24	5.54	8.51	2.70	0.38	0.06
NER-98-100	50.60	13.00	0.67	15.80	0.01	0.23	5.66	8.28	2.98	0.15	0.05
NER-98-202	53.50	14.20	0.36	15.00	0.01	0.21	4.08	7.80	2.22	0.14	0.04
NER-98-300	56.10	12.70	0.49	14.70	0.01	0.19	3.04	6.31	3.11	0.30	0.05
NER-98-451	54.40	13.60	0.39	13.80	0.01	0.20	4.46	6.50	3.04	0.24	0.04
NER-98-548	52.80	13.70	0.39	15.20	0.01	0.20	3.79	7.93	2.38	0.21	0.04
NER-99-489	53.50	13.50	0.47	15.10	0.01	0.18	3.88	6.73	3.26	0.17	0.04
NER-99-532	52.30	14.20	0.42	14.20	0.01	0.22	4.56	6.63	3.45	0.38	0.04
NER-99-602	55.90	13.00	0.46	14.90	0.01	0.17	3.01	6.04	3.32	0.28	0.05
NER-99-704	54.00	13.60	0.38	12.80	0.01	0.20	4.55	6.13	4.05	0.69	0.04
HS95M123A	58.60	16.80	0.46	6.08	<0.01	0.11	2.51	5.95	4.50	1.18	0.20
HS95M123AA	65.90	15.90	0.33	3.63	<0.01	0.05	1.91	3.64	4.78	1.49	0.10
HS95M157	65.70	15.40	0.43	4.11	<0.01	0.05	1.68	3.05	4.66	2.16	0.14
HS95M161-1	52.20	14.20	0.31	11.50	0.01	0.18	7.32	7.60	2.95	1.39	0.03
HS95M1611	52.40	14.20	0.44	14.80	<0.01	0.19	4.75	5.62	4.28	0.41	0.04
HS95M240-1	46.80	18.10	0.11	6.78	0.07	0.11	8.92	12.60	1.50	0.31	0.01
HS95M260	46.00	18.60	0.06	6.56	0.02	0.11	9.43	13.80	0.71	0.10	0.01
HS95M285	53.10	12.80	0.62	14.20	0.01	0.19	5.22	7.46	3.64	0.11	0.05
HS95M286	49.10	14.70	0.16	10.80	0.01	0.17	8.31	11.50	1.99	0.36	0.01
HS95M291-2	47.10	16.30	0.08	7.91	0.03	0.15	11.20	12.20	1.44	0.16	0.01
HS95M292	48.60	16.20	0.07	7.80	0.02	0.15	10.00	12.30	1.52	0.42	0.01
HS95M293	48.30	14.90	0.11	9.34	0.01	0.17	9.92	12.90	0.98	0.33	0.01
HS95M294	49.20	15.00	0.15	9.25	0.01	0.17	10.70	9.82	1.97	0.15	0.01
HS95M295	47.50	13.40	1.56	12.60	0.01	0.21	6.23	12.50	2.71	0.30	0.13
HS95M315-1	54.20	13.90	0.55	14.10	0.01	0.12	4.58	8.28	1.48	0.53	0.04
HS95M3151	74.00	11.30	0.24	2.45	<0.01	0.03	2.02	2.81	4.68	0.69	0.06
HS95M326	48.10	15.90	0.06	6.56	0.01	0.14	11.00	13.80	0.53	0.15	0.01
HS95M69-1	54.50	16.70	0.26	6.42	0.02	0.09	7.37	7.27	4.49	0.89	0.01
HS96M170	54.30	16.50	1.46	8.55	<0.01	0.11	4.22	7.04	3.82	0.66	0.28
HS96M298	55.50	13.80	0.41	12.40	0.01	0.18	4.34	5.58	4.61	0.28	0.05
HS96M308-1	51.00	15.10	0.20	11.70	<0.01	0.20	7.11	8.08	3.37	0.75	<0.01
HS96M309	49.30	20.30	0.31	4.75	0.01	0.08	6.67	9.39	2.67	2.13	0.04
HS96M315-3	52.30	16.50	0.28	7.70	0.01	0.08	7.34	8.73	3.32	0.72	0.02
HS96M320	48.00	15.90	0.13	7.72	0.07	0.14	10.90	10.80	1.84	0.36	0.01
HS96M322	47.50	14.90	0.06	7.52	0.03	0.14	10.90	13.10	0.93	0.19	0.01
HS96M323	47.50	16.20	0.04	5.26	0.09	0.10	12.50	12.90	1.07	0.24	0.01

Sample#	SiO <sub>2</sub> (%)	Al <sub>2</sub> O <sub>3</sub> (%)	TiO <sub>2</sub> (%)	Fe(tot) (%)	Cr <sub>2</sub> O <sub>3</sub> (%)	MnO (%)	MgO (%)	CaO (%)	Na <sub>2</sub> O (%)	K <sub>2</sub> O (%)	P <sub>2</sub> O <sub>5</sub> (%)
HS96M75-3	58.70	12.10	0.45	14.50	0.01	0.19	2.97	4.64	2.78	0.30	0.05
HS96M328	47.50	14.90	0.06	7.52	0.03	0.14	10.90	13.10	0.93	0.19	0.01
HS96M67	47.30	16.40	0.07	7.90	0.02	0.14	11.50	11.00	1.73	0.13	0.01
HS96M75-1	52.10	14.60	0.18	11.10	<0.01	0.18	7.33	8.17	3.81	0.32	0.02
HS96M75-2	62.30	11.40	0.43	13.10	0.01	0.16	2.22	5.75	2.75	0.21	0.05
HS96M76	62.20	14.60	0.48	5.47	0.06	0.08	3.94	5.46	4.84	0.79	0.13
B-87-116	52.40	13.80	0.48	13.60	0.01	0.22	2.91	8.72	2.24	0.71	0.06
B-87-154	43.70	13.30	2.53	16.80	0.01	0.20	7.21	9.11	1.66	0.61	0.23
B-87-176	58.80	13.10	0.59	9.36	0.01	0.14	2.62	5.96	4.08	0.37	0.07
B-87-220	53.70	14.00	0.57	14.10	0.01	0.18	4.55	5.90	2.47	0.33	0.05
B-87-259	65.80	10.60	0.30	13.30	<0.01	0.06	4.59	0.36	0.05	0.97	0.06
B-87-302	55.60	14.80	0.55	11.20	0.01	0.11	5.06	4.74	2.87	0.36	0.07
B-87-37	50.70	15.20	0.65	16.80	0.01	0.18	5.01	3.67	2.95	0.23	0.05
B-87-381	53.50	14.10	0.83	15.90	0.01	0.20	4.16	6.28	3.24	0.16	0.06
B-87-435	54.90	12.40	0.48	11.50	0.01	0.19	3.31	7.09	3.17	0.19	0.06
B-87-489	55.60	8.60	0.15	10.20	0.25	0.29	12.80	7.05	0.26	0.18	0.03
B-87-57	59.90	10.80	0.42	11.20	0.01	0.17	2.40	8.23	0.28	1.29	0.07
B-87-621	52.00	8.43	0.12	9.58	0.22	0.16	15.00	7.67	1.14	0.64	0.03
B-87-649	52.50	7.62	0.10	9.93	0.14	0.17	11.60	7.71	0.87	0.84	0.02
B-87-680	75.40	0.11	0.01	11.40	<0.01	0.21	0.15	10.30	0.04	0.05	<0.01
B-87-746	68.30	12.00	0.28	7.32	<0.01	0.11	1.20	3.76	4.52	0.09	0.08
B-88-1038	65.60	11.20	0.32	9.18	<0.01	0.10	2.93	2.19	3.10	0.51	0.08
B-88-1296	54.60	13.20	0.58	12.70	0.01	0.22	2.16	8.66	2.12	0.81	0.06
B-88-1497	42.70	9.45	0.39	11.40	0.01	0.23	2.03	21.80	0.53	0.77	0.06
B-88-1773	62.60	11.50	0.39	7.60	0.01	0.12	1.45	5.37	4.07	0.26	0.06
B-88-2044	50.90	14.20	0.49	13.40	0.01	0.17	6.41	6.01	2.33	0.57	0.04
B-88-2145	48.90	13.40	0.53	14.10	0.01	0.12	4.80	5.24	1.34	1.36	0.05
B-88-297	51.40	13.90	0.53	14.50	0.01	0.18	4.89	5.94	1.83	1.39	0.05
B-88-653	66.10	12.20	0.39	9.01	<0.01	0.08	2.11	4.26	2.54	0.85	0.06
B-88-847	60.60	12.40	0.45	14.90	0.01	0.23	3.35	1.20	2.55	0.10	0.05
B-89-1000	49.80	14.30	0.37	11.50	0.01	0.15	7.34	5.54	2.64	0.57	0.03
B-89-1125	56.00	12.40	0.41	12.00	0.01	0.10	4.06	4.11	1.59	1.11	0.05
B-89-1242	53.50	14.00	0.55	15.00	0.01	0.22	3.47	7.68	2.39	0.30	0.05
B-89-1424	57.90	11.70	0.41	19.60	0.01	0.18	3.82	0.67	0.53	0.14	0.04
B-89-1814	59.40	12.90	0.53	12.70	0.01	0.13	4.36	2.20	3.04	0.38	0.06
B-89-1958	55.80	13.30	0.53	14.70	0.01	0.16	4.33	5.17	2.66	0.26	0.06
FX-30-144	52.40	13.50	0.67	15.40	0.01	0.20	4.54	5.78	2.49	0.24	0.06
FX-34-W1-1048	51.30	7.91	0.09	10.80	0.23	0.17	12.70	9.53	0.90	0.44	0.03
FX-34-W1-1176	52.80	14.10	0.28	10.80	0.01	0.14	5.07	9.60	3.03	0.52	0.04
FX-34-W1-812	53.40	14.70	0.53	12.90	0.01	0.21	2.85	7.77	3.82	0.32	0.06
FX-34-W1-872	56.10	13.50	0.61	14.60	0.01	0.24	2.76	6.32	3.43	0.33	0.06
FX-35-147	56.20	13.80	0.59	12.10	0.01	0.13	4.25	4.25	4.81	0.24	0.07
FX-35-304	52.50	7.44	0.11	11.80	0.27	0.18	14.20	7.88	0.66	0.53	0.04
FX-35-420	53.50	13.70	0.59	14.40	0.01	0.20	4.38	6.72	3.09	0.23	0.06

Sample#	SiO <sub>2</sub> (%)	Al <sub>2</sub> O <sub>3</sub> (%)	TiO <sub>2</sub> (%)	Fe(tot) (%)	Cr <sub>2</sub> O <sub>3</sub> (%)	MnO (%)	MgO (%)	CaO (%)	Na <sub>2</sub> O (%)	K <sub>2</sub> O (%)	P <sub>2</sub> O <sub>5</sub> (%)
FX-36-931	53.10	13.60	0.52	12.40	0.01	0.17	3.06	9.28	2.57	0.58	0.05
CN-90-1-1061	53.00	15.10	0.27	10.40	<0.01	0.20	9.42	4.27	2.18	1.06	0.04
FX-35-456	51.90	12.90	0.54	14.50	0.02	0.20	5.68	7.58	2.60	0.23	0.05
FX-35-61	53.50	9.06	0.14	11.00	0.24	0.16	14.10	5.35	0.73	0.45	0.03
FX-36-129	69.40	14.40	0.23	2.46	<0.01	0.06	1.20	2.86	4.38	1.36	0.08
FX-36-313	51.30	14.80	1.31	13.10	<0.01	0.18	4.29	6.52	3.98	0.58	0.28
FX-36-486	49.40	11.10	0.12	9.12	0.11	0.15	11.60	6.14	1.07	0.64	0.01
FX-36-560	53.10	14.70	0.50	12.60	0.01	0.21	4.21	7.26	3.34	0.28	0.06
FX-36-694	51.80	14.30	0.60	14.40	0.01	0.19	3.34	7.45	2.18	0.57	0.06
CN-90-1-1128	43.70	19.10	0.70	13.50	<0.01	0.49	5.57	7.47	2.26	0.35	0.11
CN-90-1-270	73.10	11.40	0.24	3.87	<0.01	0.04	2.10	1.38	4.26	0.95	0.04
CN-90-1-457	52.80	14.40	0.15	11.10	0.03	0.32	10.10	5.78	1.56	0.45	0.05
CN-90-1-692	49.00	14.40	0.55	15.30	<0.01	0.12	10.30	1.05	0.30	0.52	0.06
CN-90-1-701	53.50	14.80	0.49	14.40	<0.01	0.12	10.00	0.53	0.41	0.86	0.06
CN-90-1-715	55.00	14.20	0.41	11.70	<0.01	0.08	9.75	0.29	0.18	1.26	0.06
CN-90-1-761	51.00	12.20	0.20	12.60	0.10	0.19	13.10	2.36	0.89	1.37	0.03
CN-90-1-843	50.40	15.10	0.34	11.10	0.01	0.11	10.20	3.80	3.49	0.35	0.04
CN-90-1-964	48.20	15.20	0.20	8.86	0.07	0.09	9.69	8.18	2.78	0.64	0.03
CN-90-2-163	70.90	11.90	0.27	4.84	<0.01	0.05	1.90	2.04	4.36	0.23	0.07
CN-90-2-281	56.30	14.90	0.33	9.85	<0.01	0.22	6.17	5.54	2.63	0.21	0.06
CN-90-2-291	56.50	14.40	0.43	13.80	<0.01	0.14	9.38	0.58	0.73	0.46	0.05
CN-90-2-444	49.40	13.60	0.29	16.90	0.01	0.17	9.22	1.50	1.08	0.18	0.03
CN-90-2-523	49.10	15.30	0.60	16.50	<0.01	0.12	12.20	0.98	0.58	0.47	0.06
CN-90-2-650	53.40	15.10	0.36	9.82	<0.01	0.05	8.04	6.82	2.34	0.36	0.05
CN-90-2-722	52.70	10.70	0.15	10.40	0.16	0.18	12.20	6.73	1.30	0.37	0.02
CN-90-2-848	52.40	13.80	0.23	10.20	0.02	0.23	8.02	9.29	1.09	0.57	0.03
CN-90-2-880	54.50	14.70	0.24	10.20	<0.01	0.16	6.06	7.69	2.94	0.16	0.03
CN-90-3-178	52.00	12.00	0.19	11.00	0.08	0.17	11.30	6.35	2.05	0.24	0.02
CN-90-3-225	50.00	13.20	0.42	13.70	0.04	0.17	10.10	4.33	1.77	0.40	0.04
CN-90-3-437	51.80	15.10	0.28	11.60	<0.01	0.17	7.52	5.38	3.52	0.15	0.03
CN-90-3-514	48.70	14.00	0.72	22.50	<0.01	0.17	6.73	1.24	0.64	0.81	0.09
CN-90-3-633	59.20	14.00	0.37	9.68	<0.01	0.17	2.82	6.45	2.89	0.70	0.05
CN-90-3-725	53.40	15.20	0.38	13.70	<0.01	0.18	6.72	4.21	4.02	0.06	0.05

Table A5.3. Trace element and additional components concentrations

Sample#	CO <sub>2</sub> (%)	S% (%)	H <sub>2</sub> O <sub>(+)</sub> (%)	LOI % (%)	TOTAL	FeO (%)	Rb (ppm)	Sr (ppm)	Y (ppm)	Zr (ppm)	Nb (ppm)	Ba (ppm)
HOF2-119	0.38	0.01	2.00	2.10	98.70	8.00	9	73	5	20	<2	65
HOF2-15	2.03	0.75	3.30	3.70	98.50	9.50	7	65	14	31	<2	126
HOF2-156	0.16	0.21	2.80	2.20	98.60	13.00	<2	83	17	25	<2	66
HOF-2-173	0.06	0.01	2.80	2.55	98.40	5.20	1	78	3	10	1	125
HOF2-197	0.35	0.91	1.80	1.80	98.40	8.20	<2	78	20	37	3	30
HOF2-214	0.11	0.22	2.70	2.05	98.90	11.90	<2	70	14	26	<2	60
HOF-2-290	0.53	0.02	4.30	4.25	98.80	6.20	6	102	12	18	4	258
HOF-2-32	3.32	0.10	5.50	7.75	100.20	10.90	10	44	1	20	1	101
HOF-2-33	0.22	0.04	2.20	1.55	99.60	8.00	2	77	8	17	1	243
HOF2-40	0.19	0.28	2.80	2.20	98.70	11.30	<2	70	17	33	<2	46
HOF2-68	0.06	0.04	2.00	1.65	98.20	9.10	<2	86	7	18	3	77
HOF-5-127	0.06	0.17	3.10	2.60	98.90	11.10	3	72	9	23	<2	44
HOF-5-130	0.06	0.34	3.80	2.85	100.20	12.40	1	47	9	31	1	63
HOF-5-131	0.12	0.02	3.30	2.55	99.60	7.30	4	78	8	14	1	74
HOF-5-154	0.05	0.12	1.80	0.95	99.50	11.90	1	54	5	21	1	70
HOF-5-156	0.10	0.02	2.70	2.00	99.00	8.00	13	68	5	14	1	83
HOF-5-196	0.23	0.01	2.60	2.00	98.90	9.20	17	79	6	15	1	71
HOF-5-224	0.05	0.12	2.60	1.75	98.40	12.00	<2	68	10	34	<2	44
HOF-5-268	3.20	0.01	4.40	6.15	100.20	13.00	1	25	6	25	1	55
HOF-5-272	0.31	0.01	5.90	4.50	99.60	15.70	1	38	2	16	1	33
HOF-5-297	0.06	0.03	3.40	2.50	98.30	13.10	4	61	5	15	<2	32
HOF-5-320	8.15	0.02	5.10	13.00	100.20	6.20	<2	51	1	15	<2	116
HOF-5-348	5.18	0.04	6.20	10.90	100.20	7.80	1	46	1	11	1	97
HOF-5-353	0.89	0.06	2.70	3.00	99.40	7.80	1	82	1	8	1	75
HOF-5-58	0.07	0.21	4.00	3.20	99.50	10.80	13	57	8	32	1	87
HOF-5-64	0.07	0.11	2.00	1.80	99.80	2.70	1	384	14	121	5	213
HOF-5-67	0.09	0.25	3.10	2.30	99.60	10.60	1	80	13	35	1	105
HOF-5-67.7	0.05	0.16	4.70	4.35	99.50	10.80	10	59	9	35	1	97
HOF-5-67.9	0.14	0.02	3.20	2.70	99.80	7.70	1	73	6	12	1	106
HOF-5-68	0.11	0.02	2.70	2.10	99.00	7.50	1	100	4	10	1	128
HOF-5-71	0.03	0.34	1.90	0.95	99.50	9.80	1	79	15	29	1	72
HOF-5-75	0.05	0.15	2.20	1.55	98.50	10.20	<2	90	11	28	<2	77
HOF-5-87	0.06	0.09	3.20	2.35	98.10	9.80	1	65	10	29	1	63
NER-102-104	0.21	0.44	1.40	1.05	99.30	11.10	<2	69	15	27	<2	61
NER-102-204	0.08	0.08	1.20	0.75	98.40	9.70	<2	66	13	22	7	51
NER-102-303	0.09	0.07	1.40	0.60	98.40	9.60	<2	66	13	28	<2	68
NER-102-450	0.24	0.10	1.80	1.45	98.30	9.00	<2	96	15	39	<2	63
NER-102-543	0.37	0.01	1.30	1.15	98.50	7.40	10	66	5	22	<2	145
NER-105-224	0.09	0.13	1.80	1.35	98.20	9.10	<2	75	8	20	<2	70
NER-105-305	6.33	0.01	3.60	9.10	98.80	9.10	<2	69	8	15	<2	68
NER-105-390	0.28	0.04	1.40	1.05	98.20	8.00	<2	85	1	17	<2	70
NER-105-481	0.49	0.17	1.70	1.30	98.50	10.60	<2	63	7	24	2	66
NER-105-542	8.32	0.02	4.00	11.40	99.40	8.50	<2	53	8	19	<2	162
NER-105-637	0.08	1.99	2.80	2.70	99.10	13.30	<2	67	14	24	<2	41
NER-105-724	0.32	0.01	1.90	1.70	98.30	6.90	<2	71	19	36	4	38
NER-105-76	0.29	0.17	1.70	0.85	98.30	12.10	<2	59	17	40	<2	53
NER-107-1002	0.70	0.06	2.70	2.55	98.30	9.90	6	177	19	91	4	86
NER-107-122	0.04	0.10	1.90	1.35	98.40	10.90	<2	149	12	27	<2	111
NER-107-246	1.11	0.08	2.10	2.20	98.30	12.40	<2	61	15	31	<2	61
NER-107-427	3.44	0.10	4.40	6.50	99.50	12.40	<2	61	11	28	<2	70



Sample#	CO <sub>2</sub> (%)	S% (%)	H <sub>2</sub> O <sub>(+)</sub> (%)	LOI % (%)	TOTAL	FeO (%)	Rb (ppm)	Sr (ppm)	Y (ppm)	Zr (ppm)	Nb (ppm)	Ba (ppm)
NER-107-50	0.19	0.12	1.70	1.30	98.40	10.30	<2	76	14	29	<2	61
NER-107-624	0.42	0.31	2.50	1.90	98.00	10.90	<2	78	7	27	<2	44
NER-107-722	0.39	0.05	2.10	1.40	99.40	11.10	<2	65	12	20	<2	78
NER-107-823	0.20	0.04	2.50	1.75	98.30	9.80	<2	85	8	20	<2	104
NER-107W1-43	0.20	0.11	2.20	1.50	98.00	10.50	<2	71	8	18	<2	53
NER-107W1-55	0.22	0.02	1.90	1.35	99.30	8.60	<2	77	10	19	<2	105
NER-107W1-64	0.05	0.04	2.20	1.55	98.20	9.90	<2	92	9	23	2	118
NER-107W1-76	0.35	0.03	1.60	1.10	98.50	10.00	<2	101	20	28	2	101
NER-111-157	0.12	0.18	2.60	1.95	99.20	9.50	11	85	12	39	1	64
NER-111-175	5.74	0.52	2.60	8.10	100.20	9.80	1	53	2	18	1	82
NER-111-198	0.14	0.43	3.90	3.50	99.40	9.00	1	84	9	24	1	73
NER-111-212	0.07	0.12	2.80	2.10	99.00	9.50	1	68	9	22	1	133
NER-111-228	0.13	0.02	2.80	1.90	99.00	9.00	1	63	6	13	1	127
NER-111-238	0.08	0.02	2.10	1.50	100.10	9.40	1	59	6	13	1	177
NER-116-389	0.29	0.08	2.40	2.00	99.50	10.70	1	74	17	26	1	170
NER-116-493	0.24	0.09	1.70	1.55	98.60	6.50	12	410	20	78	6	210
NER-122-135	0.82	0.18	2.20	2.40	98.30	3.80	20	532	12	121	7	226
NER-122-141	1.31	1.68	2.30	2.60	100.10	7.10	3	169	11	90	1	217
NER-122-150	0.17	0.13	3.10	2.40	98.70	11.00	1	188	21	84	5	93
NER-122-173	9.71	0.02	2.80	11.90	100.30	5.50	19	279	4	56	4	379
NER-69-19	0.10	0.03	1.70	1.35	97.70	8.90	<2	77	7	21	<2	139
NER-69-46	1.13	0.09	2.70	2.65	98.30	11.20	<2	70	15	24	2	47
NER-69-92	1.01	0.12	2.30	2.35	98.70	10.70	5	62	14	32	5	118
NER-71-176	0.08	0.15	1.50	1.00	98.00	10.80	2	67	4	17	<2	72
NER-71-31	0.16	0.05	1.80	0.90	98.50	11.40		63	11	24	<2	71
NER-71-62	0.13	0.01	1.80	1.20	98.40	7.80	<2	83	19	34	<2	59
NER-71-95	0.24	0.03	2.80	2.25	99.80	10.50	<2	72	13	27	<2	51
NER-73-109	0.11	0.02	2.00	1.55	98.90	8.10	6	77	5	21	<2	94
NER-73-28	0.30	0.21	2.60	2.35	96.30	7.50	<2	71	14	32	2	64
NER-73-74	0.54	0.18	2.10	1.90	98.00	8.80	12	82	8	20	<2	111
NER-75-130	1.05	0.25	1.60	2.10	98.10	5.40	<2	89	6	23	<2	106
NER-75-181	0.29	0.12	1.70	1.20	98.70	10.40	<2	69	13	20	<2	64
NER-75-38	0.13	0.15	1.70	1.10	98.70	10.10	<2	80	17	26	3	76
NER-75-77	0.08	0.08	3.30	2.75	99.20	10.60	<2	83	13	26	<2	59
NER-78-125	8.44	0.25	2.80	9.85	100.20	10.70	<2	57	12	27	4	154
NER-78-129	2.43	0.22	5.20	6.25	99.10	11.40	<2	54	10	25	<2	40
NER-78-168	0.10	0.01	1.90	1.45	98.50	9.90	3	63	5	17	2	110
NER-78-212	3.27	0.14	2.30	4.70	99.00	7.60	<2	84	7	18	<2	74
NER-78-279	0.28	0.04	1.90	1.45	98.90	10.00	7	66	9	25	2	110
NER-78-95	3.54	0.19	3.10	5.35	99.40	10.40	<2	96	21	29	3	85
NER-80-150	0.34	0.07	2.10	1.80	99.70	9.40	<2	61	13	21	<2	30
NER-80-201	0.17	0.22	2.60	2.10	98.60	10.50	<2	99	8	30	<2	44
NER-80-21	0.11	0.36	2.70	2.30	98.30	10.40	<2	57	14	28	4	46
NER-80-253	0.39	0.15	2.10	1.65	98.20	11.20	3	67	19	35	4	63
NER-80-75	0.41	0.06	1.50	1.05	98.50	9.30	<2	71	22	34	<2	41
NER-82-122	0.11	0.01	1.40	1.15	97.80	7.10	15	82	3	18	<2	107
NER-82-146	5.85	0.03	4.10	8.90	100.60	7.20	<2	60	8	23	<2	117
NER-82-168	0.20	0.20	2.70	2.00	99.10	10.60	5	69	4	22	<2	45
NER-82-50	0.03	1.03	1.30	0.95	99.10	11.60	<2	94	24	43	5	102

Sample#	CO <sub>2</sub> (%)	S% (%)	H <sub>2</sub> O <sub>(+)</sub> (%)	LOI % (%)	TOTAL	FeO (%)	Rb (ppm)	Sr (ppm)	Y (ppm)	Zr (ppm)	Nb (ppm)	Ba (ppm)
NER-84-301	0.18	0.02	1.90	1.65	98.60	8.80	<2	66	2	17	<2	94
NER-84-178	0.35	0.12	2.00	1.60	98.50	10.80	4	60	12	27	<2	63
NER-84-260	3.52	1.88	2.50	2.25	96.80	10.40	<2	119	29	29	19	40
NER-84-335	0.24	0.17	2.30	1.65	98.90	10.60	<2	117	18	29	4	51
NER-84-397	1.28	0.07	2.00	2.35	98.40	9.30	<2	75	9	21	<2	113
NER-84-5	1.33	0.11	2.40	2.80	98.50	11.30	<2	57	13	30	<2	129
NER-84-98	0.12	0.03	1.20	0.75	99.10	9.00	<2	54	14	32	<2	57
NER-86-143	0.49	0.05	1.90	1.25	98.40	11.10	<2	62	19	34	<2	45
NER-86-168	0.53	0.31	1.20	0.80	98.10	8.00	4	70	19	34	4	42
NER-86-21	0.14	0.29	2.80	2.00	98.60	12.70	<2	60	21	34	<2	96
NER-86-214	0.08	0.26	3.00	2.25	98.80	11.70	<2	99	18	25	<2	48
NER-86-250	0.43	0.14	1.70	1.15	98.90	13.50	<2	57	20	40	<2	51
NER-86-326	2.46	0.11	3.40	4.70	98.40	10.90	<2	85	17	25	<2	42
NER-86-40	0.10	0.14	1.60	1.15	99.00	12.30	5	61	14	32	2	77
NER-86-468	0.52	0.14	2.10	2.00	98.00	9.30	13	119	6	22	<2	247
NER-86-62	0.22	0.11	2.50	1.40	98.50	11.70	6	73	22	36	3	69
NER-98-100	0.10	0.09	1.70	0.80	98.20	11.60	3	66	16	32	2	49
NER-98-202	0.06	0.30	1.80	1.40	99.00	10.20	<2	83	7	25	<2	53
NER-98-300	0.10	0.20	1.50	0.80	97.80	10.30	<2	45	12	27	31	75
NER-98-451	0.49	0.04	2.50	2.25	98.90	10.40	2	74	12	29	<2	66
NER-98-548	0.06	0.02	2.20	1.40	98.10	9.50	<2	97	16	24	<2	59
NER-99-489	0.15	0.12	2.20	1.55	98.40	10.10	<2	79	12	26	<2	35
NER-99-532	0.06	0.13	2.00	1.70	98.10	10.10	<2	79	13	24	<2	62
NER-99-602	0.13	0.27	1.90	1.30	98.40	9.90	<2	66	19	26	<2	56
NER-99-704	0.11	0.02	1.90	1.40	97.90	9.30	7	92	9	24	<2	145
HS95M123A	0.18	0.08	1.90	1.70	98.30	3.60	12	683	15	120	8	714
HS95M123AA	1.01	0.01	1.50	2.15	100.00	2.50	10	460	14	124	7	612
HS95M157	0.26	0.06	0.50	1.75	99.30	2.70	24	593	22	158	10	717
HS95M161-1	0.04	0.01	2.40	1.70	99.40	8.20	16	65	8	17	1	195
HS95M1611	0.28	0.06	2.70	1.75	98.90	11.40	7	50	5	17	1	70
HS95M240-1	0.34	0.01	2.60	2.95	98.30	4.60	1	147	1	6	1	51
HS95M260	0.05	0.01	2.40	2.70	98.10	4.50	1	81	4	4	1	27
HS95M285	0.49	0.04	2.20	1.90	99.30	9.50	1	79	20	27	1	84
HS95M286	0.43	0.01	2.20	2.30	99.40	7.20	1	93	5	7	1	96
HS95M291-2	0.05	0.02	2.60	2.05	98.60	5.30	1	123	5	6	1	49
HS95M292	0.01	0.07	1.80	1.85	99.00	5.30	13	99	8	10	4	112
HS95M293	0.19	0.05	1.90	1.55	98.50	6.70	1	54	6	5	1	71
HS95M294	0.02	0.03	2.30	2.20	98.60	6.90	1	53	5	10	1	73
HS95M295	0.67	0.03	0.70	1.45	98.60	8.10	1	174	26	77	6	148
HS95M315-1	0.01	0.02	1.70	1.20	99.00	10.00	1	86	13	25	1	108
HS95M3151	0.73	0.01	0.70	1.30	99.60	1.60	1	63	32	85	4	128
HS95M326	0.06	0.01	1.70	2.20	98.50	4.50	4	57	12	12	5	25
HS95M69-1	0.10	0.01	1.20	1.60	99.70	4.20	23	123	20	35	9	190
HS96M170	0.01	0.01	1.90	1.60	98.60	5.90	1	358	16	149	11	376
HS96M298	0.04	0.01	1.70	1.35	98.50	9.50	1	101	12	26	1	81
HS96M308-1	0.04	0.01	1.70	1.35	98.90	8.60	1	91	1	8	1	180
HS96M309	0.23	0.01	2.00	2.50	98.30	2.80	41	649	3	34	1	492
HS96M315-3	0.04	0.01	1.70	1.45	98.50	5.60	1	116	11	22	1	140
HS96M320	0.01	0.01	3.00	2.40	98.30	5.50	4	78	6	11	1	84
HS96M322	0.02	0.01	4.10	3.45	98.70	5.30	1	52	4	6	1	44
HS96M323	0.04	0.01	2.40	2.35	98.30	3.70	1	71	10	12	4	51

Sample#	CO <sub>2</sub> (%)	S% (%)	H <sub>2</sub> O <sub>(+)</sub> (%)	LOI % (%)	TOTAL	FeO (%)	Rb (ppm)	Sr (ppm)	Y (ppm)	Zr (ppm)	Nb (ppm)	Ba (ppm)
HS96M75-3	1.29	0.08	2.50	2.70	99.40	10.80	6	34	14	34	1	76
HS96M328	0.02	0.01	4.10	3.45	98.70	5.30	1	52	4	6	1	44
HS96M67	0.01	0.01	2.90	2.40	98.60	5.70	1	56	1	5	1	62
HS96M75-1	0.03	0.01	1.80	1.40	99.20	8.40	1	53	3	7	1	97
HS96M75-2	0.10	0.30	1.10	0.60	99.00	6.00	1	43	18	36	1	58
HS96M76	0.03	0.06	1.80	1.35	99.50	3.80	1	469	17	131	5	560
B-87-116	2.30	0.07	1.90	3.35	98.50		<2	65	12	32	2	188
B-87-154	0.46	0.28	3.40	3.10	98.50		<2	158	27	158	16	203
B-87-176	1.76	0.08	1.70	3.10	98.20		<2	79	18	36	2	138
B-87-220	0.54	0.09	3.00	2.80	98.70		<2	99	14	31	<2	296
B-87-259	0.05	0.05	4.30	3.65	99.80		<2	19	21	47	<2	248
B-87-302	0.42	0.10	2.80	3.30	98.70		<2	107	18	44	<2	293
B-87-37	0.24	0.02	3.90	2.95	98.40		<2	70	19	34	<2	77
B-87-381	0.10	0.01	2.40	1.70	100.20		8	71	23	37	2	25
B-87-435	3.21	0.24	2.70	4.85	98.20		<2	121	19	33	<2	102
B-87-489	0.11	0.08	3.30	3.00	98.40		6	138	4	28	2	20
B-87-57	2.70	0.08	2.00	4.40	99.20		12	58	16	34	<2	101
B-87-621	0.22	0.06	2.90	2.40	97.40		5	45	1	27	<2	196
B-87-649	4.03	0.01	3.50	7.12	98.70		<2	72	1	24	<2	244
B-87-680	2.57	0.65	0.05	1.65	99.30		<2	55	1	9	<2	20
B-87-746	0.32	0.13	0.90	0.70	98.40		<2	90	24	51	5	90
B-88-1038	1.25	0.05	2.70	3.25	98.50		<2	66	23	45	<2	127
B-88-1296	2.17	0.08	1.60	2.90	98.00		8	66	13	35	22	149
B-88-1497	10.10	0.04	0.70	10.30	99.70		<2	89	18	29	<2	103
B-88-1773	3.56	0.14	1.80	4.85	98.30		<2	111	19	36	<2	104
B-88-2044	1.88	0.08	2.80	3.80	98.30		<2	65	17	29	<2	84
B-88-2145	7.59	0.09	3.50	10.20	100.10		2	49	13	30	<2	165
B-88-297	1.79	0.26	2.80	2.80	97.40		<2	35	13	30	<2	112
B-88-653	0.88	0.03	1.70	1.95	99.60		<2	50	20	43	<2	52
B-88-847	0.17	0.04	3.90	2.85	98.70		<2	28	13	37	<2	40
B-89-1000	3.53	0.07	3.60	6.42	98.70		<2	64	11	24	<2	90
B-89-1125	5.53	0.03	3.40	7.80	99.70		<2	42	11	33	<2	138
B-89-1242	0.66	0.05	1.80	1.70	98.90		<2	46	11	30	<2	710
B-89-1424	0.04	0.02	5.30	3.60	98.60		<2	23	13	36	<2	60
B-89-1814	0.30	0.09	3.00	2.55	98.30		<2	64	19	41	<2	101
B-89-1958	0.30	0.02	2.00	1.50	98.50		2	89	13	34	<2	88
FX-30-144	0.30	0.28	3.30	2.95	98.30		<2	155	26	37	<2	91
FX-34-W1-1048	2.55	0.10	2.70	4.50	98.60		15	53	1	25	<2	156
FX-34-W1-1176	1.24	0.04	1.80	2.55	99.00		22	133	4	30	<2	118
FX-34-W1-812	0.21	0.07	1.40	0.85	97.40		<2	119	14	33	<2	98
FX-34-W1-872	0.11	0.12	1.50	0.90	98.90		<2	96	18	32	2	61
FX-35-147	0.08	0.07	1.90	1.70	98.20		<2	131	18	41	2	77
FX-35-304	0.09	0.04	1.50	1.40	97.00		5	91	1	29	<2	99
FX-35-420	0.50	0.06	1.50	1.40	98.30		<2	134	16	33	<2	65

Sample#	CO <sub>2</sub> (%)	S% (%)	H <sub>2</sub> O <sub>(+)</sub> (%)	LOI % (%)	TOTAL	FeO (%)	Rb (ppm)	Sr (ppm)	Y (ppm)	Zr (ppm)	Nb (ppm)	Ba (ppm)
FX-36-931	2.07	0.30	1.80	3.00	98.40		<2	86	13	32	<2	103
CN-90-1-1061	0.21	0.02	1.70	1.30	97.30		<2	39	4	24	<2	240
FX-35-456	0.06	0.02	1.30	0.75	97.00		<2	90	13	32	<2	73
FX-35-61	0.11	0.01	3.60	3.45	98.20		<2	158	4	31	<2	88
FX-36-129	0.59	0.01	1.00	1.60	98.20		9	223	6	104	9	767
FX-36-313	0.15	0.20	2.20	1.80	98.20		<2	180	25	139	12	369
FX-36-486	4.87	0.20	4.80	9.65	99.10		<2	73	1	19	<2	124
FX-36-560	0.94	0.06	2.10	2.40	98.70		<2	87	11	33	<2	72
FX-36-694	2.02	0.10	2.70	3.60	98.50		<2	80	13	32	<2	158
CN-90-1-1128	1.86	0.63	4.00	3.90	97.20		<2	169	19	68	2	140
CN-90-1-270	0.13	0.02	0.90	0.95	98.40		8	68	11	57	<2	87
CN-90-1-457	0.27	0.01	1.60	1.55	98.30		14	80	1	19	<2	223
CN-90-1-692	1.40	0.02	6.10	6.70	98.30		<2	28	10	35	<2	133
CN-90-1-701	0.24	0.01	3.50	3.10	98.30		<2	22	8	31	<2	160
CN-90-1-715	0.17	0.02	5.60	5.45	98.40		<2	27	11	33	2	233
CN-90-1-761	0.53	0.46	4.60	4.45	98.50		3	123	3	26	<2	370
CN-90-1-843	0.26	0.01	3.20	3.00	98.00		<2	89	4	23	<2	159
CN-90-1-964	0.09	0.02	2.10	1.00	95.00		<2	108	5	19	<2	432
CN-90-2-163	0.58	0.10	1.30	1.55	98.10		<2	88	8	55	<2	91
CN-90-2-281	0.34	0.01	1.10	1.10	97.30		<2	89	5	32	<2	121
CN-90-2-291	0.06	0.02	2.50	2.15	98.60		<2	32	8	30	<2	121
CN-90-2-444	1.20	0.03	5.70	5.85	98.20		<2	35	3	17	<2	96
CN-90-2-523	0.51	0.01	2.90	2.85	98.80		<2	32	15	37	<2	192
CN-90-2-650	0.17	0.02	1.40	1.30	97.70		3	153	4	29	<2	188
CN-90-2-722	0.28	0.10	2.10	2.00	96.90		<2	42	1	21	<2	176
CN-90-2-848	0.16	0.28	1.50	1.55	97.50		6	159	1	23	<2	372
CN-90-2-880	1.07	0.02	1.70	2.40	99.10		4	78	1	29	<2	58
CN-90-3-178	0.05	0.01	1.90	1.55	97.00		<2	90	1	23	<2	127
CN-90-3-225	0.15	0.12	3.20	3.05	97.20		<2	61	6	33	<2	122
CN-90-3-437	0.16	0.15	2.50	2.15	97.70		<2	80	7	29	6	54
CN-90-3-514	0.06	1.38	5.10	4.45	100.10		<2	39	10	48	<2	84
CN-90-3-633	0.42	0.20	1.50	1.40	97.80		<2	115	7	35	2	312
CN-90-3-725	0.09	0.03	2.20	1.70	99.60		11	74	7	33	2	85

## **Appendix 6**

### **Estimates of analytical precision of the geochemical analyses performed at X-ray Assay Laboratories Ltd. (XRAL) on samples from the Konuto Lake, Birch Lake, Flexar and Coronation deposits**

Samples, included in the Chu Chua and the Konuto Lake data sets, were analyzed by X-RAL Laboratories in Don Mills, Ontario. Analytical errors are estimated by replicate analyses (Table A3.1). Three internal MDRU standards were used: ALB-1 (Ajax albitite), CUL-1 (Cultus Lake Shale) and MBX-1 (MBX stock, Afton). Reported data for laboratory standards as well as analytical duplicates were also used. Each of the standards was submitted up to ten times, in random order, together with samples from the Chu Chua (Chapter 3), Konuto Lake (Chapter 4) and Anderson Lake (not used in this work) data sets. The estimation involved a computer code (Stanley, 1996) performing weighed Thompson-Howarth (Thompson and Howarth, 1978) replicate error analysis. Analytical errors are expressed as the sum of an absolute error term and a relative error term.

As a form of quality control pulp duplicates were also submitted to estimate the level of analytical errors introduced during sample preparation. This step was taken because the MDRU reference materials were not prepared together with the samples, which led to concerns that they may not reflect errors introduced during sample preparation properly. The estimates of the analytical errors for the pulp duplicates (Table A6.2) and for the MDRU standards (Table A2.1) proved to be comparable.

No quality control data was available for the data donated by HBED (Konuto Lake, Birch Lake, Flexar and Coronation deposits). The data were assumed to be compatible with the main data sets, after significant and systematic differences between this data and the main data set were not observed.

Analytical precision for the samples analyzed by XRAL is discussed in Appendix 4.

Stanley, C.R., (1997b) THPLOT.MATLAB Function to Implement Generalized Thompson-Howarth Error Analysis Using Replicate Data. Lithogeochemical Exploration for Metasomatic Zones Associated with Hydrothermal Mineral Deposits. Annual Technical Report, Years 1 and 2. Mineral Deposits Research Unit, Department of Geological Sciences, The University of British Columbia, Vancouver, B.C., 51 p.

Thompson, M., and Howarth, R.J., (1978) A New Approach to the Estimation of Analytical Precision. Journal of Geochemical Exploration, 9, pp. 23-30.

**Table A6.1. Replicate analyses and precision of internal (MDRU) reference materials analyzed by X-RAL with Konuto Lake area samples**

Internal	SiO <sub>2</sub>	TiO <sub>2</sub>	Al <sub>2</sub> O <sub>3</sub>	Cr <sub>2</sub> O <sub>3</sub>	Fe <sub>2</sub> O <sub>3</sub>	MnO	MgO	CaO	Na <sub>2</sub> O	K <sub>2</sub> O	P <sub>2</sub> O <sub>5</sub>	LOI	SUM
standard	%	%	%	%	%	%	%	%	%	%	%	%	
<b>MBX-1</b>	57	0.488	17.2	0.005	4.13	0.07	2	3.85	4.94	4.71	0.23	3.55	98.3
MBX-1	56.8	0.491	17.1	0.005	4.16	0.07	2	3.82	4.91	4.7	0.23	3.7	98.1
MBX-1	57.3	0.467	17.1	0.005	4.18	0.07	1.95	3.84	4.89	4.75	0.23	3.5	98.4
MBX-1	57.3	0.48	17	0.005	4.15	0.07	1.94	3.86	4.9	4.77	0.23	3.6	98.5
MBX-1	57.00	0.49	17.20	0.01	4.13	0.07	2.00	3.85	4.94	4.71	0.23	3.55	98.30
MBX-1	56.50	0.48	17.20	0.01	4.18	0.07	2.00	3.86	5.02	4.83	0.23	3.55	98.10
MBX-1	57.30	0.47	17.10	0.01	4.18	0.07	1.95	3.84	4.89	4.75	0.23	3.50	98.40
MBX-1	57.90	0.50	17.50	0.01	4.18	0.07	2.10	3.96	5.28	5.00	0.24	3.55	100.40
<b>Mean</b>	<b>57.14</b>	<b>0.48</b>	<b>17.18</b>	<b>0.01</b>	<b>4.16</b>	<b>0.07</b>	<b>1.99</b>	<b>3.86</b>	<b>4.97</b>	<b>4.78</b>	<b>0.23</b>	<b>3.56</b>	<b>98.56</b>
<b>STD</b>	<b>0.42</b>	<b>0.01</b>	<b>0.15</b>	<b>0.00</b>	<b>0.02</b>	<b>0.00</b>	<b>0.05</b>	<b>0.04</b>	<b>0.13</b>	<b>0.10</b>	<b>0.00</b>	<b>0.06</b>	<b>0.76</b>
<b>RSTD(%)</b>	<b>0.73</b>	<b>2.39</b>	<b>0.87</b>	<b>0.00</b>	<b>0.54</b>	<b>0.00</b>	<b>2.56</b>	<b>1.10</b>	<b>2.65</b>	<b>2.08</b>	<b>1.53</b>	<b>1.80</b>	<b>0.77</b>
<b>P</b>	<b>1.46</b>	<b>4.78</b>	<b>1.73</b>	<b>0.00</b>	<b>1.07</b>	<b>0.00</b>	<b>5.11</b>	<b>2.20</b>	<b>5.30</b>	<b>4.15</b>	<b>3.06</b>	<b>3.60</b>	<b>1.53</b>
<b>ALB-1</b>	53.8	0.601	18.4	0.005	2.01	0.04	2.7	9.8	5.53	0.8	0.28	2.95	97
ALB-1	53.4	0.606	18.3	0.005	2	0.03	2.69	9.77	5.54	0.82	0.27	3.2	96.8
ALB-1	53.40	0.60	18.50	0.01	1.63	0.03	2.70	9.90	5.62	0.81	0.28	3.15	96.80
ALB-1	53.80	0.60	18.40	0.01	2.01	0.04	2.70	9.80	5.53	0.80	0.28	2.95	97.00
ALB-1	54.00	0.60	18.70	0.01	1.63	0.03	2.77	10.10	5.67	0.78	0.29	3.10	97.80
ALB-1	53.70	0.60	18.60	0.01	1.62	0.03	2.76	10.00	5.59	0.78	0.29	3.35	97.50
<b>Mean</b>	<b>53.68</b>	<b>0.60</b>	<b>18.48</b>	<b>0.01</b>	<b>1.82</b>	<b>0.03</b>	<b>2.72</b>	<b>9.90</b>	<b>5.58</b>	<b>0.80</b>	<b>0.28</b>	<b>3.12</b>	<b>97.15</b>
<b>STD</b>	<b>0.24</b>	<b>0.00</b>	<b>0.15</b>	<b>0.00</b>	<b>0.21</b>	<b>0.01</b>	<b>0.04</b>	<b>0.13</b>	<b>0.06</b>	<b>0.02</b>	<b>0.01</b>	<b>0.15</b>	<b>0.41</b>
<b>RSTD(%)</b>	<b>0.45</b>	<b>0.57</b>	<b>0.80</b>	<b>0.00</b>	<b>11.46</b>	<b>15.49</b>	<b>1.29</b>	<b>1.33</b>	<b>1.03</b>	<b>2.01</b>	<b>2.67</b>	<b>4.94</b>	<b>0.42</b>
<b>P</b>	<b>0.89</b>	<b>1.13</b>	<b>1.59</b>	<b>0.00</b>	<b>22.92</b>	<b>30.98</b>	<b>2.59</b>	<b>2.66</b>	<b>2.05</b>	<b>4.01</b>	<b>5.35</b>	<b>9.87</b>	<b>0.84</b>
<b>CUL-1</b>	52.2	0.903	14.1	0.005	10.7	0.14	2.06	7.16	2.39	0.71	0.15	7.25	97.9
CUL-1	52.3	0.91	14.2	0.005	10.6	0.14	2.05	7.16	2.39	0.71	0.15	7.15	97.9
CUL-1	52.20	0.90	14.10	0.01	11.30	0.14	2.06	7.11	2.44	0.70	0.15	7.55	98.80
CUL-1	52.20	0.90	14.10	0.01	10.70	0.14	2.06	7.16	2.39	0.71	0.15	7.25	97.90
CUL-1	52.40	0.89	14.20	0.01	10.80	0.14	2.08	7.21	2.42	0.70	0.15	7.35	98.50
CUL-1	52.30	0.91	14.20	0.01	10.80	0.14	2.07	7.23	2.39	0.68	0.15	7.22	98.20
<b>Mean</b>	<b>52.27</b>	<b>0.90</b>	<b>14.15</b>	<b>0.01</b>	<b>10.82</b>	<b>0.14</b>	<b>2.06</b>	<b>7.17</b>	<b>2.40</b>	<b>0.70</b>	<b>0.15</b>	<b>7.30</b>	<b>98.20</b>
<b>STD</b>	<b>0.08</b>	<b>0.01</b>	<b>0.05</b>	<b>0.00</b>	<b>0.25</b>	<b>0.00</b>	<b>0.01</b>	<b>0.04</b>	<b>0.02</b>	<b>0.01</b>	<b>0.00</b>	<b>0.14</b>	<b>0.38</b>
<b>RSTD(%)</b>	<b>0.16</b>	<b>0.69</b>	<b>0.39</b>	<b>0.00</b>	<b>2.30</b>	<b>0.00</b>	<b>0.50</b>	<b>0.59</b>	<b>0.90</b>	<b>1.67</b>	<b>0.00</b>	<b>1.93</b>	<b>0.39</b>
<b>P</b>	<b>0.31</b>	<b>1.38</b>	<b>0.77</b>	<b>0.00</b>	<b>4.59</b>	<b>0.00</b>	<b>1.00</b>	<b>1.19</b>	<b>1.80</b>	<b>3.33</b>	<b>0.00</b>	<b>3.85</b>	<b>0.77</b>

Internal	Sr	Zr	Y	H <sub>2</sub> O+	S	CO <sub>2</sub>	FeO
standard	ppm	ppm	ppm	%	%	%	%
MBX-1	482	100	16				
MBX-1	480	98	16				
MBX-1	488	97	18				
MBX-1	486	97	17				
MBX-1		100	16	1.00	0.24	2.83	
MBX-1		98	18	1.10	0.23	2.80	
MBX-1		97	18	1.10	0.23	2.82	
MBX-1		103	18	1.10	0.24	2.77	
<b>Mean</b>	<b>484.00</b>	<b>98.75</b>	<b>17.13</b>	<b>1.08</b>	<b>0.24</b>	<b>2.81</b>	
<b>STD</b>	<b>3.65</b>	<b>2.12</b>	<b>0.99</b>	<b>0.05</b>	<b>0.01</b>	<b>0.03</b>	
<b>RSTD(%)</b>	<b>0.75</b>	<b>2.15</b>	<b>5.79</b>	<b>4.65</b>	<b>2.46</b>	<b>0.94</b>	
<b>P</b>	<b>1.51</b>	<b>4.30</b>	<b>11.57</b>	<b>9.30</b>	<b>4.91</b>	<b>1.89</b>	
ALB-1	750	74	24				
ALB-1	749	75	23				
ALB-1		74	24	1.60	0.23	1.59	
ALB-1		74	24	1.40	0.23	1.61	
ALB-1		74	24	1.50	0.23	1.59	
ALB-1		74	22	1.60	0.23	1.59	
<b>Mean</b>	<b>749.50</b>	<b>74.17</b>	<b>23.50</b>	<b>1.53</b>	<b>0.23</b>	<b>1.60</b>	
<b>STD</b>		<b>0.41</b>	<b>0.84</b>	<b>0.10</b>	<b>0.00</b>	<b>0.01</b>	
<b>RSTD(%)</b>		<b>0.55</b>	<b>3.56</b>	<b>6.28</b>	<b>0.00</b>	<b>0.63</b>	
<b>P</b>		<b>1.10</b>	<b>7.12</b>	<b>12.56</b>	<b>0.00</b>	<b>1.25</b>	
CUL-1	253	53	18				
CUL-1	254	52	18				
CUL-1		53	30	4.10	2.02	4.09	
CUL-1		53	18	4.30	2.06	4.04	
CUL-1		54	23	4.40	2.05	3.98	
CUL-1		54	16	4.20	2.03	4.02	
<b>Mean</b>	<b>253.50</b>	<b>53.17</b>	<b>20.50</b>	<b>4.25</b>	<b>2.04</b>	<b>4.03</b>	
<b>STD</b>	<b>0.71</b>	<b>0.75</b>	<b>5.21</b>	<b>0.13</b>	<b>0.02</b>	<b>0.05</b>	
<b>RSTD(%)</b>	<b>0.28</b>	<b>1.42</b>	<b>25.39</b>	<b>3.04</b>	<b>0.89</b>	<b>1.13</b>	
<b>P</b>	<b>0.56</b>	<b>2.83</b>	<b>50.79</b>	<b>6.08</b>	<b>1.79</b>	<b>2.27</b>	



Table A6.2. Analytical precision based on duplicate pulps of Konuto Lake  
samples analyzed by X-Ray Laboratories Inc.

Sample#	SiO <sub>2</sub> (%)	Al <sub>2</sub> O <sub>3</sub> (%)	TiO <sub>2</sub> (%)	Fe(tot) (%)	Cr <sub>2</sub> O <sub>3</sub> (%)	MnO (%)	MgO (%)	CaO (%)	Na <sub>2</sub> O (%)
B-87-649	52.50	7.62	0.099	9.93	0.14	0.17	11.60	7.71	0.87
B-87-649	52.30	7.58	0.104	9.91	0.14	0.19	11.50	7.66	0.88
CN-90-1-1128	43.70	19.10	0.703	13.50	<0.01	0.49	5.57	7.47	2.26
CN-90-1-1128	43.60	19.00	0.693	13.40	<0.01	0.55	5.55	7.49	2.25
CN-90-3-225	50.00	13.20	0.420	13.70	0.04	0.17	10.10	4.33	1.77
CN-90-3-225	50.20	13.30	0.429	13.60	0.04	0.15	10.10	4.35	1.78
FX-34-872	56.10	13.50	0.609	14.60	<0.01	0.24	2.76	6.32	3.43
FX-34-872	55.90	13.40	0.613	14.50	<0.01	0.23	2.75	6.29	3.42
HOF-5-320	42.00	14.10	0.083	8.24	0.02	0.13	9.88	11.10	1.01
HOF-5-320	41.80	14.20	0.092	8.19	0.02	0.15	9.87	11.00	1.02
NER-23-78	54.50	14.20	0.473	11.20	<0.01	0.16	3.83	6.76	2.60
NER-23-78	54.80	14.20	0.475	11.20	<0.01	0.15	3.85	6.76	2.62
NER-107-823	52.10	14.70	0.324	13.20	0.19	5.51	<0.01	6.37	3.55
NER-107-823	52.10	14.60	0.326	13.10	0.19	5.48	<0.01	6.35	3.53
HOF-2-32	51.10	13.30	0.346	13.60	<0.01	0.16	4.59	4.52	3.65
HOF-2-32	51.10	13.30	0.350	13.60	<0.01	0.11	4.56	4.52	3.67
HOF-5-131	52.10	13.80	0.136	9.80	0.04	0.17	8.33	8.64	3.22
HOF-5-131	52.40	13.90	0.143	9.81	0.04	0.17	8.27	8.70	3.24
NER-116-389	53.10	13.30	0.601	14.20	<0.01	0.20	4.72	8.14	2.62
NER-116-389	52.90	13.30	0.610	14.20	<0.01	0.19	4.69	8.11	2.60
HS95M315-1	54.40	14.00	0.545	14.20	<0.01	0.12	4.60	8.29	1.47
HS95M315-1	54.20	13.90	0.550	14.10	<0.01	0.12	4.58	8.28	1.48
HS96M909	57.60	17.30	0.492	3.95	<0.01	0.06	1.96	3.83	5.16
HS96M909	58.00	17.40	0.495	3.93	<0.01	0.06	1.96	3.86	5.18
<b>Average</b>	<b>51.604</b>	<b>14.008</b>	<b>0.405</b>	<b>11.653</b>	<b>0.039</b>	<b>0.630</b>	<b>5.651</b>	<b>6.952</b>	<b>2.637</b>
<b>Error variance</b>	<b>0.02458</b>	<b>0.0034</b>	<b>2E-05</b>	<b>0.00222</b>	<b>0</b>	<b>0.00035</b>	<b>0.0007</b>	<b>0.00084</b>	<b>0.00012</b>
<b>Precision (%)</b>	<b>0.61</b>	<b>0.83</b>	<b>2.24</b>	<b>0.81</b>	<b>0.00</b>	<b>5.97</b>	<b>0.94</b>	<b>0.83</b>	<b>0.85</b>

Sample#	K <sub>2</sub> O (%)	P <sub>2</sub> O <sub>5</sub> (%)	LOI % (%)	TOTAL (%)	Sr (ppm)	Y (ppm)	Zr (ppm)
B-87-649	0.84	0.02	7.12	98.70	72.00	1.00	24.00
B-87-649	0.83	0.02	7.20	98.30	73.00	1.00	23.00
CN-90-1-1128	0.35	0.11	3.90	97.20	169.00	19.00	68.00
CN-90-1-1128	0.35	0.11	4.75	97.70	168.00	20.00	69.00
CN-90-3-225	0.40	0.04	3.05	97.20	61.00	6.00	33.00
CN-90-3-225	0.40	0.04	3.00	97.40	61.00	5.00	32.00
FX-34-872	0.33	0.06	0.90	98.90	96.00	18.00	32.00
FX-34-872	0.33	0.06	0.95	98.50	95.00	17.00	33.00
HOF-5-320	0.59	<0.01	13.00	100.20	51.00	1.00	15.00
HOF-5-320	0.59	<0.01	13.20	100.10	52.00	1.00	16.00
NER-23-78	0.17	0.06	2.35	96.30	71.00	14.00	32.00
NER-23-78	0.18	0.06	2.25	96.60	72.00	15.00	31.00
NER-107-823	0.55	0.03	1.75	98.30	85.00	8.00	20.00
NER-107-823	0.57	0.03	1.90	98.20	84.00	7.00	21.00
HOF-2-32	1.11	0.03	7.65	100.10	45.00	1.00	19.00
HOF-2-32	1.12	0.04	7.75	100.20	44.00	1.00	20.00
HOF-5-131	0.34	<0.01	2.55	99.10	75.00	6.00	12.00
HOF-5-131	0.34	<0.01	2.55	99.60	78.00	8.00	14.00
NER-116-389	0.81	0.05	1.60	99.40	71.00	16.00	26.00
NER-116-389	0.82	0.05	2.00	99.50	74.00	17.00	26.00
HS95M315-1	0.53	0.05	1.00	99.20	84.00	13.00	23.00
HS95M315-1	0.53	0.04	1.20	99.00	86.00	13.00	25.00
HS96M909	4.85	0.24	3.50	99.10	514.00	11.00	102.00
HS96M909	4.84	0.24	3.45	99.60	511.00	9.00	99.00
<b>Average</b>	<b>0.907</b>	<b>0.058</b>	<b>4.107</b>	<b>98.683</b>	<b>116.333</b>	<b>9.500</b>	<b>33.958</b>
<b>Error variance</b>	<b>3.7E-05</b>	<b>8.3E-06</b>	<b>0.04245</b>	<b>0.05333</b>	<b>1.58333</b>	<b>0.58333</b>	<b>1.04167</b>
<b>Precision (%)</b>	<b>1.35</b>	<b>9.90</b>	<b>10.03</b>	<b>0.47</b>	<b>2.16</b>	<b>16.08</b>	<b>6.01</b>

Sample#	CO <sub>2</sub> (%)	S % (%)	H <sub>2</sub> O(+) (%)	Sample#	CO <sub>2</sub> (%)	S % (%)	H <sub>2</sub> O(+) (%)
HS96M308-1	0.02	0.01	1.8	B-88-847	0.17	0.04	3.9
HS96M308-1	0.04	0.01	1.7	B-88-847	0.19	0.04	4
B-87-631	0.22	0.06	2.9	B-89-1814	0.3	0.09	3
B-87-631	0.23	0.05	2.9	B-89-1814	0.28	0.1	3
HS95M326	<0.01	0.01	2.9	CN-90-1-270	0.13	0.02	0.9
HS95M326	<0.01	<0.01	3	CN-90-1-270	0.15	0.02	0.9
HS95M285	0.56	0.04	2.3	CN-90-3-178	0.05	<0.01	1.9
HS95M285	0.49	0.04	2.2	CN-90-3-178	0.04	0.01	2
HS95M123AA	1.05	0.01	1.4	<b>Average Error variance Precision (%)</b>	<b>0.299</b>	<b>0.098</b>	<b>2.255</b>
HS95M123AA	1.01	<0.01	1.5		<b>0.00027</b>	<b>1.8E-05</b>	<b>0.00342</b>
					<b>10.89</b>	<b>8.65</b>	<b>5.19</b>
NER-111-212	0.05	0.11	2.7				
NER-111-212	0.07	0.12	2.8				
HOF-5-130	0.03	0.33	3.7				
HOF-5-130	0.06	0.34	3.8				
NER-69-19	0.1	0.03	1.7				
NER-69-19	0.11	0.03	1.7				
NER-75-130	1.05	0.25	1.6				
NER-75-130	1.05	0.26	1.7				
NER-84-301	0.18	0.02	1.9				
NER-84-301	0.19	0.02	1.8				
NER-86-468	0.52	0.14	2.1				
NER-86-468	0.52	0.15	2				
NER-98-548	0.06	0.02	2.2				
NER-98-548	0.07	0.02	2.3				
HOF-5-75	0.05	0.15	2.2				
HOF-5-75	0.04	0.15	2.2				
NER-102-104	0.21	0.44	1.4				
NER-102-104	0.21	0.44	1.5				
FX-36-560	0.94	0.06	2.1				
FX-36-560	0.93	0.06	2.1				

## **Appendix 7. Petrographic database**

### **1. Full sample descriptions**

#### **SAMPLE: M-30; Pillowed basaltic flow**

##### **LOCATION INFORMATION:**

Type	Station #/ DH	UTM E	UTM N	Elevation
Rock	30	689910	6060132	322

##### **HAND SAMPLE DESCRIPTION:**

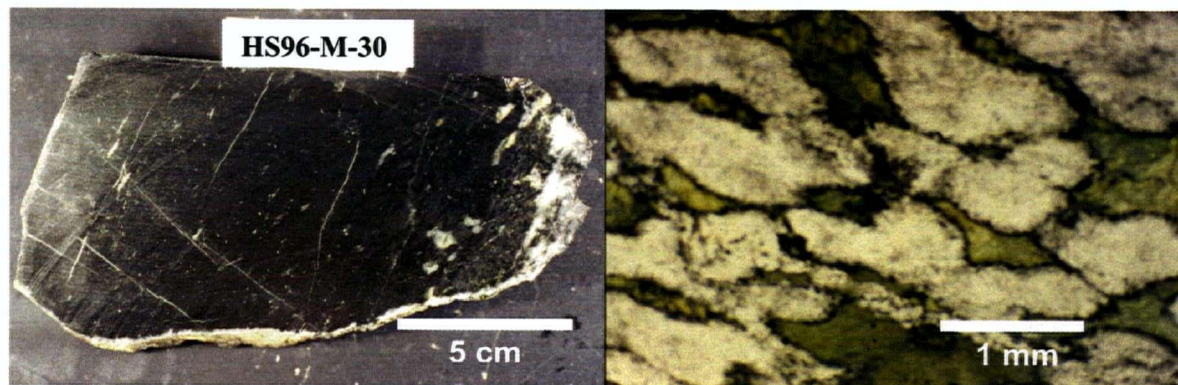
An oval structure, appr. 40 cm. long with spherulitic rind around the margin.

##### **THIN SECTION DESCRIPTION:**

Texture: Spherulitic

Mineralogy:

Mineral	Modal %	Size (mm)	Occurrence
Quartz	70	0.2-3	Abundant spherulites, stretched tangential to the pillow margin
Amphibole	30	0.05-1.5	Fine-grained masses, interstitial to the spherulites



Hand sample

PPL

**SAMPLE: HS96M75-1; Amphibolite after basalt flow**

**LOCATION INFORMATION:**

Type	Station #/ DH	UTM E	UTM N	Elevation
Rock	75	689839	6059766	318

**HAND SAMPLE DESCRIPTION:**

A massive, dark gray-green rock with sub-microscopic (barely visible) granular texture. A dense stockwork of thin (up to 2mm) veinlets of light colour cross-cut the sample with two preferential directions at 75°.

**THIN SECTION DESCRIPTION:**

Texture: Almost equigranular, hypidiomorphic

Mineralogy:

Mineral	Modal %	Size (mm)	Occurrence
Hornblende	60	0.1-0.6	Subhedral, commonly with uneven edges, dominates the sample
Plagioclase	35	0.3-0.4	Fine grained masses, interstitial to the spherulites
Zoisite	4	0.01-0.05	Subhedral, occupies the spaces between the larger and more abundant hornblende crystals
Chlorite	1	0.01-0.5	Participates in the composition of the cross-cutting veinlets

This is a typical sample of one of the varieties of the metamorphosed basaltic rocks in the region, interpreted as the bottom part of lava flows. The important features are: (1) lack of amygdulites (pipe vesicles may be present and should not be confused with amygdulites); (2) slightly granular look in hand sample and coarser texture in thin section; (3) Presence of a dense network of (usually straight) cross-cutting veinlets, in one to three (commonly two) prevailing directions. (4) Most (or all) of the leucocratic phase is in the form of plagioclase. (5) Gray-green colour on a weathered surface (hand sample scale).



PPL, FOV 5 mm.



PPL, FOV 1.5 mm.



**SAMPLE: HS96M75-2; Amphibolite after amygdaloidal basalt flow with**

**LOCATION INFORMATION:**

Type	Station #/ DH	UTM E	UTM N	Elevation
Rock	75	689838	6059766	318

**HAND SAMPLE DESCRIPTION:**

A massive, dark gray aphanitic amygdaloidal rock. Amygdules are as big as 3mm. Thin (up to 2mm) veinlets of light colour cross-cut the sample.

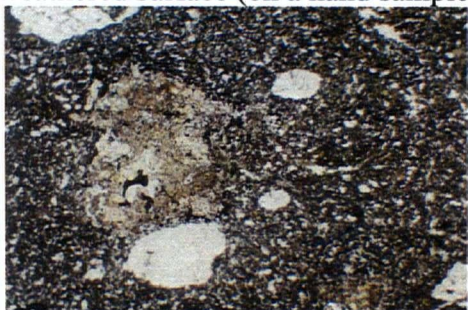
**THIN SECTION DESCRIPTION:**

Texture: Hypidiomorphic equigranular, massive, amygdaloidal (amygdules are the only feature defining a preferred direction, otherwise texture is massive)

**Mineralogy:**

Mineral	Modal %	Size (mm)	Occurrence
Hornblende	57	0.2-0.6	Subhedral, commonly with uneven edges, dominates the sample
Quartz	30	0.2-0.4	Anhedral, occupies the spaces between the larger and more abundant hornblende crystals, forms most of the amygdules (sometimes accompanied by epidote)
Epidote	7	0.03-0.15	Subhedral, constitutes the major part of the cross-cutting veinlets and a subordinate part of the amygdules
Plagioclase	5	0.2-0.1	Subhedral to anhedral, occupies the spaces between the hornblende crystals, together (but subordinated in abundance to) quartz
Opaque mineral(s)	1	0.01-0.5	Occur exclusively in the amygdules or in close association with them

This is a typical sample of one of the varieties of the metamorphosed basaltic rocks in the region, interpreted as the middle to upper parts of the lava flows. The important features are: (1) Amygdaloidal character (pipe vesicles are uncommon); (2) massive and aphanitic; (3) Presence of some (not dense) cross-cutting veinlets, usually not following a specific pattern or prevalent direction; (4) Most of the leucocratic phase is quartz; (5) dark gray colour on a weathered surface (on a hand sample scale).



PPL, FOV 10 mm.

**SAMPLE: HS96M75-3; Sheared and chloritized amphibolite after amygdaloidal basalt**

**LOCATION INFORMATION:**

Type	Station #/ DH	UTM E	UTM N	Elevation
Rock	75	689837	6059766	318

**HAND SAMPLE DESCRIPTION:**

A massive, dark gray aphanitic amygdaloidal rock. Chloritized shears and partings are common. Small (1 mm) amygdules.

**THIN SECTION DESCRIPTION:**

Texture: Intersertal, defined by slightly trachytic hornblende prisms enclosing the leucocratic phases. Crudely schistose defined by alignment of hornblende, chlorite rich shears and elongation of amygdules.

**Mineralogy:**

Mineral	Modal %	Size (mm)	Occurrence
Hornblende	57	0.05-0.2	Subhedral, dominates the sample
Quartz	30	0.03-0.1	Anhedral, occupies the spaces between the larger and more abundant hornblende crystals, forms most of the amygdules (sometimes accompanied by epidote), where size of the crystals are much bigger
Plagioclase	5	0.03-0.15	Subhedral to anhedral, occupies the spaces between hornblende crystals
Epidote	1	0.03-0.1	Subhedral, occurs in shears and veins
Chlorite	1	0.01-0.03	Rare and very fine, occurs in shears
Carbonate	1	0.01-0.1	Rare and very fine, occurs in shears
Opaque minerals	1	0.01-0.5	Occur exclusively in the amygdules or in close association with them



This is a typical sample of one of the varieties of the metamorphosed basaltic rocks in the region, interpreted as the top portion of the lava flows. The important features are: (1) Amygdaloidal character (no pipe vesicles), commonly obliterated by tectonics; (2) Abundant shears and partings; (3) Most of the leucocratic phase is quartz.

PPL, FOV 5 mm.



**SAMPLE: HS96M76; hornblende-quartz-feldspar-porphyritic dacite.**

**LOCATION INFORMATION:**

Type	Station #/ DH	UTM E	UTM N	Elevation
Rock	76	689850	6059879	314

**HAND SAMPLE DESCRIPTION:**

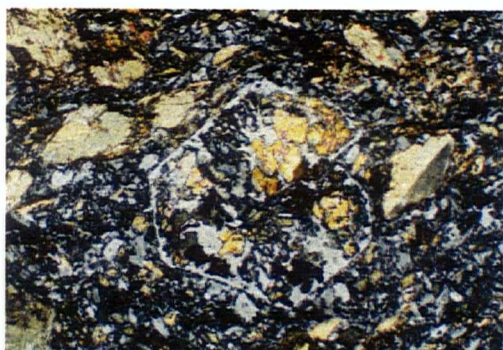
Dark porphyro-aphanitic rock, with medium-grained plagioclase phenocrysts and more scarce quartz phenocrysts, evenly distributed within the melanocratic matrix. Occurs as a 3m thick dyke intruded in basaltic rocks.

**THIN SECTION DESCRIPTION:**

Texture: Bimodal, porphyritic.

Mineralogy:

Mineral	Modal %	Size (mm)	Occurrence
Hornblende	20	0.05-2.0	Euhedral to subhedral, pale green pleochroism, bimodal distribution of sizes
Plagioclase	10	0.5-3.0	Subhedral to euhedral, An < 10 (variety albite), twinned by Carlsbad and Albite laws, occasionally forms glomerocrysts, contains inclusions of zircon, displays evidence of resorption, weakly sericitized
Quartz	5	1.0-3.0	Anhedral, oval in shape, undulatory extinction
Epidote	1	0.02-0.2	Subhedral, occurring only in resorbed plagioclase and (?) quartz phenocrysts
Sericite	<1	v. fine	Developed in plagioclase
Opaque minerals	<1	0.025-0.05	Scarce and disseminated
Ground mass	64	Sub-microscopic	Consists of quartz, plagioclase and hornblende



XPL, FOV 0.7 mm.



XPL, FOV 1.5 mm.



**SAMPLE: HS96M123-A; Hornblende-epidote schist after a hornblende-feldspar porphyritic dacite.**

**LOCATION INFORMATION:**

Type	Station #/ DH	UTM E	UTM N	Elevation
Rock	123	689949	6059566	322

**HAND SAMPLE DESCRIPTION:**

Dark porphyro-aphanitic rock, with medium grained epidote phenocrysts evenly distributed within the melanocratic matrix. Schistosity is defined by micaceous (chlorite, biotite) minerals or hornblende, aligned in one direction. Matrix is melanocratic.

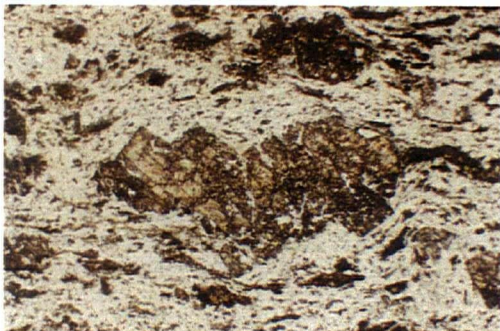
**THIN SECTION DESCRIPTION:**

Texture: Schistose, porphyroblastic

Mineralogy:

Mineral	Modal %	Size (mm)	Occurrence
Epidote	15	0.5-2	Subhedral, in porphyroblastic aggregates (?), 0.5-3 mm in size)
Hornblende	5	0.01-0.75	Subhedral, green pleochroism, forms patches elongate in the foliation direction
Biotite	<1	0.02-0.05	Very scarce
Opaque minerals	<1	0.025-0.05	Scarce and disseminated
Ground mass	80	Sub-microscopic	Dominated by quartz, also including plagioclase and hornblende

Prominent schistosity is defined by elongate aggregates of epidote and amphibole. Coarse (up to 3 mm) isometric aggregates of smaller epidote crystals display shapes characteristic of epidote. They appear as phenocrysts that have been later tectonized, some disaggregated without losing their general shape, some stretched into the foliation.



PPL, FOV 1.5 mm.

**SAMPLE: HS96M123AA; Quartz-feldspar-porphyritic dacite.**

**LOCATION INFORMATION:**

Type	Station #/ DH	UTM E	UTM N	Elevation
Rock	123	689949	6059566	322

**HAND SAMPLE DESCRIPTION:**

Light colour porphyro-aphanitic rock, with medium grained plagioclase phenocrysts and more scarce quartz phenocrysts, evenly distributed within the leucocratic matrix. Occurs as a 5m thick dyke intruded in basaltic rocks.

**THIN SECTION DESCRIPTION:**

Texture: Porphyro-aphanitic.

Mineralogy:

Mineral	Modal %	Size (mm)	Occurrence
Plagioclase	30	0.5-5.0	Subhedral to euhedral, An < 10 (variety albite), twinned by Carlsbad law and only rarely by Albite law, commonly shows zonal growth patterns, contains inclusions of epidote, intensively sericitized.
Quartz	8	1.0-10.0	Anhedral to subhedral, undulatory extinction Recrystallized where in proximity to veinlets
Epidote	2	0.02-0.2	Subhedral, occurring in plagioclase phenocrysts and scattered throughout the sample
Biotite	<1	0.02-0.1	Very scarce, along veinlets
Sericite	<1	v. fine	Ubiquitously developed in plagioclase
Chlorite	<1	v. fine	Developed in veins
Carbonate	<1	0.01-0.2	Developed in veins
Opaque minerals	<1	0.025-0.05	Scarce and disseminated
Ground mass	60	Sub-microscopic	Consists of quartz and plagioclase

Quartz-chlorite-carbonate veinlets up to 0.2mm wide cross-cut the rock

**SAMPLE: HS96M156; Silicified and sericitized hornblende rich rock.**

**LOCATION INFORMATION:**

Type	Station #/ DH	UTM E	UTM N	Elevation
Rock	156	689184	6060342	327

**HAND SAMPLE DESCRIPTION:**

The rock consists of patchy domains of light and overall dark colour. Aphanitic texture.

**THIN SECTION DESCRIPTION:**

Texture: Patchy, fine-grained, silicic alteration in an aphanitic equigranular rock.

**Mineralogy:**

Mineral	Modal %	Size (mm)	Occurrence
Quartz	45	0.05-0.5	Fine grained and anhedral, in irregular masses, flooding the rock in lobes and patches
Hornblende	17	0.05-0.7	Subhedral (fine crystals are commonly euhedral, long prismatic), green pleochroism, dominates the dark portions of the sample, enclosing the remaining phases
Plagioclase	20	0.5-1.0	Extremely sericitized and otherwise altered
Zoicite	8	0.05-0.2	Subhedral, in dense accumulations, or among fine quartz or coarser hornblende
Sericite	7	v. fine	Ubiquitously developed in plagioclase to a degree of complete replacement of the latter
Epidote	<1	0.02-0.2	Subhedral, scarce
Chlorite	<1	v. fine	Developed in veins
Opaque minerals	<1	0.025-0.05	Scarce and disseminated

**SAMPLE: HS96M157; Intensely silicified plagioclase rich rock.**

**LOCATION INFORMATION:**

Type	Station #/ DH	UTM E	UTM N	Elevation
Rock	157	689225	6060194	322

**HAND SAMPLE DESCRIPTION:**

Porphyro-aphanitic rock with rounded, medium-grained leucocratic, plagioclase phenocrysts enclosed in a matrix of intermediate colour index. Fine-grained black minerals, scattered throughout the ground mass cause a spotty appearance.

**THIN SECTION DESCRIPTION:**

Texture: Patchy texture defined by quartz flooding and alteration of the original minerals.

**Mineralogy:**

Mineral	Modal %	Size (mm)	Occurrence
Quartz	60	0.02-0.5	Subhedral, bands made up of fine grained quartz, surrounding coarser grains
Plagioclase	30	0.2-0.5	Subhedral to euhedral, An < 10 (variety albite), twinned by Carlsbad Albite laws, intensively sericitized
Hornblende	4	0.1-0.5	Anhedral remnant grains with uneven and resorbed edges, chloritized and developed in close association with epidote
Epidote	3	0.02-0.2	Subhedral, occurring in association with remnant hornblende and in thin veinlets
Chlorite	2	0.02-0.05	Developed after hornblende
Sericite	1	v. fine	Ubiquitously developed in plagioclase
Carbonate	<1	0.01-0.2	Developed in veins
Opaque minerals	<1	0.025-0.05	Scarce and disseminated

Epidote, sericite and carbonate veinlets up to 0.2mm wide cross-cut the rock, but are in turn cross-cut and obliterated by bands of fine-grained quartz.

**SAMPLE: HS96M240-1; Gabbro**

**LOCATION INFORMATION:**

Type	Station #/ DH	UTM E	UTM N	Elevation
Rock	240	690249	6061528	322

**HAND SAMPLE DESCRIPTION:**

A massive, medium gray, fine- to medium-grained phaneritic rock - gabbro.

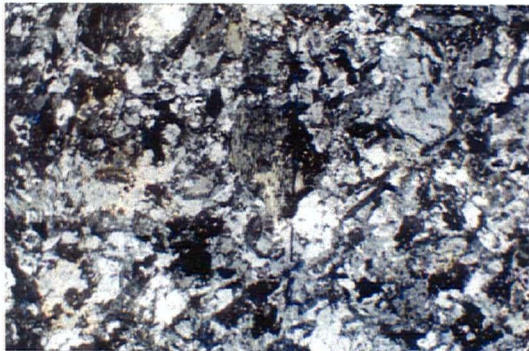
**THIN SECTION DESCRIPTION:**

Texture: Hypidiomorphic granular, bimodal

Mineralogy:

Mineral	Modal %	Size (mm)	Occurrence
Clinopyroxene	63	0.2-2.0	Subhedral, forms larger phenocrysts as well as smaller crystals, edges are commonly uneven and splintered due to alteration
Plagioclase	27	0.03-0.15	Subhedral, occupies the spaces between Clinopyroxene crystals
Zoisite	8	0.01-0.1	
Carbonate	1	0.01-0.1	Occurs in sub-horizontal lenses and shears
Opaque minerals	1	0.01-0.5	Occur exclusively in the amygdules or in close association with them

This is a typical sample of one of the varieties of the metamorphosed basaltic rocks in the region, interpreted as the top portion of the lava flows. The important features are: (1) Amygdaloidal character (no pipe vesicles), commonly obliterated by tectonics; (2) Abundant shears and partings; (3) Most of the leucocratic phase is quartz.



XPL, FOV 5 mm.



**SAMPLE: HS96M315-1; Massive, fine-grained amphibolite after a basalt precursor.**

**LOCATION INFORMATION:**

Type	Station #/ DH	UTM E	UTM N	Elevation
Rock	315	690944	6060507	326

**HAND SAMPLE DESCRIPTION:**

Very fine-grained dark green-gray rock. Possibly microgabbro or recrystallized basalt.

**THIN SECTION DESCRIPTION:**

Texture: Fine-grained, equigranular, very slightly schistose

**Mineralogy:**

Mineral	Modal %	Size (mm)	Occurrence
Hornblende	75	0.2-0.75	Subhedral (fine crystals are commonly euhedral, long prismatic), green pleochroism, dominates the sample, enclosing the remaining phases
Quartz	12	0.02-0.15	Anhedral; undulatory extinction
Epidote	2	0.01-0.05	Subhedral, in patches, commonly associated with opaque minerals
Opaque minerals	1	0.025-0.05	Scarce and disseminated, associated with epidote patches
Groundmass	10	0.01-0.5	Occur exclusively in the amygdules or in close association with them

This is a typical sample of one of the varieties of the metamorphosed basaltic rocks in the region, interpreted as the bottom part of lava flows. The important features are: (1) lack of amygdules (pipe vesicles may be present and should not be confused with amygdules); (2) slightly granular look in hand sample and coarser texture in thin section; (3) Gray-green colour on a weathered surface (hand sample scale).



PPL, FOV 1.5 mm.

**SAMPLE: HS96M315-2; Silicified intrusive contact.**

**LOCATION INFORMATION:**

Type	Station #/ DH	UTM E	UTM N	Elevation
Drill core	315	690944	6060507	326

**HAND SAMPLE DESCRIPTION:**

Aphyric, silicified rock, cut by a dense stockwork of thin dark green veinlets. The domains enclosed in the stockwork are light pink to white.

**THIN SECTION DESCRIPTION:**

Texture: Fine grained, equigranular, massive

Mineralogy:

Mineral	Modal %	Size (mm)	Occurrence
Plagioclase	50	0.025-0.15	Subhedral, An < 10 (variety albite), commonly contains inclusions of zircon (?), sericite
Quartz	45	0.02-0.15	Anhedral; undulatory extinction
Hornblende	5	0.01-0.75	Subhedral; green pleochroism, forms irregular patches
Epidote	<1	0.01-0.05	Subhedral, in scarce thin (0.08mm) veinlets
Sericite	<1	fine	Developed in plagioclase
Opaque phases	<1	0.025-0.05	Scarce and disseminated

Plagioclase and quartz are intergrown in a fine-grained massive aggregate. Hornblende forms patches up to 5mm. Scarce fine epidote cross-cutting veinlets.



PPL, FOV 5 mm.



**SAMPLE: HS96M315-3; Gabbro.**

**LOCATION INFORMATION:**

Type	Station #/ DH	UTM E	UTM N	Elevation
Rock	315	690944	6060507	326

**HAND SAMPLE DESCRIPTION:**

Equigranular fine- to medium-grained, melanocratic, phaneritic rock. Massive texture. Scarce pyrrhotite is visible as irregular patches.

**THIN SECTION DESCRIPTION:**

Texture: medium-grained, hypidiomorphic granular.

**Mineralogy:**

Mineral	Modal %	Size (mm)	Occurrence
Plagioclase	50	0.5-2.5	Subhedral, An = 45 (?), Carlsbad twinning common, albite twinning - scarce, moderate to strong sericite alteration
Hornblende	43	0.5-3.5	Pseudomorphs after clinopyroxene, some smaller grains are subhedral, green pleochroism
Epidote	1	0.01-0.1	Subhedral, scattered throughout the rock
Sericite	5	v. fine	In patches associated with plagioclase
Chlorite	<1	v. fine	Along thin veinlets, associated with epidote
Opaque phases	1	0.025-0.05	Scarce and disseminated, including several large (0.75 mm) skeletal crystals of titanomagnetite (?)



XPL, FOV 5 mm.



**SAMPLE: HS96M328-1; Intensively altered (silicified) contact between a plagioclase-rich rock (gabbro or diorite) and an aphanitic rock (possibly basalt). The gabbro-diorite part.**

**LOCATION INFORMATION:**

Type	Station #/ DH	UTM E	UTM N	Elevation
Rock	328	690498	6062570	315

**HAND SAMPLE DESCRIPTION:**

Equigranular rock (fine- to medium-grained) of intermediate colour, the prominent constituents being light-coloured small (up to 1mm) crystals, possibly plagioclase and very fine melanocratic minerals. Veinlets and pockets of dark material, possibly chlorite cross-cut the sample. Small quartz lenses subparallel to the contact. The contact itself is defined by a 1mm thick quartz-carbonate veinlet.

**THIN SECTION DESCRIPTION:**

Texture: (1) Relict, bimodal, after porphyroaphanitic

Mineralogy:

Mineral	Modal %	Size (mm)	Occurrence
Quartz	60	0.05-0.2	Anhedral, constituting the ground mass
Plagioclase	30	0.2-1.5	Subhedral to euhedral, An < 10 (variety albite), twinned by Carlsbad Albite laws, intensively sericitized, displays zonal growth, erosion of the outer surface by quartz
Carbonate	5	0.1-0.6	In pockets adjacent to plagioclase grains (increasingly abundant towards the contact and in veins)
Chlorite	2	0.02-0.2	Associated with biotite, disseminated
Epidote	1	0.01-0.1	Subhedral, disseminated
Biotite	1	0.02-0.2	Disseminated, associated with chlorite
Sericite	1	v. fine	Ubiquitously developed in plagioclase
Opaque phases	<1	0.025-0.05	Scarce and disseminated

**SAMPLE: HS96M328-2; Intensively altered (silicified) contact between a plagioclase-rich rock (gabbro or diorite) and an aphanitic rock (possibly basalt). The altered basalt part.**

**LOCATION INFORMATION:**

Type	Station #/ DH	UTM E	UTM N	Elevation
Rock	328	690498	6062570	315

**HAND SAMPLE DESCRIPTION:**

Strongly foliated rock. Colour is pale to more intense gray-green. Foliation is inclined with regard to the contact. The contact itself is defined by a 1mm thick quartz-carbonate veinlet.

**THIN SECTION DESCRIPTION:**

Texture: Foliated and banded, fine grained, equigranular

**Mineralogy:**

Mineral	Modal %	Size (mm)	Occurrence
Quartz	55	0.02-0.12	Anhedral, size varying in different bands
Chlorite	20	0.01-0.1	Forming most of some of the bands, some pseudomorphs after hornblende
Carbonate	10	0.01-0.2	Developed in veins and patches
Plagioclase	9	0.1-0.5	Subhedral
Zoisite	3	0.05-0.6	Subhedral, participates in the chlorite-rich bands
Hornblende	2	0.1-0.6	Anhedral remnant grains with uneven and resorbed edges, chloritized and with zoisite developed in close association
Sericite	1	v. fine	Ubiquitously developed in plagioclase
Opaque phases	<1	0.025-0.05	Scarce and disseminated

Contact is defined by a veinlet, about 2 mm thick, made up of relatively coarse-grained quartz, carbonate, chlorite, and zoisite.

**SAMPLE: HOF-5-67.8-2; Tectonized lava flow**

**LOCATION INFORMATION:**

Type	Station #/ DH	UTM E	UTM N	Elevation
Drill core	HOF-5; 67.8m	689580	6060065	268

**HAND SAMPLE DESCRIPTION:**

Intensely foliated and mylonitized mafic volcanic rock. Pervasively chloritized. Pyrite lenses and quartz lenses stretched in foliation. Very fine grained.

**THIN SECTION DESCRIPTION:**

Texture: Mylonitic

Mineralogy:

Mineral	Modal %	Size (mm)	Occurrence
Chlorite	5	0.01-0.1	Anhedral to pseudomorphous after amphibole
Quartz	5	0.01-0.05	Anhedral, rarely forms lenticular aggregates, possibly stretched amygdules
Opaque phases	3	0.005-0.03	Small subhedral crystals, stretched lenses up to 1-2 cm are common
Groundmass	87		Consists of amphibole, quartz

This is a typical sample of one of the varieties of the metamorphosed basaltic rocks in the region, interpreted as the top portion of the lava flows. The important features are: (1) Strong shearing and foliation; (2) Strong chloritic alteration; (3) Abundance of opaque minerals. Quartz lenses, stretched into foliation suggest amygdaloidal character of the parent rock.

## 2. Brief sample descriptions

M-1	Altered gabbro with no plagioclase remaining, appr. 20% clinozoisite
M-18	Quartz-plagioclase porphyritic dacite
M-20	Flow bottom with some quartz veining
M-21	Flow bottom with some quartz -epidote-carbonate veins and lenses
M-37	Typical flow bottom
M-43	Recrystallized (relatively coarse) hornblende-rich rock (amphibolite-basalt) containing epidosite domain
M-30	Basaltic pillow with spherulitic rind
M-108	Mylonitized and silicified rock, some hornblende remaining
M-170-2	Flow bottom (atypical - too much quartz) with epidosite
M-281	Microgabbro - basaltic flow bottom (extreme crystallization) or gabbro sill
M-286	Mylonitized and altered gabbro
M-291-2	Silicified, clinozoisite - mineralized tuff(?)
M-292	Middle parts of a basalt flow - amygdaloidal, epidote-carbonate-chlorite vein
M-293	Gabbro
M-294	Flow bottom, atypical (plagioclase-rich)
M-295	Flow bottom
M-298	Plagioclase phyric tonalite (granodiorite). (plagioclase-75%, quartz - 15%, hornblende-10%, biotite-5%)
M-308-2	Flow bottom with a pipe vesicle
M-326	Sheared and mylonitized gabbro
HOF-2-119	Flow bottom with quartz lenses
HOF-5-58	Mylonite, very fine grained - 0-0.02mm, chloritic, some coarse opaques, quartz, hornblende lenses
HOF-5-58.1	Flow bottom
HOF-5-67.8-1	Mylonite with domains and bands of less intensively tectonized amygdaloidal basalt
HOF-5-67.8-2	Mylonite with some amygdules (quartz-filled) and hornblende domains remaining as lenses
HOF-5-67.8-3	Flow bottom with quartz - carbonate - chlorite - clinozoisite veins
HOF-5-68	Flow bottom with some quartz and epidote veins
HOF-5-70.1	Flow bottom with an epidosite band (fine epidote and coarser hornblende in wavy laths), X-cut by quartz - chlorite vein.
HOF-5-127	Flow bottom
HOF-5-224	Flow bottom with abundant quartz and chlorite veinlets
HOF-5-297	Flow bottom
HOF-5-320	Carbonate-rich mylonite with some remnant pyroxene grains
HOF-5-348	Gabbro, carbonatized (30%) and chloritized
NER-73-109	Flow bottom with some quartz - epidote veins
NER-75-130	Sheared and silicified rock (no hornblende remaining), chlorite-epidote - pyrite veinlets

NER-78-129	Chloritized mylonite
NER-78-212	Flow bottom with quartz – chlorite - carbonate veinlets
NER-78-279	Flow bottom with strong silicification (domains)
NER-80-150	Mylonite, silicified, possibly tuffaceous
NER-82-146	Carbonatized mylonite
NER-84-5	Flow bottom with quartz – chlorite – carbonate - opaque mineral veinlets
NER-84-260	Carbonatized mylonite, possibly tuffaceous
NER-84-335	Flow bottom
NER-86-62	Flow bottom with quartz - epidote veinlets and x-cutting chlorite veinlets
NER-86-168	Intermediate parts of flow, quartz - epidote veinlet and amygdule
NER-86-250	Flow bottom with quartz - epidote veinlets
NER-98-100	Microgabbro - flow bottom
NER-102-204	Upper part of flow, somewhat sheared, amygdaloidal, very hornblende-rich
NER-105-224	Flow bottom with some quartz - epidote and quartz – chlorite veinlets
NER-105-390	Flow bottom with quartz - epidote veinlets
NER-105-540	Carbonate flooded mylonite, some quartz and quartz - carbonate lenses and veinlets
NER-102-450	Flow bottom
NER-102-543	Flow bottom with some quartz - epidote veinlets
NER-105-724	Intermediate or bottom part of flow - amphibolite with mostly quartz as the leucocratic phase
NER-107-246	Flow bottom
NER-107-722	Flow bottom
NER-107-823	Upper part of flow, some shearing, amygdaloidal (weakly), quartz - carbonate and epidote veinlets
NER-107-1002	Clinozoisite microgabbro
NER-107W1-764	Intermediate part of flow - some amygdules
NER-111-198	Hornblende - quartz rock, similar to flow bottom, but with mostly quartz as the leucocratic phase
NER-111-212	Silicified (with some quartz) flow bottom
NER-122-135	Gabbro with some schistosity defined by chlorite
NER-122-144	Intensively silicified rock with very little melanocratic minerals left. Quartz, plagioclase (sericitized) rock
NER-122-150	Clinozoisite - hornblende rock, very fine grained
NER-122-173	Intensively carbonatized and chloritized gabbro. No pyroxenes left

## **Appendix 8**

### **Spatial distribution of alteration according to various lithogeochemical parameters**

Study of spatial distribution of alteration was one of the major goals of this study. Various lithogeochemical parameters were used, all based on MER methodology. Because different MER plots emphasize different aspects of alteration the resulting spatial patterns differ. This appendix contains spatial patterns (Fig. 4.A.1 through 4.A.10) shown in plan view (for the Konuto Lake, Birch Lake and Flexar deposits) and cross-section (for Konuto Lake deposit only). They are based on 5 lithogeochemical parameters discussed in the text (see also Figures 4.10 through 4.14).

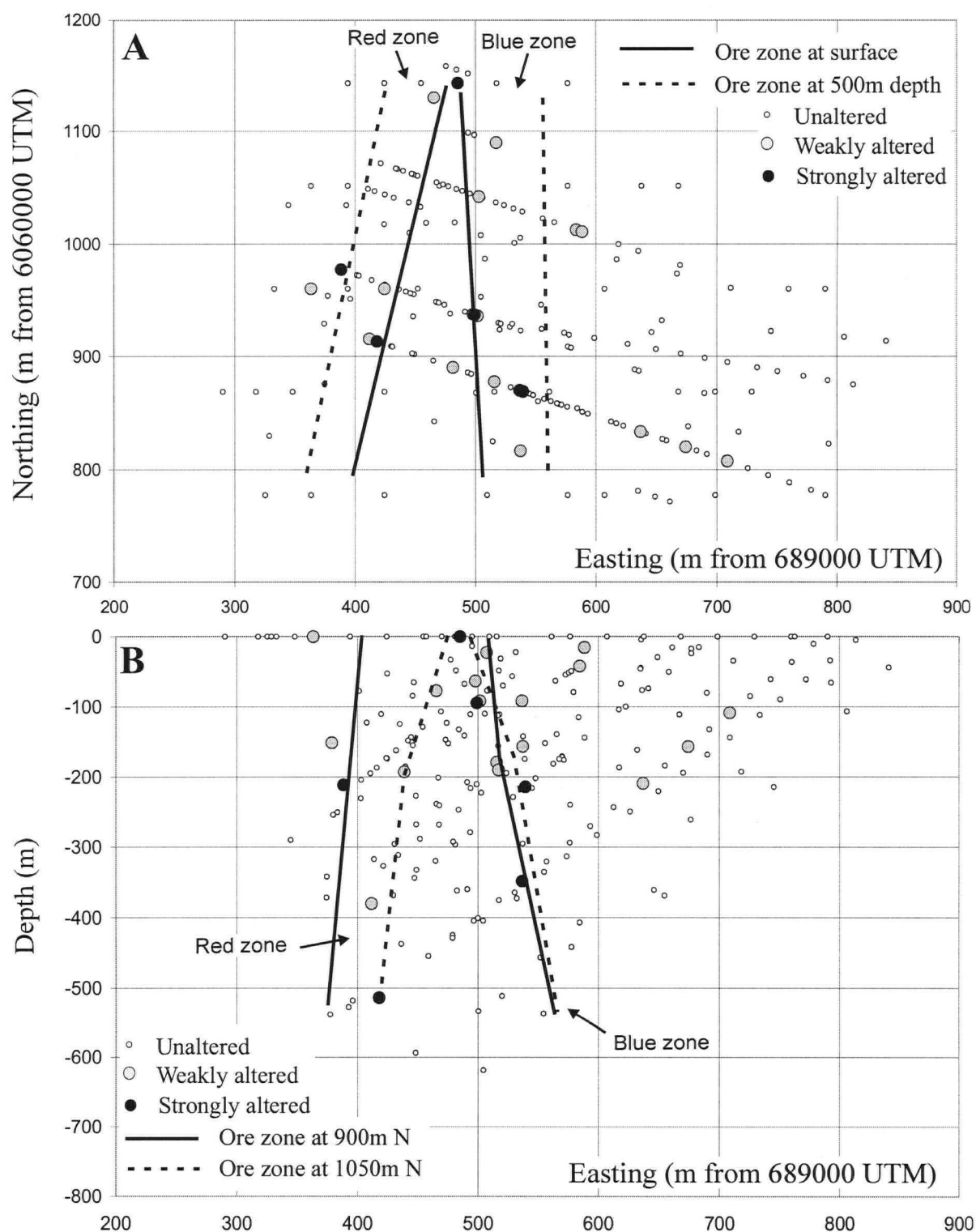


Fig. A8.1. Spatial distribution of hydrothermal alteration in the vicinity of the Konuto Lake deposit (NER claim), based on the plagioclase - clinopyroxene phase discrimination plot (Fig. 4.13). Samples with negative values for the parameter  $Ca+Na-Al$  are considered altered. Most altered samples occur between, or a short distance from the two mineralized zones. A. Plane view; B. Cross section

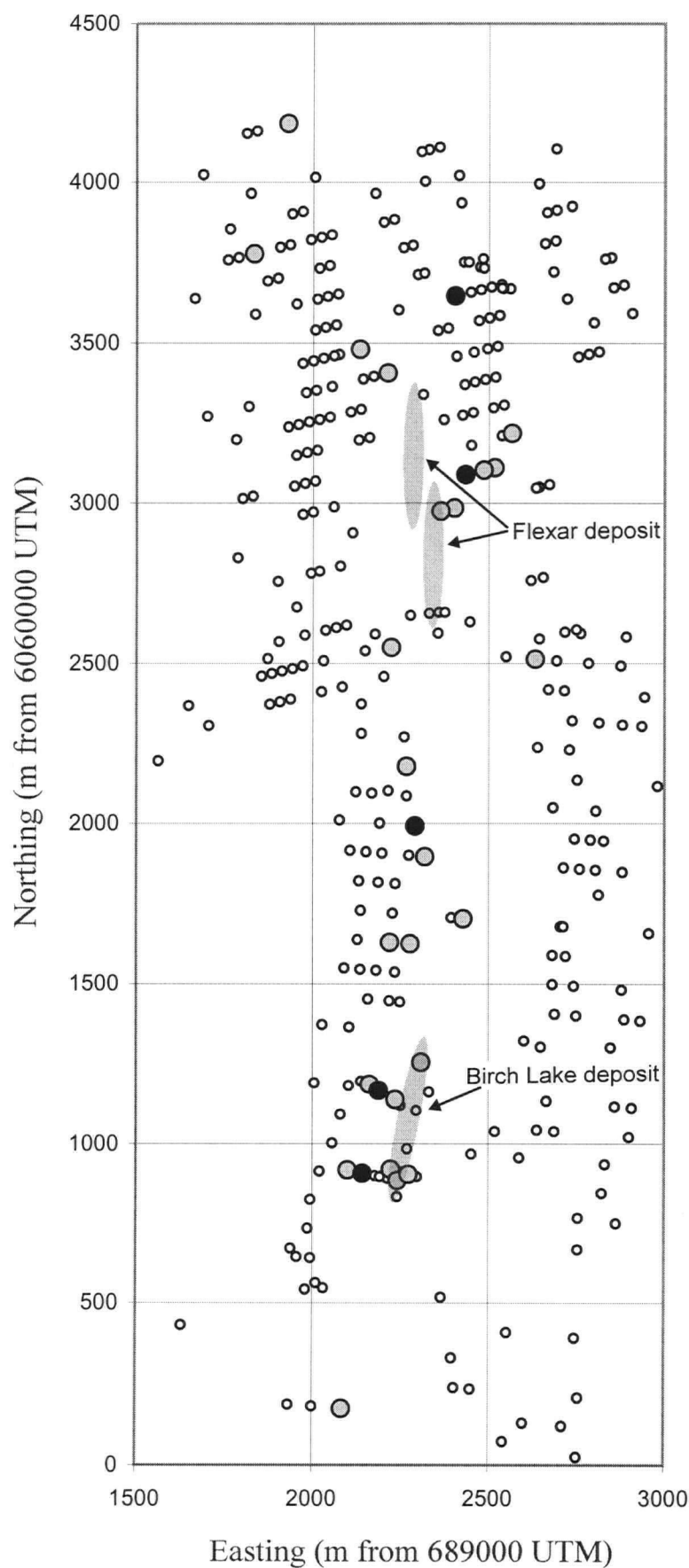


Fig. A8.2. Spatial distribution of hydrothermal alteration in the vicinity of the Birch Lake and Flexar deposits, based on the plagioclase - clinopyroxene phase discrimination plot, (Fig. 4.13). Samples with negative values for the parameter  $2Ca+Na-Al$  are considered altered. Most altered samples occur in proximity to the ore bodies.

- Unaltered
- Weakly altered
- Strongly altered
- Ore body



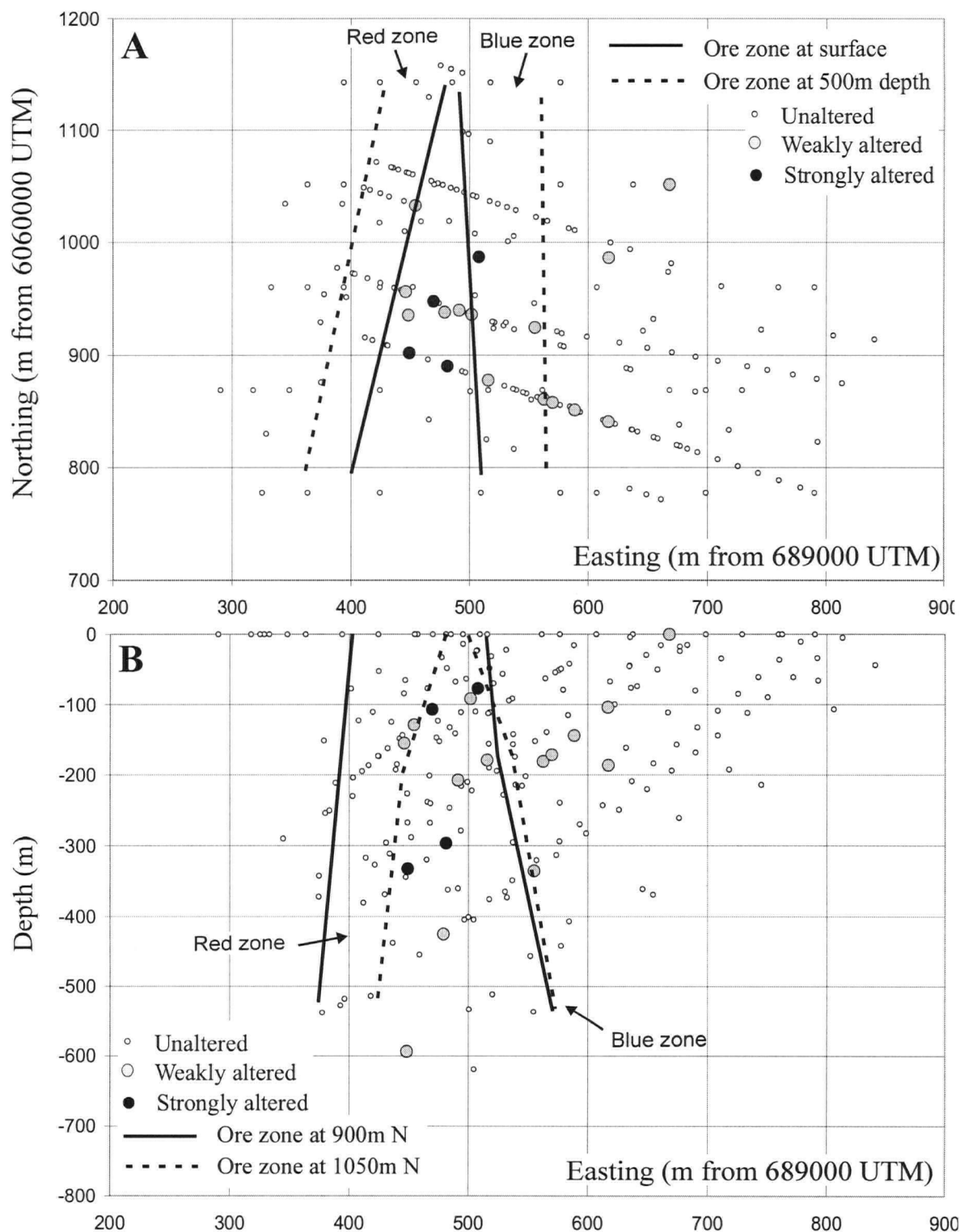


Fig. A8.3. Spatial distribution of hydrothermal alteration in the vicinity of the Konuto Lake deposit (NER claim), based on a plot projecting from plagioclase. the parameter  $(\text{Si-Ca-1/2Al-5/2Na}) / (\text{Fe+Mg})$  is used to classify samples as strongly altered, weakly altered and unaltered. Most altered samples occur between, or a short distance from the two mineralized zones.

A. Plane view; B. Cross section

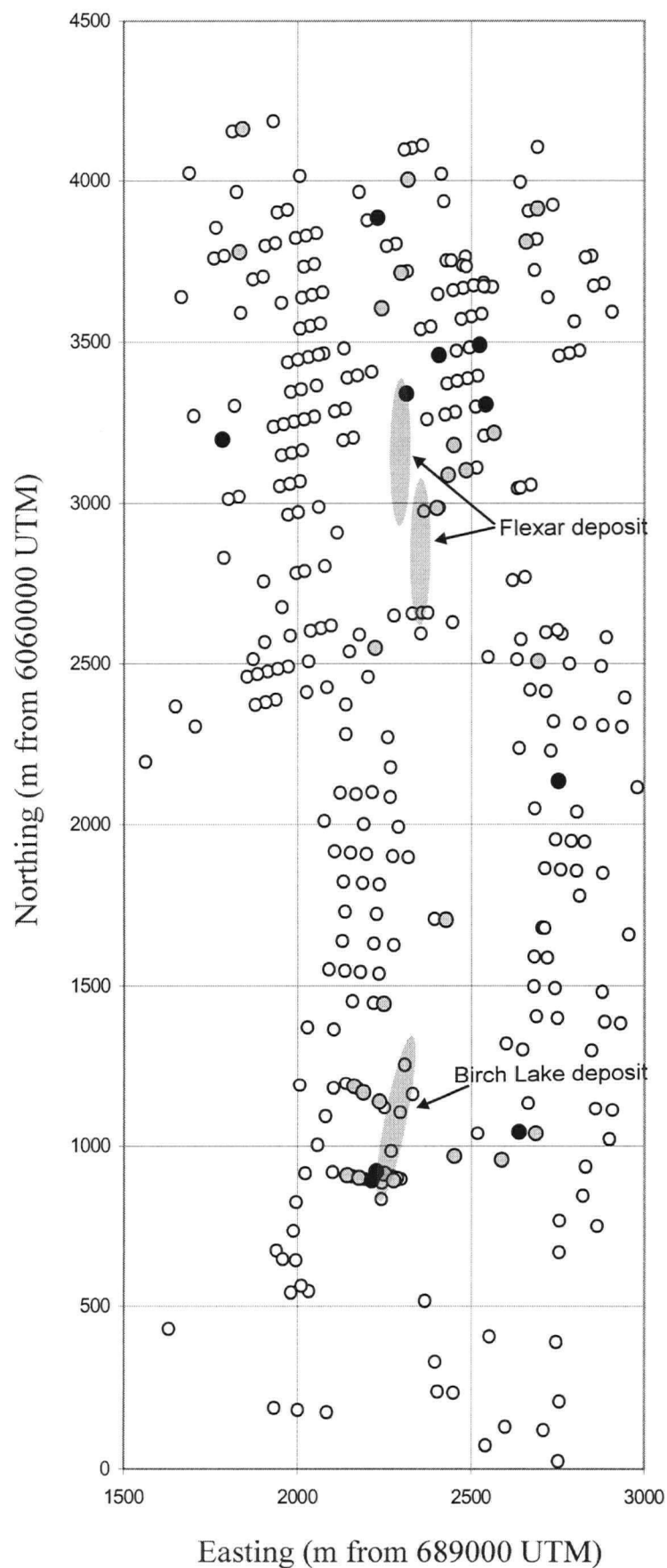


Fig. A8.4. Spatial distribution of hydrothermal alteration in the vicinity of the Birch Lake and Flexar deposits, based on a plot projecting from plagioclase, (not shown). The parameter  $(\text{Si-Ca}-1/2\text{Al}-5/2\text{Na}) / (\text{Fe}+\text{Mg})$  is used to classify the samples as strongly altered, weakly altered and unaltered. Most altered samples occur in proximity to the ore bodies.

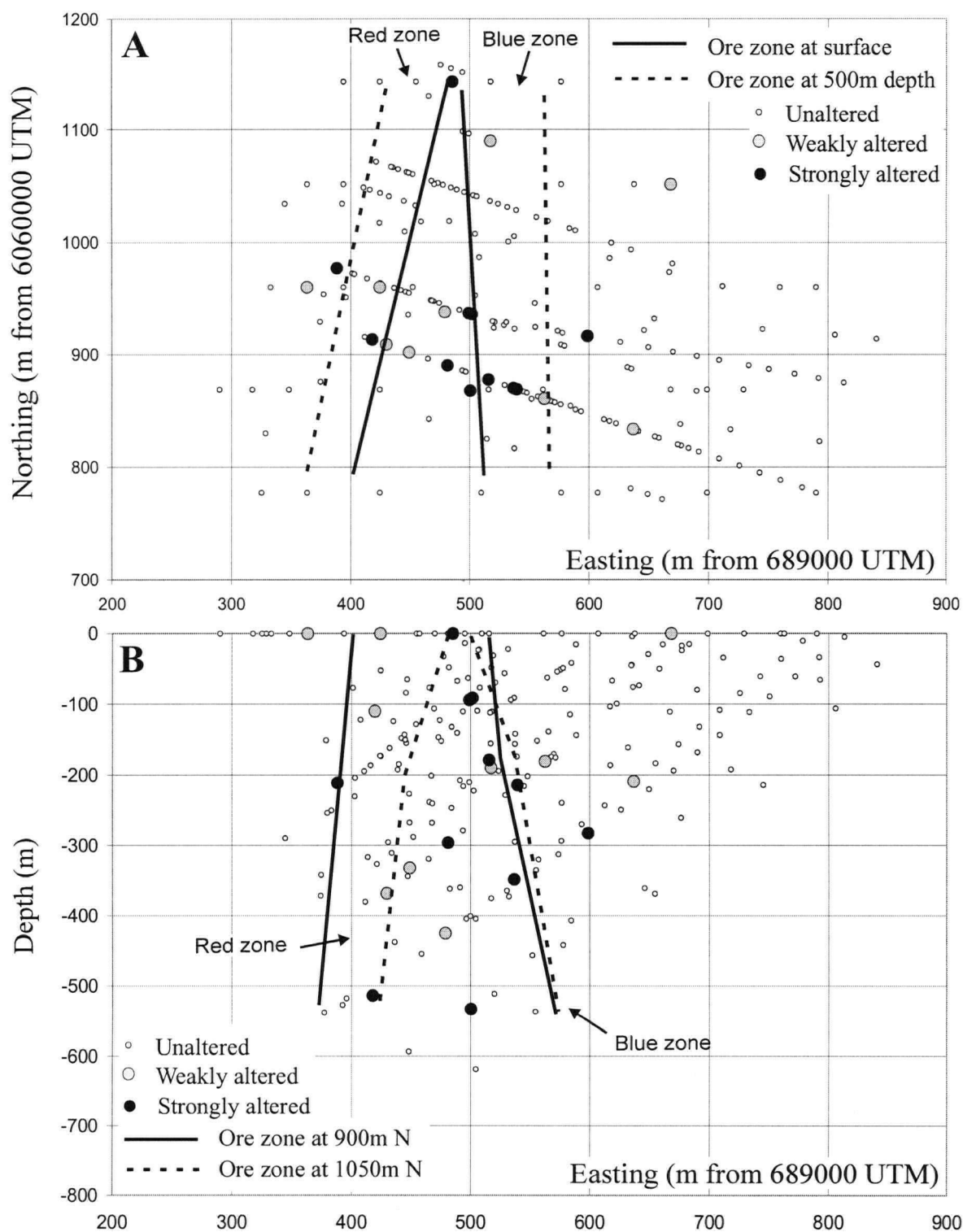


Fig. A8.5. Spatial distribution of hydrothermal alteration in the vicinity of the Konuto Lake deposit (NER claim), based on a plot modelling plagioclase and clinopyroxene fractionation (Fig. 4.11). The parameter  $\text{Si} / (3\text{Na} + 2\text{Ca})$  is used to classify samples as strongly altered, weakly altered and unaltered. Most altered samples occur between, or a short distance from the two mineralized zones.

A. Plane view; B. Cross section

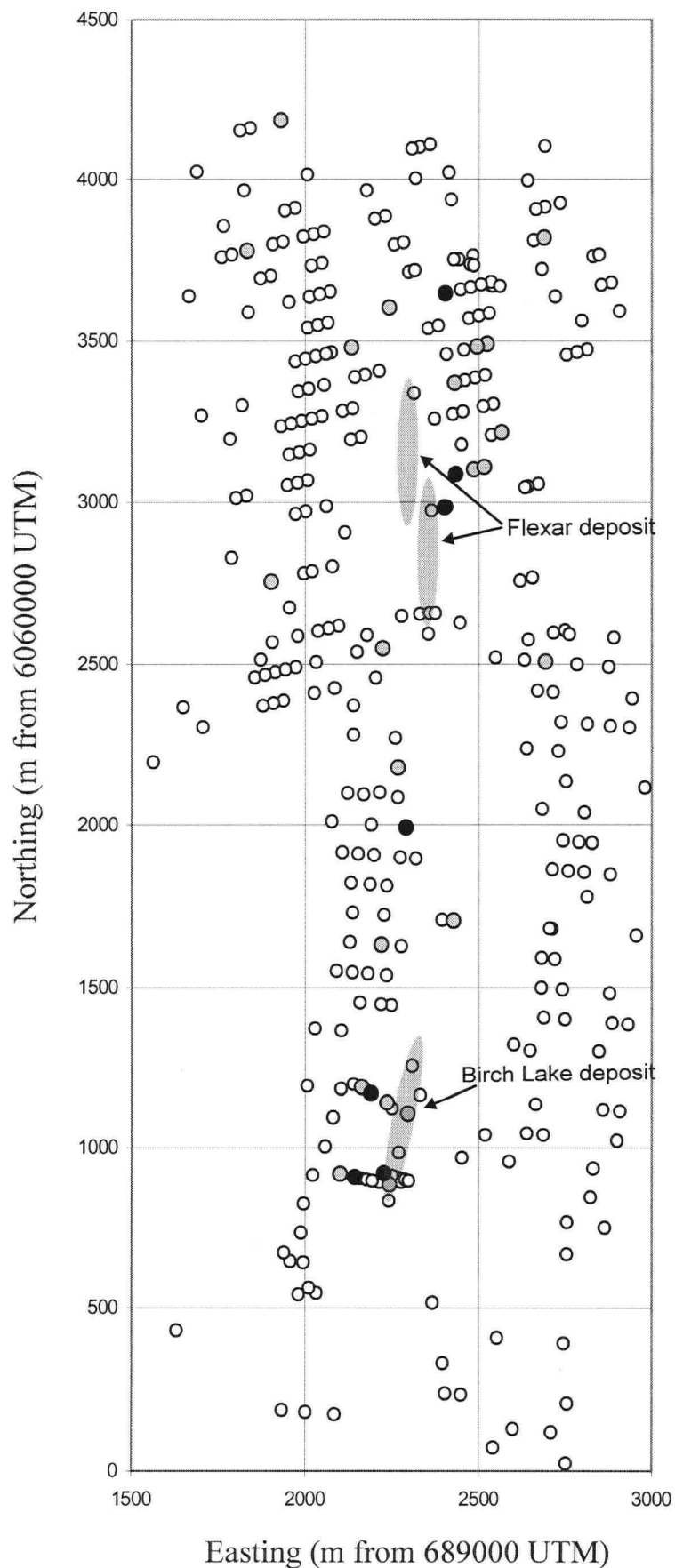


Fig. A8.6. Spatial distribution of hydrothermal alteration in the vicinity of the Birch Lake and Flexar deposits, based on a plot modelling fractionation of plagioclase and clinopyroxene, (Fig. 4.11). The parameter  $\text{Si} / (3\text{Ca} + 2\text{Na})$  is used to classify the samples as strongly altered, weakly altered and unaltered. Most altered samples occur in proximity to the ore bodies.

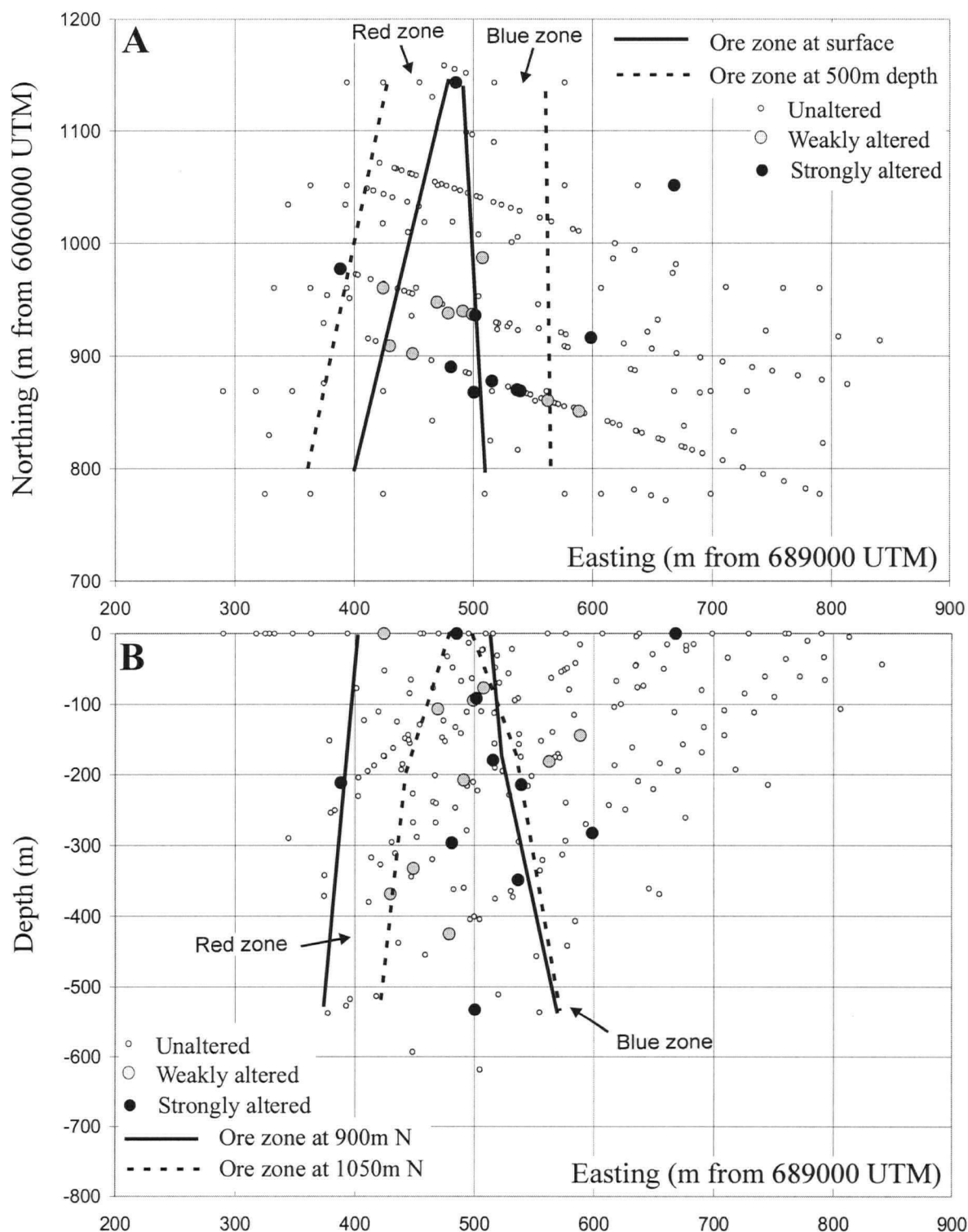


Fig. A8.7. Spatial distribution of hydrothermal alteration in the vicinity of the Konuto Lake deposit (NER claim), based on a plot modelling plagioclase, clinopyroxene and olivine fractionation (Fig. 4.12). The parameter  $\text{Si} / (1/2\text{Fe} + 1/2\text{Mg} + 1/4\text{Al} + 3/2\text{Ca} + 11/4\text{Na})$  is used to classify samples as strongly altered, weakly altered and unaltered. Most altered samples occur between, or a short distance from the two mineralized zones.

A. Plane view; B. Cross section

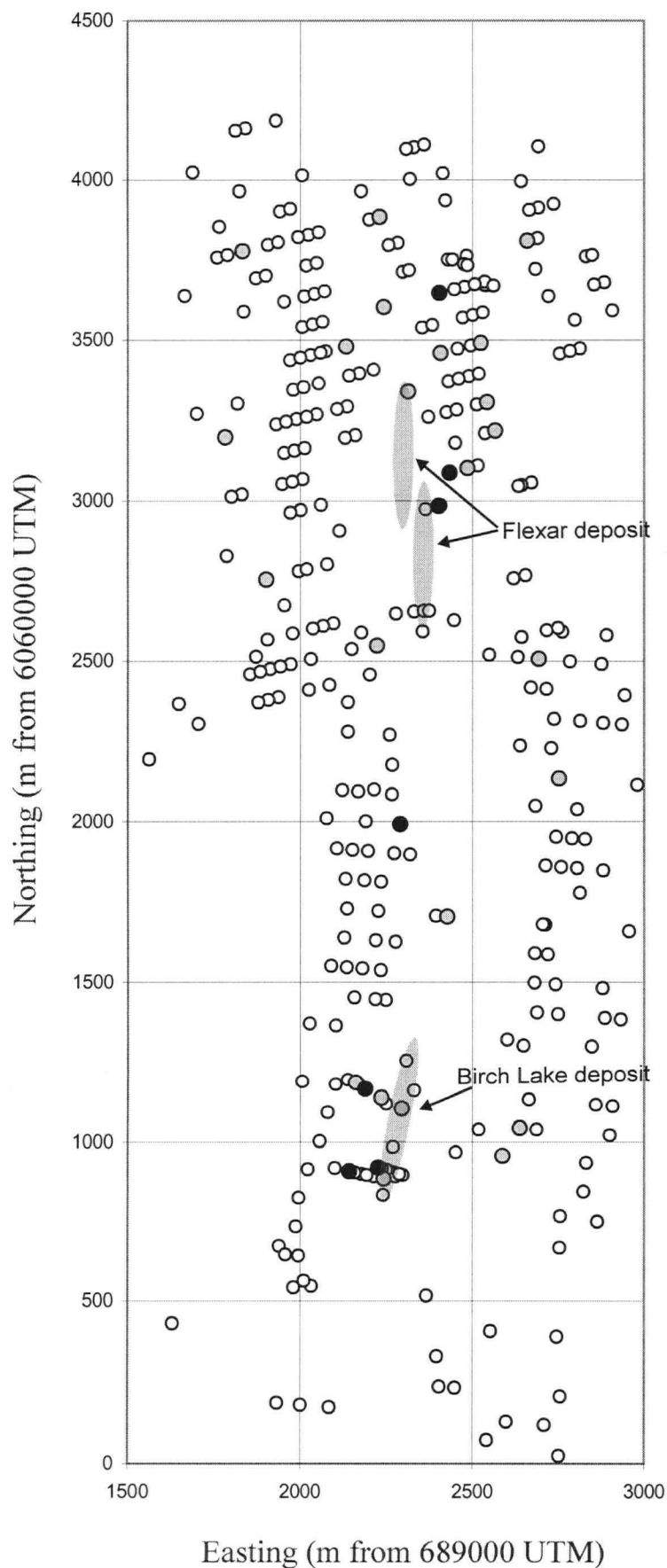


Fig. A8.8. Spatial distribution of hydrothermal alteration in the vicinity of the Birch Lake and Flexar deposits, based on a plot modelling fractionation of plagioclase, clinopyroxene and olivine (Fig. 4.11). The parameter  $\text{Si} / (1/4\text{Al} + 1/2\text{Fe} + 1/2\text{Mg} + 3/2\text{Ca} + 11/4\text{Na})$  is used to classify the samples as strongly altered, weakly altered and unaltered. Most altered samples occur in proximity to the ore bodies.

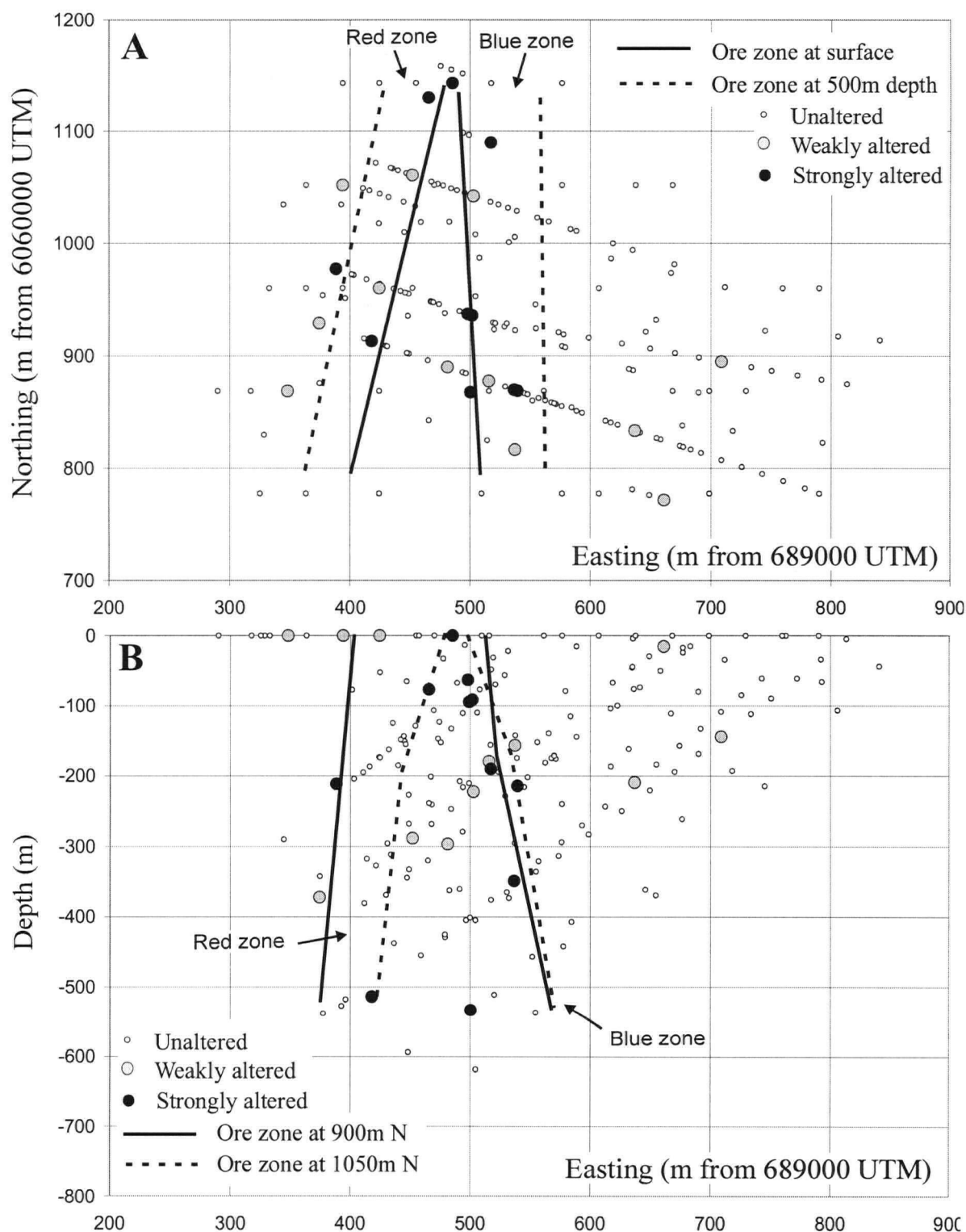


Fig. A8.9. Spatial distribution of hydrothermal alteration in the vicinity of the Konuto Lake deposit (NER claim), based on the GER plot (Fig. 4.15). The parameter  $(\text{Fe}+\text{Mg}) / (\text{Ca}+\text{Na})$  is used to classify the samples as strongly altered, weakly altered and unaltered. Most altered samples occur between, or a short distance from the two mineralized zones.

A. Plane view; B. Cross section

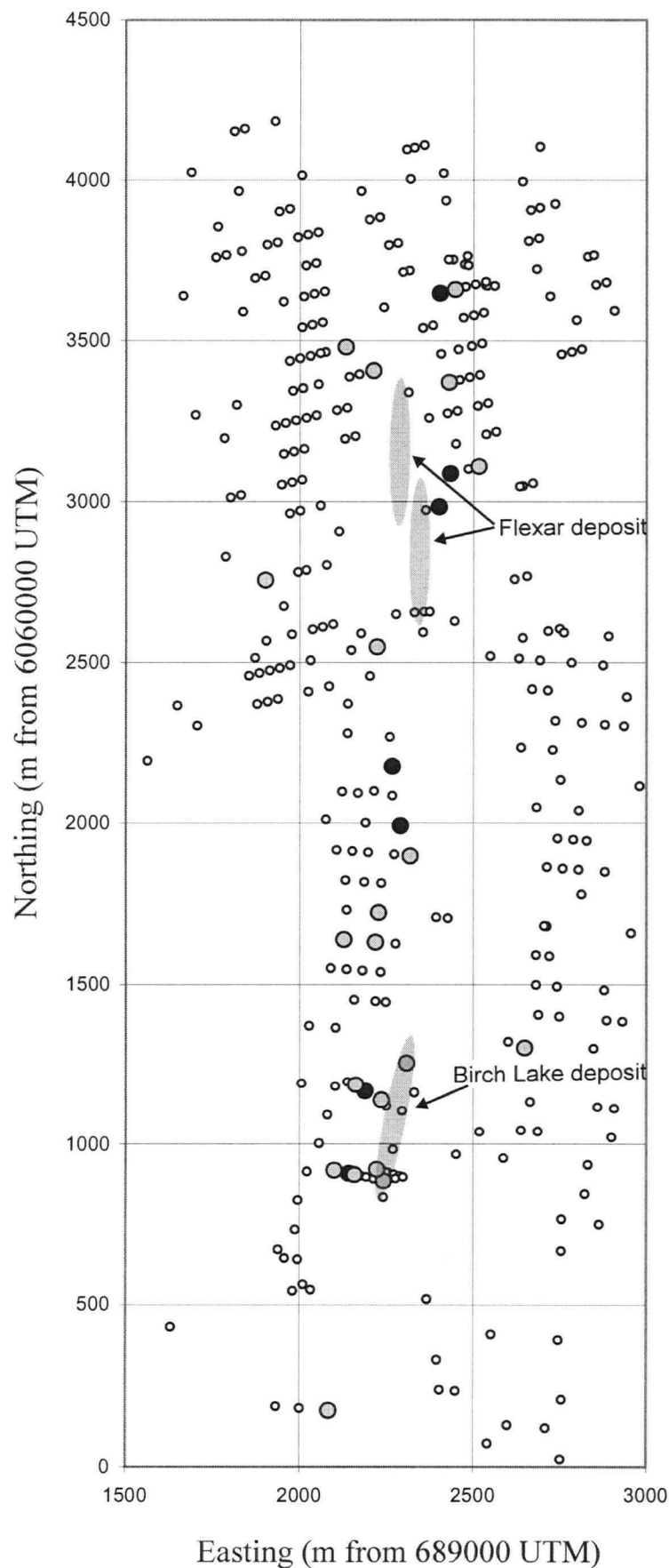


Fig. A8.10. Spatial distribution of hydrothermal alteration in the vicinity of the Birch Lake and Flexar deposits, based on the GER plot, (Fig. 4.15). The parameter  $(\text{Fe}+\text{Mg}) / (\text{Ca}+\text{Na})$  is used to classify the samples as strongly altered, weakly altered and unaltered. Most altered samples occur in proximity to the ore bodies.

- Unaltered
- Weakly altered
- Strongly altered
- Ore body



## Appendix 9

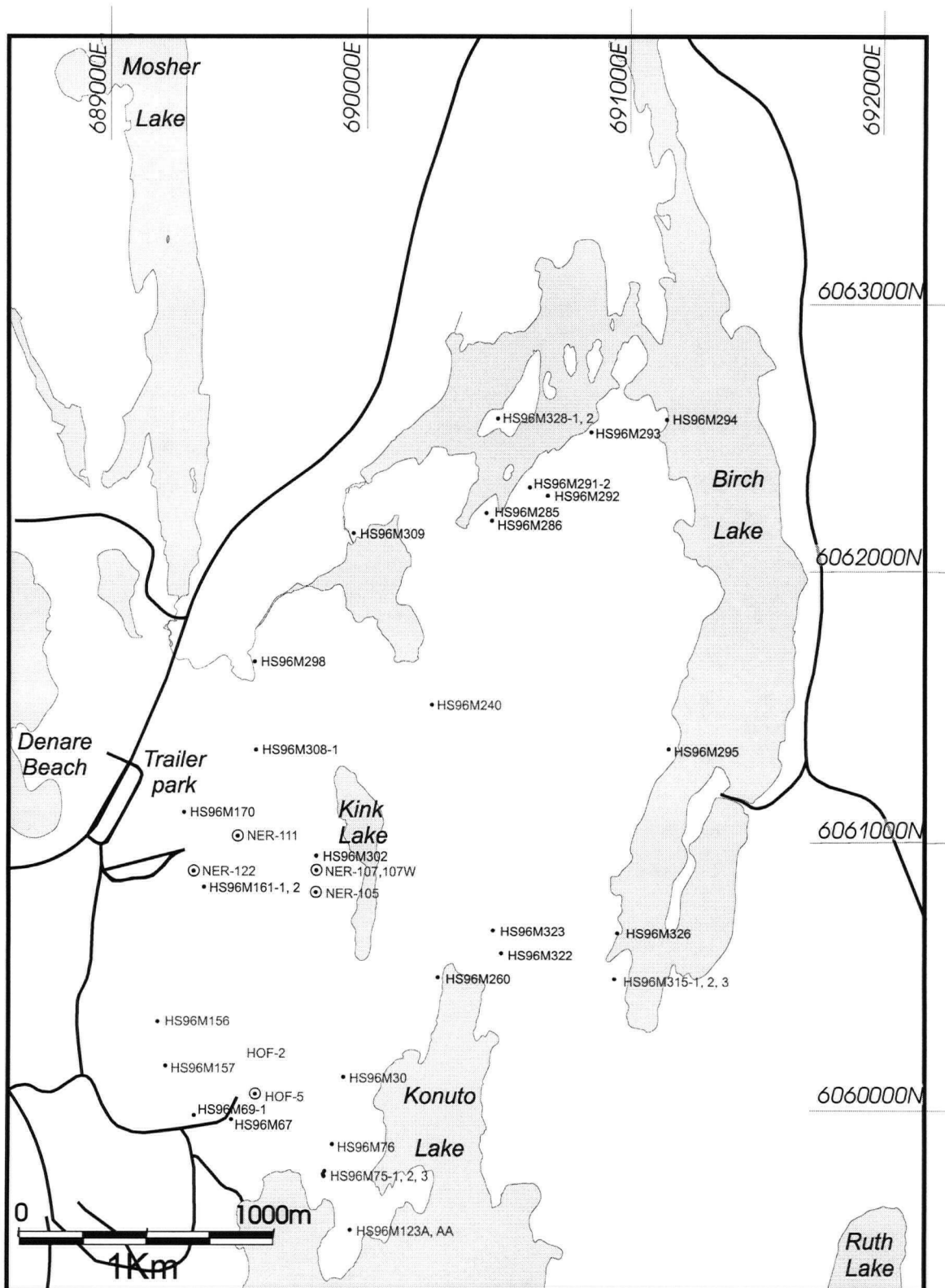


Fig. A9.1. Locations of selected mapping samples and drillholes

## Appendix 10

### Microprobe Data for Minerals from the Chu Chua and Konuto Lake VHMS Deposits

One of the main purposes of Pearce Element Ratio (PER) analysis is to identify the primary mineralogy of the studied rocks. Typically the analysis is performed under the assumption that rock-forming minerals have compositions sufficiently conforming to their idealized stoichiometric formulas. In this study, the main rock-forming minerals were analyzed by microprobe in order to ascertain their real compositions. The following conclusions were drawn from this study:

1. Plagioclase occurring in the wall rocks of the Chu Chua deposit is strongly albitized. Thirty six out of a total of 38 microprobe analyses (Table A10.2) identified the feldspar as albite ( $An_0$ - $An_{12}$ ). One grain was found to be K-feldspar and one – andesine (Fig. A10.2C). Chu Chua feldspars have near-ideal stoichiometry, a linear combination of albite and anorthite. The influence of the following components is detectable, but not significant:  $NaSiCa_{-1}Al_{-1}$ ,  $KNa_{-1}$ , and  $NaAlSi_{-1}$  (Fig. A10.2A, B).
2. In pyroxenes from Chu Chua compositional variability is restricted to the ferro-magnesian (fm,  $FeMg_{-1}$ ), tschermak (tc,  $Al_2Mg_{-1}$ ) and magnesio-calcic (mc,  $CaMg_{-1}$ ) exchanges. If ferro-magnesian exchange is neglected, because it is not usually expressed on PER plots, all the variability can be expressed on a tschermakite/magnesio-calcic plot. Thus, the pyroxenes at Chu Chua can be viewed as a solid solution ranging in composition between two end members: (1) enstatite + 0.7 mc + 0.2 tc and (2) enstatite + 0.95 mc (Fig. A10.1A). The  $(Fe+Mg)/Ca$  ratio of the pyroxenes is approximately 5/3, which is significantly different from unity (used in plots so far).
3. Plagioclase from the area of the Konuto Lake display compositions from albite to andesine (Fig. A10.4), indicating variable degree of albitization.
4. Amphiboles display ferromagnesian (fm), magnesio-calcic (cm), tschermak (tc), and edenite exchanges (Fig. A10.3). PER diagrams in this study do not discriminate between Fe and Mg and thus the ferromagnesian exchange can be ignored. Thus, most of the Konuto Lake amphiboles (85 out of 94 microanalytical points) vary between two end-member compositions: (1) tremolite – 2 cm and (2) tremolite + 0.65 ed + 1 tk.

Table A10.1. Major element concentrations in pyroxenes from the wall rocks to the  
Chu Chua deposit

Sample#	Point #	Al <sub>2</sub> O <sub>3</sub> (%)	CaO (%)	Cr <sub>2</sub> O <sub>3</sub> (%)	Fe(tot) (%)	K <sub>2</sub> O (%)	MgO (%)	MnO (%)	Na <sub>2</sub> O (%)	SiO <sub>2</sub> (%)	TiO <sub>2</sub> (%)	Ni (%)	SUM
HS952015	15-E-18	4.15	17.31	0.03	13.54	0.00	13.87	0.30	0.36	47.97	1.68	0.00	99.21
HS952015	15-E-19	0.60	23.15	0.00	14.70	0.00	8.94	0.68	0.19	50.93	0.30	0.06	99.55
HS952015	15-E-20	5.04	17.72	0.05	10.19	0.01	15.46	0.24	0.32	48.96	1.50	0.00	99.49
HS952015	15-E-22	3.77	18.94	0.13	8.01	0.00	16.53	0.19	0.29	50.32	1.00	0.02	99.20
HS952015	15-E-23	4.39	17.47	0.05	11.77	0.00	14.72	0.32	0.32	48.33	1.71	0.07	99.15
HS952015	15-E-2	4.52	17.90	0.07	11.09	0.00	14.84	0.29	0.31	48.71	1.41	0.02	99.16
HS952015	15-E-7	4.53	18.46	0.12	8.97	0.00	16.12	0.21	0.31	49.27	1.38	0.00	99.37
HS952015	15-E-8	4.32	17.45	0.01	12.33	0.01	14.32	0.34	0.37	48.39	1.45	0.01	99.00
HS952015	15-E-11	4.86	19.45	0.04	14.36	0.01	10.45	0.37	0.45	45.94	3.15	0.00	99.08
HS952015	15-E-14	4.45	16.97	0.00	15.55	0.00	12.11	0.46	0.36	47.20	2.10	0.02	99.22
HS952022	22A-1	3.28	18.96	0.00	11.80	0.00	14.24	0.35	0.24	49.43	1.19	0.00	99.49
HS952022	22A-6	1.68	19.10	0.18	8.45	0.01	16.67	0.30	0.17	51.81	0.52	0.10	98.99
HS952022	22A-7	1.63	18.92	0.30	8.34	0.00	16.99	0.26	0.14	52.26	0.50	0.00	99.34
HS952022	22A-8	2.89	19.14	0.03	10.02	0.00	15.20	0.28	0.22	50.21	0.90	0.05	98.94
HS952022	22B-1	2.53	19.50	0.01	8.53	0.00	16.38	0.28	0.17	51.37	0.67	0.00	99.44
HS952031	31C-7	2.05	22.51	0.17	10.23	0.00	12.16	0.46	0.29	50.74	0.74	0.00	99.35
HS952031	31C-8	0.65	23.58	0.06	10.73	0.01	11.53	0.49	0.20	52.12	0.12	0.05	99.54
HS952031	31d-2	1.08	23.09	0.25	10.98	0.00	11.53	0.47	0.33	51.65	0.24	0.00	99.62
HS952031	31F-3	2.09	20.74	0.10	12.64	0.01	11.62	0.49	0.32	49.92	1.23	0.04	99.20
HS952031	31-E-2	1.54	21.94	0.05	11.96	0.00	11.65	0.41	0.27	50.83	0.62	0.01	99.28
HS952031	31-E-4	5.36	18.04	0.01	12.52	0.00	13.33	0.32	0.38	47.24	2.02	0.04	99.26
HS952031	31D-5	2.27	15.75	0.00	12.73	0.02	16.05	0.43	0.26	50.58	0.89	0.04	99.02
HS952031	31D-6	5.13	17.86	0.06	10.30	0.01	14.91	0.28	0.36	48.36	1.78	0.00	99.05
HS952031	31D-7	5.76	19.27	0.15	8.58	0.01	14.99	0.21	0.34	48.23	1.61	0.04	99.19
HS952031	31D-8	4.90	18.58	0.05	11.49	0.02	13.69	0.27	0.39	47.79	2.03	0.01	99.22
HS952031	31C-1	4.54	19.78	0.12	10.85	0.00	13.29	0.24	0.36	47.95	1.88	0.01	99.02
HS952031	C2	3.77	17.61	0.19	11.47	0.06	14.04	0.25	0.31	50.63	0.83	0.00	99.16
HS952031	C5	2.10	21.52	0.24	11.55	0.01	12.08	0.44	0.34	50.39	0.70	0.00	99.37
HS952031	G1	3.82	19.36	0.06	12.59	0.01	12.60	0.34	0.41	48.20	1.62	0.00	99.01
HS952031	G2	5.76	19.33	0.07	8.41	0.00	15.03	0.20	0.30	48.66	1.34	0.02	99.12
HS952031	G3	5.46	17.80	0.19	8.54	0.01	16.15	0.21	0.30	48.90	1.43	0.03	99.02
HS952031	G5	5.68	18.40	0.25	8.83	0.01	15.52	0.17	0.33	48.39	1.65	0.00	99.23
HS952049	D1-3	5.33	19.36	0.01	10.45	0.00	13.98	0.22	0.37	47.59	2.00	0.02	99.33
HS952049	D1-5	4.39	18.50	0.02	13.34	0.02	12.24	0.40	0.39	47.75	2.00	0.00	99.05
HS952049	D1-9	4.26	18.31	0.06	13.53	0.02	12.12	0.36	0.64	48.36	1.73	0.02	99.41
HS952049	D1-10	4.58	19.02	0.04	9.52	0.02	15.27	0.21	0.34	48.91	1.44	0.04	99.39
HS952049	D1-8	5.03	17.43	0.01	11.25	0.00	14.92	0.23	0.32	47.96	1.94	0.00	99.09
HS952044	D2-1	4.54	19.53	0.36	8.28	0.00	15.39	0.19	0.30	49.64	1.25	0.00	99.48
HS952044	D2-3	0.60	23.86	0.04	12.78	0.02	9.97	0.76	0.27	51.60	0.06	0.06	100.02
HS952044	D2-5	4.56	18.75	0.00	12.44	0.00	13.16	0.29	0.37	47.54	2.04	0.05	99.20
HS952044	D2-7	5.16	18.57	0.03	13.07	0.00	12.60	0.35	0.43	46.91	2.08	0.04	99.24
HS952049	D2-8	4.56	18.45	0.15	8.66	0.00	16.07	0.23	0.33	49.43	1.24	0.00	99.12
HS952049	D3-3	5.02	19.04	0.26	7.60	0.00	16.23	0.19	0.30	49.05	1.30	0.04	99.03
HS952049	D3-5	2.16	16.64	0.44	8.02	0.00	19.21	0.23	0.21	51.97	0.50	0.05	99.43
HS952044	D3-2	4.35	19.13	0.11	8.61	0.03	15.61	0.24	0.30	49.19	1.39	0.06	99.02
HS952044	D3-3	4.47	18.49	0.07	9.77	0.00	15.61	0.27	0.36	49.17	1.27	0.06	99.54
HS952044	D3-4	0.76	23.02	0.00	12.93	0.01	10.57	0.74	0.15	51.44	0.16	0.00	99.78

Sample#	Point #	Al <sub>2</sub> O <sub>3</sub> (%)	CaO (%)	Cr <sub>2</sub> O <sub>3</sub> (%)	Fe(tot) (%)	K <sub>2</sub> O (%)	MgO (%)	MnO (%)	Na <sub>2</sub> O (%)	SiO <sub>2</sub> (%)	TiO <sub>2</sub> (%)	Ni (%)	SUM
HS952044	E1-1	4.62	19.61	0.49	7.25	0.00	16.04	0.18	0.28	49.69	1.16	0.05	99.37
HS952044	D3-5	4.45	18.70	0.39	7.80	0.00	16.44	0.19	0.32	49.93	0.91	0.00	99.13
HS952044	E1-2	4.65	19.03	0.93	6.98	0.02	16.36	0.18	0.30	49.74	1.01	0.02	99.22
HS952044	E1-3	4.89	19.50	0.08	9.16	0.02	14.93	0.25	0.30	48.59	1.55	0.05	99.32
HS952044	E1-5	4.55	18.28	0.04	9.97	0.00	15.28	0.26	0.30	49.38	1.24	0.00	99.30
HS952044	E2-3	4.50	19.25	0.04	9.57	0.01	14.83	0.24	0.33	48.75	1.58	0.00	99.10
HS952049	F1-2	4.63	18.51	0.00	13.02	0.00	12.85	0.33	0.43	47.62	1.95	0.00	99.34
HS952049	F1-4	5.07	19.51	0.03	9.47	0.01	14.30	0.31	0.38	47.99	1.89	0.09	99.05
HS952049	F2-1	2.13	17.35	0.58	7.54	0.01	18.89	0.23	0.22	52.07	0.51	0.06	99.59
HS952049	F2-2	4.52	19.03	0.83	7.11	0.00	16.46	0.23	0.31	49.94	0.87	0.08	99.38
HS952049	F2-5	4.68	19.14	0.07	9.21	0.02	15.28	0.18	0.33	48.61	1.49	0.03	99.04
HS952049	F2-7	2.04	16.72	0.30	7.99	0.00	19.29	0.21	0.22	52.11	0.53	0.04	99.45
HS952063	1	3.51	21.68	0.37	6.82	0.00	15.75	0.12	0.26	50.50	0.87	0.05	99.93
HS952063	7	3.39	21.61	0.36	6.67	0.00	15.74	0.12	0.23	50.65	0.77	0.04	99.58
HS952063	11	2.79	21.06	0.34	6.67	0.05	16.06	0.18	0.72	50.53	0.73	0.00	99.13
HS952063	12	2.75	22.02	0.04	7.27	0.02	15.65	0.24	0.24	51.46	0.78	0.00	100.47
HS952063	13	3.01	21.99	0.26	6.39	0.02	15.62	0.10	0.21	51.46	0.76	0.02	99.84
HS952063	14	3.46	21.39	0.36	6.80	0.01	15.47	0.12	0.23	51.01	0.84	0.01	99.70
HS952063	17	3.39	21.88	0.28	6.52	0.00	15.84	0.14	0.24	50.92	0.79	0.01	100.01

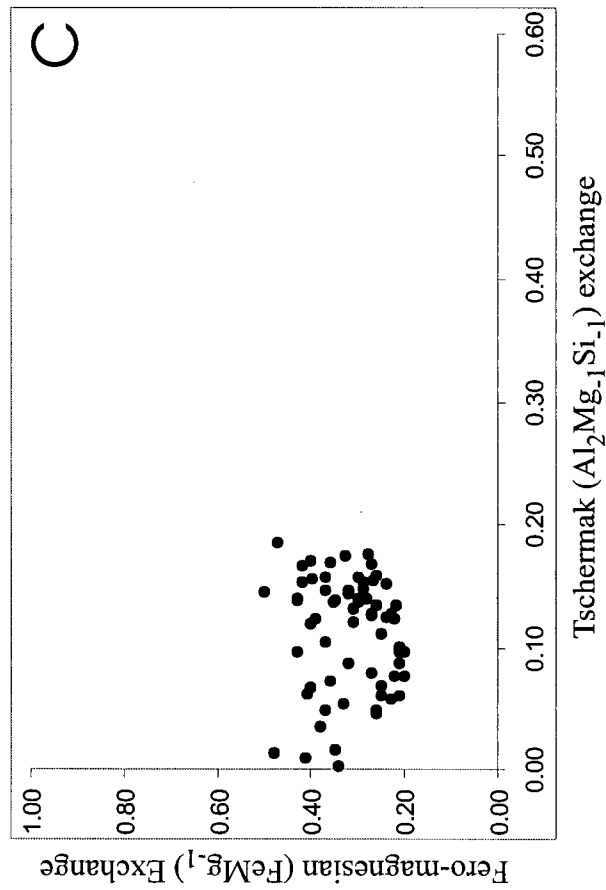
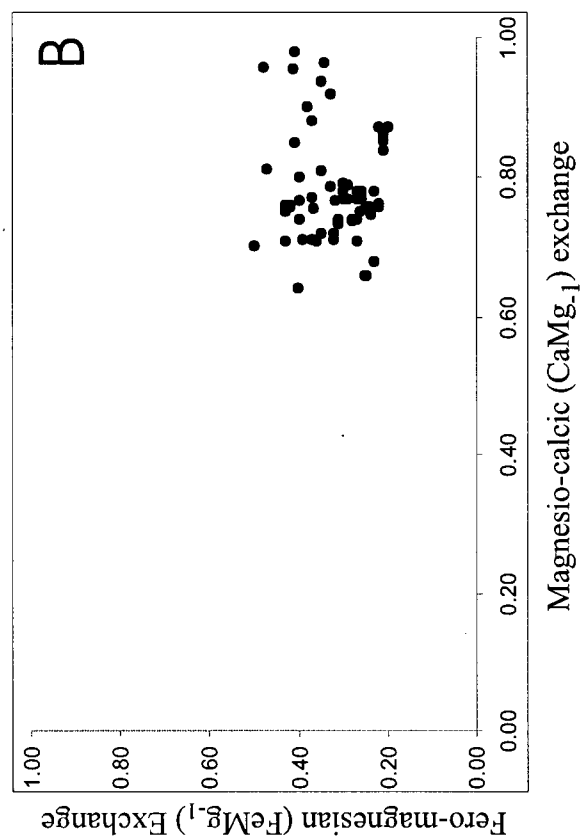
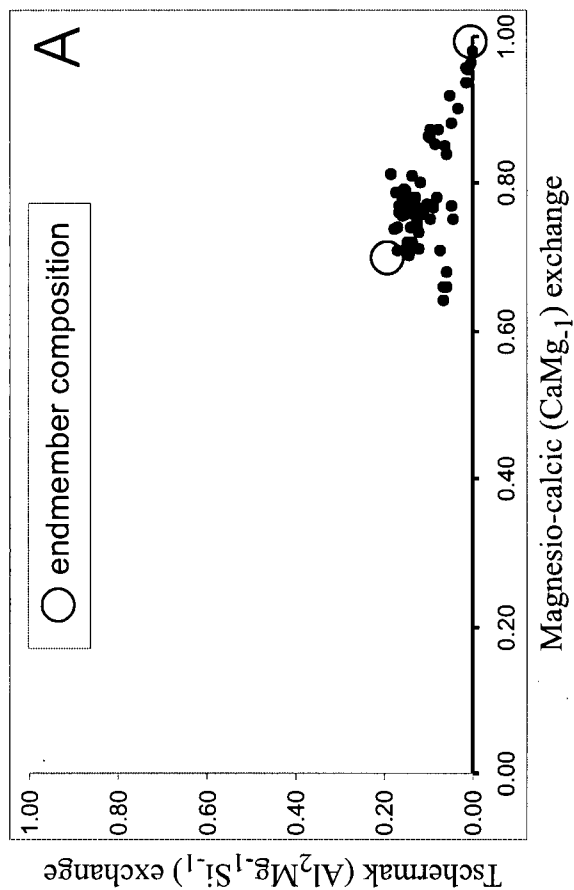


Fig. A10.1. Composition of pyroxenes from the host rocks to the Chu Chua VHMS deposit.

- A. Magnesio-calcic ( $\text{CaMg}_{-1}$ ) vs. tschermak ( $\text{Al}_2\text{Mg}_{-1}\text{Si}_{-1}$ ) exchange components.
- B. Magnesio-calcic ( $\text{CaMg}_{-1}$ ) vs. ferro-magnesian ( $\text{FeMg}_{-1}$ ) exchange component.
- C. Tschermak ( $\text{Al}_2\text{Mg}_{-1}\text{Si}_{-1}$ ) vs. ferro-magnesian ( $\text{FeMg}_{-1}$ ) exchange component.
- The exchanges modify an enstatite molecule.

Table A10.2. Major element concentrations in plagioclase from the wall rocks  
to the Chu Chua VHMS deposit

Sample#	Micro-analyt. Point #	Al <sub>2</sub> O <sub>3</sub> (%)	CaO (%)	Fe <sub>2</sub> O <sub>3</sub> (%)	K <sub>2</sub> O (%)	MgO (%)	Na <sub>2</sub> O (%)	SiO <sub>2</sub> (%)	SrO (%)	BaO (%)	SUM
HS95063	4	19.92	0.44	0.28	0.08	0.02	11.51	67.32	0.00	0.00	99.57
HS95063	6	19.07	0.59	0.51	0.08	0.01	10.44	68.95	0.00	0.00	99.65
HS95063	19	19.95	0.41	0.39	0.09	0.00	11.29	67.69	0.00	0.00	99.82
HS95063	20	20.22	0.39	0.44	0.05	0.00	11.21	67.23	0.00	0.10	99.64
HS95063	21	19.92	0.34	0.40	0.11	0.04	11.32	67.64	0.00	0.00	99.77
HS95063	22	20.06	0.33	0.27	0.08	0.01	11.28	67.57	0.00	0.01	99.61
HS95063	23	19.82	0.46	0.28	0.10	0.00	11.34	67.80	0.00	0.01	99.81
HS95063	24	20.06	0.34	0.35	0.08	0.00	11.29	67.59	0.00	0.00	99.71
HS95063	26	20.11	0.37	0.19	0.03	0.01	11.35	67.73	0.00	0.00	99.79
HS95063	28	20.13	0.53	0.22	0.10	0.00	11.23	67.22	0.00	0.00	99.43
HS95063	29	20.38	0.72	0.32	0.06	0.00	11.08	67.27	0.00	0.05	99.88
HS95063	30	20.19	0.45	0.22	0.09	0.00	10.93	67.02	0.00	0.05	98.95
HS95049	D-1	19.96	0.60	0.52	0.06	0.09	11.43	66.47	0.00	0.04	99.17
HS95049	D-3	20.75	1.23	0.24	0.08	0.05	10.89	67.24	0.00	0.02	100.50
HS95049	F-2	21.47	2.22	0.31	0.13	0.00	10.30	66.33	0.00	0.00	100.76
HS95049	F-3	21.06	1.34	0.35	0.27	0.05	10.73	67.18	0.00	0.00	100.98
HS95049	E-1	19.71	0.50	0.44	0.11	0.09	11.08	66.97	0.00	0.05	98.95
HS95049	E-4	20.11	0.98	0.49	0.09	0.07	11.12	67.05	0.00	0.00	99.91
HS95049	E-2	21.46	2.27	0.45	0.13	0.08	10.07	65.63	0.00	0.01	100.10
HS95049	F-41	20.81	1.66	0.38	0.11	0.04	10.87	66.19	0.00	0.00	100.06
HS95049	F-46	21.47	1.77	0.34	0.32	0.05	10.02	65.74	0.00	0.03	99.74
HS95049	F-47	21.34	2.45	0.35	0.13	0.05	10.10	64.47	0.00	0.01	98.90
HS95015	E-3	20.39	0.71	0.19	0.07	0.00	10.79	66.90	0.00	0.00	99.05
HS95015	E-9	27.29	10.11	0.95	0.08	0.07	5.62	54.94	0.00	0.03	99.09
HS95015	E-14	21.13	1.40	0.36	0.05	0.01	10.66	66.65	0.00	0.05	100.31
HS95022	A-2	19.69	0.31	0.22	0.07	0.04	10.74	68.57	0.00	0.00	99.64
HS95022	A-4	20.09	0.48	0.45	0.06	0.08	10.81	68.72	0.00	0.00	100.69
HS95022	A-6	19.85	0.59	0.25	0.15	0.00	10.84	68.29	0.00	0.06	100.03
HS95022	A-7	19.15	0.02	0.17	14.93	0.00	0.45	62.50	0.00	2.76	99.98
HS95022	A-11	19.94	0.34	0.32	0.04	0.03	11.29	68.85	0.00	0.00	100.81
HS95022	A-12	19.76	0.47	0.33	0.08	0.00	10.93	69.52	0.00	0.01	101.10
HS952031	C-1	20.62	0.38	0.30	0.68	0.08	10.96	67.89	0.00	0.00	100.91
HS952031	C-3	20.56	0.44	0.25	0.37	0.02	10.57	67.98	0.00	0.00	100.19
HS952031	D-1	20.34	0.33	0.30	0.37	0.01	11.17	68.47	0.00	0.00	100.99
HS952031	E-1	19.63	0.16	0.12	0.08	0.00	11.43	68.57	0.00	0.00	99.99
HS952031	E-2	20.31	0.38	0.09	0.32	0.03	11.22	68.16	0.00	0.00	100.51
HS952031	G-1	20.27	0.71	0.19	0.11	0.02	11.05	67.98	0.00	0.00	100.33
HS952031	G-4	20.36	1.17	0.14	0.13	0.00	10.21	67.43	0.00	0.01	99.45

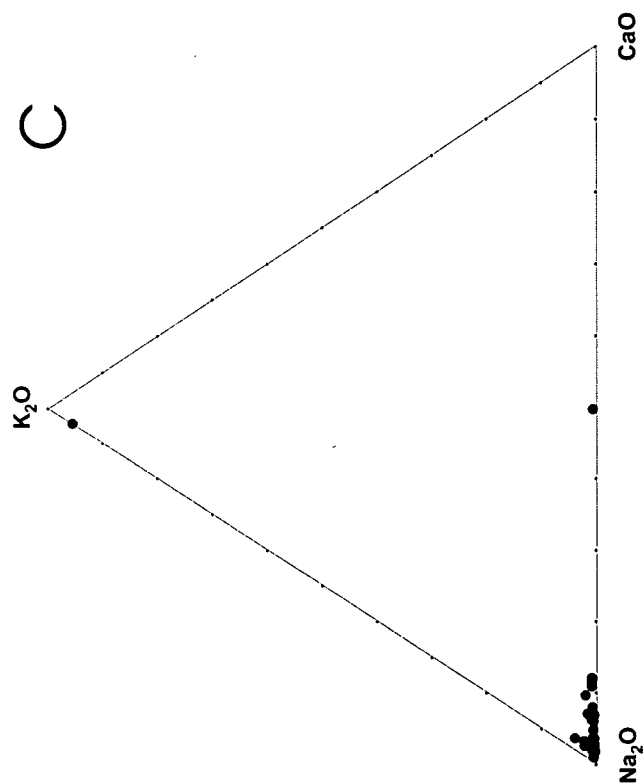
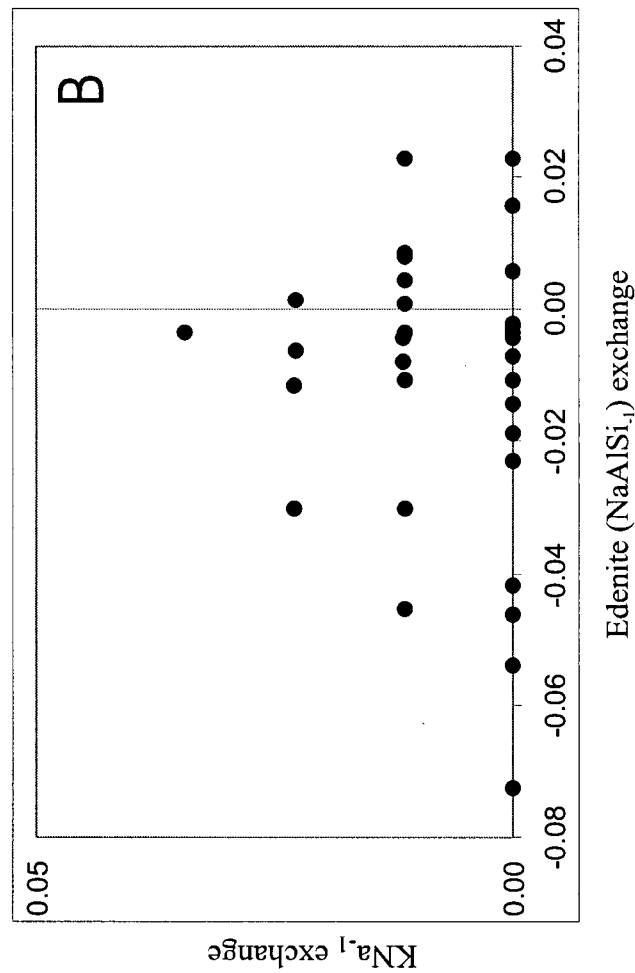
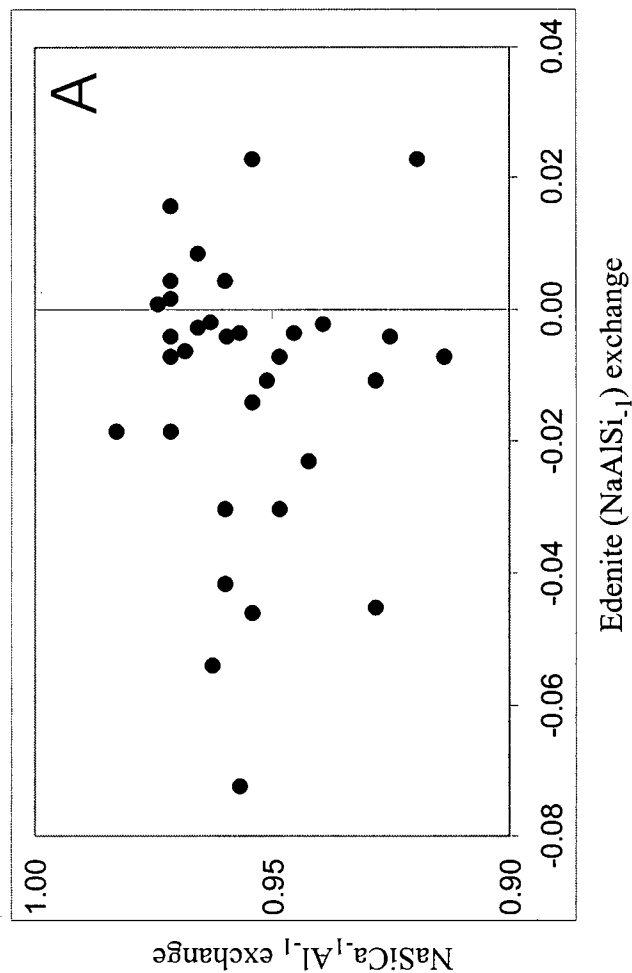


Fig. A10.2. Composition of feldspars from the host rocks to the Chu Chua VHMS deposit acquired through microprobe analysis.

A. Edenite vs. KNa-1 exchange component.

B. Edenite vs. NaSiCa<sub>1</sub>Al<sub>1</sub> exchange component.

The exchanges modify an anorthite molecule.

C. Ternary diagram showing the major oxide components in feldspars.

Table A10.3. Major element concentrations in amphiboles from the wall rocks  
to the Konuto Lake VMS deposit

Sample#	Micro-analyt. Point #	Al <sub>2</sub> O <sub>3</sub> (%)	CaO (%)	Fe <sub>2</sub> O <sub>3</sub> (%)	K <sub>2</sub> O (%)	MgO (%)	Na <sub>2</sub> O (%)	SiO <sub>2</sub> (%)	TiO <sub>2</sub> (%)	Cr <sub>2</sub> O <sub>3</sub> (%)	MnO (%)
HOF-5-70	1	7.29	11.34	21.75	0.17	8.66	0.75	45.14	0.36	0.05	0.37
HOF-5-70	2	7.42	11.49	21.20	0.13	9.47	0.70	46.95	0.24	0.02	0.36
HOF-5-70	3	8.04	11.78	22.37	0.27	8.13	0.85	45.47	0.40	0.00	0.47
HOF-5-70	4	8.32	11.73	21.52	0.20	8.63	0.80	46.39	0.24	0.02	0.32
HOF-2-127	5	5.91	9.11	16.52	0.07	14.30	0.77	49.65	0.20	0.05	0.40
HOF-2-127	6	6.16	8.16	18.12	0.08	14.16	0.81	49.71	0.27	0.12	0.45
HOF-2-127	7	7.48	10.02	16.28	0.08	13.00	0.96	48.69	0.27	0.05	0.34
HOF-2-127	8	4.84	7.05	19.17	0.05	14.47	0.60	50.61	0.23	0.00	0.66
HOF-2-127	9	6.41	10.04	15.64	0.06	13.99	0.82	49.49	0.22	0.08	0.32
HOF-2-127	10	6.82	9.47	16.11	0.08	13.81	0.92	49.34	0.24	0.02	0.40
HOF-2-127	11	5.45	8.52	16.82	0.05	14.75	0.77	50.31	0.22	0.07	0.46
HOF-2-127	12	7.66	10.67	14.97	0.12	13.17	0.97	48.68	0.29	0.04	0.31
HOF-2-127	13	6.40	8.30	17.65	0.09	14.31	0.80	50.27	0.18	0.04	0.53
HOF-5-70	14	6.58	8.92	16.97	0.05	13.63	0.88	49.30	0.25	0.10	0.46
HOF-5-70	15	7.48	9.92	15.77	0.05	13.80	0.97	49.14	0.27	0.07	0.31
HOF-5-70	16	9.48	7.63	18.40	0.05	13.97	0.62	45.09	0.21	0.07	0.34
HOF-5-70	17	8.42	11.03	21.32	0.20	8.88	1.07	45.24	0.51	0.00	0.36
HOF-5-70	18	8.84	11.10	21.67	0.27	8.38	1.20	45.13	0.40	0.01	0.36
HOF-5-70	19	7.69	11.21	21.04	0.22	9.08	1.04	46.78	0.30	0.01	0.36
HOF-5-70	20	10.67	11.04	22.88	0.37	7.24	1.50	42.83	0.43	0.00	0.41
HS96M75-1	1	8.00	9.80	13.85	0.32	13.26	0.61	48.61	0.12	0.01	0.28
HS96M75-1	2	7.91	10.05	14.15	0.17	13.32	0.54	48.73	0.13	0.00	0.33
HS96M75-1	3	13.43	6.79	20.65	0.09	13.13	0.58	39.26	0.11	0.00	0.38
HS96M75-1	4	10.39	10.97	16.08	0.19	10.34	1.70	48.11	0.18	0.03	0.24
HS96M75-1	5	4.23	12.19	14.49	0.05	13.86	0.50	51.25	0.13	0.00	0.31
HS96M75-1	6	5.34	12.04	15.56	0.08	12.70	0.64	49.91	0.12	0.03	0.30
HS96M75-1	7	14.88	7.29	13.67	0.18	7.78	3.48	46.82	0.08	0.07	0.23
HS96M75-1	9	5.26	12.18	15.85	0.09	13.09	0.64	50.16	0.15	0.00	0.31
HS96M75-1	10	4.33	12.05	15.31	0.08	13.41	0.51	50.05	0.11	0.08	0.33
HS96M75-1	11	2.90	12.27	14.74	0.02	14.24	0.42	51.19	0.07	0.03	0.30
HS96M75-1	12	2.30	12.15	14.31	0.03	14.85	0.29	52.95	0.07	0.01	0.29
HS96M75-1	13	2.20	12.18	14.44	0.03	14.93	0.28	52.66	0.07	0.01	0.34
HS96M75-1	14	8.80	11.75	16.94	0.17	11.16	1.03	47.01	0.18	0.01	0.27
HS96M75-1	15	5.53	11.75	15.50	0.11	12.85	0.73	49.68	0.15	0.04	0.34
HS96M75-1	16	8.10	8.19	27.31	0.18	6.54	1.11	44.99	0.20	0.00	0.88
HS96M75-1	17	8.13	8.10	26.96	0.18	6.55	1.09	45.23	0.17	0.03	0.93
HS96M75-1	18	9.18	8.64	26.49	0.18	6.93	1.09	44.31	0.23	0.00	0.71
HS96M75-1	20	15.84	9.82	25.23	0.36	4.57	1.65	39.18	0.33	0.00	0.38
HS96M75-1	22	14.42	10.74	25.16	0.43	4.12	1.71	40.22	0.62	0.00	0.39
HS96M75-1	23	13.29	8.60	20.30	0.58	5.22	2.23	46.78	0.11	0.01	0.27
HS96M75-1	25	14.40	9.60	23.54	0.43	5.23	1.58	41.48	0.28	0.01	0.36
HS96M30	1	11.36	10.87	23.84	0.28	6.16	1.31	43.09	0.31	0.04	0.36
HS96M30	2	9.12	10.38	23.39	0.22	7.47	1.15	44.96	0.26	0.03	0.46
HS96M30	3	7.32	9.82	23.13	0.14	8.52	1.00	46.62	0.20	0.05	0.54
HS96M30	4	9.58	10.51	22.95	0.22	7.47	1.20	44.90	0.24	0.00	0.42
HS96M30	5	9.84	11.15	22.64	0.27	7.25	1.26	44.02	0.25	0.00	0.28
HS96M30	6	8.99	10.22	23.07	0.21	7.77	1.23	44.97	0.38	0.00	0.47



	analyt.	Al <sub>2</sub> O <sub>3</sub>	CaO	Fe <sub>2</sub> O <sub>3</sub>	K <sub>2</sub> O	MgO	Na <sub>2</sub> O	SiO <sub>2</sub>	TiO <sub>2</sub>	Cr <sub>2</sub> O <sub>3</sub>	MnO
Sample#	Point #	(%)	(%)	(%)	(%)	(%)	(%)	(%)	(%)	(%)	(%)
NER-80-150	9	7.53	10.69	22.33	0.26	8.45	1.31	45.35	0.43	0.02	0.37
NER-80-150	8	7.65	10.85	21.54	0.33	8.60	1.20	46.05	0.50	0.00	0.33
NER-80-150	10	6.90	10.86	22.10	0.16	8.91	1.26	46.21	0.35	0.00	0.36
NER-80-150	11	6.23	10.78	21.66	0.17	9.23	1.11	47.05	0.37	0.02	0.33
NER-80-150	12	7.30	10.71	21.71	0.29	8.65	1.20	45.53	0.51	0.00	0.38
NER-80-150	13	7.97	11.11	21.96	0.40	8.21	1.16	45.04	0.60	0.04	0.27
NER-80-150	14	7.04	11.13	21.88	0.33	8.83	1.01	46.47	0.50	0.00	0.37
NER-80-150	15	6.92	10.84	22.22	0.32	9.03	1.06	46.33	0.51	0.02	0.36
NER-80-150	16	7.35	11.02	21.96	0.32	8.70	1.25	45.93	0.44	0.00	0.36
NER-80-150	17	7.97	11.39	22.00	0.36	8.38	1.13	45.25	0.59	0.02	0.33
HS96M30	18	7.36	11.00	21.69	0.17	8.67	1.24	45.78	0.43	0.04	0.32
NER-107-122	1	7.25	10.25	22.29	0.19	9.70	1.05	46.42	0.54	0.00	0.41
NER-107-122	2	5.40	11.53	20.53	0.25	10.12	0.62	48.38	0.29	0.00	0.28
NER-107-122	3	8.80	8.70	23.15	0.13	10.76	0.33	43.27	0.12	0.00	0.45
NER-107-122	4	7.60	10.78	21.36	0.24	9.38	1.16	45.84	0.61	0.02	0.39
NER-107-122	5	7.89	10.20	22.42	0.29	9.18	1.11	45.56	0.58	0.00	0.37
NER-107-122	6	8.85	10.88	21.75	0.36	8.78	1.30	44.90	0.57	0.01	0.33
NER-107-122	7	7.79	10.57	21.84	0.21	9.42	1.13	45.66	0.50	0.04	0.41
NER-107-122	8	3.19	11.26	19.61	0.07	11.59	0.12	50.02	0.04	0.02	0.38
NER-107-122	9	11.41	10.99	22.65	0.52	6.96	1.59	42.16	0.79	0.02	0.32
NER-107-122	10	7.81	10.24	22.17	0.25	9.20	1.07	45.60	0.47	0.00	0.44
NER-107-122	11	7.32	11.06	20.81	0.17	9.64	1.08	46.15	0.29	0.00	0.32
NER-107-122	12	6.35	9.29	22.59	0.20	10.07	0.89	47.14	0.34	0.04	0.56
NER-107-122	13	10.33	11.02	22.86	0.32	7.58	1.41	43.04	0.53	0.05	0.33
NER-107-122	14	7.73	10.60	21.82	0.27	9.02	1.04	45.71	0.57	0.02	0.48
NER-107-122	15	6.70	9.80	21.99	0.23	9.91	0.96	46.89	0.39	0.01	0.48
NER-107-122	16	10.03	11.15	21.64	0.34	8.10	1.46	43.97	0.50	0.00	0.28
NER-107-122	17	7.79	10.33	21.63	0.30	9.34	1.18	45.80	0.58	0.00	0.36
NER-107-122	18	7.48	10.53	21.74	0.25	9.33	1.08	45.86	0.66	0.01	0.37
NER-107-122	19	10.48	10.90	22.43	0.37	7.72	1.51	43.38	0.51	0.02	0.22
NER-107-122	21	7.44	10.28	21.94	0.23	9.21	0.99	46.48	0.45	0.02	0.52
NER-107-122	22	11.44	11.24	22.16	0.29	7.39	1.52	43.36	0.24	0.05	0.36
HOF-5-58	23	1.44	1.65	25.78	0.03	14.53	0.18	52.21	0.03	0.01	0.69
HOF-5-58	24	1.67	0.97	26.41	0.02	15.28	0.28	51.81	0.05	0.01	0.66
HOF-5-58	25	0.90	0.43	26.43	0.00	15.78	0.13	52.75	0.04	0.00	0.63
HOF-5-58	26	1.10	0.79	26.21	0.03	15.71	0.16	52.43	0.03	0.00	0.64
HOF-5-58	27	0.89	0.91	26.00	0.02	15.07	0.09	52.93	0.05	0.00	0.94
HOF-5-58	28	1.08	2.44	23.94	0.03	15.32	0.11	53.36	0.03	0.00	0.76
HOF-5-58	29	1.39	2.38	24.76	0.02	14.64	0.35	53.17	0.01	0.02	1.01
HOF-5-58	30	0.75	0.60	26.50	0.01	15.68	0.07	52.97	0.04	0.02	0.77
NER-78-212	1	7.80	10.68	22.64	0.41	8.32	1.04	45.40	0.34	0.00	0.31
NER-78-212	2	3.30	11.65	18.51	0.16	11.40	0.36	49.79	0.12	0.04	0.31
NER-78-212	3	8.14	10.74	22.56	0.39	8.31	1.02	45.36	0.31	0.00	0.35
NER-78-212	4	8.16	10.66	23.18	0.40	8.16	1.04	45.58	0.37	0.00	0.26
NER-78-212	5	8.19	10.59	22.92	0.44	8.07	1.07	45.08	0.31	0.01	0.35
NER-78-212	6	7.95	10.74	22.31	0.36	8.44	1.13	45.74	0.30	0.06	0.27
NER-78-212	7	8.36	10.63	23.20	0.41	8.30	1.16	45.33	0.33	0.02	0.32
NER-78-212	8	8.94	10.93	22.74	0.45	7.58	1.26	44.18	0.37	0.01	0.23

Sample#	Micro-analyt. Point #	Cl (%)	F (%)	Zn (%)	Pb (%)	SUM
HOF-5-70	1	0.37	0.08	0.08	0.02	96.44
HOF-5-70	2	0.19	0.04	0.00	0.00	98.20
HOF-5-70	3	0.13	0.04	0.02	0.01	97.98
HOF-5-70	4	0.17	0.06	0.00	0.05	98.43
HOF-2-127	5	0.00	0.01	0.00	0.08	97.06
HOF-2-127	6	0.06	0.01	0.00	0.00	98.11
HOF-2-127	7	0.06	0.15	0.03	0.00	97.40
HOF-2-127	8	0.08	0.05	0.02	0.13	97.96
HOF-2-127	9	0.06	0.01	0.00	0.00	97.13
HOF-2-127	10	0.05	0.01	0.00	0.00	97.26
HOF-2-127	11	0.06	0.01	0.01	0.00	97.52
HOF-2-127	12	0.03	0.19	0.05	0.00	97.15
HOF-2-127	13	0.08	0.01	0.09	0.05	98.79
HOF-5-70	14	0.05	0.01	0.00	0.02	97.23
HOF-5-70	15	0.01	0.05	0.02	0.00	97.86
HOF-5-70	16	0.06	0.03	0.04	0.00	95.99
HOF-5-70	17	0.25	0.18	0.02	0.04	97.52
HOF-5-70	18	0.13	0.01	0.02	0.02	97.54
HOF-5-70	19	0.08	0.01	0.00	0.00	97.81
HOF-5-70	20	0.25	0.01	0.09	0.10	97.80
HS96M75-1	1	0.09	0.35	0.06	0.00	95.36
HS96M75-1	2	0.11	0.10	0.00	0.01	95.56
HS96M75-1	3	0.02	0.08	0.04	0.11	94.68
HS96M75-1	4	0.09	0.08	0.07	0.10	98.57
HS96M75-1	5	0.04	0.05	0.03	0.12	97.25
HS96M75-1	6	0.06	0.01	0.00	0.13	96.92
HS96M75-1	7	0.24	0.20	0.00	0.12	95.04
HS96M75-1	9	0.01	0.01	0.03	0.05	97.83
HS96M75-1	10	0.01	0.01	0.07	0.00	96.36
HS96M75-1	11	0.15	0.07	0.00	0.00	96.40
HS96M75-1	12	0.05	0.02	0.00	0.00	97.34
HS96M75-1	13	0.02	0.01	0.04	0.02	97.25
HS96M75-1	14	0.10	0.01	0.00	0.00	97.42
HS96M75-1	15	0.10	0.02	0.00	0.01	96.82
HS96M75-1	16	0.23	0.01	0.00	0.02	97.75
HS96M75-1	17	0.29	0.19	0.00	0.06	97.93
HS96M75-1	18	0.27	0.14	0.00	0.08	98.25
HS96M75-1	20	0.56	0.05	0.02	0.03	98.03
HS96M75-1	22	0.77	0.01	0.03	0.10	98.70
HS96M75-1	23	0.22	0.01	0.03	0.00	97.66
HS96M75-1	25	0.43	0.09	0.00	0.06	97.49
HS96M30	1	0.10	0.06	0.04	0.06	97.88
HS96M30	2	0.14	0.01	0.02	0.00	97.61
HS96M30	3	0.02	0.07	0.07	0.00	97.50
HS96M30	4	0.11	0.01	0.03	0.00	97.64
HS96M30	5	0.31	0.01	0.00	0.07	97.35
HS96M30	6	0.13	0.08	0.08	0.02	97.64

Sample#	analyt. Point #	Cl (%)	F (%)	Zn (%)	Pb (%)	SUM
NER-80-150	8	0.14	0.03	0.05	0.00	97.04
NER-80-150	10	0.47	0.01	0.00	0.02	97.11
NER-80-150	11	0.19	0.01	0.01	0.00	97.15
NER-80-150	12	0.18	0.01	0.02	0.00	96.50
NER-80-150	13	0.11	0.01	0.00	0.04	96.93
NER-80-150	14	0.11	0.01	0.01	0.00	97.69
NER-80-150	15	0.11	0.24	0.00	0.00	97.96
NER-80-150	16	0.15	0.01	0.00	0.00	97.50
NER-80-150	17	0.21	0.23	0.08	0.00	97.95
HS96M30	18	0.24	0.01	0.06	0.13	97.14
NER-107-122	1	0.35	0.08	0.04	0.07	98.64
NER-107-122	2	0.12	0.09	0.00	0.00	97.60
NER-107-122	3	0.04	0.08	0.10	0.00	95.93
NER-107-122	4	0.28	0.04	0.00	0.00	97.71
NER-107-122	5	0.27	0.01	0.08	0.00	97.97
NER-107-122	6	0.17	0.01	0.00	0.07	97.98
NER-107-122	7	0.32	0.01	0.00	0.00	97.90
NER-107-122	8	0.02	0.14	0.05	0.06	96.56
NER-107-122	9	0.22	0.01	0.00	0.11	97.74
NER-107-122	10	0.27	0.02	0.03	0.00	97.58
NER-107-122	11	0.22	0.21	0.07	0.00	97.33
NER-107-122	12	0.15	0.05	0.00	0.03	97.71
NER-107-122	13	0.23	0.15	0.04	0.14	98.03
NER-107-122	14	0.30	0.02	0.03	0.06	97.66
NER-107-122	15	0.21	0.01	0.04	0.00	97.60
NER-107-122	16	0.13	0.03	0.05	0.08	97.77
NER-107-122	17	0.26	0.01	0.14	0.13	97.84
NER-107-122	18	0.28	0.01	0.04	0.09	97.72
NER-107-122	19	0.20	0.01	0.01	0.10	97.85
NER-107-122	21	0.18	0.19	0.10	0.02	98.06
NER-107-122	22	0.17	0.01	0.00	0.05	98.27
HOF-5-58	23	0.00	0.03	0.04	0.00	96.64
HOF-5-58	24	0.02	0.01	0.00	0.07	97.25
HOF-5-58	25	0.00	0.01	0.04	0.12	97.27
HOF-5-58	26	0.00	0.02	0.00	0.00	97.11
HOF-5-58	27	0.01	0.01	0.00	0.08	97.01
HOF-5-58	28	0.00	0.01	0.02	0.00	97.09
HOF-5-58	29	0.05	0.01	0.01	0.13	97.95
HOF-5-58	30	0.03	0.15	0.00	0.01	97.59
NER-78-212	1	0.15	0.01	0.04	0.00	97.15
NER-78-212	2	0.06	0.17	0.08	0.00	95.97
NER-78-212	3	0.16	0.01	0.09	0.00	97.45
NER-78-212	4	0.20	0.08	0.12	0.00	98.21
NER-78-212	5	0.33	0.01	0.14	0.00	97.49
NER-78-212	6	0.18	0.01	0.03	0.02	97.55
NER-78-212	7	0.21	0.01	0.10	0.00	98.37
NER-78-212	8	0.33	0.10	0.00	0.04	97.16

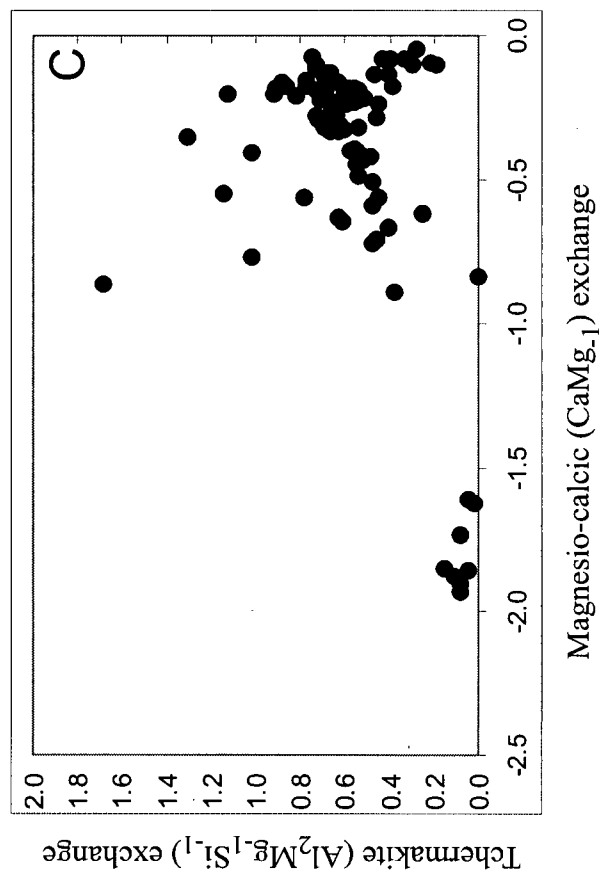
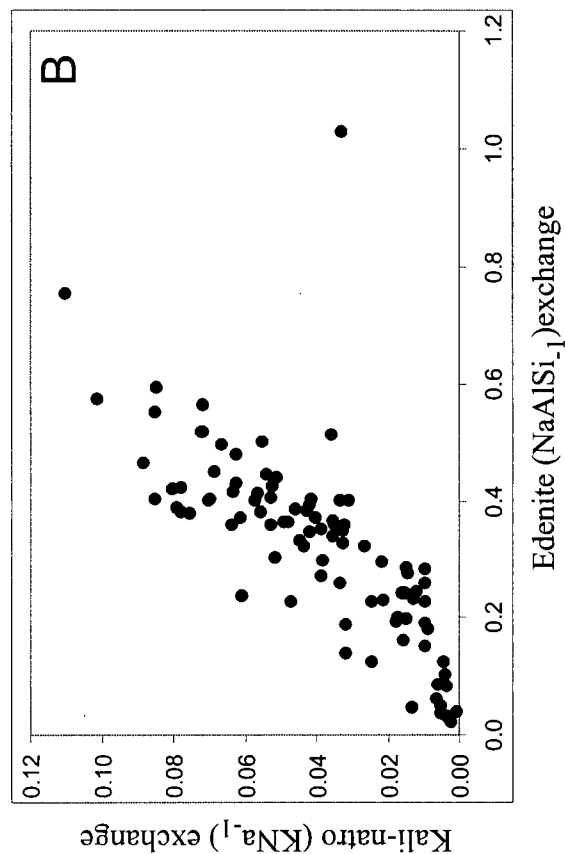
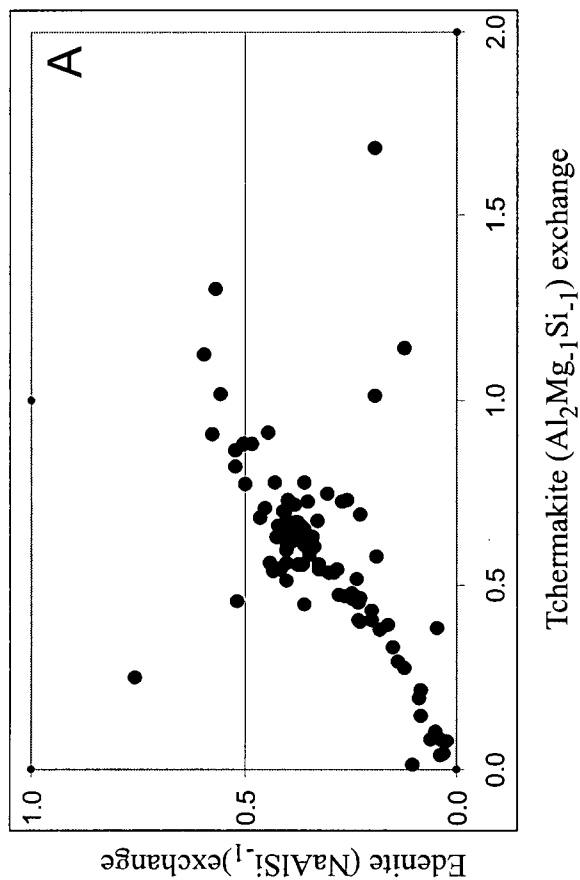


Fig. A10.3. Composition of amphiboles from the host rocks to the Konuto Lake VHMS deposit.

- A. Tschermak ( $\text{Al}_2\text{Mg}_3\text{Si}_3$ ) vs. edenite ( $\text{NaAlSi}_3$ ) exchange component.
- B. edenite ( $\text{NaAlSi}_3$ ) vs. kali-natro ( $\text{KNa}_3$ ) exchange component.
- C. Magnesio-calcic ( $\text{CaMg}_3$ ) vs. Tschermak ( $\text{Al}_2\text{Mg}_3\text{Si}_3$ ) exchange component.

Table A10.4. Major element concentrations in plagioclase from the wall rocks  
to the Konuto Lake VHMS deposit

Sample#	Micro-analyt. Point #	Al <sub>2</sub> O <sub>3</sub> (%)	CaO (%)	Fe <sub>2</sub> O <sub>3</sub> (%)	K <sub>2</sub> O (%)	MgO (%)	Na <sub>2</sub> O (%)	SiO <sub>2</sub> (%)	SrO (%)	BaO (%)	Pb (%)	SUM
HOF-5-70	12	24.96	6.48	0.19	0.06	0.00	7.62	60.48	0.002	0.002	0.019	99.82
HOF-5-70	15	20.29	0.72	0.27	0.13	0.02	11.17	68.97	0.002	0.002	0.025	101.60
HOF-5-70	17	20.25	0.73	0.07	0.08	0.00	11.22	68.69	0.002	0.002	0.002	101.07
HOF-5-70	2	19.11	1.17	0.46	0.18	0.01	8.13	69.59	0.002	0.002	0.002	98.64
HOF-2-127	C-1	27.96	10.13	0.36	0.04	0.00	5.89	56.07	0.002	0.002	0.006	100.46
HOF-2-127	C-2	26.73	8.60	0.25	0.06	0.00	6.91	57.72	0.002	0.038	0.002	100.32
HOF-2-127	C-3	27.96	10.63	0.26	0.05	0.00	5.66	55.03	0.002	0.012	0.002	99.61
HOF-2-127	CB-1	26.81	8.61	0.33	0.03	0.00	6.83	58.22	0.002	0.002	0.002	100.84
HOF-2-127	CB-2	25.77	7.38	0.45	0.06	0.01	7.40	59.57	0.002	0.002	0.169	100.81
HOF-2-127	CB-3	18.29	0.03	0.43	16.79	0.01	0.04	65.41	0.002	0.080	0.002	101.08
HS9675-1	A-12	22.73	2.22	0.31	0.35	0.07	2.96	69.62	0.002	0.051	0.002	98.31
HS9675-1	A-17	23.18	3.35	0.21	0.06	0.01	5.36	69.42	0.002	0.029	0.002	101.62
HS9675-1	A-19	23.99	5.42	0.23	0.06	0.00	8.54	62.59	0.002	0.020	0.002	100.87

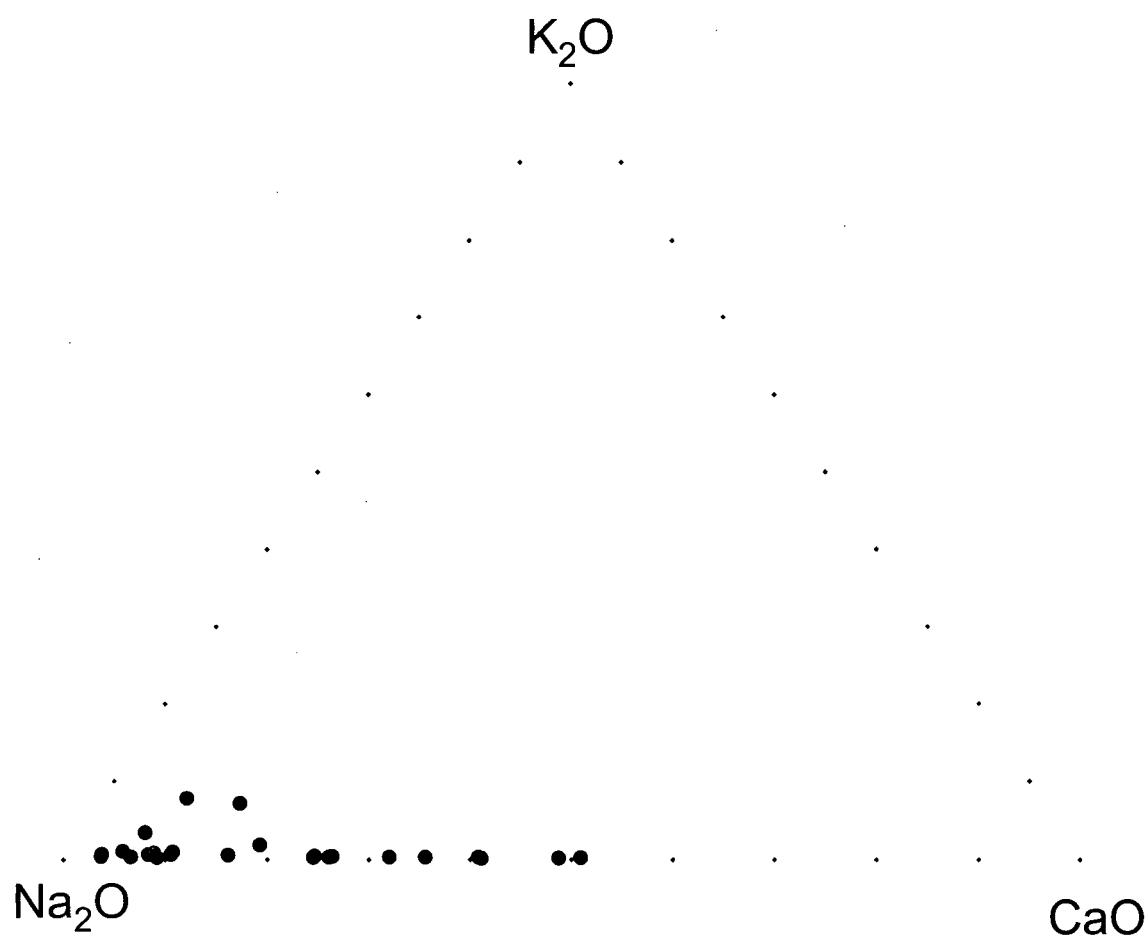


Fig. A10.4. Compositions of plagioclase from the host rocks to the Konuto Lake deposit.